Palaeoclimate reconstruction of the Northern Isles of Scotland, and Caithness, during the Last Glacial – Interglacial Transition.

Allan Alexander Cochrane

Submitted for the degree of Doctor of Philosophy

Biological & Environmental Sciences
School of Natural Sciences

University of Stirling

12th May 2020

Statement of Originality

Below I confirm that the research in this thesis, is original, has been completed by myself, the author, and all the work contained in the body of the text has been referenced and cited appropriately.

.....

Allan A. Cochrane

Date: 12-05-20

VIVA: 15-07-20

Amended Thesis Submission Deadline: 27-09-20

Word count: 77,654

“The heavens declare the glory of God; the skies proclaim the work of His hands” (Psalm 19:1, ESV)

Acknowledgments

Firstly, I would like to thank my supervisors for their continual support. Dr Robert McCulloch who has supported me throughout this research and who has bought me copious amounts of coffee. He has provided me with valuable feedback for my presentations, publications and thesis chapters even after retiring. Secondly, I would like to thank Dr Eileen Tisdall for her continual support and helpful comments on the chapters of my thesis. I would like to thank her for the support, thesis comments and guidance during our field excursions and our conference at INQUA Dublin 2019. Thirdly, I would like to thank Dr Philippa Ascough, at the Scottish Universities Environmental Research Centre (SUERC), for her guidance on radiocarbon dating, age-depth modelling and sample preparation. Fourthly, I would like to thank Dr Tom Bradwell for his help with understanding the glacial processes in the Northern Isles of Scotland and comment on my thesis.

In addition, I would like to thank Prof Jaime Toney, at the University of Glasgow, for her guidance and shared knowledge regarding the use of algal biomarkers for temperature reconstructions. I would like to thank her for the opportunity to her Biomarkers for environmental and climate science laboratory (BECS Lab). In addition, I would like to thank Mr Steve Brooks, from the Natural History Museum (NHM) for his continual guidance and experience surrounding chironomid head capsule identification and temperature modelling. Furthermore, I would like to thank Dr Rhys Timms - Royal Holloway, University of London - for preparing slides and the geochemical analysis of tephra shards. I would also like to thank Dr Richard Staff for teaching me the complexities of age-depth modelling using OxCal. In addition, I would like to thank Dr Hayworth, University of Edinburgh, for allowing me to use the EPMA and his lab for tephra analysis. I would also like to thank Dr Maarten Bleew, Queens University Belfast, for his support in Bayesian age-depth modelling. I would also like to thank Dr Steve Juggins, University of Newcastle, for providing me with a free subscription to the C2 software package. I would like to thank Lorna Goudie, Isle of Shetland, for giving us access to her land. I would like to thank Dr Mary McCulloch for making the most delicious meals I have ever tasted on our field excursions and at our conference. I would also like to thank Finn for his help with building our raft on our field trip. Lastly, I would like to thank all my fellow colleagues from my office, at the University of Stirling and University of Glasgow, and the IAPETUS cohort for their support throughout my PhD.

Several funding sources have made this research possible. I would like to thank the NERC Funded IAPETUS DTP for providing the funds and training for my PhD. I gained a lot from the IAPETUS community, felt supported from the cohort, made new friends/collaborators and I thoroughly enjoyed the annual postgraduate symposiums organised by Prof. John Wainwright (Durham University). I would like to thank the University of Stirling, Biological and Environmental Sciences, for providing the match funding for my research. In addition, I would like to thank SAGES for supporting me with the 'Small Grant Funding' which made it possible to undertake lab work at the University of Glasgow, BECS Lab (with Prof. Jaime Toney). I would like to thank Dr Julian Plancq and Ali Salik for teaching me the lab processes in the BECS Lab. I would also like to thank the NERC radiocarbon facility at SUERC for providing the funds to analyse 11 radiocarbon samples for Langs Loch, Isle of Shetland and 11 samples for the Shebster basin, Caithness (future work). Furthermore, I would to thank Dr Rhys Timms at Royal Holloway, University of London for providing the funds to analyse the geochemical signatures of tephra shards at the University of Edinburgh.

I would like to thank my family and friends for their continual support, both emotional and financial, throughout my PhD. I would like to thank John Currie, Christopher Graham, Laura Richmond, Max Smith and Dr Katrina Nilsson-Kerr for their grammatical comments and advice. I would like to thank SPACE Coffee House for allowing me to type my thesis in their shop and thank them for the lovely flat whites/v60s. I would like to thank my wife, Suzanne Cochrane, for proof reading, this very long thesis and thank her for the emotional support she has provided me with throughout this process. I'm sure all my friends and family will be glad to hear that I am no longer going to be an "eternal student".

Above all, I would like to thank the Lord Jesus Christ for giving me the opportunity to study for a PhD and for guiding me throughout my research. He gave me the will power to continue, even when I was at my lowest. Studying the world, which He created, has been awe-inspiring and a true privilege, and one which has brought me closer to Him.

Abstract

Reconstructing high-resolution records of atmospheric temperature change is necessary to better understand the oceanic-atmospheric-terrestrial systems of the North Atlantic region. Using chironomid assemblages to reconstruct mean July summer temperatures is a robust method allowing for records of climate change to be made on sub-centennial scales. No records are available for the north coast and Northern Isles of Scotland presently. Sediments from three Scottish sites (Shetland, Orkney and Caithness) spanning the Last Glacial – Interglacial transition (c.15-10k cal a BP) were analysed for chironomid assemblages, micro-XRF geochemical markers, long-chain alkenones and lithology to enhance our understand of palaeoclimate and environmental changes during this time.

These sites are located close to the North Atlantic Ocean, are highly sensitive to fluctuations in the thermohaline circulation and are prime localities to study the complex interaction between the ocean-atmosphere-terrestrial systems. Mean July summer temperature records have been inferred from chironomid assemblages found in lacustrine sediments from Orkney and Shetland (Northern Isles) and Caithness (the north coast of Scotland), complemented by the first long chain alkenone (LCA) spring lake temperature record for Scotland (Caithness). The chironomid and LCA records have provided a better understanding of seasonality in the climate records: showing that spring lake temperatures warmed earlier than summer temperatures and shows temporal, and magnitudinal, leads and lags between sites across N.W Europe.

Chironomid and alkenone inferred temperatures captured the abrupt cooling phases GI-d (6-7˚C), GI-1b (6-7˚C) and GS-1(5-6˚C) found in the Greenland ice core records. The warming phases GI-1e (10-11˚C), GI-1c (8-9.5˚C), GI-1a (10-11.5˚C) and the Holocene onset (12˚C) have also been recorded. Orkney and Caithness record the subtle three-phased event GI-1c, highlighting the warmer GI-1c (1), cooler GI-1c (2) and the warmer GI-1c (3) stage. Summer trends in Shetland are not as abrupt as those in Caithness and Orkney and trends in Shetland are more similar to those in Greenland than in other Scottish sites.

Table of Contents

LIST OF FIGURES

LIST OF TABLES

Terms and acronyms

AMOC	Atlantic Meridional Overturning Circulation
AMS	Accelerating Mass Spectrometer
B-A	Bølling- Allerød
BIS	British Ice Sheet
BRITICE project	British-Irish Ice Sheet Modelling Project
C-IT	Chironomid inferred temperatures (˚C)
DO events	Dansgaard-Oeschger
ENSO	El Niño Southern Oscillation
FIS	Fennoscandinavian Ice Sheet
GC-FID	Gas Chromatographer Flame Ionising Diffraction
GC-MS	Gas Chromatographer Mass Spectrometer
GRIP	Greenland Ice Core Project
HE	Heinrich Events
IDW	Inverse Distance Weighting
IRD	Ice Rafter Debris
INTIMATE	INTegration of Ice-core, MArine and TErrestrial records
ITCZ	Inter Tropical Convergence Zone
LGIT	Last Glacial – Interglacial Transition
LGM	Last Glacial Maximum
LLS	Loch Lomond Stadial
MAAT	Mean annual air temperatures
MAT	Modern Analogue Technique
MFM	Lake Meer Felder Maar
MIS	Marine Isotope Stage
NGRIP	North Greenland Ice Core Project
NPF	North Polar Front
OxCal	Oxford radiocarbon calibration
SIC	Shetland Ice Cap
SST	Sea Surface Temperatures (˚C)
SMOW	Standard Mean Ocean Water (‰)
TMC	Thermohaline Circulation
YD	Younger Dryas Period

Chapter 1 - Thesis outline

High resolution temperature reconstructions for the Northern Isles of Scotland and Caithness are lacking and as a result there is a need for independent, reliable and robust paleoclimate records for the region. Chironomid head capsules, long-chain alkenones and micro-XRF geochemical analysis have been implemented to better understand the leads and lags, magnitude and, when possible, synchronicity of climate change across the north of Scotland during the Last Glacial – Interglacial Transition (LGIT). Using a multi-proxy approach to reconstruct the environmental and climate history of the region, provides one with a fuller image of climate change throughout the LGIT. This thesis is organised into 10 chapters. This section, Chapter one, will provide an outline to the thesis.

Chapter two will provide an overview of the literature, titled a '*Palaeoenvironmental history of the North Atlantic region during the Quaternary period'.* Here, will focus on the last glacial cycle, the periods of climate warming and cooling from the termination of the LGM to the onset of the Holocene period. A more detailed depiction of the LGIT in Scotland will be included to highlight the spatial focus of this investigation. A summary of the major palaeoclimate proxies used for environmental and temperature modelling will be included, highlighting the pros and cons for each.

Chapter three, *Chironomid Assemblages: an overview of their taxonomy and application in palaeoclimate reconstructions,* will provide an overview of the life cycle of chironomid larvae, their biodiversity, their application to palaeoclimate research and the pros and cons of using this method.

Chapter four, '*Thesis rationale, site selection and aims/objectives/hypotheses'* highlights, the rationale for conducting the research in the Northern Isles of Scotland and Caithness with the aims and objectives for the project.

Chapter five, includes the methods and materials used in this research. Showing the measures taken in the field, laboratory and during analysis of the results. A description of the sediment coring, lithological analysis (both non-destructive and destructive) and geochemical analysis will be shown. An in-depth description of the methodologies used in extraction, preparation, identification and modelling of chironomid head capsules will be highlighted. Furthermore, the methods used in statistical analysis of the temperature inference models will be included. Next, the

methods used in the preparation, extraction and modelling spring lake temperatures using algal lipids, in particular long chain alkenones, will be shown, highlighting the reasoning for including this proxy. A description of the laboratory work and technical modelling used in the construction of the robust chronology will be included, focusing on the use of tephrochronology and AMS radiocarbon dating. An overview of the software and approach used in constructing geographical maps and palaeo-isotherms for each site will be included to conclude this chapter.

Chapter six, '*Palaeoclimate and environmental reconstruction of Shetland during the LGIT'*, will highlight the palaeoenvironmental history and chironomid inferred temperatures for Lang Lochs mire using an independent chronology and high resolution chironomid sub-sampling. This chapter will compare the onset of the Holocene period with the pollen record from Hulme & Shirriff (1994) and the chironomid record in Lang Lochs mire.

Chapter seven, '*Palaeoclimate and environmental history of Orkney during the Last Glacial – Interglacial Transition'*, will highlight the major findings for the second site located on Orkney in the Sabiston basin. Here, an independent, AMS and tephra based, chronology was used, combined with a high-resolution record of chironomid inferred temperatures to assess the leads and lags in climate change across Orkney. This chapter will compare the temporal fluctuations in temperature, ecology and landscape evolution across the Isle of Orkney, by comparing this record with diatom and pollen records from the literature.

Chapter eight, '*Multi-proxy palaeoclimate and environmental history of Caithness, Northern Scotland, during the Last Glacial-Interglacial Transition.*' This chapter will highlight the palaeoenvironmental findings from the Shebster basin in Caithness, from northern Scotland. This will assess the leads and lags between the mean July summer temperatures, inferred from the chironomid assemblages, and the spring lake surface temperatures inferred from the long chain alkenone records.

Chapter nine, '*A synthesis of the inferred temperatures for the Northern Isles of Scotland and Caithness during the Last Glacial – Interglacial Transition*' will combine all the results from this project. Here, an overview of each of the sites will be included and the implications for climate change across the North Atlantic Ocean will be highlighted. Chapter 10 with conclude the thesis and highlight the future work required.

Chapter 2. Palaeoenvironmental history of the North Atlantic region during the Quaternary period

2.1 Quaternary climate change

The Quaternary period constitutes last 2.6 million years to present day (Lowe & Walker, 2014). Evidence from deep ocean sediments indicates there were 50 interstadial - stadial cycles (Lisiecki & Raymo, 2005) and within the last 800,000 years there have been 10 cycles (Lowe & Walker, 2014). The final cycle will be focus of this research – known as the last glacial-interglacial transition (LGIT).

2.2 Last Glacial – Interglacial Transition (LGIT)

High-latitude summer insolation is believed to have led to the destabilisation of northern hemispheric ice sheets at the end of the Last Glacial Maximum (Rodrigues et al., 2010) triggering the onset of the LGIT. Reduced sea ice cover in the southern hemisphere is thought to have led to the transportation of heat northward into the North Atlantic Ocean (Bianchi & Gersonde, 2004). Which would have led to the rapid retreat of ice sheets at this time [Fig.1]. Shown through the release of ice-rafted debris (IRD), during Heinrich event 1, between c.17.5k cal BP to c.15k cal BP (Lowe & Walker, 2014). This coincided with an abrupt reignition of the Atlantic Meridional Oscillation Circulation (AMOC) and deep-water formation in the North Atlantic Ocean (NADW). The reorganisation of oceanic currents in the North Atlantic are thought to have led to increased atmospheric temperatures of 10˚C in less than a century (Steffensen et al., 2008). Warming is thought to have occurred synchronously across the Northern Hemisphere however more evidence suggests that this may not be the case. Bradwell et al. (2019) highlights that the onset of the LGIT varied temporally across the Northern Isles of Scotland with early deglaciation of the LGM occurring at 19ka BP on the north coast of Scotland and c.15-16k BP in parts of the Northern Isles. Furthermore, the magnitude of temperature change has been shown to vary spatially and temporally across this region throughout the LGIT (Brooks & Langdon., 2014).

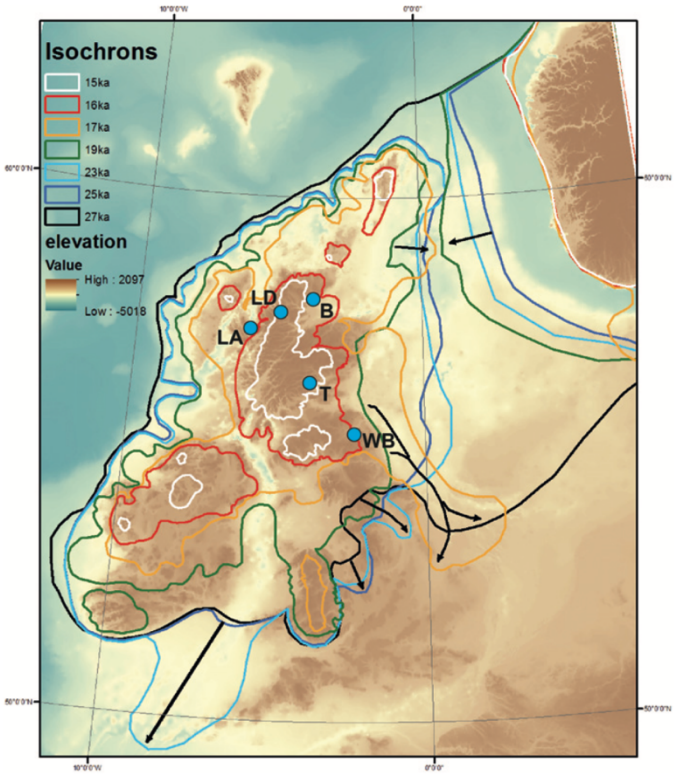

Figure 1. Isochrons of glacial retreat after the termination of the LGM (Walker & Lowe, 2019 citing Clark et al., 2012)

The LGIT was a unique time of increased climatic instability, with high amplitude climate oscillations and extensive environmental change (Denton et al., 2010; Brooks et al., 2016) across the North Atlantic (Peterson et al., 2000), North America (Iversen, 1954) and Europe (Naughton et al., 2007) and as a result, it is the most documented time period throughout the Quaternary. Climate scientists have been fascinated with this period as the rapid changes in the environment and climate have been readily recorded in terrestrial and marine archives making this a unique time frame to study the complex interactions between the atmosphere-ocean-terrestrial systems. High-resolution records and climate models have been developed, enhancing our understanding of this time (Meehl et al., 2007; Heiri et al., 2014) however they are spatially disparate across N.W Europe with gaps in the North Atlantic. Notably, the Faroe Islands, Iceland, Greenland and the Northern Isles of Scotland have a lack of records (Brooks and Langdon., 2014). The high amplitude climate fluctuations altered between stadial (cold) and interstadial (warm) conditions, and at times on sub-centennial scales (Rasmussen et al, 2014). Notably, there was a period of abrupt warming at the end of the LGM, c. 15k cal BP, known as the Bølling-Allerød in Europe (Hoek, 2008), and GI-1 in Greenland (Rasmussen et al., 2014).

2.2.1 **Bølling-Allerød Interstadial/ GI-1**

The Bølling - Allerød interstadial/GI-1 is a period of climate warming which began at c.14.7k cal BP and lasted until c.12.9k cal BP (Blockley et al., 2012). This marked the end of the Last Glacial Maximum/GS-2 and temperate conditions prevailed across the British Isles and N.W Europe during this time (Brooks and Langdon., 2014; Brooks et al., 2016)

Warm water began to rise from the bottom of the North Atlantic Ocean, combined with the release of CO_2 into the atmosphere, which is believed to have triggered the onset of the interstadial (Thiagarajan et al., 2014). During this time, sea ice retreated in the northern hemisphere, the Atlantic meridional overturning circulation (AMOC) restarted (McManus et al., 2004) and heat rose through the stratified water column (Denton et al., 2005; Thiagarajan et al., 2014).

This period of warming was named after the field localities - Bølling and Allerød in Denmark (Hoek, 2008). Hartz and Milthers (1901) first identified these sites and noticed that an organic layer, rich in birch (*Betula*) and elk fossils, was found between two layers of clay. This clay layer was rich in *Dryas octopetela* macrofossils which was evidence of significant environmental cooling. This sequence suggests that vegetation switched from a tundra-like environment, to a forest and later returned later to a tundra (Hartz and Milthers, 1901). This transition between minerogenic rich clays to macrofossil rich organic sediments indicated that rapid environmental fluctuations occurred between this transition. As the climate and environment changed rapidly this has been reflected in the vegetation across N.W Europe (Birks et al., 1978), diatom (Birnie, 2000; Dalton et al., 2005; Whittington et al., 2003) and coleoptera beetle records (Walker & Lowe., 2019).

Temperatures have been largely inferred from pollen assemblages which have led to large temperature uncertainties and lags in the records (Brooks et al., 2016). For instance, the percentage of Arboreal pollen increased during the Bølling-Allerød throughout N.W Europe which suggests that the warmest part of the LGIT was at the latter end of the Allerød interstadial (Hoek, 2001). However, this conflicts with the Greenland ice cores (Johnsen et al, 1992; Grootes et al., 1993) and Coleoptera beetle assemblages (Atkinson et al., 1987; Coope et al., 1998), which suggest that the warmest part of the LGIT was during the Bølling interstadial. Therefore, high resolution single variable temperature records are required to assess the magnitude of climate changes during this time.

2.2.2 **Younger Dryas/Loch Lomond Stadial/GS-1**

The Younger Dryas Stadial, or cold reversal, (c.12,900 - 11,600 BP cal BP) was a short-lived period of intense cooling which lasted for approximately 1,000 years (Golledge et al., 2008(b); MacLeod et al 2011). The Younger Dryas occurs during a time of increased summer insulation. Nevertheless, glacial re-advance prevails across the North Atlantic region (Golledge et al., 2008(b)).

The current hypothesis postulates that catastrophic drainage of Lake Agassiz, dammed by the Laurentide Ice Sheet, slowed down the thermohaline circulation in the North Atlantic (MacLeod et al., 2011), which in turn ceased the flow of warm water from the Gulf of Mexico (Johnsen et al., 1992; Alley et al., 1993; Clark et al., 2001). This inhibited warm salty water from the Southern Ocean rising to the surface, thus causing a 'breakdown' in the thermohaline circulation (also known as the Atlantic meridional overturning circulation - AMOC) (Broeker, 1997). Secondly, due to the lack of convection, cold freshwater is thought to have collected on the ocean surface, preventing transfer of heat to the atmosphere (Fiedel, 2011) leading to a reduction in atmospheric temperatures. Three factors are thought to have influenced the onset of the Younger Dryas Stadial: ocean circulation, atmospheric circulation (Seager and Battista, 2007) and solar radiative forcing (Fiedel, 2011). The third scenario is that solar radiative forcing reduced, due to a weakening of the sun, which caused a reduction in insolation and as a result lower atmospheric and oceanic temperatures (Goslar et al., 2000).

The magnitude of the YD was not uniform throughout the Northern Hemisphere (Fiedel, 2011) as winter temperatures in the Grand Canyon fell to 3˚C (Cole and Arundel, 2005) whereas temperatures in Greenland fell by 10˚C (Alley, 2000; Grachev and Severinghaus, 2005). The North American Great Basin (Liu and Broeker, 2008) and Florida (Grimm et al., 2006) had wetter climates during this time whereas In China climate was wet and summer monsoons were frequent (Zhou et al., 1997).

In N.W Europe the YD has been recorded in a high-resolution record from Meerfelder Maar, in Germany. These lake sediments are continuously varved and constrained by 69 radiocarbon samples and the Laacher See Tephra layer forming a robust age-depth model (Brauer et al., 2008). This record indicates that falling temperatures lag behind Greenland by 200 years suggesting that climate and environmental change differed between regions across N.W Europe during this period. In addition, Lake Kråkenes has a continuous YD record which has been constrained

by 96 calibrated AMS dates which has been tied to the Greenland Ice Core record by the Vedde Ash tephra layer and indicates that the North Polar Front (NPF) moved northwards throughout the YD (Lane et al., 2013). Evidence from the Nordic Sea suggests that the surface waters were frozen during the early YD. It is thought that the North Polar Front propagated northwards leading to increased sea surface temperatures and ice-free conditions at c.12.15 k BP (Bakke et al., 2009). This occurred 400 years earlier than the onset of the YD in Greenland. Further indicating that possible asynchronies occurred in the North Atlantic region during this time.

2.2.3 **Holocene Period**

The Holocene period marks the end of the Younger Dryas/GS-1 (Walker et al., 2009) and the beginning of rapid temperature warming throughout the Northern Hemisphere, with an average increase of ~10 ± 4˚C (Buizert et al., 2014; Grachev and Severinghuas., 2005). Risebrobakken et al (2011) highlights that the onset of the Holocene period was due to increased summer insolation due to orbital forcing. Crucifix et al (2002) and Helmans et al (2007) highlight that local and regional variations in oceanic and atmospheric currents controlled the magnitude and timing of warming, combined with the destabilising of ice sheets at the end of the YD. Throughout the early Holocene there were notable short-lived drops in atmospheric temperatures called the 11.4k event and the 8.2k event (Rasmussen et al., 2007; Rasmussen et al., 2014). These events are thought to be a result of an influx of cold freshwater into the North Atlantic Ocean which briefly stopped the thermohaline circulation (THC) (Wiersma and Rensen., 2006). Although short-lived cold events have been identified in the early Holocene; temperatures do increase sharply on the whole. This led to highly stable temperatures (Brooks et al., 2012) resembling what we see today. A chrono-stratigraphical framework has been recently formed to highlight the main climatic events that occurred throughout this time (Walker et al. 2019). A tripartite sequence has been formulated with the first being the warm Greenlandian Stage/Age (11,650 cal BP), the second being the cooler Northgrippian Stage/Age (8186 cal BP) and thirdly, the drier Meghalayan Stage/Age (4250 cal BP).

2.2.4 **Modern-day climate**

2.2.4.1 North Atlantic Oscillation (NAO)

Understanding present day climate processes is key to infer the palaeoclimate history of the North Atlantic. Weather and climate across the Northern Hemisphere are controlled by fluctuations in the North Atlantic Oscillation (NAO) (Hurrell and Deser, 2010). The NAO is a term used to describe the redistribution of air masses between the Arctic and the sub-tropics (Hurrell and Deser, 2010) [Fig.2]. The NAO alternates between negative and positive phases and is used as an indicator for increased storminess, changing winds and alternating levels of precipitation (Hurrell and Deser, 2010). The NAO has been shown to also impact fluctuations in ocean heat content, circulations, salinity values, deep water formations and sea ice cover extents. When climate modes, such as the NAO, consistently change they lead to significant changes in weather patterns over long temporal periods ("climate change").

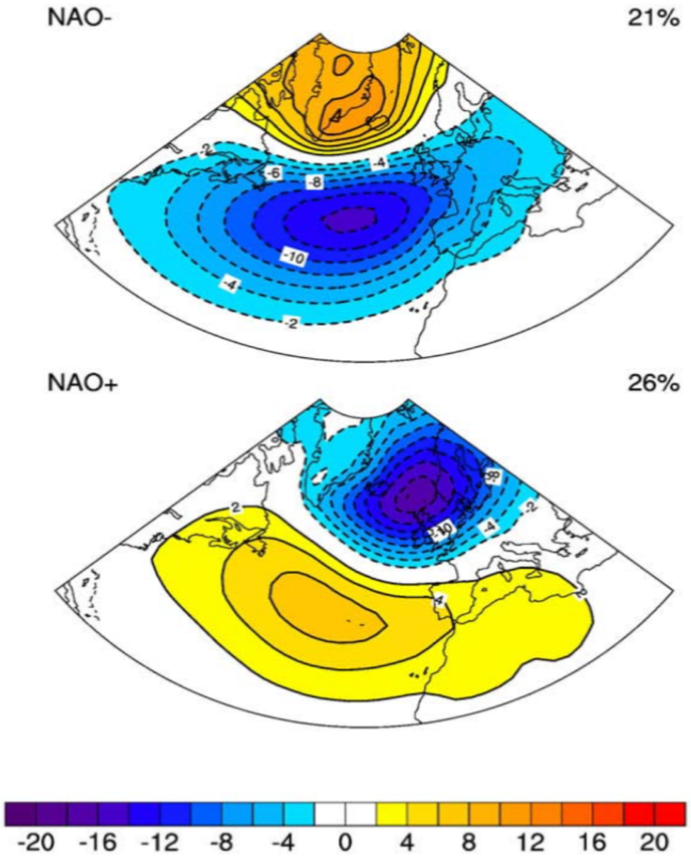

Figure 2. Boreal winter North Atlantic Oscillation indices between 1950-2006 geospatially shown through cluster analysis. This map shows the spatial variability of the NAO across the North Atlantic region (Hurrell and Deser, 2010)

The NAO indices have been used to better understand the relationship between atmospheric variability and ecosystem functions through large temporal scales. Rapid magnitudinal, frequential and altitudinal shifts in climate modes have been shown to influence the temporal and spatial distribution of marine and terrestrial ecosystems (Stenseth et al., 2003; Wang and Schimel, 2003). These climate changes are then recorded through time by the marine and terrestrial climate proxies which are mentioned throughout this research. The NAO indices have been recorded from 1860 to present day and can be used as a proxy for understanding variations in atmospheric and ocean conditions through time (Hurrell and Deser, 2010) [Fig.3]

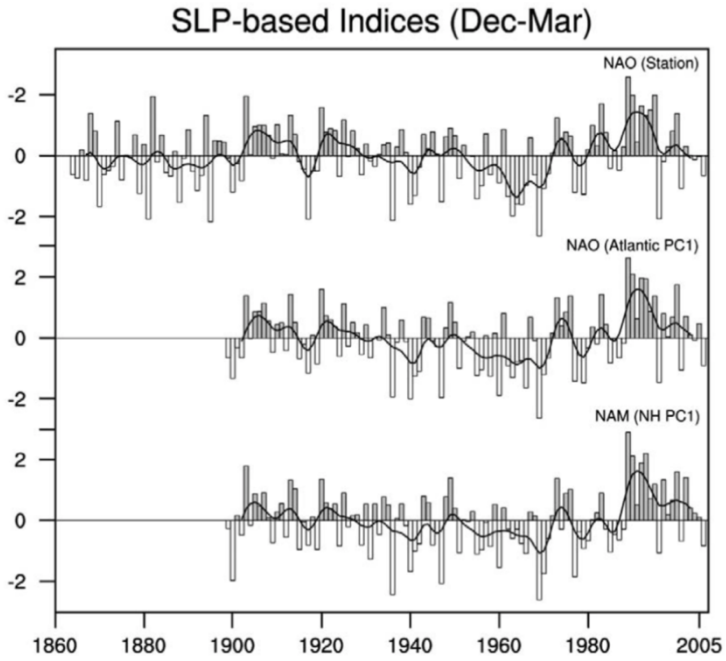

Figure 3. North Atlantic Oscillation indices recorded through time (1860-2005) (Hurrell and Deser, 2010)

Variations in the NAO is known to be a dominant control in winter temperatures across the Northern Hemisphere with sea surface temperatures and surface air temperatures being positively correlated with the NAO (Hurrell and Deser, 2010). Studies have shown that multidecadal fluctuations in the NAO can induce poleward ocean heat transfer in the North Atlantic Ocean and influence the downturn of the Atlantic Meridional Overturning Circulation (AMOC) (Delworth et al.,2016) [Fig.4]. Therefore, understanding modern-day atmospheric processes are vital to better understand climate change through time. It is also important to understand what forced particular climate events through time, what the geospatial extent of atmospheric temperatures was and the implications of climate change on terrestrial ecosystems. Variations in the NAO and atmospheric circulation patterns have been shown to impact terrestrial and

marine ecosystems today (Mysterud et al., 2003; Straile et al., 2003). Atmospheric pressures tend to be larger during the winter months are more stable during the summer which leads to more stable conditions (Wallace et al., 1993). As a result, as the interpretations made from this research are based on summer intervals the inferences are likely to be more reliable as seasonal pressure variations are not a factor to consider.

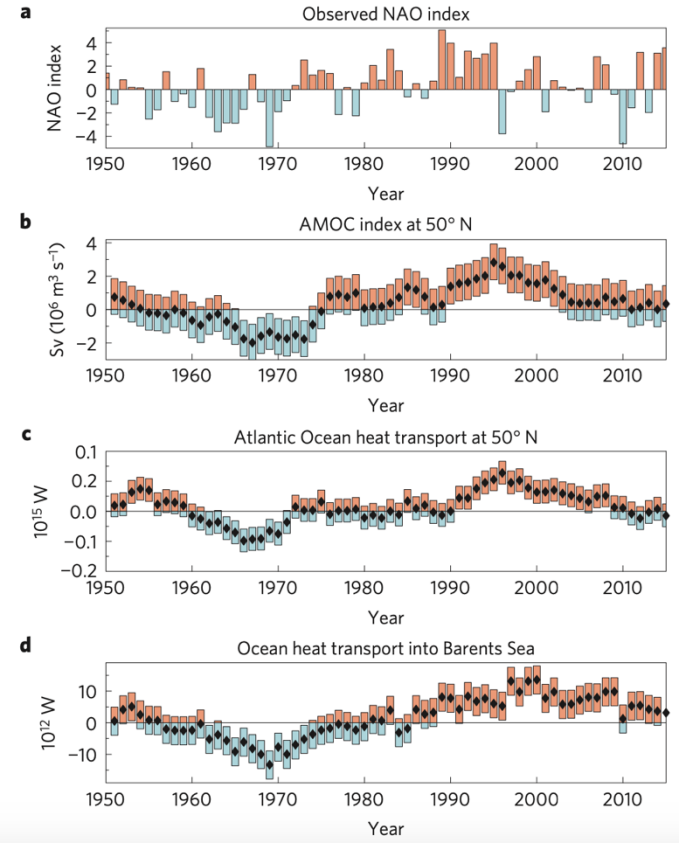

Figure 4. Graphs below show the relationship between the observed NAO index (a), the AMOC index at 50˚N (b), the Atlantic Ocean heat transport at 50˚N (c) and the ocean heat transport into the Barents Sea (d) between 1950-2010 (Delworth et al., 2016)

2.2.4.1 North Atlantic Current

The North Atlantic Current is an important driver of atmospheric warming and cooling in the Northern Hemisphere. It is an essential system which regulates the transportation of heat from sub-tropical latitudes and transporting deep water carbon northward (Holliday et al., 2020). Highly saline waters from the sub-tropics flow northward to higher latitudes in the North Atlantic Ocean, cool and then sink, forming the North Atlantic Overturning Meridional Circulation (AMOC) (Buckley and Marshall, 2016; Ferreira et al., 2018). Modern-day climate studies have shown that atmospheric winds can drive fluctuations in the AMOC and slow the circulation down (Holliday et al., 2020).

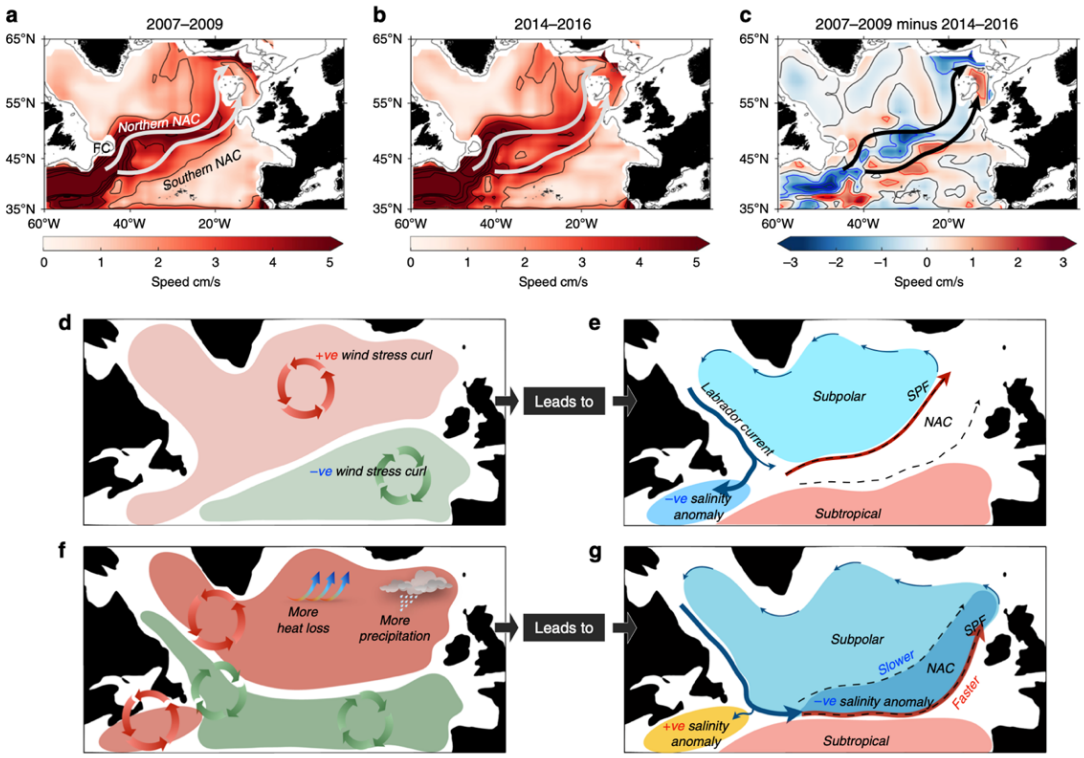

Figure 5. Schematic from Holliday et al (2020) highlighting the complex relationship between heat transport, salinity, the sub-polar gyre and the North Atlantic Current for controlling climate in the North Atlantic Ocean.

Holliday et al (2020) have shown that more heat loss and increased precipitation in the North Atlantic Ocean, combined with decreased wind stress curl, leads to a slower sub-polar gyre and a faster North Atlantic Current [Fig.5]. Regional scale ocean circulation is thought to explain the centennial and decadal scale temporal climate changes seen across the North Atlantic (Holliday et al., 2020). Studies have shown that a weaker AMOC is linked to a decline in heat transport northwards and reduced sea surface temperate and heat storage (Knight et al., 2005; Delworth & Zeng, 2012; Smeed et al., 2018). Furthermore, 20th century salinity measurements have likened reduced values to a reduction in wind forcing in the North Atlantic region (Häkkinen et al., 2002). There is a complex relationship between the ocean-atmosphere and when researching the palaeoclimate history of the region it is important to understand what drives fluctuations in climate in present day. Uniformitarianism underpins the temperature inferences and environmental reconstructions made in this research. The assumption is that, like today, the AMOC and the NAO/atmospheric circulations were the main drivers of climate change throughout the LGIT.

2.2.5 **Chronological nomenclature**

Throughout N.W Europe and the North Atlantic Ocean the literature suggests that the LGIT spanned c.15-8 k cal BP (Hoek, 2008). This time frame has been known as the Weichselian Lateglacial (in Europe), the Wisconsian (in North America) and the Devensian (in Britain) (Lowe & Walker et al., 2014). There is a general agreement that each nomenclature used relates to the LGIT. However, there is uncertainty regarding the timing of the formal subdivisions throughout this period. On the British Isles two events are highlighted during the LGIT, the Windermere Interstadial and the Loch Lomond Stadial event. Whereas, on the European mainland these events are known as the Bølling and Allerød periods (Hoek, 2008). Further confusion arises when the Greenland Ice Core records are considered. Here, the stadial/cold events are known as GI-1d, GI-1b and GS-1; whereas the interstadial events are known as GI-1e, GI-1c and GI-1a (Rasmussen et al., 2014). Work has been done by the INTIMATE working group to build a chrono-stratigraphical framework that prescribes up-to-date descriptors and event horizons for the LGIT and beyond. (Rasmussen et al, 2014 Walker et al, 2019) [Table 1.].

Table 1. INTIMATE event stratigraphy for the Last Glacial-Interglacial Transition (Rasmussen et al., 2014)

INTIMATE-Event Stratigraphy			
Event	NGRIP depth (m)	Age (b2k)	Maximum counting-error (years)
Onset of 8.2 ka BP Event	1234.78	8300	49
End of 9.3 ka BP event	1322.88	9240	68
Onset of 9.3 ka BP event	1331.65	9350	70
End of 11.4 ka BP event	1476.16	11400	96
Onset of 11.4 ka BP event	1482.32	11520	97
Onset of Holocene	1492.45	11703	99
Onset of GS-1	1526.52	12896	138
Onset of GI-1a	1534.5	13099	143
Onset of GI-1b	1542.1	13311	149
Onset of GI-1c1	1554.75	13600	156
Onset of GI-1c2	1557.08	13660	158
Onset of GI-1c3	1570.5	139854	165
Onset of GI-1d	1557.08	14075	169
Onset of GI-1e	1604.64	14692	186
Onset of GS-2.1a	1669.09	17480	330

2.2.6 **Greenland Ice Core Record**

The Greenland ice-cores provide an archive of the environmental and climatic changes that occurred during the LGIT for the Northern Hemisphere (Rasmussen et al., 2014). The cores record the isotopic ratios of oxygen atoms ($\partial^{18}O/\partial^{16}O$), from gas bubbles locked in the ice. These gas bubbles record the chemical composition of the Earth's atmosphere at the time the ice precipitated. Based on these isotopic ratios, it has been shown, that during the Last Glacial Maximum (LGM) temperatures were ~20˚C lower than present day (Daansgaard et al., 1993). The Greenland ice cores have the highest resolution of all terrestrial records in the Northern Hemisphere and are therefore used as a stratotype of temperature fluctuations across the North Atlantic region. Currently, there are 6 ice core projects in Greenland: the NGRIP, GRIP, GISP2, Camp Century, Dye-3 and Renland archives (Johnsen et al., 2001; Rasmussen et al., 2014) [Fig.6]. The nomenclature from the NGRIP ice core (Rasmussen et al., 2014) will be used to compare the climate changes found in this research. Although there are gaps in the Greenland ice core records, the archive is the highest resolution of all terrestrial records, and as a result can be useful to compare the timing of events between sites.

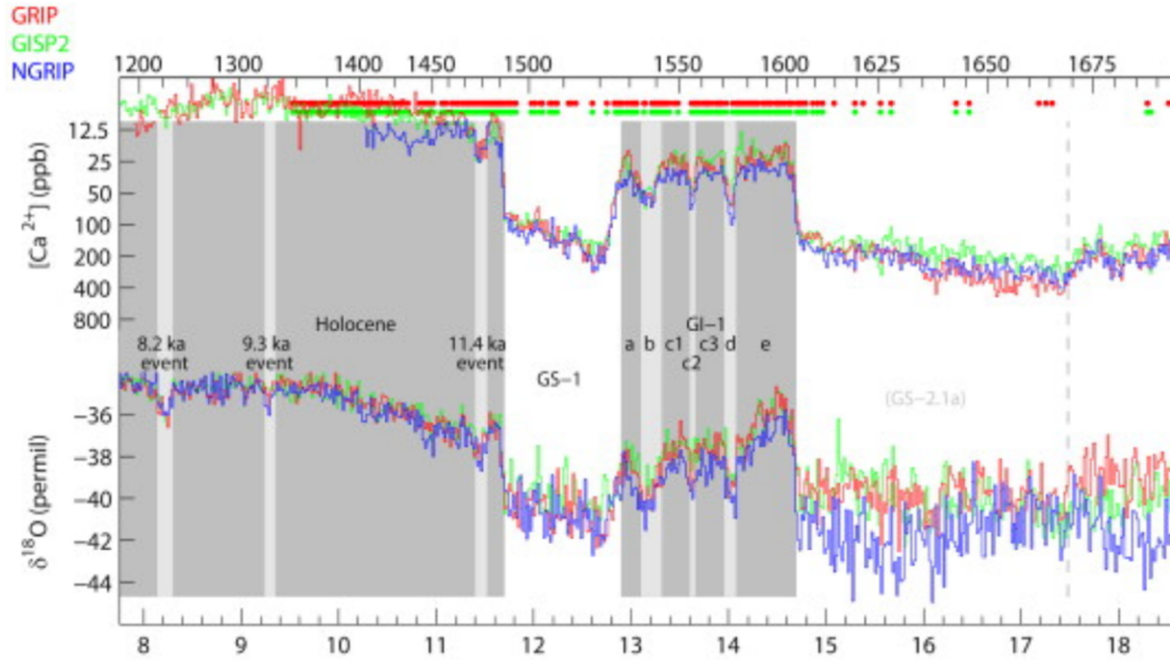

Figure 6. The ∂18O (permil) and Ca2+ (ppb) records for the last 18-8ka using the Greenland Ice Core records (NGRIP, GISP2 and GRIP records). The diagram above highlights the main geological events, using the INTIMATE stratigraphy highlighted in Rasmussen et al (2014)

2.2.7 **Whitrig Bog: a British strato-type (Walker & Lowe, 2019)**

The Greenland NGRIP record has been regarded as the North Atlantic stratotype for the Quaternary period (Rasmussen et al., 2014). However, growing evidence suggests that climate oscillations were not synchronous across the North Atlantic, notably during the YD/LLS (Lane et al., 2013; Lowe et al., 2019).

Walker & Lowe (2019) highlight that there is no one site in the British Isles which is regarded as a strato-type for the LGIT. They suggest that Whitrig Bog should be a contender for this position due to the wealth of data available from the site. They highlight the following strengths for Whitrig Bog to be considered as a strato-type for the LGIT:

- At present the site has the longest sequence of the LGIT in Scotland, spanning approximately 2m.
- Multi-proxy analysis has been undertaken on the same core and therefore does not require cross-correlation between cores.
- There is a large quantity of sediment available for processing, as a trial pit was dug for the site, which allows for multiproxy analysis to be undertaken for the site.
- High resolution sub-sampling has been undertaken at this site: 75 sub-samples for chironomid and pollen assemblages (Brooks et al., 1997). With an average sampling interval of 36 years.
- There is a close resemblance to the NGRIP oxygen isotope record with the chironomid inferred temperatures for this site. With high temperatures being recorded at the onset of the late-glacial interstadial.
- Two tephra layers have been identified which allows for cross-correlation to be made.
- Multiproxy analyses used: chironomids, pollen, micro-XRF and sediment stratigraphy.

Although Whitrig Bog has many strengths to be considered for the British strato-type, it does have a major limitation. The lack of a robust chronology for the site and the lack of tephra tie-points makes determinations of climate synchronicity difficult (Walker & Lowe., 2019).

2.3 Scotland during the Last Glacial – Interglacial Transition

2.3.1 Glacial history of Scotland

The last glacial period is the most studied period of the Quaternary, occurring between c.15k cal BP to c.11k cal BP (Rasmussen et al., 2014). As a result, there is a wealth of data spanning this time. Particularly so in Scotland where the landscape has been carved by glacial activity (Walker & Lowe., 2019).

The glacial history of the north of Scotland and the central Highlands is contentious with some studies suggesting that there were remnants of the British Ice Sheet (BIS), or localised ice-caps in the flat plateaus, of the N.W Highlands and the eastern Cairngorms (Everest & Kubik 2006; Bradwell et al. 2008). Walker and Lowe (2019) highlight that recalibrations of AMS and cosmogenic dating suggests that the majority of the Scottish Highlands had no significant glacial ice. Fabel et al. (2012) goes further by suggesting that prior to the deglaciation of the LGM, the BIS was thinning, prohibiting the expansion of ice into the LGIT [Fig.7]. Glacial erratics on the summits provide exposure ages of c.16-15k cal BP showing that before the BIS ice sheet retreated, ice thinned, and down wasting occurred. However, Small et al. (2012) has shown that localised re-advance did occur in the N.W Highlands during the 'Wester Ross Re-advance' and that the BIS had a remnant ice sheet on Skye that lasted until c.14.3 $\pm$ 0.9ka BP. They suggest that this glacier remained active until the middle of the first interstadial phase (GI-1e).

The glacial history of the Scottish Highlands is complex, and further work is needed to better understand the processes and the landscape evolution during this time. For the most northern point of Scotland and the Northern Isles the glacial history is less clear. During the LGM, it is believed that the north of Scotland, remained ice free and was subsequently named the 'moraine-less Buchan' (Phillips et al., 2008). However, evidence now suggests that the complete Scottish mainland was covered by glacial ice during the LGM (Chiverell & Thomas, 2010) and that deglaciation of the LGM occurred a-synchronously across the Northern Isles and Caithness (Bradwell et al., 2019).

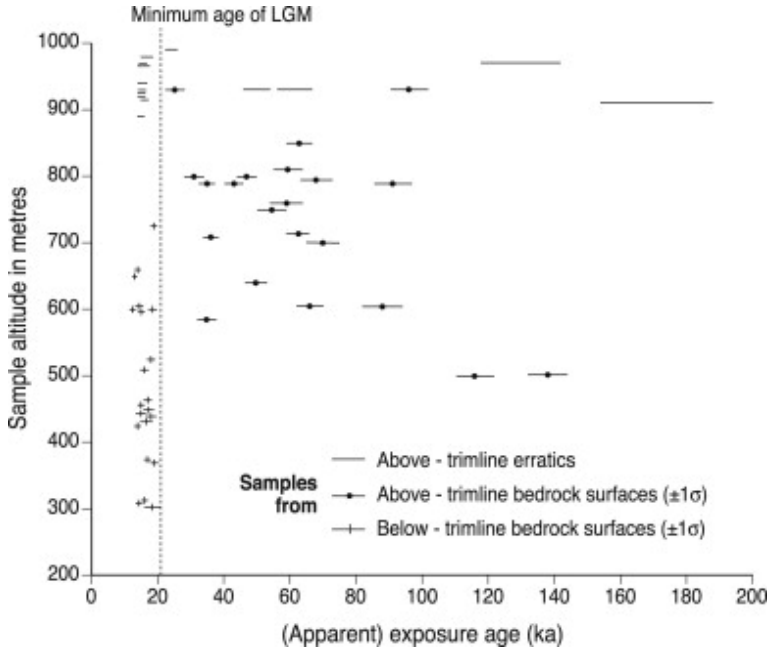

Figure 7. The onset of thinning of the British Ice Sheet constrained by cosmogenic exposure ages (ka) (Fabel et al., 2012)

The last glacial activity in Scotland was during the Loch Lomond Stadial/Younger Dryas period. Golledge et al (2010) and Ballantyne et al (2007) mapped the extent of the Loch Lomond Stadial (LLS) ice sheet to a high resolution using geomorphological evidence and cosmogenic exposure dating [Fig.8]. They combined this with chironomid inferred temperatures to calculate the amount of summer ablation (melting) and winter accumulation. Studies have used cosmogenic, radiocarbon and geomorphological evidence to track the retreat and advance of ice across Scotland during the LLS (Benn & Ballantyne., 2005; Ballantyne & Stone 2012; Golledge et al., 2010; Ballantyne et al., 2007; Fabel et al., 2012).

Throughout the Loch Lomond Stadial meltwater channels, hummocky moraines and glacial trimlines indicate that ice extended to palaeo Lake Blane, located near the village of Croftamie in the southern Scottish Highlands (Lowe & Walker, 2014). For the LLS some exposure dates suggest that there was an early glacial retreat at c.12.5k cal BP (Ballantyne & Stone 2012). However, other sites suggest that the LLS ice remained until c.11.5ka (Small et al., 2016). The extent of ice is varied between glaciers in Scotland. Some reached a maximum position towards the latter end of the LLS whilst others reached a maximum ice thickness at the early stages of the LLS (Golledge, 2010; MacLeod et al., 2010). Golledge et al (2008(b)) simulated the time taken for glaciers to have formed in Scotland and found that 400 years was enough time for the glaciers to advance.

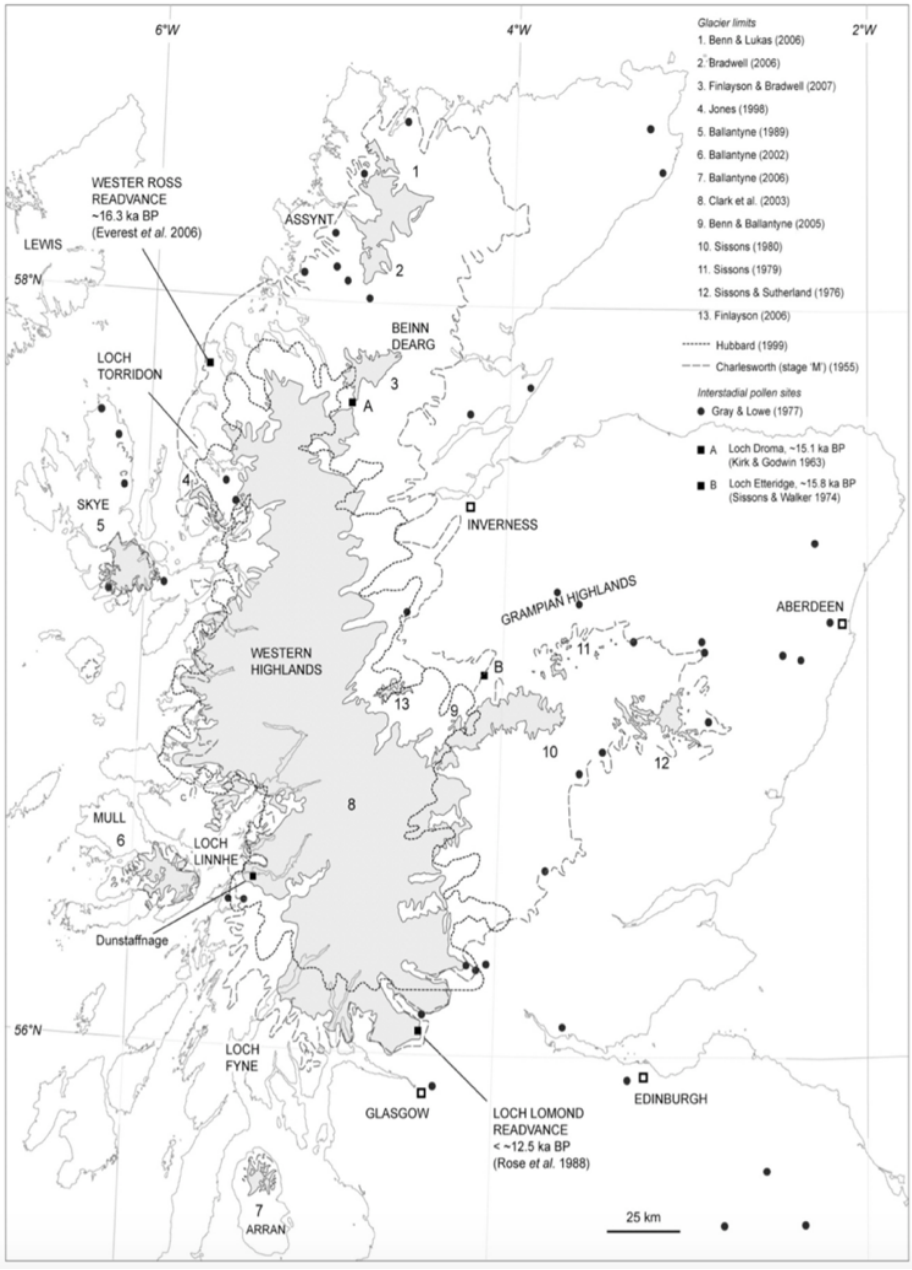

Figure 8. Map of the Scottish Highlands and the extent of the Younger Dryas glacial re-advance. (Golledge et al, 2008 (b))

Although there is a wealth of information surrounding glacial activity in Scotland there is still work needed. In particular, a combination of palaeoenvironmental data and temperature reconstructions need to be recorded to build a bigger picture of the environmental and glacial history of the LGIT in Scotland. With temperature sensitive climate proxies, it may be possible in the future to assess if it was possible for ice to have lasted into the LGIT in the Northern Isles and Caithness. It is of particular interest during the cold reversals, GI-1d and GI-1b.

2.3.2 **Palaeoenvironmental history of Northern Scotland and the Northern Isles.**

This section will highlight the main proxies used to reconstruct the palaeoenvironmental and climate history of Scotland. The pros and cons of using these proxies will be shown for environmental and climate reconstructions. To begin, a summary of the vegetation history of Scotland will be shown through the use of pollen and plant macrofossils. Followed by the use of oxygen isotope analysis and the palaeoclimate histories inferred from speleothem records. This will be followed by an overview of the use of diatoms to reconstruct aquatic ecosystem change and then finish with the use of coleoptera for summer temperature inferences.

2.3.2.1 **Pollen and plant macrofossils records**

Pollen grains and plant macrofossil assemblages are often used to reconstruct environmental change during the LGIT and are the most widely adopted method (Isarin et al., 1999; Lowe and Walker, 2014). Palynological studies throughout Scotland have expanded throughout the last century, exceeding 100 sites (Walker and Lowe., 2019), many of which show the ‘tripartite’ last glacial interstadial sediment stratigraphy, indicating periods of cooling and warming [Fig.9]. These sites are found largely in the north west of Scotland (Boomer et al., 2012), the western isles (Walker & Lowe., 1990; Tipping, 1991), the Grampians (Donner, 1958) and central Highlands (Godwin & Willis., 1959). There have been advances in the record, particularly in the Northern Isles of Scotland with recent studies coming from Loch of Sabiston, Crudale Meadow and Quoyloo Meadow in Orkney (Bunting, 1994; Whittington et al., 2015; Kingsbury et al., 2018; Abrook et al., 2019). Furthermore, Shetland has pollen records from Sel Ayre (Birks et al., 1979) and Clattnadal (Whittington et al.,2003) spanning the LGIT. With records of Holocene environmental change from Lang Lochs (Hulme & Shirriff., 1994) and Catta Ness (Bennett et al., 1992).

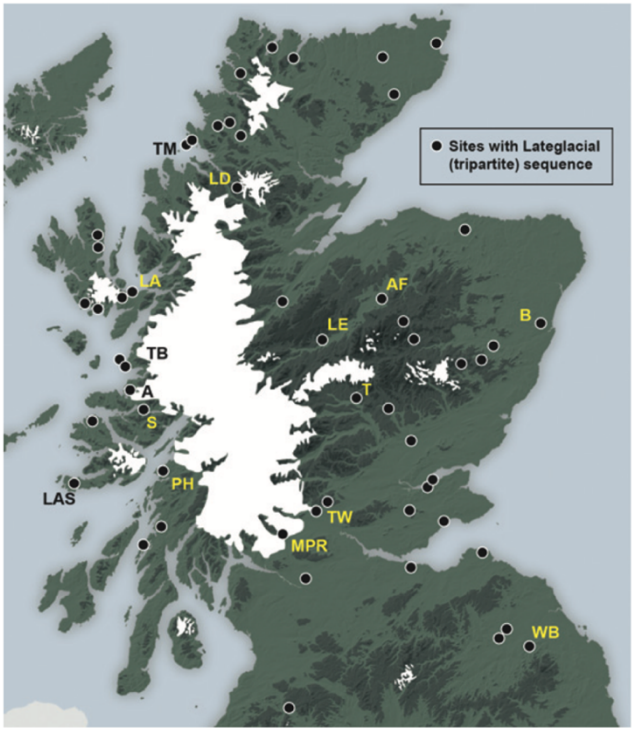

Figure 9. Sites in yellow: AF (Abernethy Forest), WB(Whitrig Bog), MPR (Muir Park Reservoir), LA (Loch Ashik), LD (Loch an Drium) and T (Tirnie). The black dots highlight the tripartite sequence of cooling and warming during the interstadial (Walker & Lowe., 2019)

The best and highest-resolution pollen record from Orkney has been analysed from Quoyloo Meadow (Abrook et al., 2019) [Fig.10]. Abrook et al (2019) records subtle cold reversals, during the 'tripartite' phase of the interstadial. However, as pollen often lags behind more sensitive temperature proxies the magnitudinal scale of these events is currently unknown, thereby stressing the need for single-variable atmospheric temperature proxies. With the advancement of radiocarbon dating these cold events have been dated to be c.14.05-13.63k cal BP and c.10.94-10.8k cal BP in Orkney (Abrook et al., 2019), likely corresponding to GI-1d and GI-1b from the NGRIP chronology from Greenland (Rasmussen et al., 2014).

To date, no records of atmospheric temperatures have been recorded for this region. The vegetation history indicates that Orkney was dominated by open grasslands and heathland during the interstadial (Abrook et al., 2019), suggesting that temperatures were high enough to support these plants. Whilst during the LLS open grasslands prevailed, suggesting that temperatures were significantly cooler. The study of pollen has been shown to provide high resolution climate records (Seppä & Bennett, 2003) and records of vegetation change at local and regional scales (Gajewski, 2008). Pollen grains are wind dispersed to maximise the likelihood of fertilisation. As a result, they may not be deposited *in-situ* and may not reflect the

vegetation of the local catchment (Brooks et al., 2016). Therefore, evidence of plant macrofossils is necessary to determine if a species of plants inhabited the catchment or if it was wind-blown. For instance, at Lochan Druim there is a dominance of *Betula* in the record, however no birch macrofossils have been found indicating that the pollen grains have been transported from afar (Birks, 2003(b)). Therefore, this limitation as pollen assemblages can reflect false environmental change signatures if the grains were transported far via wind.

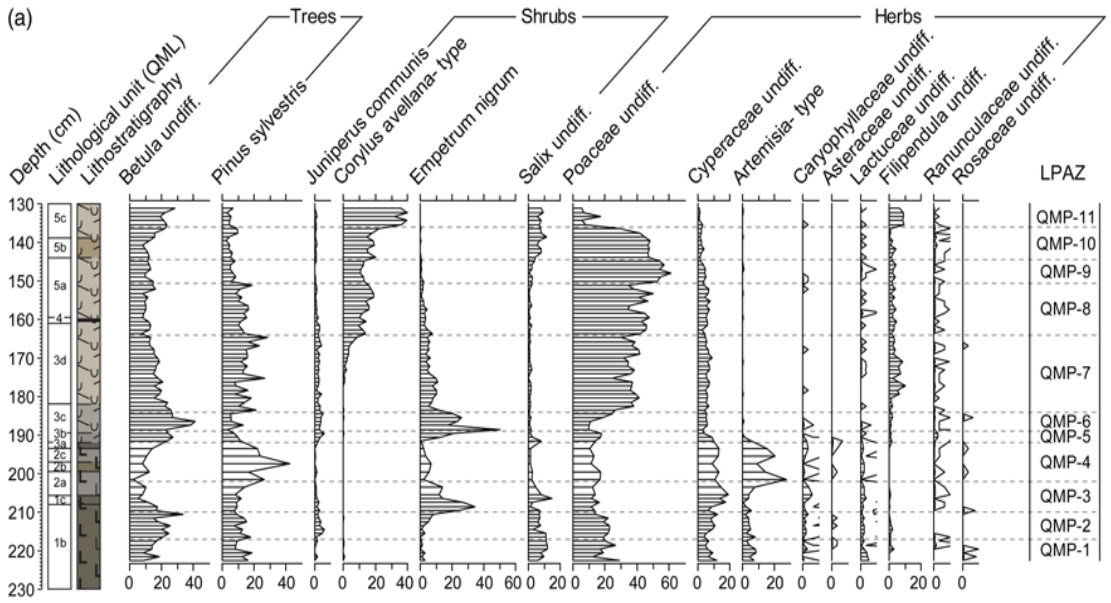

Figure 10. The main pollen assemblages indicating the presence of trees, shrubs and herbs for Quoyloo Meadow. (Abrook et al., 2019)

2.3.2.2 **Stable isotope records: marine and terrestrial**

Stable isotope analysis off planktonic foraminifera, *N. pachydermia*, have been used to reconstruct sea-surface temperatures (SST) across the North Atlantic Ocean (Eldevik et al., 2014). Based on foraminifera stable isotope analysis a warming of 2˚C is seen in the North Atlantic basin at the end of the LGM. This led to the collapse of the Laurentide Ice Sheet (LIS) and inundation of freshwater to the North Atlantic (Marcott et al., 2011; Àlvarez-Solas et al., 2011). The melting of the Feno-Scandinavian ice sheet (FIS) is also believed to be a major contributor to the termination of the LGM and the associated a breakdown of the Atlantic Meridional Overturning Circulation (AMOC) (Àlvarez-Solas et al., 2011). This warming of the North Atlantic Ocean is thought to be a major contributor to the termination of the LGM and the retreat of the British Ice Sheet (BIS) (Rasmussen and Thomsen, 2008).

Eldevik et al (2014) compared the stable isotope SST to the July surface air temperature anomaly from a pollen-based record and the alkenone SST record (for the Holocene onset) [Fig.11]

It is clear from their work that SST reconstructions, using stable isotope analysis on planktonic foraminifera, provide high resolution records of quantitative warming and cooling than compared to the pollen assemblages. This is likely due to the lower sensitivity of vegetation to climate change and the larger temperature ranges pollen-based models provide (Brooks et al., 2016). The diagram below shows the range of data points and the large errors recorded when using pollen-based records (Eldevik et al., 2014) [Fig.12].

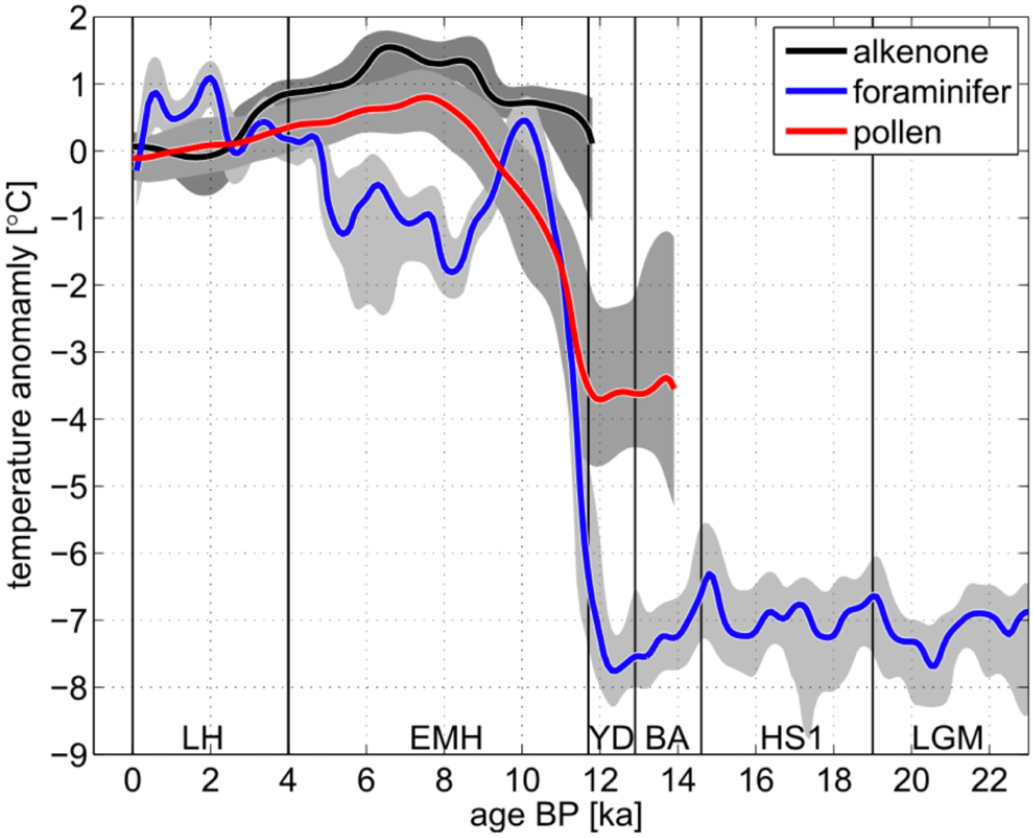

Figure 11. The SST (˚C) records from planktonic foraminifera in the North Atlantic Ocean, compared to a pollen record from Norway and an alkenone SST (˚C) record for the Holocene (Eldevik et al., 2014)

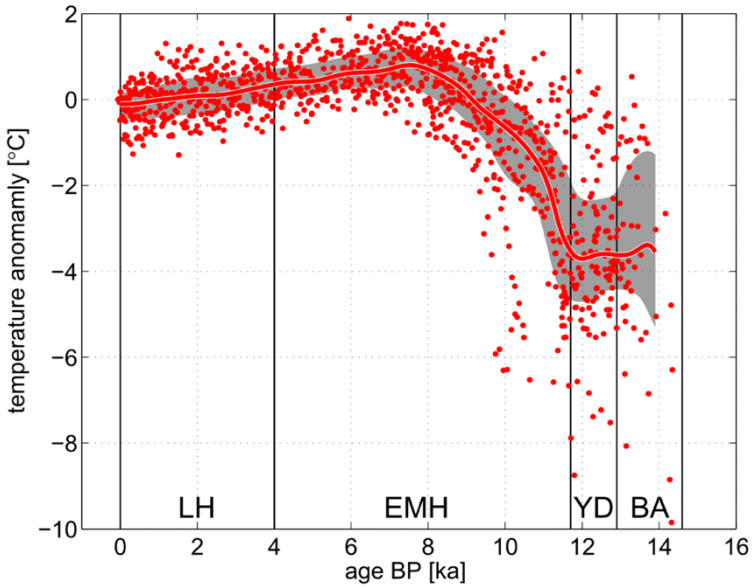

Figure 12. Pollen temperature reconstruction for the last 16k years BP. Highlighting the large temperature ranges inferred from the pollen records (Eldevik et al., 2014)

Stable isotope analysis of lake sediments can provide high resolution records of temperature change (Walker & Lowe., 2019). To date only 3 stable isotope records are available for Scotland: Crudale Meadow on the Isle of Orkney (Whittington et al., 2015), Tirinie in the Grampians (Candy et al., 2016) and Lundin tower in the east of Scotland (Whittington et al., 1996). Tirinie, in the central Grampians, of the Scottish Highlands (Candy et al., 2016) records five distinct $\partial^{18}O$ isotope events, indicating warming and cooling, likely corresponding to GI-1e to GI-1a at this site. Crudale Meadow in Orkney has also been analysed for $\partial^{18}O$ isotopes (Whittington et al., 2015). This study however only records 4 events between GI-1e to GI-1a as there was insufficient carbonate available for analysis. This is a limitation of this proxy as sufficient quantities of calcium carbonate are required to use this method. Where marl rich sediments are found this proxy can be used. However, minerogenic rich lake muds, low in calcium carbonate, often do not record any fluctuations in the record thus leaving gaps in the model [Fig.13] and therefore limits the lakes that can be assessed using this method. Furthermore, the isotope records do not provide a quantitative measure of atmospheric temperature change highlighting the continual need for quantitative single-variable climate proxies.

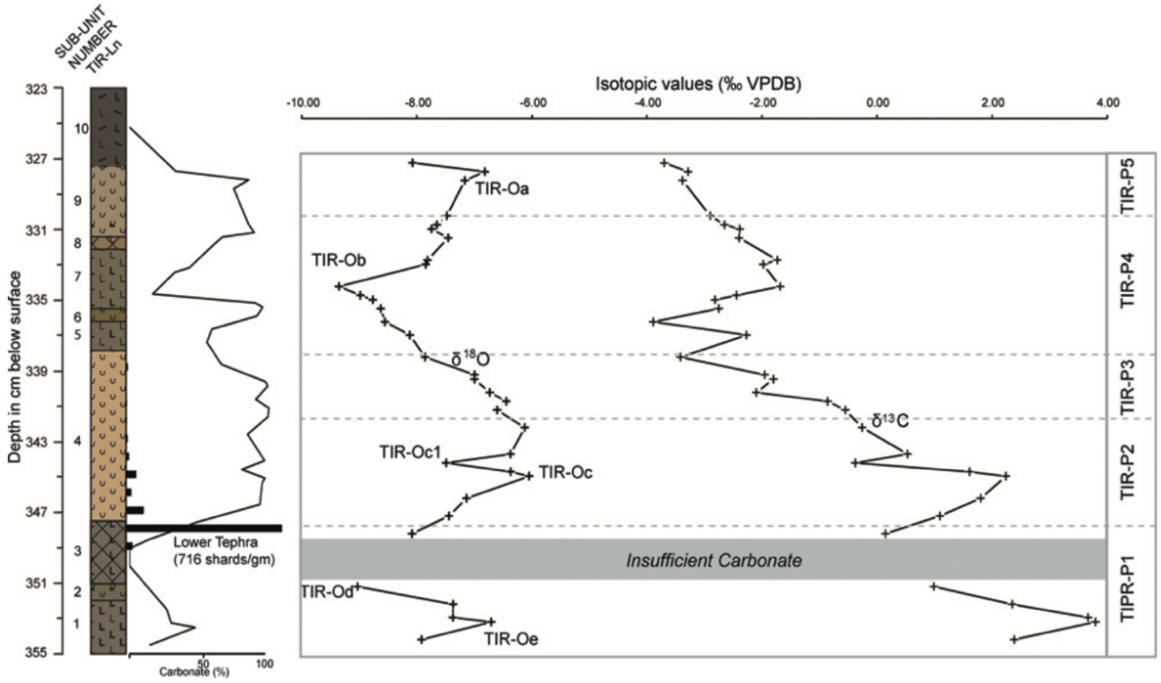

Figure 13. Calcium and oxygen isotope ratios for Tirinie, eastern Grampian Highlands in Scotland (Candy et al., 2016). The diagram shows the area of insufficient carbonate for isotopic analysis.

2.3.2.3 **Speleothem records**

Speleothem records are lacking in Scotland. However, there is one recorded site in the N.E Scotland in Assynt, close to Caithness (Atkinson et al., 1986). The site highlighted below is the only Scottish record spanning the LGIT.

In order for calcite to form speleothems there has to be a consistent supply of calcite rich ground water entering into a karstic cave system (Atkinson et al.,1986). Ford (1983) highlights that the dominance of ice-cover and permafrost interrupts the flow of water into cave systems, thereby inhibiting the precipitation of calcite. By using the ratio of $^{230}Th/^{234}U$ the growth bands in the stalactite can be dated and as a result it is possible to date periods of warming. Atkinson et al (1986) records no calcite growth between 26-15k BP, due to the dominance of ice-cover and permafrost during the LGM. Therefore, this limits the use of speleothems during periods of intense cooling and lack of precipitation.

2.3.2.4 **Diatom records**

Diatoms are single celled silica-based algae found in freshwater and marine settings (Kingsbury, 2018). They can be used to assess lake depth and provide water quality reconstructions (Kingsbury, 2018). Records of diatom assemblages for the Northern

Isles, have been analysed from Clettandal (Robinson, 2004) and Loch of Clumlie (Kingsbury, 2018) in Shetland.

Diatoms have also been recorded for Loch of Sabiston, in Orkney, which is one of the three sites in this research. Kingsbury (2018) records high levels of minerogenic in-washing and oligotrophic waters during the cold reversals, such as the LLS. As a result, diatom species richness and abundance decline, and at times disappear from the record (Kingsbury 2018). This limits the use of this proxy during times of ultra-low nutrient levels as the diversity and abundance of the diatoms are too low to measure. Diatom assemblages are controlled by a combination of variables, including depth, pH, fertility and salinity and as a result do not provide single-variable environmental records.

However, as diatoms are often useful indicators of water chemistry, depth and pH, they can be used to infer isostatic rebound (Bradley et al., 2011). Bradley et al (2011) shows that by identifying the dominant species of diatoms, a reconstruction of sea-level can be made as some species are indicative of freshwater lakes and others of saltwater systems (Shennan et al., 2006). As a result, they are useful indicators for tracking isostatic rebound after the LGM in Scotland. At the termination of the LGM, approximately 16.0k cal BP, relative sea level fell from a high of 35m to 4m by c.4.0k cal BP indicated by the diatom assemblages in Scottish lakes (Shennan et al., 2006).

2.3.2.5 **Coleoptera records**

Coleoptera assemblages (beetles) are the most diverse group of Quaternary fossils found in the sediment records (Lowe & Walker, 2014). They have been widely used in Quaternary research as they are sensitive to changes in atmospheric temperature change, ubiquitous and contemporaneous to the local environment (Coope et al.,1998, Walker & Lowe., 2019). Each species of coleoptera often reflect the communities of plants in the area and as a result provide a good reflection of the environmental conditions at the time (Walker & Lowe., 2019). Coleopteran beetles are a highly mobile species and therefore can inhabit a wide geographical range (Coope, 1977). However, this does suggest that due to their increased mobility they may not reflect in-situ atmospheric temperatures. Coleoptera beetles require a lot of sediment to be processed in order to find sufficient quantities for temperature inference modelling and as a result low-resolution high error records of climate change are often

achieved as fewer individuals can be picked from a small sample of sediment (Brooks et al., 2016). To date there are many sites in England and some in Scandinavia, however there are a lack of beetle records for Scotland, and none spanning the whole LGIT, and as a result quantitative records of temperature change are lacking using this proxy (Coope et al., 1998; Walker & Lowe, 2019). Sites that are available are from the Lowlands of Scotland which indicate that mean July summer temperatures were 15˚C during the last glacial interstadial (Bishop & Coope, 1977) and fell to 10˚C during the LLS (Merrit et al., 1990). Beetle records at Croftamie, in the southern Highlands indicate that mean annual temperatures fell to an unlikely low of -5˚C (Coope & Rose, 2008). Coleoptera temperatures have largely been interpolated across Scotland between Croftamie near the outskirts of Loch Lomond and the western edge of Norway. As a result, the temperatures inferred between these two data points are unlikely to be accurate or reliable. To determine the reliability of these temperature records for the British Isles, Brooks and Langdon (2014) compared the chironomid inferred temperatures for N.W Europe with the available coleoptera records in the literature (Coope et al., 1998). They found that on the whole coleoptera assemblages tend to record temperatures which are warmer than those of the chironomids [Fig.14]

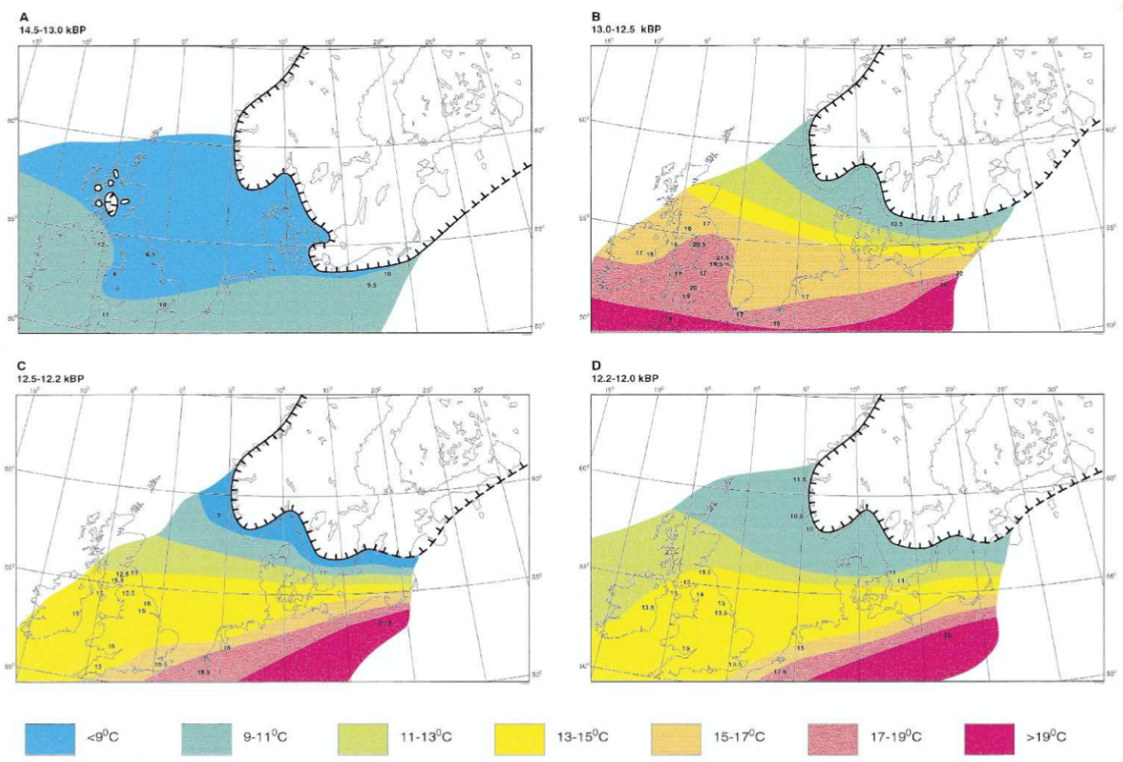

Figure 14. Coleopteran temperature records spanning 4 times slices (14.5-13.0k BP, 13.0-12.5k BP, 12.5-12.2k BP, 12.2-12.0k BP) (Brooks and Langdon., 2014)

2.3.3 **Proxy limitations**

The proxies highlighted above, individually provide a high-resolution record of palaeoenvironmental change. Like all available proxies they do have limitations. Birks (2003(b)) shows that pollen grains can be transported over long distances and can lead to false records of vegetation change. It is then required to find macrofossil evidence to substantiate the pollen records. However, plant macrophytes are often not preserved well due to sediment reworking and degradation. Furthermore, Eldevik et al (2014) has shown that the mean annual air temperatures (MAAT) inferred from pollen records often have large temperature ranges due to the breadth of niches that the flora can inhabit.

Speleothems are useful proxies to infer past climate change however they are spatially limited to localities that have (1) underlying karst lithologies and (2) have a supply of calcite rich ground water (Atkinson et al., 1986). Ford (1983) highlights that the dominance of ice-cover and permafrost interrupts the flow of water into cave systems. Therefore, this limits the use of speleothems during periods of intense cooling and lack of precipitation. Furthermore, this record does not provide a quantitative record of temperature change but rather the ratio of oxygen isotopes, which in turn reflect atmospheric temperature change.

Coleopteran beetles are a highly mobile, require a lot of sediment to be processed reliable and robust temperature inferences to be modelled (Brooks et al., 2016) and there is a lack of beetle records for Scotland, and none spanning the whole LGIT. As a result, quantitative records of temperature change are lacking using this proxy (Coope et al., 1998; Walker & Lowe, 2019). It is therefore necessary to use a robust temperature proxies to reconstruct the palaeoclimate history of the Northern Isles and Caithness.

This research proposes the use of chironomids, the ‘non-biting midge’, to reconstruct the palaeoclimate and environmental history of the Northern Isles and Caithness. Chironomids are abundant, being found in all freshwater aquatic environments, they inhabit a wide geographical range over varying temperature gradients and are found in-situ due to their short life cycle (Brooks et al., 2016). Most importantly, chironomids are single variable temperature proxies which can reconstruct mean July summer temperatures on a millennial and centennial scale (Brooks et al., 2016).

2.4 Chronological uncertainty during the LGIT

Determining if climate was synchronous or not during the LGIT is one of the most interesting and sought-after questions facing quaternary scientists. Presently, research has focused on synchronising the marine-terrestrial-ice records across the North Atlantic region however this assumes that atmospheric warming and cooling occurred simultaneously across a large region. The large scale Dansgaard–Oeschger (D-O) events, shown by fluctuations in ∂18O in Greenland ice cores, are believed to be synchronous with terrestrial records (Dansgaard et al., 1993; Blaauw et al.,2010). However, the inference of synchronicity between regions is dependent on numerous factors: (1) the sensitivity of marine and/or terrestrial proxies to environmental change, (2) the temporal resolution of the sedimentary profile and (3) the applied age-depth models (Blaauw et al., 2010). In order to assess if climate and environmental change was synchronous between sites robust, high resolution and low error age-depth models are necessary.

One hypothesis of this research is that climate changes were not synchronous across the LGIT between the Northern Isles of Scotland and across N.W Europe (see section 4.3) however to determine how accurate this is, it is necessary to limit chronological uncertainty. The LGIT was a time of high amplitude climate change with periods fluctuating on decadal and centennial scales (Brooks et al., 2016). This is problematic as chronological uncertainties can often exceed 100 years and some chronological errors have been known to exceed 2000 years pre-LGIT (Blaauw et al., 2009). This is difficult when trying to answer questions surrounding synchronicity between records. This project will aim to overcome this by implementing both AMS radiocarbon dating of terrestrial plant macrofossils and using tephra layers, where available, in order to decrease the uncertainty and increase the temporal resolution of the climate inferences.

2.4.1 Tephrochronology and age uncertainties

Tephrochronology enhances the temporal resolution of sedimentary profiles as the ages of each eruption are well researched. These layers can be compared to profiles which contain the same tephra layers allowing tie-points to be made between localities across large regional scales. With the addition of tephra layers these enhance the temporal resolution of sedimentary profiles.

The low-error ages of the tephra layers are inferred through identifying the same layer in high resolution records across the globe, such as the Greenland ice core records, the Hulu cave speleothem records and marine isotope records, to infer a robust age for that dated layer (Bond et al., 1993; Cacho et al., 1999; Lisiecki and Raymo, 2005; Hughen et al., 2006). Therefore, the age of tephra layers can have low temporal errors, and as a result if the same layer is found in other sites, the age-depth model for that locality can be more robust for that point in time. However, one limitation is the lack of tephra layers across the globe as layers are only deposited by volcanic eruptions. Where sites are far from volcanic hot zones there are no guarantees that atmospheric circulation patterns will allow for the deposition of ash at each site researched [Fig.15].

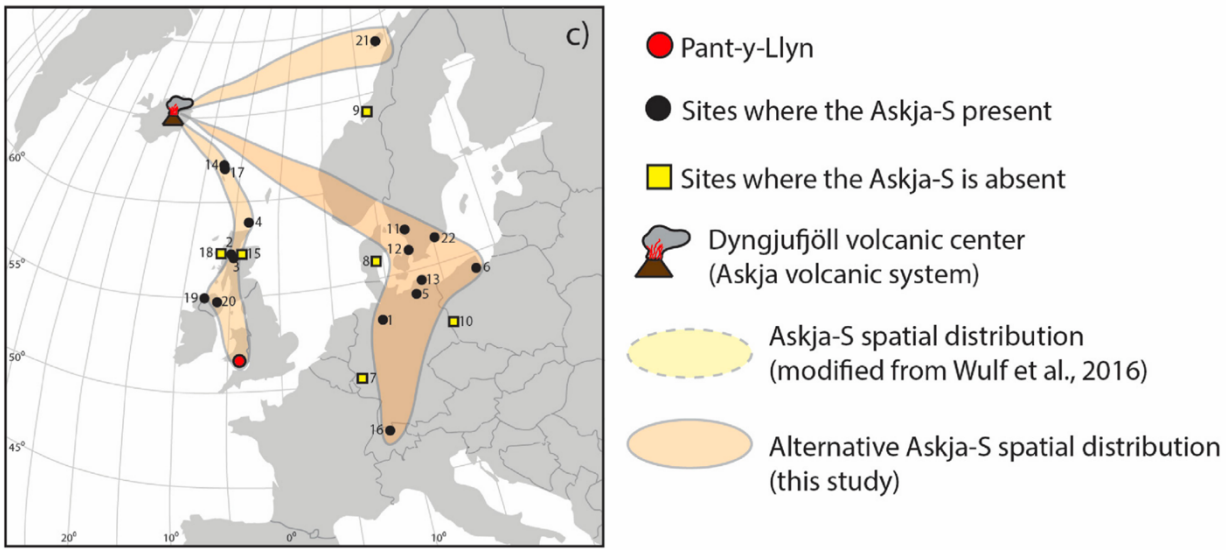

Figure 15. Sites where the Askja-S tephra is present across N.W Europe. Tephra layers dictated by volcanic eruptions and atmospheric circulation (Jones et al.,2017)

2.4.2 Lake varves and age uncertainties

Lake varve records are one of the most sought-after sedimentary profiles as they allow the reconstruction of high-resolution low temporal error records of environmental change across annual timescales. Few varve records are available, with only two encompassing the full Younger Dryas period during the LGIT (Lake Meerfelder Maar in Germany and Lake Gosciaz and Perespilno in Poland) (Brauer et al., 2008; Goslar et al., 1999).

Varves form when calcite precipitates within the epilimnion of lakes throughout the summer months during algal blooming seasons and is then deposited in the lake bottom, often recording a lighter/creamier sedimentary profile (Neugebauer et al., 2012). Throughout the winter months darker sediments are deposited during phases of decreased organic deposition (Lowe & Walker, 2014). These couplets of alternating sediments form what are known as 'varves' [Fig.16]. However, not all lakes are contusive to record annual records of warming and cooling due to sediment reworking (Lowe & Walker, 2014) and therefore limiting the use of varve records. To date, only one varve record has been recorded for Scotland (Glen Roy) and this sequence only encompasses a partial record of the LGIT (Sissons, 2017).

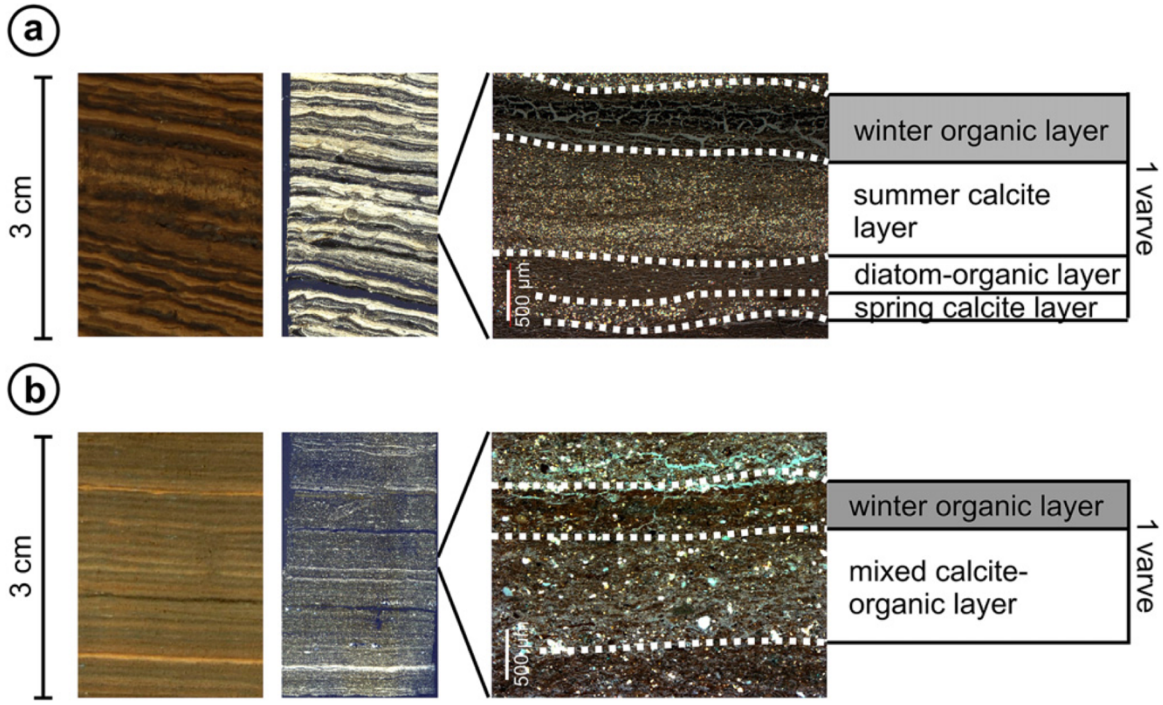

Figure 16 (a) varves formed by winter organic deposition, summer calcite precipitation and spring calcite formation. (b) coupled varve sequence showing winter and summer deposition of organic/calcite layers. (Neugebauer et al., 2012)

2.4.3 Radiocarbon contamination, reservoir age uncertainties and radiocarbon plateaus

An assumption when using radiocarbon dating is that the concentration of ^{14}C has not changed in the atmosphere through time (pre-industrial revolution) (Lowe and Walker, 2014). This has been shown to be false as dendrochronological studies have shown that there is an offset between the tree ring ages (5.0k BP) and radiocarbon ages (5.8k BP) for the same site (Clark & Renfrew, 1973). Furthermore, studies have shown that

during 10.4k BP, 10.0k BP and 9.6k BP there are constant radiocarbon ages, known as radiocarbon plateaus, where the concentration of ^{14}C remained stable [Fig.17]. Due to this temporal offset this therefore requires a clear distinction to be made when using either radiocarbon years or calendar ages.

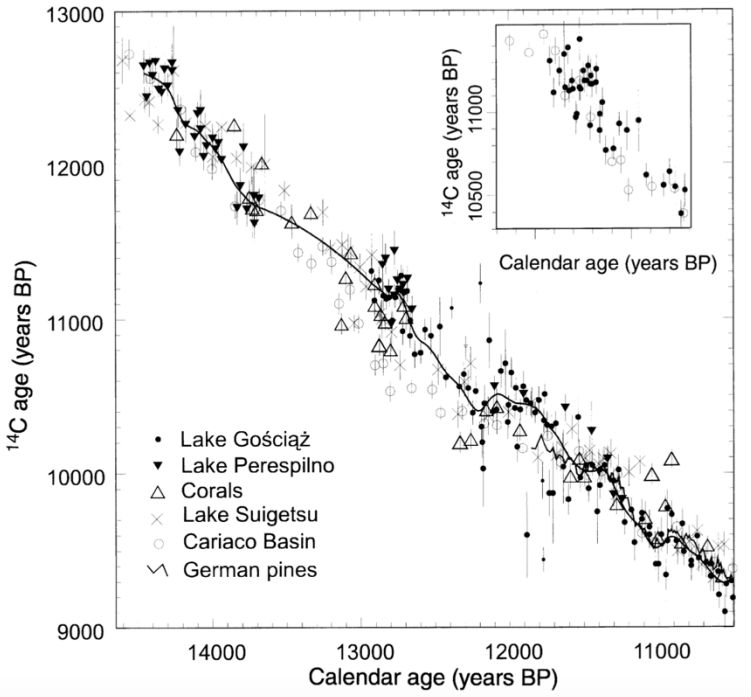

Figure 17. 14C age (years BP) vs Calendar age (years BP) from Goslar et al (2000) showing the radiocarbon plateau during the Younger Dryas period.

Contamination can also be a factor which leads to high temporal errors when using radiocarbon dating. Contamination can occur when older or younger sediments have been reworked into the sample of sediment that is analysed. This can occur though bioturbation, the percolation/infiltration of humic acids from younger sediments downcore or through root penetration (Lowe and Walker, 2014). The influence of glaciogenic sediments during phases of minerogenic in-washing can also lead to erroneous age reconstructions due to the transportation of old carbon into the lake system (Walker et al.,2001). Furthermore, the precipitation of calcite into the water column by freshwater organisms has also been linked to increased contamination, leading to what is known as a hard water error (Lowe and Walker, 2014). This can be overcome though through only analysing in-washed terrestrial plant fibres/fragments as these are unlikely to be negatively impacted by any hard-water errors (Marty and Myrbo, 2014).

Chapter 3 - Chironomid Assemblages: an overview of their taxonomy and application in palaeoclimate reconstructions

3.1 Introduction

This chapter will describe what chironomids are, the nature of their life cycle, their biodiversity and their function in lake ecosystems. This section will highlight their application to palaeoclimate reconstructions, show why chironomids are useful indicators of climate change and how they can be used to model mean July summer temperatures. Examples will be shown from the sites across the British Isles and N.W Europe. This will be followed by an overview of long chain alkenone records and their applications to spring lake temperature inferences.

3.2 Holarctic chironomid larvae

Chironomids are 'two-winged flies' from the family of Diptera and are colloquially known as the '*non-biting midge'* (Brooks et al., 2016). They are ubiquitous in nature, found in large quantities (50-100 individuals in $1cm^{-3}$of sediment) and are found in all freshwater environments (Brooks et al., 2016). Approximately 5000 species of chironomids have been described globally and it is believed that 15,000 may exist (Cranston & Martin, 1989; Cranston, 1995; Brooks et al., 2007). There are 10 sub-families with a proposed number of 355 chironomid genera (Ashe., 1983). The following are the most common sub-families in British Isles and the North Atlantic: Tanytarsinae, Orthocladinae, Diamesinae, Chironominae, Prodiamesinae and Tanypodinae. Chironomids are holometabolous, meaning that they transform from their pupal stage to adult forms, through metamorphosis (Gullan & Cranston., 2010). Each chironomid has 4 unique stages to their life cycle [Fig.18]. Each instar phase is characterised by a set of unique morphological characteristics. Identification of the specific taxa of chironomid are usually done with the final 4^{th} instar stage (Cranston., 2013).

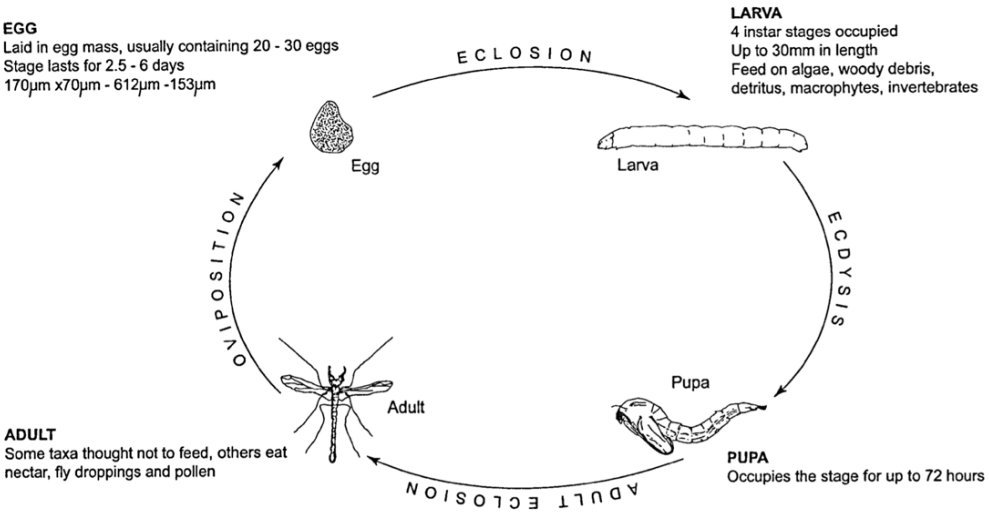

Figure 18. Chironomid life cycle diagram (Gilchrist., 2004)

This stage of the chironomid life cycle has the most developed and the most complete chitinous head capsule. As a result, this is the most effective stage to identify the chironomids apart from one another. Once the larval stage is completed, the pupa escapes via weaknesses in its sclerotised cranium (Cranston., 2013), leaving behind the chironomid head capsule in the lake sediments which can be sub-sampled and identified. Chironomids have features on their head capsule which allow one to separate and identify each taxon.

3.2.1 **Chironomid biodiversity, geography and trophic status**

Chironomids have a wide geographical range, being found at both the tropics and the arctic (Brooks et al., 2007). They inhabit most freshwater systems, can live in wet terrestrial environments and in some extreme cases have been known to live inside other organisms (Chernovskii, 1949). Their preferred temperature range is dependent on the species. Some species can live in hot springs that exceed 40˚C (Pinder, 1995) whilst others only inhabit water bodies with high levels of acidity (Yamamoto, 1986).

Chironomids are detritivores, getting their nutrients from bacteria, algae and/or graze on the surface of plants (Brooks et al., 2007). Chironomids are versatile as they use various feeding styles: predate on other chironomids, scrape vegetation, filter-feed from the water column, deposit-feed or use a combination of these feeding methods (Berg, 1995). Chironomini larvae have a distinctive red appearance, due to the presence of haemoglobin in their blood – allowing them to thrive in anoxic substrates through anaerobic respiration (Nagell & Landahl, 1978; Brooks et al.,

2007). *Tanytarsini* are unable to use anaerobic respiration as the levels of haemoglobin in their blood is lower and therefore live in oxygen-rich lake systems (Walshe, 1948). Chironomids from the Orthocladinae family are green in appearance (as they feed on algae) and are generally less tolerant to anoxic conditions (Brooks et al., 2007). They thrive in oligotrophic waters, in sandy streams or rivers dominated by gravel (Brooks et al., 2007) [Table 2.]. Similarly, Diamesinae are found in mostly colder waters and are indicative of proglacial lakes and streams fed by glacial runoff (Brooks et al., 2007). Chironomids are stenotopic, meaning they have a narrow ecological maximum, preferring a particular environment and temperature optimums over others (Brooks et al., 2007). It has been shown that pH generally leads to a reduction in the diversity of chironomid assemblages found in lakes (Henrikson et al., 1982; Brodin, 1990). At low pH levels metal oxides can begin to form and precipitate onto the macrophytes and lake substrates, leading to a reduction in the number of Diamesinae and Orthocladinae species (Rasmusssen and Lindegaard., 1988). However, principle component analysis (PCA) shows that chironomids are more influenced by water temperature than other environmental factors (such as pH), making them useful palaeoclimate proxies for modelling temperature change (Brooks et al., 2000; Brooks et al., 2012; Brooks et al., 2016; Watson et al, 2010). See methods chapter for more information on the main drivers of chironomid distributions.

Table 2 Chironomid taxa indicative of trophic status (Brundin., 1949; Saether 1975, Lindegaard., 1995) (adapted from Brooks et al (2007).

Lake Trophic Status	**Indicator species**
Ultra-oligotrophic	*Heterotrissocladius subpilosus*
Oligotrophic	*Tanytarsus lugens*
Mesotrophic	*Stictochironomus rosenschoeldi & Sergenita coracina*
Moderately eutrophic	*Chironomous anthracinus*
Strongly eutrophic	*Chironomous plumosus*
Dystrophic	*Zalutschia*

The most common species of chironomids breed in water bodies high in nutrients with a warm ambient temperature (Brooks et al., 2007). Temperature is known to determine the rate of egg development and the quantity of larvae that hatch from the lake substrate (Williams, 1981). During the larval stage of the chironomids life cycle they live within the lake sediments consuming detritus, macrophytes and epiphytes until they have matured and then leave their aquatic home.

3.3 Chironomid inferred temperature records (C-IT)

Chironomids have been shown to be effective indicators of past environmental change and are able to record high-resolution archives. Gilchrist (2004) and Brooks (2016) highlight the main attributes that make chironomids reliable proxies for palaeoclimate reconstructions and indicators of environmental change (see below).

Attributes:

- Taxa are stenotopic that withstand narrow ecological temperature optimums and niches.
- Chironomids are ubiquitous in nature and found in all aquatic environments (excluding the marine setting) (Brooks et al., 2016)
- Highly abundant in lacustrine sediments (50-100 individuals in $1cm^3$) (Walker, 2001; Brooks et al., 2016; Porinchu & MacDonald, 2003).
- They are known to provide a low error mean July summer temperature records (Brooks et al., 2012; Brooks et al., 2016).
- Well preserved chitinous head capsules

Chironomids are a single variable climate proxy with the ability to quantify mean July summer air temperatures (Brooks et al., 2016). Fossil chironomids are compared to modern assemblages, their temperature optimums are derived, and a transfer function is used to model past atmospheric temperatures based on their similarity. A weighted-average partial least squares (WAPLS) regression is modelled, with a boot-strapped (cross validated) root mean squared error prediction (RMSEP) (Heiri et al., 2011; Brooks et al., 2016). This transfer function enables atmospheric temperatures to be inferred with an error of 1.04˚C (Heiri et al., 2011). Currently, transfer functions have been developed for Norway (Brooks et al., 2000) and Switzerland (Heiri et al., 2005)

in N.W Europe. The Norwegian calibration data set contains 157 lakes and the Swiss data set contains 117. A combination of both data sets, known as the Swiss-Norwegian data set, has also been developed. This contains a suite of 274 lakes across N.W Europe (Heiri et al., 2011). Transfer functions are mathematical functions that statistically compare modern biological data with fossil assemblages. They are used in palaeo-ecology to reconstruct environmental conditions based on variants within multiple linear regression models (Lowe and Walker, 2014). Throughout the British Isles and Ireland 22 sites (shown in the sub-sections below) have been recorded for chironomid assemblages and temperature inferences have been made for each (Brooks et al., 2001; Brooks et al., 2012; Brooks et al., 2016; van Asch et al., 2012; Watson et al., 2010) [Fig.19].

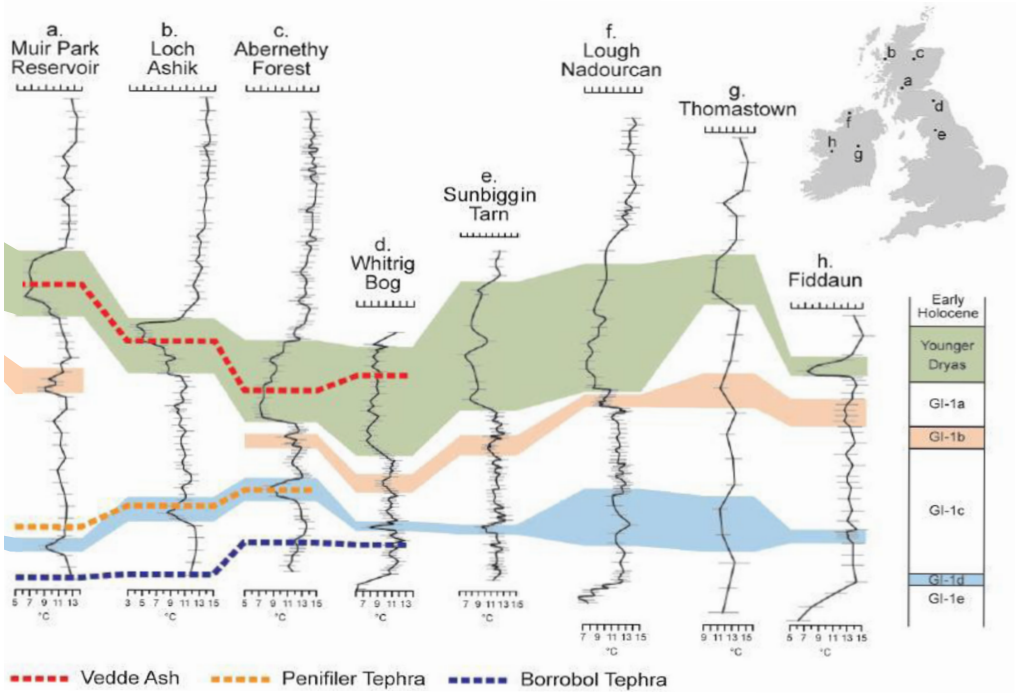

Figure 19. Chironomid inferred temperature models for the British Isles and Ireland constrained by cryptotephra layers (Brooks et al., 2016)

It has been noted that temperature changes across the British Isles, whilst similar to Scandinavian and Greenland records, differ in magnitude due to regional scale climatic forcing (Brooks et al., 2012). Chironomid assemblages have two important advantages over other proxies for temperature inferences. Firstly, they can be used to reconstruct single variable temperature records to a high resolution. Secondly, compared to other climate proxies, such as Coleoptera, chironomids are found in large concentrations within lake sediments (Brooks at al., 2016).

3.3.1 **Chironomid record for Muir Park Reservoir (MPR), southern Highlands**

Brooks et al (2016) developed a chironomid inferred temperature reconstruction and environmental history for the Muir Park Reservoir (56˚5'51.73" N, 4˚25'58. 50" W), in the west-central Scotland [Fig.20]. The site is on the periphery of Palaeolake Blane and the southern limit of the Loch Lomond Stadial re-advance glacier (7km east of Balmaha on the eastern edge of Loch Lomond).

The cool events, GI-1b and GI-1d, are well resolved in this core and are clearly apparent throughout the temperate interstadial (Brooks et al., 2016). They notice that these events are not widely reported throughout the British mainland and Ireland, likely due to a suppressed climatic signal from the North Atlantic Ocean (Brooks et al., 2016). Similar to Loch Ashik, on the Isle of Skye, the MPR site has a C-IT model which indicates temperatures were lower in the second phase of the LLS (Brooks et al., 2012). Both of these sites were located close to icefields or glaciers. Therefore, the influence of these ice masses is likely being represented.

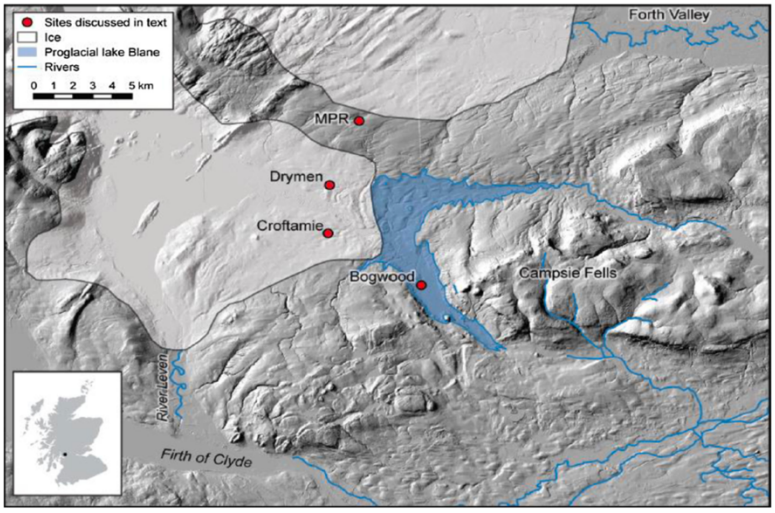

Figure 20. Brooks et al (2016) site Muir Park Reservoir and its proximity to palaeo Lake Blane

3.3.2 **Chironomid record for Loch Ashik, Isle of Skye**

Brooks et al (2012) analysed 83 samples from a core from Loch Ashik, on the Isle of Skye. Late glacial and Holocene temperature records were recorded using the identified chironomid head capsule assemblages. The core from Loch Ashik was analysed for tephra shards to build a robust age-depth model for the site, and at the time, was the first to do so for the region. They found a clear signature, thought to be synchronous with GI-1d, where temperatures fell by 2.8˚C. In addition, Brooks et al

(2012) record a gradual decline in mean July summer temperatures by 1˚C throughout the interglacial period until the onset of the YD/LLS - with a peak in temperatures at the onset of the deglaciation.

The chironomid inferred temperature record suggests that the second half of the LLS was cooler than the first, which Brooks et al (2012) believe to be a result of the close proximity of the site to the Skye-ice field (Ballantyne.,1989). Subsequently, the work done by Golledge (2010) indicates that this ice field was 10km from Loch Ashik. The close proximity to this icefield would have influenced the local climate through catabatic winds (Golledge et al., 2007). This is different from their other site, e.g. Abernethy Forest, which saw an increase in temperatures during the second phase of the LLS/YD. *Microspectra radialis* and *Paracladius* dominate this assemblage indicating that lake productivity was low, and temperatures were sub-arctic. At Loch Ashik there appears to be a 300-year lead in chironomid inferred temperatures before the lithology and geochemistry changes. This further supports the highly sensitive nature of chironomids for temperature reconstructions (Brooks et al.,2016).

3.3.3 **Chironomid record for Abernethy Forest, Cairngorms**

Brooks et al (2012) analysed a site in the Scottish Highlands (Cairngorms) where they identified 123 chironomids in order to reconstruct summer temperatures during the LGIT [Fig.14]. The chronology for Abernethy forest was developed through AMS dating of terrestrial plant fragments from the lake substrate. At the Abernethy site temperatures indicate that the interstadial period was punctuated by three cooling events. These events are GI-1d, GI-1c and GI-1b and were believed to be synchronous with the Greenland climate-stratigraphy (Brooks et al., 2012; Rasmussen et al., 2014) [Fig.21]. Based on the chironomid inferred temperature models (C-IT) (˚C) an event thought to be synchronous with GI-1d fell by 5.9˚C. In addition, the C-IT model suggests that temperatures fell by a further 2.8˚C. Lastly, their chironomid inferred temperatures indicate a fall in temperatures by 2.8˚C during GI-1b.

Unlike their Loch Ashik site, temperatures at the latter stage of the Younger Dryas period appear to rise at Abernethy Forest. Brooks et al (2012) suggests that this is due to local icefields on Skye. However, the YD ice fields in the Cairngorms were small and far from the lake. Calculated precipitation values for eastern Scotland

indicate that rainfall was similar to values today (Golledge, 2010; Benn and Ballantyne, 2005), in contrast to the Isle of Skye which calculated rainfall in excess of 1600 mm yr^{-1} at the equilibrium line altitude (ELA) for this time period. Therefore, the nature and magnitude of temperatures at Abernethy Forest are typical of climate oscillations seen across the rest of the British Isles and Ireland (Watson et al., 2010; van Asch et al., 2012; Brooks et al. 2016).

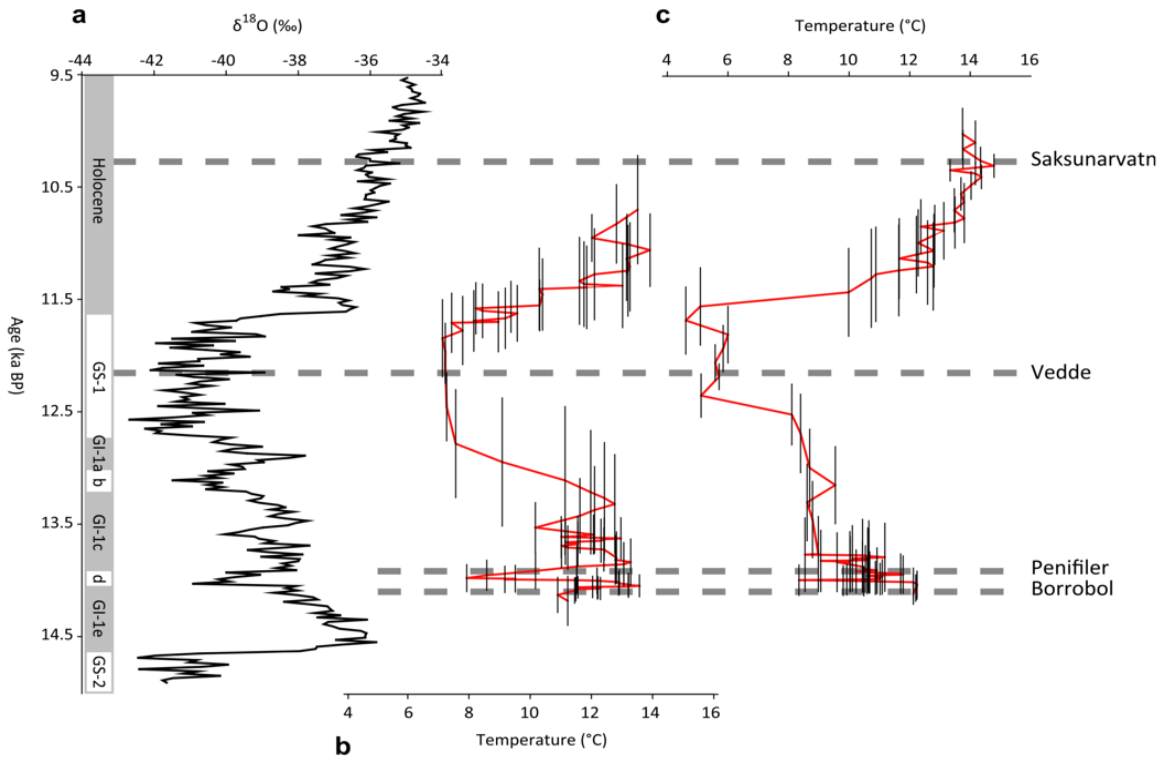

Figure 21. Chironomid inferred temperatures for Abernethy Forest (b) and Loch Ashik (c) for the LGIT (Brooks et al., 2011) against (a) NGRIP record (ka BP).

3.3.4 **Chironomid record for Whitrig Bog, Central Scotland**

One of the first sites to use chironomid head capsule assemblages for temperature reconstructions was at Whitrig Bog in Central Scotland. At the time research into the use of chironomids for temperature inference modelling was in its infancy and as a result low resolution records were built. However, there is a clear indication of the warm interstadial event, shown by the dominance of *Chironomous spp, Procladius* and the *Tanytarsus* groups. The Younger Dryas period is also evident in the core due to the presence of *Microspectra radialis, Paracladius,* and *Sergentia coracina*. Quantitative temperature reconstructions were not possible at this time due to the lack of a chironomid training set.

3.3.5 **Chironomid record for Lough Nadourcan, North of Ireland**

Watson et al (2010) retrieved a sediment core from Lough Nadourcan, on the north of mainland Ireland (55˚ 3' N, 7˚ 54' W). This was the first study to use chironomids as a proxy for mean July summer temperatures for Ireland that spanned the LGIT. Similar to the sites on mainland Britain, this Irish site shows a rapid warming at the end of the LGM with punctuated cool events throughout the interstadial [Fig.22]. These oscillating events throughout the interstadial are thought to represent the events GI-1e-a from the Greenland event stratigraphy. Loch Ashik and MPR (Brooks et al., 2012; Brooks et al., 2016) temperatures increase at the latter end of the Younger Dryas period from a low of 10˚C from a low of 7˚C (Watson et al., 2010). They show patterns that are similar to records from mainland Britain. In particular, they show a striking resemblance to the records from Hawes Water, England (Bedford et al., 2004) and Whitrig Bog from central-eastern Scotland. Watson et al (2010) conclude that both Britain and Ireland were subjected and responded to the same climatic influences. Notably, the influence of the North Atlantic Ocean and its relationship to atmospheric circulation patterns and temperature change.

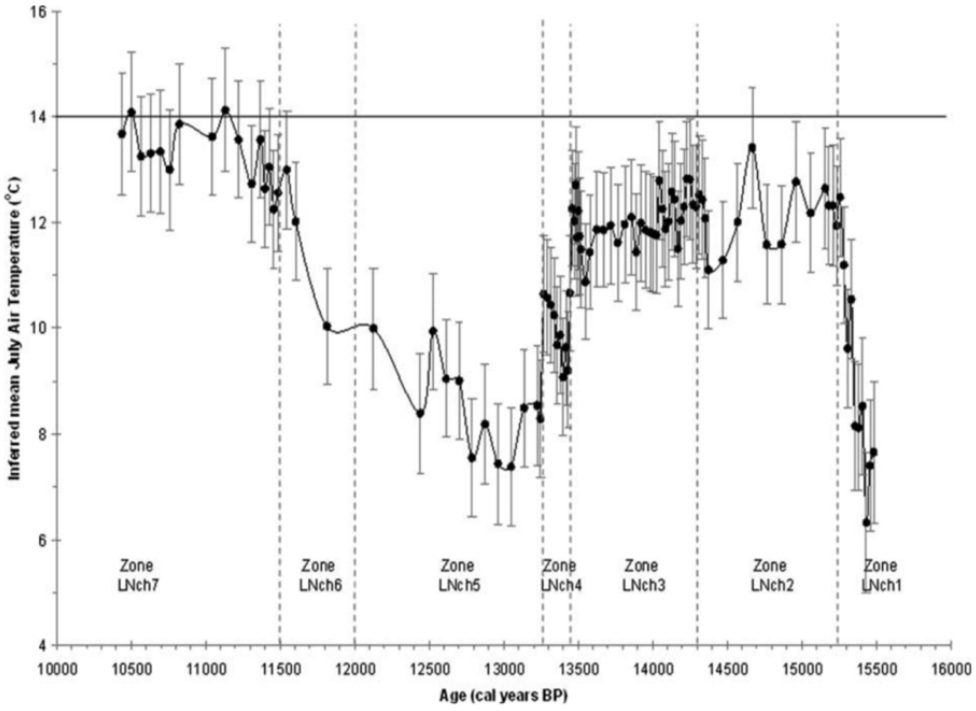

Figure 22. Chironomid inferred temperatures from Lough Nadourcan against time (based on 24 AMS dates) (Watson et al., 2010)

3.3.6 **Chironomid record for Thomastown, Central Ireland**

Turner et al (2015) modelled chironomid inferred temperatures for Thomastown Bog, in Ireland spanning the LGIT. In addition, they used a multiproxy approach to infer the environmental history of the lake by using micro-XRF, pollen and stable isotopes [Fig.23]. Furthermore, they identified 12 climatic events which spanned the LGIT, encompassing regional events, e.g. GI-1b, to sub-centennial local fluctuations. They found a resemblance of their C-IT model (˚C) to those found across the British Isles and Ireland. In addition, after the onset of the Holocene period they record a 2˚C drop in temperatures which likely represents the Preboreal Oscillation (Björck et al., 1997).

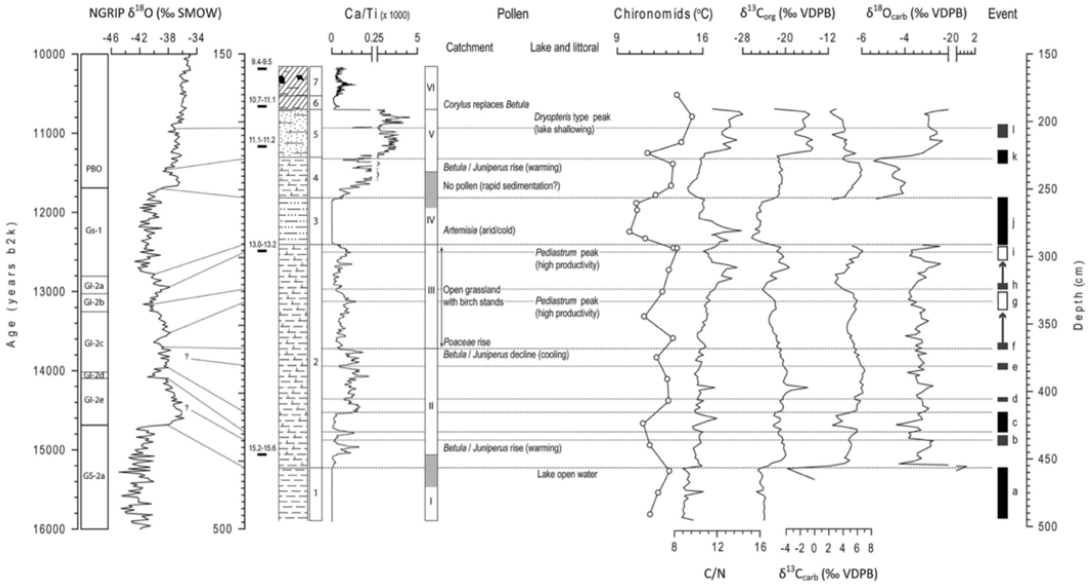

Figure 23. The multiproxy study of Thomastown Bog highlighting the geochemical, pollen and lithological record for the site. Combined with the chironomid inferred summer temperatures (˚C) (Turner et al., 2015)

3.3.7 **Chironomid record for Fidduan, Western Ireland**

A lake core was taken from Fidduan, in the west of the Irish mainland to record changes in summer temperature change across the LGIT (van Asch et al., 2012) [Fig.24]. Due to its close proximity to the North Atlantic Ocean this site was chosen to assess the sensitivity of chironomids to temperature change as a result of oceanic circulation fluctuations.

As with Turner et al (2015) they also use a multi-proxy approach to reconstruct the environmental history of the site. They found that the $\partial^{18}O$ values and the chironomid inferred temperatures were similar which suggests that both proxies are controlled by the same factor, atmospheric temperature change. Similar to the

previous sites across the British Isles and Ireland they record a rapid warming straight after the termination of GS-2, a sharp decline in temperatures throughout the Younger Dryas and again a rapid warming at the onset of the Holocene. Temperatures during the interstadial range between 12.5-14.5˚C and fall to a low of 7.5˚C during the Younger Dryas. Based on the C-IT model, at the onset of the Holocene, temperatures sharply rise to 15˚C. Van Asch et al (2015) suggests that these events, like the others recorded throughout the North Atlantic, are synchronous with the Greenland chrono-stratigraphy (Rasmussen et al., 2014).

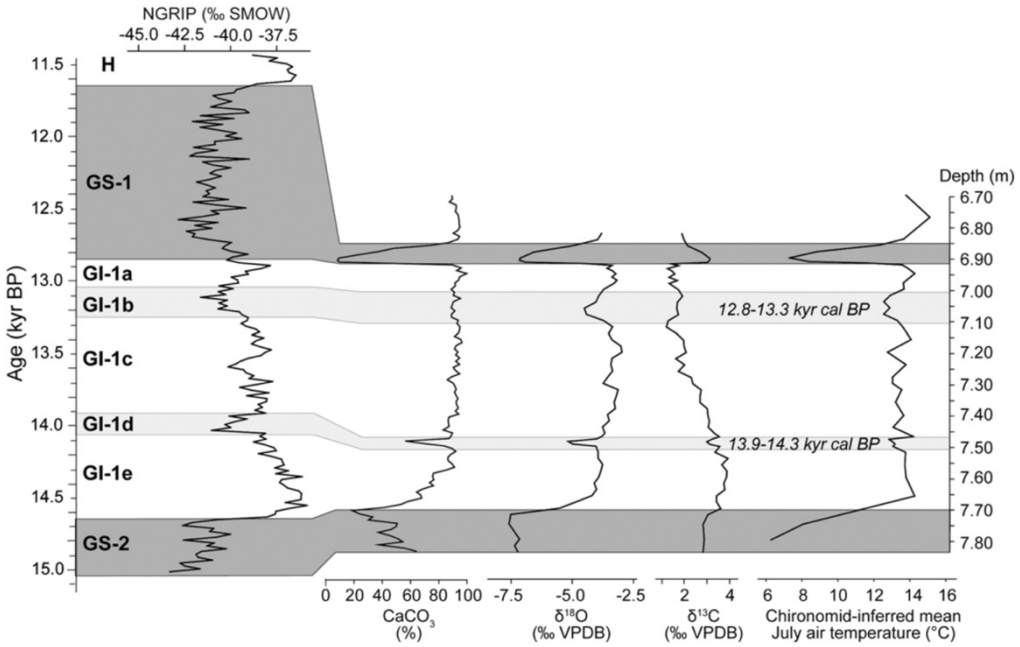

Figure 24. Fidduan chironomid inferred temperatures (˚C) with the ∂18O and ∂13C values against the NGRIP (‰ SMOW) values. All of the proxies were plotted against age (kyr BP) (van Asch et al., 2012)

3.3.8 **Chironomid records for N.W Europe**

Across N.W Europe local variations in mean July summer temperatures have been recorded for 31 sites as of 2014 (Heiri et al., 2014). Since, then Muir Park Reservoir in Central Scotland has been analysed (Brooks et al., 2016) and the 3 sites from this project. Each of the 31 C-IT models were spliced and stacked to form regional temperature reconstructions were for 8 regions: North Norway, West Norway, Baltic Region, British Isles, Alpine Region, Southwestern Europe and East/South Central Europe (Heiri et al., 2014) [Fig.25 and 26]. Subsequently, these records were then compared to the modern-day climate model (ECHAM-4), with the aim to reconstruct the same temperatures recorded by the chironomids. There was an excellent agreement between both methods, however the ECHAM-4 model tended to model

slightly warmer temperatures than the proxy record (Heiri et al., 2014) [Fig.27]. However, what is less known is if climate changes in N.W Europe were the same across the Northern Isles of Scotland and Caithness. Likewise, what is not known is if the climate drivers in N.W Europe, were the same as those in the north of Scotland.

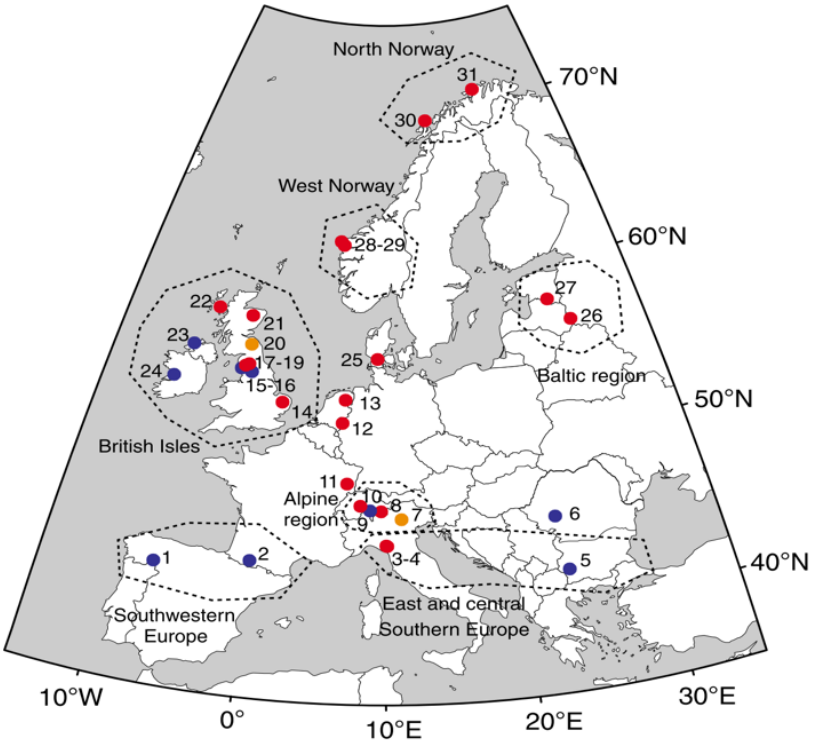

Figure 25. Location of all the chironomid inferred temperature records for N.W Europe (Heiri et al., 2014)

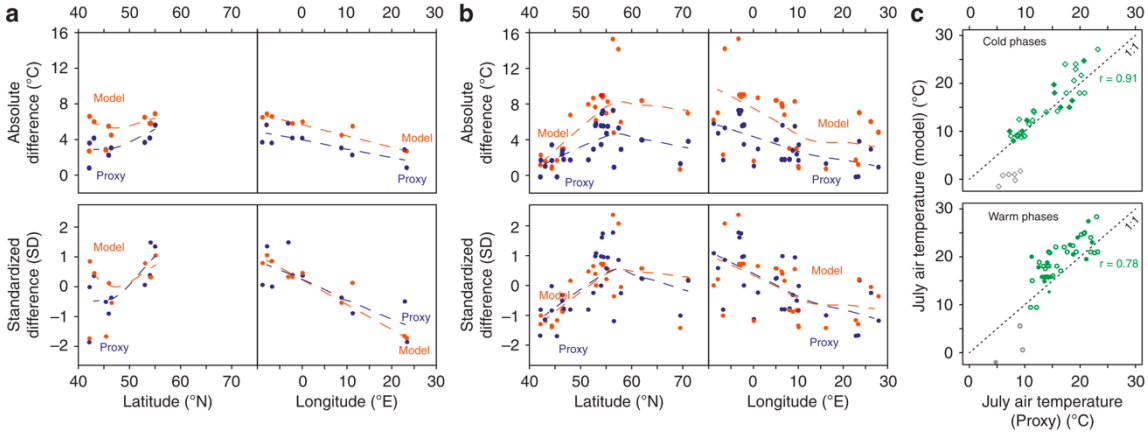

Figure 26.Chironomid inferred temperatures compared to the ECHAM-4 climate model (Heiri et al., 2014)

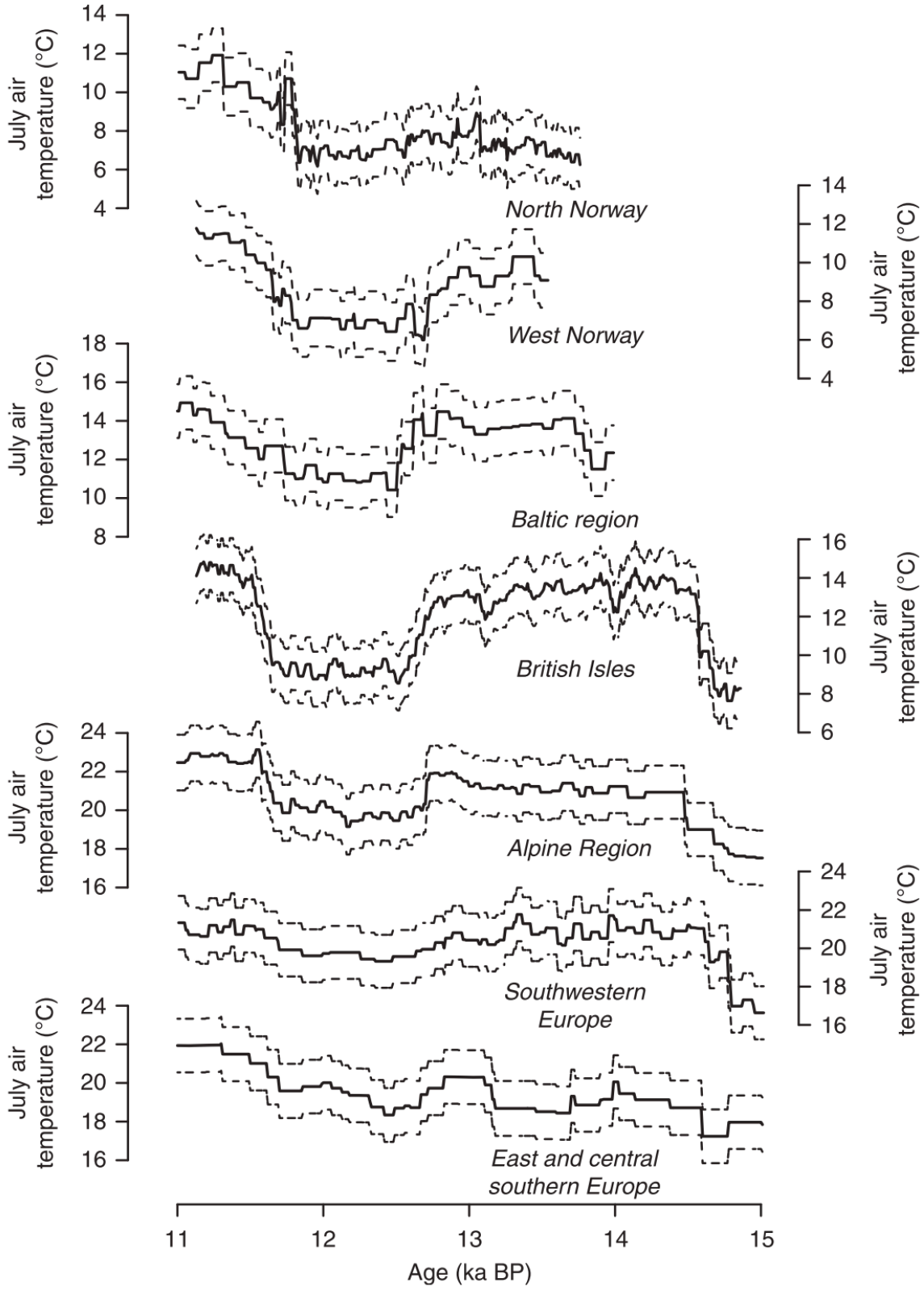

Figure 27. Each of the 31 C-IT models were spliced and stacked to form regional temperature reconstructions for 8 across N.W Europe: North Norway, West Norway, Baltic Region, British Isles, Alpine Region, Southwestern Europe and East/South Central Europe (Heiri et al., 2014)

3.3.9 **Chironomid isotherms across the North Atlantic**

Brooks and Langdon (2014) collated the C-IT and coleopteran temperature models across N.W Europe and spatially plotted them through time, spanning the LGIT (see chapter 2). Their study reaffirms the robustness of C-IT models in palaeoclimate reconstructions as they on the whole agreed with the coleopteran record to within 1˚C (with an exception for GI-1e and GI-1C where a 2˚C offset was recorded). This also underlines the influence of atmospheric temperatures, rather than other environmental variables, on the distribution of chironomid assemblages.

Combining chironomids with geographical information software (ArcGIS) one can track the position and magnitude of temperature oscillations through time. To date, computer models (Brooks & Langdon, 2014) have inferred temperatures for the Northern Isles and Caithness during the LGIT. However, these are based on 22 data points across the N.W Europe of which none are present in the Northern Isles [Fig.28]. Therefore, by combining the C-IT models from this project, with those recorded throughout the British Isles and Ireland, a better understanding of the position of palaeo-isotherms can be resolved.

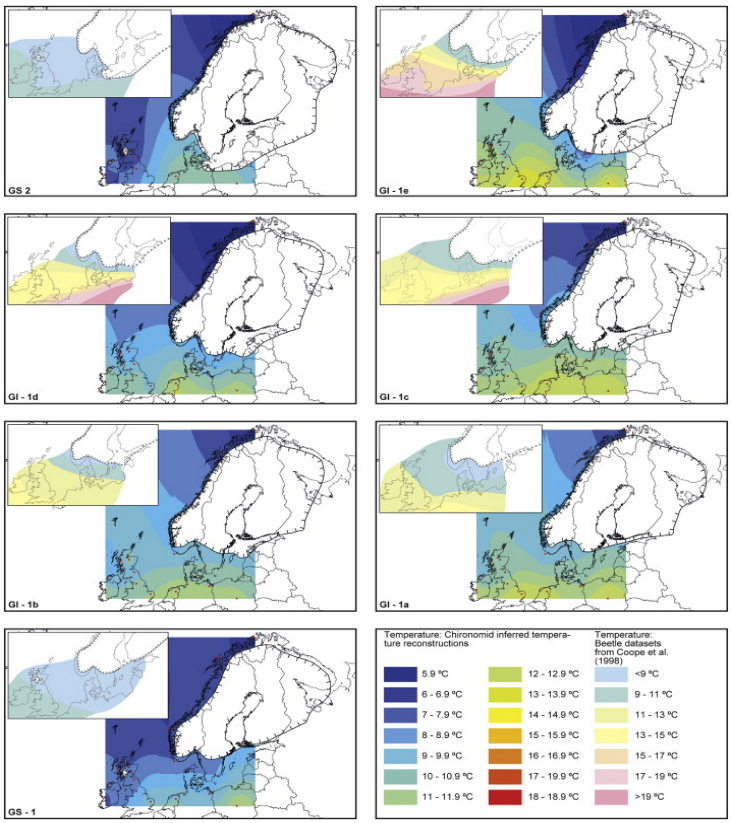

Figure 28. A comparison of the Coleoptera inferred summer mean temperatures (Coope et al, 1998) and the chironomid inferred mean July temperatures for N.W Europe (Brooks & Langdon, 2014)

3.3.10 **Chironomid inferred temperatures and glacial reconstructions**

The mean July summer temperatures inferred from chironomid assemblages have been used to reconstruct palaeo-precipitation levels for the LLS in Scotland (Ballantyne, 2007; Golledge et al., 2010) [Fig.29]. Ohmura et al (1992) identified a relationship between summer temperatures (T) with winter ice accumulation (P_a) (see the equation below). The equilibrium line ablation (ELA) is responsible for determining the advance and retreat of glacial ice masses. Therefore, with the addition of mean July summer temperatures it is possible to calculate palaeo-precipitation levels through time.

$$P_a = 645 + 296T_3 + 9T_3^2$$

Ballantyne (2007) used chironomid inferred mean July summer temperatures to reconstruct the annual precipitation levels in North Harris, in the Outer Hebrides. Temperatures were used from Whitrig Bog, central Scotland (Brooks & Birks, 2000) as this was the closest site available at the time. However, by doing so they assume that the temperatures in the Outer Hebrides and N.W Scotland were the same as the central belt of Scotland. Ballantyne (2007) was able to reconstruct the temperatures at the Equilibrium Line Altitude using the C-IT model from Whitrig Bog:

$$T_3(ELA2) = \left[0.97\,Tj - \left(\Delta H\; x \frac{dt}{dH}\right)\right] - 1.11$$

The $T_3(ELA2)$ at the ELA2 considers glacial hypsometry, variable mass balance gradients and the ELA together (Benn and Gemmell., 1997). The ELA2 has a direct relationship with July summer temperatures (Tj) minus the difference in altitude, between Whitrig Bog and North Harris (∆H), multiplied by the mean summer environmental lapse rate ($\frac{dt}{dH}$). The result is then subtracted by 1.11 which is the difference in summer temperatures between Whitrig Bog and the extrapolated temperatures in North Harris. Ballantyne (2007) assumes an environmental gradient of 0.42˚C per 100km, which implies a mean July summer temperature of 7˚C. With local temperature record one can assess if the implied precipitation/temperatures at the ELA are realistic.

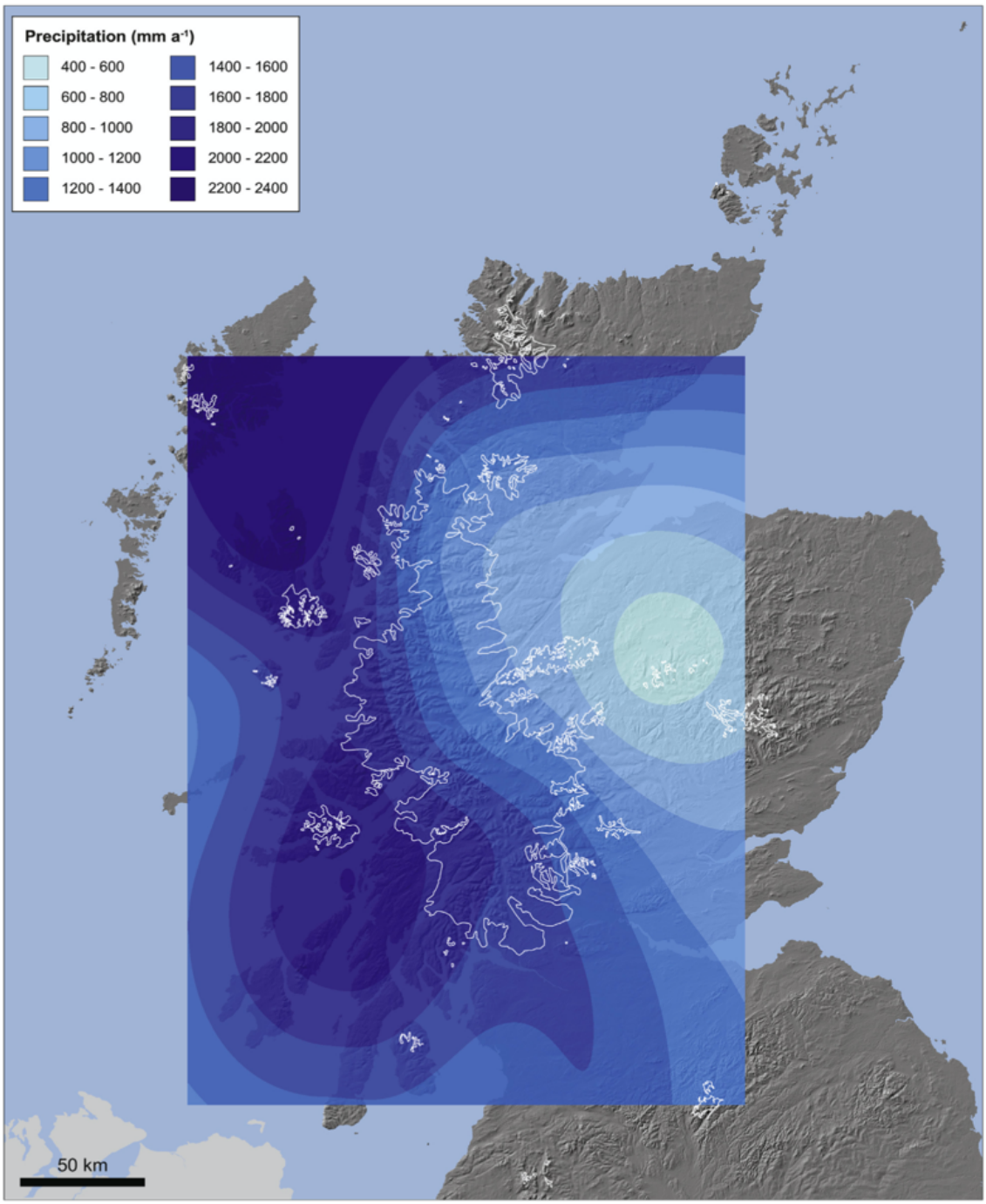

Figure 29. Inferred palaeo-precipitation levels from the temperature at the Equilibrium Line Altitude for the Loch Lomond Stadial. Inferred by the chironomid temperature records for Scotland (Brooks et al., 2016) (Chandler et al., 2019)

Chapter 4 - Thesis rationale, site selection and aims objectives

4.1 Thesis rationale

The Last Glacial – Interglacial Transition (LGIT) was a time of high amplitude climate change, where temperatures oscillated between warm and cold phases on millennial and centennial scales (Brooks et al., 2016). However, in order to track these climate shifts high resolution single variable temperature proxies are required.

Chironomid assemblages can be used to infer high resolution records of mean July summer temperatures by comparing the environmental conditions that modern day species inhabit to fossilised taxa (Brooks et al., 2000). Chironomids are found in large abundances in terrestrial lake sediments; have narrow temperature optimums and are ubiquitous in nature (Brooks et al., 2016). As a result, they are useful proxies to record temperature change for the LGIT (Brooks et al., 2000). In addition, long-chain alkenones, derived from algal biomarkers, are able to reconstruct spring lake temperatures. The peak area of the LCA chromatograms can be used to calculate the UK^{37} index for each lake (Toney et al., 2010). This index is known to have a linear relationship with spring lake temperatures, which can be tracked through time.

Chironomid inferred temperatures have been modelled for the Last Glacial – Interglacial Transition for British Isles, Ireland and across N.W Europe (Watson et al., 2010; Brooks et al., 2012; Heiri et al., 2014; Brooks et al., 2016). However, there are clear spatial gaps in the temperature records across the North Atlantic region. Brooks and Langdon (2014) modelled the spatial extent of temperature change throughout the LGIT for N.W Europe. They highlighted that there are significant gaps in the Scottish records, particularly so for the Northern Isles and Caithness. Temperatures currently are being inferred from Loch Ashik, on the Isle of Skye to Western Norway. Therefore, local records of temperature change are required to assess the accuracy of these models for these northern Scottish sites.

Currently, the literature suggests that climate changes across the North Atlantic were synchronous throughout the LGIT (Rasmussen et al., 2014). However, recent studies have suggested that the magnitude, spatial extent and timing of these climate events differed by locality (Lane et al., 2013; Lowe et al., 2019). New evidence from

this study suggests that events may have varied spatially and temporally across northern coast and Northern Isles of Scotland.

The rationale of this project is to utilise chironomid assemblages to assess how mean July summer temperatures changed across the Northern Isles of Scotland and Caithness during the LGIT. Long chain alkenones and chironomid inferred temperature records have been modelled, for one of the sites in this project. This has been done to critically assess the synchronicity between both proxies, in order to highlight seasonal variations in temperatures throughout the LGIT and provide a better understanding of the paleoecology of the lake.

Researching the impacts of these climatic oscillations will provide one with a better understanding of how atmospheric temperatures affect environmental and climate changes across the North Atlantic region. Determining the magnitude and timing of these events will provide scientists, and policy makers, with a better understanding of the forcing's, magnitude and temporal scale of climate change and how this can lead to a better understanding of anthropogenic climate changes today. However, to do this high-resolution climate records are required to precisely determine when, and to what degree, temperatures changed throughout time.

4.2 **Overview of Sites**

The Northern Isles and the north coast of Scotland have been chosen for this research. These regions are separated into Shetland, Orkney and Caithness [Fig.30]. The Northern Isles are located off the coast of mainland Scotland in the North Atlantic Ocean.

The Northern Isles of Scotland are positioned between the North Atlantic Ocean and the North Sea which means the sites are particularly sensitive to fluctuations in the North Atlantic Thermohaline Circulation (THC) and the position of the North Polar Front (NPF) (Eldevik et al., 2015). This region experiences higher rates of temperature change to continental Europe (Willis & MacDonald, 2011) and saw rapid high amplitude atmospheric fluctuations throughout the LGIT (Whittington et al., 2003). However, to date no records of atmospheric and/or lake temperatures have been made for this region from the LGIT. To date, no high-resolution single variable records of atmospheric temperatures are available for these sites. See below a description each locality for this project:

Figure 30. The location of the three sites: Caithness, Orkney and Shetland (Google Earth)

4.2.1 **Isle of Shetland: Overview**

The Isles of Shetland (60.5297° N, 1.2659° W) total over 100 individual islands, spanning 113km N-S with a width of 47km W-E and extend 1446km^2 (Hulme & Shirriff, 1994). The Isle of Shetland is located 340km east of Bergen, Norway, and 160km to the Scottish mainland (Fenton, 1977; Hulme & Shirriff, 1994). Mean annual precipitation levels are approximately 1053mm. The islands are dominated by a hyper-oceanic climate system ranging from humid to lower boreal (Birse, 1971). In relation to other sites across the North Atlantic Ocean, at similar latitudes, mild summers (~11.9˚C) and cool winters (~3.3˚C) dominate due to the influence of heat transfer from the THC (Hulme and Shirriff, 1994). As a result, Shetland is particularly sensitive to fluctuations in the THC and the NPF, which have been recorded in terrestrial lake sediments. The geology of Shetland is complex, consisting of a wide range of rock types, spanning all the major lithological types (igneous, metamorphic and sedimentary lithologies (Mykura, 1976). Eustatic sea level changes, since the termination of the Last Glacial Maximum, have caused many of the valleys to be inundated with water forming present day voes (Flinn 1964)

4.2.1.1 **Last Glacial Maximum**

Shetland has been under scrutiny for the past century, with many believing that it supported a local ice cap during the LGM (Home, 1881; Hall, 2013). However, some studies have suggested that there was a lack of evidence for this (Finlay, 1926). Shetlands ice cap likely interplayed with the Norwegian Channel Ice Stream (NCIS) (Merrit et al., 2019), the Fennoscandinavian and the British Ice sheet (Bradwell et al., 2019). Marine bedform imagery highlights that ice retreated towards the south of the Isles throughout the end of the LGM (Bradwell et al., 2008) with of moraines on Unst marking the position of deglacial ice retreat (Golledge et al., 2008). Bradwell et al (2019) highlights that ice retreated offshore at c.22k BP reaching the interior by c.15-16k forming the localised ice cap [Fig.31]. Merritt et al (2019) suggests the independent Shetland ice cap began to retreat at ca. 15 ka due to warming atmospheric temperatures at the start of the interstadial.

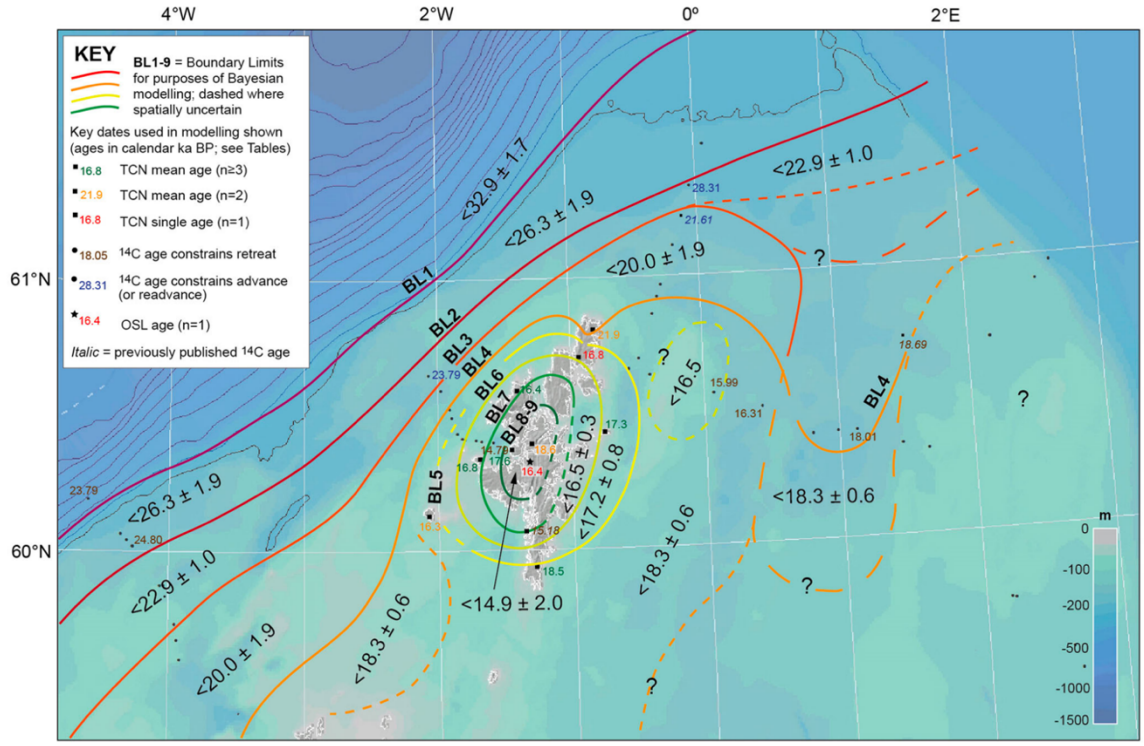

Figure 31. Bayesian modelling of glacial retreat for the LGM to GI-1. The coloured lines highlight the boundary limits of ice. Ages are in calendar ages (ka BP) and error. (Bradwell et al., 2019).

4.2.1.2 **The Interstadial**

Whittington et al (2003) highlights that sedimentation at Clettandal in Shetland began between c.15.79-14.37k cal BP. This is consistent with an onset of deglaciation at c.15k BP (Bradwell et al., 2019). Their sediments and diatoms indicate that there were rapid successions of minerogenic in-washing and organic rich autochthonous sediments during periods of cooling and warming (Whittington et al., 2003). Bradwell et al (2019) highlights that there are no records of glacial activity after the LGM in Orkney.

There are few sites on Shetland that record the LGIT with many focusing on the Holocene period e.g. Lang Lochs (Hulme and Shirriff, 1994). One of the few records is in Clettandal on the Shetland mainland. Whittington et al (2003) does not record any significant change in the fauna or vegetation during the interstadial and the LLS at this site. This is consistent with Birks and Peglar (1979) who highlight that tree growth was non-existent due to the lower summer atmospheric temperatures and exposure to high winds. Birnie (2000) records a slow response of the vegetation to atmospheric warming with *Salix herbacea* and *Rumex* dominating the landscape. They show that tall herbs and dwarf shrubs were abundant during this time. Furthermore, the palynological evidence from Shetland shows a dominance of *Betula* in the records however there is no macrofossil evidence to support this, indicating that these pollen grains were windblown and do not represent the in-situ vegetation at the time (Birnie, 2000). Other palynological studies been undertaken in Shetland which record a succession of vegetation similar to N.W Europe (Iversen, 1958; Birks and Peglar, 1979).

Whittington et al (2003) highlights that it is unlikely the short-lived cooling events, GI-Id and GI-1b, would be recorded in Shetland where there are unstable landscapes. They stress the need for varved sedimentation in order to record these short-lived fluctuations in the environment. The palynological and diatom records for Shetland are vast however there are no records of atmospheric temperature change. To date, they have been largely inferred by spatial computer modelling (Brooks and Langdon, 2014). Therefore, it would be necessary to use high-resolution single variable climate proxies to overcome this and to identify short-lived centennial climate oscillations.

4.2.1.3 **Loch Lomond Stadial/Younger Dryas**

At present there are no records of glacial activity on Shetland during the Loch Lomond Stadial. However, one of the aims of this thesis is to assess if mean July summer temperatures were low enough to support localised ice caps. With the use of chironomid inferred temperature records it may be possible to do this.

Whittington et al (2003) records the presence of cold indicator species of Coleoptera: *Apatania muliebris* and *Pyncnoglypta lurida*. Whereas, the diatom record from their study show little variance in the record at this transition from warm to cold conditions. Birnie (2000) also records little variation in the vegetation record from the interstadial to the onset of the Loch Lomond Stadial which suggests that there was no environmental or climate fluctuations at this point. However, this does not support the clear shift from organic rich lake sediments to minerogenic rich clays, at the onset of the LLS/YD, recorded by Birnie (2000), Whittington et al (2003) and Hulme & Shirriff (1994). With the addition of chironomid inferred temperatures a clearer image of the mean July temperatures can be made for this time frame.

4.2.1.3 **Holocene Onset**

Deep peat units overlay the sediments from the LGIT which were formed during the interglacial Holocene period (Birks & Ransom, 1969). These units have provided continuous records of environmental change spanning the Holocene (Bennett et al., 1992, Whittington and Edwards, 1993). Hulme and Shirriff (1994) record a sharp transition in minerogenic rich clays to organic rich muds at the transition to the Holocene. Johansen (1975) and Bennett et al (1992) record a dominance of shrubs and herbaceous vegetation such as grass and sedge. They record a drop in the abundance of plants that thrive in unstable landscapes. This highlights that the Holocene was significantly warmer, and the landscape was more stable to support a greater diversity of flora. Hulme and Shirriff (1994) show that during the Holocene period *Pinus* abundances drop sharply and they conclude that these taxa did not return after the LLS.

Whittington et al (2003) used a multiproxy approach which indicates a sharp warming at the transition into the Holocene. However, they do not record any subtle fluctuations in temperatures or environmental change that are known to occur in the early Holocene e.g. 11.4k event (Rasmussen et al., 2014).

4.2.2 **Isle of Orkney: Overview**

The Isle of Orkney (58°42-59°25' N, 02° 22'- 03° 24' W) is low-lying, and closer to the Scottish mainland than Shetland. The climate is controlled by oscillations in the North Atlantic current and has an intermediate climate system between the north of Scotland and Shetland (Berry, 2000; Whittington et al., 2015). The onset of sedimentation is thought to have occurred at c.15k BP (Whittington et al., 2015). The majority of the landscape of Orkney lies beneath 270m and consists of undulating Devonian sedimentary rocks (Ballantyne et al.,2007) from the Caithness Plateau. The landscape is covered by a blanketing of peat bogs, underlain by unconsolidated glacial sediments (Bennett et al, 1997).

Orkney has robust palaeoenvironmental records. Sediment cores, spanning the LGIT, have been found in Orkney and provide a better understanding of the palaeoenvironmental history of the isles (Bunting et al., 1994; Whittington et al., 2015; Kingsbury, 2018; Abrook et al., 2019). More importantly, a core from Loch of Sabiston, with a high-resolution robust chronology spanning the LGIT, was taken in 2009 and has been subsequently analysed for diatoms and pollen assemblages, to better understand the palaeoecological conditions of the lake basin (Kingsbury, 2018). As a result, this region was chosen as there is a wealth of robust, high resolution multi-proxy records that allow for a better understanding of environmental change in the region.

Orkney has been shown to have high-resolution records of tephra deposition for the LGIT (Kingsbury, 2018; Timms et al., 2018), recording the Borrobol Tephra, Penifiler Tephra, Vedde Ash, Hässeldalen Tephra, Askja-S Tephra and Saksunarvatn Tephra (Timms et al., 2018). This site is prime locality to study the synchronicity of climate changes with other sites across N.W Europe as these tephra markers allow for robust age tie-points to be constructed between sites.

4.2.2.1 **Last Glacial Maximum**

The Isle of Orkney has a complex glacial history (Hall & Whittington, 1989, Hall et al., 2016(a)). Based on cosmogenic exposure and optical stimulated luminescence dating, Bradwell et al (2019) shows that deglaciation occurred at c.23k BP offshore and terminated at c.16-17k BP [Fig.32]. This is consistent with Phillips et al (2008) who highlights that the onset of deglaciation occurred <c.20k BP.

There are believed to be three stages of glacial till deposition throughout the LGM based on the formation of stacked till sequences, highlighting a complex interplay with the FIS and BIS ice sheet (Hall & Riding, 2016) [Fig.33(a)]. The oldest glacial morphological features are raised rock platforms and cliffs which were inundated with a blanketing of Digger Till (Crampton & Carruthers, 1914). The Digger Till contains Carboniferous and Permian palynomorphs suggests that ice flowed from the east of Orkney to the N.W (Merritt et al., 2019) [Fig.33(b)]. Evidence suggests that the Isle of Orkney had a vast dome of accumulated ice and snow on the mainland. (Merritt et al., 2019).

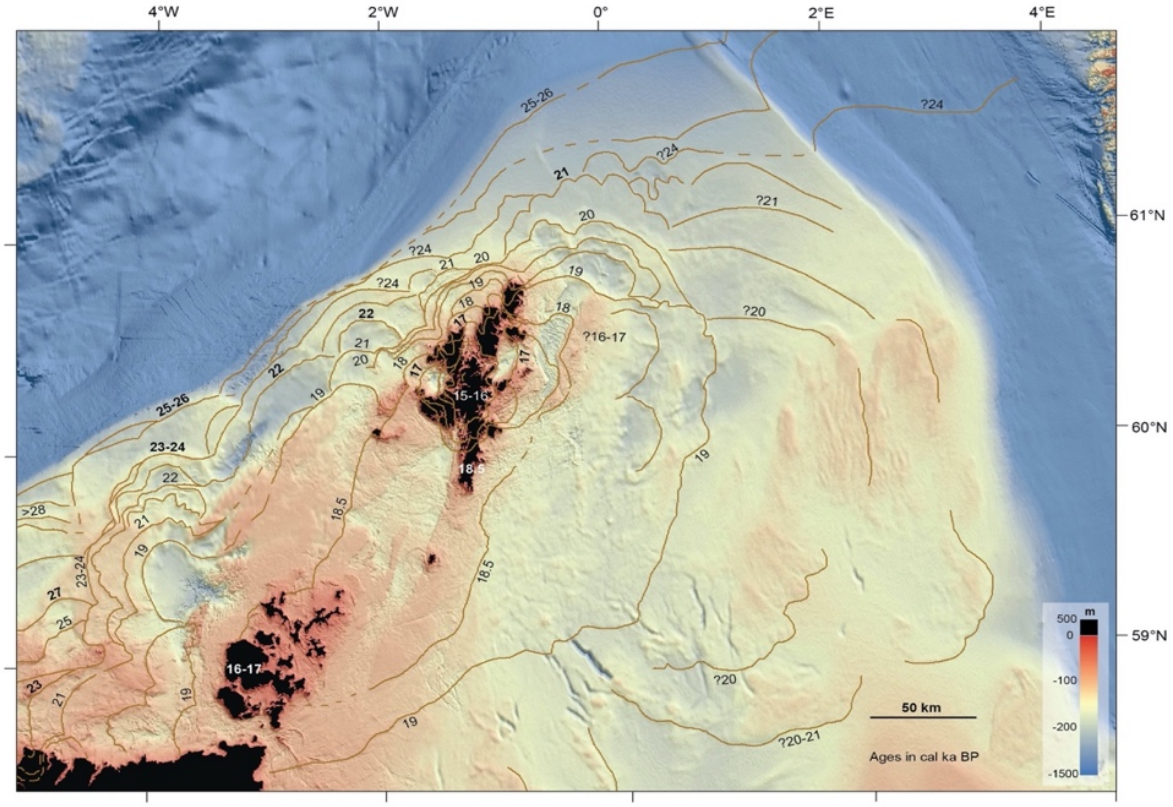

Figure 32. Northern Isles of Scotland and Caithness exposure dating ages of deglaciation after the LGM (Bradwell et al., 2019)

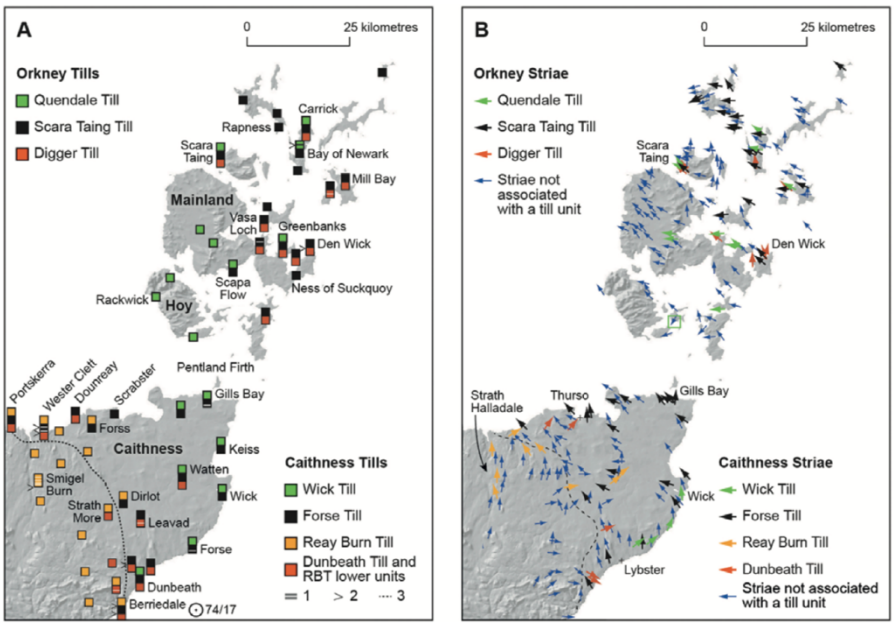

Figure 33. (A) Cited from Merrit et al (2019). Evidence of three stages of till formation on the Isle of Orkney and Caithness (Hall & Riding (2016) and Hall et al., 2016.

4.2.2.2 **The Interstadial**

Whittington et al (2015) reconstructed the environmental history of Crudale Meadow on Orkney using stable isotope analysis, pollen studies and mollusc identifications. They recorded two clear indicators of climate cooling corresponding to the Older Dryas (GI-1d) and the Inter-Allerød cold period (GI-1b). They also record a subtle cooling event between GI-1d and GI-1b, likely corresponding to GI-1c (2) (Rasmussen et al., 2014). However, as the lake is currently dried, they were unable to model a quantitative measure of temperature change. They record vegetation indicative of an open landscape composed of herbs and low shrubs. Whittington et al (2015) record a sharp drop in the abundance of arctic mollusc assemblages which suggest that the climate warmed during the interstadial. Kingsbury (2018) analysed the palaeoenvironmental history of Loch of Sabiston (the same lake for this project) They record a sharp transition in the abundance of the diatom *Fragilaria* between the calcium rich marls and the minerogenic rich clays during the short-lived cold phases GI-1d and GI-1b. Kingsbury (2018) also record the transition between the warm and cold phases throughout the interstadial in their geochemical record. However, quantitative records of atmospheric temperatures have not been recorded for this region. The rationale for choosing this region was to quantitatively assess the magnitude and timing of these mean July summer temperature fluctuations.

4.2.2.3 **Loch Lomond Stadial/Younger Dryas/GS-1**

Whittington et al (2015) records a sharp transition from marl rich sediments to minerogenic rich clays. They show that the pollen grains, in this clay unit, were greatly eroded suggesting that the landscape was unstable at this time. Unlike Shetland, glacial activity returned during the LLS in Orkney. Two small glaciers, named the Dwarfie Hamars Glacier and the Enegars Glacier, have been recorded in the hilly regions of Hoy, based on exposure dating (Ballantyne et al., 2007) [Fig.34]. Equilibrium Line Altitude (ELA) calculations have been modelled to reconstruct the ice extent on Hoy during this time, using chironomid inferred summer temperatures from Whitrig Bog, Central Scotland (Ballantyne et al., 2007). With the addition of C-IT records from Loch of Sabiston, from this project, more reliable temperature inferences could be applied to this model to assess if the extent of glacier advance was greater.

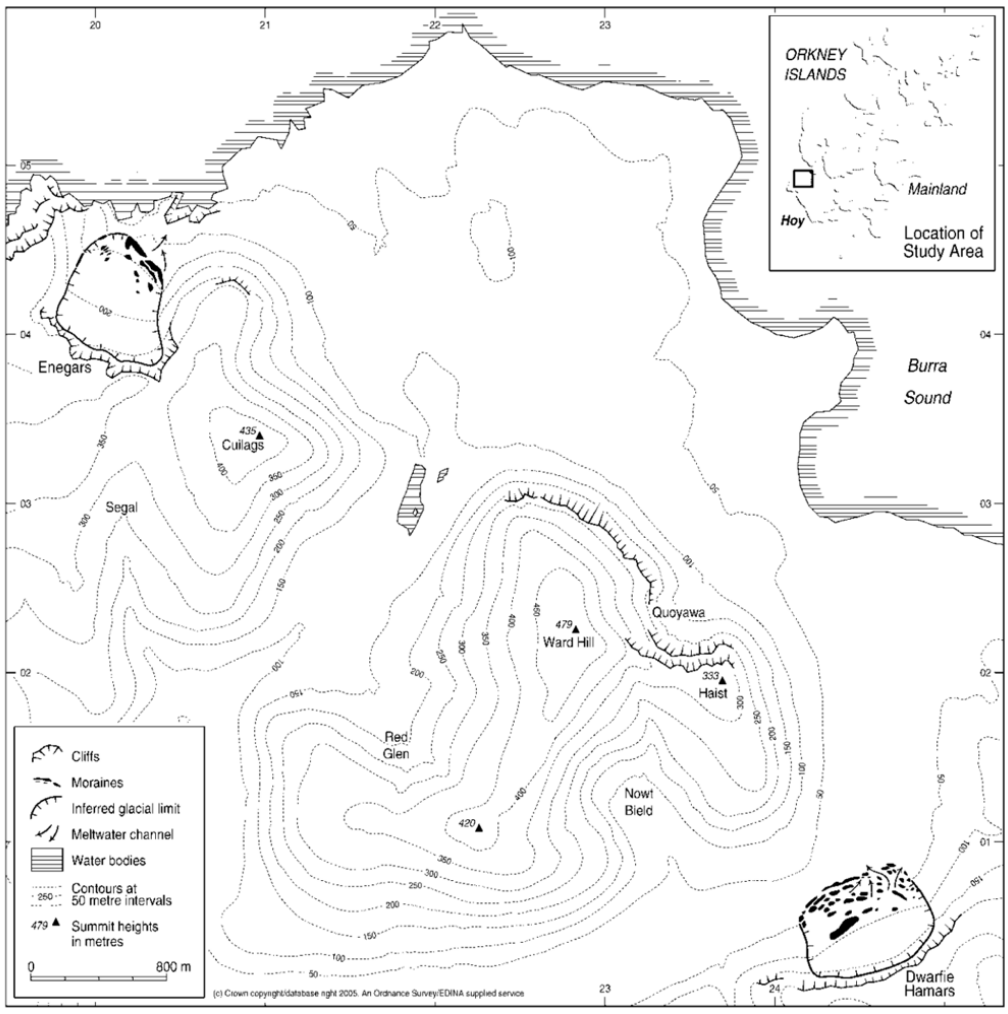

Figure 34. The location of the two small glaciers on the Isle of Hoy, off the coast of mainland Orkney (Ballantyne et al., 2007)

4.2.2.4 **Holocene Onset**

In Crudale Meadow the $\partial^{18}O$ values rapidly rise at the onset of the Holocene period. Indicating a sharp rise in carbonate precipitation. This coincides with an increase in the abundance of the warm thermophilic species Corylus (Hazel). The stratigraphy in Crudale Meadow indicates that there was a short-lived cooling event after the onset of the Holocene period, likely corresponding to the 11.4k Event (Rasmussen et al., 2014; Whittington et al., 2015), although, as the event was short-lived it is not reflected in the pollen assemblages. Throughout the Holocene there is a continuous increase in the abundance of Poaceae indicating that there was an expansion of grasslands and lake mires (Whittington et al., 2015).

4.2.3 **Caithness: Overview**

Caithness (58°24'59.99" N -3°29'59.99" W), although not within the Northern Isles of Scotland, is the closest part of the Scottish mainland to the archipelagos. This area lies close between the North Atlantic Ocean to the west and the North Sea to the east (Golledge et al., 2009). Due to the close proximity of Caithness to the North Atlantic Ocean it too is influenced by changes in the North Atlantic circulation and the thermohaline circulation (Golledge et al., 2009). This area has been colloquially named the 'flow country' due to the flat lying undulating peat bogs that blanket the landscape (Stroud et al., 1987). Presently, the region has 900-1000mm of rain annually with temperatures also ranging between 11.5-3.5˚C from summer to winter (Birse, 1971; Golledge et al., 2009).

4.2.3.1 **Last Glacial Maximum**

Hall & Riding (2016) and Hall et al (2016) highlight that the glacial history of Caithness is complex. Glacial erratics from the East Sunderland Granites, near Caithness, have been found on the Isle of Stronsey within the archipelago of Orkney. Likewise, upper Cretaceous chalk, from the North Sea have been found in Caithness [Fig.35]. The evidence above highlights that there was a complex relationship between the BIS and the FIS (Merritt et al., 2019).

Golledge et al (2009) dated the onset of sedimentation and subsequent deglaciation at c.18k cal BP in the Shebster basin. They highlight that this date is likely too old due to an influx of old carbon into the reservoir system. The same hard water

errors were recorded by Peglar (1979) at Loch of Winless, eastern Caithness. The Caithness region has a wealth of palynological data to help to understand the environmental history of the LGIT. The chronology of these records is low due to the time that the projects were conducted. AMS dating had not been developed when the projects were conducted.

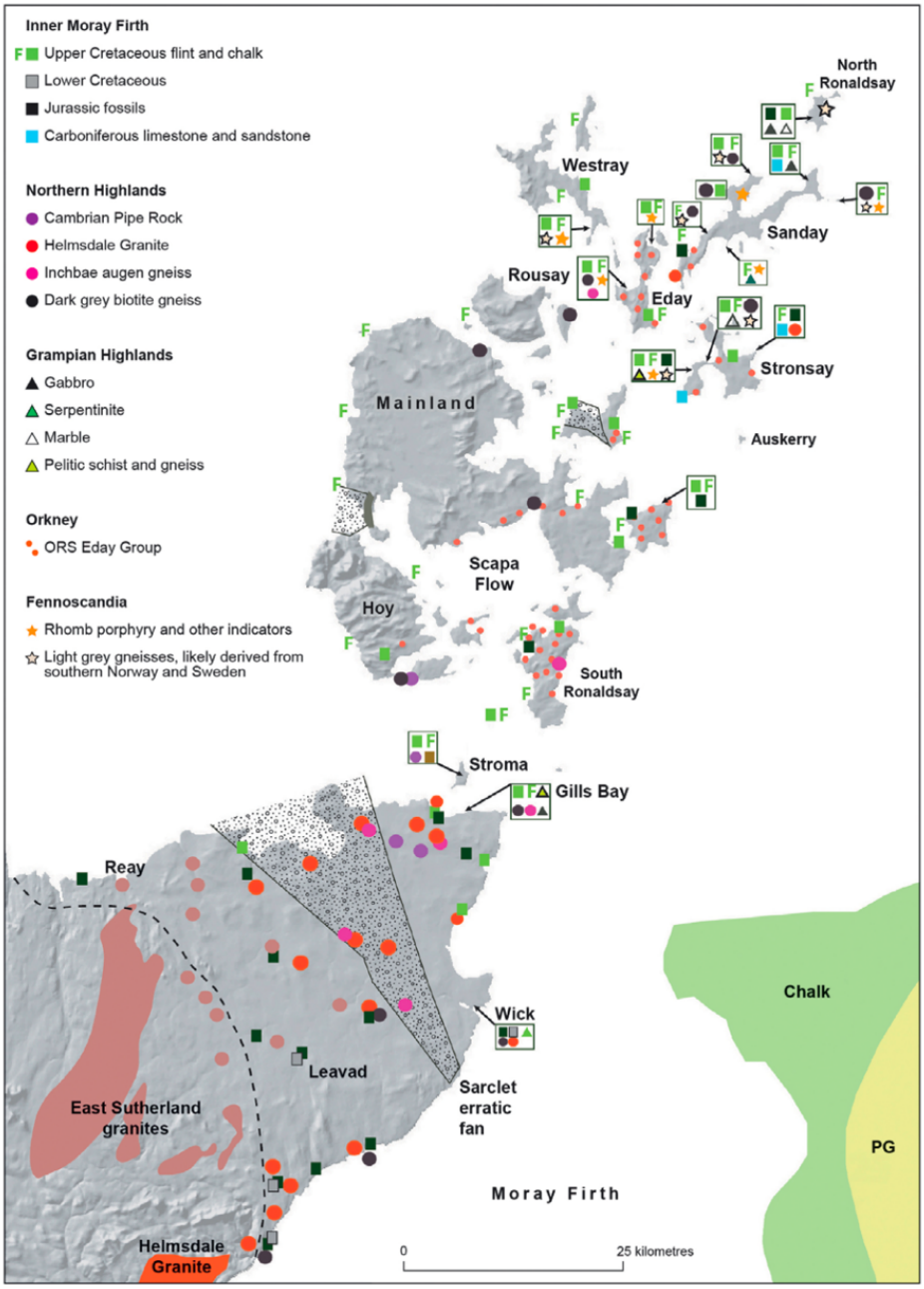

Figure 35. Records of glacial erratics on the north coast of Scotland and Orkney. Highlighting the interprlay with the BIS and FIS (Merrit et al., 2019 citing Hall & Riding (2016) and Hall et al (2016))

4.2.3.2 **The Interstadial**

Moar (1969) and Peglar (1979) record a dominance of *Empetrum* throughout the interstadial at Loch of Winless, suggesting that heathland was widespread throughout the North of Scotland. This is reaffirmed by Birks (1984) and Pennington et al (1972) who also record heathland extending to Sutherland in the North of Scotland. Their pollen records show little variation in vegetation during the interstadial. Productivity in the lakes in the region increased, with Loch of Winless seeing a rise in the concentration of algae and aquatic plants (Peglar., 1979). Before the onset of the LLS there is a rise in the abundance of tall-herbs and dwarf shrubs which required nutrient rich-soils (McVean & Ratcliffe, 1962).

4.2.3.3 **Loch Lomond Stadial/Younger Dryas**

Currently, there is no record of glacial activity spanning the LLS for the Caithness region. The closest locality which is known to have glacial activity was in Sutherland (Assynt) to the west (Golledge et al., 2008) [Fig. 36]. The Loch Lomond Stadial is not represented well in the palynological records for Caithness. Peglar (1979) records little variation in the vegetation record which spanned this cold phase. However, there is a subtle decrease in the number of tall herbs recorded which represents a phase of increased catchment instability and soil erosion. At Loch of Winless the catchment has been likened to a mosaic/patches of vegetation (Peglar, 1979).

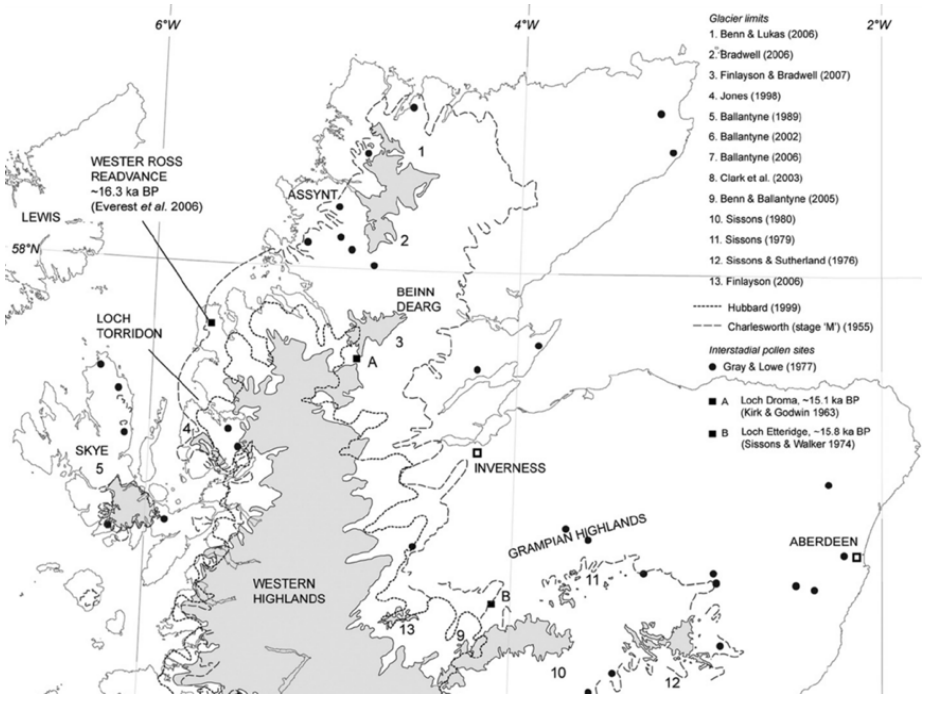

Figure 36. The northward extent of the Loch Lomond Stadial ice sheet (Golledge et al., 2008)

4.2.3.4 **Holocene Onset**

The onset of the Holocene is marked by a sharp transition from minerogenic rich clays to calcium carbonate rich marls sediments in the Shebster basin (Golledge et al., 2009). At Loch of Winless there is significantly less woodland vegetation than at the Shebster basin. At Loch of Winless the onset of peat accumulation occurs at c.9k cal BP (Peglar, 1979). To date, there are no quantitative records of atmospheric or lake temperature change for this timeframe.

4.2.4 **Summary**

In summary the Northern Isles of Scotland and Caithness were chosen for this research as they currently lack high resolution single variable temperature records. Due to their close proximity of Scotland to the North Atlantic Ocean they are highly dependent upon and influenced by fluctuations in the thermohaline circulation (Brooks et al., 2016; Kingsbury, 2018). They are in a are prime locality to study the relationship between the ocean-atmosphere-terrestrial systems. Brooks and Langdon (2014) highlighted that this region in the North Atlantic has a low-resolution record of climate change and future work should be focused here. Furthermore, each of the three locations have a wealth of palaeo-environmental data. This data could be used to better understand how the environment changed throughout the LGIT for these regions, thereby aiding interpretations of how synchronous palaeoenvironmental change and atmospheric temperatures were during the LGIT.

4.3 Aims, Objectives & Hypotheses

This research will reconstruct a high-resolution record of palaeoclimate and environmental change for the Northern Isles of Scotland and Caithness spanning the Last Glacial-Interglacial Transition (LGIT). This research will address the following aims and use the objectives below:

(1) **Reconstruct the palaeoclimate history of the Northern Isles of Scotland and Caithness during the LGIT**.

- Objectives:
  - Use high-resolution, chironomid inferred mean July temperature reconstructions to record summer temperature change for the LGIT.
  - Use long chain alkenone spring lake temperature record for Scotland to reconstruct spring lake temperatures for the LGIT.

(2) Determine, if it is possible to assess, the degree of climate synchronicity between sites during the LGIT?

- Objectives:
  - Use a robust AMS radiocarbon and tephra-based chronology combined with age-depth modelling in OxCal to determine the degree of synchronicity between sites.

(3) Determine the seasonal variations in temperatures for Caithness during the LGIT.

- Objectives:
  - Compare the mean July summer temperatures from the chironomid head capsules with spring lake temperatures derived from long chain alkenones.

(4) Determine the spatial extent and magnitude of climate changes during the LGIT.

- Objectives:
  - Geospatially plot palaeotemperature isotherms to determine the temperature trends and gradients for the LGIT

The following hypotheses have been made at the onset of this research. Using the aims and objectives highlighted above one will assess the accuracy of these assumptions:

(1) **Chironomids can reliably reconstruct mean July atmospheric temperatures for the Northern Isles and Caithness during the LGIT.**
(2) **Atmospheric temperature change is the main driver of chironomid assemblages during the LGIT.**
(3) **Climate changes were not synchronous across the North Atlantic Ocean during the LGIT**
(4) **Long-chain alkenones record cooler temperatures than that of chironomid inferred temperature record for the LGIT in Caithness**
(5) **Ocean circulation changes drove atmospheric warming and cooling during the LGIT**

Chapter 5-Methodology & Materials

5.1 Introduction

This chapter highlights the methodologies used within this project. Chironomid head capsule assemblages, algal biomarkers (long chain alkenones), tephrochronology and geochemical analysis was undertaken throughout this research.

Firstly, this chapter will describe the method of coring followed by the non-destructive and destructive geochemical analysis. Secondly, the methods used to sample, extract and separate the chironomid head capsules will be shown. Fourthly, the methods used to identify each chironomid and the process to model the temperature inferences will be shown. A description of the preparation, separation and analysis of algal biomarkers will be shown. Lastly, the methods used in building a robust chronology of the sites will be shown using tephrochronology, radiocarbon dating, and age-depth modelling.

5.2 Coring

Each lake was chosen due to their close proximity to the North Atlantic Ocean and influence of the North Polar Front. Cores were taken previously from Loch of Sabiston (Orkney) (Kingsbury, 2018) and the Shebster basin (Caithness) (Stewart et al., 2017). However, for Lang Lochs (Shetland) the core was retrieved for this project.

A small raft was constructed to reach the centre of the lake for Loch of Sabiston where the sedimentation rate was higher and most concentrated (Kingsbury, 2018). Stewart et al (2017) retrieved a core from the Shebster basin near the original coring site of Golledge et al (2009) to maximise continuity between projects. This was taken on a blanket peat bog/surface mire however the site was previously a lake.

The Lang Lochs core was taken on the fen edge of the lake. The stratigraphy of the basin was assessed using trial cores to determine where the highest sedimentation rate and fullest record of the LGIT was. The site was previously cored by Hulme & Shirriff (1994) however their record only encompassed the end of the LLS/Holocene. The GPS coordinates of their site was used to retrieve a core close to the original site to maximise the similarity of stratigraphical tie-points between projects.

Cores were retrieved using a 1m Russian D-section corer to retrieve a continuous core, limit smearing and therefore reduce the likelihood of contamination

[Fig.37]. Each core included a 10cm overlap to maximise retrieval and continuity in the lithological sequence [Fig.38]. Once retrieved each core was placed in plastic guttering and sealed with lay-flat tubing to prevent desiccation. Each section of core was archived and stored at 4˚C to limit additional moisture. Straight after retrieval the sedimentary characteristics of the cores were described, the depth (cm) of each stratigraphical boundary was recorded and the potential areas for radiocarbon dating were noted.

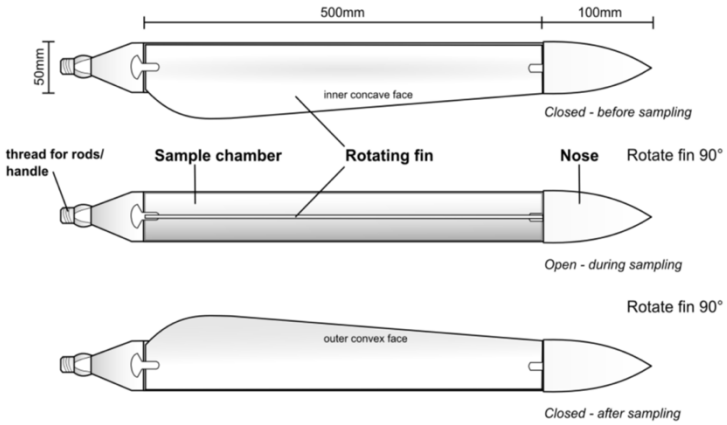

Figure 37. Image of a Russian D-Section corer and its dimensions (mm) (image cited by ARCO, 2014)

Loch of Shebster, Caithness (965-875cm)

Loch of Sabiston, Isle of Orkney (420-180cm)

Lang Lochs, Isle of Shetland (405-270cm)

Figure 38. Image of each core including sampling depths (cm). Image includes a continuous sequence from Caithness, the Isle of Orkney and the Isle of Shetland.

5.3 Non-destructive analysis

5.3.1 Micro- XRF and lithological descriptions

Micro-XRF was used to provide a high-resolution record of the geochemical and compositional characteristics of each core. Major and minor element profiles were retrieved for the following: Si, S, P, Ca, Ti, K, Fe, Pb, Mn, Zn, Rb, Sr and Zr. However, for this research only the silica, calcium, potassium, titanium and phosphorus counts will be used.

The calcium counts will be used to infer increased productivity as a result of lake warming (Balasacio et al., 2011; Lauterbach et al., 2011); the titanium counts will be used to infer basin in-washing and potential tephra layers (Kylander et al., 2012), iron counts will be used to determine the levels of anoxia and also for tephra identification (Kylander et al., 2012), silica counts will be assessed to determine the diatom abundances and minerogenic inputs (Croudace & Rothwell; 2015). Phosphorus levels will also be used to infer lake nutrient levels. Titanium values are useful indicators of allochthonous inputs from the catchment (Cohen, 2003). The relationship between Si-/Ti can be used to infer the production of biogenic silica which would enable one to separate biogenically dominated sediments from inorganic silica (Brown et al. 2007).

The instrumentation used a step size of 500μm, resolution of 200μm and a voltage of 60kV was used for each 1m core. Each core was joined together and an overlap of 10cm was allowed to account for sediment smearing and inaccurate readings at the ends of each core. Micro-XRF core scanning has long been known to be a useful method to determine the geochemical properties of marine and lacustrine sediments (Croudace & Rothwell, 2015). It has been widely used in chemostratigraphy (Pearce and Jarvis, 1995). Using the methods highlighted above a fuller interpretation of the lake chemistry, basin dynamics and productivity will be assessed. This method has been used to better understand the palaeo-lake chemistry for each site and to build a more robust chronology by identifying possible layers for radiocarbon and tephra dating. Sub-samples were taken every 1cm to assess the loss on ignition (LOI) for the Lang Lochs. The Loch of Sabiston core was sub-sampled previously for LOI (Kingsbury, 2018). The Shebster basin core was not sub-sampled. However, Golledge et al (2009) recorded the LOI for an adjacent core. Where stratigraphical correlations were available between cores the LOI from Golledge et al (2009) was used.

5.4 Chironomid assemblages and temperature inference

5.4.1 Sampling and extraction

Sub-samples were taken from each of the three cores following the method outlines in Brooks et al (2007). Contiguous samples were taken every 1-2cm over stratigraphical boundaries in order to track sub-centennial changes in chironomid assemblages for all of the three sites. Areas of uniform sedimentation rates and no lithological changes were sub-sampled at a lower resolution (4cm). This was routinely checked by pilot runs which indicated that the composition of the chironomids remained largely unchanged. Each sample was reacted with 10% HCl, in a 50˚C bath, to remove any organic matter from the sediment to allow for the head capsules to be picked with ease. The samples were then sieved at 212µm to remove the adult chironomids and 90µm to extract the juvenile fractions following Brooks et al., 2007 for subsequent identification. The samples were then transferred into vials and archived until the separation stage.

5.4.2 Slide preparation

Separation of the chironomid head capsules, from the concentrated samples, was undertaken using a Borgorov sorting tray (Brooks et al., 2007). Samples were pipetted into the tray and subsequently picked, using tweezers, under a dissecting microscope. Head capsules were picked from the treated sample and mounted onto thin-section slides using Hydromatrix© mounting medium (Brooks et al., 2007). Initial mounting was undertaken using Euparal essence to dry the head capsules, removing trapped moisture, and subsequently mounted using Euparal mounting gel. This method was replaced with Hydromatrix as it was less time consuming. Cover slips were then placed on the samples to aid identification and the samples were left to dry.

5.4.3 Fossil identification and analysis

A minimum of 50 chironomid head capsules were identified per sub-sample in order to provide a statistically robust temperature inference model (Brooks et al., 2007). The diagnostic features found on the head capsule: the ventromental plates, mandibles, mentum (teeth), pedestals and the post-occipital plates of each chironomid were used to separate each family and identify each species. The key identifying characteristics

of the head capsules were analysed following Brooks et al (2007) [Fig.39]. See below the main diagnostic features used to separate out the chironomid taxa:

- ***Setae***. The posterior to anterior of the head capsule, have features that are unique to each species. Each area has cephalic setae present on the surface of the capsule (Cranston., 2013). However, the setae often fall off during deposition in the lake, leaving behind circular indentations on the surface of the capsule. These are located throughout and are unique to each species (Cranston., 2013). These diagnostic features are particularly valuable when identifying taxa within the family of Tanypodinae (Rieradevall & Brooks., 2001). In addition, Vallenduuk & Moller-Pillot (2007) highlight the importance of using the posterior section of the Tanypodinae head capsule to separate these taxa.

- ***Antennae.*** Chironomid larvae have distinctive antennae visible on the anterior section of the head capsule. The antennae can be retracted back within the head of the Tanypodinae head capsule (Cranston et al., 2013). However, the other sub-families have stationary antennae which are supported on a pedestal on the top of the head capsule. These features can trail behind the chironomid in some taxa, whilst in others, such as Podonominae, they are positioned in the posterior segment of the head capsule (Cranston et al., 2013).

- ***Mandibles & Pre-mandibles.*** Pre-mandibles are paired, mobile and have small teeth on their surface (Brooks et al., 2007). Tanypodinae and Podonominae lack these features which makes them good identifiers for separating out taxa (Cranston et al., 2013). The mandibles are larger and are one of the most prominent features on the chironomid head capsule, located on the anterior of the capsule. The taxa of chironomid will depend on the number of teeth on the surface of the mandible. Usually, the mandible has one dominant dorsal tooth, an apical tooth and numerous surface teeth on the edge of the mandible (depending on the taxa) (Brooks et al., 2007., Cranston., 2013)).

- ***Mentum:*** the mentum is a feature of the mouthpart and the most distinctive part of the head capsule. The mentum, in most species, resembles a serrated edge of a

saw, whilst others such as *Corynocera ambigua*, have one large tooth. Each species of chironomid have a unique mentum morphology and as a result is often the first part that micro-palaeontologists and entomologists to use for identification.

- ***Ventromental plates:*** the ventromental plates are a continuation of the mentum. Within these plates are where the chironomid holds its silk sack. These plates are found beneath the mentum, lying horizontally across the head capsule. Often striations, are found on the surface of the plate which can be used to identify species apart. E.g. 'Eye-lash' striations on *Chironomous anthracinus* (Brooks pers comm). In Orthocladinae the purpose of these are unknown (Cranston et al., 2013). In this taxon they are found at a diagonal lineation from the edge of the mentum.

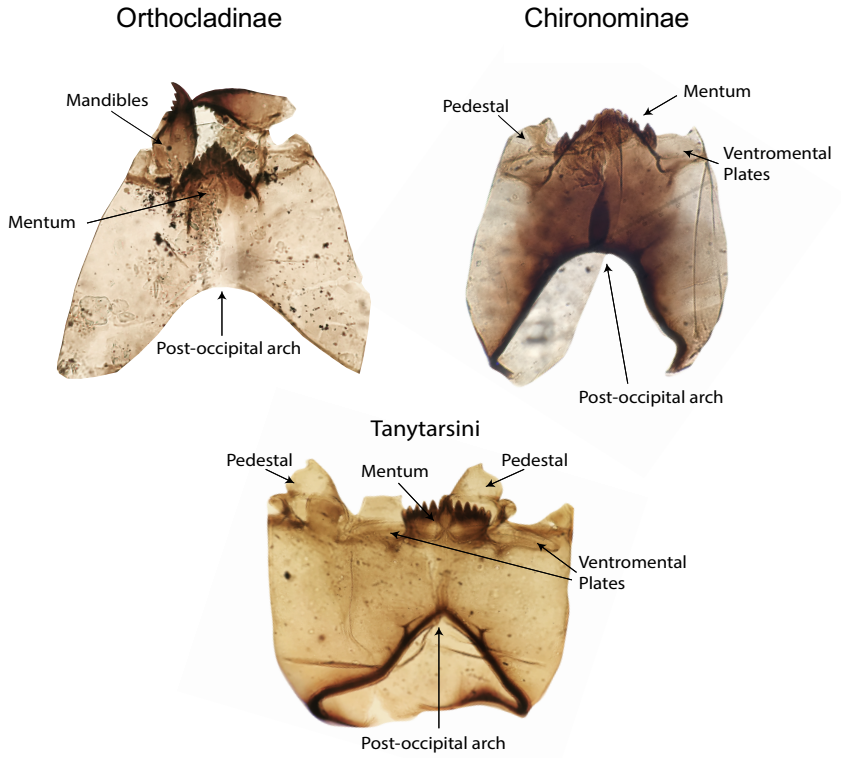

Figure 39. Chironomid head capsules indicating the key characteristics to identify each species.

Chironomid assemblages were plotted using Tilia v2.1.1 and significant zones were plotted by stratigraphically constraining the assemblages with cluster analysis by incremental sums of squares (CONISS) (Grimm, 1987). This was done in order to highlight significant shifts in chironomid assemblages within the core and in turn infer changes in environmental history.

5.4.4 Chironomid identification challenges and decision making

The key diagnostic features highlighted above were used to distinguish genera apart from one another and where possible samples were separated further into species morphotypes using keys from Cranston et al (1983), Cranston (1995), Cranston & Martin (1989), Cranston (2013) and Brooks et al (2007). 59 taxa were identified for Lang Lochs (Shetland), 56 for Loch of Sabiston (Orkney) and 47 for the Shebster basin (Caithness). The vast majority of the fossils were able to be reliably identified however some presented difficulties as some taxa, if identified incorrectly, would lead to an unreliable and inconsistent temperature inference model. Below, the taxa which were important in the decision making and/or which presented challenges for identification will be highlighted:

1) *Paratanytarsus austriacus / Paratanytarsus penicillatus*

Paratanytarsus are often confused with other Tanytarsini but can be easily distinguished by the sharply incised post-occipital arch and short pedestals. Difficulty arises when trying to separate them out to species morphotypes. *Paratanytarsus austriacus* and *Paratanytarsus penicillatus* are respectively cold and warm stenotherms therefore it is essential that both are accurately identified as poor identification would result in an inaccurate temperature reconstruction. It is possible to separate both by using the mandible as *P. penicillatus* has two inner teeth whilst *P. austriacus* has three [Fig.40]. These morphotypes are only found in the Shetland site.

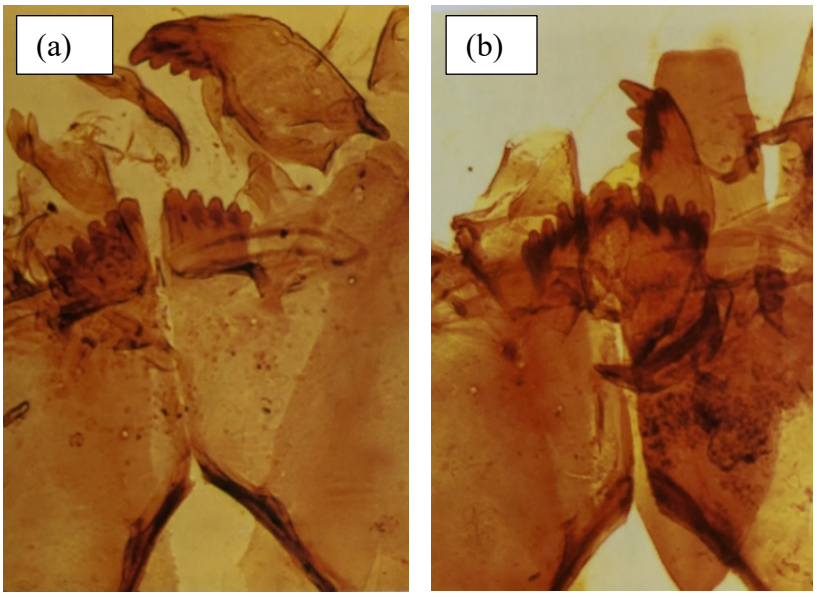

Figure 40. (a) Paratanytarsus austriacus showing three inner teeth on the mandible (b) Paratanytarsus penicillatus showing two inner teeth on the mandible. Both taxa show a sharply incised post-occipital arch and short pedestals (Brooks et al.,2007)

2) *Tanytarsus lugens/Corynocera oliveri*

Often *Tanytarsus lugens* and *Corynocera oliveri* can be confused due to their similar morphological features. Both taxa can be reliably separated as *T.lugens* is known to have a large surface tooth on the mandible and a curved pedestal, whereas *C. Oliveri* has overlapping outer lateral teeth on the mentum [Fig.41]. This is important to distinguish as *T.lugens* is a cold stenotherm which inhabits oligotrophic high latitude lakes (Brooks et al.,2007).

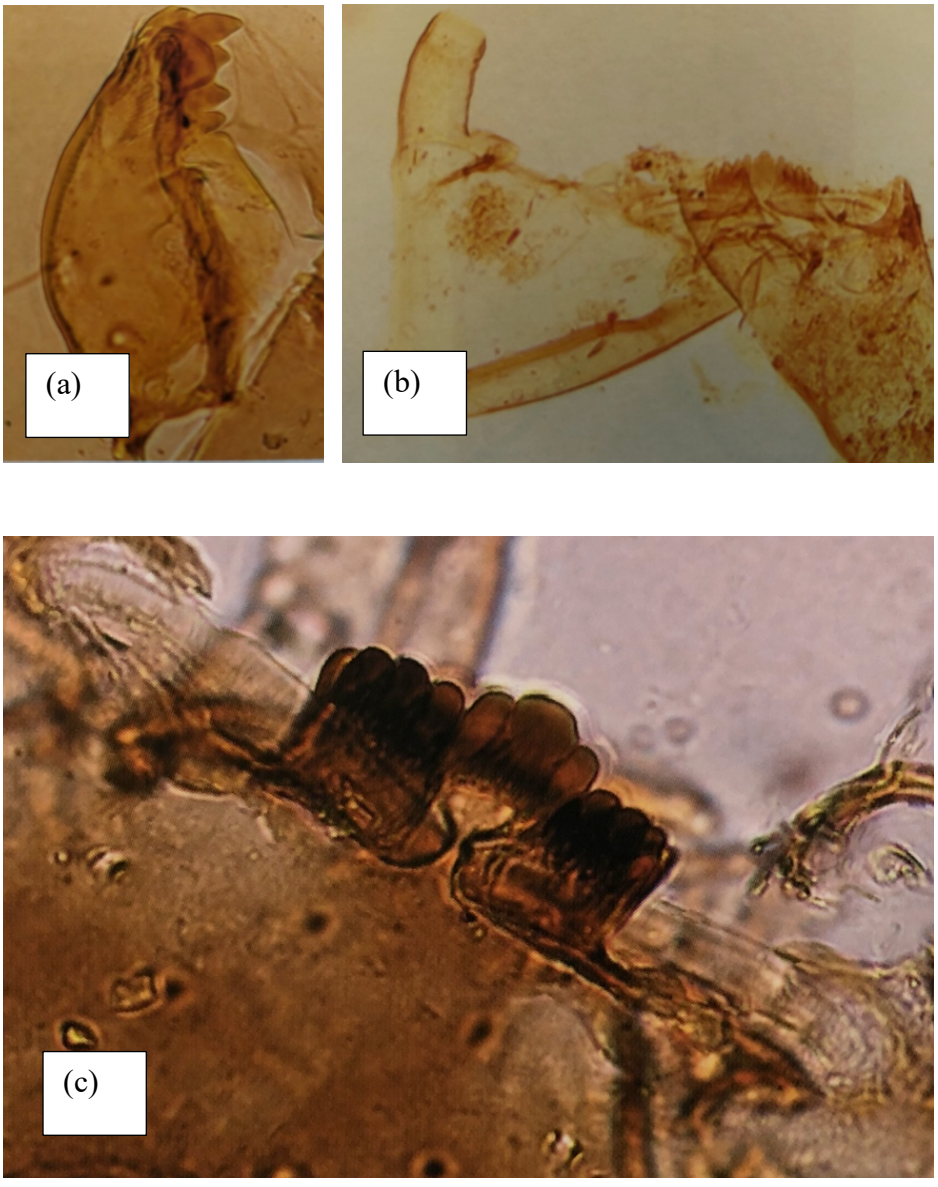

Figure 41. (a) Large surface tooth on Tanytarsus lugens and (b) curved elongated pedestal indicative of Tanytarsus lugens. (c) overlapping outer median teeth of Corynocera oliveri (Brooks et al., 2007)

3) Microspectra radialis/Microspectra insigniloblis/Microspectra contracta

The Microspectra genera are easily separated from other Tanytarsini, such as Paratanytarsus, by the presence of a sharp spur on the pedestal (Brooks et al., 2007) [Fig.42]. However, within the Microspectra genera distinguishing species apart can be more problematic. Microspectra radialis, is a cold stenotherm indicative of oligotrophic conditions, whereas Microspectra insigniloblis and Microspectra contracta are cold-temperate taxa, therefore it is important to identify these taxa apart. Microspectra contracta can be distinguished from Microspectra insigniloblis by its narrower post-occipital arch and its a-symmetrical spur (Brooks et al., 2007). Whereas, Microspectra insigniloblis can be distinguished from Microspectra radialis as it has a much narrower post-occipital arch and lacks the black highlight on the spur.

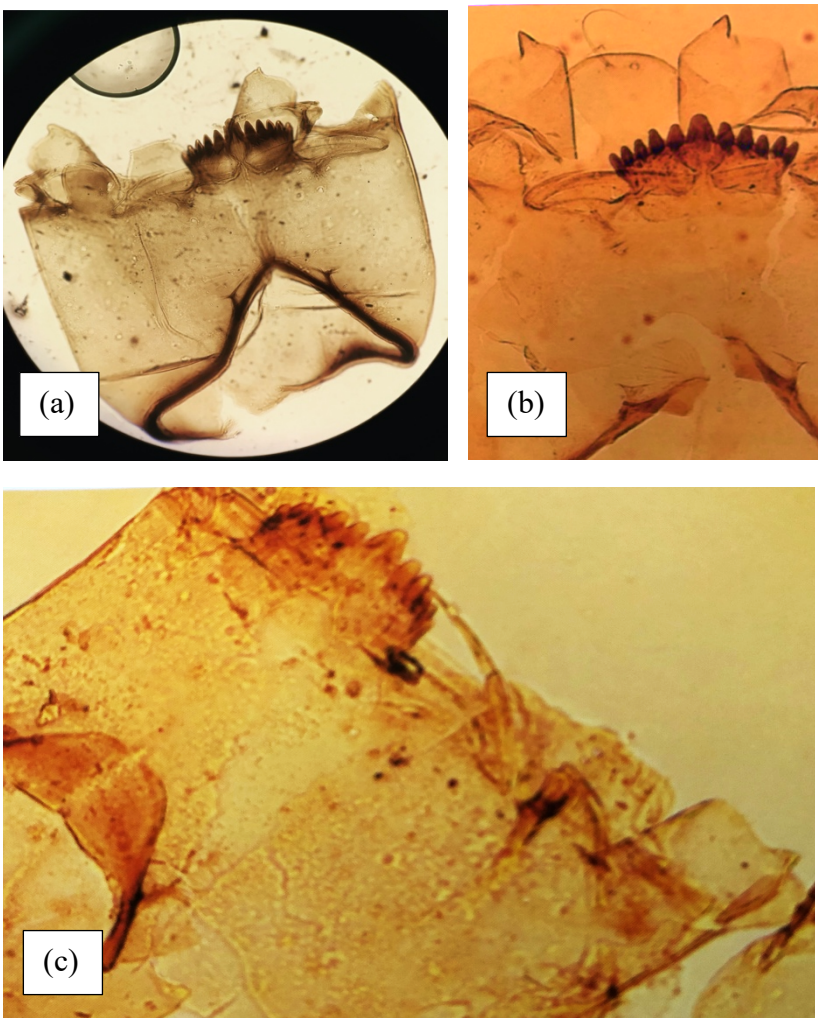

Figure 42. (a) sharp/acute post-occipital arch found in Microspectra insigniloblis (b) black highlight found in Microspectra radialis spur (c) large post occipital plate found in Microspectra contracta (Brooks et al., 2007)

4) *Psectrocladius septentrionalis/ Psectrocladius sordidellus/ Psectrocladius calcaratus*

The Psectrocladius genera occur in large abundances throughout all three of the sites in this project and therefore have to be identified correctly to increase the reliability of the temperature inference models. The morphotype Psectrocladius septentrionalis has a median single tooth and has a ventromental plate which is not as narrow to that found on Psectrocladius calcaratus. Moreover, the median tooth on P. calcaratus is singular and in the shape of a triangle (Brooks et al., 2007). Whereas, the median tooth on Psectrocladius sordidellus is paired and longer than the lateral teeth and has a triangular ventromental plate at its apex (Brooks et al., 2007) [Fig.43]

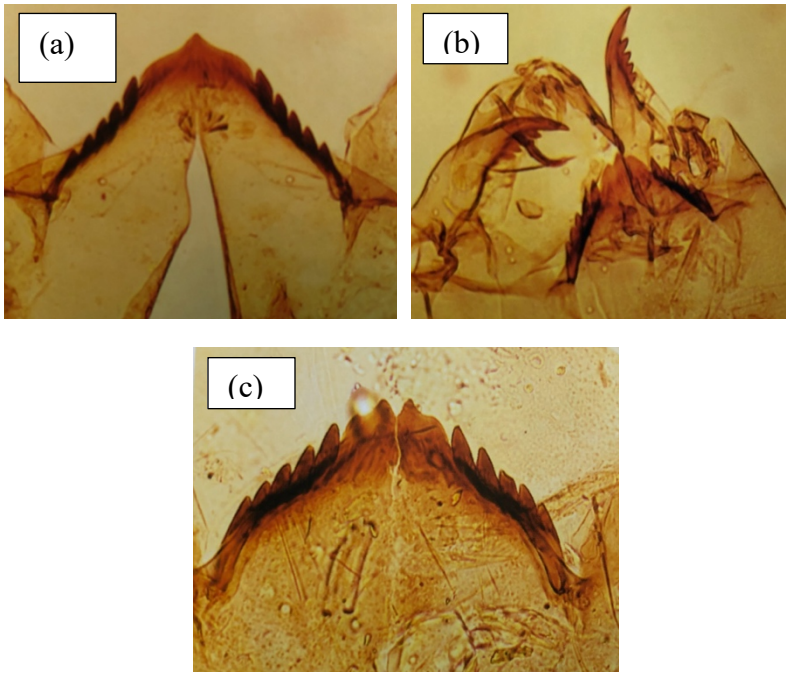

Figure 43. (a) Psectrocladius calcaratus with a single median tooth (b) Psectrocladius septentrionalis with a single median tooth and triangular ventromental plate (c) Psectrocladius sordidellus with paired median teeth (Brooks et al., 2007)

5) *Corynocera ambigua*

Corynocera ambigua occurs in large abundances within two of the records (Caithness and Orkney). Therefore, it was important to reliably identify this chironomid as it is particularly rare in the Norwegian training set (Brooks and Birks, 2000). This species can be easily identified as it has a mandible which has both dorsal and inner teeth absent, has a prominent single tooth on the mentum and is heavily pigmented brown - black (Brooks et al., 2007) [Fig.44].

6) Chironomous anthracinus/Einfelda dissidens type

Chironomous anthracinus is a chironomid which occurs abundantly throughout each of the three cores. This taxon is an early colonising species indicating rapid changes in environmental change however can resemble *Einfelda dissidens*. Therefore, it is important to reliably identify these taxa apart. The surface texture of Einfelda is reminiscent of an orange-peel (Brooks et al., 2007) which is not found on *Chironomous. Chironomous anthracinus* is easily distinguished as it has a short 4th lateral tooth on the mentum and has only two inner teeth on the mandible. Both chironomids are often misidentified as they have vertical striations in the shape of a eye-lash on their ventromental plates [Fig.44].

Figure 44. (a) Chironomous anthracinus showing a single median tooth with lower 4th lateral teeth and 'eye-lash' striations on the ventromental plate. (b) Einfelda showing the same striations on the ventromental plate (c) Single median tooth found on Corynocera ambigua (Brooks et al., 2007; Personal image collection)

5.4.5 Chironomid diversity drivers

This research has used the well-established method of inferring mean July atmospheric temperatures with chironomid head capsule assemblages. Principle component analysis of the Norwegian training set (Brooks and Birks, 2000) highlights that July and water temperatures explain ~40% of the overall variance in chironomid assemblages and are the primary drivers of chironomid assemblages [Fig.45]. However, there are other factors that need to be considered which have been known to influence the biogeographical distribution of chironomids throughout N.W Europe. The PCA analysis highlights that pH, salinity and calcium levels account for some variation, approximately 22%, on the assemblages of chironomids.

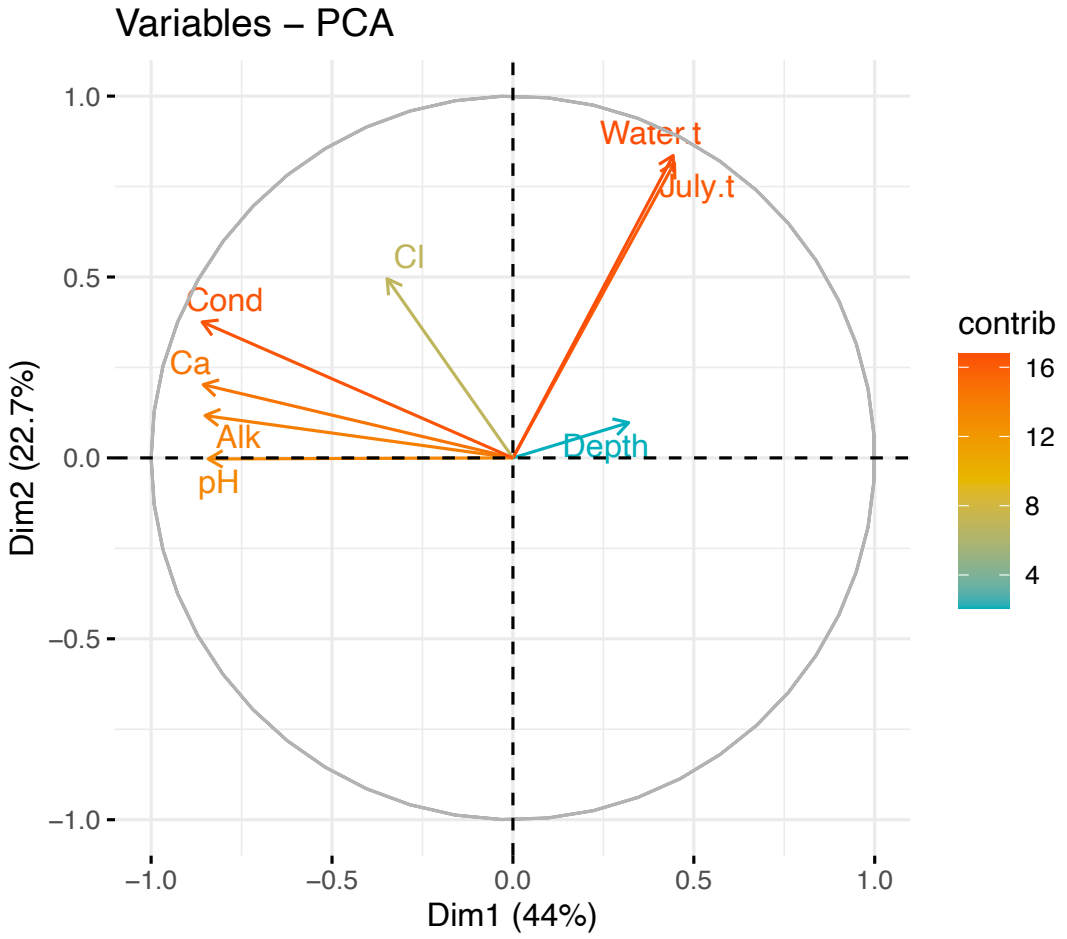

Figure 45. Principle component analysis highlighting the drivers of chironomid distributions: Water temperatures, July air temperatures and depth (cm) account for 44% of the variance in chironomid distributions (Brooks and Birks, 2000).

5.4.5.1 Other drivers of chironomid assemblages

Whilst temperature is believed to be the main driver of chironomid distributions. Where areas have had rapid shifts in atmospheric temperatures this has been the primary driver in the composition of assemblages. However, during periods of stable climate conditions other variables need to be considered (Pinder, 1995; Zhang et al., 2011). Zhang et al (2011) assessed if temperature was still the main driver of chironomid assemblage compositions during phases of stable mean July summer temperatures which were heavily influenced by anthropogenic activities. They showed that over short time scales the chironomids were primarily controlled by fluctuations in bottom water dissolved oxygen and lake depth [Fig.46]. Where lakes have been rapidly altered by anthropogenic processes, e.g. acid mine discharge, this can also lead to a change in the dominance of chironomid taxa (Lindegaard, 1995).

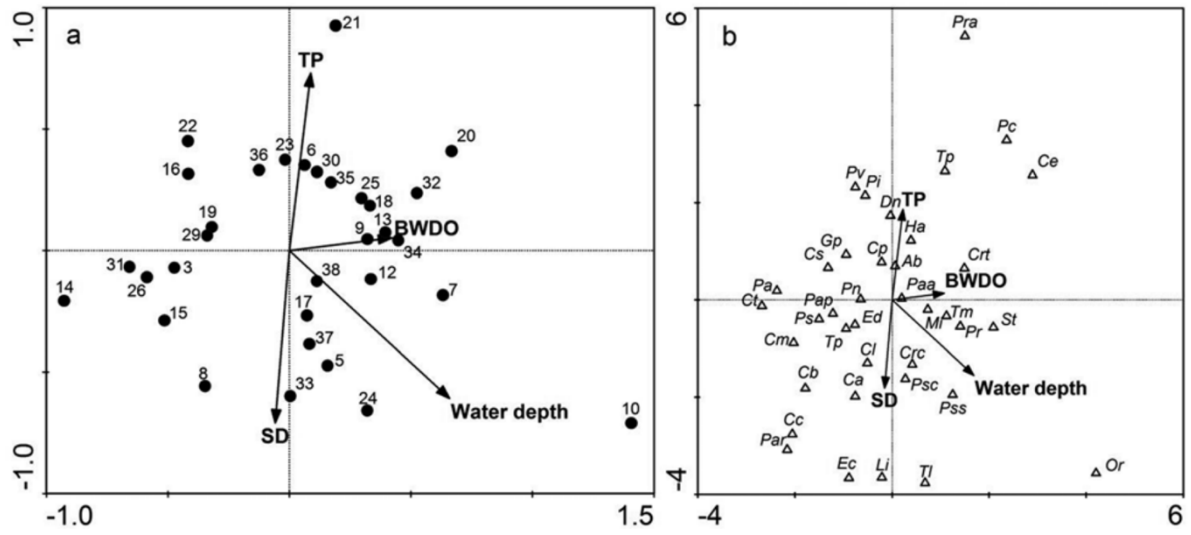

Figure 46. Principle component analysis showing the variance of bottom water dissolved oxygen (BWDO), total phosphorus (TP), water depth and seechi disc depth (SD) with regards to the composition of modern day chironomids (Zhang et al., 2011). The plots show environmental drivers other than temperature which drive chironomid communities.

However, over longer temporal periods Zhang et al (2011) found a strong relationship with atmospheric temperatures being the primary driver. Other studies have shown that variables such as pH and nutrient levels also influence the composition of assemblages (Velle et al., 2005). Whilst, Korhola et al (2000) and Nyman et al (2005) have shown that there may also be a relationship between organic content, substrate composition and lake depth with chironomid compositions. Attempts have been made to use chironomid assemblages as a proxy for total phosphorus concentrations

through time to assess when lakes have been impacted by increased anthropogenic activity (Cao et al., 2014) [Fig.47].

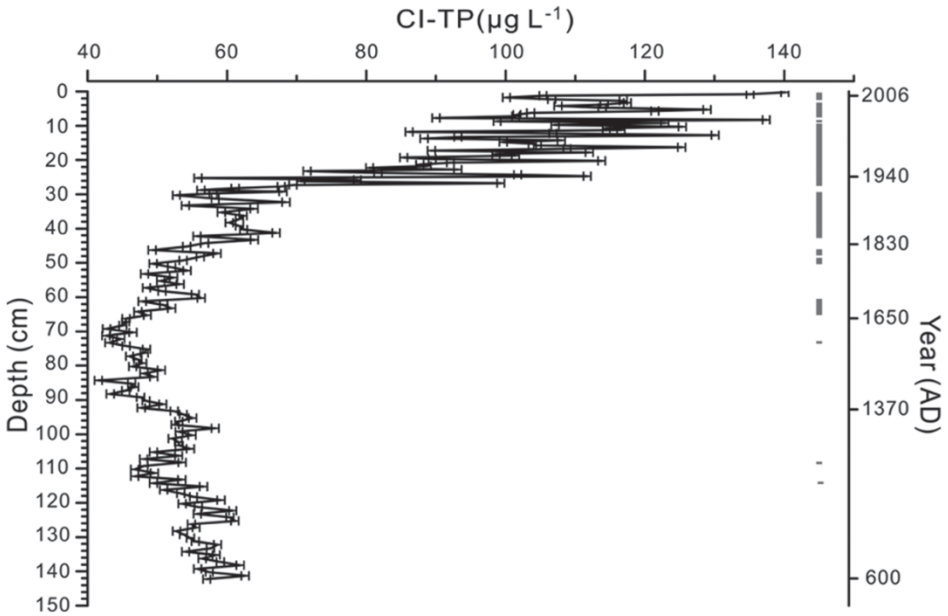

Figure 47. Chironomid inferred total phosphorus concentrations for Taibi Lake (south east China) spanning 1400 years (Cao et al., 2014).

As a result of this co-variance between environmental parameters this presents a problem to which training set or transfer function is used when modelling atmospheric temperatures (Langdon et al., 2008). Langdon et al (2008) promote the use of an Icelandic training set to reconstruct Holocene July temperatures as the environmental conditions in this region are distinctly different to that of Norway. They show that lake nutrient levels and organic content are primarily controlled by minerogenic in-washing and deposition of volcanic ash which in turn influences the composition of the chironomid assemblages.

This research has chosen to use the Norwegian Training set (Brooks and Birks, 2000; Brooks and Birks, 2004) as the latitudinal gradient is similar to the Northern Isles of Scotland, both locations are controlled by the same maritime climate system and both regions are in closer proximity to one another when compared to other training sets e.g. the Swiss-Norwegian (Heiri et al., 2014) or the North American (Porinchu et al,. 2009) (see section 5.4.6). Unlike the Swiss-Norwegian training set which contains marl rich lakes (Heiri et al., 2014), like those found in Orkney and Caithness, the Norwegian dataset does not. This presents a problem for this research as both Orkney and Caithness are dominated by calcium carbonate rich marl during the warmer

phases. However, this is not apparent in the Shetland site and therefore ideally a Scottish training set would have been used. Statistical analysis will be undertaken to highlight the reliability of using the Norwegian training set for this research.

5.4.6 Transfer function

The fossilised chironomid head capsules from each core were compared to a dataset of 142 modern chironomid taxa from N.W Europe using a transfer function (Brooks and Birks, 2000) [Fig.48] (Steve Brooks (NHM, London) taught me the methodology and chironomid identification procedures). Chironomid inferred temperatures (C-IT) were modelled using C2 v1.5.1 (Juggins, 2005) using a minimum of 50 head capsules to reliably reconstruct mean July summer temperatures (Heiri and Lotter, 2001). The chironomids included in this dataset are appropriate to use in this transfer function as the taxa of chironomids are similar to those found in the Northern Isles of Scotland (Heiri et al., 2011; Brooks et al., 2012). However, there are species which are found in each core that are not present in the modern-day training set [Table.3] and as a result will influence the reliability of the temperature inference models (see section 5.5.2 and 5.5.3 on how this is accounted for).

Table 3. Species found in the cores but are not present in the modern-day Norwegian training set

Species present in **Lang Lochs** and **Loch of Sabiston** but not found in the Norwegian training set.	1) Larsia 2) Microspectra ryd 3) Microspectra A 4) Cricotopus intersectus 5) Polypedilum A 6) Paracricotopus 7) Stictochironomous 8) Tanytarsus lactenscens 9) Psectrocladius barb. 10) Stictochironomous B 11) Orthocladius riv. 12) Parametriocladius 13) Cricotopus obnixus
Species present in the **Shebster basin** but not found in the Norwegian training set.	1) Cricotopus intersectus 2) Psectrocladius calcaratus 3) Psectrocladius barb 4) Sympocladius 5) Orthocladius I 6) Chaetocladius B

This Norwegian training set consists of 154 lakes, expanded from an original set of 109 lakes, spanning latitudes of 80˚N to 58˚N and temperature ranges of 3.5-16˚C (Brooks and Birks, 2000) [Table 4.] A swiss training set has also been developed (Heiri et al., 2011) however was not chosen for this study as the latitude of the Scottish sites is more similar to that of Norway and both regions are controlled by a dynamic marine influenced climate system. See below a map showing the location of the C-IT records across N.W Europe [Fig.50]. See the dominant taxa found in the training set [Fig.49].

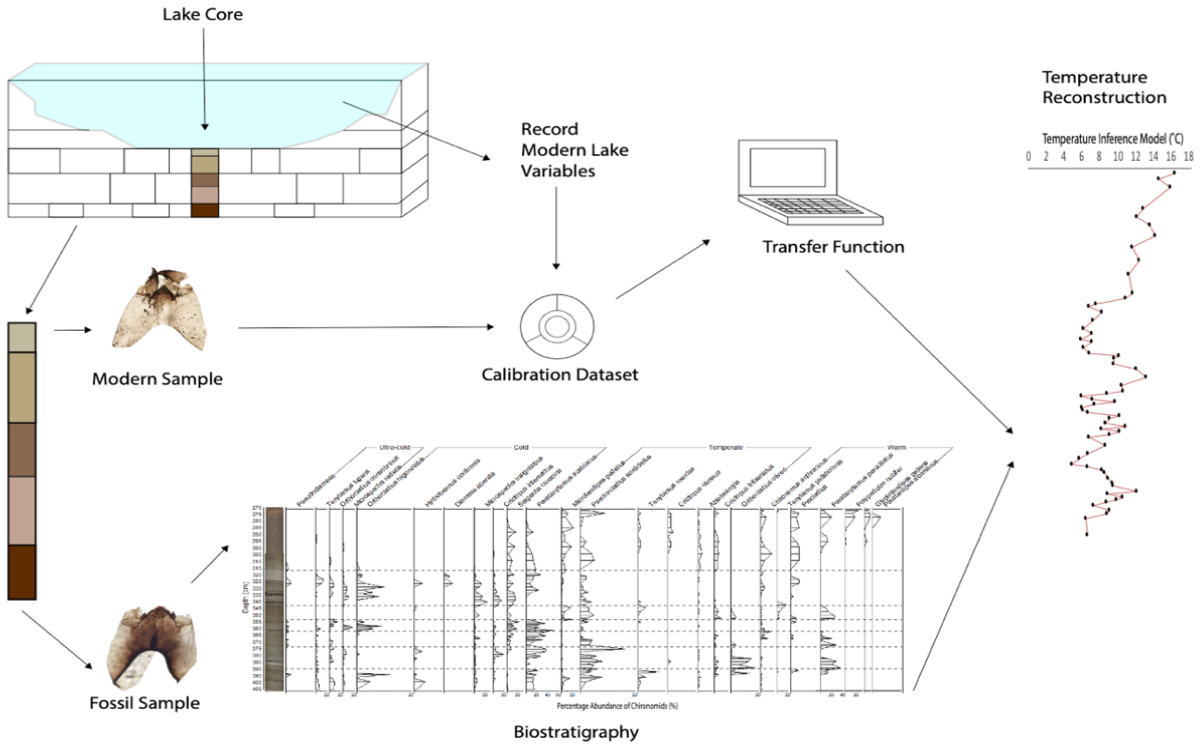

Figure 48. Schematic diagram of the process to extract, process and infer temperature reconstructions using chironomid head capsule assemblages (inspired by Lowe & Walker, 2014)

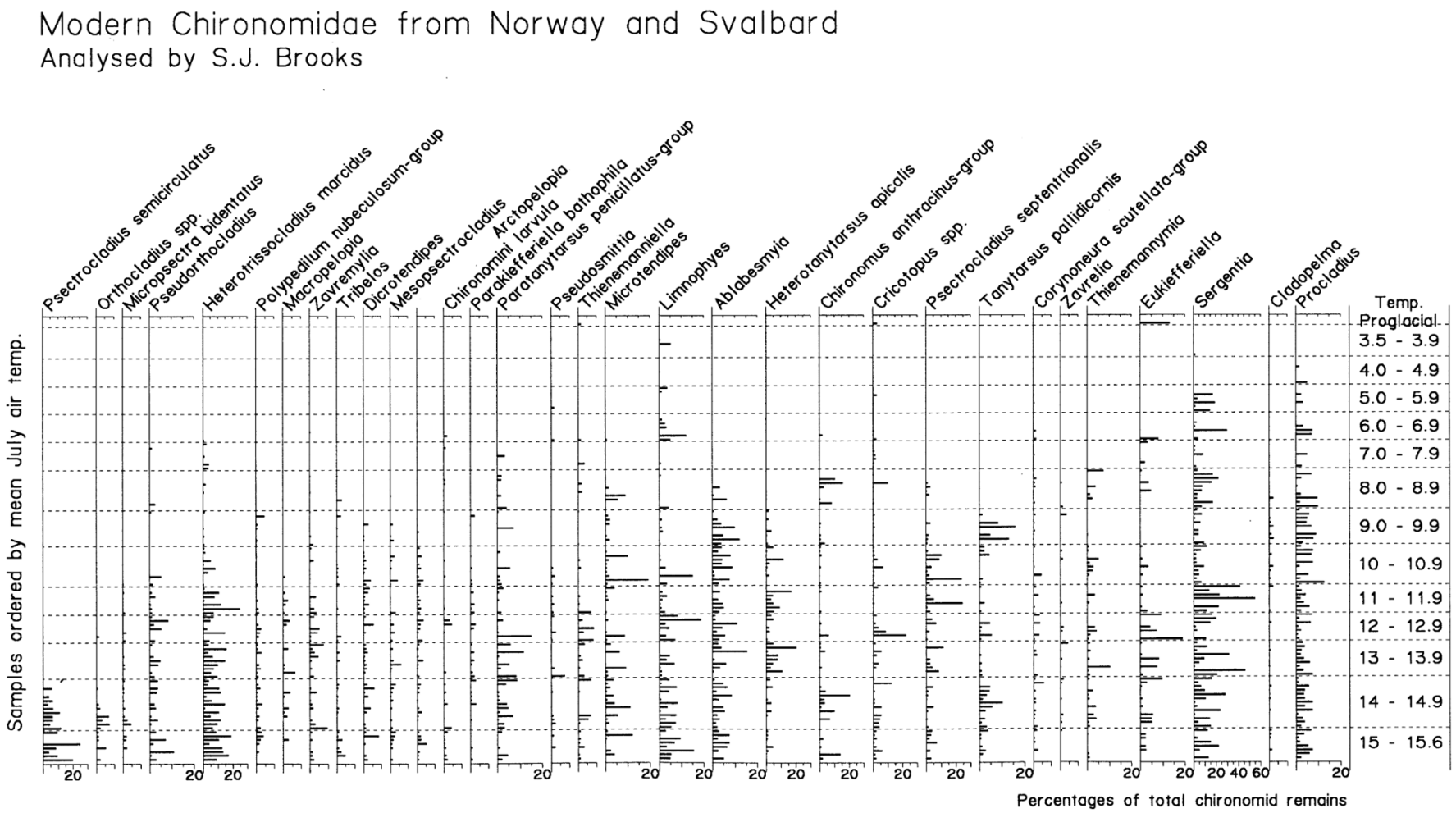

Figure 49. Dominant chironomid taxa found in the Norwegian and Svalbard training set (Brooks and Birks, 2000)

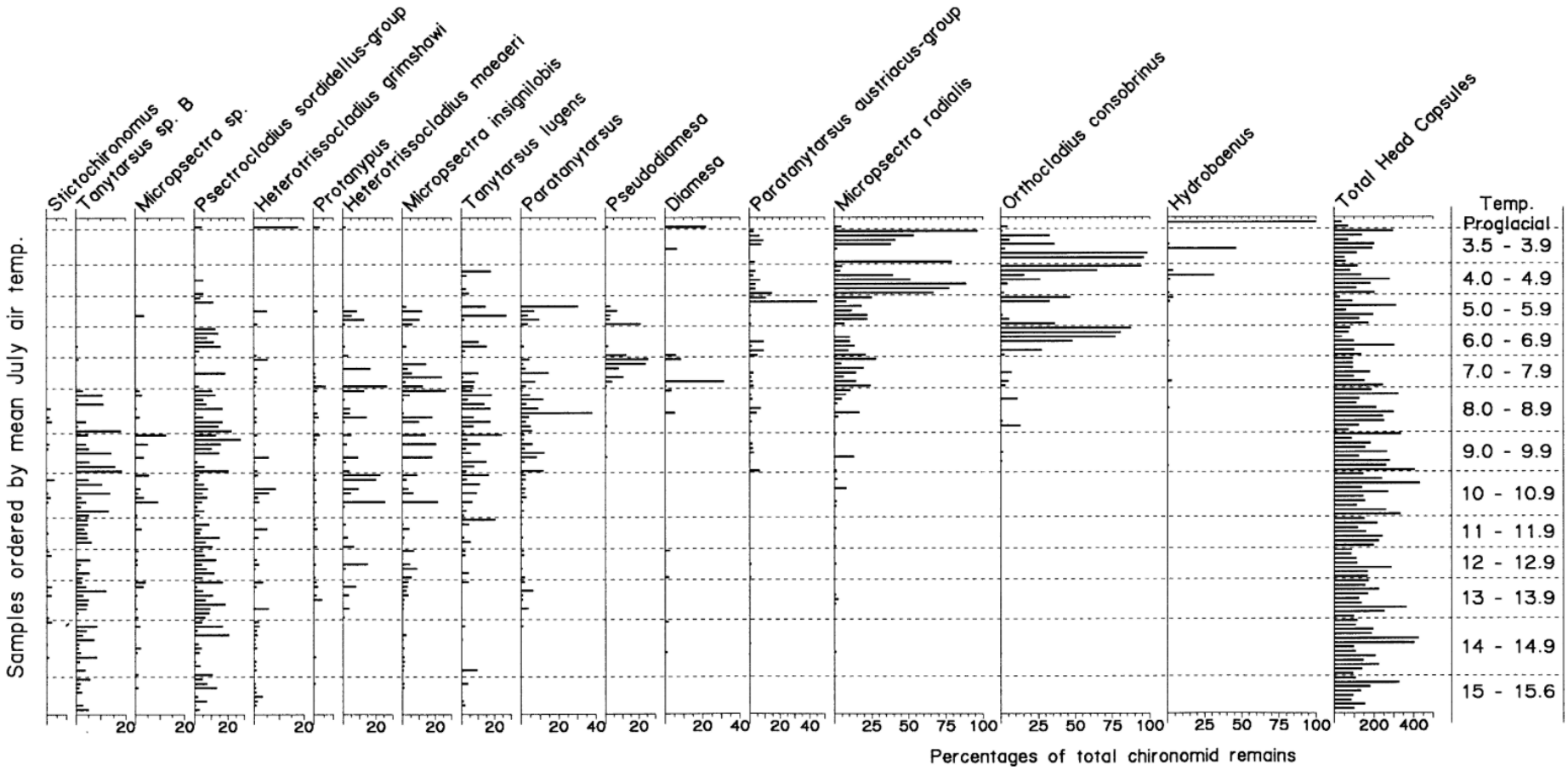

Continuation of figure 49.

Table 4. Coordinates, altitude, July summer temperatures, water depth and vegetation zones for the Swiss and the Norwegian Training sets (Heiri et al., 2011)

	Swiss calibration data-set	Norwegian calibration data-set
No. of lakes sampled	117	157
Latitude (°N)	46.1–47.6	58.1–79.8
Longitude (°E)	5.9–10.3	5.0–31.0
Altitude (m a.s.l.)	418–2815	5–1594
July air temperature (°C)	5.0–18.4	3.5–16.0
Water depth (m)	2.1–85	0.9–29
Vegetation zones	Temperate deciduous to alpine	Temperate deciduous to middle alpine and high arctic

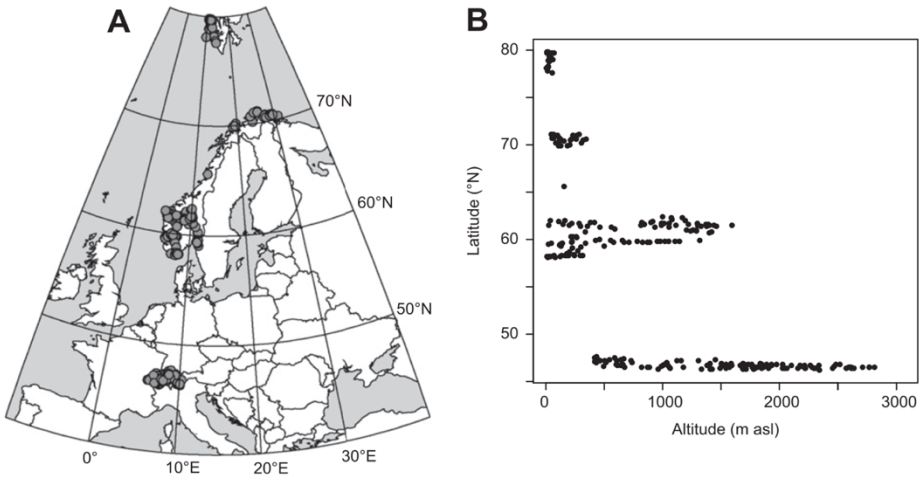

Figure 50. Location (A) and latitude (B) of the Swiss and Norwegian chironomid training set localities (Heiri et al., 2014)

5.5 Chironomid inferred temperatures

5.5.1 Mean July summer temperature modelling:

The mean July summer temperatures for each of the three sites, Caithness, Orkney and Shetland, were modelled following the methodology below. The model outputs are highlighted in table 5 & 6.

1) Upload the chironomid data set for the specific lake in question (e.g. Loch of Sabiston), the Norwegian environmental dataset and the Norwegian chironomid training set (Brooks & Birks, 2000)
2) Analyse data using the transfer function within C2. 1.5.1 (Juggins, 2005).
3) Use an inverse weighted-average partial least square regression (WAPLS) function with leave one out cross validation.
4) Remove lake number 13, 111, 134 and 136 as these have environmental conditions which force chironomid distributions other than temperature.
5) Transform the data to square root
6) Use July temperature (JulyT) as your reconstruction
7) Use the 2-component model as your temperature reconstruction (WAPLS_C2X).

5.5.2 Calculating sample specific temperature errors (SSE):

The sample specific temperature errors were modelled for each of the chironomid samples for each of the cores using the following steps within C2. 1.5.1 in order to calculate the uncertainty in the temperature models for each sample. The following methods were used to calculate the sample specific errors:

1) Use a weighted average partial least squares function
2) Remove lakes 13, 111, 134 and 136
3) Transform the data set to square root
4) Use July temperature (July T)
5) Use the 2-component model as your sample specific temperature error (WAPLS_C2X)

5.5.3 Modelling the reliability of each temperature reconstruction

The reliability of the mean July summer temperature records was tested using a good modern analogue technique (MAT), a goodness to fit to temperature function and by

calculating the number of rare chironomids in the core. The following methods were used to assess the reliability of the mean July summer temperatures:

1) Use the good modern analogue technique (MAT) function
2) Remove lakes 13, 111, 134 and 136
3) No transformation of the data
4) Use a squared chord distance dissimilarity co-efficient
5) Extract the relevant data from the output: Squared chord distance (MAT) and the squared residual distance (Goodness of fit to temperature)

5.5.4 Statistical Evaluations

Samples exceeding a squared chord distance dissimilarity co-efficient of 65% were deemed as having no good analogues, following Velle et al (2005). This was used as an indicator for which samples were dissimilar to the modern day chironomid assemblages from the Norwegian training set. Rare chironomid taxa with a Hills N2 value ≤ 5 indicate a rare species exceeding 5% of the overall assemblage (Birks et al., 1990). These parameters were set in order to enhance the robustness and statistical significance of the temperature inference models. The Goodness of fit to temperature was determined, following Brooks et al., 2016, by passively positioning the fossilised species, against present-day July summer temperatures (˚C) by principle component analysis (PCA) on the modern training set [Fig.45]. Samples with a squared residual distance within the top 10% are highlighted as having a poor fit to temperature. See below a summary of the number of fossil taxa identified, the number of taxa not found in the modern-day training set that were in the fossil records and the sample specific temperature ranges [Table.5]

Table 5. Number of fossils in each core (Lang Lochs, Loch of Sabiston and the Shebster basin), number of taxa not found in the training set and sample specific temperature errors (˚C)

	No. Fossil Taxa	**No. of fossil taxa not found in training set (N2=0)**	**Sample specific temperature errors (˚C)**
Lang Lochs	59	13	0.35 – 1.10
Loch of Sabiston	56	12	0.50 – 1.11
Shebster basin	47	6	0.51 – 1.11

Table 6. Model specifications for chironomid inferred temperature reconstructions for this research

Model Specifications: Lang Lochs C-IT (Norway)
Model name : Lang Lochs Temperatures (15-07-20)
Model type : Weighted Averaging Partial Least Squares
Species data : Norway_TS_spp
Environmental data : NorENV
Environmental variable : July t
Total number of samples : 157
Number of samples in model : 153
Total number of variables : 141
Number of variables in model: 140
Fossil data : Lang Lochs Species (15-07-20)
Total number of samples : 65
Total number of variables : 59
Number of variables in model: 45
Results for model: Loch of Sabiston C-IT (Norway)
Model name : Loch of Sabiston C-IT (Norway)
Model type : Weighted Averaging Partial Least Squares
Date : 30 July, 2019: 12:02:23
Species data : Norway_TS_spp
Environmental data : NorENV
Environmental variable : July t
Total number of samples : 157
Number of samples in model : 153
Total number of variables : 141
Number of variables in model: 140
Fossil data : Loch of Sabiston Species
Total number of samples : 103
Total number of variables : 56
Number of variables in model: 42
Results for model: Shebster C-IT (Norway)
Model name : Shebster C-IT (Norway)
Model type : Weighted Averaging Partial Least Squares
Species data : Norway_TS_spp
Environmental data : NorENV
Environmental variable : July t
Total number of samples : 157
Number of samples in model : 153
Total number of variables : 141
Number of variables in model: 140
Fossil data : Shebster Species
Total number of samples : 93
Total number of variables : 47
Number of variables in model: 41

5.6 **Algal lipid biomarkers**

Long-chain alkenones were extracted and analysed following the BECS, University of Glasgow Laboratory protocol guide. The practises and methods used have been adapted Toney et al., 2010, D'Andrea et al., 2016 and Longo et al (2018).

5.6.1 **Preparation**

Sediments were sub-sampled at a resolution of 1-2cm over stratigraphical boundaries and 4cm throughout homogenous sediments. A pilot run of 4 samples was undertaken to assess which core (Shebster basin or Lang Lochs) had Long-chain Alkenones present. Samples were chosen from organic and inorganic sediments to assess the varying concentration of algal lipids. Based on the initial pilot study it was highlighted that the Shebster basin was the only core suitable for further analysis as the Lang Lochs core from Shetland did not have any LCA present in the sediments. Subsequently, 50 samples were taken, and later freeze dried for 2-3 days at -50˚C, at a pressure of 0.006 bar. All the glassware used in the process was combusted at 450˚C for 8 hours to remove any organic contaminants.

5.6.2 **Extraction**

Total Lipid Extraction (TLE) was undertaken following the methods highlighted in Toney et al., 2010, D'Andrea et al., 2016 and Longo et al (2018). Firstly, an accelerated solvent extractor (ASE350) was used to extract the TLE following the ASE350 procedure guide. Samples were homogenized using a mortar and pestle to ensure the sample was extracted in full when passed through the ASE. The TLE was subsequently evaporated in 40ml iChem vials until dried using a Turbovap, with Nitrogen (N_2) to remove any left-over solvents. The TLE residue was transferred in to pre-weighed 8ml vials using dichloromethane and dried once again under N_2. The samples were weighed to determine the mass of TLE. This stage is vital to allow temperature inference calculations to be made at the analysis stage.

5.6.3 **Silica gel separation**

5.6.3.1 **Neutral Fractions**

The neutral fractions contain the algal biomarkers that are subsequently analysed for long chain alkenones (LCA). Glass pipettes were filled with 4cm of dry LC-NH_2 silica

gel. Quartz wool was placed at the stem of the pipette to prevent the silica gel from escaping. A small amount of combusted sand was then put on top to prevent the upmost layer of silica gel drying. The pipettes were cleaned with Dichloromethane (DCM) (x3) and the samples were then transferred into the columns. The Total Neutral Fraction (TNF) was extracted with 4ml of 1:1 DCM:ISO(Isopropanol) and collected into vials (8ml) [Fig.51].

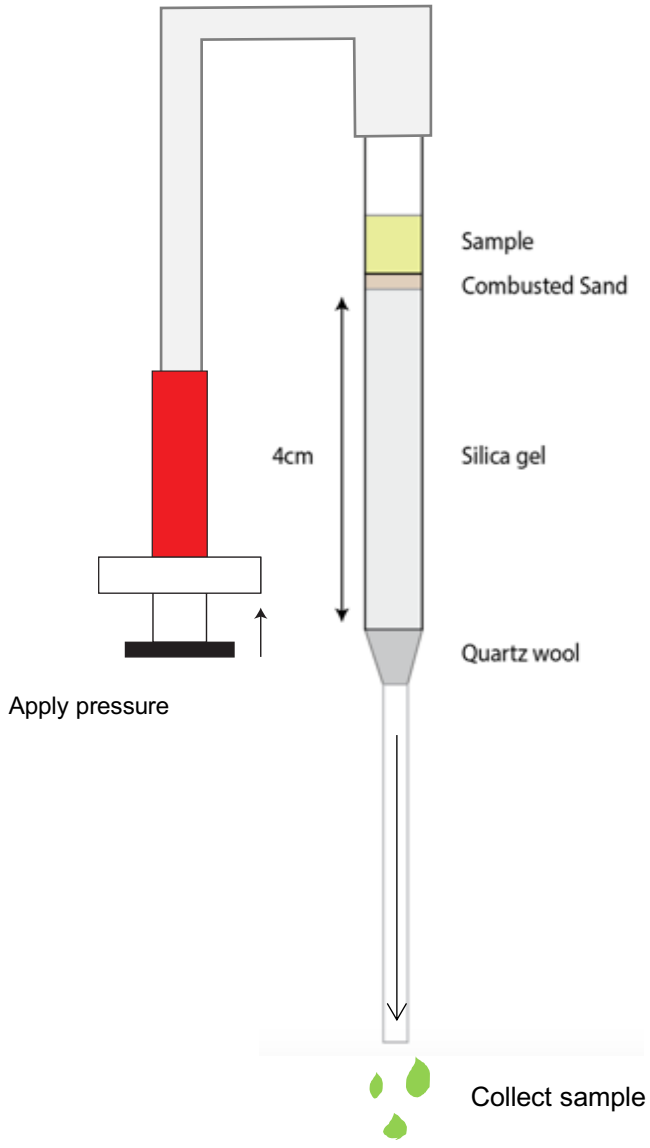

Figure 51. Diagram of the silica gel separation method

5.6.3.2 **Acid Fractions**

The acid fractions contain fatty acids which contain leaf waxes (another proxy used to infer precipitation values (Toney pers comm). The process to remove the acid fractions is similar. Glass pipettes were filled with 4cm of dry LC-NH_2 silica gel. Quartz wool was placed at the stem of the pipette to prevent the silica gel from escaping. A small amount of combusted sand was then put on top to prevent the upmost layer of silica gel from drying. The pipettes were cleaned with DCM (x3) and the samples was then transferred into the columns. The Total Acid Fraction (TAF) was extracted with 4ml of ether (with 4% acetic acid). The samples were subsequently collected into 8ml vials. The TAF fraction was archived for analysis at a later date. The lipids in this fraction were not suitable for analysis at this stage due to time constraints and lack of appropriate instrumentation.

5.6.3.3 **Derivatization**

The TAF is methylated to allow for the samples to be run on the gas chromatographer. The samples undergo Fischer esterification and were dried in an 8ml vial.

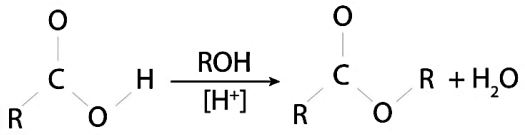

100µl of MeOH was combined with 12% BF_3 and transferred into the 8ml sample vials. The vials were sealed with Teflon-lined screw caps and dried for 1 hour at 70˚C. The samples were taken out and allowed to cool naturally. Further clean-up is necessary to derivatise the TAF. The columns were cleaned with hexane. The TAF was loaded into the columns using hexane (x3). The samples were eluted with 4ml of hexane, collected in 8ml vials and further eluted with 4ml of DCM. The samples were further blown down, transferred into GC-vials and dried under N_2. The samples were labelled and stored in cryoboxes until required for analysis.

5.6.3.4 **Separation of the TNF**

35-70 µm silica powder was used for the TNF separation stage (instead of the LC-NH_2 used previously). Columns were assembled again for this part of the process with 4cm of silica gel, combusted sand and quartz wool. The TNF was added to the columns

and eluted with four solvents (Hexane, DCM, Ethyl acetate: hexane (25:75) and methanol) to remove the organic content of the TNF [Table.7]. The solvents were dried under N_2 for the 4 fractions. The aliphatic and aromatic fractions were transferred into GC-vials using DCM and were ready for analysis in the gas chromatographer flame ionizer (GC-FID)

Table 7. Solvents, volumes and TNF fractions

Fraction	Solvent	Volume (ml)	Organic Content
N1	Hexane	4	Aliphatic
N2	Dichloromethane	4	Aromatics
N3	Ethyl-acetate: hexane	4	Alcohols
N4	Methanol	4	Polar

5.6.3.5. **Procedures for BSTFA Derivatisation**

The N3 & N4 fractions went under further derivatisation with BIS (trimethylsilyl) trifluoroacetamide (BSFTA) in order to analyse on the GC-FID. The samples were dried under N_2. The samples were combined with 15µL of BSFTA and 20µL of pyridine. The vials were subsequently heated at 80˚C for 2 hours in order to complete the chemical reaction. The vials were naturally cooled and transferred into GC-vials with DCM.

5.6.3.6. **Gas Chromatography: GC-FID and GC-MS**

Standards were set and the appropriate concentrations were determined in a pilot run before the samples were ran on the GC-FID and GC-MS. Only the N2 fractions, which contained the Long-chain Alkenones, were analysed on the instruments. At a later date it would be possible to analyse the other fractions for additional climate and environmental proxies. The $C_{37:2}$alkenone ,$C_{37:3}$alkenone and $C_{37:4}$alkenone correspond to freshwater Group I Haptophytes. Whilst, the $C_{38:2}$alkenone ,$C_{38:3}$alkenone and $C_{38:4}$alkenone correspond to brackish Group II Haptophytes (Longo et al., 2018) [Fig.52].

Once analysed on the GC-FID Alkenone peaks were integrated, calculating the area under each curve, to determine the concentration of each type of alkenone in the

samples. The samples were analysed on the GC-MS to make sure each integrated peak corresponded to the correct alkenone. In order to quantify the alkenones relationship with temperature the U^{k}_{37} index was calculated, using the area under each peak. Once the peak areas of each alkenone (C37:4, C37:3 and C37:2) have been integrated onto the Gas Chromatographer - Flame Ionising Diffractor (GC-FID) the index can be calculated by using the equation above (D'Andrea et al., 2016). One must manually integrate the peaks and record each peak area.

To assess if the peaks correspond to the correct alkenone analysis on a Gas Chromatographer Mass Spectrometer (GS-MS) is required (Toney et al., 2010). Each peak corresponds to a known mass of molecules present in each alkenone. By determining the mass of each compound, it is possible to determine what its composition is and subsequently identify the specific alkenone (Toney et al., 2010).

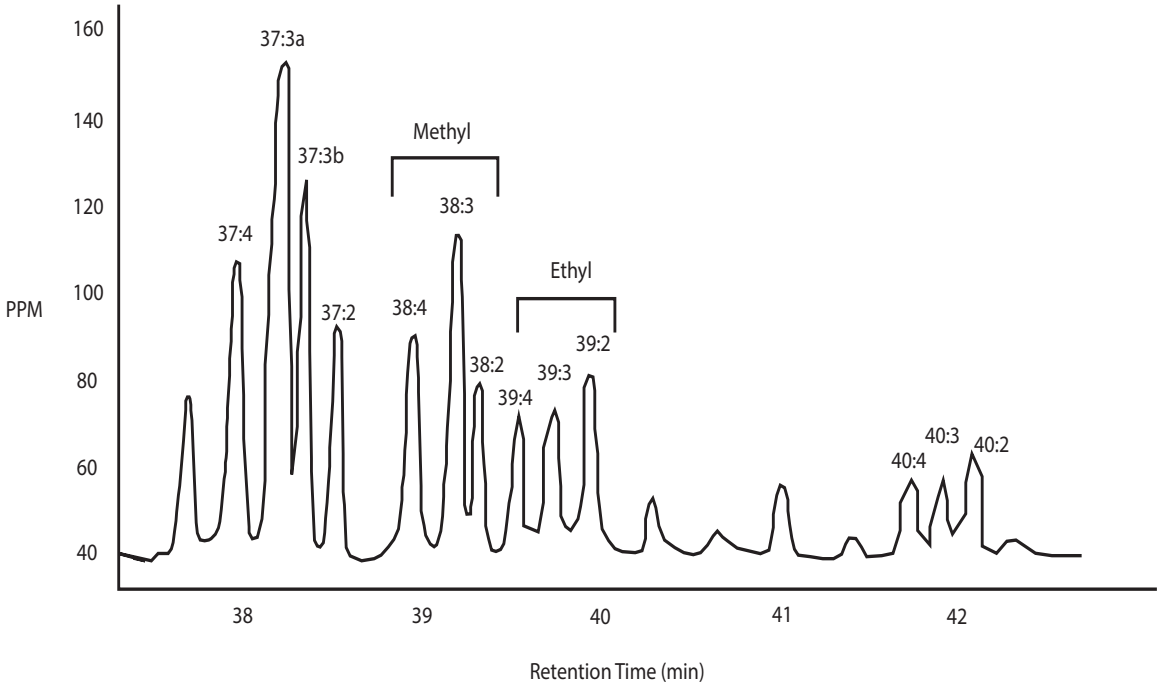

Figure 52. An example of an interstadial sample on the gas chromatographer (GC-FID)

5.6.4 Long-chain Alkenones: An overview of their application and the methods used in this research

Algal biomarkers, in particular long chain alkenones, are another climate proxy used for reconstructing environmental change. Haptophyte algae, produced in aquatic environments, contain lipids within their cells and these lipids can be separated into Long-chain Alkenones (LCAs) which contain carbon-based molecules ranging from C_{36} to C_{39} (Toney et al., 2010). The degree of unsaturation of these molecules in marine sediments has been shown to be a function of water temperature (Toney et al., 2010). Previously, studies have been focused on the use of LCAs on sea surface temperature reconstructions (Brassell et al., 1986). *Emiliani hueyii and Gephyrocapsa oceanica* are the main LCA producing Haptophyte algae within the marine environment and they are well preserved in marine sediments (Volkman et al., 1980; Prahl et al., 1987; Prahl et al., 1988). Using the $U\frac{K\prime}{37}$ index and the ratio of C_{37} Alkenones in each sample, a linear relationship can be seen with SSTs and therefore temperature inferences can be made (de Bar et al., (2017)) using the relationship below.

$$U_{37}^{K\prime} = \frac{[C_{37:2}\text{alkenone}]}{[C_{37:2}\text{alkenone}] + [C_{37:3}\text{alkenone}]}$$

Prahl et al (1987) accurately predicted the linear relationship between the unsaturation of alkenone concentrations with sea surface temperatures by culturing algae in the lab. They pioneered the first linear calibration shown below:

$$U_{37}^{K\prime} = 0.033T + 0.043$$

Subsequently, a worldwide calibration has been developed using 370 surface samples across the world's oceans spanning 60˚N and 60˚S (Müller et al., 1998). However, this calibration was not statistically different from the function developed by Prahl et al (1987) which allowed for the original calibration to be used. As a result of this study the use of alkenones for palaeothermometry reconstructions has expanded. One such study reconstructed three high resolution records of temperature change for the South China Sea spanning the Holocene period (Wu et al., 2017) [Fig.53]

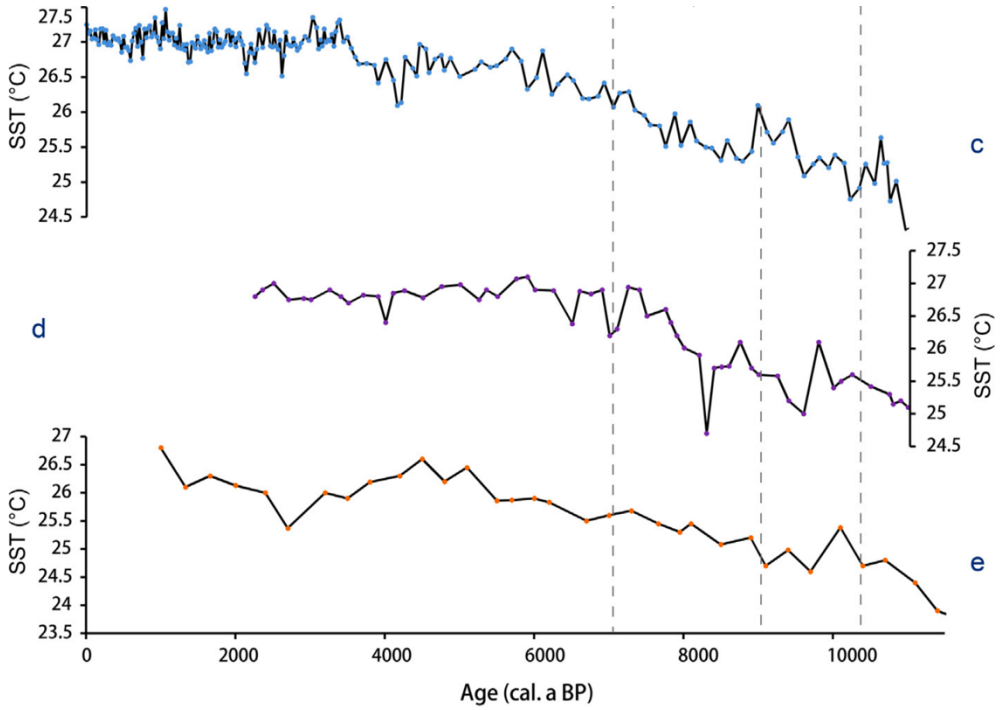

Figure 53. Three alkenone inferred sea surface temperature records from marine sediments in the South China Sea (Wu et al., 2017)

Until recently, LCAs have been infrequently used for lacustrine palaeoclimate reconstructions as the abundance of LCAs were believed to be small in lake sediments (Coolen et al, 2004). However, studies have shown that this may not be the case as LCAs have been shown to be present in various lakes from around the world (Cranwell, 1985; Zink et al., 2001; Chu et al., 2005; Pearson et al., 2008). Progress has been made allowing temperature inferences to be modelled in lacustrine environments (Toney et al., 2010; D'Andrea et al., 2016; Longo et al., 2018). However, it appears a global temperature calibration for lakes is not possible as each system has different water chemistries, which have been shown to impact the distribution of the lipid producing freshwater haptophytes (Longo et al., 2018). Only local calibrations have been shown to statistically reflect palaeotemperatures in lakes using the U_{37}^{K} index. Calibrations have been developed around the globe: from Alaska (Longo et al., 2018), Germany (D'Andrea et al., 2006), Norway (D'Andrea et al., 2016), Western Greenland (D'Andrea et al.,2011) mainland USA (Toney et al., 2010) and the Canadian Prairies (Plancq et al., 2018). Research has also been undertaken to grow

algal cultures in the lab in order to determine a global lake calibration (Nakamura et al, 2014; Toney et al 2010, 2011; 2012).

Once each of the sediment samples have been processed and analysed on a GC-MS and GC-FID the peak area under each of the alkenone chromatograms can be calculated. The area under the peak profiles, for each of the 3 types of C_{37}Alkenones, can be inserted into the equation below to reconstruct the U_{37}^{K} index for each sample in each lake core.

$$U_{37}^{K} = \frac{[C_{37:2}\text{alkenone}] - [C_{37:4}\text{alkenone}]}{[C_{37:2}\text{alkenone}] + [C_{37:3}\text{alkenone}] + [C_{37:4}\text{alkenone}]}$$

The U_{37}^{K} index has been shown to have a linear relationship with spring lake temperatures in Alaskan and Norwegian lakes (Lake Vikvatnet) (D'Andrea et al., 2016, Longo et al., 2016). Site specific spring lake temperature calibrations can be formed by recording modern day temperatures from present day water bodies and comparing them to the index value (Toney et al., 2010; Longo et al., 2016). Once the modern-day temperatures, and the present in situ U_{37}^{K} index, have been calculated then a relationship can be developed. An example of one such calibration is from D'Andrea et al (2016) who recorded the $U_{37}^{K}\,\text{index}$ for Lake Vikvatnet in Norway and compared it to present day lake temperatures. A linear relationship was shown to exist between the index and temperature (R^2=0.94, n=10, p<.0001) [Fig.54]. Palaeotemperatures can be inferred by inserting the calculated U_{37}^{K} value for each sample depth in the equation below.

These studies underpin the research done in this project and the same linear relationship with spring lake temperatures is assumed to be the same in the Shebster basin as the region is located in a similar latitude to the Norwegian site from D'Andrea et al (2016) and has a combination of Group I and Group II Haptophyte algae found in the Alaskan site (Longo et al., 2018). Therefore, the Shebster basin is regarded as being a similar analogue to the studied sites highlighted above. Although an independent lake calibration would have been preferred (see section 5.6.4.1).

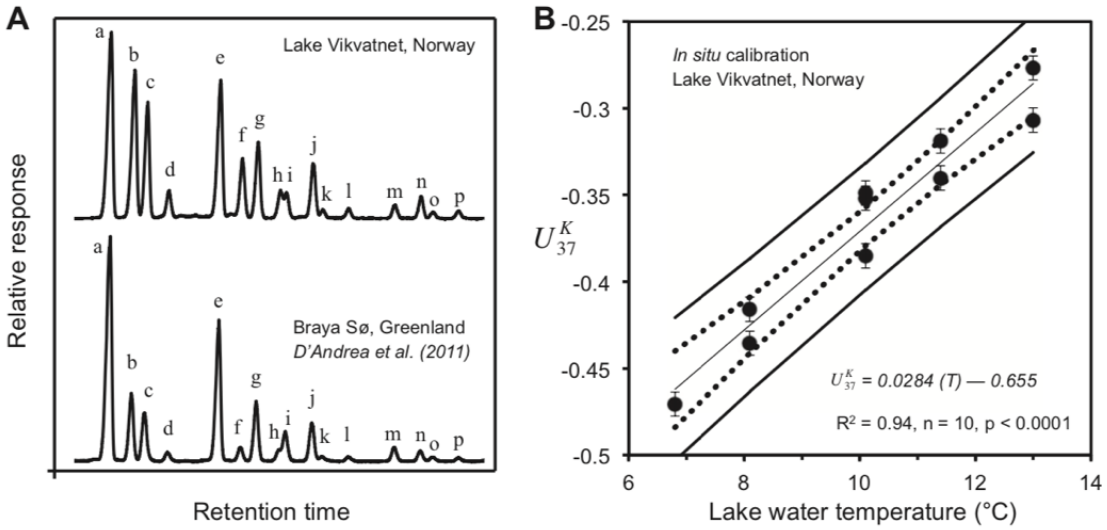

Figure 54. A) shows the peaks of the alkenones for Lake Vikvatnet in Norway (D'Andrea et al., 2016) and Braya Sø in Greenland (D'Andrea et al., 2011). (B) Shows the linear relationship between temperature (°C) and the UK37 index for Lake Vikvatnet

5.6.4.1 **Uncertainties and methodological challenges**

Ideally, an independent lake calibration would have been used for this project. However, in order to do this present-day lake temperatures were needed and as the lake is currently dried, and is now a blanket peat bog, this was not possible. A spatial analogue, from a nearby lake that represented the conditions of the Shebster basin could have been chosen, however there was no guarantee that the conditions in that water body would have the same modern day and paleo-environmental conditions found in the Shebster basin. Therefore, this presented a problem and limits the reconstruction of lake temperatures to bodies of water which are still active lakes today.

Furthermore, the chemical composition of the sediments, and in turn the water column, of the Shebster basin palaeo-lake led to a mixture of both the Group I and Group II alkenone forming haptophytes. Sites with varying pH and salinities have been shown to support a different and more complex community of freshwater haptophyte algae and as a result this required another index to be used in conjunction with the U^K_{37} *index*. (Longo et al.,2016; Longo et al., 2018). The R3b index was chosen to be used to quantify the mean spring lake temperatures for the samples that were known to have a mix of group I and group II haptophytes (Longo et al., 2016). They showed that this index below reliably reconstructed spring lake temperatures for an Alaskan lake where both groups of haptophytes were present.

$$\mathrm{R3b} = \frac{[\mathrm{C_{37:3b}}]}{[\mathrm{C_{38:3b}alkenone}] + [\mathrm{C_{37:3b}}]}$$

The $R3b$ index was converted into lake temperatures following the Alaskan Group I and Group II spring lake water temperature calibration from Longo et al (2018) shown below:

$$\mathrm{R3b} = 0.0081\ (\mathrm{T}) + 0.44$$

Initial studies have thought that freshwater lakes only had Group I haptophytes present in the lake which led to studies only using the $\mathrm{U}^{\mathrm{K}}_{37}$ index and lake specific calibrations. This has been shown to be an oversimplification as Longo et al (2018) has shown that lakes with varying pH and salinities can have a mix of haptophyte groups and therefore requires caution when any lake is analysed as species effects have been shown to be a factor which can compromise the reliability of temperature inferences when using LCA. Uniform pH and salinity values through time cannot be assumed (Longo et al., 2018) and therefore other methods of determining pH/salinity should be used to aid any temperature inferences, such as micro-XRF geochemistry and micropaleontological. Group I Haptophytes are known to inhabit freshwater systems whilst Group II Haptophytes inhabit brackish environments (Longo et al., 2018). Where this is the case the *R3b index* is used to account for the input of Group II Haptophytes (Longo et al., 2018). The figure below shows the clear distinction, in the peak profiles, for both of the algal Haptophytes [Fig.56]. Although temperature is regarded as being the main driver of alkenone saturation in sediments other drivers are thought to influence the distribution of the alkenone producing haptophytes, such as nutrient loading and trace element availability (Thiel et al., 1997), indicating that long-chain alkenones are not single variable temperature proxies. Toney et al (2010) also attributed lake stratification to altering the distribution and abundance of LCA in lake ecosystems. Plancq et al (2017) hypothesised that summer lake temperatures were the main driver for LCA distributions however found that salinity explained the majority of the variance for their site [Fig.55].

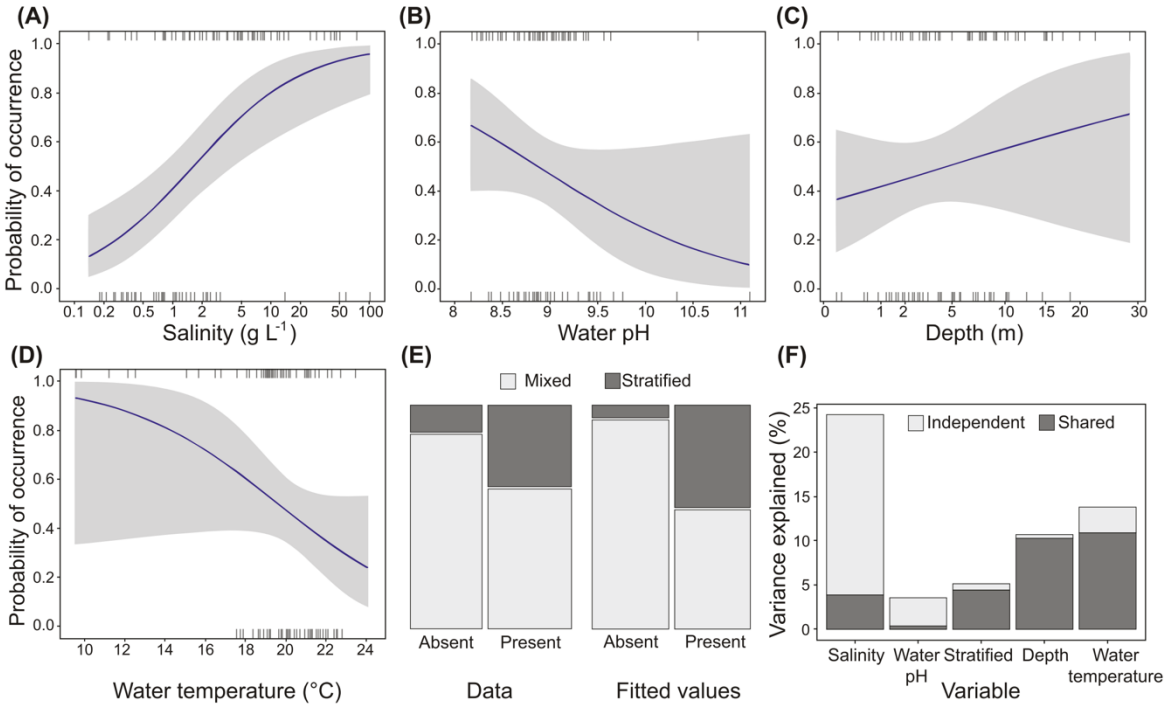

Figure 55. Statistical models highlighting the probability of occurrence of alkenones in lakes with (A) salinity, (B) water pH (C), depth (m), (D) water temperature (˚C), (E) lake stratification and (F) the percent variance explained (Plancq et al., 2017).

Plancq et al (2017) and Toney et al (2010) also record a surprising lack of LCAs recorded in regions where they have already been found to be present. Highlighting, why another lake in the Caithness region was not chosen as an analogue for the area and to why other calibrations were used for this project. Toney et al (2010) also records an unknown compound found in Canadian lakes that coelutes with the alkenones on the GC-FID, which if thought to be an LCA, would infer unreliable temperature inferences. Therefore, highlighting the need to use a GC-MS to accurately identify the chemical composition of the samples being identified and not assuming the identification of alkenones based on their chromatographic profile.

At present the exact species of the haptophyte algae which produces the alkenones is unknown, which makes inferences of seasonality difficult to reliably assess. Plancq et al (2017) suggests that this species does not grow in the summer months as there is no statistically significant relationship between the U_{37}^{K} *index* and summer lake temperatures for their site (Canadian Prairies). As a result, they infer that the spring is the likely time that which this species blooms. The exact month at which this algae bloom is important to know as this is the month at which modern-day lake sampling and temperature readings will be taken. By doing this a much more reliable

lake calibration and temperature inference model will be made. Furthermore, their study highlights that only 55% of all the studied lakes had alkenones present in the sediments. This was a challenge for this research as Lang Lochs (Shetland) was also chosen for this research however after initial pilot studies it was determined that no alkenones were found in the lake. It is not known if they are present until the samples are fully processed and analysed which is time consuming.

Furthermore, due to the nature of LCA analysis, studies can be limited by resources, technology and by time. Processing vast quantities of samples can be costly and requires specific and expensive equipment, unlike chironomid methodologies which are relatively inexpensive, this does limit the use of this proxy. This can result in lower resolution records of palaeoclimate change, e.g. only one site in this research could be analysed for alkenones opposed to the three sites analysed for chironomids.

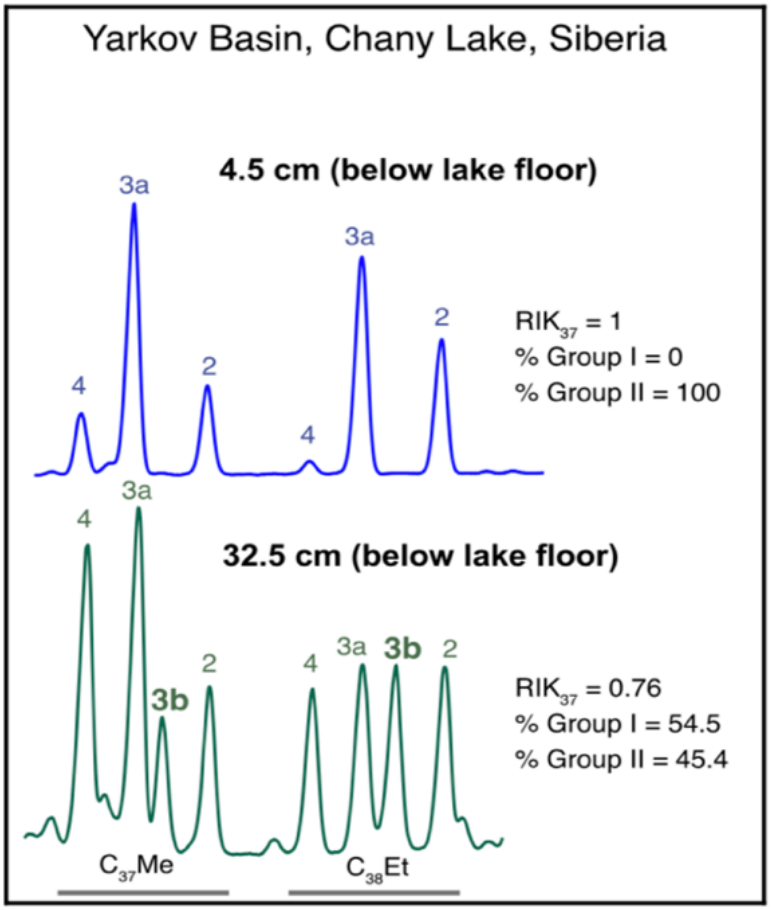

Figure 56. Alkenone profiles for the Group I and Group II haptophytes from Chany Lake, Siberia (Longo et al., 2018)

5.7 Tephrochronology

5.7.1 Preparation and extraction

Sub samples were taken throughout each of the three cores in areas that were thought to have high concentrations of ash shards. The extraction of the tephra shards was undertaken at Royal Holloway, University of London by Dr Rhys Timms.

The extraction phase followed the works highlighted by Pilcher & Hall (1992) and Turney (1997). The sub-samples were burned in the furnace at 550˚C, in crucibles, to remove any organic matter from the sediment and later heated at 110˚C, cooled and weighed (Turney, 1998). The burned samples were then transferred into centrifuge tubes, with HCl to separate the ash from the sediment and dissolve any unwanted inorganics (Turney, 1998). The sediment, combined with the solution, was sieved at 75 & 24µm. The residue which remained was centrifuged (x2) in polytungstate (with a density of 2.50gcm^{-3}) at 2500rpm for approximately 20 minutes (Turney, 1998). The 'float' was subsequently decanted, as the top layer had the highest concentration of cryptotephra shards and was put into distilled water to be centrifuged again at 2500 rpm for 15 minutes (Turney, 1998). This kinetically separated out the heaviest shards from the lightest: gradually concentrating the heaviest at the surface (exceeding 2.50gm^{-3}). Once the tephra shards were concentrated through these centrifuging stages the shards were picked and then mounted onto thin section slides for geochemical analysis.

5.7.2 Tephra geochemical analysis

The geochemical composition of the tephra grains was analysed at the University of Edinburgh under supervision of Dr Hayward and Dr Timms (RH, University of London). Analysis was undertaken using electron probe micro-analysis (EPMA) and 10 major elements, in the form of oxides, were analysed. Once analysed each sample was plotted onto Total Alkali Silica plots (TAS), using the R based software GCDkit 5.0, in order to differentiate each ash layer based on a unique geochemical signature and composition (Vojtěk et al., 2006).

5.8 Radiocarbon dating

The Lang Lochs and Loch of Sabiston core have been sub-sampled to build robust independent age-depth models following the method below. However, for the Shebster basin an independent age-depth model was not possible. Golledge et al (2009) previously dated the Shebster basin however these dates were not useable as they record age-reversals and too old basal ages. Due to the high-resolution record in Loch of Sabiston the age-depth model was transferred to the Shebster basin (section).

5.8.1 Preparation

Each sediment core was pre-screened, and specific sub-samples were chosen to be extracted based on stratigraphical boundaries visible to the eye, changes in chironomid head capsule assemblages and fluctuations in the temperature inference models. 12 sub-samples were taken from Loch of Sabiston and 11 sub-samples from Lang Lochs to build a robust age depth model.

5.8.2 Extraction & Processing

Analysis was undertaken at SUERC, Radiocarbon dating facility. Each core was sub-sampled for terrestrial plant macrofossils/bulk sediments using a dissecting microscope and tweezers. Each sample had a carbon content ranging between 25-30‰ to allow for radiocarbon best-age estimates. Sub-samples were digested in 2M HCl at 80˚C for 4 hours and subsequently washed with deionised water to remove mineral acids and then further digested with 0.5M HCL at 80˚C for 4 hours. The process was repeated until no more humic acid was extracted from the sample. The residue was further rinsed to remove any excess alkalis, digested further with 1M HCL at 80˚C for a reduced time of 2 hours and subsequently rinsed with deionised water, dried and homogenised. The total amount of carbon, compared to the known weight of the sample before treatment, was retrieved in the form of CO_2 by heating the sample with CuO in a vacuum sealed quartz tube. The collected gas was subsequently converted to graphite using Fe/Zn reduction.

5.9 **Age-depth modelling**

The calculated AMS Radiocarbon ages were calibrated using the IntCal 13 Calibration curve (Stuiver et al., 2013). Age-depth modelling was undertaken using OxCal v4.3 (Ramsey et al, 2017). Best age estimates were modelled by P-sequencing, constraining the top to ≤ 2012 AD and the basal boundaries to the bottom of the core, in order to provide realistic age iterations. The age-depth model for the Shebster basin was constrained to Loch of Sabiston using the matched chironomid inferred temperatures from both sites (section 8.3.3). Ages were modelled independently from the Greenland ice core records to assess synchronicity between sites.

5.10 **Geographical Information Systems**

Chironomid inferred temperatures (C-IT) (˚C) for each site were plotted using ArcGIS. A geographical projection of WGS 1986 was used for the base map - with each point plotted at the same projection. Golledge (2010) Loch Lomond Stadial glacial extent shapefile was used and plotted on top of the C-IT (˚C) temperatures. For this map the British National Grid geographical projection was used. Subsequent, temperature Isotherms were modelled for each INTIMATE event throughout the LGIT using Inverse Distance Weighting (IDW).

Chapter 6 - Palaeoclimate and environmental reconstruction of Shetland during the LGIT

6.0 Introduction: Overview of Shetland

The Shetland archipelago has a complex glacial history and as a result many studies have been undertaken to better understand the advance and retreat of ice masses of the island and the surrounding region (Sejrup et al., 2009; Bradwell et al., 2008; Graham et al., 2011; Clark et al., 2012; Becker et al., 2018). Throughout the LGM the landscape was strongly influenced by the interaction of the British Ice Sheet (BIS), the Fennoscandinavian Ice Sheet (FIS) and the Shetland Ice Cap (SIC) (Golledge et al., 2009; Bradwell et al., 2019). Recently, the timing of deglaciation has been reconstructed for the archipelago (Bradwell et al., 2019). However, to date no records of glacial activity have been recorded for the Last Glacial – Interglacial Transition (LGIT) (Ross et al., 1997). Glacial reconstructions for the LGIT have been modelled for N.W Highlands of Scotland using local chironomid inferred temperature records (Ballantyne et al., 2007). With the addition of a C-IT record for Shetland this may be possible in the future.

Records of palaeoenvironmental change have focused on the Holocene period (Bennett et al., 1992; Whittington and Edwards, 1993; Hulme and Shirriffs, 1994; Birnie, 2000). To date, there are limited records spanning the LGIT: two palaeoenvironmental records (Whittington et al., 2003; Kingsbury, 2018), one radiocarbon range finding study (Hall, 1993), two diatom studies (Robinson, 2004; Kingsbury, 2018) and one record of the fire history of Shetland (Edwards et al., 2000). Currently, there are no records of atmospheric temperature change for the Isle of Shetland.

Brooks and Langdon (2014) highlight that the northern regions of the North Atlantic have no chironomid inferred temperature records. They geospatially plotted time slices across N.W Europe, highlighting the major climate transitions across the LGIT. They show that temperature records are needed for the Northern Isles to increase the spatial resolution of the present temperature inferences. The map below shows the lack of temperature inferences in N.W Europe and Scotland [Fig.57]. As a result, this is why Shetland was chosen to infer atmospheric temperature change.

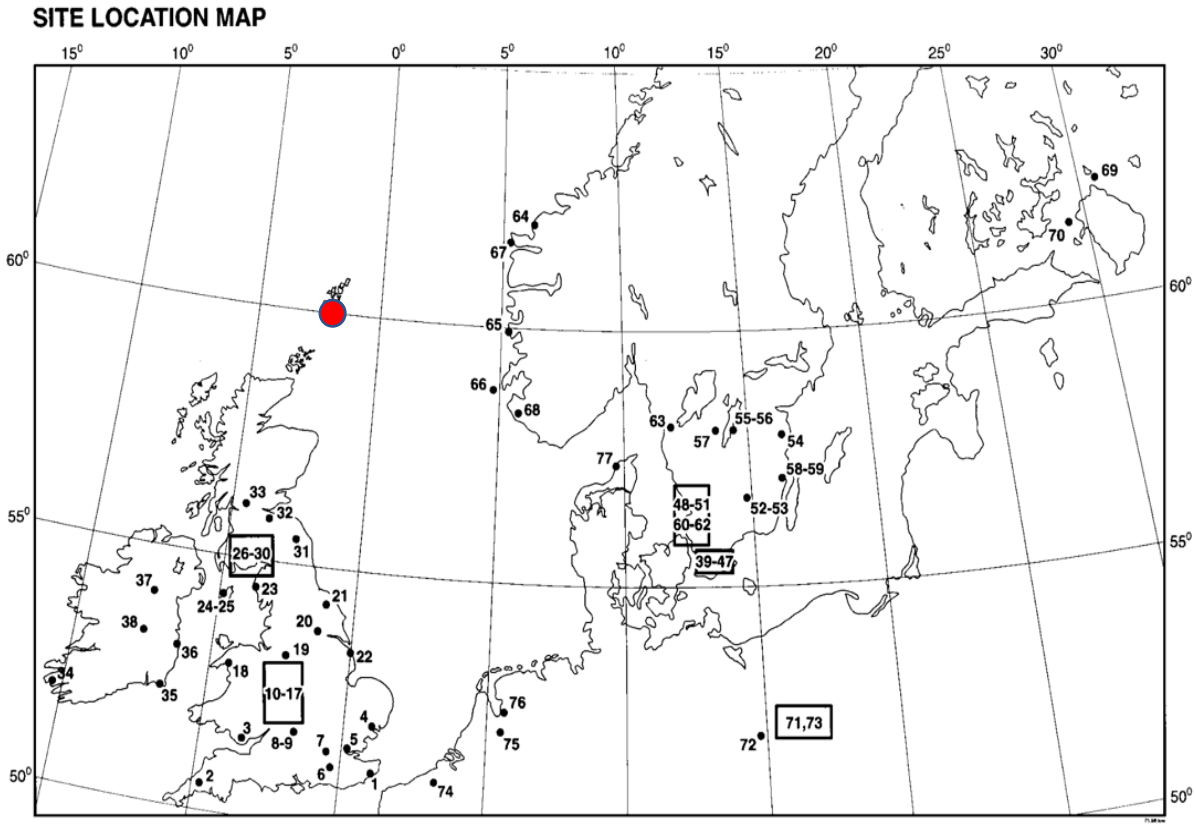

Figure 57. The 76 chironomid and coleoptera inferred temperature records for north-west Europe (Brooks and Langdon., 2014). The position of the Isle of Shetland is shown (red dot).

6.0.1 **Introduction: Lang Lochs mire**

Hulme & Shirriff (1994) previously cored Lang Lochs mire, south of Lerwick, to assess the vegetative history of the catchment. Although a record of the entirety of the LGIT was known to exist, this study was focused on the transition of the LLS and into the Holocene period. Consequently, there are no records of palaeoenvironmental change for this site spanning the end of the LGM and the interstadial, providing another reason as to why this site was chosen. Furthermore, as a continuous sedimentary sequence spanning the LGIT was known to exist this site was a prime location (Hulme & Shirriff, 1994).

This is the first mean July summer temperature record for the Isles of Shetland. A high resolution palaeoclimate history of the LGIT has been reconstructed using chironomid head capsule assemblages. Combined with micro-XRF analysis, a fuller image of the palaeoenvironmental history of the catchment has been made

6.1 Aims & Objectives

This project will aim to reconstruct the palaeoclimate and environmental history of Shetland spanning the Last Glacial-Interglacial Transition (LGIT) using the following objectives:

- Reconstruct mean July summer temperatures using chironomid assemblages for the Lang Lochs basin.
- Use a multiproxy approach to reconstruct the environmental conditions throughout the LGIT in Shetland.
- Compare the data from Lang Lochs to other palaeo-environmental sites in Shetland.

6.2 Site description

6.2.1 Lang Lochs, Shetland

The Lang Lochs field site was chosen for this study as it has a continuous record of sedimentation spanning the end of the LGM to the onset of the Holocene period (Hulme & Shirriff, 1994). An initial walkover survey was done to scope a potential coring location. A gently sloping hill was located to the west of the lake. From the top it was clear that the lake was more extensive in the past with the remnants of a palaeo-lake edge being visible

During the survey old posts were found which pinpointed previous trial cores taken by Hulme & Shirriff (1994). Using a combination of GPS and the position of the marker posts from Hulme & Shirriff (1994) study, five continuous trial cores were taken to assess the basin stratigraphy. In order to maximise continuity between both projects and to identify a site which maximised the record of the LGIT, these trial cores were taken in order to identify where sediment was being focused and where the deepest part of the lake was located. The deepest part of the lake had an extensive Holocene record, however, did not have the longest sedimentary record for the LGIT. Rather, the surface mire/fen edge had the longest record of the LGIT and as a result was chosen as the core site [Fig.39]. A continuous, undisturbed sedimentary record was retrieved [Fig.40].

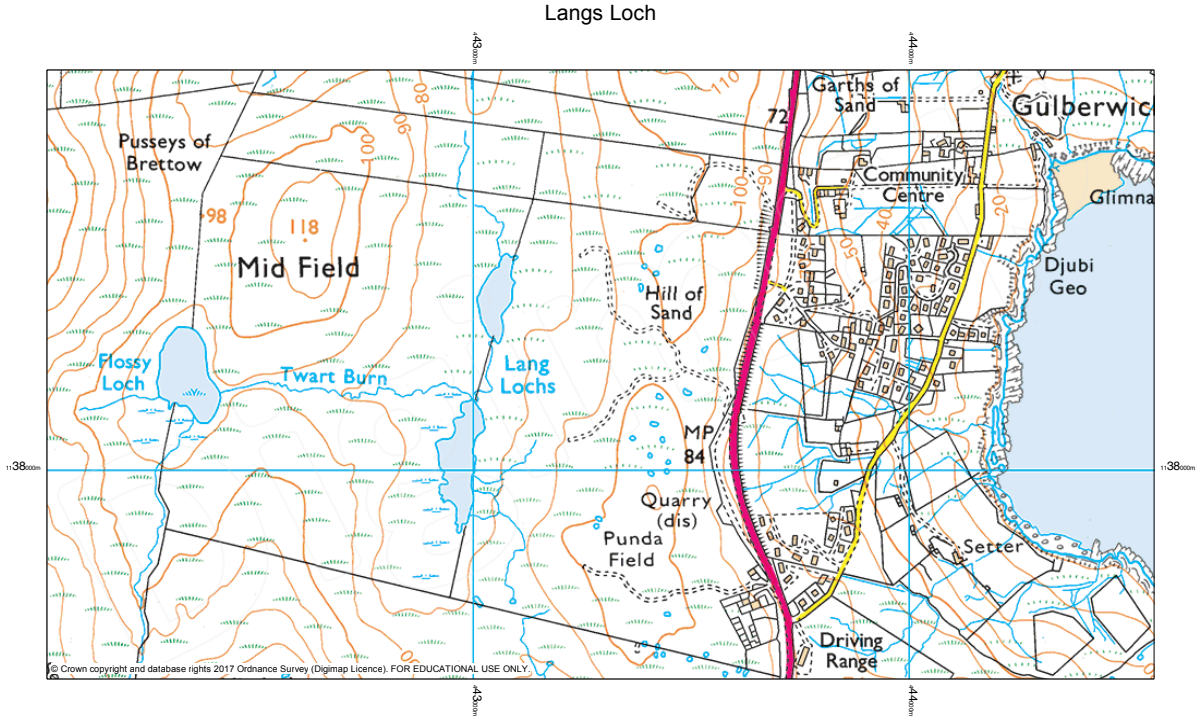

Figure 58. Ordnance survey map of the Lang Lochs basin. Scale 1:10000m (Edina Digimap)

Figure 59. Lang Lochs image of the sedimentary core straight after coring

6.2.2 **Regional Geology**

The Isle of Shetland has a complex geological history [Fig.61]. The basal lithology is dominated by Lewisian Gneiss, Mica Schist and Hornblende from the ancient continent of Laurentia which deformed between 2.9-1.7 billion years ago (McKirdy, 2010). Flash flooding and river sediments overlay the basal lithology. These have undergone metamorphism, and subsequent uplift, and form the basis of the ancient Caledonide mountain range. The largest mélange of metamorphic rocks is from the Dalradian and Moine supergroups which are associated with cross-cutting faults seen across Shetland (McKirdy, 2010). Devonian sandstones are also present on Shetland representing a dry arid environment which was once close to the equator. Between 200-66 Ma the Atlantic Ocean opens which leads to the formation of the volcanic features on the island (McKirdy, 2010). The hard geology is overlain by unconsolidated Quaternary sediments indicating an environment with a complex geological history (section 6.0.).

6.2.3 **Site Geology**

The Langs Loch basin is underlain by the ‘Rova Conglomerate’ and metamorphosed mafic intrusive rocks. These are overlain by unconsolidated glacial till, diamicton, organic peat layers and alluvial sediments composed of silt and clays [Fig.60]. At Lang Lochs, the underlying geology is composed of igneous and metamorphic rocks, and as a result the unconsolidated sediments are dominated by clay rich minerogenic layers during the phases of allochthonous sedimentation in the lake. The kyanite and andalusite minerals found in the metamorphosed rocks are responsible for giving the minerogenic rich sedimentary layers a light blue colour.

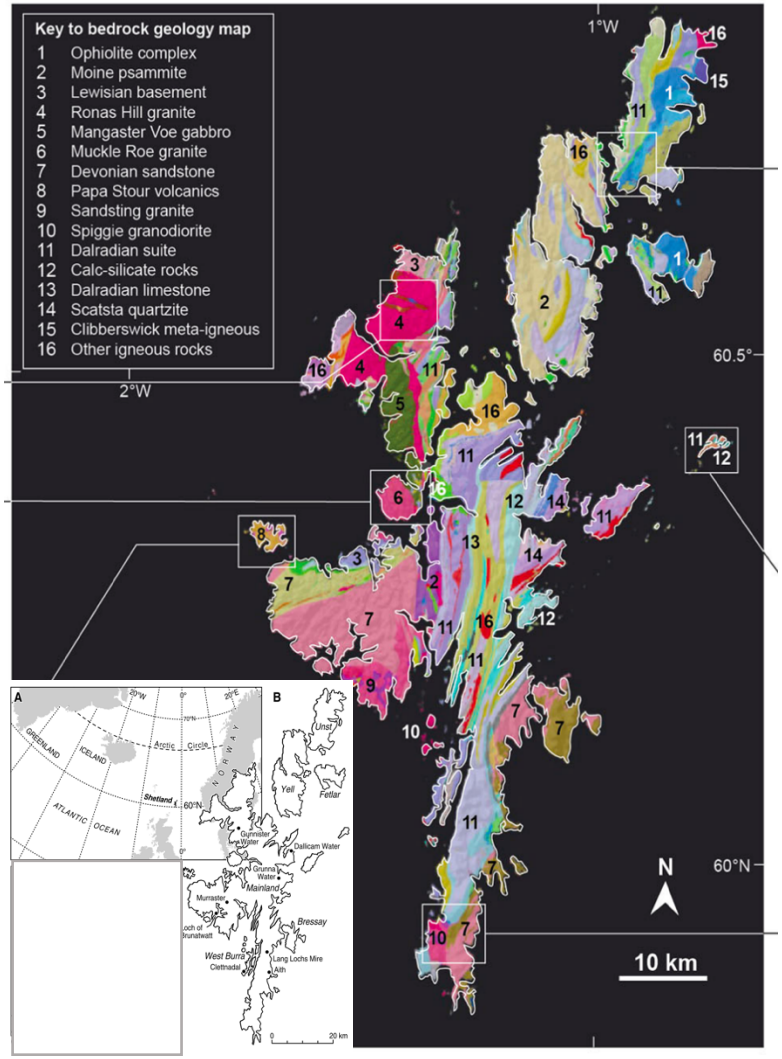

Figure 61. The main geological units throughout Shetland, the location of the archipelago in the North Atlantic and position of the site in relation to other paleo-environmental study sites (adapted from Bradwell et al (2019) and Whittington et al (2003))

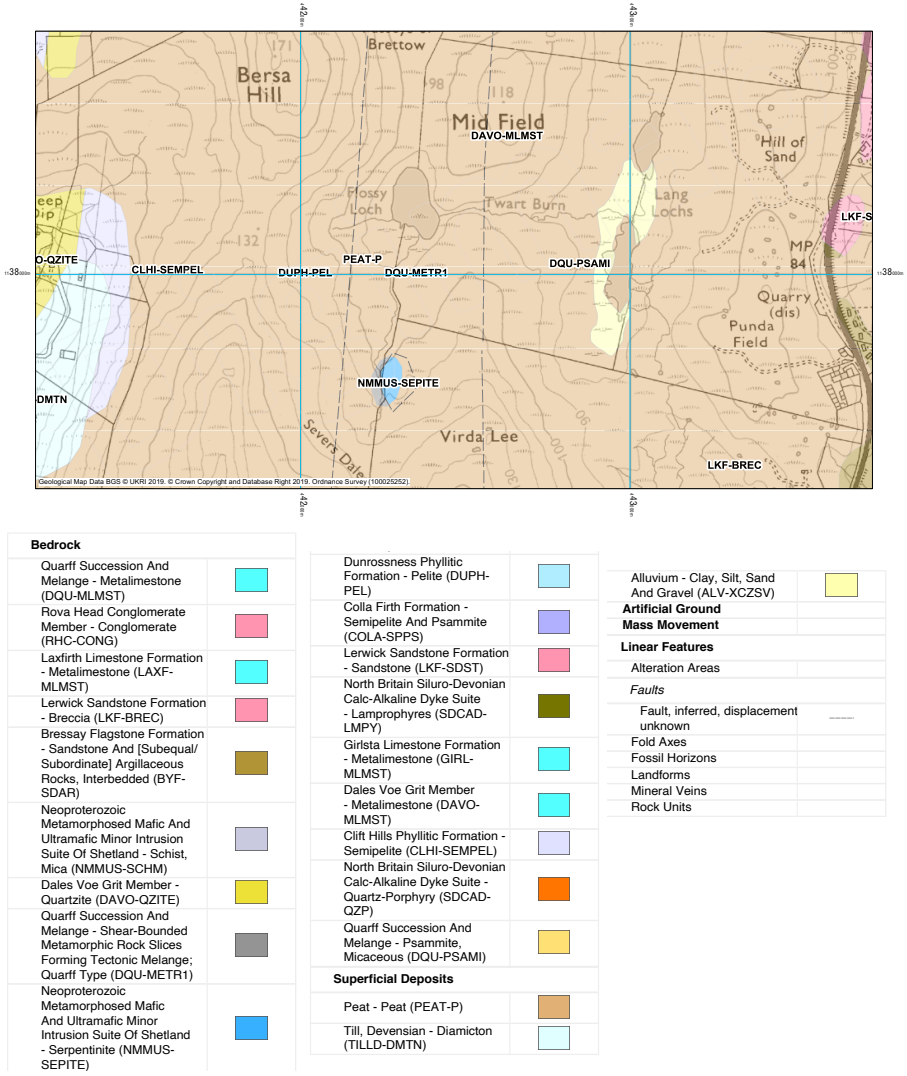

Figure 60 The geology and associated legend of the Lang Lochs mire (Edina Digimap, 2019)

6.2.4 **Basin characteristics, Land-use & Vegetation**

The basin stratigraphy and the topography indicate that the loch was likely bigger in the past. There is a clear palaeolake edge in the south of the catchment. To the east of Lang Lochs there is a disused aggregate mine. Lang Lochs is surrounded by land used for sheep and cattle grazing. The lake edge is surrounded by a blanket mire and peat bog [Fig.62]. The eastern half of the catchment is dominated by heather and grassland. Twart Burn enters the loch by the western bank. However, the loch is mainly fed by precipitation, groundwater and runoff from the sloping hills (called 'Hill of Sand' on the map). The lochs are found on low-lying ground with a gradual slope located to the west and east of the catchment.

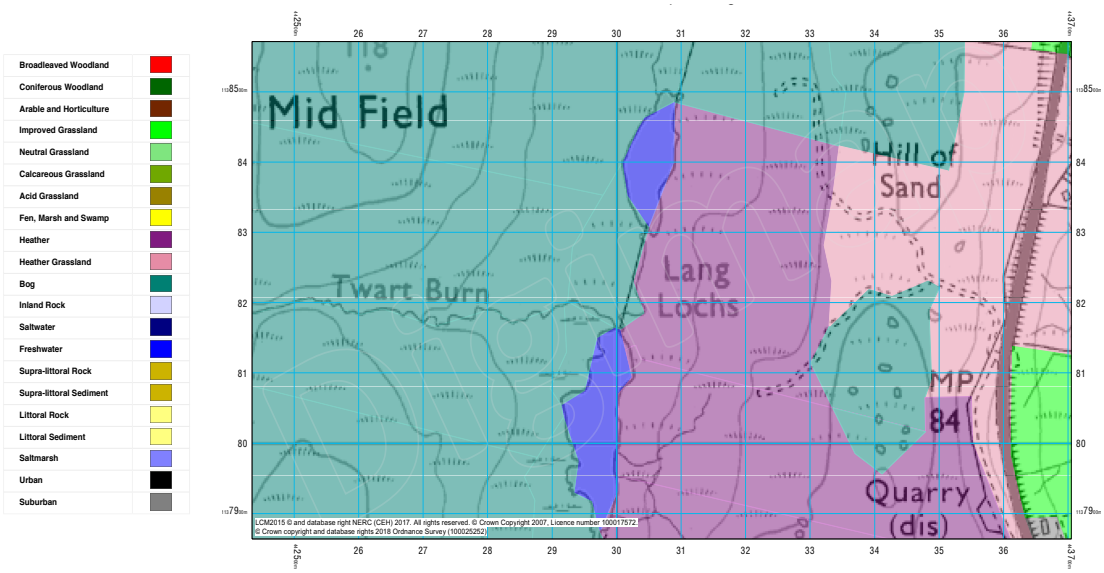

Figure 62. The environmental biomes recorded at present day for the Lang Lochs mire (Edina Digimap (2019) citing the Centre for Ecology and Hydrology land cover map)

6.2.5 **Present-day climate**

Present day climate in the Isle of Shetland is controlled by the interaction between the cold NPF, the THC and the warmer Azores high (Walker, 1924). The interaction between these two air masses forms a pressure dipole which can be quantified in the form of an index known as the North Atlantic Oscillation (NOA). A positive NAO results in stronger winds whilst a negative NAO leads to weaker winds. The NAO can vary annually shown by an extreme low throughout 2009-10 (Chafik., 2013) [Fig.63]. The minimum average winter temperatures are 2˚C and the maximum summer temperature is 13˚C in July (based on the record spanning 1947-2009) (Dawson et al., 2010).

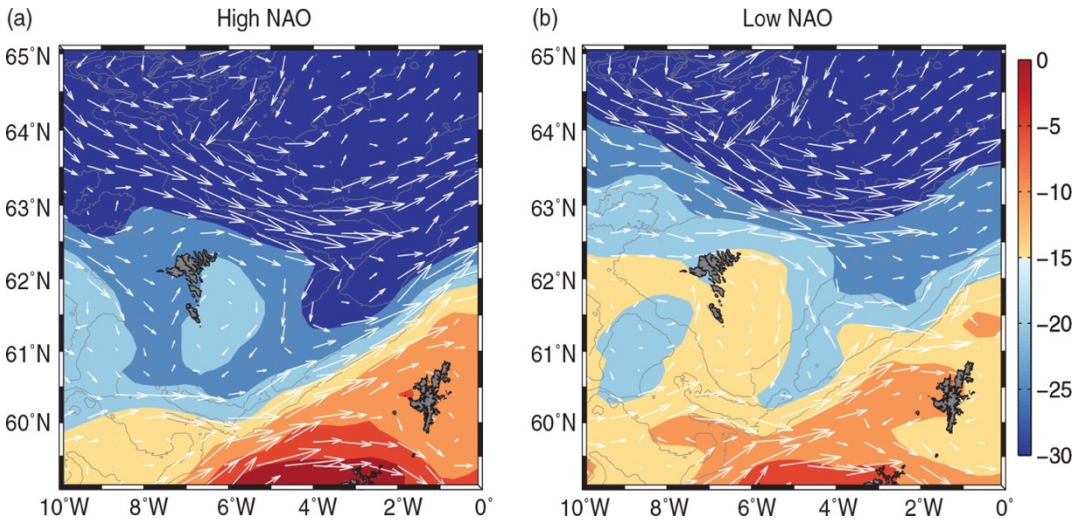

Figure 63 A comparison between a low and high North Atlantic Oscillation index for the Isle of Shetland (Chafik., 2013)

The North Atlantic Oscillation is influenced by changes in deep water formation, SST (˚C) and the THC. Between the months of October and December in 2009 SST(˚C) changed rapidly. Modern sea surface temperatures are 8˚C in the winter and 12˚C in the summer (Zumaque et al., 2012) [Fig.64], showing the dynamic ocean and atmospheric changes that occur in the Faroe-Shetland channel (Chafik., 2013). When considering palaeoenvironmental change throughout the LGIT it is important to consider the present-day influences on the Shetland climate as the oceanic and atmospheric drivers today are thought to be similar to those recorded in the past. The chironomid transfer functions assume that atmospheric temperatures, and chironomid assemblages, interact the same way today as they did during the LGIT (Brooks and Birks, 2001). Therefore, understanding present day climate is necessary to make reliable inferences about climate during the LGIT and early Holocene.

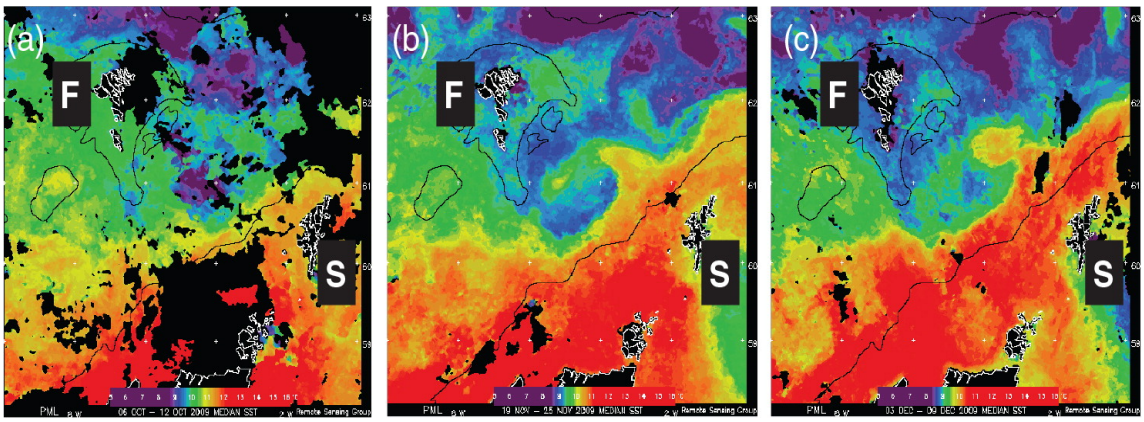

Figure 64. SST records between October and December 2009 (Chafik., 2013)

6.3 Results & Interpretation

6.3.1 Lithology and Geochemical Analysis

A core spanning 410cm was recovered from the fen edge of the Lang Lochs mire. Five continuous cores, overlapping by 10cm, were taken and contiguous samples were taken for organic content (LOI). The lithological properties and geochemistry were recorded and analysed (section 5.3) [Fig.66 & 67]. *Micro*-XRF (ITRAX) analysis was undertaken at Aberystwyth University, Wales. This analysis offers a geochemical record down core, highlighting the elemental ratios of trace elements, both organic and inorganic. An analysis of the counts of Iron (Fe), Titanium (Ti), Silicon (Si), Calcium (Ca), Phosphorus (P) and Potassium (K) were recorded to assess lake nutrient levels, productivity, underpin potential crypto-tephra layers and determine the sources of organic and minerogenic material (section 5.7) [Fig.67].

410-395cm: First minerogenic layer. The sediments in this layer are blue-grey fine grained minerogenic clays. The levels of silica, potassium and titanium reach medium counts. Calcium values remain low within this unit. The organic content within this zone is low reaching a maximum of 5%. *Salix herbacea* and *Betula nana* plant fragments throughout, located at 403cm, 397cm and 394cm.

395-379cm: First lacustrine mud layer. Brown-grey fine-medium grained lacustrine lake muds are found in this unit. These layers are indicated by drops in the counts of minerogenic sediments. There is a spike in organic content in the sediment at 385cm indicating a layer of organic matter. The organic content rises from a low of 5% to a high of 30%.

379-370cm: Second minerogenic layer**.** This layer is composed of texturally mature fine blue-grey minerogenic rich sediments. This organic layer is indicative of higher calcium counts. The counts of silica, potassium, iron and titanium increase subtly in this zone to medium counts. The loss on ignition falls within this sedimentary unit. The organic content falls to 15% within this layer.

373 to 357cm: Second lacustrine mud layer**.** This unit is composed of fine-medium grained brown lake mud. This unit gradates into the minerogenic rich clays above. Shown also by the gradual decrease in the counts of titanium, iron, potassium and silica. The levels of calcium spike to higher counts in this unit. The organic content remains similar to the previous layer with a slight increase to 20%.

357 to 351cm: Third minerogenic layer. A blue-grey layer of minerogenic rich sediment is found in this unit. Counts of calcium remain low. However, there are spikes in the counts of potassium, silica, iron and titanium. The organic content falls from a high of 20% to 10% in this layer.

351 to 341cm: Third lacustrine mud layer: finely laminated brown-grey organic rich lake muds grading into the unit above. Throughout this unit there are spikes in potassium, silica and titanium indicating minerogenic inputs. Calcium levels remain low throughout this unit. At 343cm there is a layer of organic matter indicated by high counts of calcium.

341cm to 318cm: Fourth Minerogenic Layer. This layer is composed of finely laminated blue-brown clays mixed with organic fragments. This minerogenic layer has high spikes in the counts of calcium, highlighting two layers of organic rich lenses of plant macrofossils. This layer has medium counts of silica, titanium, potassium and iron. The organic content is lower in this layer (10%). There is a spike in the LOI values at 330cm indicating a layer of plant fragments of *Betula nana* and *Salix herbacea*.

318cm to 270cm: Fourth lacustrine mud layer: This layer is composed of fine-medium grained blue-grey clays grading into organic rich finely laminated brown lake muds. The layer has spikes in the counts of calcium at 270cm, 290cm and 300cm. There is a spike of titanium at 273cm indicating a possible tephra layer. Calcium levels gradually increase throughout this zone to medium counts. Whilst the counts of iron, titanium, potassium and silica gradually drop as minerogenic sediments fall. At 315cm there is a sharp reduction in the organic content to 8%.

In summary, the basal sediments are dominated by fine to medium grained minerogenic rich clays which sharply transition into finely laminated brown lacustrine muds. There are clear transitions throughout the core from minerogenic rich clays to organic rich lake muds indicating rapid environmental change occurred. There are notable black-brown bands which highlight organic rich layers abundant in macrofossils, *Betula nana* and *Salix herbacea*. Throughout the core there are spikes in the counts of titanium which indicates potential tephra layers.

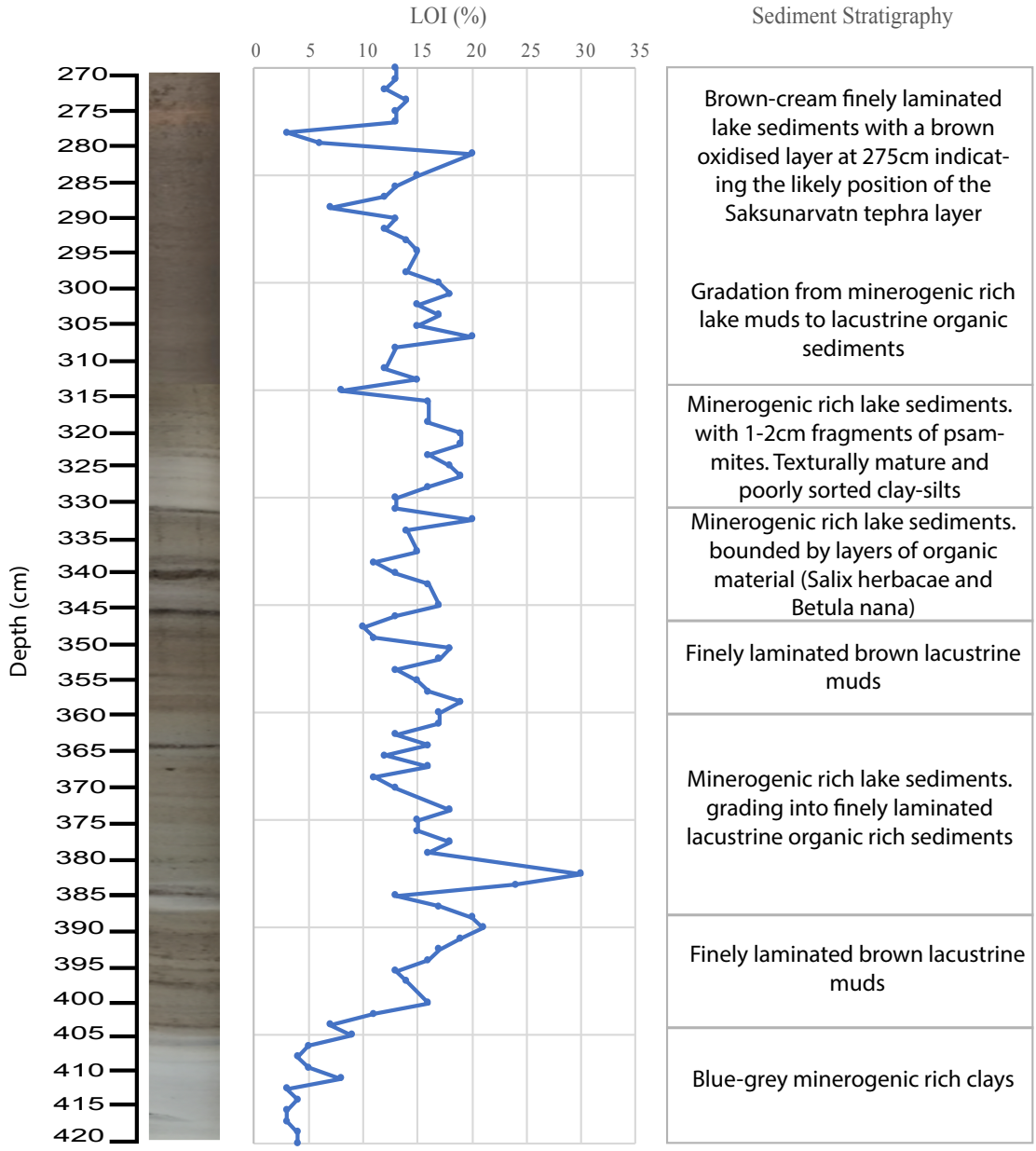

Figure 65. The organic content of the Lang Lochs core was assessed and recorded below.

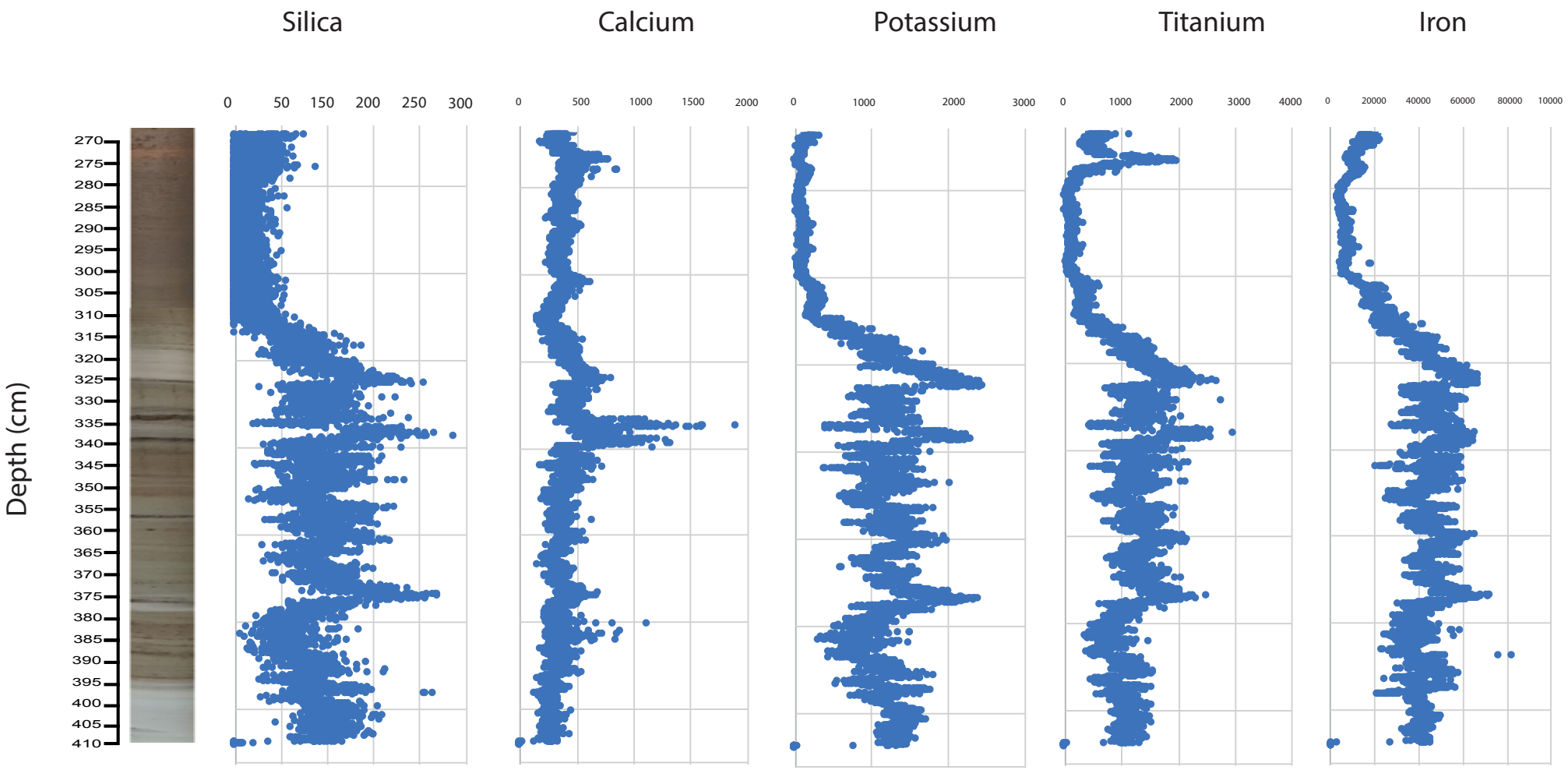

Figure 66. Micro-XRF analysis was undertaken for the core and the silica, potassium, iron, titanium, silica and calcium values were recorded.

6.3.2 **Chronology**

An age-depth model was constructed using 8 AMS dates [Fig.69]. 11 AMS dates were granted by the NERC Radiocarbon committee (Autumn 2018), however 3 were removed from the model due to age reversals and calibrated dates being too old for the position in the stratigraphy. This site is known to have a tripartite sedimentary sequence and as a result it is possible to assess the reliability of the calibrated ages, allowing for ages to be removed from the age-depth model. The $\partial^{13}C$ values were also used to determine the likelihood that terrestrial plant fragments were analysed where plant fragments were not able to be identified. Samples with values <-25‰ suggest that aquatic macrophytes were analysed instead of terrestrial species (Marty and Myrbo, 2014). However, in Lang Lochs some samples were included in the model, even though they had lower isotopic values, as the samples were identified as being *Salix herbacea* and/or *Betula nana* [Fig.68]. The median age was used for the temperature reconstructions later in the thesis [Table.8 & Fig.67]. See section 5.8 for the model used in the project.

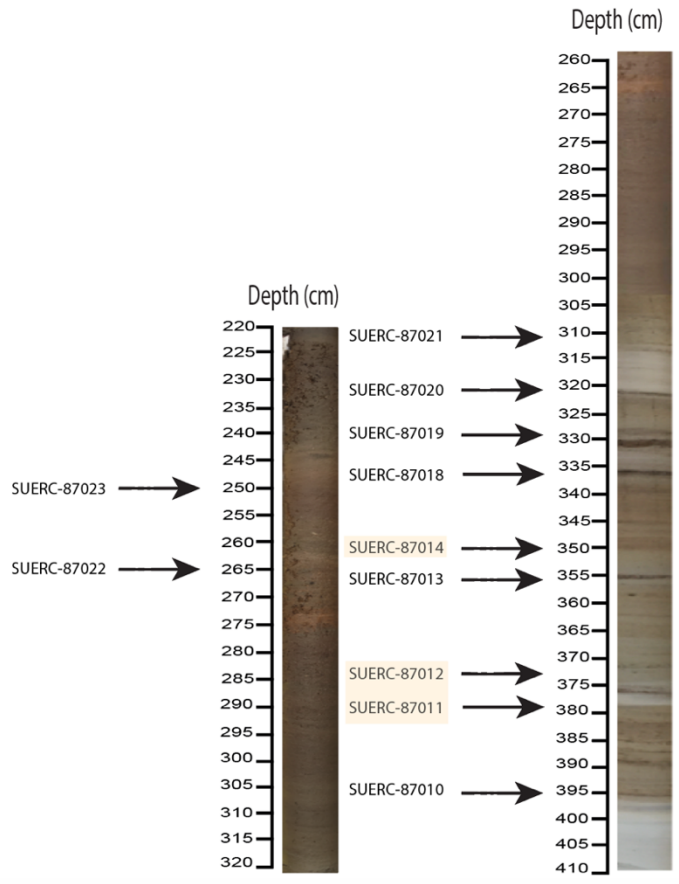

Figure 67. Position of the samples taken for AMS Radiocarbon dating. The three samples in yellow were removed from the model.

Table 8. The unmodelled and modelled ages for Lang Lochs. Showing the AMS dates and tephra's used in the model. The median age is included in the table. Modelled using OxCal. The samples highlighted in yellow were not included in the age-depth model

Laboratory code	Depth (cm)	Material	$\delta^{13}C_{VPDB}$‰ (± 0.1)	^{14}C yr (1σ)	Calibrated age range (95.4%) cal yr BP with median*
SUERC-87010	395	Plant fibres	-33.7	13410 ± 52	15933-(16136)-16316
SUERC-87011	379	Plant fibres	-29.0	13616 ± 51	16210- (16407)-16638
SUERC-87012	374	Salix herbacea	-23.6	11790 ± 46	13534-(13626)-13740
SUERC-87013	356	Plant fibres	-25.3	12003 ± 45	13743-(13854)-14003
SUERC-87014	350	Plant fibres	-19.3	12642 ± 55	14751-(15035)-15230
SUERC-87018	336	Salix herbacea	-26.9	11479 ± 45	13225-(13330)-13438
SUERC-87019	330	Salix herbacea	-25.5	11402 ± 45	13125-(13239)-13338
SUERC-87020	320	Plant fibres	-22.9	11236 ± 44	13030-(13101)-13194
SUERC-87021	310	Plant fibres	-16.8	10003 ± 42	11668-(11470)-11703
SUERC-87022	265	Plant fibres	-18.2	8825 ± 40	10056-(9880)-10151
SUERC-87023	249	Plant fibres	-21.3	7325 ± 39	8019-(8116)-8200

Figure 68. Betula nana and Salix herbacea plant macrofossils from the Lang Lochs core

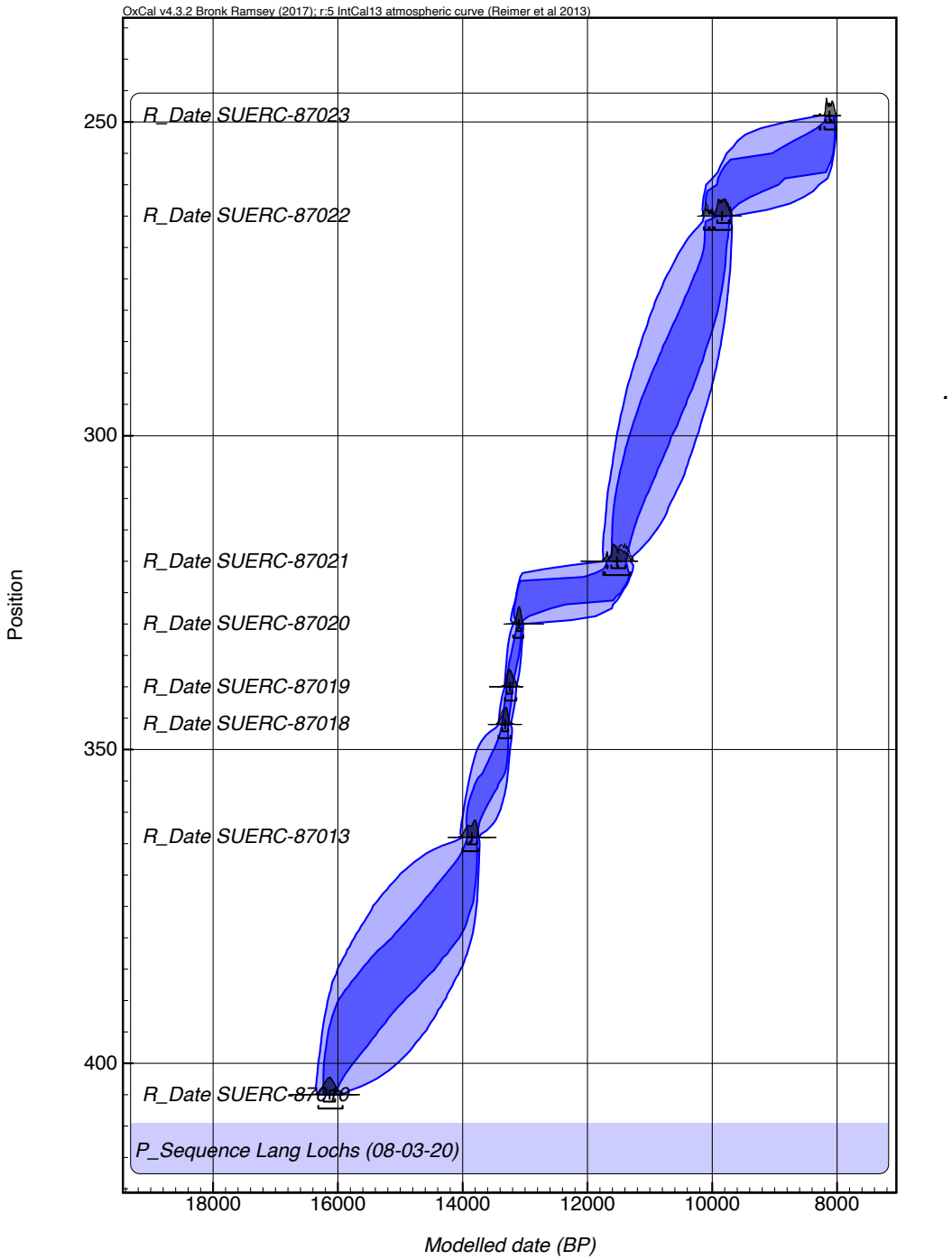

Figure 69. Calibrated OxCal age depth model (cal Yr BP) for the Lang Lochs core highlighting the position of the AMS dates and tephra layers. Depth (cm) on the y-axis and age on the x-axis.

6.3.3 **Chironomid assemblages**

A high-resolution record of mean July summer temperatures has been modelled for the Lang Lochs. Based on the composition of the chironomid communities the palaeoclimate and environmental history of the core has been assessed. A total of 59 chironomid taxa were identified to genus level for the Lang Lochs core, with many being sub-divided to species level (see Appendix for the full list of the chironomid taxa). Nine significant assemblage zones were determined with CONISS cluster analysis (section 5.4.3). Samples were sub-sampled every 1-2cm for the full core. Across lithological boundaries samples were taken every 1cm. Throughout areas of uniform deposition and stable assemblage counts samples were taken at a 2cm resolution.

The chironomid assemblage diagram only highlights the 31 most abundant species of chironomid. Rare taxa which were less than 5% of the overall sample assemblage were not included in the plot. However, some stenothermic taxa were included which were <5% which were rare species that had a narrow ecological optimum that supported the interpretations of the palaeoclimate history of the region. In the basal sediments, and the minerogenic rich clays found between 285-316cm, there were insufficient chironomid head capsules for statistically reliable temperature reconstructions. This led to some samples being combined, where it was not possible to exceed the desired count of 50 head capsules. Between 285cm-316cm there is a lower resolution due to the lack of chironomid fossils with samples being separated by 3-4cm. However, high resolution 1cm sub-sampling was possible between all the lithological boundaries in order to maximise the timing of environmental/climate change and to reliably assess the leads and lags in the records. The diagram below highlights the dominant chironomid taxa and assemblage zones found within the Lang Lochs core. [Fig.70].

Based on the identified chironomid taxa mean July summer temperatures were reconstructed for this site using the Norwegian training set and transfer function (Brooks and Birks, 2001) [Fig.71]. See the methods section for the species which were found in the Lang Lochs core that were not found in the Norwegian training set [Table 5]. A modern analogue technique (MAT) was used to assess the likeness of the modern day chironomid assemblage to the fossils from the Norwegian training set. A goodness of fit determination was used to assess the chironomid assemblages fit to modern temperatures (Brooks and Birks, 2001). The MAT highlights that 14 samples have no modern analogues, whereas the rest of the samples have poor modern

analogues or good modern analogues. The goodness of fit determination function indicates that 9 of the samples have a poor fit to temperature. Largely there is a good reliability that the reconstructions are indicative of palaeotemperatures throughout the LGIT, as the majority of the samples have a squared chord distance, of the good modern analogue, do not exceed 60% indicating that there is a close resemblance between the species found in Shetland to the training set [Fig.72].

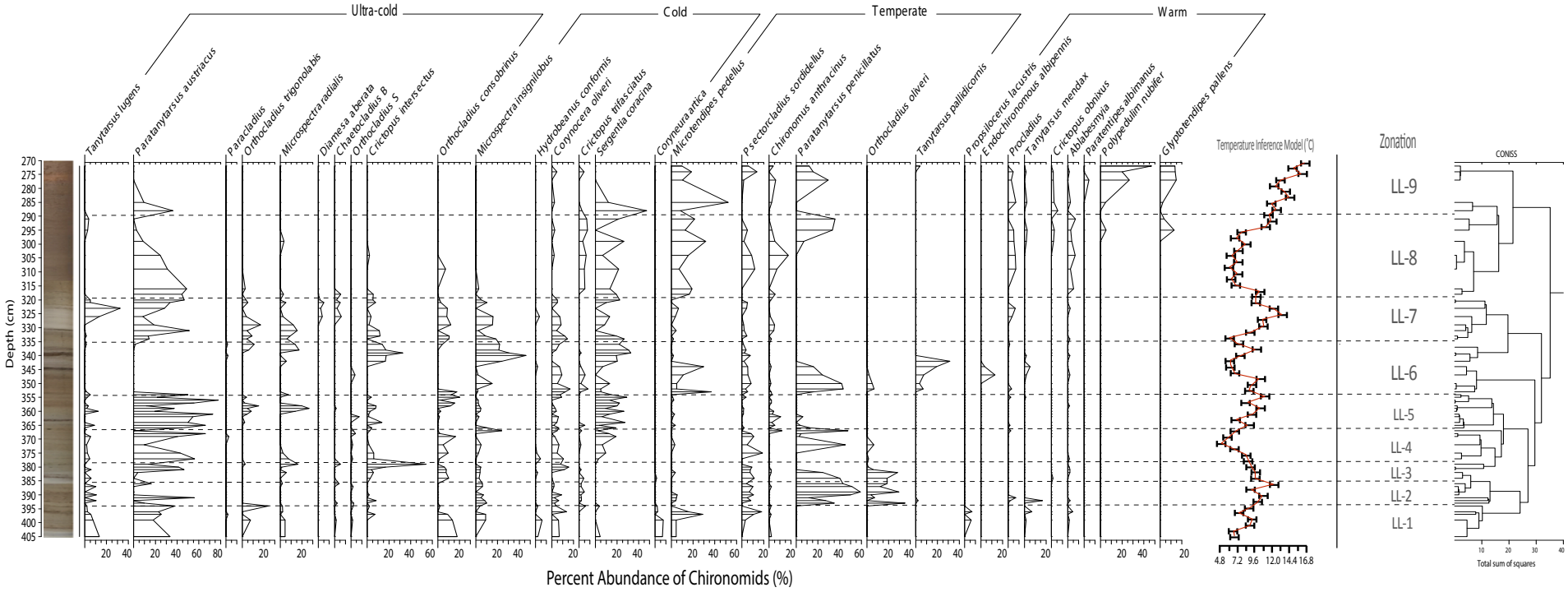

Figure 70. Lang Lochs chironomid assemblage plot (%), C-IT (°C) model and zone partitioning (CONISS). The species are organised from ultra-cold to warm (left to right)

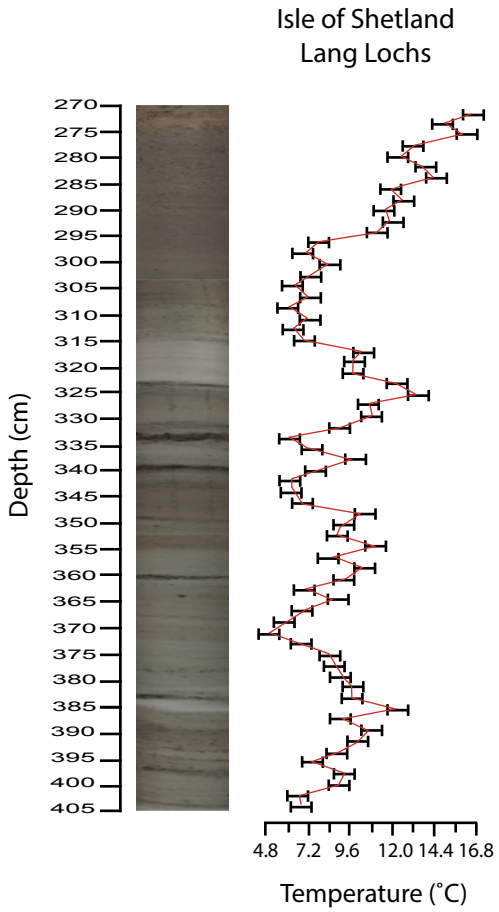

Figure 71. Lang Lochs C-IT (˚C) model with sample specific errors.

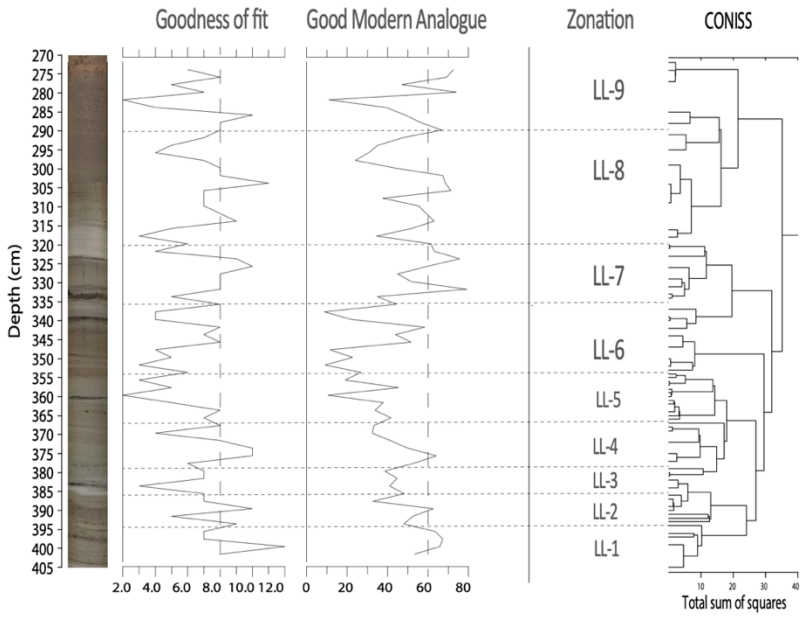

Figure 72.Lang Lochs good modern analogue and goodness of fit to temperature. Samples to the right of the dotted line have no good modern analogues and have a poor fit to temperature.

Zone LL-1 (405-395cm) records the point at which the chironomid communities are supported in the lake. Between 410-405cm the environment was too harsh for the chironomids to survive and as a result no chironomid head capsules were detected. The productivity in the lake increases which allows cold oligotrophic chironomid species to dominate. Notably, *Paratanytarsus austriacus* (30-40%), *Orthocladius consobrinus* (20%), *Microspectra radialis* (10-21%), *Chaetocladius B* (<5%) and *Tanytarsus lugens* (5-18%) are found within this section of the core. These chironomids are indicative of cold sub-arctic conditions (Brooks et al., 2007). It is worth noting that this is the only section of the basal clays that had sufficient chironomid head capsules to allow quantification. However, chironomids are only found from 405cm onwards even though the basal clays reach 410cm. Throughout, LL-1 mean July summer temperatures range from 6-8˚C.

Zone LL-2 (395-385cm) consists of cool-temperate chironomid taxa: *Microspectra pedullus, Tanytarsus mendax, Tanytarsus lugens, Psectrocladius sordidellus* and *Chironomous anthracinus*. The presence of *Microtendipes pedullus* and *Psectrocladius septentrionalis* indicates an environment low in organics composed of littoral to sublittoral sediments (Brodersen & Lindegaard, 1997). The presence of *Ablabesmyia* and *Tanytarsus* spp. indicates that the lake was acidic and composed of aquatic vegetation for the chironomids to graze on the associated epiphytic algae (Pinder & Morley, 1995; Brodersen et al., 2001). *Chironomus anthracinus* suggests that intermediate temperatures dominated (Brooks et al., 2007). This species is also an early coloniser and is an indicator of changing lake nutrient conditions (Brundin, 1949; Brooks et al, 2007). Notably, this is the only zone which contains a dominance of *Orthocladius oliveri*. At times this species exceeds 35-40% of the overall assemblage. Between 395-385cm these temperatures increase to a high of a 12.5˚C.

Zone LL-3 (385-380cm) the assemblage consists of chironomids indicative of cooler oligotrophic conditions (Brooks et al., 2007). *Paratanytarsus austriacus, Pseudodiamesa, Orthocladius consobrinus* and *Crictopus intersectus* are found in this zone with the assemblage being dominated by *Paratanytarsus austriacus* (exceeding 40-45% of the overall assemblage). This species is a cold stenotherm indicating a return to cold sub-arctic conditions. LL-3 has temperatures ranging between 5-6˚C.

Zone LL-4 (380-365cm). There are subtle changes in the inferred temperatures throughout this zone indicated by the mix of cold and warm species. This zone is dominated by cool-temperate species of chironomids such as *Paratanytarsus penicillatus* (40%), *Sergentia coracina* (15-20%), *Corynocera oliveri* (10-15%) and *Paratanytarsus austriacus* (50-60%). This assemblage is mixed with both oligotrophic cold stenotherms and warm-temperate species (Brooks et al., 2007). According to the Norwegian training set (Brooks and Birks, 2000), *Sergentia coracina* and *Corynocera oliveri* have wide temperature optimums thus possibly explaining their presence in the zone. Interestingly, when *Paratanytarsus austriacus* rises *Paratanytarsus penicillatus* falls and vice versa. Both species are stenotherms indicative of cold and warm conditions respectively, therefore highlighting subtle cool and warm events throughout LL-4. Between 380-365cm temperatures gradually rise to 10-11˚C throughout zone.

Zone LL-5 (365-355cm) is dominated with ultra-cold to cold species of chironomids. The assemblage contains the following: *Paratanytarsus austriacus, Pseudodiamesa, Orthocladius consobrinus, Microspectra radialis, Sergentia coracina* and *Orthocladius trigonobalis*. *Paratanytarsus austriacus* is a cold stenotherm and is the dominant species within this assemblage, constituting 44-72% of the sample. The abundance of this species increases throughout this zone reaching the highest abundance at the end of the LL-5 (361cm). *Crictopus intersectus* and *Psectrocladius sordidellus* are rare species in this assemblage constituting 1.4% and 4.7% of individuals in each sample. These species are cool-temperate taxa (Brooks et al., 2007) indicating that the conditions of the lake changed subtly to support these taxa. Between 368-361cm, the C-IT(˚C) model indicates that summer temperatures ranged between 4-6˚C

Zone LL-6 (355-335cm) is composed of temperate-warm species of chironomids such as *Paratanytarsus penicillatus* (50% at the onset), *Microtendipes pedullus* (35% at the onset), *Tanytarsus mendax* (5-10%), *Tanytarsus pallidocormis* (10-30%) *Crictopus trifasciatus* (10-15%) and *Psectrocladius sordidellus* (10-15%). Within this zone *Paratanytarsus austriacus* disappears again and is replaced by the warm stenotherm *Paratanytarsus penicillatus* (Brooks et al., 2007). The abundance of *Paratanytarsus penicillatus* is high at the start of the zone (50%), falling gradually until it disappears from the assemblage at 340cm. Throughout the core there is an apparent abrupt switch in these two taxa, indicating a change from cool to warm phases and vice versa.

The onset of this zone is dominated by *Microtendipes pedullus* highlighting an abrupt change in the environmental conditions at this time. Temperatures rose to a high of 10-14˚C.

Zone LL-7, **(**335-320cm) significantly alters from temperate-warm species to ultra-cold chironomids. This assemblage is dominated with *Paratanytarsus austriacus, Pseudodiamesa, Tanytarsus lugens, Orthocladius consobrinus, Diamesa aberata, Microspectra radialis* and *Microspectra insignilobus*. *Paratanytarsus austriacus* again is the dominant taxa, constituting 40-51% of the assemblage. The cold stenotherm *Diamesa aberata*, although rare throughout the core, occurs in larger abundances than previously seen (2-5.5%) indicating that the environment became much colder, resembling a lake system similar to high latitude Icelandic lakes (Oliver., 1983; Brooks et al., 2007). *Orthocladius consobrinus* is another cold stenotherm which increases in abundance throughout this zone from a low of 4% to a high of 11% by 329cm. Temperatures throughout this zone fall from a high of 12˚C to a low of 4-5˚C

Zone LL-8 (320-290cm) is the next significant zone which is dominated by chironomids indicative of mesotrophic temperate-warm conditions. The assemblage is composed of the following species: *Sergentia coracina, Psectrocladius sordidellus, Crictopus trifasciatus, Microtendipes pedullus* and *Procladius*. The cool-temperate acidophilic species *Sergentia coracina* increase in abundance from a low of 10.3% to 26% of the assemblage by 299cm. *Microtendipes pedullus* appears, dominating the assemblage (14-16%) indicating that there was abrupt environmental change at this zone from cold to temperate conditions. Temperatures rise gradually from 8˚C to 13˚C.

Zone LL-9 (290-270cm) is composed of the warmest species of chironomids throughout the Lang Lochs core. This zone is dominated by the following chironomids: *Paratanytarsus penicillatus, Ablabesmyia, Microtendipes pedullus, Crictopus obnixus, Paratendipes albimanus, Glyptotendipes pallens, Polypedulum nubifer* and *Glyptotendipes severini*. This is the first appearance of Paratendipes albimanus, Glyptotendipes pallens, *Polypedulum nubifer* and *Glyptotendipes severini* which suggests that conditions became markedly warmer and nutrient rich (Walker & MacDonald., 1995; Brooks et al., 2001). Temperatures rise further to a high of 16˚C.

6.4 **Palaeoclimate & environmental history of Lang Lochs**

A high-resolution temperature record, geochemical markers and a robust chronology have been used to infer the palaeoclimate and environmental history of the Lang Lochs basin for the LGIT [Fig.74]. The local climate of the Lang Lochs basin will be the focus of this sub-chapter. However, comparisons will be made to other sites located on Shetland to gain a fuller image of the regional scale climate and environmental changes seen throughout the LGIT [Fig.73].

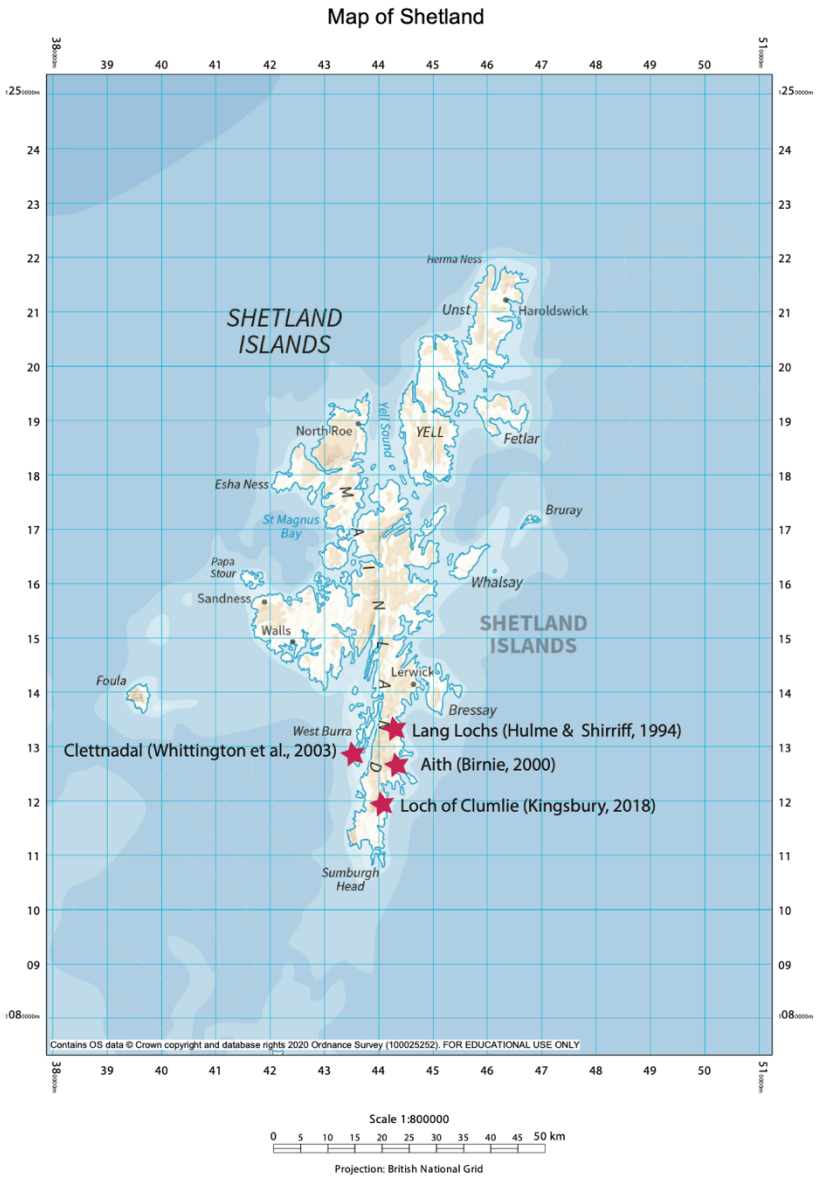

Figure 73.Location of the palaeo-environmental sites for Shetland spanning the LGIT. Lang Lochs (Hulme & Shirriff, 1994; this project), Clettnadal (Whittington et al., 2003), Loch of Clumlie (Kingsbury, 2018) and Aith (Birnie, 2000)

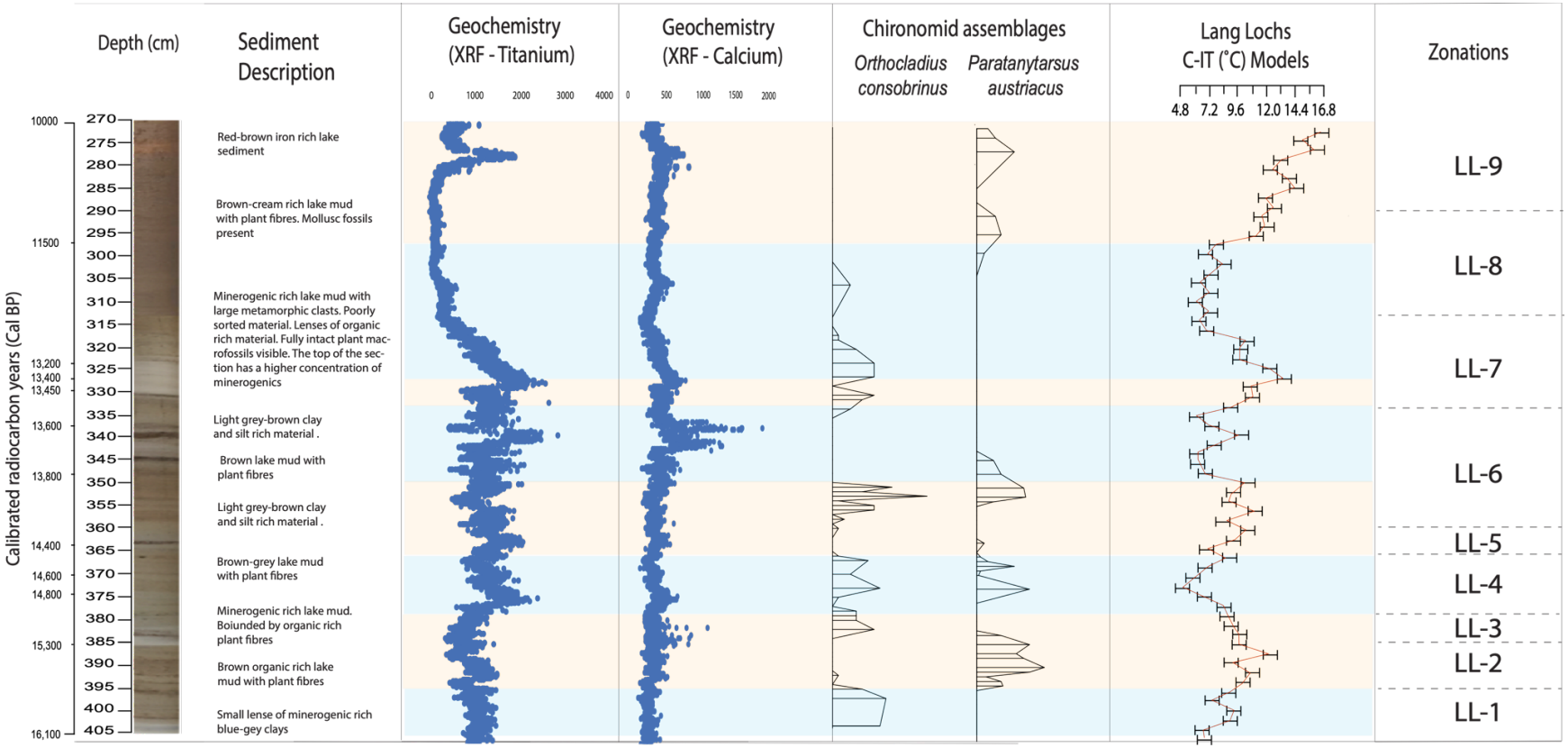

Figure 74. Synthesis diagram combining the chironomid assemblages of Orthocladius consobrinus and Paratanytarsus austriacus. The C-IT (°C) model is shown with the chronology (cal Yr BP) and the geochemical data (Calcium and Titanium). The sediment description is included on the left hand side.

The climatic events shown by the C-IT (˚C) model will be compared to the NGRIP chronology. However, the timing of these cold and warm events will be based on the independent chronology from this project. This will make it possible to assess the possible leads and lags between both records. The nature and magnitude of each climatic event will be described below, constrained by the independent chronology for the site [Fig.75]

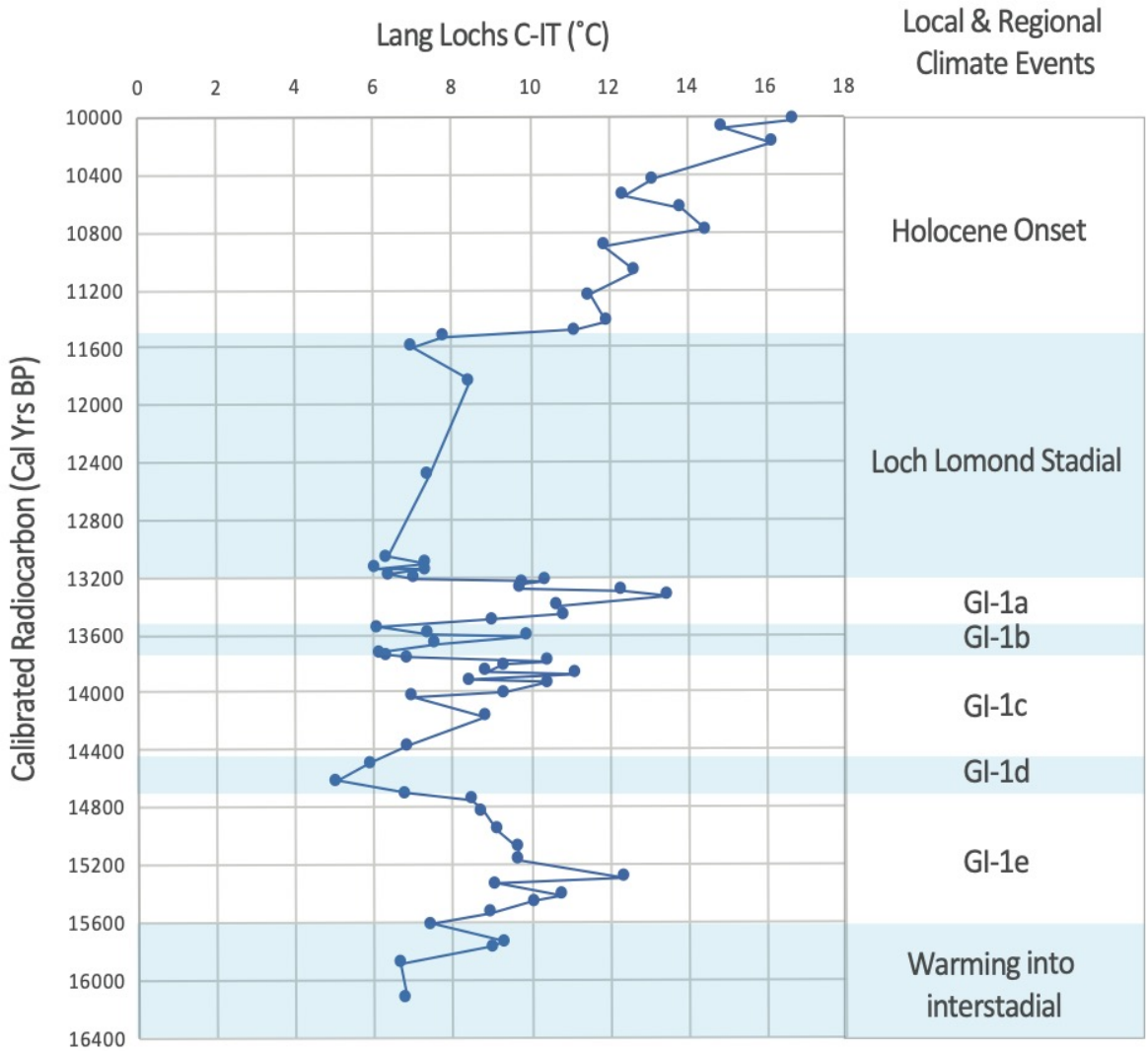

Figure 75. Chironomid inferred mean July summer temperatures for Lang Lochs with time (cal yr BP). The blue bars highlight the cold events throughout the LGIT. Local and regional climate descriptors are used to highlight the cool events (Rasmussen et al., 2014; Lowe et al., 2019)

6.4.1 **Warming into the interstadial (<c.15.6k cal BP)**

The chironomid inferred temperatures indicate that, for approximately 800 years, cold arctic temperatures are recorded in Lang Lochs after the onset of sedimentation. The beginning of sedimentation is inferred to be c.15.6k cal BP. There was a lack of organic matter of the base of the core to take an AMS sample. Temperatures range between 6-8˚C during this time and show that temperatures gradually warm until the onset of the interstadial (GI-1e). Bradwell et al (2019) and Peacock and Long (1994) highlight that the deglaciation of the LGM occurred gradually throughout the Isle of Shetland. first beginning offshore at c.24k cal BP and terminating at the interior at c.15-16k cal BP [Fig.75]. This supports the date of sedimentation from this project of 15.6k cal BP for Lang Lochs.

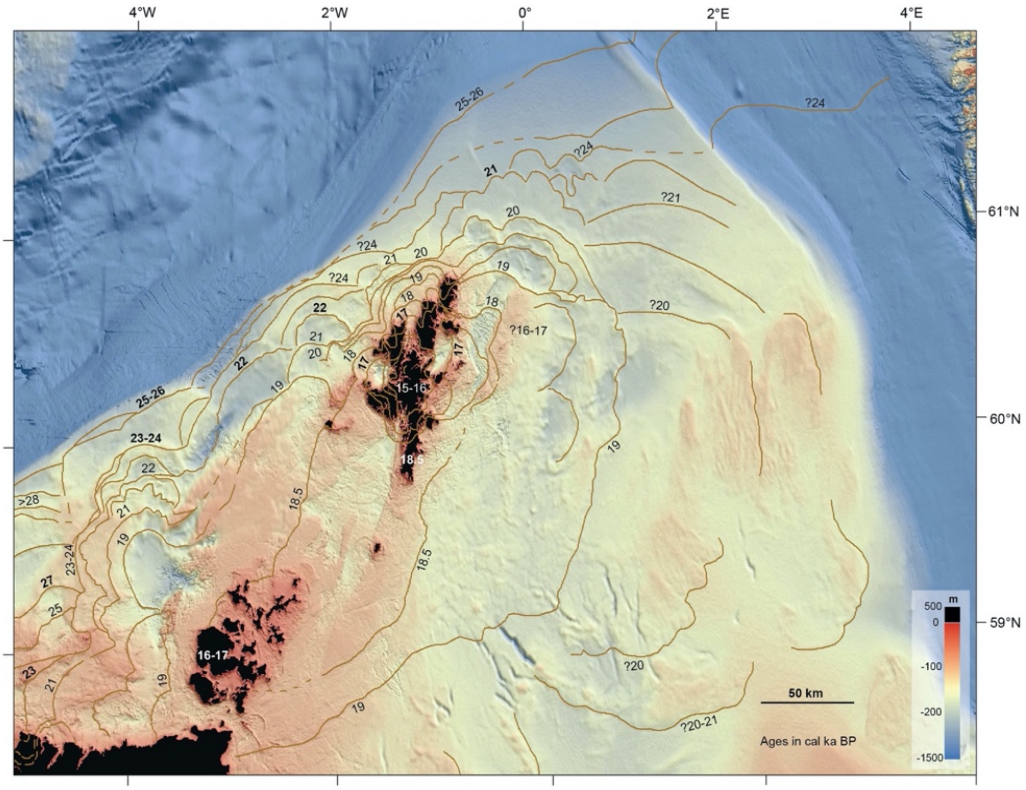

Figure 76. Timing of deglaciation at the end of the LGM for the Isle of Shetland and Orkney (Bradwell et al., 2019)

The C-IT (˚C) record begins at 405cm whereas sedimentation occurs at 410cm. The environment was likely not inhabitable by chironomids at this time. The geochemistry suggests that minerogenic in-washing was high, indicated by increased titanium counts (Kylander et al., 2012). The lake was likely too unstable to support a community of chironomids. Furthermore, Greffard et al (2012) highlights that chironomid assemblages are often found near aquatic macrophytes. Increased turbidity in the lake

would lead to reduced photosynthesis and as a result lower lake productivity, which would limit chironomid habitation in the lake. Both Robinson (2003) and Kingsbury (2018) record the dominance of the pioneering diatom species *Fragilaria* at this stage. This species is dominant in cold oligotrophic alkaline lakes with low visibility supporting the hypothesis that the environment was too turbid to support macrophyte-associated chironomid taxa until the organic content rose sufficiently at 405cm.

Cold oligotrophic-associated chironomids dominate at this time. This is the only site in this project which records cold arctic conditions at the base of the core and the only one that records warming into the interstadial. The Lang Lochs core contains the following dominant chironomid assemblage: *Chaetocladius B, Paratanytarsus austriacus, Tanytarsus lugens, Orthocladius consobrinus* and *Microspectra radialis*. These chironomids are indicative of cold, sub-arctic and oligotrophic conditions. *Paratanytarsus austriacus* is also present at this time. This is a cold stenotherm abundant in oligotrophic lakes at high latitudes or altitudes (Buskens, 1987; Brodersen et al., 2001

Chaetocladius B is a species of chironomid which is known to inhabit Icelandic lakes and other regions across the Holarctic, sub-arctic and arctic (Cranston et al., 1983; Brooks et al., 2007). Currently, Icelandic lakes have a lower chironomid biodiversity due to the harsher and cooler climates. Gathorne-Hardy et al (2008) identified only 19 chironomid morphotypes opposed to the 59 found throughout entirety of the Lang Lochs core highlighting the impact that climate cooling has on chironomid species richness. Mean lake temperatures were recorded for Lake Mývatn in N. Iceland between 1991-1998 and ranged 13-14˚C (July) (Olafsson, 1999) [Fig.77]. The results from Lang Lochs recorded mean July summer temperatures of 6-8˚C which is more comparable to temperatures in late spring and early autumn in Iceland today. This highlights that the climate was considerably cooler in the past on Shetland after the end of the LGM.

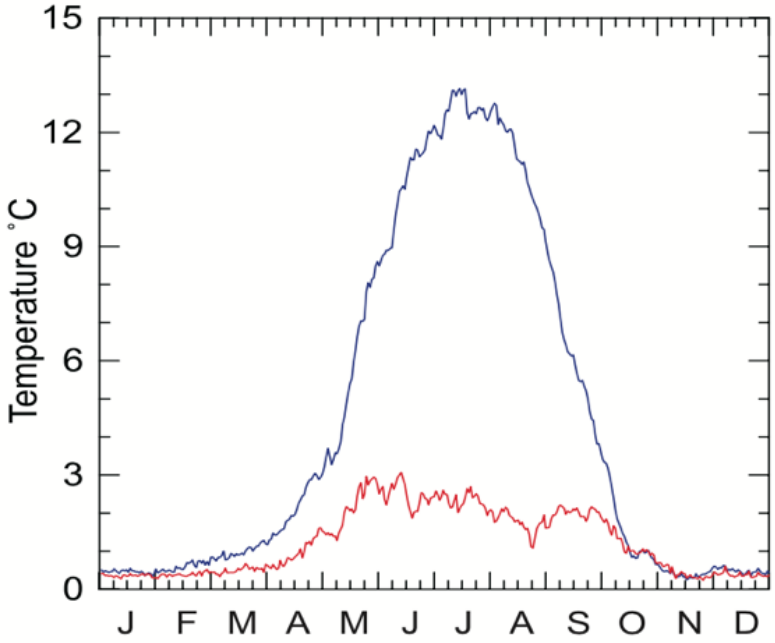

Figure 77. Mean lake temperatures (˚C) for Lake Myvatn, Iceland from 1991-1998 (Olafsson., 1999)

Based on the assemblage it is apparent that conditions were low in organics, vegetation was limited, and lake productivity was low (Saether, 1979; Hoffman, 1984). This is also suggested by the low calcium counts which show that productivity levels fell (Lauterbach et al., 2011). Although the environment became conducive to support this assemblage the counts of titanium and iron were still relatively high which suggests that minerogenic in-washing was ongoing (Moreno et al., 2011; Marshall et al., 2011) which is likely a result of the on-going snow/ice melt from the termination of the LGM.

Whittington et al (2003) and Birnie (2000) do not record any vegetation changes in Shetland from end of the LGM into the interstadial. It is clear from this research that mean July summer temperatures were as low as 6.5˚C <c.15.6k cal BP [Fig.56]. Therefore, here we can see the importance of using chironomid inferred temperature inferences for palaeoclimate reconstructions since they can capture aspects of environmental change which were not identified by the pollen records.

6.4.2 **Warm interstadial/GI-1el (c.15.6-14.8k cal BP)**

The onset of the warm interstadial occurs at c.15.6k cal BP in Lang Lochs. This warm event is thought to be synchronous with GI-1e in Greenland. This event occurred c.14.7k cal BP in Greenland, which was 900 years later than Lang Lochs. The onset

of warming occurs at 15.2k cal BP in Loch of Clumlie (Kingsbury, 2018). Furthermore, Whittington et al (2003) dated the warming and subsequent onset of sedimentation at c.15.79k cal BP for Clettnadal. These three sites indicate a-synchronous warming may have occurred at this time across the North Atlantic.

There is a gradual change in the dominance of sub-arctic oligotrophs to temperate mesotrophic indicator species. The following taxa dominate the assemblage: *Chironomous anthracinus, Tanytarsus mendax, Paratanytarsus penicillatus* and *Psectrocladius sordidellus*. These chironomids are indicative of an environment which has a higher nutrient status, likely being mesotrophic, where macrophytes are present (Brooks et al., 2007). The abundance of *Microtendipes pedullus* falls significantly between the stratigraphical boundary between the clay and lacustrine muds. This species occurs in low abundances throughout this zone (2-5%) which indicates that the organic content of the lake increased at this time (Brodersen & Lindegaard, 1997). *Ablabesmyia* and *Tanytarsus* species are found within this section of the core highlighting that the lake was likely acidic with aquatic vegetation present for the chironomids to graze on epiphytes (Pinder & Morley, 1995; Brodersen et al., 2001).

Paratanytarsus penicillatus and *Orthocladius oliveri* dominate this assemblage. At times these species exceed 35-40% of the overall assemblage. These species are indicative of warmer climates. This is the first appearance of these taxon in the core. However, there are still cooler chironomid species found in this assemblage (*Tanytarsus lugens* and *Microspectra insigniloblis*) which suggests that the climate was still conducive to cooler taxa, and there was a gradual transition between stadial and interstadial conditions. As a result, the chironomid inferred temperatures are not as abrupt as at other sites across the British Isles during this time. Temperatures gradually warm from a low of 8.5˚C to 12˚C by c.15.25k cal BP [Fig.75], coinciding with a gradual reduction in the counts of titanium which suggests that in-washing reduced throughout this time. At c.15.25k cal BP there is an increase in the abundance of cooler taxa (e.g. *Microspectra radialis* and *Paratanytarsus austriacus*). This coincides with a stratigraphical change from lacustrine muds to minerogenic rich clays indicating cooling occurred and minerogenic in-washing resumed. The abundance of cool taxa increases, recording a gradual decline in the mean July summer temperatures to 8˚C by c.14.8k cal BP. This shows the need for chironomid temperature inferences as they are able to record quantitative measurements of environmental change that other

proxies cannot (e.g. pollen). Whittington et al (2003) pollen record does not show conclusive warming and/or early cooling throughout this time but rather a dominance, and stability, of *Rumex and Betula*. Robinson (2004) records diatoms which are indicative of cold environments at Clettandal during this time, with no suggestion of warming. Here, this project has been able to record the warming into the interstadial and subsequent early cooling before the onset of GI-1d. Therefore, more highly sensitive climate proxies are required to record these small shifts in atmospheric temperatures and highlight aspects of environmental change that have not been previously recorded for Shetland.

6.4.3 **Abrupt cooling/GI-1d (c.14.8-14.4k cal BP)**

Between c.14.8-14.4k cal BP cold sub-arctic temperatures prevail. It has been shown in the previous section that the chironomids indicate an early gradual cooling until the onset of this event (thought to be GI-1d). At c.14.8k cal BP temperatures fall further to a low of 6.8˚C, indicating abrupt climate cooling occurred at this time. Temperatures fall further to 5˚C at c.14.6k cal BP[Fig.75]. This is approximately 700 years earlier than in the Greenland ice core record. Temperatures in Greenland abruptly fall at 14.03k cal BP.

Paratanytarsus austriacus, Pseudodiamesa, Orthocladius consobrinus and *Crictopus intersectus* are found in this zone, with the assemblage being dominated by *Paratanytarsus austriacus* (exceeding 40-45% of the overall assemblage). *Paratanytarsus austriacus* is an oligotrophic cold stenotherm indicative of nutrient deficient sub-arctic conditions (Brooks et al., 2007). *Pseudodiamesa* suggests that the lake was oligotrophic (Saether & Andersen., 2013). This sharp increase in the abundance of this taxa highlights that there was abrupt environmental change between 14.8-14.4k cal BP (Buskens, 1987; Brodersen et al., 2001). There is a sharp increase in the counts of iron, potassium, silica and titanium suggesting that there was an increase in the amount of in-washing and detrital inputs (Kylander et al., 2011).

This cooling is not recorded in the pollen record by Whittington et al (2003) and Robinson (2003). However, there is a subtle distinction between the diatom record by Whittington et al (2003) who records phases of succession and reversion. As the chironomids are influenced primarily by atmospheric temperatures they are more sensitive to environmental change whereas the diatom and the pollen records are

influenced by in-direct climate variables (Whittington et al.,2003). As this cool event only lasts for approximately 400 years it is likely that it is too short to be recorded by the pollen record explaining why there is no record of climate cooling at this time. However, it is possible that the cooling was too small for it to be recorded by the vegetation due to their environmental tolerance thresholds.

By the mid stage of this cold event, c.14.6k cal BP, the chironomids record a gradual warming from a low of 5˚C to 7˚C. This warming continues until the onset of the GI-1c. Here, it is clear that the chironomids are responding earlier than the stratigraphy which highlights the sensitivity of chironomids to summer temperature change.

6.4.4 **Climate warming/GI-1c (c.14.4-13.8k cal BP)**

The onset of this event is marked by a gradual rise of mean summer temperatures to 8˚C at c.14.4k cal BP. Temperatures reach a high of 10.2˚C by c.13.8k cal BP. With 11˚C being recorded at 13.9k cal BP [Fig.75]. This warm phase lasts for approximately 600 years. This zone is dominated by cool and temperate species of chironomids such as *Paratanytarsus penicillatus, Sergentia coracina, Corynocera oliveri, Orthocladius consobrinus* and *Paratanytarsus austriacus*. This assemblage is mixed with both oligotrophic cold stenotherms and warm-temperate species (Brooks et al., 2007). *Sergentia coracina* is a species indicative of cold conditions, whilst *Chironomous anthracinus* indicates warm temperate conditions. Both species have wide temperature optimums which could explain why both species occur in the same assemblage. However, with closer inspection, the abundance of both *Sergentia coracina* is greater at the start and end of this warm phase, whilst *Chironomous anthracinus* is greater during the mid-stage of this warming event. However, this is more evident with the sharp change in the abundance of *Paratanytarsus austriacus* and *Paratanytarsus penicillatus*. Both species are stenotherms indicative of cold and warm conditions respectively (Brooks et al., 2007).

This is reflected in the C-IT(˚C) model which records a short-lived, sharp drop in temperatures during the early and latter stages of this warm phase highlighting that subtle cool and warm events occurred between c.14.4-13.65k cal BP [Fig.75]. In Greenland these small scale climate fluctuations are found during the warm phase GI-1c, known as GI-1c (1), GI-1c(2) and GI-1c(3) (Rasmussen et al., 2014). Unlike the

other sites in this project these small-scale climate events are not recorded in Shetland. Higher resolution sampling may be required to locate these fine scale climate fluctuations. Although these events are not recorded there are abrupt temperatures fluctuations, with warm spikes and abrupt cooling throughout this time, indicating that the climate was unstable at this time. With higher resolution sampling it may be possible to constrain these fluctuations to particular climate events. Temperatures continue to rise throughout this warm phase reaching a high of 11˚C.

Kingsbury (2018) did not record any significant change from the previous cold stage and this warming event in Loch of Clumlie. She recorded a dominance of grasses, dwarf willows and sedges in the catchment which suggests that an alpine arctic environment prevailed. Whittington et al (2003) also sees a dominance of *Rumex* and *Salix* at this time with little variation in the assemblage counts. The catchments likely remained stable with little change in the plant community structures whereas the climate was more variable This is likely a result of the lower sensitivity and lagged response of vegetation to atmospheric temperature changes (Brooks et al., 2016). Kingsbury (2018) records a stabilised diatom species richness and evenness, indicating increased biological diversity and maturity throughout this stage in Loch of Clumlie. She also recorded increased bromine counts which are a proxy for increased productivity (Gilfedder et al., 2011). The lake ecosystems too remained stable during this time and do not reflect the variability shown in the chironomid temperature record. Although, the productivity in Lang Lochs increases also it is evident that there are small scale climate cooling and warming events during this time which are not reflected in the geochemical trace elements in the Lang Lochs core, the stratigraphy or from other lake records across Shetland. This highlights the importance of using single-variable climate proxies to better understand palaeotemperature change.

6.4.5 **Abrupt cooling/GI-1b (c.13.8 cal-13.5k cal BP)**

There is a short-lived cooling event that lasted for approximately 300 years during this phase. Mean July summer temperatures fall to a low of 6.1˚C at c.13.6k cal BP [Fig.75]. This cold event has been described as the Inter-Allerød Cold Period in the amphi-Atlantic (Lowe et al., 1994) and the Gerzensee fluctuation in Denmark (Andresen et al., 2000). In Greenland this event corresponds to GI-1b (Rasmussen et

al., 2014). This event is believed to be synchronous with the NGRIP however in Greenland this event begins at c.13.2k cal BP. This cooling occurs 600 years earlier in Shetland than in Greenland. Andressen et al (2000) highlights that high-resolution records of this cold reversal are unlikely to be recorded as the stratigraphy is often too short. However, the C-IT (˚C) record from Lang Lochs captures this event.

This time frame is dominated by ultra-cold chironomid taxa: *Orthocladius trigonobalis, Orthocladius consobrinus, Paratanytarsus austriacus, Pseudodiamesa* and *Microspectra radialis*. The presence of *Orthocladius trigonobalis* and *Orthocladius consobrinus* indicate that the lake system was oligotrophic with a low nutrient status. Both species are cold stenotherms that are dominant in environments similar to that in the sub-arctic (Brodin, 1986, Hoffman, 1984; Brooks et al., 2007). There is a return of *Paratanytarsus austriacus* which indicates that cooler conditions, similar to those found in oligotrophic lakes in higher latitudes, prevailed (Buskens, 1987; Brodersen et al., 2001). *Pseudodiamesa* and *Microspectra radialis* are found in the profundal zone of cold oligotrophic lakes, indicating that the lake was deep at this time, likely a result of the increased snow and meltwater (Walker et al., 1991; Bitušik & Kubovcík, 1999). This is supported by increased counts of titanium, iron and silica, at the onset of this cold phase, highlighting a return to minerogenic in washing (Moreno et al., 2011; Martin-Puertas et al., 2011; Aufgebauer et al., 2012). *Microspectra radialis* is the dominant species found in this assemblage. Brodin (1986) records a similar dominance of this taxa during this cold phase and suggests that the environment was like those of ultraoligotrophic alpine and arctic lakes. This further suggests a return to cooler conditions at this time.

These findings are supported by Whittington et al (2003) who record the presence of three individual species of Staphylinid: *Pycnoglypta lurida, Olophrum boreale and Boreaphilus heningianus* during this cold phase. These species are no longer found in the British Isles but are common in Late Glacial environments indicative of cold conditions. Along with these beetles, layers of *Salix herbacea* were recorded from their site implying that the conditions at this time were also cold and indicative of sub-arctic conditions. *Pycnoglypta lurida* is a boreal to sub-arctic species (Gusarov, 1995) and *Olophrum boreale*, and *Boreaphilus heningianus*, are known to inhabit cold high alpine regions of Scandinavia (Campbell, 1983; Østbye and Hågvar, 1996). Due to the lack of beetle remains a quantitative measure of temperature change was not possible. Kingsbury (2018) also records a return to cooler conditions during

this phase with a sharp drop in species richness and a return in the dominance of the cold pioneering diatom *Fragilaria*.

6.4.6 **Short-lived warming/GI-1a (c.13.5 cal-13.4k cal BP)**

It is evident that there is a sharp transition from ultra-cold to temperate-warm conditions. Based on the C-IT (˚C) models temperatures reach a high of 13.0˚C [Fig.56]. This is an abrupt rise in temperatures from a low of 6˚C at c.13.5k cal BP. The age-depth model indicates that temperatures rose markedly by 7.6˚C within ~150 years. This warm phase lasts for 100 years in Shetland. It is believed to be synchronous with GI-1a in Greenland. However, this event began 400 years later in Greenland than in Shetland (c.13.1k cal BP). Although the timing of the onset and termination varies between sites the duration of the warm phase is the same. This may indicate a northward transgression of polar air masses across the North Atlantic leading to asynchronous warming.

The dominating species of chironomids are *Crictopus trifasciatus, Psectrocladius sordidellus, Paratanytarsus penicillatus, Microtendipes pedullus* and *Tanytarsus mendax*. The species highlighted above are indicative of temperate-warm conditions. The environment changed considerably from a nutrient deficient to productive lake ecosystem during this time. *Paratanytarsus penicillatus* indicates that the lake had aquatic macrophytes and was a productive ecosystem (Buskens, 1987; Brodersen et al., 2001). *Microtendipes pedullus* is an early colonising species found in large abundances between this lithological boundary and indicates that there was significant environmental change during this time. The nutrient status becomes eutrophic indicated by the presence of *Crictopus trifasciatus* (Brooks et al. 2007). This taxon is also found in the littoral zone of the lake indicating that the water depth was likely lower (Brooks et al., 2007). There is a gradual reduction in the counts of silica, iron, titanium and potassium. This suggests that the input of minerogenic sediments fell (Martin-Puertas et al., 2011; Moreno et al., 2011; Kylander et al., 2011). Due to the reduction in titanium there is an indication that in-washing and detrital inputs fell (Balascio et al., 2011; Corella et al., 2012; Stansell et al., 2013). As a result of increased summer temperatures, reduced in-washing and increased productivity in the lake, the biodiversity of the chironomid assemblages likely expanded in Lang Lochs during this warm phase.

6.4.7 **Loch Lomond Stadial (c.13.4-11.50k cal BP)**

There is a sharp drop in temperatures at c.13.4k cal BP [Fig.75] from a high of 13.8˚C to 6˚C within 100 years. This cold event lasts between c.13.4k-11.50k cal BP and based on the age-depth model this abrupt cold phase corresponds to the LLS in Scotland (Lowe et al., 2019). This assemblage is dominated with the following species: *Diamesa aberata, Microspectra radialis, Microspectra insignilobus Paratanytarsus austriacus, Pseudodiamesa, Tanytarsus lugens* and *Orthocladius consobrinus*. These species are indicative of ultra-cold temperatures similar to those recorded from the sub-arctic (Brooks et al., 2007).

The presence of *Diamesa aberata* is indicative of cold oligotrophic conditions This species is found in the surf zone of Icelandic lakes (Brooks et al., 2007) further suggesting that the environment returned briefly to cold oligotrophic conditions (Oliver, 1983; Hoffman, 1984). This is concurrent with an increase in the counts of silica and titanium which highlights that in-washing and detrital inputs increased (Kylander et al., 2011; Corella et al., 2012). *Diamesa aberata, Microspectra radialis* and *Paratanytarsus austriacus* dominate the early stage of the LLS whilst the latter stage is composed of *Microspectra insignilobus, Psectrocladius sordidellus and Microtendipes pedullus.* From the mid LLS onwards the chironomids transition from ultra-cold to cool-temperate taxa. This same mid-phase is recorded throughout N. W Europe (Lane et al., 2013) and in the other chironomid inferred temperature records from Scotland (Brooks et al., 2016). However, some sites across Scotland, such as Abernethy Forest, show a warming throughout the LLS, and others show cooling in the latter stages, for example Loch Ashik (Brooks et al.,2012) (see chapter 9) Whittington et al (2003) identifies two distinct assemblages of beetles, indicative of cold conditions, throughout the LLS further highlighting a two-staged subdivision.

The pollen record in Clettandal however does not show any sufficient change in vegetation at this time. Whittington et al (2003) highlights that the onset of the LLS is not reflected by the pollen recorded although it is clear from the stratigraphy that there is sharp alteration in the sediment profile, from organic rich lake muds to minerogenic clays. Similarly, this is apparent in Lang Lochs as there is an abrupt rise in the counts of titanium, iron and silica at this stage which indicates that there was increased in-washing and landscape instability. However, at Loch of Clumlie (Kingsbury, 2018) the onset of the LLS is clear with a dominance of *Salix* and *Cyperaceae* indicating a return to cooler conditions. The diatom record also does not

show any assemblage change at the onset of the LLS. Whittington et al (2003) suggests that this is a result of the beetles reacting to atmospheric temperature change and the diatoms being forced by indirect climate variables such as pH and water depth. It is clear that the onset of the LLS is marked by a sharp fall in atmospheric temperatures at c.13.4k cal BP by the chironomids which highlights their usefulness for understanding environmental change throughout the LGIT.

The second phase of the LLS occurs between c.12.4-11.5k cal BP in Lang Lochs. The assemblage of chironomids is similar to the previous however there is an increased species diversity. Temperate species of chironomids increase in abundance whilst colder species gradually decline. This assemblage is composed of the following taxa: *Crictopus trifasciatus, Crictopus intersectus, Microtendipes pedullus, Microspectra insigniloblis Sergentia coracina, Psectrocladius sordidellus* and *Procladius. Microtendipes pedullus* is a species which is indicative of intermediate temperatures and is found in abundance in Holocene sediments across Europe (Brooks & Birks, 2001). The nutrient status of the lake increases to mesotrophic-eutrophic levels based upon the presence of *Procladius* (Brooks et al., 2007). Furthermore, the lake likely became more acidic as this species can tolerate decreased pH levels (Il'yashuk & Il'yashuk, 2000).

There is a sharp rise in the counts of titanium and iron, at c.12.96k cal BP, which suggests that there was an abrupt period of in-washing and allochthonous sedimentation. However, this is short lived and gradually declines until 11.6k cal BP. This in-washing phase coincides with a gradual increase in summer temperatures. Perhaps increased summer temperatures lead to an increase in snowmelt and resulted in increased sediment deposition into the lake. As the minerogenic input falls it is replaced by autochthonous sedimentation again. The organic content rises to 20% which suggests that lake productivity increased. This is affirmed by the dominance of biologically derived lacustrine muds and layers of macrofossils (*Betula nana* and *Salix herbacea*) found in the lake core. Robinson (2003) also records the presence of these plant macrofossils at this stage. This shows that other sites across Shetland saw this increase in lake productivity and macrophyte growth. Kingsbury (2018) also records this mid LLS transgression from colder to warmer conditions. *Salix* disappears from the record at Loch of Clumlie highlighting that the climate was warmer and snow cover disappeared (Wijk, 1986).

Interestingly, when the sediment core was retrieved from the field, and visually inspected, it was thought that the LLS was located between 330-325cm. However, this does not align with the chironomid inferred temperatures. Rather the C-IT model indicates that the LLS encompassed 327-298cm [Fig.75]. However, the stratigraphy locates the blue-grey clays at 330-325cm and gradually transitions into lacustrine-minerogenic rich muds. At this point the stratigraphy suggests that the LLS period ends and the Holocene begins. The chironomid record indicates that this is not the case and in fact temperatures remain cool for a further 1000 years. When combined with the titanium counts from the ITRAX it is clear that minerogenic in-washing and detrital inputs continue to enter the lake system (stopping at 298cm when the chironomids indicate warming). This highlights the need to use a multi-proxy approach to palaeo-environmental histories. Using the stratigraphy alone is not enough to record environmental change. This highlights the importance of using of chironomids for palaeoclimate reconstructions, as they clearly record aspects of environmental change that stratigraphy does not.

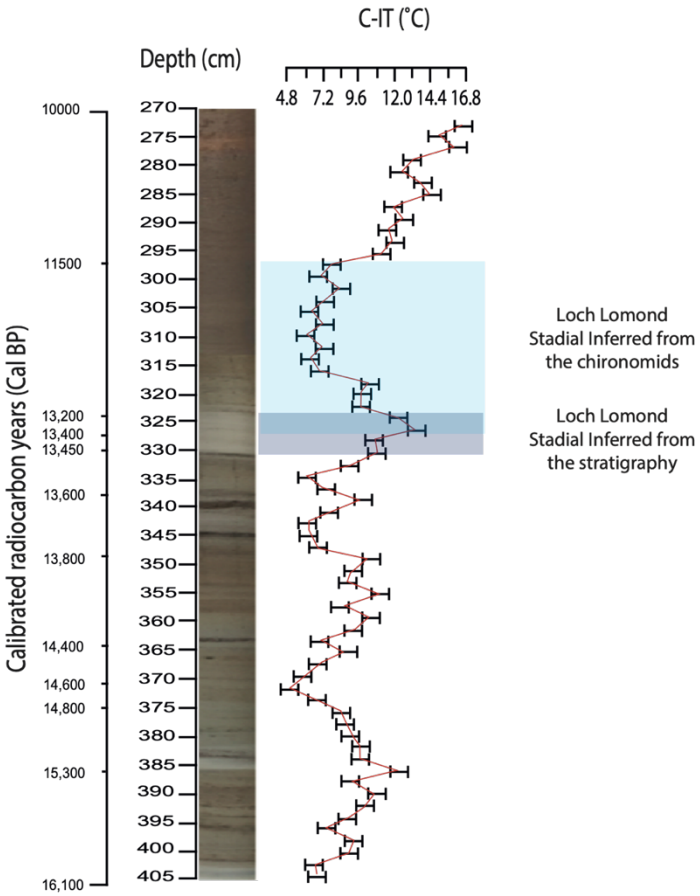

Figure 78. Offset between the stratigraphy and the chironomid inferred temperatures (˚C) for the Lang Lochs core, against the calibrated ages (cal yr BP).

6.4.8 **Holocene onset (c.11.58-10.02k cal BP)**

Temperatures sharply rise from a low of 7˚C, at the end of the LLS, to a high of 11.9˚C by c.11.58k cal BP within less than c.200 years [Fig.75]. The onset of the Holocene occurs approximately 200 years earlier in Greenland, at c.11.7k cal BP, than it does in Shetland. At Clettandal the onset of the Holocene period occurred between c.12,181-11,333 cal BP. This highlights the likelihood that this warming event corresponds to the onset of the Holocene period.

This zone is dominated by the following chironomids: *Ablabesmyia, Crictopus obnixus Glyptotendipes pallens, Glyptotendipes severini, Paratanytarsus penicillatus, Microtendipes pedullus, Paratendipes albimanus* and *Polypedulum nubifer*. The environmental conditions of the lake rapidly from sub-arctic oligotrophic conditions to temperate-warm conditions. The pH of the lake fell during this time indicated by *Glyptotendipes pallens* (an acidophilic species) (Brodin, 1986). Lake detrital levels increased during this stage suggested by the presence of *Glyptotendipes spp* (Pinder & Reiss, 1983). This species of chironomid is found in lakes which are dominated by aquatic macrophytes (Vallenduuk, 1999; Brodersen et al., 2001). This is consistent with the LOI values which gradually rise to 15-20%. Further indicating that the productivity of the lake increased. Based on the presence of this species the lake was likely mesotrophic – eutrophic during this phase (Brooks et al., 2001). *Polypedulum nubifer* is a species which is indicative of eutrophic, vegetation rich lakes (Brodersen et al., 2001; Klink, 2002).

There is a clear spike in the counts of titanium and an oxidised layer found at 275cm. Based on the timing and the position of this layer this likely corresponds to the Saksunarvatn tephra layer (Bronk Ramsey, 2015). Further tephra analysis may find this layer which would increase the resolution and robustness of the age-depth model. This puts the AMS age for Langs Loch in the same time frame, with a best age-estimate of c.11.26k cal BP. The timing of this transition is likely synchronous across Shetland and this offset is likely a result of uncertainties in the age-depth model. They record a dominance of open woodlands, grasses and herbs. At Clettandal there is no clear transition from the LLS to the Holocene period in the pollen record. As a result, the small scale pre-boreal events located in the early Holocene, found in other Scottish sites (Edwards & Whittington., 1997; Björk et al., 1997) do not appear in the record in Clettandal. The chironomid record from Langs Loch does show these small-scale

temperate changes. Between c.11-10k cal BP there are clear fluctuations in atmospheric temperatures indicated by a fall from 14.5˚ to 12.4˚C.

Between c.11.58-10.02k cal BP there is one clear short-lived abrupt cooling event at c.10.57k cal BP which lasts for approximately 400 years. Temperatures fall from a high of 14.5˚C to 12.4˚C. This is marked by a sharp increase in the abundance of the cold oligotroph *Paratanytarsus austriacus* and *Sergentia coracina.* The presence of *Microtendipes pedullus* also affirms the onset of this cold stage as it sharply increases in abundance. This species is an early colonising opportunist, highlighting that there was sufficient environmental change at this time. During this time the abundance of the temperate species drops markedly. Rasmussen et al (2014) records two cold reversals in the Early Holocene, 11.4ka event and the 9.3ka event. It is likely that this cold episode recorded in Lang Lochs corresponds to one of these two events. However, due to the low-resolution chronology at this part of the core it is not possible to name this cold stage at this point.

Hulme & Shirriff (1994) record a sharp transition between the LLS and the Holocene from their pollen record. They showed a dominance of dwarf shrubs during the cold phase which were later replaced by grasses, herbs and an open woodland at the onset of the Holocene. However, based on their record this did not occur until c.10,500 cal BP [Fig.79].

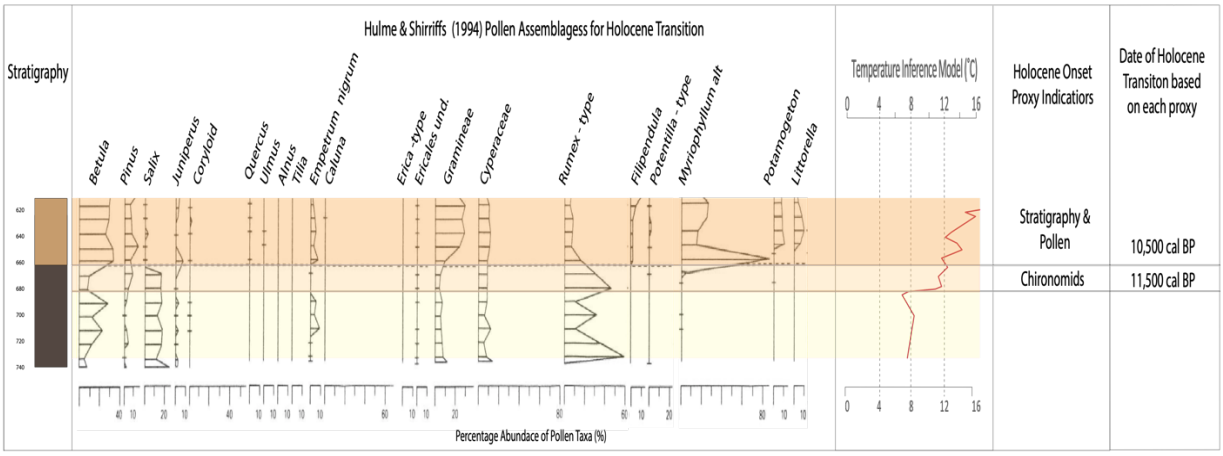

Figure 79. A synthesis diagram comparing the pollen record and the chironomid inferred mean July summer temperatures for the Holocene transition (Hulme & Shirriff, 1994)

The age-depth model, from this project, suggests that the onset of the Holocene occurred at c.11.58k cal BP, c.1k cal BP before Hulme & Shirriff (1994) pollen record. Based on stratigraphical markers, the transition from minerogenic rich clays to lacustrine lake muds and the chironomid inferred temperatures, from this study, it is clear that the chironomids respond to atmospheric warming ~1000 years earlier than the pollen record from Hulme & Shirriff (1994) [Fig.79]. This highlights the sensitivity of chironomids for palaeoclimate and environmental reconstructions.

6.4.9 **Summary**

Chironomid inferred temperatures have been modelled for Shetland, the first time for the Northern Isles of Scotland. The main climate events recorded in the Greenland ice core have also been recorded in Lang Lochs. However, the timing, duration and the magnitude of these events differ. See below the main findings from this chapter:

- The warming and cooling events throughout the LGIT occur gradually in Lang Lochs
- This is the only site in the project which records warming into the interstadial (GI-1e). Temperatures are 8.5˚C, at 15.7k cal BP, and rise gradually to 12˚C by 15.45k cal BP. Greenland lags behind Lang Lochs by 900 years at the onset of this warm phase.
- Temperatures fall again at the onset of GI-1d, occurring between c.14.8-14.4k cal BP in Lang Lochs, to sub-arctic temperatures of 6.8˚C.
- Temperatures reach a high of 10.2˚C by c.13.65k cal BP corresponding to the onset of GI-1c. Rasmussen et al (2014) divides GI-1c into three stages. However, these sub-divisions are not clear in the Lang Lochs record. The climate during this time was unstable with high amplitude short lived warming and cooling events during this time.
- There is a sharp transition into GI-1b to ultra-cold temperatures (c.13.65k cal BP). Temperatures fall to a low of 6.1˚C and the lake is dominated by oligotrophic chironomids.
- Temperatures gradually rise between c.13.5-13.4k cal BP (GI-1a) to 10.8-13.5˚C.

- Temperatures sharply fall to 6.38˚C at the onset of the Loch Lomond Stadial c. (c.13.2k cal BP). This extensive cold period lasts until c.11.6k cal BP. Halfway through the LLS temperatures gradually rise until the onset of the Holocene period. Indicating a two-staged phase of the LLS.
- Throughout the Holocene temperatures reach a maximum of 16˚C however there appears to be a short-lived cold event, lasting 500 years between c. 10.7-10.2k cal BP, where temperatures fall to 12.4˚C from 14.5˚C.

Chapter 7 - Palaeoclimate and environmental history of Orkney during the Last Glacial – Interglacial Transition.

7.0 **Introduction**

A multi-proxy analysis of Loch of Sabiston, in Orkney, was undertaken using chironomid head capsule assemblages and *m-XRF* geochemical analysis. This is the first chironomid inferred mean July summer temperature record for Orkney spanning the LGIT. This project will reconstruct the environmental and palaeoclimate history of the Sabiston basin, spanning the end of the LGM to the onset of the Holocene period in order to assess how lake chemistry, atmospheric temperature change and chironomid assemblages have changed throughout.

The Isle of Orkney is an archipelago located off northern mainland Scotland (58°42-59°25' N, 02° 22'- 03° 24' W) and due to its close proximity to the North Atlantic Ocean it is particularly sensitive to oscillations in the ocean-atmosphere systems (Brooks et al., 2016). Therefore, any climatic signals will be recorded within the terrestrial sediment archives. Sediment cores, spanning the LGIT, have been found from lakes and peat bogs in Orkney and provide a better understanding of the palaeoenvironmental history of the isles (Bunting et al., 1994; Whittington et al., 2015; Kingsbury, 2018; Abrook et al., 2019) (section 4.2.2) [Fig.80].

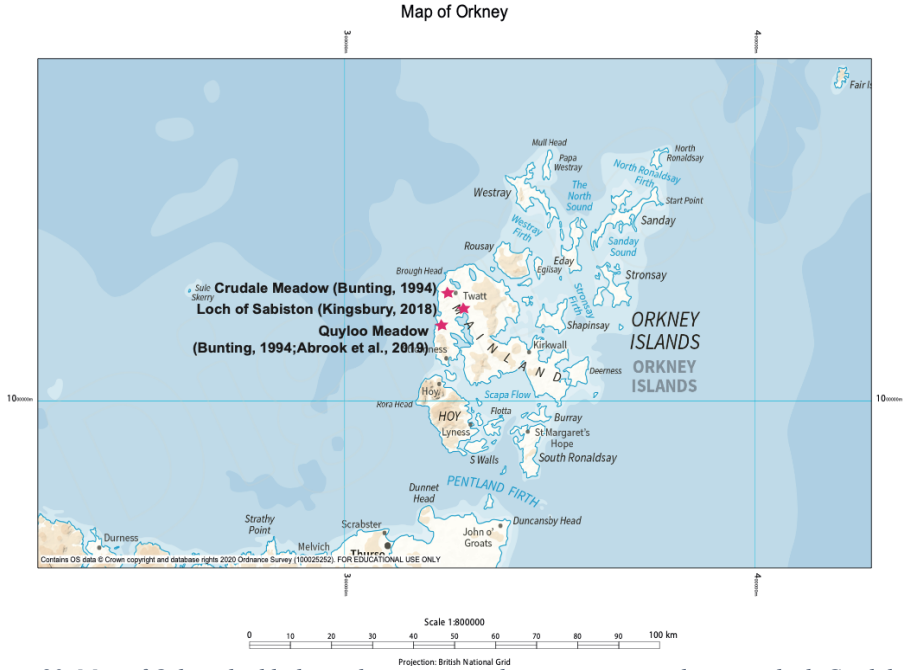

Figure 80. Map of Orkney highlighting the previous palaeo-environmental sites studied: Crudale Meadow (Bunting, 1994), Loch of Sabiston (Kingsbury, 2018; This project) and Quoyloo Meadow (Bunting, 1994; Abrook et al., 2019)

A core from Loch of Sabiston was retrieved in 2009 and has been subsequently analysed for diatoms and pollen assemblages, to better understand the palaeoecological conditions of the lake basin (Kingsbury, 2018). Currently, the Vedde and Saksunarvatn tephra's have been identified and combined with previously subsampled AMS dates to build a robust chronology (Kingsbury, 2018). As a result, this core was chosen as it has a multi-proxy record; it has a robust age-depth model and has a high sedimentation rate to allow for a high sub-sampling resolution. With the addition of a chironomid inferred temperature reconstructions a better understanding of the interaction between climate and lake ecology can be determined.

The British Isles and Ireland have a wealth of chironomid inferred temperature reconstructions (Brooks et al., 2000; Watson et al., 2010; Brooks and Langdon, 2014; Brooks et al., 2016). However, to date there are no records from Orkney. Instead, palaeotemperatures have been inferred from Loch Ashik, on the Isle of Skye (Brooks et al., 2012). Isotherm computer modelling has been the predominant method of reconstructing temperatures for the region (Brooks & Langdon, 2014). However, high-resolution independent temperature reconstructions are required to assess the accuracy of these models.

Contiguous assemblages have been identified and robust, high-resolution, sub-centennial scale records of mean July summer temperatures have been recorded for this site. Loch of Sabiston is the best constrained chronology for the Isle of Orkney. As a result, determinations of climate synchronicity are made possible (section 9.4). However, this sub-chapter will focus on the local climate and environmental history for the isle.

7.1 **Aims & Objectives**

This chapter aims to reconstruct the palaeoclimate and environmental history of the Loch of Sabiston basin by using the following objectives:

1. Reconstruct mean July summer temperatures using chironomid assemblages for the Loch of Sabiston, Orkney.
2. Use a multiproxy approach to reconstruct the environmental conditions for Orkney during the LGIT.
3. Determine the degree of similarity between the record from Loch of Sabiston and other records across the British Isles and Ireland.

7.2 Site description

7.2.1 Loch of Sabiston

As this site was previously studied by Kingsbury (2018), a full record of the LGIT is known to exist. With a full diatom, pollen and geochemical record already available this allows direct comparisons between proxies to be made. This is a prime locality to use chironomid assemblages as it will allow an assessment of synchronicity between environmental change and summer temperature fluctuations for the LGIT. Kingsbury (2018) assessed where the fullest record of the LGIT was located by taking a transect of cores across the lake using a small raft and anchors.

Loch of Sabiston (58°42-59°25' N, 02° 22'- 03° 24' W) is on the N.W coast of Isle of Orkney mainland [Fig62.], approximately 2km from the North Atlantic Ocean, making it strongly influenced by oscillations in the AMOC (Golledge et al., 2009). Loch of Sabiston has a surface area of 26 hectares, a mean depth of 0.5m, a maximum depth of 0.9m and an elevation of 17m above sea level (UK Lakes Portal, 2020) (Fig.81 & 82]. The basin is approximately 1.8km by 1.2km. To the north of the loch stands a steep sided hill which rises to 105m. The lake is runoff and groundwater fed as there are no rivers present in the basin. There are small streams to the south-east of the catchment surface feeding into the lake and a spring located to the east of the loch. The topography is flat which has been recently used for agriculture and peat cutting.

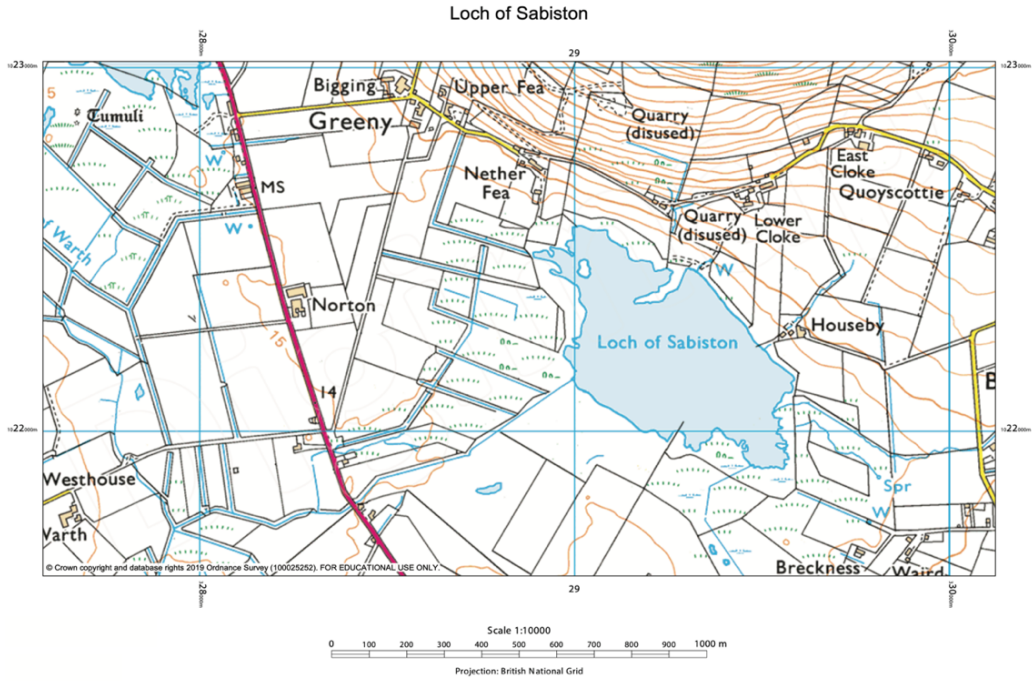

Figure 81. OS map of the Loch of Sabiston. Scale 1:10000m (Edina Digimap, 2020)

Figure 82. Aerial view of the Loch of Sabiston basin. Steep sided hill to the north and stripped farmland surrounding the loch (Google Earth, 2020)

7.2.2 **Geological setting: local and regional**

Across Orkney, peat bogs and unconsolidated glacial sediments overlie Devonian sedimentary rocks, from the Caithness Plateau, (Bunting, 1996; Ballantyne et al.,2007). The sediments in the basin are composed of glacial alluvial and till which have been reworked from the underlying calcium carbonate rich siltstones and shales (of the Lower Stromness Flagstone formation).

To the north of Loch of Sabiston lies the Sandwick Fish Bed Member formation [Fig.83]. This lithological unit is rich in calcium carbonate which leads to the precipitation of marl in the lake. Runoff and erosion from the surrounding hills likely transport carbonate rich material into the basin which dissolves into the water column. Combined with the percolation of groundwater, from the water table, calcium is transported into the lake. During periods of warming the calcium precipitates out of solution and forms the calcium carbonate rich marls seen throughout the core.

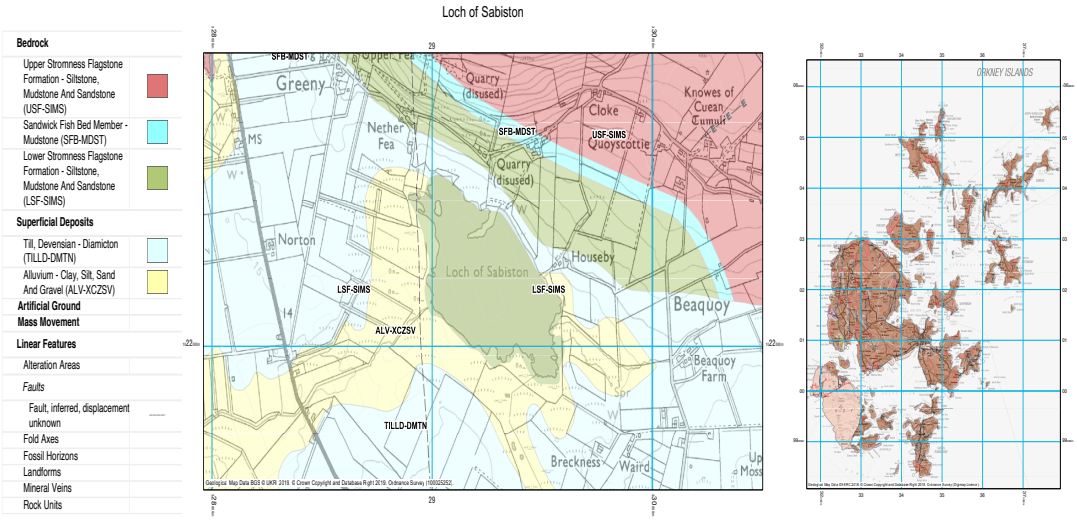

Figure 83. Site specific geological map for the Loch of Sabiston catchment. Upper Stromness Flagstone group (red), Sandwick fish beds (blue) and siltstone (green). Linear features highlighted to show the position of fault lines. An overview of the geology of the Isle of Orkney is also shown on the right highlighting that it is dominated by old red sandstone with the Island Hoy being composed of Igneous rocks.

7.2.3 **Basin characteristics, Land-use & Vegetation**

Loch of Sabiston is dominated by a fen edge to the west, with natural grassland and marsh surrounding the rest of the lake. The depth at which the core was taken was at 0.72m (Kingsbury, 2018). The water temperature was recorded to be 11.9˚C with a pH of 8.18 (Kingsbury, 2018). See the table below for the environmental conditions recorded in June (2012) when the lake core was taken [Table.9]

Table 9. The lake variables recorded by Kingsbury (2018) in June (2012) for Loch of Sabiston. Highlighting the depth(m), area (ha), temperature (˚C), conductivity (µS cm^{-1}), altitude (m a.s.l) and pH

Depth (max)	0.72 m
Area	~ 24 ha
Temperature	11.9 °C
Conductivity	347 µS cm^{-1}
Altitude	27 m a.s.l.
pH	8.18

At present the lake is dominated by autochthonous sedimentation and aquatic macrophytes. The main vegetation which dominate are the following: *Phragmites*

australis and Cyperaceae spp. In addition, charophyte algae are also abundant in the lake (Kingsbury, 2018). Charophytes are known to inhabit lakes that are dominated by calcium in the water column (Wiik et al., 2013).

The slopes are gentle in the catchment. However, there is a hill to the north-east which may channel run-off into the lake. There is evidence of past human activity in the lake and at the lake edge with the remnants of a crannog and steppingstones (Kingsbury, 2018). In addition, a disused quarry to the north of the loch and farms surround the edge of the basin, which are used to this day. Land-use at present is intensive with the catchment being separated into fields for various agricultural purposes [Fig.84]. As a result, the drainage system is man-made currently. The fields are primarily used for grazing livestock.

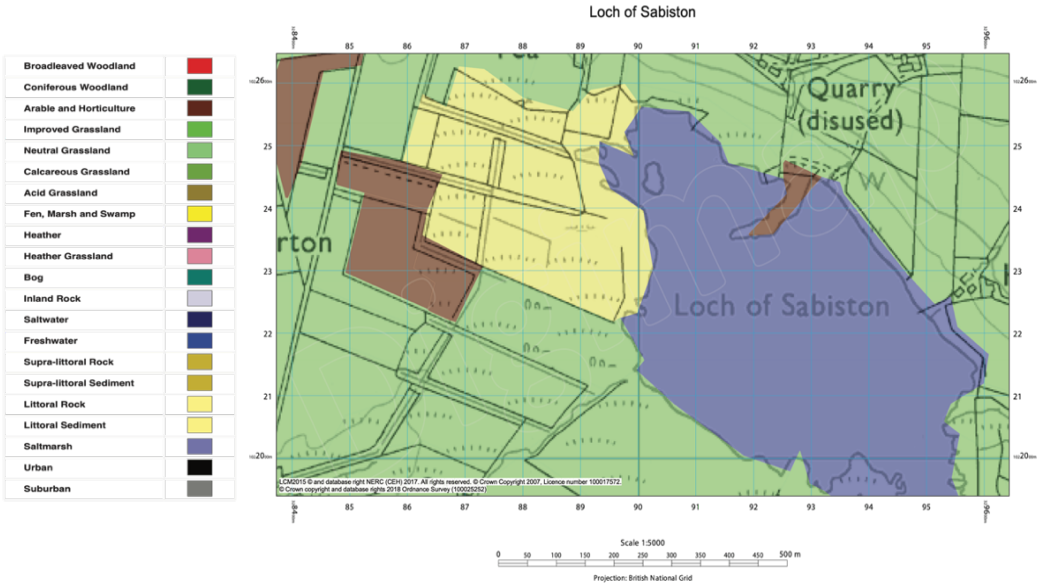

Figure 84. Environmental biome map and soil characteristics of the Loch of Sabiston catchment area (CEH Land Cover Map, Edina Digimap, 2020)

7.2.4 **Present Climate**

Temperatures range between 1.9˚C in the winter and rise to a high of 16˚C in the summer, wind speeds reach a high of 13.5 knots and the region has an average rainfall of 1039mm per year (Kingsbury, 2018; Windfinder., 2020). The high winds are a result of low-lying relief and a lack of vegetation. Presently, the climate can substantially vary between the summer and winter months. As a result, this highly sensitive region is a prime locality to study past climate oscillations. At the time of the field excursion (June 2012) summer atmospheric temperatures were 11.9˚C (Kingsbury et al., 2018). This

provides a baseline of modern-day temperatures to compare to those inferred from this project. The climate of the Isle of Orkney is strongly influenced by fluctuations in the North Atlantic Current, thermohaline circulation and the North Polar Front resulting in wet mild summers and cool winters (Bunting, 1994).

7.3 Results & Interpretation

7.3.1 Lithology and Geochemical Analysis

Kingsbury (2018) recorded the organic content of the core through LOI [Fig.85] and analysed the geochemical composition of the sediments through *Micro*-XRF (ITRAX) analysis, highlighting the trace composition of the inorganic and organic trace elements. However, the graphical visualisations and interpretations made in this research is original. An analysis of the counts of Iron (Fe), Titanium (Ti), Silica (Si), Calcium (Ca), Phosphorus (P) and Potassium (K) were recorded to assess lake nutrient levels, productivity, underpin potential crypto-tephra layers and determine the sources of organic and minerogenic material (section 5.7) [Fig. 86].

(1) **First organic rich layer** (420-365cm): the first section of the core is dominated by fine-medium grained lacustrine silts. The sediments are fine brown-grey and have low counts of calcium. The counts of iron are high at 420cm which indicates a dominance of minerogenic sediments. Iron counts fall gradually from 420cm to 365cm. There are notable spikes in iron at 380cm and 370cm possibly indicating tephra layers (Kylander et al., 2012). Phosphorus counts rise abruptly from 420cm and reach a maximum at 385cm. Potassium, silica and titanium counts are high at 420cm and gradually fall at 380cm. The organic content of this unit is low (2-4%) as it is dominated by minerogenic-lacustrine rich muds. There is a spike in the organic content at 375cm and the geochemistry indicates that there is a gradual increase in the productivity in the lake system throughout this time.

(2) **First Minerogenic Layer (**365-350cm): this minerogenic rich layer is dominated by blue-grey fine silts and clays. Calcium counts begin to increase at the end of this unit (360cm) from low to intermediate counts. A gradual increase in the levels of calcium suggests that the lake was beginning to warm

gradually coinciding with an increase in productivity in the lake (Lauterbach et al., 2011). Between 365-350cm there is a sharp rise in the counts of potassium and titanium indicating an increase in minerogenic in-washing and erosion into the lake (Kylander et al. 2011). Phosphorus counts remain at similarly high levels to the previous layer. At 375cm there is a layer of undifferentiated plant fragments which is recorded by a rise in organic content to 10.2% at 375cm.

(3) **First Marl Layer** (350 to 330cm): this unit is dominated by fine-medium grained yellow-brown calcium carbonate rich marl. There is a sharp reduction in the levels of iron, titanium, phosphorus and silica. The increase in calcium values suggest that lake temperatures increased also leading to the precipitation of the calcium carbonate rich marls found in this unit. A sharp increase in the levels of calcium coincide with an increase in productivity within the lake system (Lauterbach et al., 2011). Phosphorus counts are low in this sedimentary unit also. The organic content of this unit starts low and rises at the end of the unit to 8% further indicating that lake productivity began to rise.

(4) **Second Minerogenic Layer** (330 to 324cm): this unit consists of fine-grained blue-grey silts. Calcium values sharply fall at the onset of this layer. A reduction in the levels of calcium is noted which suggests that the lake temperatures and primary productivity within the lake decreased (Lauterbach et al., 2011). This is synchronous with an increase in titanium, iron, silica and potassium values, indicating a return to minerogenic in-washing into the lake catchment at this time (Kylander et al., 2011). Furthermore, there is a single sharp peak of phosphorus within this layer which may correspond to an unidentified layer of cryptotephra. The organic content of this unit is low ranging between 4-5% which suggests that primary productivity and autochthonous sedimentation was lower.

(5) **Second Marl Layer** (324 to 314cm): this layer is dominated by fine-medium grained calcium carbonate rich marl. Once again there is a sharp reduction in the levels of iron, titanium, phosphorus and silica within this unit. The calcium increases markedly, highlighting an increase in the concentration of autochthonous sedimentation (Balascio et al., 2011) and increasing lake

temperatures (Lauterbach et al., 2012). The organic content of this unit rises to 6.5-8%. Lake productivity was still relatively low however, an increase in the LOI suggests that there was a gradual increase in organic matter in the lake at this time.

(6) **Third Minerogenic Layer** (314cm to 275cm): this layer is composed of fine-medium grained blue-grey silts and clays. Calcium values sharply fall at the onset of this layer. This reduction in the levels of calcium is evidence that lake temperatures began to fall which coincides with a drop in primary productivity (Lauterbach et al., 2011). This is synchronous with an increase in titanium, iron, silica and potassium values. Potassium and silica values are high at the onset of this unit and gradually fall whereas, silica values remain consistently high. Increased counts of titanium suggest an increase in catchment run-off (Haberzettl et al., 2005). This change in environmental conditions is believed to be linked to increasing inputs of detrital material (Kylander et al., 2011). Phosphorus levels are high at the onset of this unit and gradually increase by 275cm. At 290cm there is a noticeable brown layer which has high levels of titanium and iron with a subtle rise in calcium values. The organic content is low, with values of 4%, throughout this unit however it rises to 8% by the end of this minerogenic layer. Primary productivity and vegetation increase throughout this time.

(7) **Third Marl Layer** (275cm to 180cm). This layer is composed of fine-medium grained calcium carbonate rich marl. There is a gradual change from minerogenic rich sediments to the onset of the final marl unit. Calcium values abruptly rise highlighting an increase in lake temperatures and associated primary productivity. Similar studies have shown that this can correlate with a rise in autochthonous material (Balascio et al., 2011; Lauterbach et al., 2012). Whereas, there is a sharp reduction in the values of titanium, silica and potassium. This zone has low counts of silica which suggests that detrital inputs decreased also (Martin-Puertas et al., 2011; Marshall et al., 2011). At 250cm, 235cm, 230cm, 220cm and 210cm there is a sharp rise in the values of iron and titanium which may indicate the presence of potential tephra shards.

(Kylander et al., 2012). LOI values range between 2.8-4.2% which suggests that the lake was low in macrophytes and had reduced productivity.

(8) **Summary.** The Loch of Sabiston core is split into distinctive bands changing between minerogenic rich clays and marl lacustrine muds, indicating a sharp transition between minerogenic in-washing and autochthonous sedimentation. Increased calcium counts indicate a warm productive lake ecosystem prevailed. The organic content of the core is relatively low throughout the marl rich sediments and the minerogenic rich clays. There are notable spikes at 270cm, 275cm, 290cm, 325cm, 336cm and 372cm indicating layers of organic rich material which have been used for AMS dating. Throughout the core there are spikes in phosphorus and titanium indicating the presence of potential cryptotephra layers not yet identified.

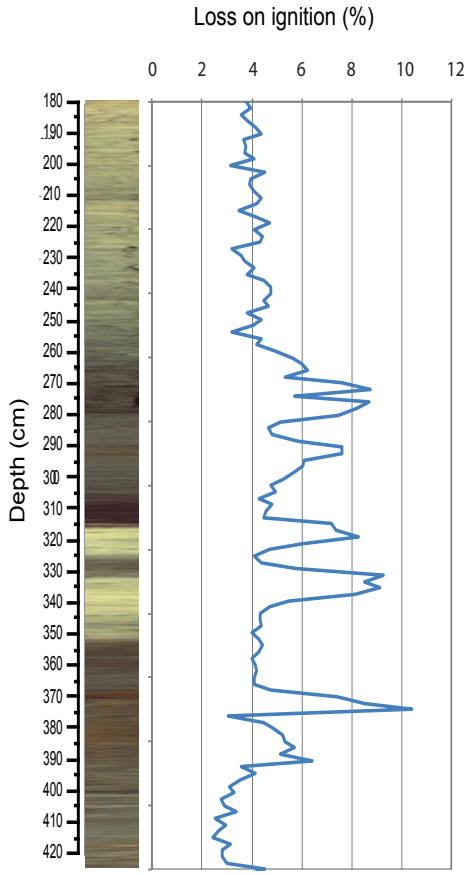

Figure 85.. Loss on ignition for the Sabiston core. Depth (cm) and the lithology shown on the right (Kingsbury, 2018)

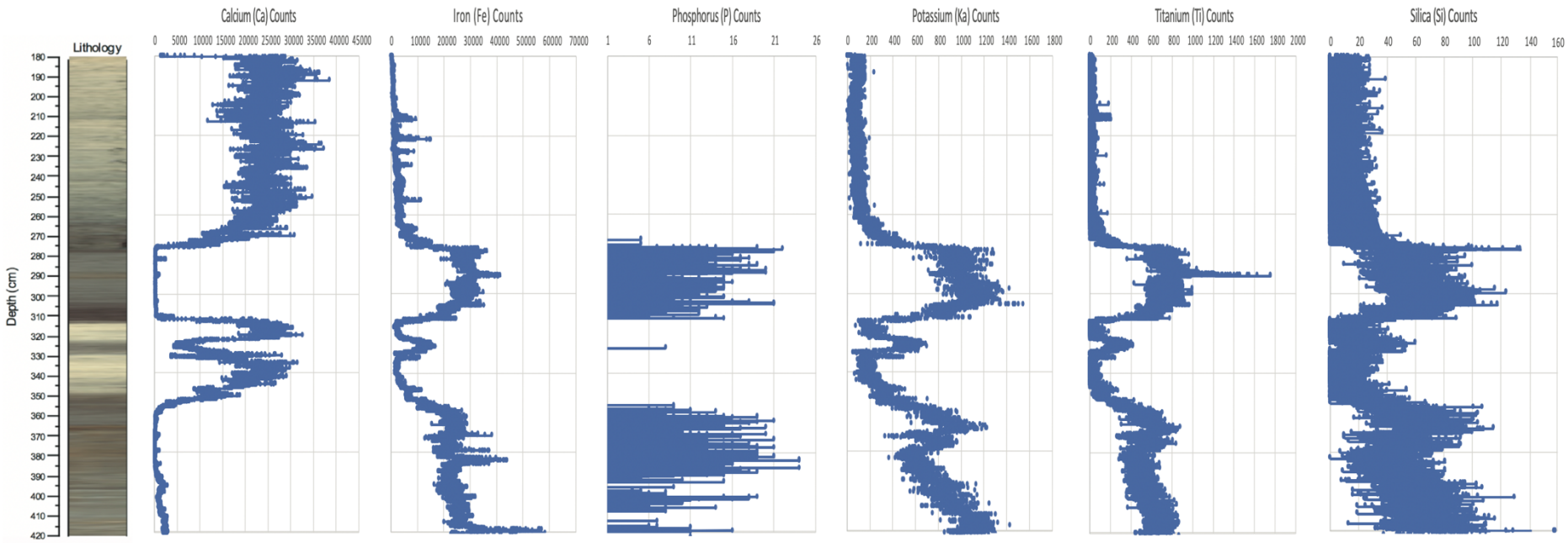

Figure 86. Micro-XRF analysis (undertaken at Aberystwyth University, Wales) highlighting the major trace elements, both organic and inorganic, for the Loch of Sabiston core. Depth (cm) is highlighted on the Y-Axis and the number of counts of each element is shown

7.3.2 **Chronology**

Four AMS dates and four tephra layers were used in the construction of the independent age-depth model for Loch of Sabiston [Table.10 & Fig. 87]. The calcium carbonate rich marl sediments have been known to provide inaccurate ages due to the influence of old carbon into the lake. This has been shown from a core taken from Clettnadal on Orkney (Whittington et al., 2015). Furthermore, the dates were calibrated using Calib 7.10 (Stuiver and Reimer, 1993) to assess what samples were outliers, age-reversals or had dates that were too old. The AMS dates used in the project were known to be composed of terrestrial plant fragments and/or had isotopic values indicative of terrestrial plant fragments (ranging between -25-30‰) (Ascough et al., 2010). These dates were subsequently modelled to determine if they had reliable ages by comparing them to known stratigraphical boundaries in the core and the NGRIP record (Rasmussen et al., 2014).

Table 10. AMS radiocarbon samples. Sample ID, depth (cm), measured age, calibrated years (95.4%) (with median), ∂12C/13C and sample code.

Laboratory code	Depth (cm)	Material	$\delta^{13}C_{VPDB}$‰ (± 0.1)	^{14}C yr (1σ)	Calibrated age range (95.4%) cal yr BP with median*
BORO-TEPHRA	383	TEPHRA			**14098± 47**
PEN-TEPHRA	361	TEPHRA			**13939 ± 66**
SUERC-67380	355	Plant Fibres	-23.6	11988 ± 48	13731-(13838)-14003
SUERC-67381	330	Plant Fibres	-25.3	11074 ± 44	12807-(12941)-13061
VEDD-TEPHRA	293	TEPHRA			**12023 ± 43**
SASK-TEPHRA	212	TEPHRA			**10176 ± 49**
SUERC-67388	115	Plant Fibres	-25.5	4790 ± 38	5465-(5519)-5601
SUERC-67389	100	Plant Fibres	-22.9	3460 ± 36	3638-(3730)-3832

Cryptotephra were also used as tie-points to constrain the chronology (section 5.8). The geochemical analysis and morphology of the shards confirmed the presence of four tephra layers: the Borrobol tephra (c.14.10k cal BP), the Penifiler tephra (c.13.94k cal BP), the Vedde ash (c.12.02k cal BP) and the Saksunarvatn tephra (c.10.18k cal BP) [Fig.87 & 88]

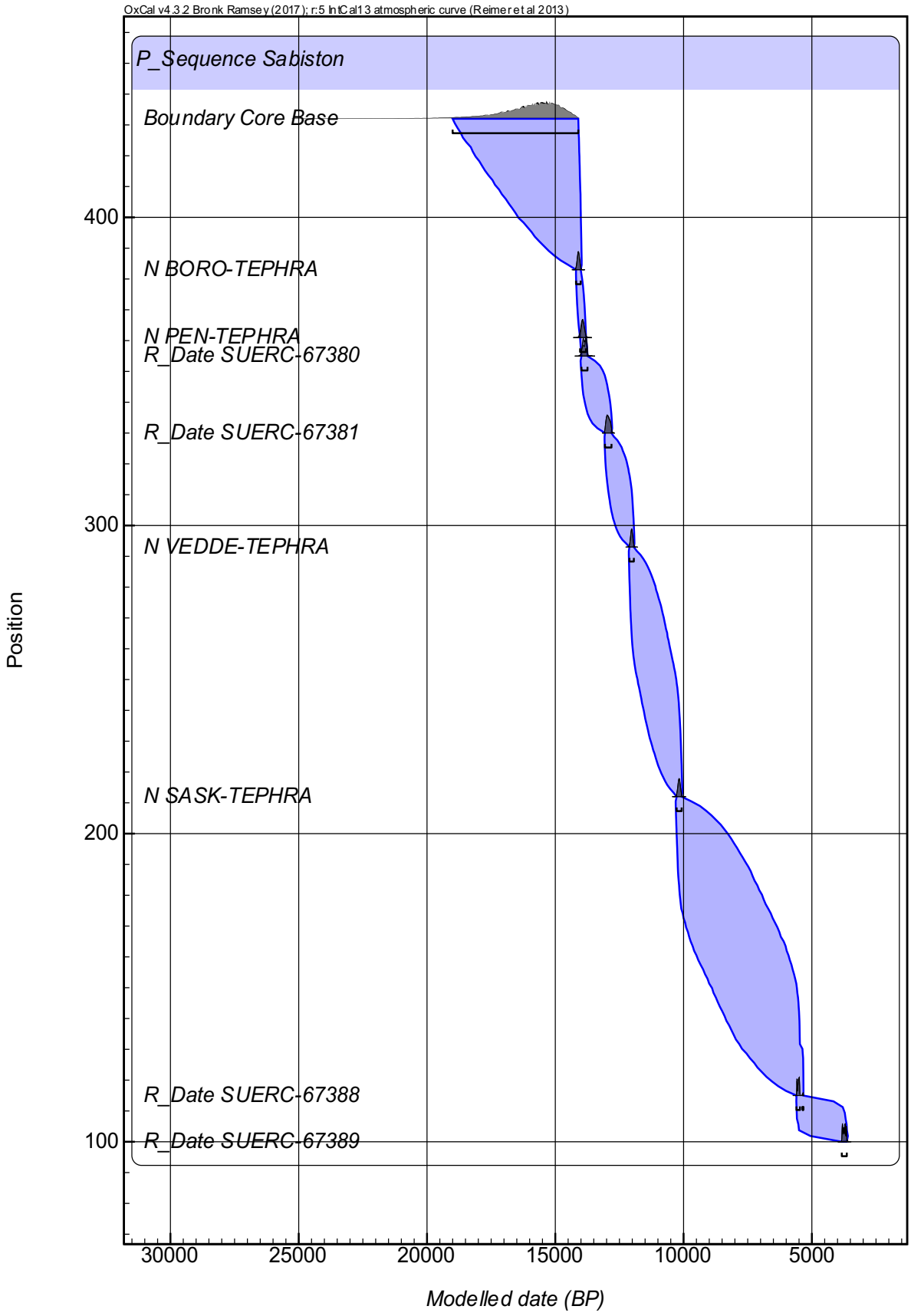

Figure 87. Age-depth model for Loch of Sabiston. Depth on the Y-axis and the modelled age (cal yr BP) on the x-axis. The blue lines highlight the extent of the 2 sigma errors.

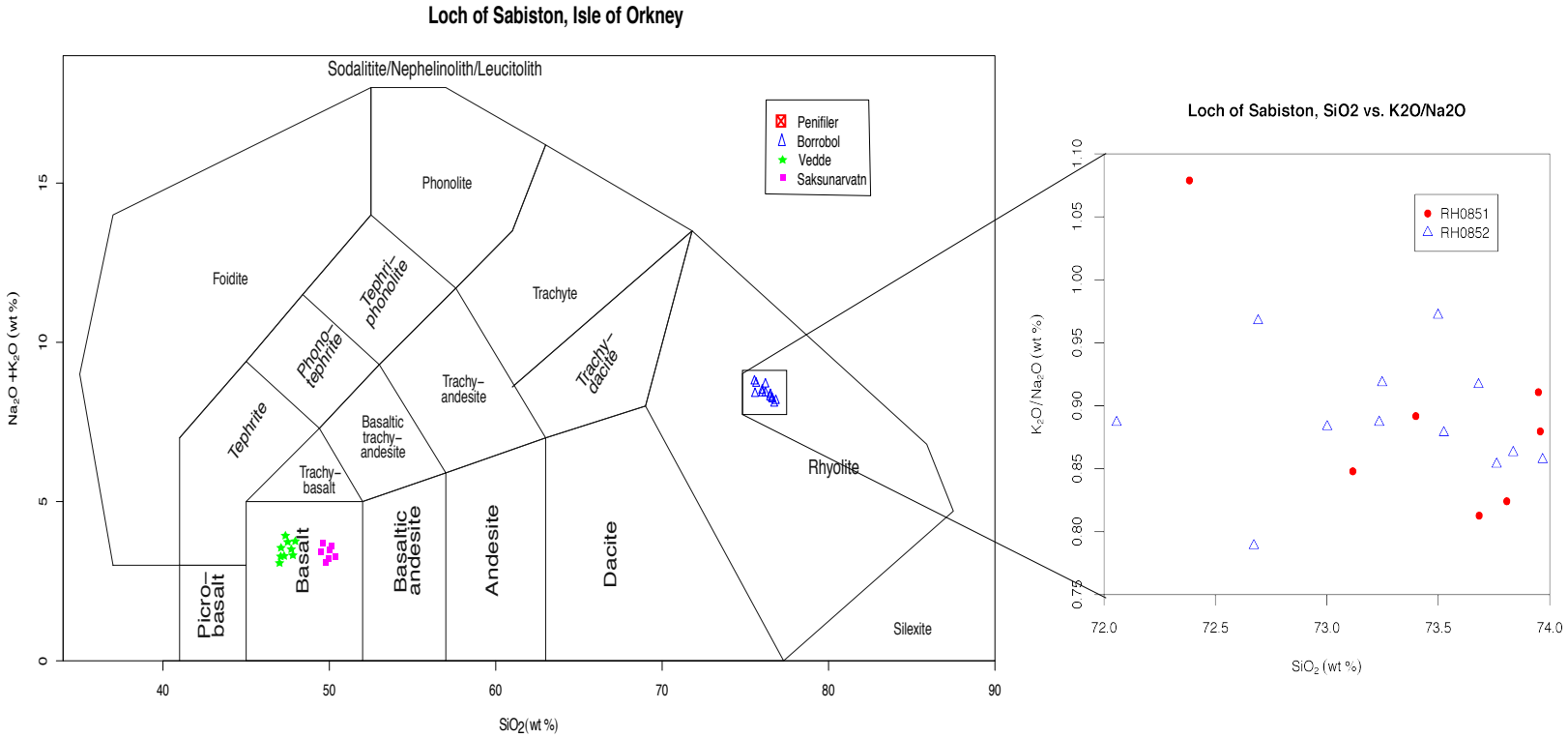

Figure 88. TAS geochemical plots indicating the composition of the Penifiler, Borrobol, Vedde and Saksunarvatn tephra layers for Loch of Sabiston. The composition of the Penifiler and Borrobol tephra are similar and have to be identified using their stratigraphic position in the core, shard morphology and characteristic geochemistry.

7.3.3 **Chironomid head capsule assemblages**

A total of 58 chironomid taxa were identified to genus level [see Appendix], with many being sub-divided to species level. Eight significant zones were determined, with 3 sub-divisions, using a statistical assemblage partitioning function (CONISS) [Fig.89]. From 420cm to 385cm samples were taken (every 4-8cm) at a lower resolution due to low numbers of chironomids being retrieved and a lack of change in the overall composition of the assemblage. From 385cm until 215cm, samples were taken at 2cm intervals in order to track the changes of chironomid assemblages throughout each zone. Between lithological boundaries samples were taken every 1cm, to assess high resolution assemblage changes across varying environmental gradients. Each zone is partitioned using CONISS and the modelled environmental conditions are shown.

- **Zone Sab-1 (420-365cm)** is dominated by cool-temperate chironomid taxa: *Ablabesmyia* (10%), *Microspectra pedullus* (25-58%), *Tanytarsus pallidocormis* (18-24%), *Psectrocladius septentrionalis* (5-25%) and *Chironomous anthracinus* (20-40%). The presence of *Microtendipes pedullus* and *Psectrocladius septentrionalis* indicate an environment low in organics with a dominance of littoral to sublittoral lithologies (Brodersen & Lindgaard, 1997). The presence of *Ablabesmyia* and *Tanytarsus pallidocormis* indicates that the lake was acidic and that aquatic macrophytes were found in the lake (Pinder & Morley, 1995; Brodersen et al., 2001). The presence of *Psectrocladius septentrionalis* and *Chironomous anthracinus* suggests that intermediate temperatures dominated (Brodin, 1949; Brooks et al, 2007). During zone Sab-1 temperatures have been inferred to be intermediate-warm ranging between 11-13˚C.

- **Sab-2 (365-315cm)** there are 3 significantly distinctive zones (Sab 2a-c).
    - The first subdivision, Sab-2a, is found between the depths of 365-350cm. The assemblage consists of chironomids indicative of cool-temperate taxa. The dominant taxa are *Microspectra radialis* (30%), *Paracladius* (20-25*%), Corynocera oliveri* (10-25%), *Microspectra pedullus* (10-20%), *Chironomous anthracinus* (10-18%) and *Microspectra insignilobus* (10-18%) are present. These species indicate an environment similar to ultraoligotrophic arctic lakes found in the present day and are often found

during cold events across the LGIT (Brooks et al., 2007). The abundance of *Microspectra pedullus* increases at the onset of this zone indicating an abrupt change in the environment. The C-IT model indicates that temperatures reached a low of 6.5˚C.

- Zone Sab-2b (330-350cm) is the next significant zone which contains cool-temperate chironomid taxa including *Microtendipes pedullus* (5-10%), *Sergentia coracina* (20-45%), *Psectrocladius septentrionalis* (10-30%), *Corynocera ambigua* (35-60%), *Procladius* (15%) and *Ablabesmyia* (5-10%). The abundance of early colonisers (*Microtendipes pedullus* and *Corynocera ambigua*) spikes at the onset of this zone indicate a sharp change in the environment. Both species fall in abundance throughout this zone indicating a stability in the environment and increase in chironomid diversity. The abundance of *Sergentia coracina* and *Psectrocladius septentrionalis* increases, indicating cold oligotrophic lake conditions. Temperatures start low at 7˚C and rise gradually to 9.5˚C

- Sab-2c (315-320cm) contains a mix of both of the previous subdivisions. These chironomids indicate that warm and cold conditions prevailed. With cooler temperatures occurring at the start of the zone and warmer conditions at the end. The assemblage is dominated by *Orthocladius consobrinus* (10%), *Microspectra radialis* (18%), *Orthocladius trigonobalis* (16-18%), *Paracladius* (20%), *Sergentia coracina* (15-40%) and *Corynocera ambigua* (15-60%). *Microspectra pedullus* (22%), *Tanytarsus mendax* (10%), *Ablabesmyia* (10%) and *Procladius* (15-18%) are found at the top of this zone. *Ablabesmyia* is a species of chironomid which indicates that the lake was acidic and that macrophytes dominated (Brodin, 1986; Brodersen et al., 2001). Sab-2c is indicated by a sharp increase in the presence of *Corynocera ambigua*. This is an opportunistic species which has been known to be an early coloniser, often occurring in large concentrations between environmental and lithological boundaries (Brooks et al., 2007). The species dominates 40-60% of the overall assemblage suggesting that there was a significant change in the nutrient status and chemical composition of the lake (Brooks et al., 2007).

- Sab-2 has been separated into three distinct zones. Temperatures fall at the onset of Sab-2a to a low of 6˚C which suggest that stadial conditions were apparent. Whereas, Sab-2b shows a very gradual decline in temperatures from a high of 11˚C to a low of 7˚C at its termination. Sab-2c is the third distinct zone which is further split into 2 stages. The first half of Sab-2c has low temperatures ranging from 7-8˚C whereas the latter half reached a high of 12˚C.

- **Sab 3 (315-280cm)**. This assemblage is composed of *Orthocladius consobrinus* (15-20%), *Hydrobeanus conformis* (10-35%), *Microspectra radialis* (30-40%), *Orthocladius trigonobalis* (30-40%), *Paracladius* (5%), *Microspectra insignilobus* (10-20%), *Crictopus intersectus* (15-30%), *Sergentia coracina* (15-20%) and *Tanytarsus lugens* (5-10%). These species indicate the lake was low in nutrients and was similar to lakes found in the sub-arctic (Brooks et al., 2007; Andersen et al., 2013). This zone is split into two distinct zones inferred by the dominance of ultracold oligotrophic chironomids at the latter half of the zone. An increase in *Orthocladius consobrinus* and *Microspectra radialis* concentrations indicates that colder temperatures prevailed. The cold stenothermic chironomids (*Paracladius, Orthocladius consobrinus* and *Orthocladius trigonobalis*) increase in the latter half of the zone and suggest that an oligotrophic lake with sub-arctic conditions prevailed (Brooks et al., 2007). Within Sab-3 temperatures fall, ranging between 5-6˚C in this zone.

- **Zone Sab-4 (255-280cm)** is the next significant zone. Sab 4 indicates a sharp increase in the quantity of warm-temperate taxa such as *Microtendipes pedullus (20-30%), Tanytarsus glabrescens (10-15%), Dicrotendipes nervosus (5-10%), Procladius (15-20%), Ablabesmyia (10%) and Tanytarsus lactescens (10-15%). Psectrocladius sordidellus and Psectrocladius septentrionalis* are also present which suggests that colder water conditions prevailed. The chironomids *Ablabesmyia, Tanytarsus lactescens* and *Microtendipes pedullus* and *Chironomous anthracinus* are found before stratigraphical changes as they are known to be an early colonising species (Watson et al., 2010). The abundance of *Tanytarsus lactescens* increases throughout this zone indicating temperatures

increased further. Throughout Sab-4 the C-IT model shows that temperatures significantly increase from a low of 5-6˚C to a high of 13˚C.

- **Zone Sab-5 (255-215cm)** has a similar composition as Sab-4, as cold-temperate species of chironomids dominate the overall assemblage: *Psectrocladius septentrionalis (15-40%), Microtendipes pedullus (8-18%) Tanytarsus glabrescens (25-55%), Dicrotendipes nervosus (20%), Procladius (10-20%), Ablabesmyia (10%) and Tanytarsus lactescens (5-20%)*. There is a gradual increase in the counts of *Tanytarsus glabrescens* which indicates that temperatures rose throughout this zone. However, there are also cold oligotrophs found at 240cm and 215cm indicating short-lived cooling occurred. Temperatures fall to 10.5˚C during these cold phases. The dominance of these cold taxa at these points coincide with a reduction in the abundance of *Tanytarsus lactescens*. Temperatures steadily rise in Sab-5 reaching higher temperatures ranging between 15-16˚C.

- **Zone Sab-6 (180-215cm)** is composed of the warmest chironomid species found in the Loch of Sabiston core: *Tanytarsus glabrescens* (10%), *Dicrotendipes nervosus* (10%), *Procladius* (10%), *Ablabesmyia* (5-8%), *Tanytarsus lactescens* (25-35%) and *Polypedulum nubifer* (22%). *Tanytarsus lactescens* is found in carbonate rich lakes (Brooks et al., 2007). These species are indicative of nutrient rich eutrophic lakes in temperate-warm settings. Throughout Sab-6 temperatures fall from 16˚C to 10˚C. Higher resolution sub-sampling is required to record the small-scale temperature changes in this part of the core.

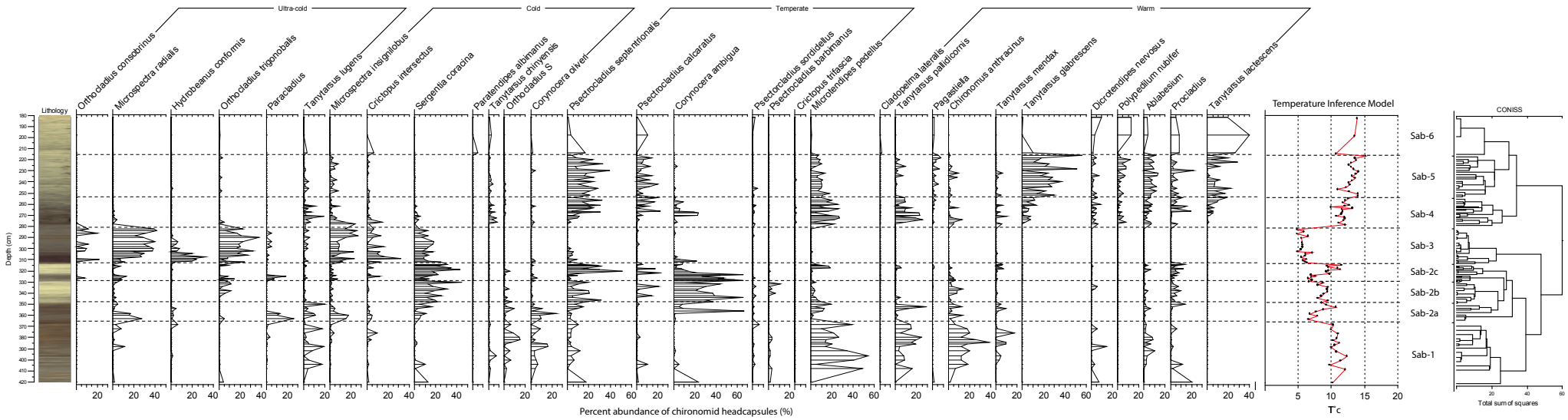

Figure 89. The chironomid assemblage plot highlighting the dominant species. Ultra-cold species are shown to the left of the graph, transitioning to cold, then temperate and finally showing the warm species to the right (%). Zones separated by CONISS

7.3.4 **Reliability of the C-IT model**

To assess the reliability of the chironomid inferred temperature inference model the occurrence of modern-day chironomids were compared to the fossilised species in the Loch of Sabiston core using the Norwegian training set (Brooks and Birks, 2001). A modern analogue technique (MAT) was used to assess if the chironomid fossil assemblage was similar to those found in present day. Also, a goodness of fit determination was used to assess if the chironomids in Loch of Sabiston had a good fit to temperature (Birks et al., 1990; Brooks and Langdon, 2001; Brooks et al., 2016). The results indicate that 67 out of 103 chironomid assemblages had either a good or poor analogue with the modern-day Norwegian training set. 28 samples are in the range of the 2nd and 5th percentile, indicating poor modern analogues. There are 36 chironomid assemblages that have no modern analogue. Samples which have no modern analogues are have a no similarity to the Norwegian training set. Regardless, samples can have no modern analogues but can still have a reliable fit to temperatures (Birks et al., 1998). Therefore, the reliability of the temperature inference model is still thought to be good even though 36 samples have no modern analogue. The samples with no modern analogues are found in the marl rich sediments in Loch of Sabiston. This may suggest that the calcium in the lake is having a greater control of the chironomid assemblages than temperature at this time and/or that marl lochs are rare in Norway.

Finally, of the 103 samples taken from the Loch of Sabiston core, only 2 of the samples have rare types which exceed 5% of the overall head capsule assemblage. These two samples have a high abundance of *Corynocera ambigua*. This species is rare in the Norwegian training set however common in the Isle of Orkney at this time. Where species have a narrow ecological/ temperature optimum they have a greater impact on the inferred temperature models. They are known to skew temperature inference models if the species is rare in the training set however common in the fossil assemblages. This is one of the downsides of using the weighted-average partial least squares (WAPLS) function [Fig.90]. The sample specific inference errors are shown below highlighting the narrow temperature ranges modelled.

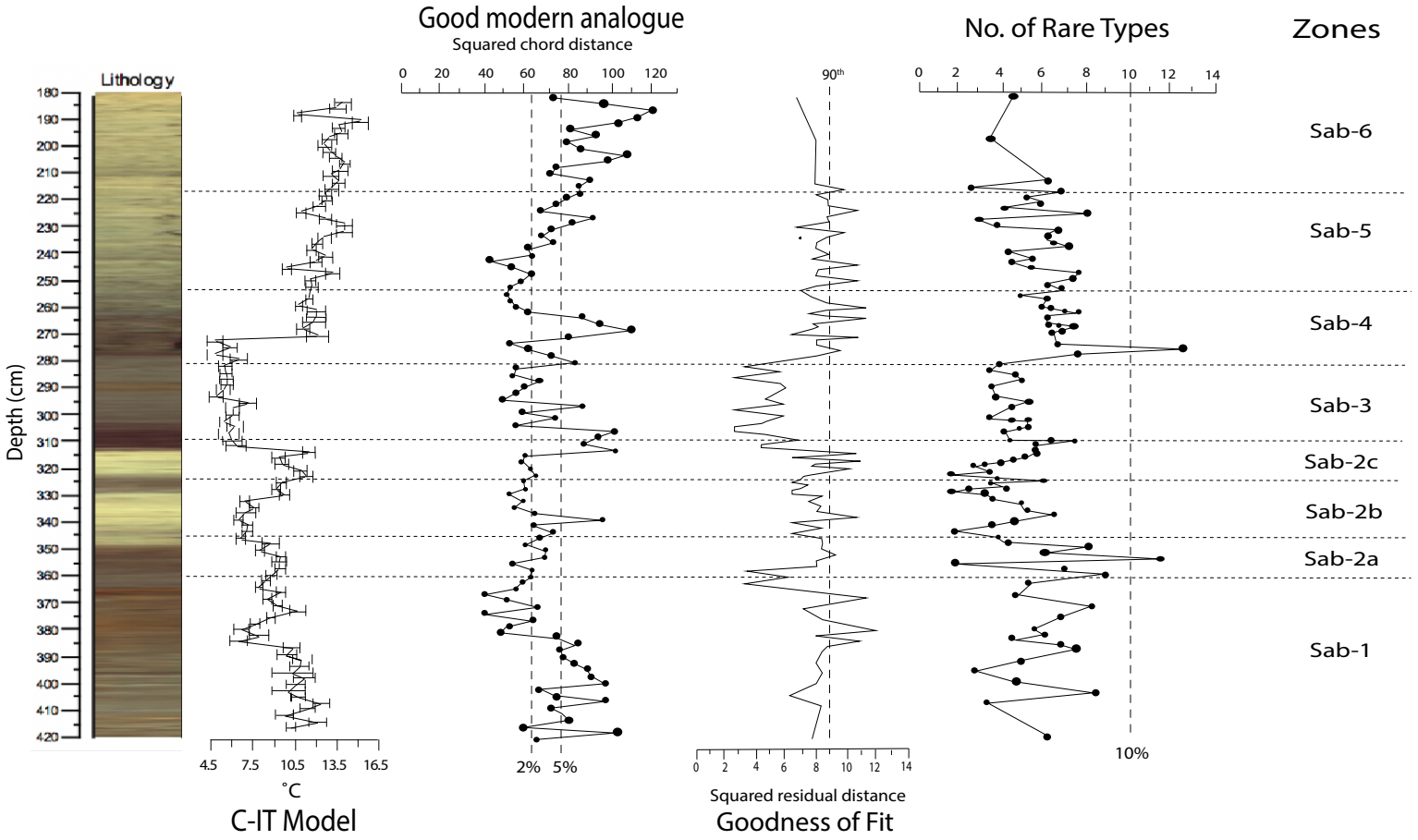

Figure 90. The C-IT model (˚C) with the sample specific errors, Good modern analogue (2% and 5% cut-off), Goodness of fit to temperature and the number of rare types. Zonation built with CONISS. Depth (cm) and core shown to the left

7.4 Discussion

7.4.1 Palaeoclimate & environmental history of Loch of Sabiston, Orkney

The paleoclimate and environmental history of Loch of Sabiston was assessed using a combination of chironomid inferred temperatures and micro-XRF from this project [Fig.92]. Chironomid assemblages have provided a high-resolution image of the mean July summer temperatures, for Loch of Sabiston, combined with a robust high resolution, AMS and tephra-based, chronology [Fig.91].

The discussion will focus on the relationship between chironomid assemblages, the inferred mean July summer temperatures and the geochemistry of the lake basin with the overall aim to record the palaeoclimate and environmental changes across the LGIT for the Sabiston catchment. It will now also be possible to determine if climate fluctuations were synchronous with the diatom and pollen record from Kingsbury (2018) for the same core. By comparing the records from Loch of Sabiston to the other studied localities, it is possible to gain a better understanding of regional scale climate and environmental changes [Fig.93] (Whittington et al., 2015; Kingsbury, 2018; Abrook et al., 2019). Below in-depth interpretations of the main climatic events will be shown using the proxies/literature highlighted from Orkney and compared to the Greenland ice core chronology (Rasmussen et al., 2014).

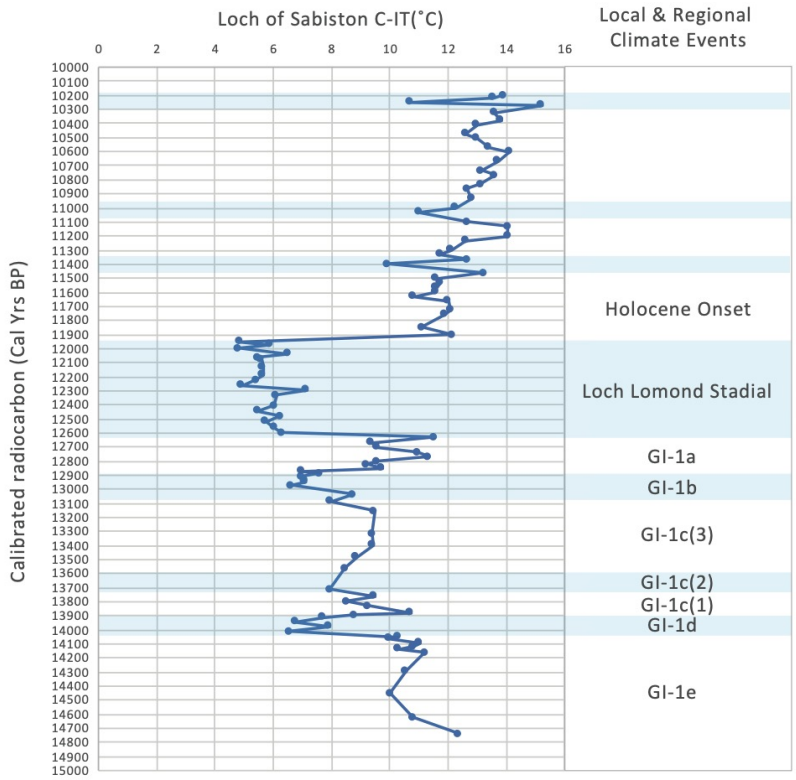

Figure 91. Chironomid inferred temperature reconstruction for Loch of Sabiston against calibrated radiocarbon ages (Cal Yr BP). Rasmussen et al (2014) NGRIP chronology local climate descriptors have been used to distinguish each cold (blue bars) and warm phase

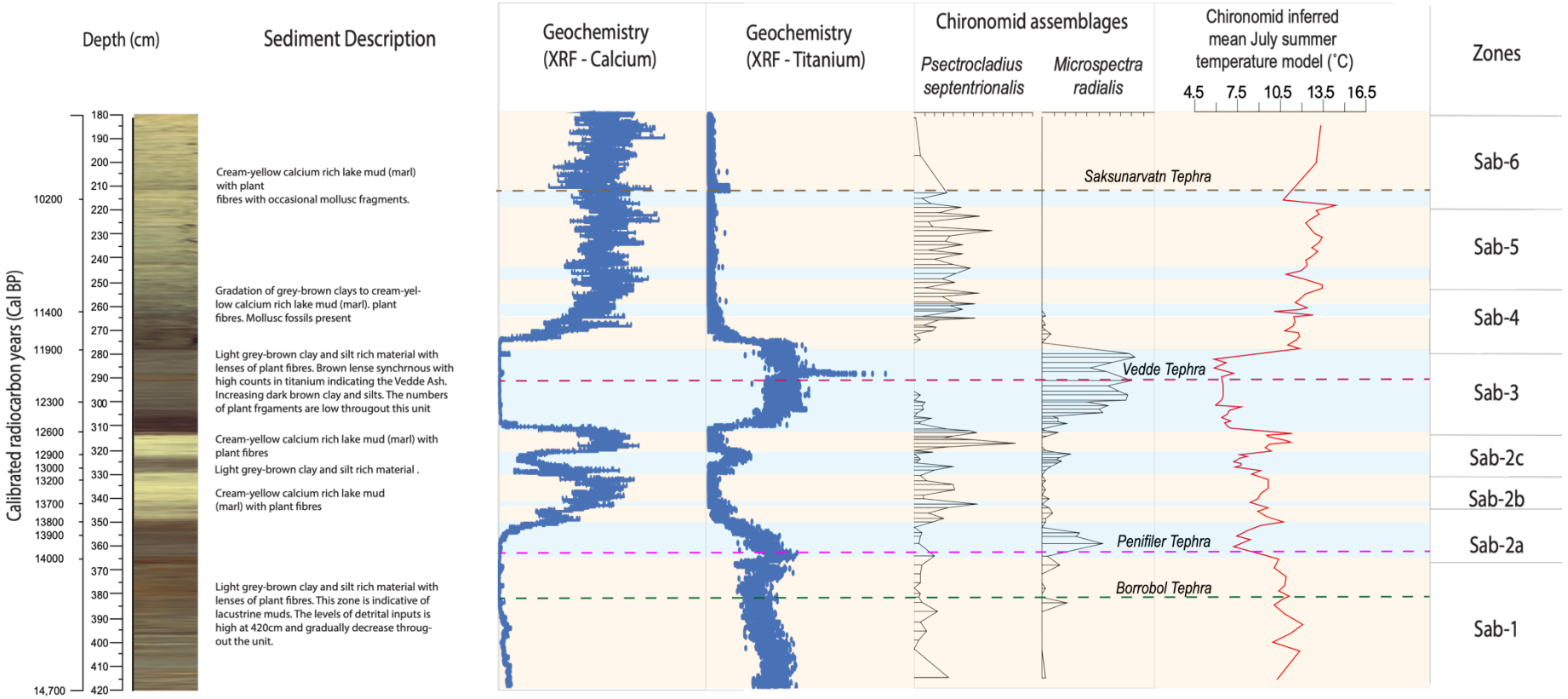

Figure 92. Synthesis diagram combining the chironomid assemblages of Psectrocladius septentrionalis and Microspectra radialis. The C-IT (°C) model is shown with the chronology (cal Yr BP) and the geochemical data (Calcium and Titanium). The sediment description is included on the left

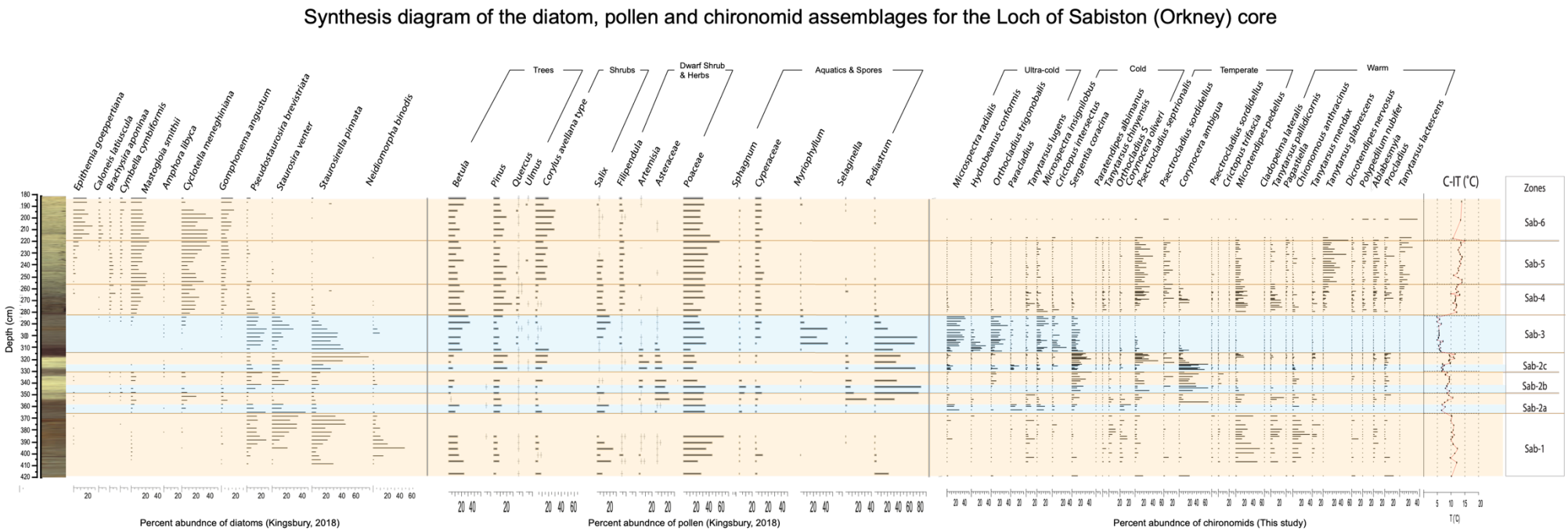

Figure 93. The percentage (%) abundance of the diatom, pollen and chironomid records for the Loch of Sabiston core, spanning the LGIT. This graph is a synthesis of the work from this project and the previous work of Kingsbury (2018)

7.4.2. **The end of the LGM**

Bradwell et al (2019) indicate that deglaciation began offshore between c.22-19k cal BP and reached the coastline by c.19-18k cal BP. Based on their model, the ice sheet subsequently disappeared from Orkney by c.17-16k cal BP. The chironomid temperature records start to record warming at around c.14.7k cal BP. However, there is a small lens of minerogenic sediments at the base of the core highlighting that sedimentation began just before c.14.7k cal BP. However, this is consistent with the ages inferred from Bradwell et al (2019). This is also consistent with Whittington et al (2015) who indicate that sedimentation began c.14.2k cal BP. The basal sediments of Loch of Sabiston lack an abundance of chironomid head capsules, indicating that the lake was either frozen over/ice was present, or the water column was not conducive to support chironomids. However, this may relate to a lack of plants in the lake at this time. Many chironomids rely on aquatic macrophytes for food however with increased minerogenic in-washing, and as a result increased lake turbidity, plants would not be able to photosynthesise (Greffard et al.,2012), thereby limiting the abundance and diversity of chironomids in the lake at this time. As a result, an interpretation of the environment at the end of the LGM is difficult to assess.

Previously, palaeoenvironmental studies from other sites on Orkney, have been analysed. Each of the three sites are located in the same N.W corner of mainland Orkney which likely suggests that environmental changes would have been similar between localities. Abrook et al (2019) noticed a lack of pollen at the end of the LGM, within Quoyloo meadow in Orkney, and also had difficulty interpreting the environmental conditions during this time. The absence of pollen assemblages in their site indicates there was a lack of vegetation in the catchment and as a result limited landscape development. This is reaffirmed by Bunting (1996) who noticed the same lack of pollen grains in the record. They concluded that this was a result of high wind speeds and an unfavourable dominance of minerogenic sediments which inhibited the growth of plants in the catchment. Abrook et al (2019) suggest that productivity was low and minerogenic inputs were still high as a result of continual glacial and landscape weathering. Therefore, an unfavourable environment resulted in the lack of chironomids and pollen at this time from both sites. This is also shown by Kingsbury (2018) who did not record any assemblages of diatoms in the basal sediments of Loch of Sabiston.

7.4.3. **Onset of interstadial/GI-1e (c.14.8-14.2k cal BP)**

The onset of sedimentation, after the termination of the LGM, is inferred to be c.14.8k cal BP in the Sabiston basin. This warm phase is likely synchronous with the onset of GI-1e in Greenland (Rasmussen et al., 2014) The assemblages during this time are dominated by temperate species of chironomids: *Ablabesmyia, Tanytarsus pallidocormis, Chironomous anthracinus, Microspectra pedullus,* and *Psectrocladius septentrionalis*. The presence of *Microtendipes pedullus* indicates that the Sabiston basin was low in organic matter and dominated by littoral to sublittoral sediments. (Brodersen & Lindegaard, 1997). This suggests that although the chironomids increase in biodiversity and abundance the vegetation in the lake was still limited. This is affirmed by the low LOI values at this time. Although temperatures are in the temperate-warm range some cooler species still thrive. *Psectrocladius septentrionalis* is a cool-temperate species of chironomid however is found at the colder end of the temperature range (Brooks et al., 2007). In addition, *Ablabesmyia* and *Tanytarsus pallidocormis* are found in this zone which suggests the lake had a lower pH. Kingsbury (2018) records the presence of the diatom *Fragilaria* in this zone. highlighting that the lake was low in nutrients, had lower pH levels and light was limited. The diatoms suggest that during this time there was a gradual stabilisation of the catchment, encouraged by the development of soils in the basin (Fritz and Anderson, 2013). *Chironomous anthracinus* is an early colonising species suggesting that the environmental conditions of the lake changed sufficiently to create a new niche for this species to fill. The resolution is low throughout this time. However, temperatures appear to be stable ranging between 10-12˚C.

The chironomid assemblages above rely on aquatic macrophytes and their attached algae for a food source (Pinder & Morley, 1995; Brodersen et al., 2001). The organic content is low but gradually increases at this time suggesting that lake productivity and macrophyte growth slowly increased too. This plant growth and increasing diversity of chironomids is synchronous with a reduction in minerogenic in-washing indicated by falling titanium counts (Moreno et al., 2011; Kylander et al., 2011; Aufgebauer et al., 2012) and affirms the work of Greffard (2012) that records a relationship between macrophytes, chironomid abundance and lake turbidity. Abrook et al (2019) concluded that, at c.14.3 $\pm$ 0.33 cal BP, vegetation was sparse, and the landscape had yet to stabilise and was dominated by grasslands. They record a

dominance of minerogenic clays-silts in the catchment which coincides with an increase in algal blooms (high abundance of *Pediastrum*) (Weckström et al., 2010). This increase in algal bloom activity leads one to believe that temperatures were higher. However, the chironomids from Sabiston show that the lakes were likely oligo-mesotrophic, nutrient deficient and atmospheric temperatures were temperate-cool at this time. The single variable nature of the chironomids provides a fuller image of the atmospheric temperatures at this time. Therefore, it is important to remember that many proxies, i.e. diatoms, are controlled by multi-variables. Where stable environmental conditions prevail chironomid composition is primarily controlled by atmospheric temperature. However, other variables such as pH, nutrient status and salinity are known to covary and, to a lesser degree, also drive chironomid communities (Langdon et al., 2008)

During this time, Kingsbury (2018) and Abrook et al (2019) record an increase in the abundance of *Betula nana* pollen. However, there is no macrofossil evidence to support the colonisation of birch on the island at this time. This has been shown to be the case by Paus (2010).

7.4.4. **Abrupt cooling/GI-1d (c.14.2-13.9k cal BP)**

Climate cooling occurs at c.14.05k cal yr. BP. This event is likely synchronous with the cold phase GI-1d in Greenland (Rasmussen et al., 2014). Cool-temperate species of chironomids dominate with temperatures falling to 6.5-7˚C. The following species are the main taxa found in this zone: *Microspectra radialis, Microspectra insigniloblis, Paracladius, Corynocera ambigua* and *Corynocera oliveri*. There is a sharp increase in the abundance of *Corynocera ambigua* at the onset of this cold phase. This abundance of this species has been known to increase rapidly between lithological boundaries as it is an early colonising taxon it is a good indicator species of rapid environmental change (Brooks pers com, 2017).

Brooks et al (2007) highlights that these species are found in ultra-oligotrophic arctic lakes and are indicative of cold conditions. Furthermore, *Microtendipes pedullus* and *Chironomous anthracinus* and found in this assemblage as they are found in environments low in organics (Brooks et al., 2007). These species are often found in temperate lakes which suggests that the environment was still contusive to support these taxa. This is likely due to the wide temperature ranges that these species have

(Brooks and Birks, 2001). Although there are temperate species, the abundance of these fall at the onset of this cold phase. As temperatures decline and the lake becomes more oligotrophic the abundance of the temperate species reduces and is replaced by cold oligotrophs. This cold event is short lived, lasting no more than 300 years, and as a result the temperate species of chironomids do not completely disappear. Chironomid abundance falls sharply at the onset of this cold stage which appears synchronous with an increase in minerogenic inputs. The levels of iron, silica, titanium and potassium rise sharply highlighting increased inputs of allochthonous inorganic detritus (Moreno et al., 2011; Kylander et al., 2011; Aufgebauer et al., 2012) and increasing in-washing (Kylander et al., 2011). The C-IT model indicates that temperatures fell from 10˚C to 6.5˚C.

At 14.05k cal BP Kingsbury (2018) records a sharp reduction in the abundance of the diatoms *Pseudostaurosira brevistriata, Staurosira venter* and *Staurosirella pinnata* at the onset of this cold phase. However, the overall species richness increases throughout this zone increase from this point onwards which indicates that the environment stabilised to support a wider variety of diatom species (Kingsbury, 2018). Kingsbury (2018) records little change in the abundance of the diatoms *Brachysiria aponinaea* and *Gomphonema angustum* from this point onwards unlike the chironomid assemblages which rapidly change at the onset of this cold phase. Furthermore, Kingsbury (2018) does not record this short-lived cold phase but rather a stability in the pollen record with little variation in the abundance of *Betula, Pinus* and *Quercus*. This is likely due to low-resolution sub-sampling throughout this time. The sampling resolution at Quoyloo Meadow on Orkney, from Abrook et al (2019), is higher and shows there was an abrupt colonisation of heathland and dwarf shrubs in the region. This shows the importance of using high resolution contiguous sub-sampling when using pollen assemblages. Pollen assemblages often lag behind climate change and as a result may miss short lived events in the climate record (Brooks et al., 2016). The pollen record for Sabiston suggests that the environment remained stable at this time when in fact the chironomid temperatures record climate instability throughout the interstadial. This further highlights the usefulness of chironomid temperature inference modelling as they are able to identify short lived cooling events which may not be recorded by other proxies.

7.4.5. **Three phase climate warming/GI-1c (c.13.9-13.2k cal BP)**

Between c.14.05-13.16k cal BP temperatures rise and range between 7.9-10˚C. This warming likely corresponds to GI-1c in the NGRIP record (Rasmussen et al., 2014). Abrook et al (2019) shows that the same zone in their record, spanning c.14-13.2k cal BP. Sedimentation rates in in Quoyloo Meadow and Loch of Sabiston are low at this time, and are likely a result of the low-lying basin, the lack of erosion and reduced sediment transport (Abrook et al., 2019).

Chironomids indicative of cool-temperate conditions dominate at this time: *Corynocera ambigua, Procladius, Microtendipes pedullus, Sergentia coracina, Psectrocladius septentrionalis* and *Ablabesmyia*. The taxa listed above are suggestive for an environment that is in an interstadial phase (Brooks et al., 2007). Once again, *Corynocera ambigua* is found here in large concentrations between lithological boundaries. This early colonising species indicates that the environment markedly altered at this time. Often found after significant environmental change, greater numbers of this species opportunistically fill an environmental niche (Brooks et al., 2007). *Microtendipes pedullus* and *Sergentia coracina* indicate that the lake was low in organics and had a low nutrient status. Although atmospheric temperatures increased at this time, the lake was still nutrient deficient, indicated by a low organic content (4%). Similar to GI-1e, the presence of *Psectrocladius septentrionalis* indicates intermediate temperatures prevailed. This species is on the cooler end of the gradient and has a wide temperature optimum (Brooks and Birks., 2001; Brooks et al., 2007).

Increased atmospheric temperatures led to the formation of calcium rich marl sediments precipitating out of the water column (Lauterbach et al., 2011). Based on the C-IT (˚C) model temperatures began to increase, from a low of 7.9˚C to 11˚C, at 355cm. Yet, the lithology does not change from minerogenic clays to marl rich sediments until 349cm. This highlights that the chironomids are more sensitive to atmospheric temperature change than the lake sediments are (Brooks et al., 2016). The cool-temperate conditions throughout this zone promote an increase in diatom species richness (Kingsbury, 2018). The Loch of Sabiston pollen assemblages do not show any rapid changes from cool to warm conditions. Rather, there is a continuous dominance of trees and dwarf shrubs which suggests that the catchment was open at this time. This warm phase lasts for approximately 700 years and due to the low-

resolution sampling of the pollen assemblages this event is not distinguished from the rest of the interstadial (Kingsbury., 2018).

Although there was low sedimentation rate at this time, it is clear that there were 3 subtle climate events occurring during this time. Whittington et al (2003) highlights that it is unlikely that proxies will be able to reconstruct these short-lived climate fluctuations. This project has shown that chironomids have been able to identify these subtle climate cooling and warming events. This warmer stage is thought to be synchronous with the GI-1c in the Greenland ice core record. The NGRIP record is also records this 3 part subdivision: (1) warmer early phase (GI-1c (1)), cooler mid-phase (GI-1c(2)) and a warmer latter stage (GI-1c(3)) (Rasmussen et al., 2014). See below an interpretation of these three subdivisions:

- **Phase 1/GI-1c (1)**. Abrupt atmospheric warming occurs at c.13.9k cal BP and lasts until c.13.7k cal yr BP. Temperatures rise to a high of 10.7˚C. The temperate species *Psectrocladius septentrionalis* increases in abundance at this time. The end of this warming is marked by a sharp rise in the abundance of the early colonising species *Corynocera ambigua*, indicating that there was a significant change in the environmental conditions at this time
- **Phase 2/GI-1c (2).** Subtle climate cooling occurs at c.13.7k cal BP and lasts until c.13.6k cal BP. Temperatures fall to 7.9˚C during this cooler phase. There is spike in the abundance of the cold stenotherm *Microspectra radialis* indicating a return to cooler conditions at this time.
- **Phase 3/GI-1c (3).** Abrupt atmospheric warming occurs at c.13.6k cal BP and lasts until c.13.2k cal BP. Temperatures rise to 9.5˚C and the abundance of *Corynocera ambigua* increases which again indicates that there was abrupt environmental change occurring at this time.

7.4.6 **Abrupt climate cooling/GI-1b (c.13.2-12.97k cal BP)**

Between c.13.2-12.7k cal yr. BP there is another high amplitude abrupt cold phase which lasts for approximately 200 years. Temperatures fall to a low of 6.6˚C by c.12.97k cal BP. This event is thought to be synchronous with GI-1b in the Greenland ice core records (Rasmussen et al., 2014).

Sergentia coracina, Orthocladius trigonobalis, Orthocladius consobrinus, Microspectra radialis and *Paracladius* are present during this time. There is also a sharp increase in the presence of *Corynocera ambigua* to 40-60% of the assemblage. Once again, indicating a sharp transition between the previous warm phase and this cold reversal. The cold stenotherms *Microspectra radialis, Orthocladius trigonobalis* and *Orthocladius consobrinus* are present at this time. They are indicative of sub-arctic and high latitude oligotrophic conditions (Brodin, 1986; Hoffman, 1984; Brooks et al., 2007). The organic content of the core drops at this stage indicating a fall in lake productivity. Minerogenic in-washing increases at this time which suggests that the landscape was unstable, and erosion was prevalent (Stansell et al., 2013; Kylander et al., 2011; Balascio et al., 2011). Environmental conditions sharply changed from temperate to arctic conditions based on the community of chironomids and increasing minerogenic and detrital inputs. Kingsbury (2018) records a sharp drop in the diversity of diatoms during this time due to the increasing minerogenic in-washing. *Brachysiria aponinaea* and *Gomphonema angustum* disappear from the assemblage highlighting that rapid environmental change occurred at this time.

7.4.7 **Abrupt climate warming/GI-1a (c.12.97-12.6k cal BP)**

Mean July summer temperatures increase rapidly to a high of 11.3-11.5˚C during this warm phase. The onset of this event is thought to be synchronous with the warm GI-1a phase in the Greenland ice core record.

Microspectra pedullus and *Corynocera ambigua* abundances increase at this time. These early colonisers indicate that there was abrupt environmental change between c.12.97-12.6k cal BP. *Tanytarsus mendax, Procladius, Psectrocladius septentrionalis, Corynocera ambigua* and *Ablabesmyia* dominate at this time highlighting that temperate conditions prevailed. This assemblage indicates that the lake was likely a larger body of water where aquatic mosses prevailed (Epler et al.,2013). Furthermore, plants became abundant in the lake at this time, indicated by the presence of *Ablabesmyia.* This species is known to graze on aquatic macrophytes (Brodin, 1986; Brodersen et al., 2001). The organic content of the sediments increases at this point indicating a rise in lake productivity.

7.4.8 **Loch Lomond Stadial (c.12.6-11.9k cal BP)**

Rapid cooling occurs at c.12.6k cal yr BP, lasting for approximately 700 years, terminating at c.11.9k cal BP. The C-IT model suggests mean July summer temperatures fell to a low 6-7˚C. This cold phase is likely synchronous with GS-1 in Greenland (Rasmussen et al., 2014), the YD in Norway (Romundset et al., 2019) and the LLS in Scotland (Lowe et al., 2019). Temperatures fall from a high of 11.5˚C to 6.9˚C within ~40 years.

This abrupt environmental change is recorded in the chironomid assemblages with a rapid decline in the abundance of temperate taxa to ultra-cold oligotrophs. *Microspectra radialis, Orthocladius consobrinus, Paracladius, Orthocladius trigonobalis, Crictopus intersectus and Hydrobeanus conformis* are found in higher abundances during this cold phase. They are known to inhabit cold oligotrophic lakes in northern latitudes (Andersen et al., 2013). These taxa are symptomatic of a cold oligotrophic sub-arctic/alpine environment (Walker et al., 1991; Brooks et al., 2007).

Sergentia coracina occurs in higher abundances at the onset of this cold phase, and gradually falls throughout. This is a cold stenotherm which is indicative of oligo-mesotrophic lakes (Epler et al., 2013), showing that the lake initially had a higher nutrient status at the onset of the LLS and rapidly became nutrient deficient by the mid LLS. This is affirmed by the presence of *Psectrocladius septentrionalis* as it is a species found in cold-temperate lakes. The abundance of this species drops markedly from the end of the previous warm phase and disappears midway through the LLS. *Hydrobeanus conformis* also occurs in large abundances (comprising 30% of the overall assemblage) between 311-300cm. This is the first instance where this taxon occurs in such high abundances. It is known to inhabit lakes in Svalbard and in northern Norway (Cranston et al., 1983). Gradually, the abundance of *Hydrobeanus conformis* falls and is replaced by the cold stenotherms *Microspectra radialis* and *Orthocladius trigonobalis*. This shows that there was a two stepped phase mid-way through the LLS where subtle environmental and climate change occurred.

The C-IT (˚C) model indicates that temperatures fell to a low of 4.5-5˚C at the onset of the second phase of the LLS. The second stage has a discernible increase in the following taxa: *Orthocladius consobrinus, Microspectra radialis* and *Orthocladius trigonobalis* (at 299-300cm). An increase in the concentrations of *Orthocladius consobrinus*, *Paracladius, Orthocladius trigonobalis* and *Microspectra radialis* indicates that much colder temperatures prevailed similar to the sub-arctic in the

present day (Brooks et al., 2007). *Microspectra radialis* is also an acidophilic and ultra-oligotrophic taxon (Brooks et al., 2007). With a decreased pH and lower organic content, the lake likely became deficient in nutrients and accounts for the sharp decrease in species diversity. Decreased calcium counts, combined with the sharp fall in lake temperatures, indicates that lake productivity fell also.

Lane et al (2013) records a mid-YD transitional phase across N.W Europe (see chapter 9). This same transition is recorded in Loch of Sabiston with cold oligo-mesotrophic conditions being recorded at the onset of the LLS and ultra-cold oligotrophic conditions being recorded in the latter stages. This is consistent with Muir Park Reservoir and Loch Ashik (Brooks et al., 2011; Brooks et al., 2016) in Northern Scotland. Abrook et al (2019) records an expansion of *Artemesia and Rumex* during the first stage of this cold phase indicating an establishment of dry, cold and tundra vegetation with a reduction in woody plants. Combined with an increase in the abundance of *Salix* from the Loch of Sabiston core, this suggests that the landscape was exposed and dominated with snow much later in the year (Wijk 1986). Lake productivity reduced in Loch of Sabiston, indicated by lower LOI values (2%). Abrook et al (2019) also records a reduction in the LOI during this stage, suggesting a limited organic input entering the lake system across the Isle of Orkney.

At 290cm there is a noticeable increase in the counts of calcium and titanium (which coincides with a brown staining in the lithology) indicating the presence of the Vedde ash layer. Tephra layers in the Faroe Islands have been identified by using increased calcium and titanium counts (Kylander et al., 2012). Combined with the EMP analysis and the sediment lithology this layer has been identified as containing the Vedde Ash cryptotephra. The presence of this tephra layer allows direct comparisons of the timing and magnitude of climate change across the North Atlantic making it possible to track the movement of the mid transgressional phase of the LLS (see chapter 9).

7.4.9 **Abrupt warming/Onset of the Holocene (c.11.9-10.03k cal BP)**

Abrupt warming occurred at c.11.9k cal BP, rising from a low of 4.5˚C to a high of 12˚C. *Ablabesmyia, Microtendipes pedullus, Dicrotendipes nervosus, Procladius, Tanytarsus lactescens and Tanytarsus glabrescens* dominate at this time. This event is thought to be synchronous with the onset of the Holocene period (Rasmussen et

al., 2014). Brooks et al (2012) records a sharp increase in temperatures, by 9˚C, on the Isle of Skye (Loch Ashik), and across the British Isles and Ireland (Brooks et al., 2016), although, the magnitude and timing of this warming has been known to vary between localities (Lane et al., 2013; Brooks et al., 2016).

Warming at the onset of the Holocene period occurs before any lithological changes. The chironomids indicate warming at 282-283cm however the lithology does not switch from minerogenic silts to calcium rich marls until 270-275cm. The chronology indicates that temperatures rapidly rose at c.11.9k cal BP however the precipitation of marl did not occur until c.11.6k cal BP, indicating a clear lag in the geochemical record when compared to the chironomids. This reaffirms the work done by Brooks and Birks (2000), Brooks et al (2016) and Watson et al (2010) that show that chironomids are highly sensitive to atmospheric temperature change and often lead other environmental proxies.

A rapid increase in the abundance of the early colonisers *Chironomous anthracinus* and *Corynocera ambigua* is recorded by Watson et al (2010) before the lithological boundary of the LLS and Holocene. This is the first instance where *Tanytarsus lactescens* is found in the core. This is a species of chironomid which is often found in marl rich sediments from the Holocene period (Brooks et al., 2007). Which further indicates that this is likely the onset of the Holocene. Throughout this zone there is a sharp reduction in the counts of iron and titanium which suggests that minerogenic in washing fell (Stansell et al., 2013). Calcium counts rapidly increase throughout this zone indicating lake that temperatures rose, and the nutrient status of the lake altered sharply from an ultraoligotrophic to mesotrophic-eutrophic conditions (Lauterbach et al., 2011).

The pollen record from Abrook et al (2019) highlights that there was an expansion of *Rumex* and *Salix* which suggests that the catchment opened, and the tundra disappeared. They also suggest that the soil in the catchment developed further as dwarf shrubs became prevalent in the area. Abrook et al (2019) record an increase in the organic content within this zone however this is not recorded in Loch of Sabiston. Kingsbury (2018) noticed that the abundance of diatoms increases markedly at the onset of this zone with a transition from pioneer species to increased species richness and a change to epiphytic taxa. This zone is dominated by *M. lacustris* and *C. menehiniana* which are indicators of high alkaline waters. This is to be expected as the concentration of calcium carbonate rich marl sediments increase at this stage.

At c.11.4k cal BP, c.11.03k cal BP and c.10.02k cal BP there are spikes in the abundance of the following cold oligotrophic taxa: *Psectrocladius septentrionalis, Microspectra insignilobus*, *Crictopus intersectus and Orthocladius trigonobalis* and *Sergentia coracina.* Although, temperatures had increased rapidly there appears to be short lived cold reversals during the early Holocene. *Corynocera ambigua and Microtendipes pedellus* abundances increase sharply indicating abrupt environmental change occurred at the onset of these cold phases. Based on the independent chronology for this site this cooling event is likely highlights the 11.2k event (Rasmussen et al., 2014). However, the age-depth model for this site indicates that this occurs at 11.4k yrs. BP. This coincides with spikes in titanium which indicates increased in-washing and detrital inputs (Metcalfe et al., 2010; Balascio et al., 2011; Kylander et al., 2012). The abundance of *Polypedulum nubifer, Tanytarsus glabrescens, Dicrotendipes nervosus, and Tanytarsus lactescens* increase further from c.10.4k cal BP onwards. As previously stated, *Tanytarsus lactescens* is found in carbonate rich lakes. As the abundance of this species increases one can assume this is a result of increasing productivity and calcium in the lake (Brooks et al., 2007). The abundance of *Polypedulum nubifer* increases indicating that Sabiston had a eutrophic nutrient status. Also, *Polypedulum nubifer* is often found living and consuming aquatic vegetation which indicates a productive lake system prevailed (Brodin & Gransberg, 1993; Buskens, 1987). Calcium values reach a maximum count highlighting that the lake became highly eutrophic and productivity rose. Furthermore, there is a sharp rise in the counts of titanium at 210cm which is consistent with the geochemical signature of the basaltic Saksunarvatn tephra layer found at this depth (Shane & Smith, 2000).

Abrook et al (2019) records a development of grasslands at this time indicated by the presence of Poaceae. Poaceae occur in high abundances in the Sabiston core and as a result suggests that the development of grasses was apparent across all of Orkney. Abrook et al (2019) suggests that conditions were wetter due to the presence of *Filipendula*. Kingsbury (2018) pollen record is low-resolution in this section of the core and as a result these short-lived cool phases are not recorded. However, their record does record a drop in the abundance of the diatoms *Cyclotella meneghiniana* and *Mastogloia smithii*. The reduced diversity of diatoms is likely a result of increased turbidity due to a return of minerogenic in-washing.

7.5 **Summary**

This is the first high resolution chironomid inferred temperature reconstruction for the Isle of Orkney. Combined with a robust AMS and tephra-based chronology the main palaeoclimate and environmental fluctuations across the LGIT have been reconstructed:

(1) Between c.14.8-14.05k cal BP the chironomid record indicates that mean July summer temperatures ranged between 10-13.5˚C and was dominated by temperate species indicative of low productivity lakes ecosystems.

(2) There is a sharp fall in the temperatures at c.14.05k cal BP which lasts until c.13.7k cal BP. Temperatures fall to 6.5˚C from a high of 10˚C. The assemblage is composed of cold stenotherms such as *Microspectra radialis* and *Paracladius* which are indicative of oligotrophic sub-arctic conditions. This coincides with heathland expansion and a dominance of low-lying herbs across Orkney (Kingsbury., 2018; Abrook et al., 2019).

(3) Between 13.9-13.7k cal BP there is a warmer phase which is split into three distinct sections:

- **Phase 1/GI-1c (1)**. Abrupt atmospheric warming occurs at c.13.9k cal BP and lasts until c.13.7k cal yr BP. Temperatures rise to a high of 10.7˚C.
- **Phase 2/GI-1c (2).** Cooling occurs at c.13.7k cal BP and lasts until c.13.6k cal BP. Temperatures fall to 7.9˚C during this cooler phase. There is spike in the abundance of the cold stenotherm *Microspectra radialis*.
- **Phase 3/GI-1c (3).** Abrupt atmospheric warming occurs at c.13.6k cal BP and lasts until c.13.2k cal BP. Temperatures rise to 9.5˚C and the abundance of *Corynocera ambigua* increases which again indicates that there was abrupt environmental change occurring at this time.

(4) Between c.13.2-12.7k cal BP there is a sharp fall in temperatures to a low of 6.6˚C. This event is believed to be synchronous with the GI-1b event in Greenland (Rasmussen et al., 2014)

(5) Between c.12.7-11.9k cal BP ultra-cold oligotrophic species of chironomids dominate. This time period corresponds to GS-1 in Greenland (Rasmussen et al., 2014) and the LLS in Scotland (Lowe et al., 2019). Split into two phases temperatures fell to a low of 6-7˚C during the first stage and later fell to 4.5˚C during the second stage. The chironomid assemblages indicate that there was abrupt fall in temperatures at this time. Productivity was low, gradually falling throughout the LLS, which coincides with a drop off in the cool temperate species of chironomids and an establishment of cold oligotrophs. Minerogenic in-washing rises throughout this zone, reaching a maximum in the latter stage of the LLS.

(6) Abrupt warming occurred at 11.9k cal BP, rising from a low of 4.5˚C to a high of 12˚C. This warming phase appears to be synchronous with the onset of the Holocene period throughout the British Isles (see chapter 9). Throughout this time there are subtle short-lived cold phases indicated by a drop-in temperature to 10.5˚C. Although the chironomids show that temperatures continued to warm throughout this period (from 14-15.5˚C).

This study has provided a high-resolution comprehensive reconstruction of the palaeoclimate and environmental history of Orkney during the LGIT. This chapter has highlighted the unique sensitivity of the chironomid assemblages to pick out subtle environmental changes that other palaeoenvironmental proxies cannot.

Chapter 8: Multi-proxy palaeoclimate and environmental history of Caithness, Northern Scotland, during the Last Glacial-Interglacial Transition.

8.0 Introduction

A multi-proxy analysis of the environmental and climate history of Caithness has been undertaken on a continuous lacustrine core spanning the LGIT. This is the first research to use chironomid head capsule assemblages and long chain alkenones in parallel to reconstruct summer and spring temperatures respectively. Palaeotemperature records are lacking in this area and as a result temperature have been largely inferred from computer simulations (Brooks & Langdon, 2012). Currently, this is the first study to use long chain alkenones in freshwater lakes for the British Isles. Combining the C-IT and the LCA records one can begin to better understand seasonality in Caithness throughout the LGIT. Combined with micro-XRF analysis a better understanding of the environmental processes in the lake catchment can be inferred in order to gain a fuller image of the palaeoenvironmental history of the site.

Caithness is located on the N.E of Scotland (58°24'59.99" N -3°29'59.99" W) and is the closest part of the Scottish mainland to the archipelagos. Temperature and precipitation levels in Caithness are therefore influenced by changes in the THC (Golledge et al., 2009). This area is known as the 'flow country' due to the flat lying undulating peat bogs that overlay the region (Stroud et al., 1987). These sediments form continuous records of the climatic and environmental history of the Caithness during the LGIT.

8.0.1 Previous research

The LGM in Caithness reached its largest extent between 24-18k cal BP (Hall et al., 2016(b)). Evidence suggests that deglaciation of the ice margin began at 17.5k cal BP (Sejrup et al., 2014) and retreated into the Moray Firth. Hall and Jarvis (1989) dated the retreat of the Moray Firth glacier lobe to be 15.32 ± 200 ^{14}C. Minor glacier advances are believed to have occurred at 14k cal BP near Elgin (Merritt., 2000), and further advance at Ardersier around 13k cal BP (Merritt., 1995). However, Ballantyne & Stone (2012) refute this and argue that glacial activity was limited to the end of GS-2 and the start of GI-1e rather than lasting into the interstadial. Bradwell et al (2008) provides evidence that glacial activity in the north west of Scotland did last into the

Older Dryas/GI-1d. They highlight that glacial retreat was likely not abrupt at the end of GS-2 as the warming of GI-1e lasted for 600 years before temperatures cooled into GI-1d [Fig.94]. Ballantyne & Stone (2012) do conclude that localised ice caps may have persisted in the higher altitudes of N.W Scottish munros.

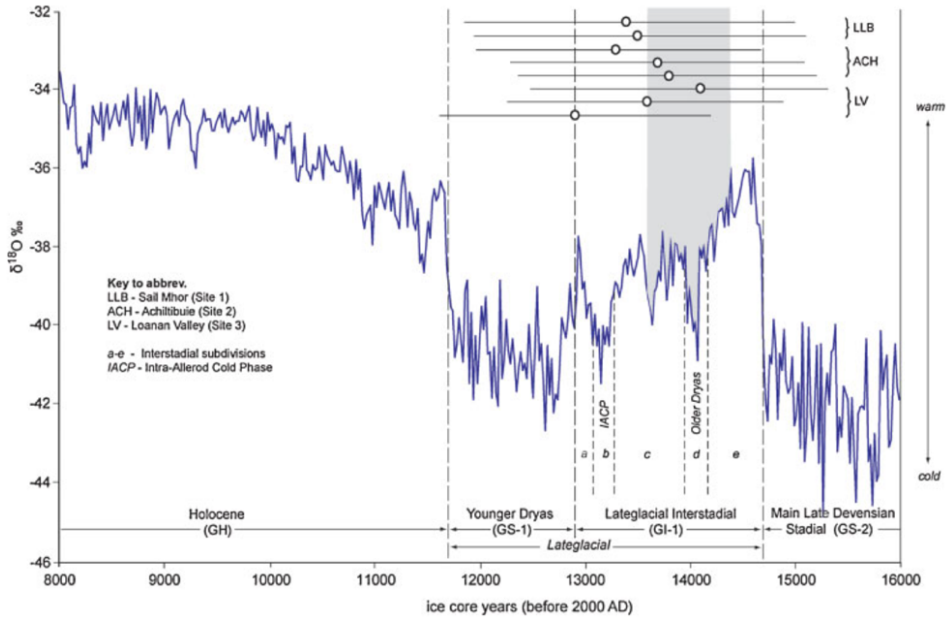

Figure 94. Evidence of glaciers surviving into the early interstadial in N.W Scotland based on cosmogenic exposure dating (Bradwell et al., 2008)

The North of Scotland has a wealth of palynological data to help to understand the environmental history of the LGIT [Fig.95]. Moar (1969) and Peglar (1979) record a dominance of *Empetrum* on Caithness and Orkney in Loch of Winless suggesting that heathland was widespread throughout the North of Scotland and the Northern Isles. Birks (1984) and Pennington et al (1972) also record this dominance of heathland extending to Sutherland in the North of Scotland. Each of these records do record the tripartite warming and cooling in the sedimentary record. Yet, it is missing from the palynological records. Therefore, with the addition of a chironomid and alkenone based temperature record it is now possible to distinguish the abrupt high amplitude warming and cooling events record throughout the LGIT (Brooks et al., 2016). It is likely that the environment was not as stable as the pollen records suggest. With the addition of the chironomid and alkenone temperature reconstructions we are now able to understand what the magnitude and timing climate change was during the LGIT for this region. Moreover, it is now possible to better understand the complexities of seasonality in the climate records when using the summer C-IT record and the spring LCA record.

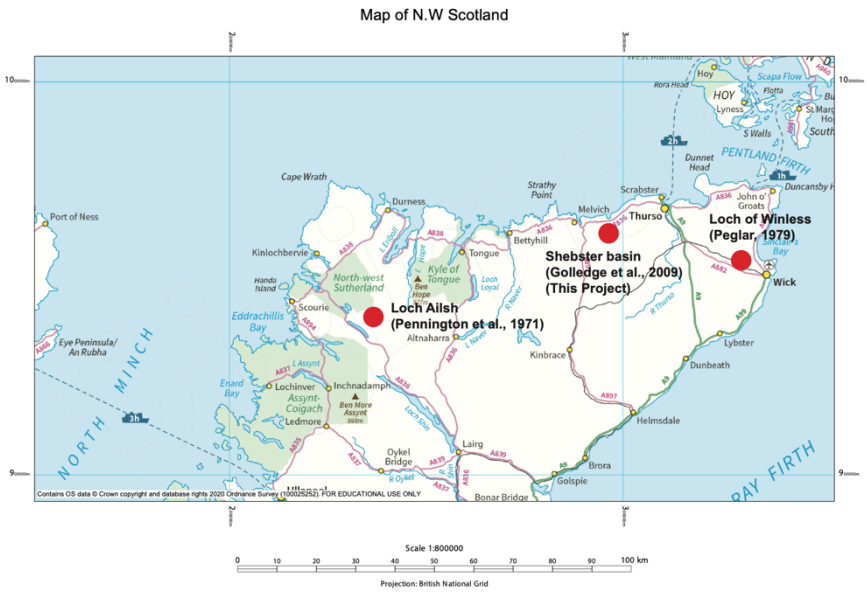

Figure 95. Map of the pollen and macrofossil sites in the N.W Scotland: Loch Ailsh (Pennington et al., 1972), Shebster basin (Golledge et al., 2009) and Loch of Winless (Peglar, 1979)

However, to date, there are no temperature records for this region of Scotland. Brooks and Langdon (2011) highlight that this area lacks temperature reconstructions and have been largely interpolated from the closest site on the Isle of Skye, Loch Ashik (Brooks et al.,2012). In order to assess the accuracy of this inferred model high resolution, independent and single variable records of temperature change are required for this region. Therefore, with the addition of chironomid inferred temperatures, and long chain alkenone surface water temperatures, they will provide a fuller image of the climate, environmental history of Caithness during the LGIT.

8.1 **Aims & Objectives**

This project aims to reconstruct palaeotemperatures, throughout the Last Glacial-Interglacial Transition (LGIT), for the North of Scotland, using the following objectives:

1. Reconstruct mean July summer temperatures using chironomid assemblages for the Shebster basin.
2. Reconstruct mean spring temperatures using Long-chain Alkenones for the Shebster basin.
3. Critically assess the use of chironomids for temperature inferences by comparing the results to the Long-chain Alkenone records
4. Use a multiproxy approach to reconstruct the environmental conditions throughout the LGIT in Caithness.

8.2 Site description

8.2.1 Shebster basin, Caithness

The Shebster basin, is situated on the North-Eastern tip of Scotland (58°24'59.99" N -3°29'59.99" W). The basin is in a close proximity to the North Atlantic Ocean, and the North Sea, and therefore is influenced by oscillations in the Atlantic Meridional Oscillation Circulation (AMOC) (Golledge et al., 2009; Brooks et al., 2016) [Fig.96]. Temperature and precipitation levels in Caithness are influenced by changes in the THC (Golledge et al., 2009). Any changes in atmospheric circulations and climate change will recorded within the lake and peat sediments. Caithness is influenced by a hyperoceanic to hemioceanic climate system (Birse, 1971) and is also controlled by fluctuations in the North Polar Front (Brooks et al., 2016). This a perfect location to study the influence of the THC and NPF on the climate of the north of Scotland due to the basin's close proximity to the North Atlantic.

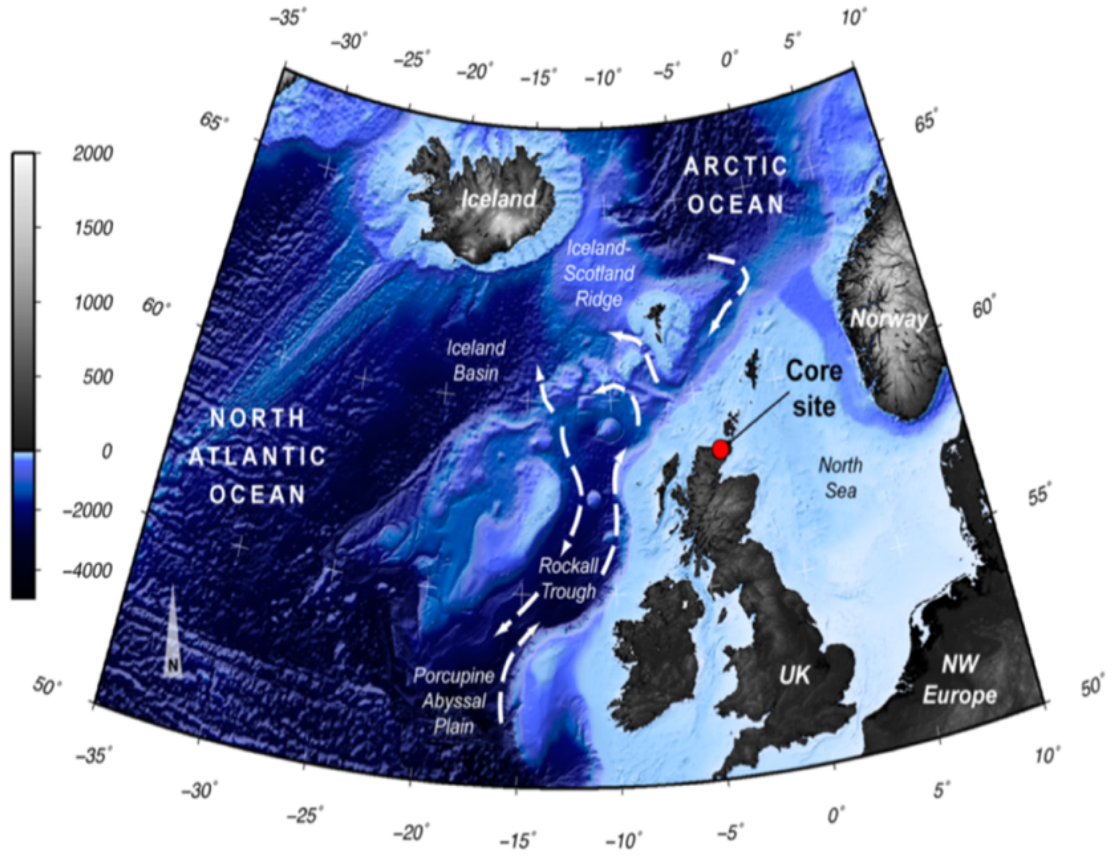

Figure 96. The location of the Shebster basin in relation to the UK and the North Atlantic Ocean highlighting the climate sensitivity of the site (Golledge et al., 2009; McIntrye & Howe, 2009)

Golledge et al (2009) previously cored the Shebster basin to investigate the palaeoenvironmental history of Caithness, to gain a better understanding of how long the site had been ice-free and how the environment changed over the LGIT [Fig.97]. Shebster is known to have a complete last glacial and early Holocene sedimentary sequence. The site has a robust high resolution palynological record spanning the LGIT and a record of the organic content. Furthermore, radiocarbon analysis was undertaken which recorded a basal age of ~18 k cal BP for the site. If this is accurate, it is one of the oldest ages of deglaciation in the British Isles.

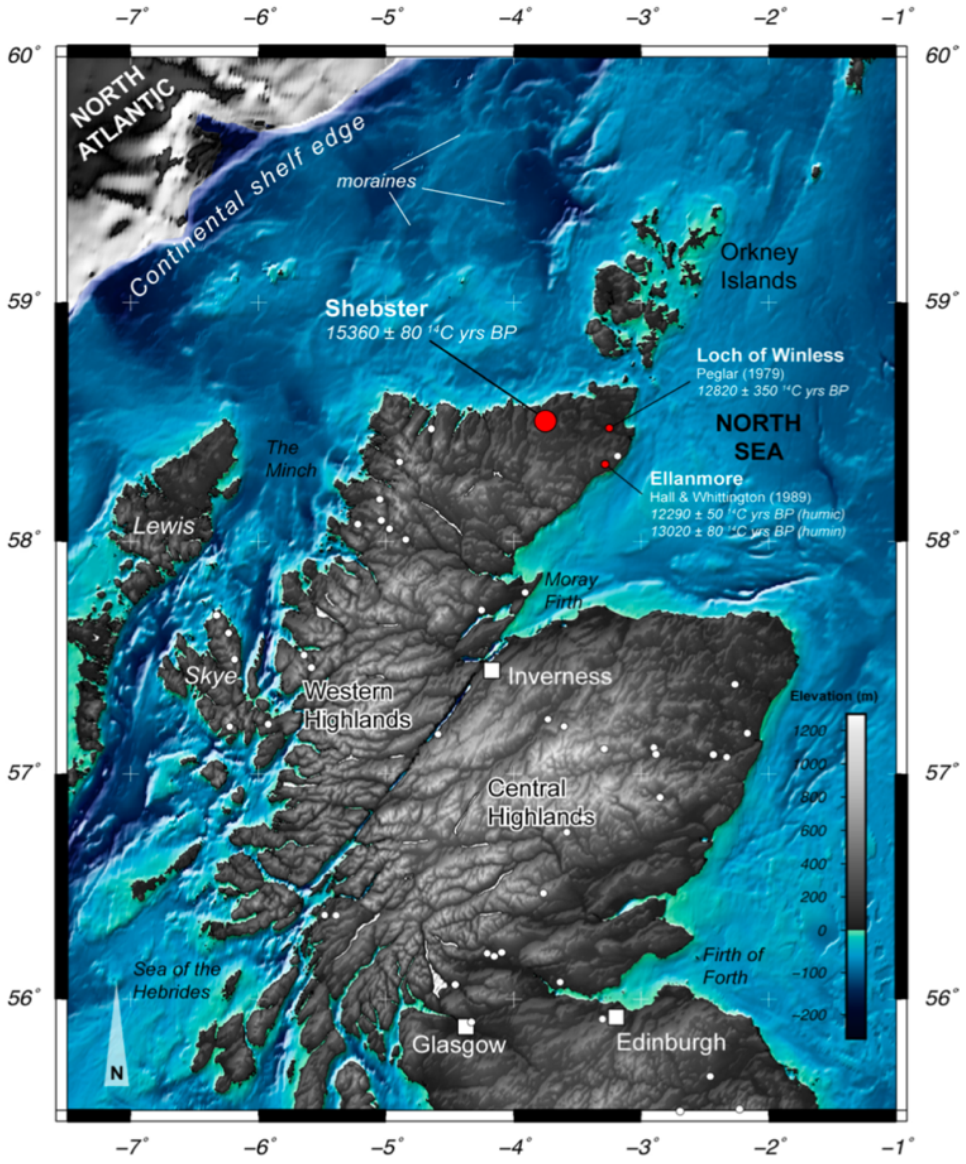

Figure 97. The location of the Shebster basin in relation to the Northern Isles of Scotland and the Scottish Highlands. The unmodelled ages of deglaciation are shown at three sites Ellanmore, Shebster and Loch of Winless (Golledge et al., 2009)

The site has been ice free since approximately 15k cal BP (and potentially 18k cal BP based on the works of Golledge et al (2009)). Therefore, there has been sufficient time for sediments to accumulate and record climatic fluctuations spanning the LGIT. The Shebster basin is known to have a fully intact continuous record of environmental change from the termination of the LGM throughout the LGIT, and into the Holocene (Golledge et al., 2009). The site is a prime locality as pilot studies indicated that long chain alkenones were present in the minerogenic and organic rich sediments throughout the LGIT. Toney (pers comm) records a 52% chance of successfully finding long chain alkenones in lakes. Therefore, the site may allow an interpretation of seasonality to be made for the LGIT in Caithness.

To the north-west of the Shebster basin a steep-sided hill rises to 133m [Fig.98]. The burn of Shebster flows into the basin from the west. These indicate that the palaeolake was likely runoff-precipitation fed. At present the basin consists of many undulating peat bogs (Stroud et al., 1987). However, throughout the LGIT lacustrine muds-minerogenic sediments dominated. Once a palaeolake sequence, until approximately 8.7 ka BP, the Shebster basin is currently now a peat bog (Golledge et al., 2009) [Fig.99]. A core was taken near the original coring location to maintain continuity between the two projects. In order to maximise the reliability of stratigraphical tie-points between the two cores.

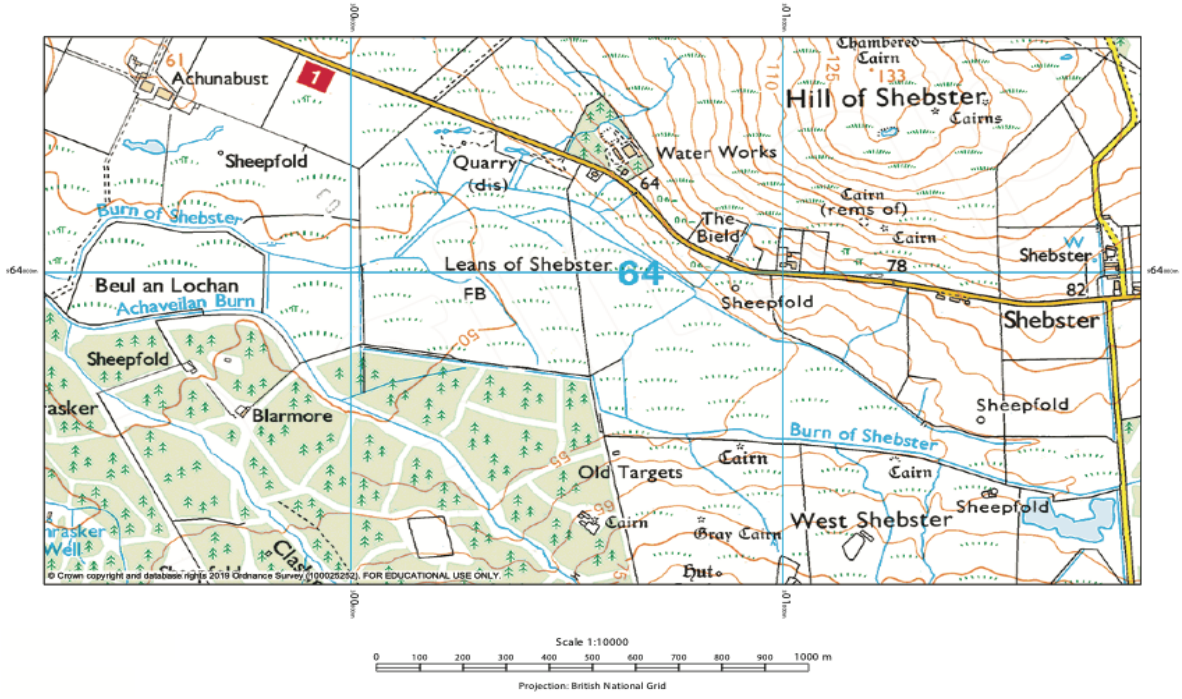

Figure 98. An Ordnance survey map of the Shebster basin. Scale: 1:10000m (Edina Digimap, 2019)

Figure 99. An aerial view of the Shebster basin in Caithness. The site is highlighted in blue. (Google Earth, 2020)

8.2.2 Geological setting

Caithness is underlain by Devonian sandstone from the Caithness Flagstone Group. Whilst the west and the south of the area is dominated by Silurian granites and Neoproterozoic metamorphic sedimentary rocks (Golledge et al., 2009). The North western area of the Shebster basin is dominated by the Porkskerra psammite formation. The underlying geology is overlain by Broubster Till which is composed of silty sand, with a moderate brown to red colour. Clasts of the underlain Devonian sandstone are found throughout the till. Rare shell fragments are also present in the till thought to have been formed in the Mesozoic mudstone formations (Hall & Whittington, 1989

The Shebster basin is on top of the Sandside Bay Formation which is composed of sandstones and siltstones with lenses of limestone throughout [Fig.100]. Surface runoff and groundwater processes transport calcium, from the underlying geology, into the lake. During phases of warming, the lake precipitates the available calcium leading to the formation of calcium carbonate rich marls and organic rich lacustrine sediments. This may lead to potential hardwater errors and perhaps older AMS radiocarbon dates.

8.2.3 **Catchment, Land use and vegetation**

The Shebster basin was originally a shallow, freshwater lake where it was dominated by small aquatic plants and algal blooms during the summer months (Golledge et al., 2009). These plants precipitated out biogenic carbonate during the summer months which was also responsible for the formation of the marl units present in the sediment core. From 8.4 ka BP the lake dried out and vegetation continued to grow leading to the formation of the peat bogs seen today (Golledge et al., 2009). At present the

Shebster basin is dominated by natural grassland, heather and coniferous woodland [Fig.101]. Currently, the northern section of the basin has a disused quarry and a sheepfold to the east and west. To the north of the Shebster basin is the Dounreay nuclear power plant.

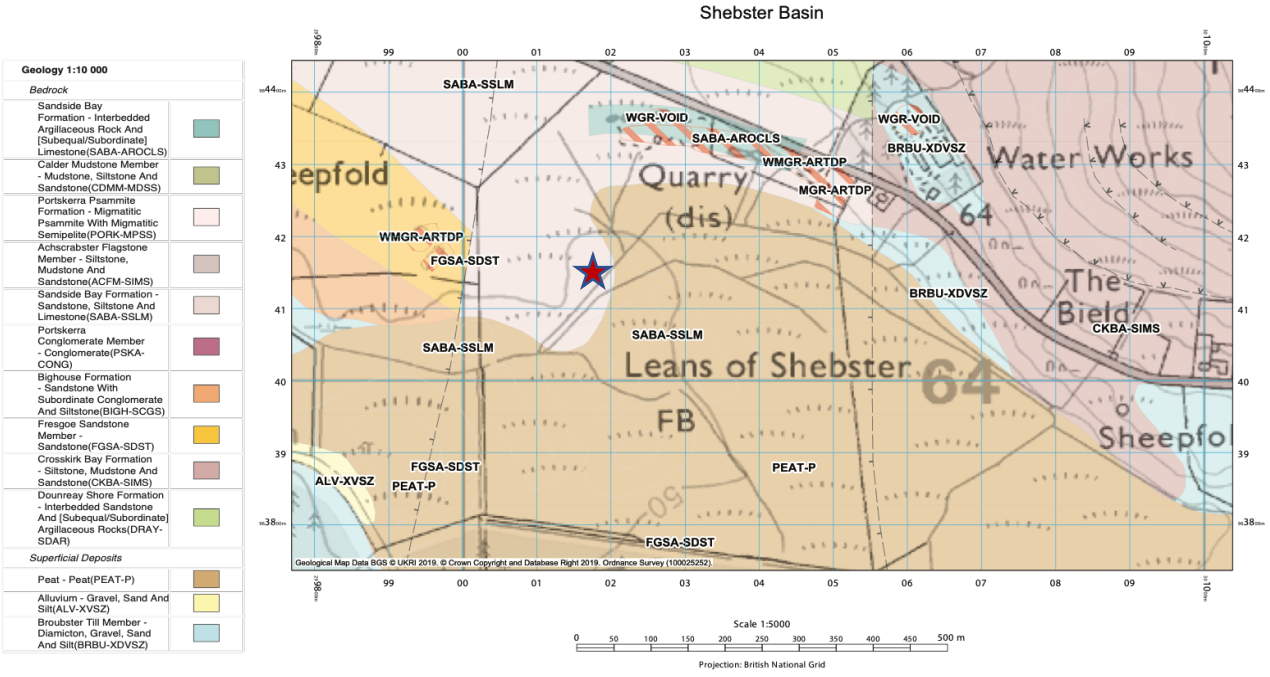

Figure 100. Geological map of the underlying lithology of the Shebster Basin. The red star indicates the coring site. Scale 1:1000m (Edina Digimap)

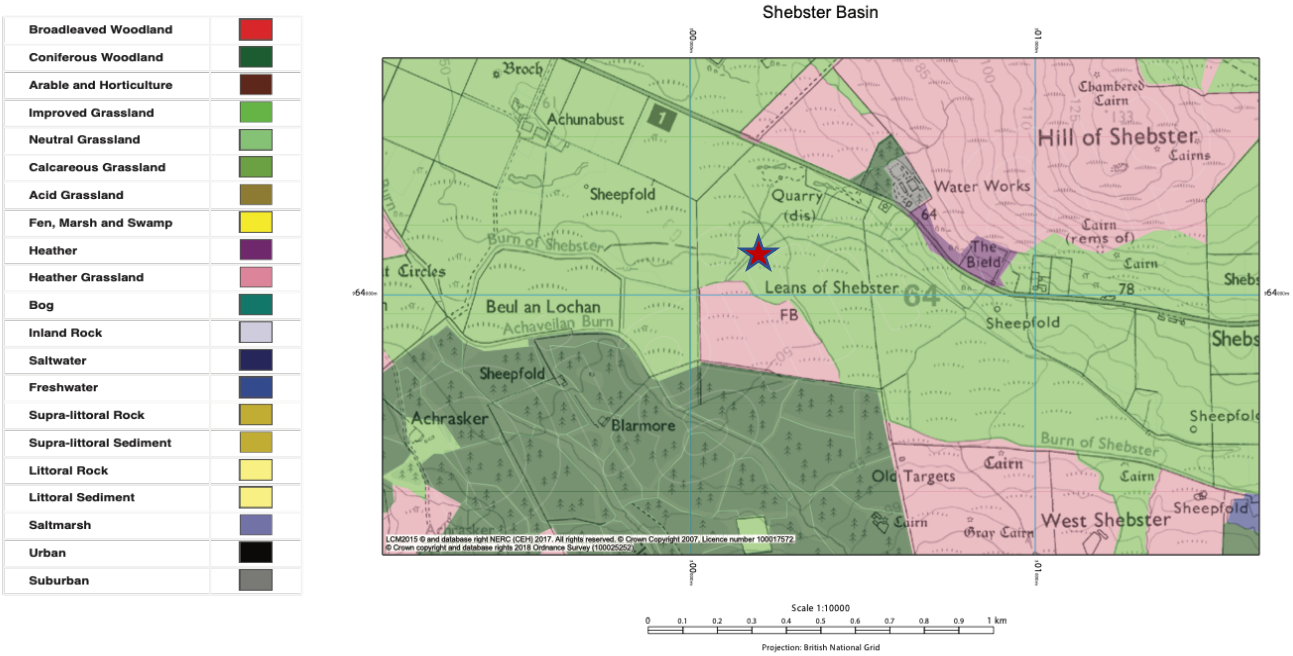

Figure 101. Land-use map for the Shebster Basin. The red star indicates the coring site. Scale 1:1000m (Edina Digimap, CEH land cover map, 2020)

8.2.4 **Climate**

Currently, the Shebster site is located c.50m above sea level and receives 900-1000mm of rain annually with temperatures also ranging between 11.5-3.5˚C from summer to winter (Birse, 1971; Golledge et al., 2009). Annually, the region has approximately 177 days of rain with mean annual maximum and minimum temperatures of 3.5-11.5˚C.

8.3. **Results and Interpretation**

8.3.1 **Lithology and Geochemical Analysis**

The Shebster core has distinctive lithological units and boundaries which have unique geochemical signatures. The LOI from their core shows little variation in the organic content of the LGIT sedimentary units with values ranging between 10-20% throughout [Fig.102]. The geochemical composition of the core was assessed using an ITRAX micro-XRF core scanner at Aberystwyth University [Fig.103]. Loss on ignition is not available for this core however was done on the adjacent core taken by Golledge et al (2009). As both cores have the same stratigraphical markers it is possible to transfer the organic content across. In summary the core is split into two distinctive lithologies: calcium carbonate rich marl units and minerogenic rich clays. Both units indicate climate warming and cooling respectively. Unidentified mollusc fragments and layers of organic rich plant fragments are found throughout. Each unit has been separated by depth and described below in detail:

(1) **Basal Sedimentary Layer** (965-963cm): Fine minerogenic rich blue-grey clay unit with intermediate counts of silica, iron and low counts of calcium. Higher counts of titanium indicate that minerogenic in-washing was high at this time. Higher iron values also indicate inorganic detritus entered the lake during this time. Low counts of calcium suggest that temperatures and productivity was low (Lauterbach et al., 2011). Based on the adjacent core from Golledge et al (2009) the organic content is 5%.

(2) **First Marl Sedimentary Layer** (965-945cm): Fine-medium grained yellow-cream calcium carbonate rich marl with occasional layers of plant remains and molluscs. From 965cm to 940cm there is a decrease in the counts of silica, titanium and potassium. However, silica is still present in the unit indicating that it may have

been reworked into the carbonate rich lake mud (marl). The presence of the calcium carbonate rich marl layer indicates higher temperatures prevailed to precipitate the calcium from solution. The higher temperatures promote the growth of $CaCO_3$ dependant organisms in the water column resulting in layers of biogenic marl found in the lakes (Pentecost, 2009; Willby, 2005). The organic content drops to 2-4% throughout this unit (Golledge et al., 2009).

(3) **First Minerogenic Layer (**945-930cm): from 945-939cm there is a graded contact from the previous marl to this silt rich brown-grey minerogenic unit. From 945 to 939cm there is a reduction in the levels of calcium whereas the levels of titanium, phosphorus, titanium, silica and potassium increase (all of which show a bimodal distribution). The titanium counts indicate that sediment transportation and minerogenic in-washing was high (Kylander et al., 2011). At 940cm there is a spike in the counts of potassium. Franke (2016) analysed a core from Lake Ohrid, Albania-Macedonian border, and found that peaks in potassium correlated with 6 tephra layers. Therefore, tephra maybe present at this depth, however further investigation is required. Based on the similarities in lithology and stratigraphy with the Loch of Sabiston core these spikes likely correspond to the Borrobol and Penifiler tephra. The organic content is 5% for this layer (Golledge et al., 2009)

(4) **Second Marl Layer** (930 to 902cm): this layer is composed of fine-medium grained calcium carbonate rich marl, with occasional lenses of organic rich material and mollusc fragments. There is a sharp reduction in the levels of iron, titanium, phosphorus and silica whereas the levels of calcium increase. Lauterbach et al (2011) suggests this increase in calcium reflects increased temperatures in the lake and, as a result, an increase in productivity. At 920cm there is a reduction in the amount of calcium which corresponds to an increase in the amount of phosphorus, titanium and potassium. The organic content falls again to 2-4% (Golledge et al., 2009)

(5) **Second Minerogenic Layer** (902 to 895cm): this layer is composed of fine-grained brown-grey minerogenic rich silts and clays. There is a fall in calcium levels with an increase in the levels of iron, phosphorus, silica and potassium. Increased levels of titanium, iron and silica occurs in this layer, highlighting that in-washing

and inorganic detrital inputs dominated the lake at this time (Kylander et al., 2011). There is a graded contact from marl rich sediments to brown-grey silts from 902 to 892cm. The organic content rises to 15% indicating an increase in lake productivity (Golledge et al., 2009).

(6) **Third Marl Layer** (892 to 865cm): fine to medium grained, creamy-yellow, marl and lenses of organic rich macrophytes. There is also a high concentration of mollusc fragments present, and occasionally whole specimens. From 895 to 865cm there is a gradual decline in the concentration of silica, iron and titanium suggesting that the environmental conditions were indicative of a temperate lake system (Croudace & Rothwell, 2015). Although, the levels of iron and titanium greatly fall there are some isolated peaks found between 890-884cm perhaps suggesting crypto-tephra layers (Kylander et al., 2011). The organic content gradually drops to 12% (Golledge et al., 2009).

(7) **Third Minerogenic Layer** (865 to 860cm): there is a graded contact from the calcium rich marl sediment to the fine-medium grained minerogenic rich clays. Silica, potassium, iron and titanium counts sharply rise throughout this unit and gradually decrease until the onset of the next marl layer. Increased levels of titanium, iron and silica occurs in this layer, highlighting that in-washing and inorganic detrital inputs dominated (Kylander et al., 2011). The organic content of the sediments gradually increases to 20% (Golledge et al., 2009).

(8) **Fourth Marl Layer** (860 to 850cm). From 860 to 850cm there is a sharp transition to fine-medium grained, creamy-yellow, calcium rich marls with occasional lenses of plant fragments indicating increased productivity in the lake. Calcium counts increase throughout this zone whereas silica, titanium, iron and potassium fall in this unit. This suggests that minerogenic in-washing fell at this stage (Kylander et al., 2011). Increasing calcium counts indicate that lake warming occurred which promoted lake productivity (Lauterbach et al., 2011). The organic content of the sediment remains stable at 20% (Golledge et al., 2009).

(9) **Fourth Minerogenic Layer** (850cm to 820cm) there is a sharp rise in the content of iron and titanium indicating the onset of in-washing (Kylander et al., 2011). This change in environmental conditions is believed to be linked to increasing inputs of detrital material (Kylander et al., 2011). A reduction in the levels of calcium is noted which suggests that the temperature of the water column fell and as a result primary productivity also reduced (Lauterbach et al., 2011). From 850cm to 820cm there is a sharp transition in to grey-brown clay rich lake mud with a silty texture. This zone increases in the concentration of silty material down core. In addition, the levels of phosphorus increase, reaching a maximum count at 830cm. The levels of potassium increase sharply, with a bimodal distribution, with the minimum counts found at 830cm. Increased counts of titanium suggest that the landscape was wetter resulting in increased catchment run-off (Croudace and Rothwell., 2015). Sediment transportation and minerogenic in-washing was high at this time (Kylander et al., 2011). There are layers of unidentified plant fibres visible throughout this zone. The organic content of the core falls to 5% indicating a fall in the abundance of organic matter and lake productivity (Golledge et al., 2009).

(10) **Fifth Marl Layer** (825cm to 795cm). This layer is composed of fine-medium grained marl rich cream-brown marl. There are high counts of calcium, suggesting that there was an increase in lake temperatures which led to an increase in the primary productivity within the lake and allochthonous material (Balascio et al., 2011; Lauterbach et al., 2011). From 825cm to 795cm the sediment is creamy-yellow, rich in plant fibres and with fragmented and whole molluscs remains. The iron counts start low and increase towards 820cm as the lithological boundary is met where there is a gradation into the clay-rich minerogenic unit beneath. The levels of calcium increase markedly, further supporting the hypothesis, that a productive lake system dominated. Throughout the zone there are peaks in iron at 805 and 815cm also highlighting possible layers of tephra (Kylander et al., 2012). Spikes in phosphorus at 799cm and 804cm suggest that there was an increase in the nutrient enrichment within the lake (Croudace & Rothwell, 2015). However, these short-lived spikes in phosphorus may highlight layers of cryptotephra (Timms et al., 2019). P_2O_5 levels increase where trachydacite and basaltic rich tephra's are present. This zone has low counts of silica which suggests that detrital inputs decreased (Martin-Puertas et al., 2011) and concentration of quartz rich sediments

decreased. Titanium counts are low however between the depths of 805-820cm there are spikes which may indicate possible cryptotephra layers (Kylander et al., 2012). The majority of this unit has low counts of titanium suggesting that in-wash was low (Czymzik et al., 2013). The organic content remains low at 5% (Golledge et al., 2009).

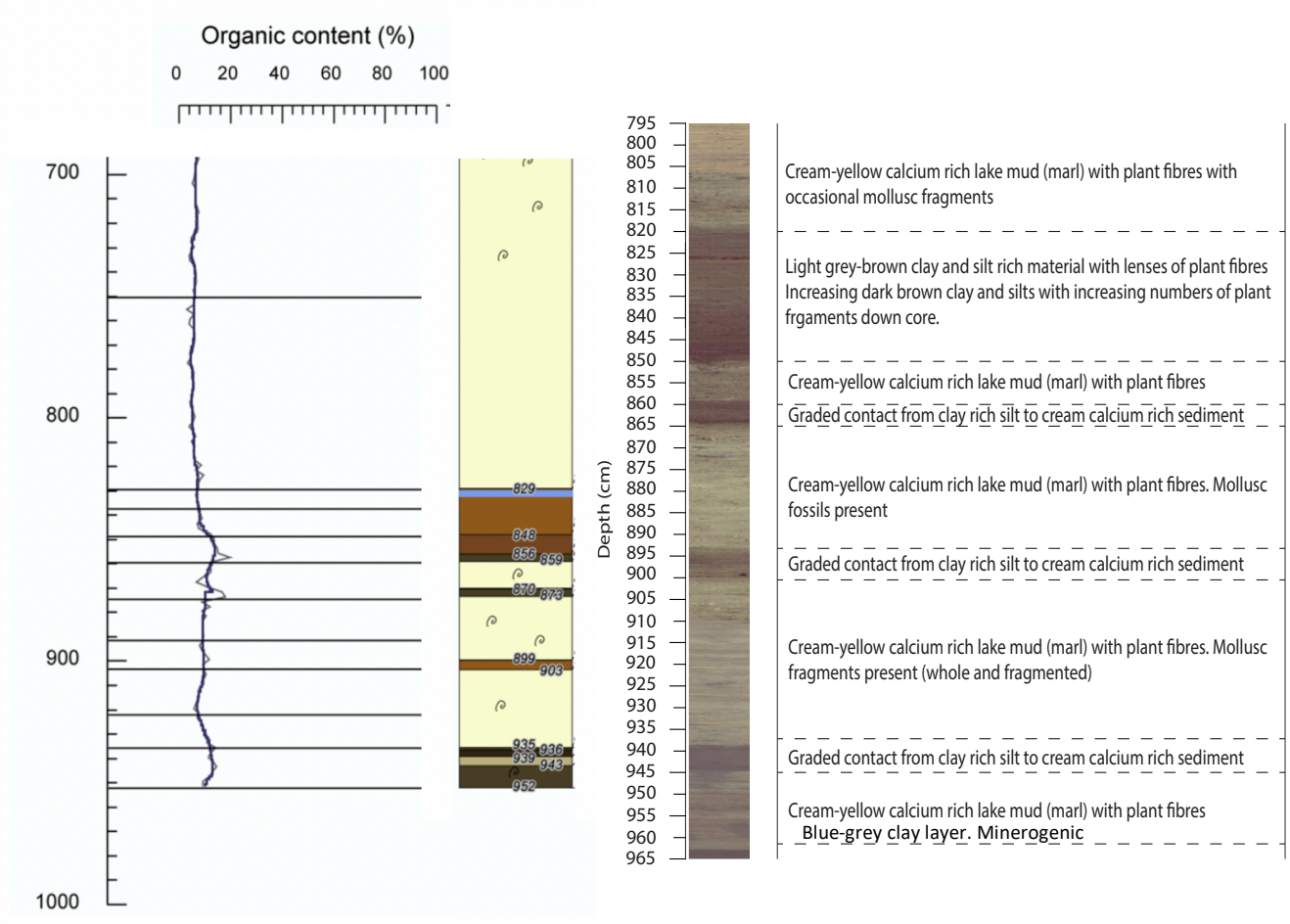

Figure 102. Loss on ignition (LOI) from the Shebster basin. The stratigraphy is shown on the right with the depth (cm) on the left (Golledge et al.,2009) (b) Lithological description of the Shebster basin core against depth. 9 distinct lithological zones have been identified

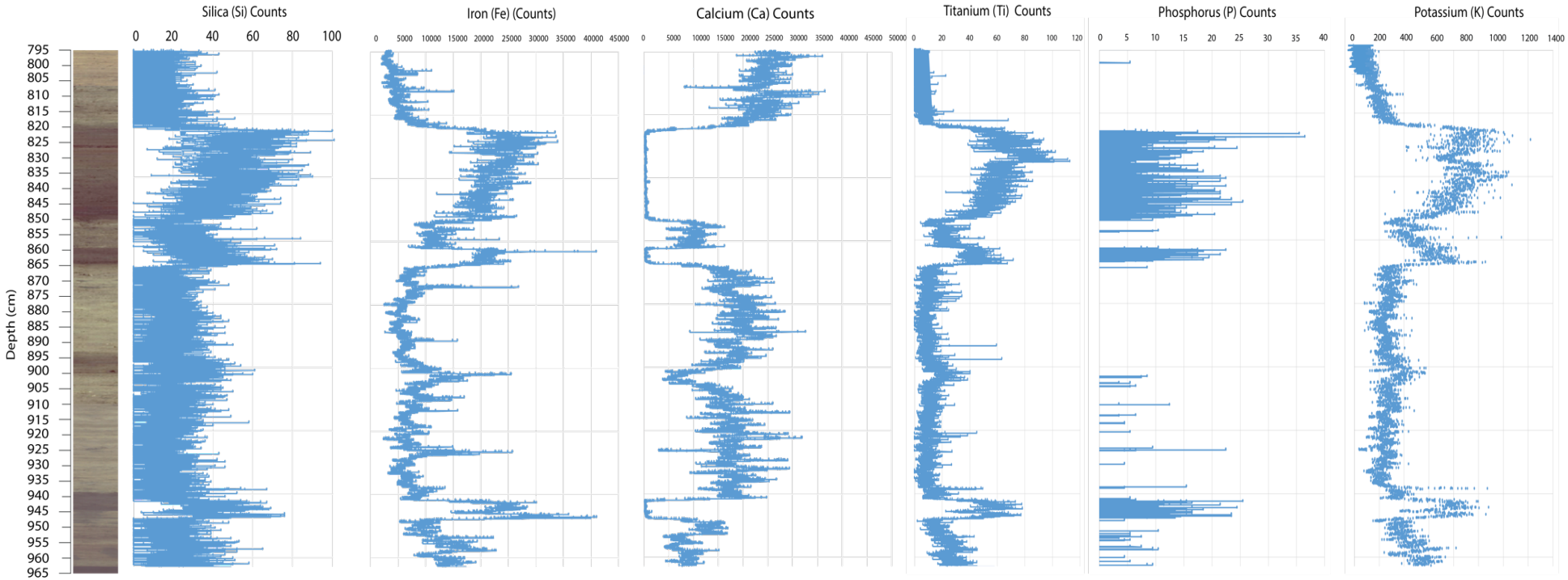

Figure 103. The XRF geochemical counts of Silica (Si), Iron (Fe), Calcium (Ca), Titanium (Ti), Phosphorus (P) and Potassium (K) are shown. The sediment core and subsequent depths are shown on the Y-axis.

8.3.2 **Chironomid head capsule assemblages**

Chironomid assemblages have been recorded for each sedimentary unit, spanning the LGIT, that encompasses depths of 965-875cm. A full list of all the species identified in the core will be shown in the appendix. Each sample is recorded as a percentage (%) of each species recorded in that sample [Fig.104]. Only the main taxa >5% are shown in the diagram below. Some species are shown that have an abundance <5% as they thrive in specific environments which aid the interpretation of the record. All of the species identified were included in the transfer function to reconstruct reliable mean July summer temperatures [Fig.105. The 109 Norwegian lakes calibration data set has been used to model the palaeo-temperatures across the LGIT (mean July summer temperatures (˚C) (section.). Cluster analysis was undertaken to separate the significant chironomid taxa into zones using CONISS. See the chironomid diagram below which contains the dominant chironomid taxa in the Shebster core [Fig.104].

- **Zone Sheb-1** (965-946cm) is dominated by temperate-warm species of chironomids. *Psectrocladius sordidellus, Chironomous anthracinus, Microtendipes pedullus, Procladius* and *Tanytarsus mendax* constitute the largest percentage of the overall assemblage. These taxa are indicative of temperate conditions (Brundin, 1949) and are associated with aquatic macrophyte communities (Brodersen et al., 2001; Brooks et al., 2007). Furthermore, *Psectrocladius sordidellus* is a species of chironomid that is found in acidified lakes (Brodin & Gransberg, 1993). *Chaetocladius piger* is a rare species in this assemblage (accounting for 2.3% of the overall assemblage) and is found predominantly in the Holarctic (Cranston et al., 1983). *Crictopus sylvestris* is another rarer species found in this zone corresponding to 0.7-1.5% of the assemblage. Although dominated with temperate species of chironomids there are also occurrences of colder species. Throughout this zone *Paracladius,* a cold dominant species is found, and constitutes 2.3-4.9% of the assemblage. This species is found in oligotrophic lakes in the sub-arctic (Walker et al., 1991). Based on the species recorded mean July temperatures have been inferred between 11-13˚C.

- **Zone Sheb-2** (946-934cm) is composed of ultra-cold to cold species of chironomids at the onset of the zone. *Microspectra radiallis* is found in higher abundances at the start of the zone (12.9% of the assemblage) and falls throughout (to a low of 8.2%). This is a cold stenotherm species is indicative of arctic conditions (Brooks et al., 2007). *Tanytarsus lugens* (4.8%), *Paracladius* (1.0-11.3%). *Sergentia coracina* also occur in high abundances in this zone, averaging 17% of the assemblage. These species are also indicative of cold arctic conditions (Walker et al., 1991; Brooks et al.,2007). *Microspectra insignilobus* is the most dominant species of chironomid in this zone reaching a high of 45.2% of the assemblage. *Orthocladius trigonobalis* is a cold stenotherm (Brooks et al., 2007) ranging between 1.8 - 8% of the assemblage. At the latter half of the zone the composition of chironomids alters, promoting communities of temperate species such as *Psectrocladius sordidellus* and *Chironomous anthracinus* grading into the next significant zone. Modelled mean July temperatures range between 6-7˚C for this zone in the earlier stage of this zone and gradually rise to 8˚C at the end.

- **Zone Sheb-3** (934-900cm) is separated into 3 parts (a-b-c). The statistical package, CONISS, inferred 3 distinctive zones within Sheb-3. Overall, the zone is dominated by temperate species of chironomids however there are three subtle subdivisions.
    - Zone Sheb-3a (934-924cm) is dominated by temperate-warm species of chironomids such as *Psectrocladius sordidellus, Microtendipes pedullus, Ablabesmyia* and *Tanytarsus pallidocomis*. Based on the assemblage of these chironomids temperatures have been inferred to range between 10.0-10.5˚C which are indicative of temperate-warm summer conditions. The presence of *Microtendipes pedullus* indicates that the lake was littoral and low in organics (Pinder & Reiss, 1983; Hoffman, 1984).
    - Zone Sheb-3b (924-910cm) has a similar composition to the previous subdivision however colder species of chironomid begin to appear. *Orthocladius trigonobalis* dominates the assemblage ranging between 11-14.3% of the assemblage. This species is a cold stenotherm indicative of cold arctic conditions (Brodin, 1986; Saether, 1979). *Hydrobeanus conformis, Paracladius* and *Microspectra radialis* appear also with an

abundance of 1.4% are other species which are present and are indicative cold oligotrophic condition (Cranston et al., 1983). The presence of these species suggests temperatures ranged between 9˚C and that nutrient levels in the lake fell considerably.

- Sheb-3c (910-900cm) has a similar composition to Sheb-3a. *Pagastiella* and *Dicrotendipes nervosus* (11.4%) is often found in littoral sediments of lentic waters (Pinder & Reiss, 1983). This species is also associated with aquatic plants (Moller Pillot & Buskens, 1990; Brodersen et al., 2001). This species is classed as a thermophilic species which is often found in warmer temperate lakes (Brooks et al., 2007). This assemblage indicates that mean July temperatures rose again to 10-11˚C.

- **Zone Sheb-4** (903-892cm) is dominated by cold-temperate species of chironomids. The presence of *Corynocera ambigua* spikes within this zone, constituting 37.9% of the assemblage. Indicating a sharp transition from temperate to colder conditions (Brooks et al., 2007). *Microspectra insignilobus* is also found in cold lake systems however this species has a wider temperature range and can occur in warmer conditions (Brundin, 1956; Brooks et al., 2007). This species is also acidophilic, preferring lakes with lower pH. *Sergentia coracina* is found in this assemblage and is indicative of cold oligo-mesotrophic lake conditions (Brodin & Gransberg, 1993). The temperature inference model suggests that mean July temperatures fell to 7-8˚C.

- **Zone Sheb-5** (892-867cm) is composed of temperate species of chironomids. This is indicated by the dominance of *Chironomous anthracinus, Psectrocladius sordidellus, Corynocera ambigua and Orthocladius type-S*. There is a sharp rise in the abundance of *Corynocera ambigua* which indicates a rapid change in the environment occurred at this time (Brooks et al., 2007). Although this zone is dominated by temperate species, *Microspectra radialis and Paratanytarsus austriacus* also occur in low-moderate abundances (5 to 10% respectively). Mean July temperatures range between 9-10˚C.

- **Zone Sheb-6** (867-860cm) is dominated by ultra-cold to cold species of chironomids. This is shown by the presence of *Tanytarsus lugens* (10%), *Sergentia coracina* (10%) and *Microspectra insignilobus* (10-20%). The species above are indicative of a sub-arctic/arctic environment that is nutrient deficient (Brooks et al., 2007). *Tanytarsus lugens* is a cold stenotherm which is found in the profundal of nutrient deficient lakes in the arctic (Brundin, 1956; Brodin, 1986). *Corynocera ambigua* occurs in high abundances (50-69.8% of the assemblage). Mean July temperatures have been inferred to range between 6-7˚C.

- **Zone Sheb-7** (860-849cm) This zone is dominated by the presence of *Microtendipes pedullus (20%), Corynocera ambigua (40%), Dicrotendipes nervosus (10-15%), Chironomous anthracinus (20%) Tanytarsus mendax* and *Orthocladius type-S. Dicrotendipes nervosus* indicates a return to a lake system dominated by aquatic plants (Moller Pillot & Buskens, 1990; Brodersen et al., 2001) and warmer temperate lakes (Brooks et al., 2007). The sharp rise in *Corynocera ambigua* indicates that rapid environmental change occurred during this time (Brooks et al., 2007). The presence of *Microtendipes pedullus* suggests that the lake was low in organics (Hoffman, 1984). This species is abundant in Holocene and Late Glacial sediments and is associated with intermediate temperatures in the Norwegian training set (Brooks & Birks, 2001). Based on the overall assemblage, mean July temperatures have been inferred to range between 8-9˚C.

- **Zone Sheb-8** (849-824cm) is composed of ultra-cold species of chironomids: *Microspectra insignilobus, Crictopus intersectus, Sergentia coracina, Paratanytarsus austriacus, Protanypus, Pseudodiamesa, Microspectra radialis and Tanytarsus lugens*. All of these species are found in cold oligotrophic lakes in the sub-arctic/arctic (Walker & MacDonald, 1995; Oliver, 1983). The abundance of *Microspectra radialis* is high at the start of the zone (40%) and falls to 10-15%. Whilst the abundance of *Sergentia coracina* is 20% at the start of the zone and rises to 40% replacing *Microspectra radialis* mid-way through the minerogenic sediments. These species are indicators of cold arctic conditions (Brooks et al., 2007). Mean July temperatures ranged between 5-7˚C.

- **Zone Sheb-9** (824-785cm) is dominated by a sharp rise in warm species of chironomids. The assemblage indicates a marked change in the environmental conditions shown by the presence of *Corynocera ambigua* (20-60%), *Microtendipes pedullus, Psectrocladius sordidellus* (20-50%), *Ablabesmyia* (5-20%), *Tanytarsus mendax, Endochironomous albipennis* (15%), *Dicrotendipes nervosus* (10-20%), *Cladopelma lateralis* (5%), *Paratanytarsus albimanus* (<5%) and *Polypedulum nubifer* (<5%). This is the first time that *Cladopelma lateralis*, Paratendipes albimanus and Endochironomous albipennis occurs in the core. *Cladopelma latteralis* is indicative littoral and muddy lakes (Hoffman, 1984; Walker & MacDonald, 1995). *Endochironomous albipennis* and *Paratendipes albimannus* are abundant in lakes which have a mesotrophic-eutrophic nutrient status and in lakes where there are aquatic plants (Pinder & Reiss, 1983; Saether, 1979; Brodin, 1986; Brodersen et al., 2001). Mean July temperatures have been inferred to have risen abruptly from 5-13˚C at the boundary between these two assemblages.

8.3.3 **Reliability of chironomid inferred temperatures**

Mean July summer temperatures have been modelled for the Shebster basin and the sample specific errors have been included [Fig.105]. The majority of the samples within the Shebster core have a good fit to temperature, with the exception of 5. The samples on the right-hand side of the dashed line indicate the assemblages which have a poor fit to temperature and have been identified with red markers [Fig.106]. The good modern analogue technique indicates that the samples have no modern analogue, as the squared chord distance cut-off exceeds 60. However, the samples have a good fit to temperature [Fig.106] Birks et al (2010) and Brooks et al (2012) highlight that these temperatures should be treated with caution. However, they show that the temperature reconstructions can still have a good fit to temperature when there are no modern analogues. The rare chironomid species, *Corynocera ambigua*, is present in large quantities (constituting 40-60% of the overall chironomid assemblage) between the depths of 900-890cm and 790-820cm. Although rare in the Norwegian training set this species is quite common in the marl rich lakes from Caithness and the Isle of Orkney.

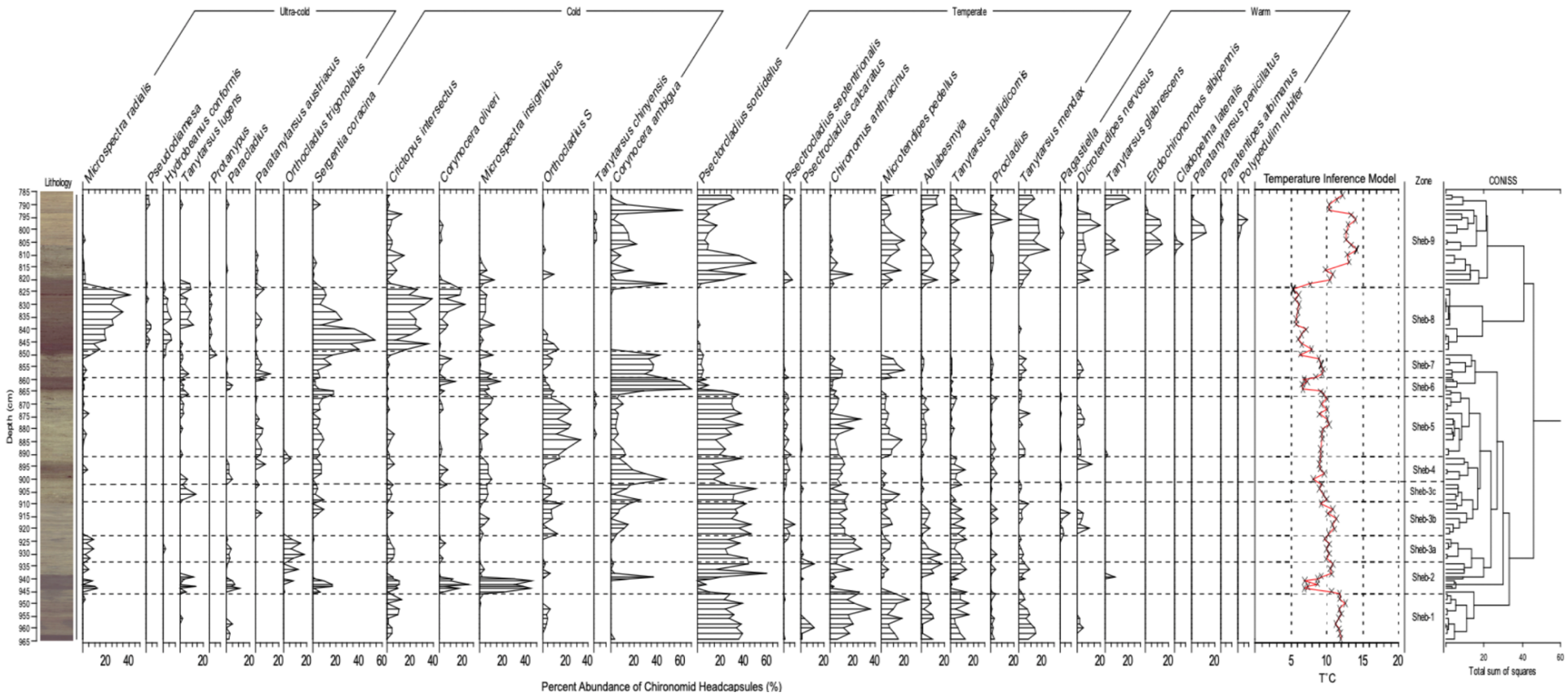

Figure 104. Chironomid assemblage plot for the Shebster basin. The diagram shows the species of chironomids, separated by different temperature optimums. The temperature inference model (°C) is included on the diagram above with the CONISS plot highlighting the statistically significant assemblage zones

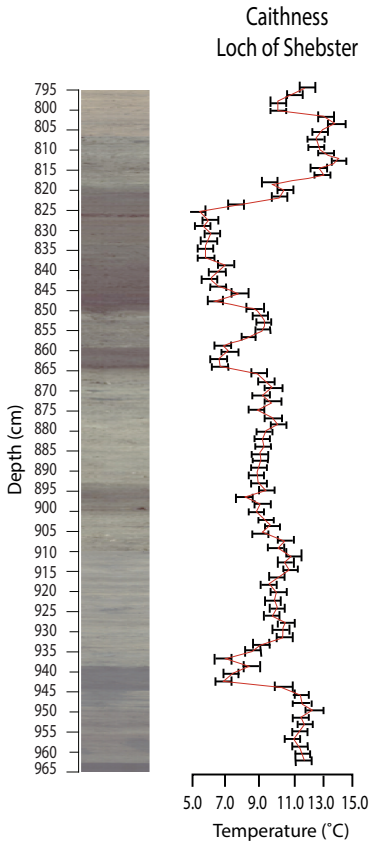

Figure 105. Shebster C-IT (°C) model with sample specific errors.

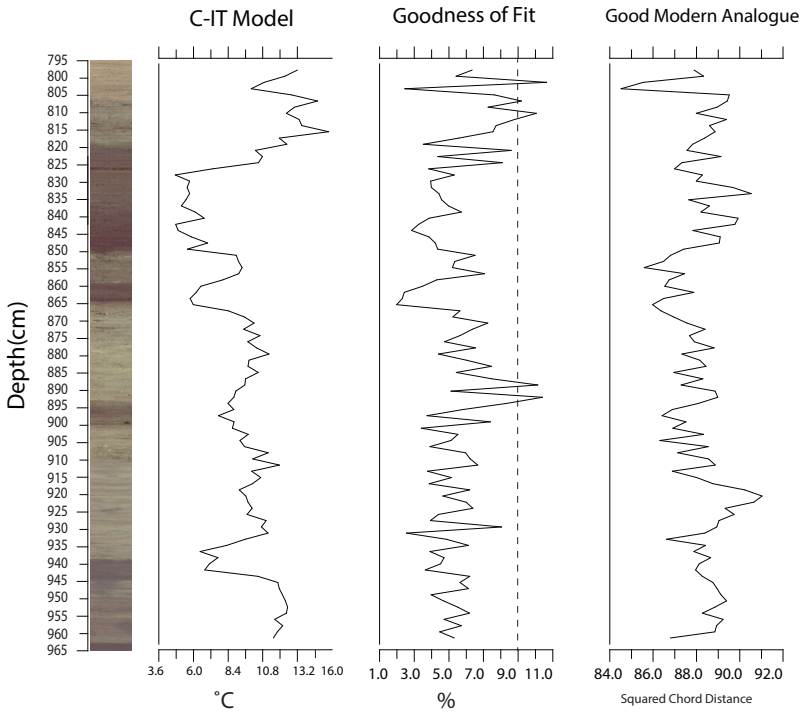

Figure 106. Chironomid C-IT model (°C), Goodness of fit (%) with rare types highlighted above to the right of the dotted line and the Good Modern Analogue (squared chord distance)

8.3.4 **Long-chain Alkenone temperature reconstructions**

The long-chain alkenone temperature proxy has been shown by D'Andrea et al (2016) and Toney et al (2010) to reconstruct palaeo-spring lake temperatures. For the Shebster basin temperatures were calculated using a Norwegian lake calibration from Lake Vikvatnet (D'Andrea et al., 2016) (section 5.6.4). Long chain alkenones have a unique gas chromatography profile [Fig.107]. The area underneath the peaks are used to calculate the sample specific U_{37}^{k} index. The first stage is to calculate the peak area of the 37:4, 37:3a, 37:3b and the 37:2 alkenones. The calculated independent U_{37}^{K} index is recorded for each sample and shown in the supplementary table provided [Appendix.]. The index has a maximum value of -0.05 and a minimum value of -0.72. See below a diagram showing the chromatogram peaks indicating the presence of alkenones in minerogenic and organic rich sediments [Fig.107] The following equation is used to calculate the U_{37}^{K} index:

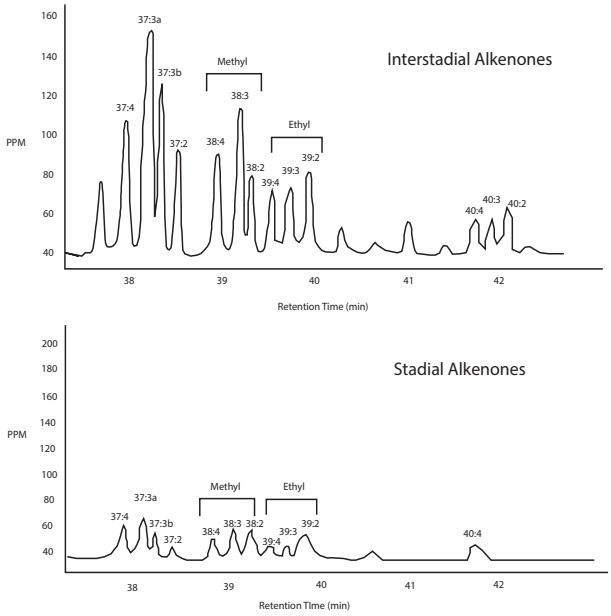

Figure 107. The GC-FID profile for interstadial and stadial sediments found in the Shebster basin core are shown above. The peaks for the 37:4, 37:3a, 37:3b and the 37:2 Long-chain Alkenones are shown with the retention time noted on the x-axis (minutes)

$$U_{37}^{K} = \frac{[C_{37:2}\text{alkenone}] - [C_{37:4}\text{alkenone}]}{[C_{37:2}\text{alkenone}] + [C_{37:3}\text{alkenone}] + [C_{37:4}\text{alkenone}]}$$

Where samples had a mix of Group I and Group II haptophyte algae a lake calibration from Alaska was used (Longo et al., 2018). At present this is the only calibration that takes into consideration a mix of haptophyte algae. See below the relationship to calculate the R3b index:

$$\mathrm{R3b} = \frac{[\mathrm{C_{37:3b}}]}{[\mathrm{C_{38:3b}alkenone}] + [\mathrm{C_{37:3b}}]}$$

An independent lake calibration was unable to be built due to the fact, that at present, the Shebster basin does not currently have a lake or body of water to analyse (see section 5.6.4 for justifications of the methodology.) Therefore, the water temperature in Shebster cannot be recorded and the linear temperature model required to model spring temperatures cannot be built. Hence, why the following two relationships have been chosen to reconstruct the spring lake temperatures (1) Norwegian Lake Vikvatnet calibration (D'Andrea et al., 2016) and (2) an Alaskan lake calibration (Longo et al., 2018). The inferred LCA temperatures are shown in the supplementary table along with the independent $\mathrm{U}^{\mathrm{k}}_{37}$ index and R3b for the Shebster basin [Appendix].

$$(1)\mathrm{U}^{\mathrm{K}}_{37} = 0.0284\ (\mathrm{T}) - 0.655$$
$$(2)\mathrm{R3b} = 0.0081\ (\mathrm{T}) + 0.44$$

The diagram below records the $\mathrm{U}^{\mathrm{k}}_{37}$ index only temperature reconstructions. When this index was applied to the Norwegian calibration (equation 1) temperatures were exceedingly large during the warmer phases of the LGIT and recorded spring temperatures which were larger than the mean July summer temperatures recorded by the chironomids. Furthermore, during the coldest stage of the LLS the temperatures recorded were -0.7˚C which is not possible as this would indicate that the lake was frozen. Haptophyte algae require photosynthesis to thrive (Longo et al.,2018). When a combination of both indices and both lake calibrations were used (equation 1+ 2) then the temperatures became more realistic. The temperatures during the warmer phases still record higher values than the mean July temperatures from the chironomids. However, these are more realistic now (ranging between 10-15˚C). There is a closer agreement with the temperatures during the cold phases of the LGIT between the LCA and C-IT reconstructions [Fig.108 & 109]. However, during the LLS there is a hiatus in the LCA record.

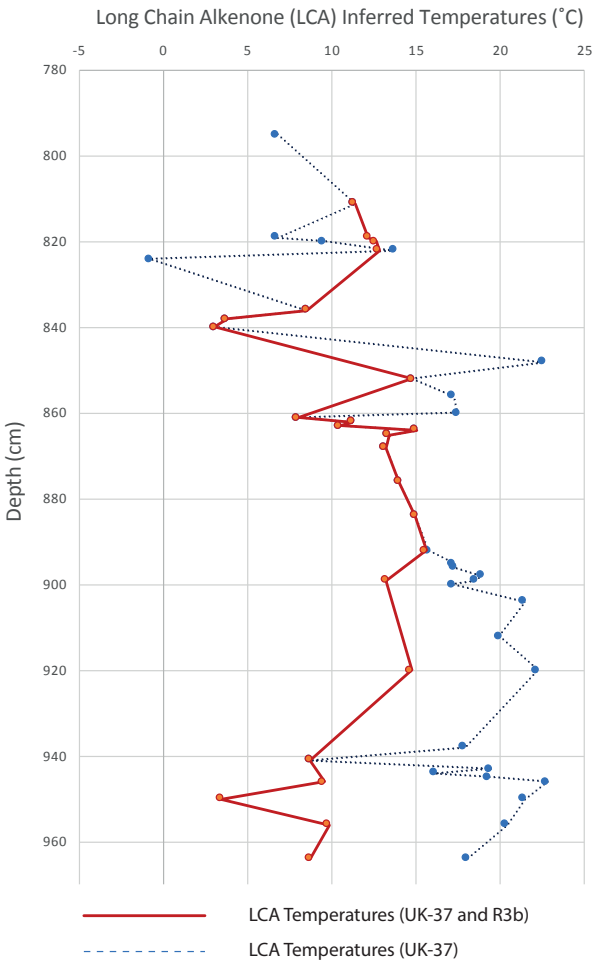

Figure 109. Graph showing the temperatures reconstructed with the UK37 index and Norwegian lake calibration (D'Andrea et al., 2016)(Blue dotted line) and the combined Uk37/R3b index and lake calibration from Alaska (Longo et al., 2018)(Red line).

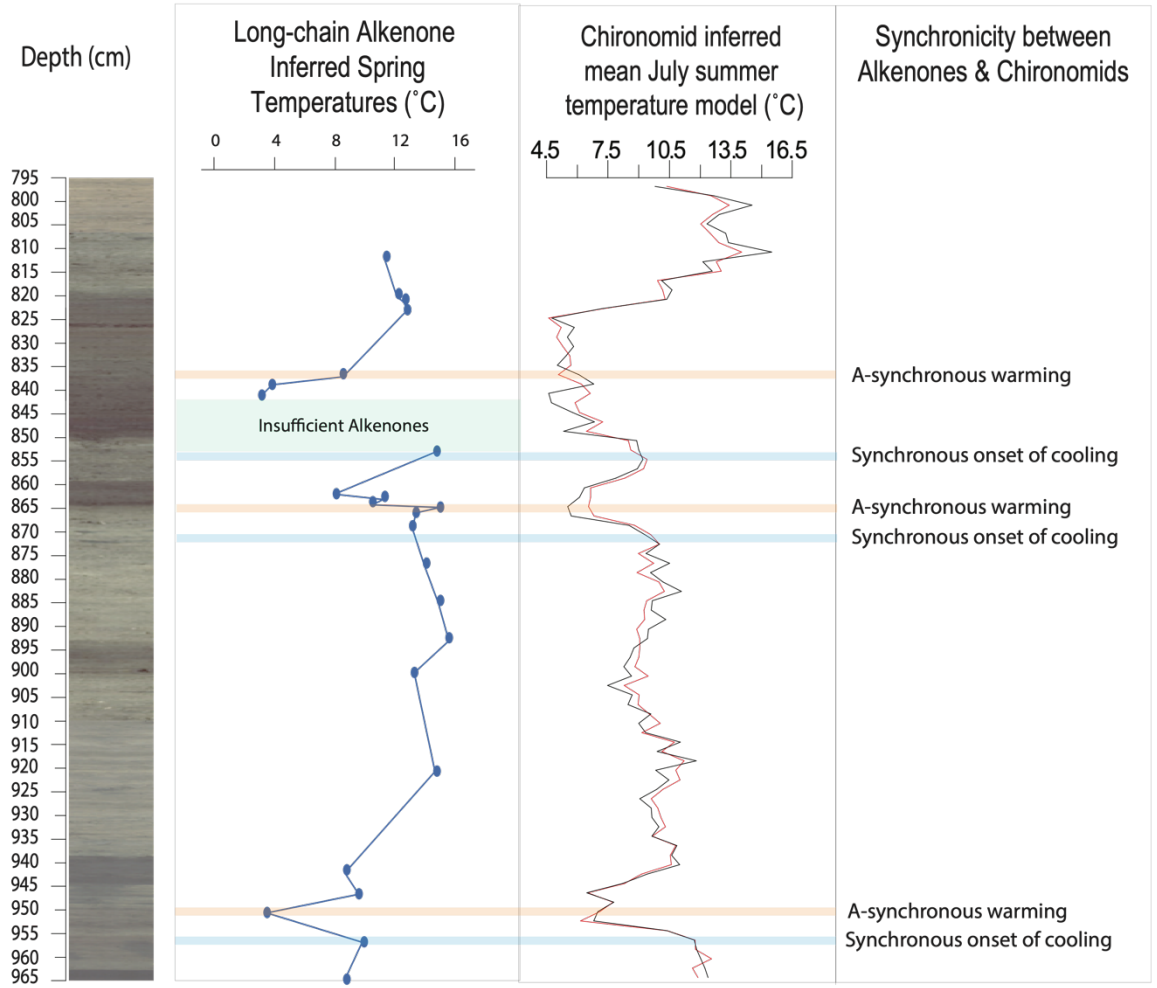

Figure 108. Graph combining the chironomid inferred mean July summer temperatures (˚C) with the spring lake temperatures from the alkenone record (˚C). Samples are plotted by depth (cm) and the synchronicity of the proxies are shown on the right.

8.3.5 **Offset between C-IT and LCA records**

The long chain alkenone record indicates that temperatures during the colder phases were similar to those recorded by the chironomids which highlights the robustness of the LCA temperatures during these periods. However, during phases of organic sedimentation temperatures range between 14-15˚C whereas the C-IT model indicates temperatures range between 10-11˚C. See below a fuller description of the offsets between both records. This is problematic as the LCA temperature record is inferring spring temperatures which are higher than the chironomids inferred summer temperatures. Below are two possible explanations which may explain the apparent offsets throughout warm phases of the LGIT:

(1) **Lack of an independent lake calibration.** Due to the lack of an independent lake calibration for the Shebster basin temperatures have been inferred from the D'Andrea et al's (2016) Norwegian Lake Vikvatnet. However, due to the presence of both group I and group II haptophytes a lake calibration from Alaska (Longo et al., 2018) was used to account for this mixed distribution. The environmental conditions in Alaska are not subjected to the same environmental forcing as in N.W Europe, (e.g. North Atlantic thermohaline circulation). The chironomid inferred temperatures are likely more accurate as they represent assemblages found in the region of N.W Europe. The chironomid training set considers average temperatures, over varying latitudes, encompassing 154 lakes and 142 species, (Brooks and Birks, 2001). However, the calibration used in this study is independent to Lake Vikvatnet in Norway, and Alaska, meaning that the environmental conditions, whilst they may be similar to Caithness, will not directly represent the absolute inferred temperatures during the LGIT. The output from this research, until an independent calibration can be found, should be interpreted in a relative sense of warming and cooling.

(2) **Saline intrusion**: As there are a mixture of Group I Haptophytes (indicative of freshwater/shallow environments) and the Group II haptophytes (found in deeper coastal-saline environments) this suggests that there may have been a marine influence in the lake system that skewed the temperature inference models. The Shebster basin is in close proximity to the North Atlantic Ocean. Shennan et al.,

(2006) indicates that Wick, 48km from the Shebster basin, had a relative sea level change of -20m between 14-10 ka yr. BP meaning that the lake may been strongly influenced by marine incursion. This is not unreasonable to assume as presently the lakebed is found approximately 60m above sea level today.

8.3.6 **Chronology**

Golledge et al (2009) constructed an age-depth model for the Shebster basin. However, the modelled ages were too old and there were age-reversals found throughout. They recorded one of the earliest ages of deglaciation at c.18k cal BP. Furthermore, the material that was analysed was not reliably identified. It was not possible to determine if aquatic or terrestrial plant fragments were analysed from their study. An independent chronology would have been preferred and 11 AMS radiocarbon dates have been successfully awarded from the NERC Radiocarbon Committee (2019) however the samples were not available for the submission of the thesis due to time and COVID-19 restrictions. However, they will be used for future research and publications.

For this research the high-resolution chronology from Loch of Sabiston will be transferred to this research [Fig.91 & 92]. Loch of Sabiston has a combination of AMS and tephra tie-points which constrain the main climatic events during the LGIT. Loch of Sabiston is the closest chironomid inferred temperature record to the Shebster basin and temperature fluctuations present in Loch of Sabiston are also present in the Shebster basin. Therefore, it is possible to match the climate oscillations to this site. There are 6 main temperature transitions recorded in both Loch of Sabiston and the Shebster basin: Abrupt cooling at 14.09k cal BP, abrupt warming at 13.90k cal BP, abrupt cooling at 13.16k cal BP, abrupt warming at 12.91k cal BP, abrupt cooling at 12.63k cal BP and abrupt warming at11.90k cal BP. Both lake cores have a similar diversity of chironomids and have similar geochemical compositions. Both switch from minerogenic rich sediments to calcium carbonate rich marl during periods of warming and cooling.

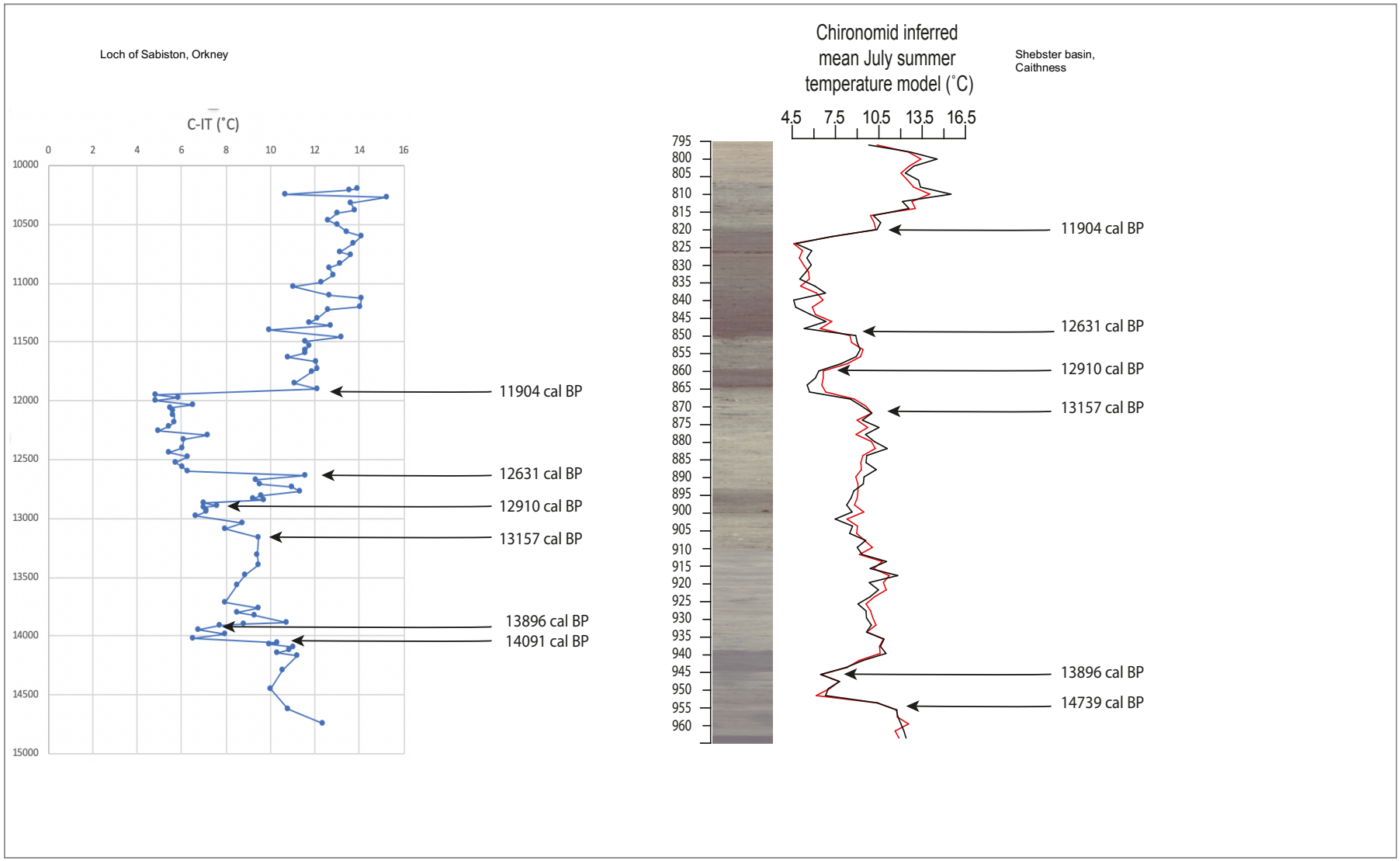

Figure 110. Loch of Sabiston (C-IT˚C) with age (cal yr BP). The dates transferred over are shown below. The same dates are shown on the C-IT(˚C) for the Shebster basin. Black arrows highlight the matched calibrated radiocarbon ages and the red/black lines correspond to the inferred temperature reconstructions from the Norway & Norway-Swiss Combined training sets.

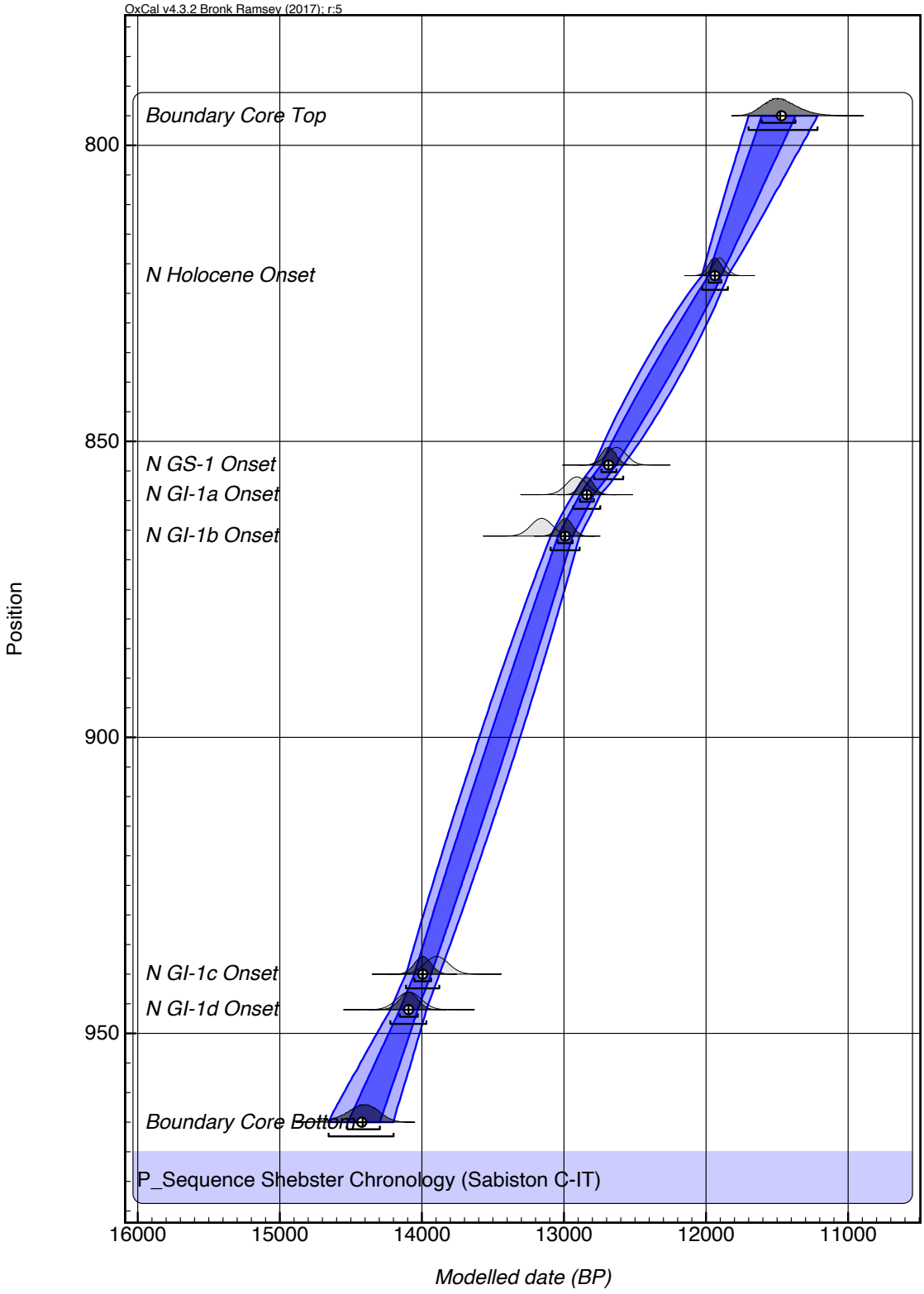

Figure 111. Age-depth model (modelled cal Yr. BP) based on dates based on the chronology of the Loch of Sabiston. The main climatic events were used as tie-points between sites: GI-1d onset, GI-1c onset, GI-1b onset, GI-1a onset, GS-1 onset and Holocene onset.

8.4 Discussion

8.4.1 Palaeoclimate & environmental history of Caithness

A high resolution of the palaeoclimate and environmental changes of the LGIT have been made for the north coast of Scotland using a multiproxy approach [Fig.112]. This is the first high-resolution mean July summer temperature record for the northern region of Scotland and the first Scottish long chain alkenone spring lake temperature record. By combining both records, and a robust chronology, it is now possible to better understand seasonality in the temperature records [Fig.114]. Wagner-Cramer & Lotter (2011) suggests that warming spring temperatures lead temperature changes in the summer months. Therefore, it is important to understand how spring and summer temperatures forced environmental change during the LGIT. This research indicates that there is a close similarity between the warming and cooling trends between both proxy records. However, there are distinct and important differences in the records [Fig.114]. With a high-resolution chronology, it is possible to determine when the main climatic events of the LGIT occurred in Caithness [Fig.113]. Combined with a high-resolution geochemical record one can better understand the relationship between the chironomids, alkenones and processes within the lake through time. See below an interpretation of the main warm and cold phases during the LGIT for the Shebster basin (each of the main climate events will be compared to the Greenland ice core chronology and local climate descriptors [Fig.113]).

8.4.2. LGM deglaciation of the Shebster basin

Bradwell et al (2019) highlights that glacial retreat occurred between 17-18k cal yr. BP in Caithness. However, radiocarbon dates from marine and terrestrial records nearby suggest deglaciation occurred at 18.5k cal BP (Sejrup et al., 2009). With the basal clays being deposited at c.14.2k cal BP there appears to be an offset of 3000 years between deglaciation and the onset of sedimentation. The intermediate counts of titanium in the basal sediments indicates that the lake was unstable and minerogenic in-washing was prevalent at this time (Kylander et al., 2011). The lake was not established, which accounts for the lack of chironomid inferred temperatures during this period. Any bodies of water would have been highly turbid, unstable and would likely be frozen over. As a result, the environment would not be able to support a community of chironomids.

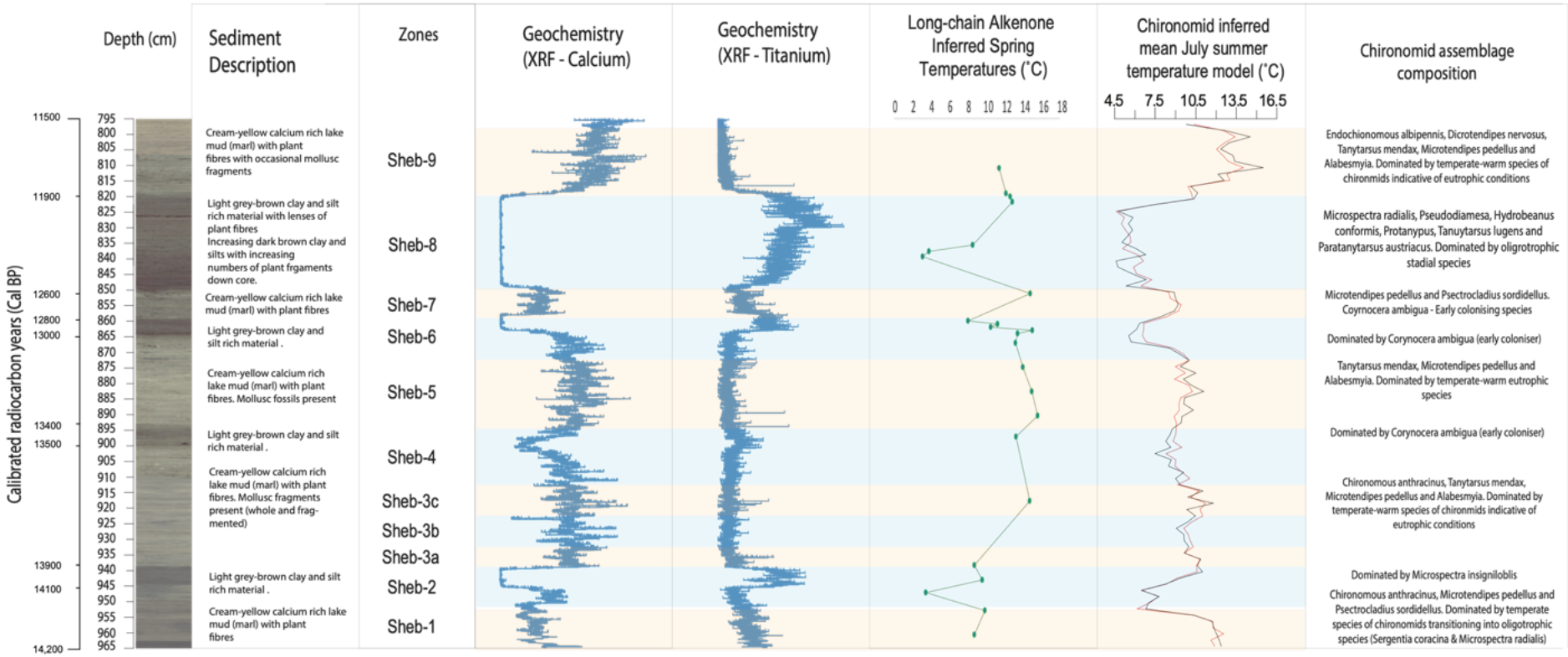

Figure 112. Sediment description, geochemical data (calcium and titanium), chironomid inferred mean July summer inferred temperatures (˚C), Long-chain Alkenone inferred spring temperatures (˚C), age-depth model (cal Yr. BP), chironomid assemblage plot and the climatic INTIMATE event stratigraphy.

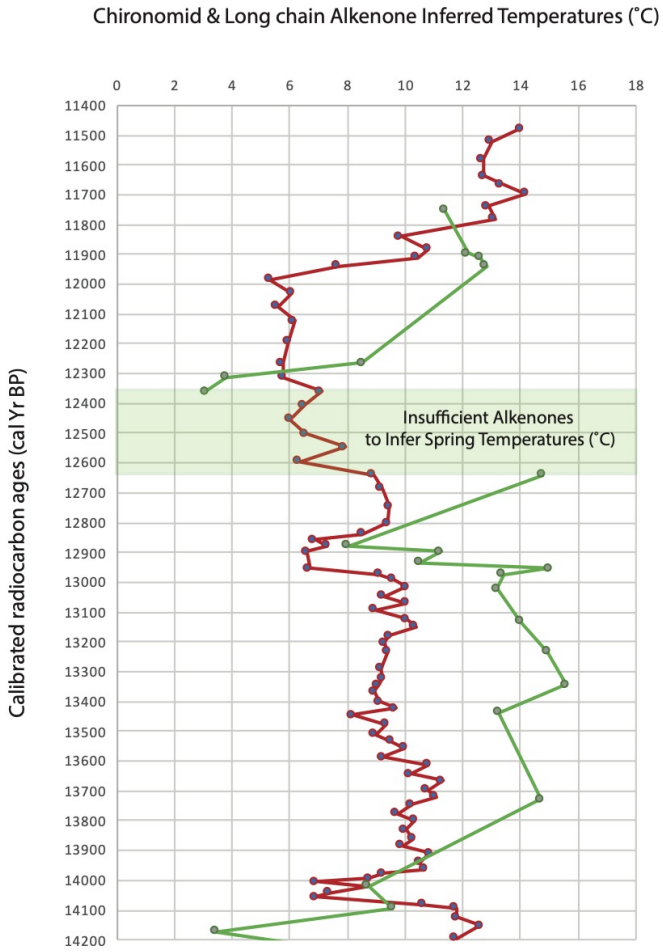

Figure 114. C-IT (˚C) and LCA (˚C) palaeotemperatures for the Shebster basin showing the temporal offsets in cooling between both records. Alkenones (Green) and Chironomids (Blue).

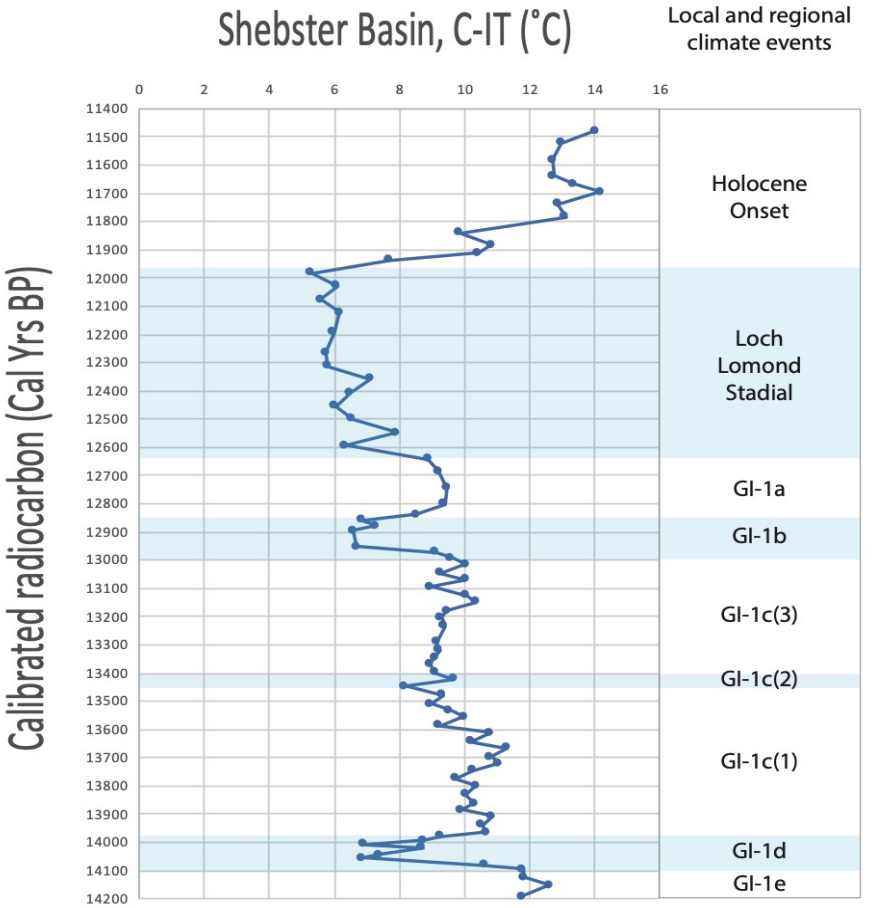

Figure 113. C-IT(˚C) for the Shebster basin with calibrated radiocarbon ages (cal yr BP). The local and regional climate descriptors are shown to the right (Rasmussen et al., 2014; Lowe et al., 2019). The cold events are highlighted in blue

8.4.3 **GI-1e (< c.14.2-14.1ka cal yrs. BP)**

The onset of sedimentation and climate warming occurs at c.14.2k cal BP and lasts until 14.1k cal BP. Temperatures appear stable during this time and range between 12-12.5˚C. However, the LCA record shows that spring lake temperatures were significantly lower, reaching 3.8˚C. This apparent offset is likely a result of the chironomids recording the warming air temperatures during GI-1e whilst the alkenones are recording localised melt water. The LCA record here was constructed using the combined temperature model as both group I and group II haptophytes were found here. Longo et al (2018) highlights that a mix of haptophytes are found in environments where salinities abruptly change, for instance where lake basins are fed by glacial meltwater allowing oligohaline conditions to prevail. However, this may also be a result of seasonality. It is likely that spring water temperatures were lower than those in the summer, which accounts for this offset between the records.

Temperate-warm species of chironomids dominate: *Psectrocladius sordidellus, Chironomous anthracinus, Orthocladius S, Microtendipes pedullus, Procladius* and *Tanytarsus mendax. Psectrocladius sordidellus* has the largest abundance in the assemblages during this time. Indicating that the lake was acidic (Brodin & Gransberg, 1993; Brodersen et al., 2001). This species is associated with macrophyte plant communities highlighting that between c.14.2-14.1k cal yr. BP the lake was productive and nutrient rich (Brooks et al., 2007). *Chironomous anthracinus* is also found at this time highlighting that littoral sediments dominated with macrophyte plants present (Brodersen et al., 2001). It is clear that there is a sharp transition from an unstable turbid lake system to one which can support a community of chironomids within a short period of time. *Psectrocladius sordidellus* and *Microtendipes pedullus* are abundant and are indicative of temperate conditions (Brooks & Birks, 2001; Brooks et al., 2007). The lake became more productive, being able to support a variety of chironomid taxa and aquatic plants. Although chironomid taxa diversity did increase it is still relatively low at this stage.

The assemblage is dominated by early colonising species e.g. *Chironomous anthracinus* and taxa which are indicative of high levels of acidity. There are still occasional appearances of colder taxa such as *Paracladius*. This presence of this taxa indicates that the environment was still cold enough at times to support predominantly sub-arctic species (Walker et al., 1991). This is supported by Birks (1984) who records

the presence of *Salix herbacea* and a move to bare soil colonists in Caithness during this time frame. This species has been known to inhabit sub-arctic regions where snow prevailed further into the year (Birks., 1994). The geochemical record indicates that in-washing still was on-going at this time which supports the lower diversity of chironomids, the dominance of early colonisers and the influence of melt water on the haptophyte algae. Birks (1984) records the appearance of *Rumex,* which is able to inhabit unstable soils and environments where in-washing persists.

Birks et al (2003) revisited Lochan an Drium, near Caithness, and found a lack of birch macrofossils in the record, to support this abundance of *Betula* pollen they initially identified in their 1984 study. Instead they recorded a dominance of shrubs and herb macrofossils suggesting that arctic vegetation prevailed at this time. They concluded that the *Betula* pollen grains were windblown to the site. As a result, they remodelled lower summer temperatures during the interstadial to <10˚C. Based on the C-IT(˚C) model for Shebster temperatures were on average 2.5˚C higher than inferred by the pollen and macrofossil assemblages by Birks et al (2003).

8.4.3.2 **GI-1d (c.14.1-13.9 cal yr. BP)**

Between c.14.1-13.9k cal BP mean July summer temperatures fall markedly from a high of 11.8˚C to a low of 6.9˚C. Similarly, the LCA record suggests that spring lake temperatures also fell to 8.7˚C. Both proxies indicate that temperatures abruptly fell, lasting for no more than 200 years, in the spring and summer months [Fig]. This event is thought to be synchronous with GI-1d in Greenland (Rasmussen et al., 2014).

Ultra-cold/cold species of chironomids dominate at this time. Many species are cold stenotherms and indicative of cold conditions similar to the sub-arctic to arctic (Brooks et al., 2007). These are the dominant taxa during this cold phase: *Paracladius, Microspectra radialis, Tanytarsus lugens, Protanypus and Orthocladius trigonobalis. Tanytarsus lugens, Paracladius, Protanypus and Microspectra radialis* are abundant in littoral sub-arctic lakes where oligotrophic conditions prevail (Brundin, 1956; Brooks et al., 2007). There is a stark contrast with this cold phase and the previous warm phase. The productivity and nutrient status of the lake fell at this time. Due to the harsh cold conditions' species diversity falls at this time. This cold phase lasts no more than 200 years however it is clear from the chironomid record that the environment changed sufficiently to support cold tolerant taxa. This cold event is short lived and there is a

gradual reestablishment of temperate species throughout the latter half of the zone. There is a notable increase in abundance of temperate chironomids such as *Psectrocladius sordidellus* and the earlier coloniser *Chironomous anthracinus* before the lithological boundary into the next marl layer.

The geochemistry indicates an increase in the amount of silica, titanium and iron in the lake. Suggesting there was an increase in the amount of detrital inputs and lake in-washing at this time (Marshall et al., 2011; Martin-Puertas et al., 2011). Calcium counts are low which indicates a reduction in temperatures likely leading to a drop in primary productivity (Lauterbach et al., 2011; Jouve et al., 2013). This suggests that autochthonous sediment production fell and was replaced with allochthonous inputs due to the increasing run-off (Lauterbach et al., 2011). This emphasises that abrupt environmental change occurred at this time, from temperate lacustrine conditions supporting an abundance of chironomids to a cold oligotrophic lake environment.

8.4.4 **GI-1c (c.13.9-12.9k cal BP)**

Between c.13.9k cal BP and c.12.9k cal BP cool-temperate conditions prevail with temperatures ranging between 8-11˚C.C This warm phase is thought to be synchronous with GI-1c in Greenland (Rasmussen et al., 2014). In Greenland this phase is split into three distinct climate events. These subtle temperature fluctuations are also recorded by the chironomids and the alkenones from this study.

(1) The first phase is found between c.13.9-13.6k cal BP. It is thought to be synchronous with GI-1c(1) in Greenland (Rasmussen et al., 2014). Cool-temperate species of chironomids dominate at this time: *Microspectra radialis, Orthocladius trigonobalis Ablabesmyia, Psectrocladius sordidellus, Microtendipes pedullus* and *Tanytarsus pallidocomis*. Based on the assemblage of these chironomids temperatures have been inferred to range between 10-11˚C. The LCA record indicates lake temperatures also rose during this time, ranging between 13-15˚C. This assemblage suggests that the lake system was oligo-mesotrophic, and the productivity of the lake was gradually rising (Brooks et al., 2007). Although, the productivity increased it was still on the lower end of the scale due to the presence of *Microtendipes pedullus* which thrives in

lakes low in organics (Pinder & Reiss, 1983; Hoffman, 1984). Species diversity and abundance gradually increases at this time too, likely due to increasing productivity in the lake and organic matter. Abrupt environmental change occurs at this time indicated by a spike in the abundance of early colonisers (*Corynocera ambigua* and *Microtendipes pedullus*). Cold stenotherms are found during this time frame, indicating that summer temperatures were still increasing. *Tanytarsus pallidocomis* indicates that the lake was likely acidic too (Bilyj & Davies, 1989).

(2) The second phase records subtly cooler temperatures between c.13.6-13.2k cal BP. This event is thought to be synchronous with GI-1c(2) in Greenland (Rasmussen et al., 2014). Cooler species of chironomid taxa begin to appear. This colder phase is dominated by cold-temperate species of chironomids. The presence of *Corynocera ambigua* markedly rises at the onset of this section. This indicates a sharp transition from temperate to colder conditions (Brooks et al., 2007). *Microspectra insignilobus* and *Sergentia coracina* are return indicating a drop in the nutrient status of the lake and acidity increased (Brodin, 1986). Both *Sergentia coracina* and *Microspectra insignilobus* are regarded as being cold stenothermic chironomids. These species are abundant in sub-arctic lake systems (Brundin, 1956). *Paracladius* is also found during this time indicating that the lake began to resemble lakes in Scandinavia (Brooks et al., 2007) and became more oligotrophic (Walker et al., 1991). This coincides with an increase in titanium levels suggesting a return to increased detrital run-off and in-washing (Lauterbach et al., 2011; Kylander et al., 2011). This cooler stage is also recorded by Peglar (1979) who records an increase in the abundance of the, snow loving, *Salix herbacea*. They also record a return to a mosaic landscape, with a decrease in the amount of flowering plants coinciding with increasing montane vegetation.

(3) The third stage is warmer, with temperatures ranging between 10-10.3˚C, throughout c.13.2-12.9k cal BP. This event is thought to be synchronous with GI-1c (3) in Greenland (Rasmussen et al., 2014). The

assemblage indicates that the lake was experiencing a period of increased acidity, as *Pagastiella* an acidophilic species, increases in abundance (Moller Pillot & Buskens, 1990). *Dicrotendipes* is a thermophilic species which is often found in warmer climates and is also found during this time. This further indicates a significant alteration to the environment at this time. There is an increase in the levels of calcium indicating higher productivity levels (Lauterbach et al., 2011). The levels of titanium and iron are reduced throughout this section highlighting that there was a reduction in detrital inputs and in-washing (Moreno et al., 2011; Marshall et al., 2011; Martin-Puertas et al., 2011). As the landscape stabilised through GI-1c species abundance and diversity increases indicated by an increase in the abundance of *Psectrocladius sordidellus, Chironomous anthracinus* and *Orthocladius type-S.* The abundance of early colonisers, e.g. *Corynocera ambigua,* falls too as the lake became more stable. The presence of *Chironomous anthracinus* and *Psectrocladius sordidellus* highlights that the lakebed was littoral, and the water column had a mesotrophic nutrient status in the latter stages of this warm phase (Brooks et al, 2007). *Psectrocladius sordidellus* is often found grazing on macrophytes which suggests that the temperate lake system was more productive, and the abundance of vegetation increased during this time.

Peglar (1979) records a dominance of *Pediastrum* and *Botryococcus* algae during this time which further suggests that the lake became more productive during this stage. There is a noticeable increase in the counts of calcium which highlights that temperatures rose at this time which would have led to increased productivity in the lake (Lauterbach et al., 2014). This coincides with reduced in-washing and detrital inputs (Moreno et al., 2011; Marshall et al., 2011; Martin-Puertas et al., 2011).

Peglar (1979) affirms this by recording a move from unstable bare soils to an open landscape dominated by small shrubs. This is supported by Birks (1984) who records an increase in temperatures and more diverse vegetation due to the presence of flowering plants (e.g. *Juniperus*). The lakes appear to be productive, dominated by aquatic vegetation, shown in Loch of Winless, on the east coast of Caithness. The vegetation records above are not able to identify these subtle climate fluctuations

during this time frame. Whittington et al (2003) highlights that it is unlikely that the pollen records can distinguish the cold and warm phases apart during the interstadial.

At the depths of 890cm and 871cm there are peaks in iron, when the background levels are low. This may indicate possible tephra layers which have yet to be identified (Kylander et al., 2011). Due to the position of the peaks in the core they may correspond to the Borrobol and/or the Penifiler tephra layers found in Loch of Sabiston. Further analysis would be useful to assess if more tephra tie-points are possible to build a more robust age-depth model.

8.4.5 **GI-1b (c.12.9-12.8k cal BP)**

There is a sharp transition to colder conditions at c.12.9-12.8k cal BP. This event is thought to be synchronous with GI-1b in Greenland (Rasmussen et al., 2014). This cold phase only lasts for 100 years yet temperatures fell to a low of 6.6˚C from a high of 10-11˚C. The LCA temperatures fall from 15˚C to 8˚C during this cold phase. However, it is clear that the LCA record lags behind the C-IT record by c.50 years.

This zone is dominated by species of chironomids that indicate a marked boundary from temperate-warm to cool conditions. *Tanytarsus lugens, Microspectra insigniloblis* and *Sergentia coracina* are cold stenotherms and thrive in sub-arctic conditions (Brooks et al., 2007). *Tanytarsus lugens* indicates sub-arctic and sub-alpine lakes where oligotrophic conditions prevail. *Sergentia coracina* too is a cold stenotherm however it is also acidophilic which indicates that pH fell during this time (Brodin, 1986; Brundin & Gransberg, 1993). This zone is highlighted by a sharp increase in the abundance of early colonising species, e.g. *Corynocera ambigua,* indicating that the lake altered significantly at this time (Brooks et al., 2007). The taxa signify the onset of oligotrophic sub-arctic conditions (Brundin, 1956; Brodin, 1986; Brooks et al., 2007).

The titanium counts indicate that there was in increase in minerogenic in-washing during this time and that the catchment became more unstable. This is supported by Charman (1995) who also records increased minerogenic in-washing at this time. They also record an unstable landscape dominated by the snow indicating *Salix herbacea*.

8.4.6 **GI-1a (c.12.8-12.6k cal BP)**

At c.12.8-12.6k cal BP there is a sharp transition to temperate-warm conditions. Temperatures range between 9-9.5˚C during this phase. This event is thought to be synchronous with GI-1a in Greenland (Rasmussen et al., 2014). The LCA temperature record indicates that temperatures ranged between 14-15˚C during this zone. These temperatures are larger than expected, likely due to the lack of an independent lake calibration, however they do indicate an abrupt warming trend at this time which supports the C-IT record.

The early colonising species *Corynocera ambigua* occurs in large abundances throughout this zone indicating that a significant switch in environmental conditions from cool to temperate temperatures occurred (Brooks et al., 2007). *Microtendipes pedullus* is another early colonist which is dominant in this zone. It is suggestive of intermediate temperatures and is known to inhabit lakes throughout north-western Europe (Brooks & Birks, 2001). The thermophilic species *Dicrotendipes nervosus* is also present which is indicative of warm conditions (Brooks et al., 2007). It is found in mesotrophic lakes which have an intermediate nutrient status (Brodin, 1986). The productivity of the lake increases at this time, coinciding with increasing lake and atmospheric temperatures during the summer and spring months. *Orthocladius type-S* indicates that the lake was littoral and that macrophyte communities, prevailed in the lake at this time (Cranston et al., 1983; Brodersen et al., 2001). This further suggests that the productivity, nutrient status and the temperatures in the lake rose during this time.

The levels of silica fall during this time which suggests that detrital inputs fell (Balascio et al., 2011; Marshall et al., 2011). In addition, the levels of potassium and titanium fell which suggests that the levels of in-washing halted (Metcalfe et al., 2010; Aufgebauer et al., 2012). This coincides with increased calcium counts which indicates an increase in lake temperatures and productivity (Lauterbach et al., 2011). The organic content of the core remains low which does suggest that although productivity and the abundance of plants increased, they were limited.

8.4.7 **Loch Lomond Stadial (c.12.6-11.9k cal BP)**

There is a sharp reduction in mean July summer temperatures, between c.12.6-11.9k cal BP, to a low of 6˚C. This is also demonstrated by the LCA record which suggests

temperatures were between 3.5-5˚C. This event is thought to be synchronous with GS-1 in Greenland (Rasmussen et al., 2014) and the Loch Lomond Stadial in Scotland (Lowe et al., 2019). Evidence suggests that the LLS in Scotland, was split into two stages (Brooks et al., 2012; Lane et al., 2013).

Between c.12.6-12.35k cal BP there are no alkenones present in the lake. It is not until c.12.35k cal BP, mid-way through the LLS, until the record begins which clearly indicates a two staged LLS, as proposed by Lane et al (2013). Longo et al (2016) shows that lake freezing can inhibit the growth of LCA producing algae which may account for the break in the record. Perhaps the lake became ice-free mid-way through the LLS. The chironomid record does indicate that temperatures spiked from 6˚C to 7˚C halfway through the LLS. This coincides with the return of haptophyte algae. This short-lived warm phase during the LLS may have provided enough warming to melt surface ice to promote the growth of algae in the lake. However, this increase in temperatures is followed by further climate cooling with the latter half of the LLS recording colder temperatures, falling to a low of 5.3˚C. Also, minerogenic in-washing increases in the latter stages which suggests there was increasing instability and turbidity in the lake during this time, which would have limited the growth of algae in the lake (Toney, pers comm). The reason for this increase in the abundance of haptophyte algae is unknown. The lake was likely still frozen during the spring and open during the summer, hence why there is no hiatus in the chironomid record. Regardless, it does clearly highlight that mid-way through the LLS significant environmental change occurred.

Ultra-cold species of chironomids dominate: *Sergentia coracina, Paratanytarsus austriacus, Protanypus, Pseudodiamesa, Microspectra radialis* and *Tanytarsus lugens*. The species listed above are indicative of a sub-arctic environment (Brooks et al., 2007). *Protanypus* is a rare species of chironomid in the record. However, it occurs in large abundances in profundal oligotrophic lakes in the sub-arctic (Walker & MacDonald., 1995). The presence of *Sergentia coracina* indicates that the lake was acidic (Uutala, 1986). *Corynocera oliveri* has been identified in this section. This species is indicative oligotrophic conditions and lakes from Scandinavia. This emphasises that the lake had a lower nutrient status and that it was similar to sub-arctic conditions today (Brooks et al., 2007). Another species of chironomid which is quite rare in the record, yet abundant in this section of the core, is *Pseudodiamesa*.

This species is a cold stenotherm and inhabits lentic and lotic lakes which have an oligotrophic nutrient status (Oliver, 1983).

Pennington et al (1972) records a dominance of *Artemisia* pollen during this stage in Lochs Sionascaig, Tarff and Borralan. They conclude that the disruption of the biological assemblages and a dominance of minerogenic material were due to intense environmental change and landscape instability. Furthermore, they also record plants which are indicative of alpine-arctic conditions which supports the interpretation above.

8.4.8 **Holocene Onset (c.11.9 -11.5k cal BP)**

There is a sharp transition to warmer climates at c.11.9k cal BP. Mean July summer temperatures rise from a low of 5.3˚C to 10.8˚C. During the Holocene period there is a similar agreement in temperatures from both temperature records. The LCAs show an increase spring lake surface temperature from 2˚ to 12˚C. However, the LCA record shows a rise in temperatures at c.12.3k cal BP. The chironomids record this warming at c.11.9k cal BP. This is likely a result of the lack of alkenone samples available for the LLS.

This event is believed to be synchronous with the onset of the Holocene period in Greenland (Rasmussen et al., 2014). This time frame is dominated by warm species of chironomids some of which have not been present in the core thus far. The main taxa found in this section of the core are as follows: *Microtendipes pedullus, Psectrocladius sordidellus, Tanytarsus mendax, Endochironomous albipennis, Dicrotendipes nervosus,* and *Polypedulum nubifer, Paratanytarsus albimanus and Cladopelma lateralis*. The abundance of *Corynocera ambigua* spikes once again indicating a dynamic change in the environmental conditions of the lake (Brodersen & Lindegaard, 1999) The occurrence of *Microtendipes pedullus* and *Psectrocladius sordidellus* is indicates that intermediate temperatures prevailed (Brooks et al., 2007). This is the first occasion where *Polypedulum, nubifer, Paratanytarsus albimanus*, *Endochironomous albipennis* and *Cladopelma lateralis* are found. All of these species are warm stenotherms. *Cladopelma lateralis* is indicative of lakes with a mesotrophic nutrient status (Walker et al., 1991; Brodin, 1986). Calcium counts increase at this stage indicating that there was a rise in temperatures and productivity in the lake (Lauterbach et al., 2011). At 820cm there was a significant decrease in the counts of

titanium and potassium in the sediments. This shift suggests minerogenic in-washing fell at this time (Aufgebauer et al., 2012).

However, at c.11.6-11.48k cal BP there is a sharp reduction in temperatures falling from a high of 14˚C to a low of 12˚C. The abundance of the cold stenotherms increases at this time. Indicating that a short-lived cold phase occurred at this time. There is a sharp increase in the abundance of *Corynocera ambigua*, indicating that there was significant environmental change at this time. There is a sharp fall in calcium counts and an increase in titanium highlighting that minerogenic in-washing restarted (Kylander et al., 2011). This event is likely synchronous with the 11.4k event in Greenland (Rasmussen et al., 2014).

8.5 **Summary**

This is the first study to directly compare the use of chironomid head capsules with long chain alkenones for the British Isles. The results indicate that chironomids reliably reconstruct mean July summer temperatures for the region and show similar trends to those recorded across the British mainland and Ireland. The overall trend of the long chain alkenone record, when compared to that of the chironomids, has a striking resemblance. This correlation between both records leads one to support the idea that LCAs can be effective proxies for lake temperature modelling in lacustrine environments (Toney et al., 2010). Whilst, the long chain alkenone record is in agreement with the chironomid record for the onset of the cold events it is apparent that there is a significant offset between the onset of warming between the two proxies. Temperatures appear to be warmer by 2-4˚C throughout the LGIT, when comparing the alkenone record with the chironomid inferred temperatures. See below the main findings from this research for each of the main climate events throughout the LGIT:

(1) **GI-1e**: Temperatures appear stable c.14.2k cal BP (12-12.5˚C). However, the LCA record shows that spring lake temperatures were significantly lower, reaching 3.8˚C.

(2) **GI-1d**: Between c.14.1-13.9k cal BP mean July summer temperatures fall markedly from a high of 11.8˚C to a low of 6.9˚C. Similarly, the LCA record suggests that spring lake temperatures also fell to 8.7˚C.

(3) **GI-1c**: Between c.13.9k cal BP and c.12.9k cal BP temperatures ranged between 8-11˚C. This event is split into three subtle distinct climatic phases.

(4) **GI-1b**: Temperatures fell to a low of 6.6˚C from a high of 10-11˚C between c.12.9-12.8k cal BP. The LCA temperatures fall from 15˚C to 8˚C during this cold phase. There is clear lag between the LCA and the C-IT by c.50 years.

(5) **GI-1a**: Between c.12.8-12.6k cal BP temperatures range between 9-9.5˚C. The LCA temperature record indicates that temperatures ranged between 14-15˚C.

(6) **Loch Lomond Stadial**: there is a sharp reduction in mean July summer temperatures, between c.12.6-11.9k cal BP, to a low of 6˚C. This is also demonstrated by the LCA record which suggests temperatures were between 3.5-5˚C. Loch Lomond Stadial split into two-phases. It is apparent that the LCA producing haptophytes are not present in the lake during the onset of the Loch Lomond Stadial and return halfway through the LLS. Significant environmental change occurred during the second phase of the LLS to support the growth of algae in the lake system.

(7) **Holocene onset**: there is a sharp transition to warmer climates at c.11.9k cal BP. Mean July summer temperatures rise from a low of 5.3˚C to 10.8˚C. The LCAs show an increase spring lake surface temperature from 2˚ to 12˚C.

Chapter 9 - A synthesis of the inferred temperatures for the Northern Isles of Scotland and Caithness during the Last Glacial – Interglacial Transition.

9.1 Introduction

Chironomid inferred temperature reconstructions have been inferred for the Northern Isles and Caithness for the LGIT. Independently, each record provides a high-resolution time series of temperature and environmental change for each locality. When considering the three sites it is now possible to better understand the magnitudinal, spatial and temporal differences across varying latitudes across the North Atlantic. To date, eight chironomid inferred temperature reconstructions have been developed for the British Isles and Ireland (Lang et al., 2010; Watson et al., 2010; Brooks et al., 2012; van Asch et al., 2012; Brooks et al., 2016). However, until now no mean July summer temperature records had been developed for the Northern Isles of Scotland or Caithness.

The Greenland ice core chrono-stratigraphy (Rasmussen et al., 2014) will be used to separate out the main climatic events for the interpretation of the three sites. Where possible independent ages will be shown to highlight the leads and lags between regions across the British Isles and N.W Europe. By combining this research with the available records across the British Isles one can better assess if climate changed synchronously during the LGIT. Although synchronicity is difficult to determine without annually resolved sedimentary profiles; it may be possible to use the periods where tephra layers and terrestrial plant fragments were analysed. Furthermore, combined with a long chain alkenone record, from Caithness, it is now possible to better understand seasonality in the climate records.

This research will provide a clearer image of the drivers of climate change for the LGIT by assessing temperature trends and gradients geospatially. This will allow one to assess if the forces that drove climate change across the British Isles and further afield were the same in the Northern Isles of Scotland and Caithness. This research will attempt to track the movement of the north polar front northwards during the Loch Lomond stadial cold phase. By using local chironomid inferred temperatures this may also make glacial and precipitation reconstructions more reliable and robust.

9.2 Aims & Objectives

This synthesis chapter will answer the main aims of this PhD research. The overall aim of this research is to reconstruct the mean July summer temperatures of the Northern Isles of Scotland and Caithness during the Last Glacial – Interglacial Transition. Another aim was to determine the magnitudinal and temporal changes in seasonal temperatures in Caithness for the same time period. The final aim was to assess how synchronicity of the temperature records compare to the Greenland ice core and other C-IT models from across the British Isles. This was achieved by using the following objectives:

- Where chronological uncertainty is reduced, use the C-IT records for Northern Isles of Scotland and Caithness to assess the leads and lags in temperatures across Scotland and the British Isles.

- Where chronological uncertainty is reduced, use the C-IT records for Northern Isles of Scotland and Caithness to assess the leads and lags in temperatures across N.W Europe.

- Use the C-IT record from Orkney to assess the degree of synchronicity with the NGRIP record where chronological uncertainty is low.

- Geospatially assess the temperature gradients, for the main climate events, in spanning the LGIT for the Northern Isles and Caithness

- Use the titanium geochemical markers to track the movement of the mid-YD/LLS transgression across N.W Europe.

9.3 Palaeoclimate synthesis of the Northern Isles and Caithness

This research has provided high-resolution palaeoenvironmental records for Caithness, Orkney and Shetland which has helped us to better understand environmental change during the LGIT for these regions. However, the palaeoclimate records are the main focus and the novelty of this research. Until now, no chironomid or alkenone inferred temperatures have been reconstructed for this region. Three high resolution mean July summer temperature records have now been developed for Caithness, Orkney and Shetland [Fig.115]. This chapter will compare these records to other sites across Scotland [Fig.116] and N.W Europe [Fig.117] In order to assess the magnitudinal, temporal and spatial differences between regions for the LGIT.

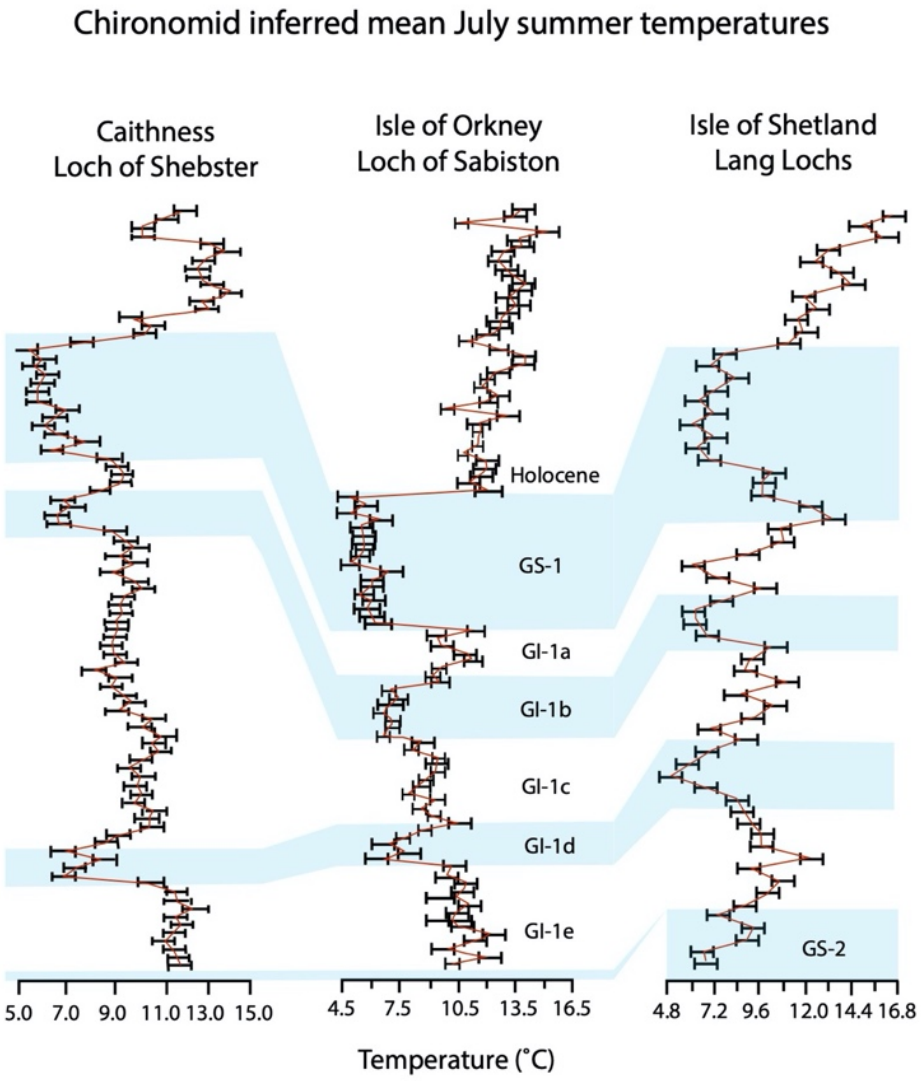

Figure 115. C-IT (°C) records for the Northern Isles and Caithness by depth (no scale). The Greenland chronology is used to highlight the warm and cool phases throughout the LGIT (Rasmussen et al., 2014)

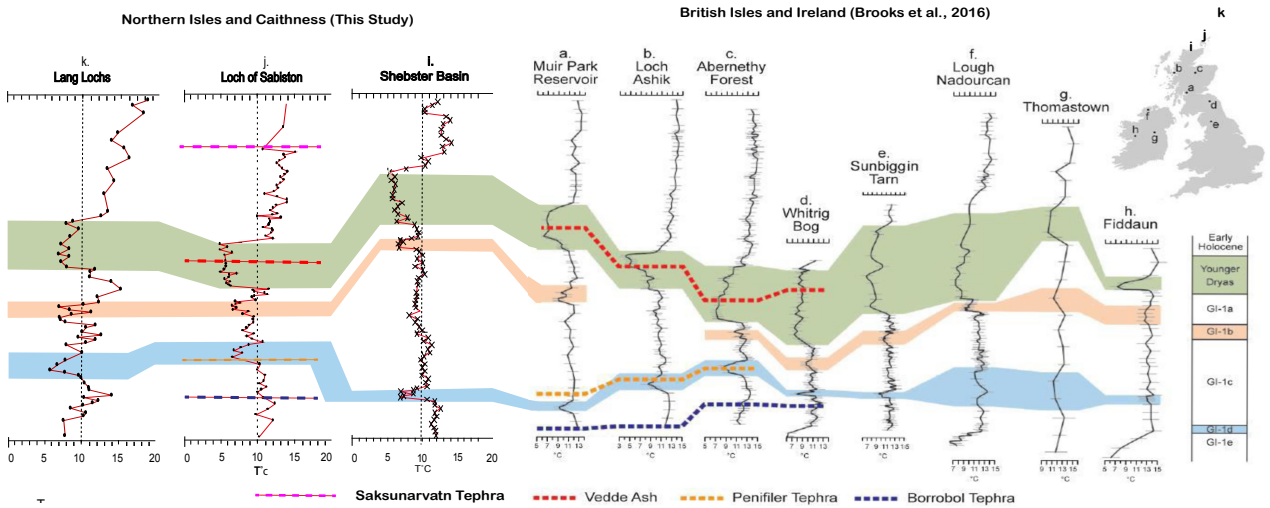

Figure 116. The temperature inference models for this project combined with the records from the British Isles and Ireland (adapted from Brooks et al., 2016)

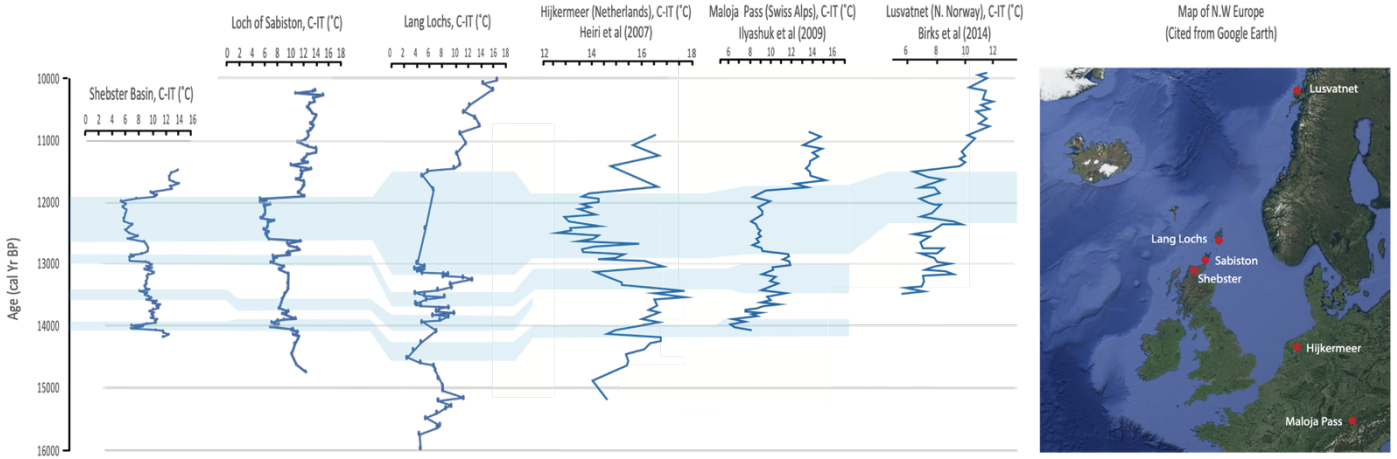

Figure 117. C-IT models with time for the Shebster basin, Loch of Sabiston and Lang Lochs. Combined with a record from Hijkermeer in the Netherlands (Heiri et al., 2007); Maloja Pass (Swiss Alps)(Illyashuk et al., 2005) and Lusvatnet (N.Norway)(Birks et al., 2014)

9.3.1 **Palaeoclimate history of Scotland**

9.3.1.1 **Termination of the LGM and Pre-interstadial**

All three sites have a complete record of the LGIT, from the end of GS-2/LGM to the onset of the Holocene period. However, Shetland is the only site in the Northern Isles record which records warming into the interstadial after the end of GS-2. The chironomid inferred temperatures suggest that mean July temperatures ranged between 5.5˚C to 10˚C, at c.15.88k cal BP, before the end of GS-2. This suggests that sedimentation and deglaciation occurred earlier in Shetland than in Greenland. Temperatures in Shetland increase gradually highlighting that warming into the interstadial was not abrupt.

There are two short-lived cooling events at c.15.6k cal BP and c15.3k cal BP where temperatures fell from 9˚ to 7.4˚C and 10.7˚C to 9˚C respectively in Shetland before the onset of GI-1e [Fig.115], highlighting that the warming into the interstadial was not rapid. This increase in temperatures appears to occur in stages rather than one abrupt temperature shift from cold to warm. The only other chironomid sites which record warming into the interstadial are from Whitrig Bog, Lough Nadourcan and Fidduan. At Whitrig Bog temperatures gradually rise from a low of 6˚C to 11˚C (Brooks et al., 2000); at Lough of Nadourcan temperatures gradually rise from 7˚C to 13˚C (Watson et al., 2010) and at Fidduan temperatures gradually rise from 6˚C to 15˚C (van Asch et al., 2012) [Fig.116]. These temperatures are similar to those found in Lang Lochs where temperatures gradually rise from 5.5˚C to 10˚C. The Greenland ice core record suggests that warming was abrupt into the interstadial (Rasmussen et al., 2014) however this does not appear to be the case in these sites. Millet et al (2012) records a similar gradual response at the end of GS-2 in the French Pyrenees. They suggest this is due to a gradual decline in cold optimum taxa with a replacement of warm stenotherms as climate gradually changed. This gradual warming is also found in the oxygen isotope records from Ammersee (Grafenstein et al.., 1999) and northern England (Marshall et al., 2002) [Fig.117].

The retreat of the BIS, and warming, occurred asynchronously across the British Isles with Shetland being ice-free early before the other sites in this project. Bradwell et al (2019) affirms this by recording a gradual retreat of ice from c.22k BP to c.18k BP off the Shetland coastline to the interior of the archipelago with a rapid collapse and ice-retreat occurring between c.18.3k - 16.5k cal BP of the Shetland Ice

Cap (SIC) (Bradwell et al., 2019). The final deglaciation of the SIC occurred between c.16.5-14.9k cal BP. Which coincides with climate deterioration in the Northern Hemisphere during GS-2a (Lowe et al., 2008). The influence of the THC and the NPF is known to be a control of temperature change for this region during this time (Brooks et al., 2016). However, there are local influences that need to be considered too.

Hall (2013) suggests that Shetland, during GS-2, had its own ice cap due to the position of Shetland in the North Atlantic Ocean. The climate here was controlled by a combination of the local Shetland Ice Cap (SIC), the British Ice Sheet (BIS) and the Fennoscandia Ice Sheet (FIS). Whereas, the Isle of Orkney and Caithness did not have these complex interactions as there was no ice cap on the Orkney mainland or in Caithness, and the FIS was too far from Caithness and Orkney to influence its climate, unlike in Shetland. The FIS persists throughout the LGIT, gradually retreating between c. 22-11k cal BP (Stroeven et al., 2016). There was little retreat of the western edge of the FIS between 10-11.5 cal BP and as a result this would have continued to be a major control of summer temperatures on Shetland [Fig.118].

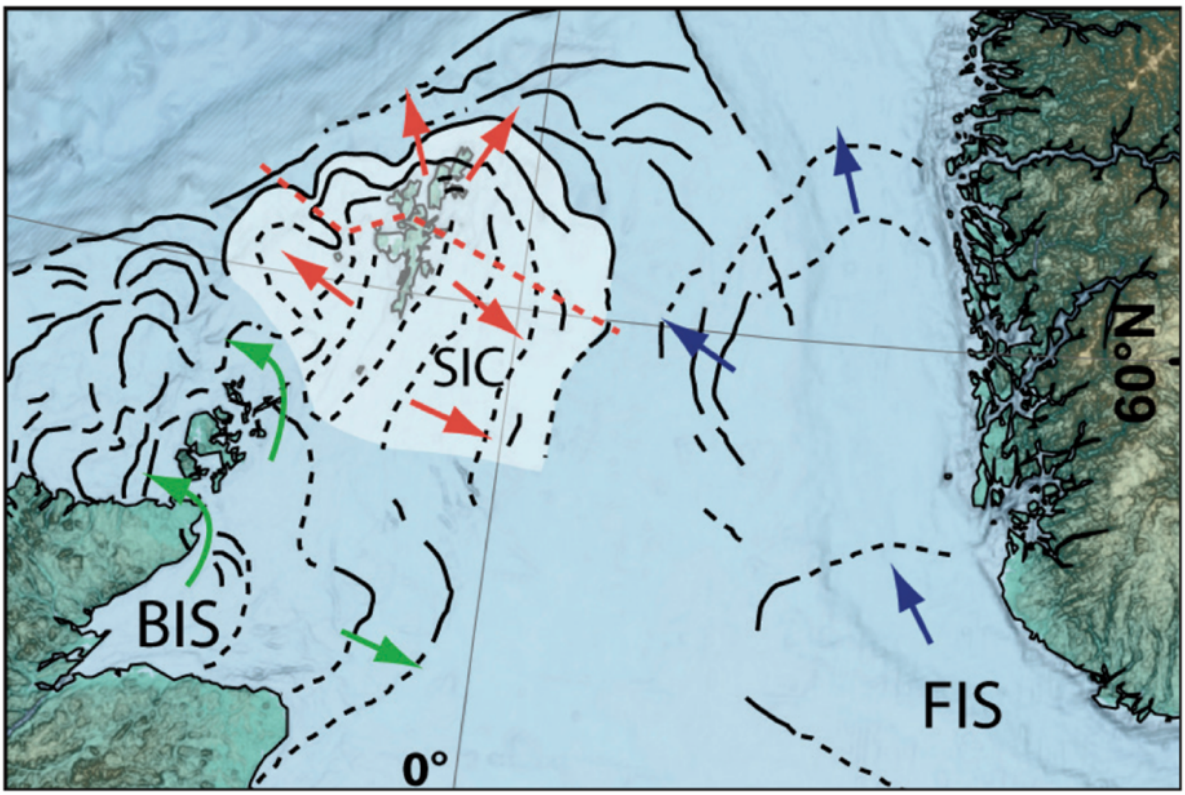

Figure 118. The position of the British Ice-Sheet (BIS), the Fennoscandia Ice Sheet (FIS) and the Shetland Ice Cap (LGIT) at the end of the LGM (Hall et al.,2013)

It is worth comparing the C-IT records from this project to sites across the N.W Europe to assess the spatial extent and intensity of this climate warming. The chironomid record from Hijkermeer in the Netherlands, also indicates warming into the interstadial from 14˚C to 16.4˚C (Heiri et al., 2007). Although the temperatures are higher than those found in the Northern Isles, the maximum temperature in the Netherlands, is only c.2˚C higher than the maximum found in Lang Lochs in Shetland. This highlights the vast spatial extent and high magnitudinal climate changes that occurred across N.W Europe during this time.

9.3.1.2 **Warmer Interstadial (GI-1e)**

At the onset of the interstadial temperatures reach 12˚C in Caithness, c.14.7k cal BP, and 10.5˚C in Orkney, c.14.1k cal BP. Whereas, in Shetland, temperatures are 8˚C at c.15.6k cal BP. In Caithness and Orkney temperatures appear more stable with values ranging between 12-12.5˚C and 10.5-12˚C respectively [Fig.115], whereas Shetland temperatures range between a low of 8.7˚C and high of 12.3˚C, with temperatures reaching a maximum at the start of GI-1e and gradually falling throughout the interstadial.

The LCA record from Caithness indicates that the surface of the lake was colder, ranging from 3.4˚C to 9.6˚C. The alkenone record records cooler spring temperatures during the onset of GI-1e. At c.14.2k cal BP there is a difference of c.9˚C between summer and spring temperatures. Throughout the interstadial the difference in temperatures falls to c.2.5˚C by c.14.1k cal BP. Within approximately 100 years the difference between spring lake temperatures and summer temperatures minimises. This affirms the work of Wagner-Cramer & Lotter (2011) who suggests that warming spring temperatures lead temperature changes in the summer months.

In MPR, Loch Ashik, Abernethy Forest, Whitrig Bog, Lough Nadourcan and in Thomastown temperatures range between 11-13˚C during GI-1e (Brooks et al., 2016) [Fig.116]. These temperatures are in the same range as those in Orkney and Caithness. This suggests that the climate system across mainland Britain and Ireland was similar to the drivers in Orkney and Caithness whereas, there was more climate variability in Shetland.

Magny et al (2006) records temperatures ranging between c.14-18˚C in the French Jura mountains and Lotter et al (2014) records temperatures of 14˚C in the

Swiss alps [Fig.98]. This highlights the warm GI-1e phase had a wide geographical extent and was enough to alter the climate in the alpine regions of mainland Europe and the Northern Isles of Scotland. In Orkney there are two small-scale cooling events between GI-1e and GI-1d which are not found in the Greenland, Caithness or Shetland. However, they are recorded in Lake Lautrey, in the French Jura Mountains (Magny et al.,2006). They record two cold phases named the 'Intra-Bølling Cold Periods' (IBCP) found at c.14.5k cal BP and c.14.35 k cal BP. In Orkney the same cooling events are found at c.14.45k cal BP and c.14.13k cal BP and record temperatures falling from c.12.3 to c.10˚C respectively [Fig.119]. Orkney has the highest resolution chironomid record and the most robust chronology which may explain why these events have only been identified here and not the other northern Isles sites. This also highlights the usefulness and reliability of chironomids to detect small scale and short-lived cooling phases that other proxies may not be sensitive enough to record. These two climate cooling events have also been recorded in Meer Felder Maar in Germany (Brauer et al., 2000) and the Norwegian sea (Karpuz and Jansen., 1992).

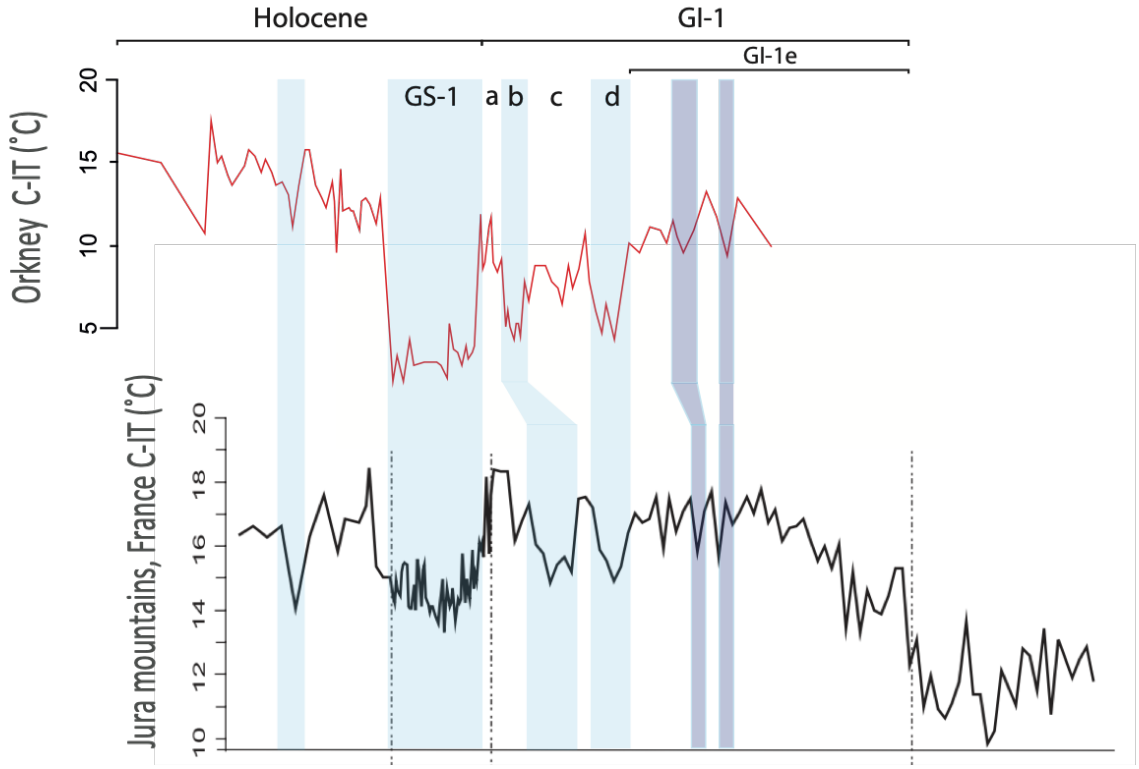

Figure 119. Adapted chironomid inferred temperature model from the French Jura Mountains (Magny et al., 2006) and the C-IT(˚C) model from Orkney. The climate cooling events found in both records are recorded in blue. The same unidentified cold phases from both cores are highlighted in purple

9.3.1.3 **Abrupt cooling (GI-1d)**

The onset of GI-1d is marked by an abrupt drop in mean July summer temperatures in Caithness, with temperatures falling markedly from a high of 11˚C to 6.8˚C at c.14.1k cal BP. In Orkney, temperatures fall from 11˚C to 6.5˚C by c.14.1k cal BP [Fig.115]. The LCA record from Caithness indicates that spring lake temperatures fell to a low of 8.7˚C by c.14.02k cal BP. The onset of GI-1d is more abrupt in Caithness and Orkney compared to Shetland. Although these sites are still considered to be maritime, they are located closer to the mainland of Britain and as a result have more continentality. When compared to Lang Lochs, temperatures gradually fall from 12˚C, c.15.3k cal BP, to 4.8˚C, c.14.6k cal BP. Shetland is located at the fringe between two climatic zones (temperate and subarctic) and is dominated by a maritime climatic system (Whittington et al., 2003). Therefore, the climate moderating effect may lead to shorter temperature ranges and fewer temperature extremes when compared to the other sites (Whittington et al., 2003). Temperatures are on average 2˚C warmer in Orkney and Caithness compared to Shetland.

At Fidduan and Lough Nadourcan temperatures fell by c.2˚C (Brooks et al., 2016) [Fig.116]. However, here this short-lived cooling event is subtle when compared to the other sites in the British Isles. At Abernethy Forest and Whitrig Bog temperatures fell by c.4-5˚C (Brooks et al., 2012; Brooks et al., 2016) which is consistent with Caithness and Orkney where temperatures fell by c.4˚C [Fig.115]. Although temperatures fall by a similar amount across the British Isles and the Northern Isles sites, the absolute temperatures are much lower in Caithness, Orkney and Shetland. Caithness and Orkney record minimum temperatures of c.6˚C. This is 3-4˚C lower than those recorded in Loch Ashik, Abernethy Forest (Brooks et al., 2012) and Muir Park Reservoir (Brooks et al., 2016). Brooks et al (2016) suggests that this is a result of an increasing oceanic-continental gradient with decreasing latitude. As you decrease in latitude temperatures expectedly increase throughout this cold event and the event becomes more abrupt. Sunbiggen Tarn, in the north of England is the most southern chironomid inferred temperature record. This site reaches a minimum of 9˚C and the transition appears more abrupt than in Shetland (Turner et al., 2015).

Consistently, the minimum temperatures recorded throughout GI-1d are lower than GI-1b across the British mainland and Ireland. This same event is highlighted by a sharp oscillation in the GICC05 ice core records in Greenland (Brooks et al., 2012). However, sites in central Europe show the opposite with GI-1b having the coolest

temperatures. Brooks et al (2012) suggests that this is a result of regional differences. As Scotland and Norway are closer to the North Atlantic Ocean they are greatly influenced by fluctuations in oceanic and atmospheric circulations whereas, sites in central Europe have a continental climate system which subdues the temperature signal.

In the Netherlands there is rapid drop in temperatures from a high of 17˚C to a low of 15˚C (Ilyashuk et al., 2009; Larocque-Tobler et al., 2010). Millet et al (2012) record a drop of c.2˚C in the French Pyrenees from 17.5˚C to 15.2˚C [Fig.117]. Therefore, this cold event had a large spatial scale spanning many sites in N.W Europe, although the magnitude varied between sites due to the latitude, altitude and closeness of the site to an ice-sheet (Renssen and Isarin., 2001). This cold event is synchronous with the Aegelsee Oscillation in Europe (Lotter et al., 2012).

The climate cooling signature in Shetland closely resembles that of the Greenland ice core record [Fig.120]. Rasmussen et al (2014) shows that there was a gradual fall in the oxygen isotope record from the middle of GI-1e to the onset of GI-d. The southern tip of Greenland is at the same latitude as Shetland (60˚N) therefore likely had a similar climate at the time. As a result, it may be more appropriate to use the Greenland ice core chronology to constrain climate changes for higher latitudinal sites like Shetland, as opposed to the remainder of the British Isles and N.W Europe.

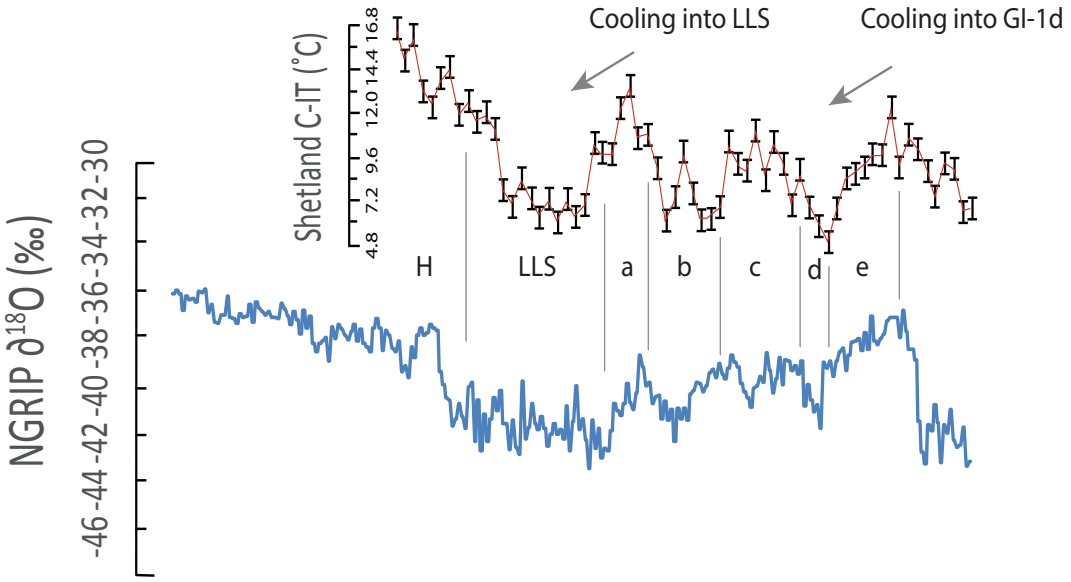

Figure 120. Comparison of the NGRIP record (Rasmussen et al., 2014) with the C-IT (˚C) record from Shetland. The cooling into the LLS and GI-1d is shown on the diagram highlighting the similarities in the records

9.3.1.4 **Abrupt Warming (GI-1c)**

Abrupt warming occurs in Caithness and Orkney at c.13.9k cal BP. Temperatures rise to 10.6˚C and 10.7˚C respectively [Fig.116] indicating that a temperate climate system replaced the previous sub-arctic conditions. At both sites warming occurs within 40-50 years which shows how rapid this warming was in this region. When compared to Shetland, temperatures rise to 8.9˚C by c.14.2k cal BP. The transition from cold to warmer climates is less abrupt in Shetland taking approximately 400 years, 8 times slower than in Orkney and Caithness.

Throughout GI-1c summer temperatures range between 10.5-11.5˚C in Caithness and 9-10.5˚C in Orkney. Temperatures in Shetland are more subdued than those in Orkney and Caithness. The C-IT (˚C) models from Caithness and Orkney record the small-scale climate fluctuations known as GI-1c (1-2-3) shown in the Greenland records [Fig.96]. However, on Shetland these events are not apparent. See below an interpretation for these small-scale climate events:

(1) **GI-1c(1)(c.13.9k cal BP).** In Caithness mean July summer temperatures were 11.3˚C and in Orkney temperatures were 10.7˚C. The LCA record from Shebster also records lake temperatures of 14˚C during GI-1c(1)
(2) **GI-1c(2) (c.13.7k cal BP).** During this subtle cold phase temperatures fall to 8.1˚C in Caithness and 7.9˚C in Orkney. The LCA record from Shebster also records lake temperatures of 13˚C during GI-1c(2)
(3) **GI-1c(3)(c.13.4k cal BP).** Temperatures begin to rise again to 10.4˚C in Caithness and 9.5˚C in Orkney. The LCA record from Shebster also records lake temperatures of 15˚C during GI-1c(3)

The LCA record from Shebster also records these subdivisions. However, the likelihood that these are the absolute lake surface temperatures is low due to the lack of an independent lake calibration. However, it does suggest that lake temperatures were high in GI-1c(1), fell during GI-1c(2) and then rose again during GI-1c(3). The only other sites in the British Isles which records the three-stage GI-1c warm phase is Abernethy Forest in the Scottish Cairngorms [Fig.117] (Brooks et al., 2012) and Whitrig Bog in Central Scotland (Brooks et al., 2000).

To date, no records in N.W Europe show these subtle distinctions in temperatures. The chironomid records at Kråkenes, western Norway, and Lusvatnet in North West Norway, do not record any mean July summer temperatures until the termination of GI-1c. Norway at this stage was still glaciated which inhibited lake formation and chironomid communities. As a result, the spatial extent of this climate cooling was likely isolated to Northern Scotland and Greenland. The other sites across Britain and Ireland do not record any sub-divisions due to (1) low resolution sampling and/or (2) no environmental response from the chironomids (Brooks et al., 2016).

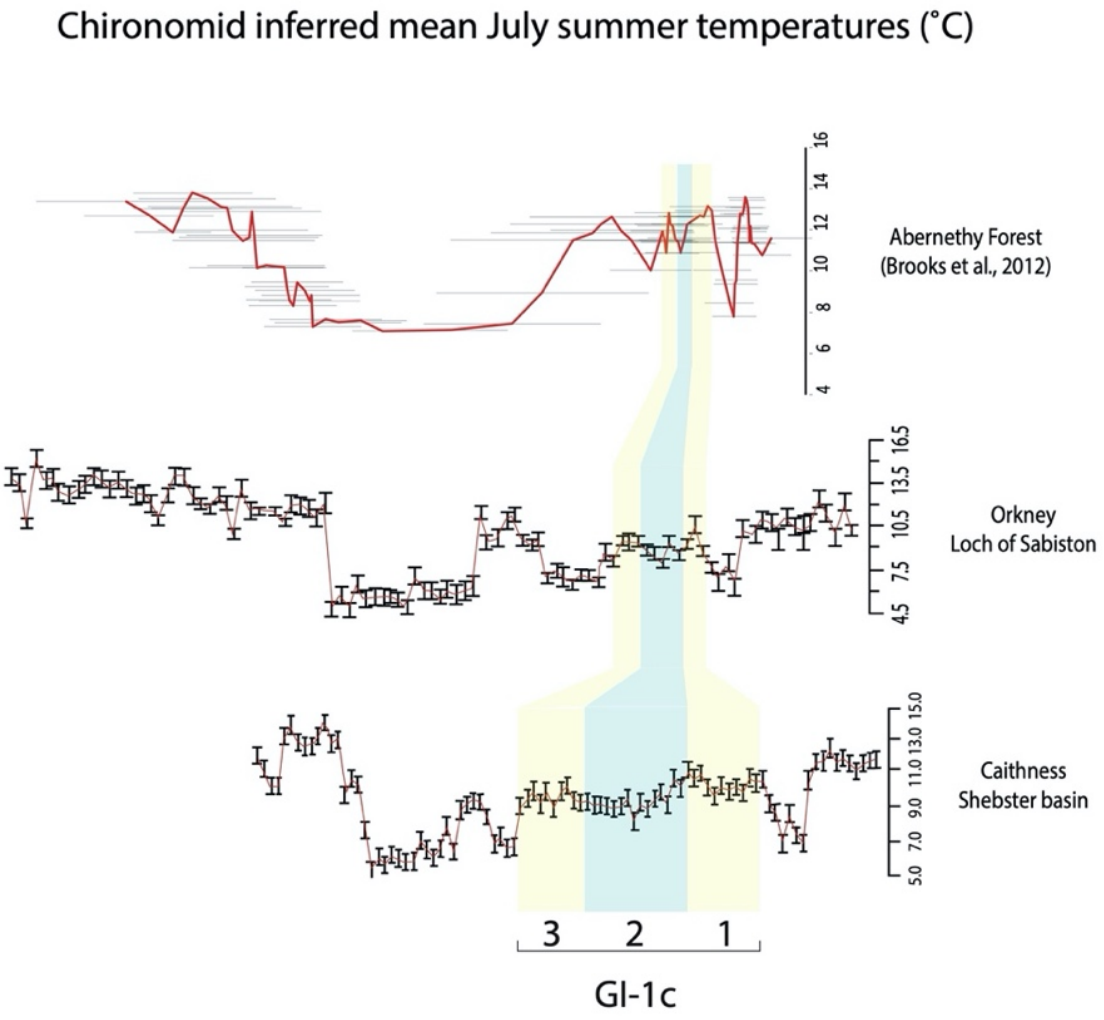

Figure 121. The chironomid inferred temperatures for Caithness, Orkney and Abernethy Forest (Cairngorms)(Brooks et al., 2012). The warm phases of GI-1c are shown in yellow with the cold mid phase shown in blue.

9.3.1.5 **Abrupt cooling (GI-1b)**

Abrupt cooling occurs in Caithness and Orkney at c. 13.0k cal BP. Mean July summer temperatures fall to a low of 6.6˚C in both locations [Fig.116] highlighting that the sites had a similar magnitude during this cold phase. This abrupt cold phase occurs in Shetland at c.13.8k cal BP and temperatures drop to 6.11˚C. The LCA record from Caithness indicates an abrupt drop in spring lake temperatures to a low of 8˚C.

This cold phase is not clear at Loch Ashik (Isle of Skye), as temperatures only fall by c.1˚C, whereas Abernethy Forest (Cairngorms), Whitrig Bog (central Scotland) (Brooks et al., 2016) and in Muir Park Reservoir (Loch Lomond and the Trossachs) temperatures fall by 2-3˚C (Brooks et al., 2012) [Fig.117]. This is similar to Caithness, Orkney and Shetland where there is also clear drop in temperatures by 3-3.5˚C. The greatest drop in temperatures is recorded in Shetland where there is a fall of 4˚C. It is clear that abrupt environmental change occurred at this time. However, it is evident that the magnitude differed between localities. This research suggests that sites at a higher latitude (e.g. Shetland) have a greater magnitudinal change than sites at a lower latitude (e.g. Abernethy Forest).

This abrupt cold event appears to happen at the same time in the three sites in this research. However, GI-1b is relatively warmer than the previous GI-1d cold phase. G-1d differed, as the event appeared to influence Orkney and Caithness in a similar way. However, it was more gradual in Shetland suggesting that the climate forcing mechanisms may have differed between these two events. The drop-in temperatures and the temporal scale of GI-1b appears to be similar in the three Northern Isles sites.

The Scottish sites on the whole show a larger decrease in temperatures during this GI-1b. Hawes Water in northern England only shows a subtle drop of 1˚C and the Irish Sites Fidduan and Lough Nadourcan only show a drop of 1.5-2˚C (Brooks et al., 2016). Therefore, this supports the assumption above that sites at a higher latitude had a greater temperature drop than sites at a lower latitude. However, other local factors need to be considered.

Lang et al (2010) suggests that local differences in wind exposure and catchment size can influence the temperatures recorded at each site. Also, the calibration used for each site needs to be considered. For Fidduan the combined Swiss-Norwegian training set was used (Heiri et al., 2011) which has larger atmospheric temperature ranges (5-18.4˚C); whereas Lough Nadourcan used the Norwegian training set which has temperature ranges between 3.5-16˚C (Watson et

al., 2010). This event is known to have a wide geographical extent, reaching mainland Europe. Heiri et al (2007) records a sharp drop in temperatures by 2.1˚C during this cold phase at Hijkermeer in the Netherlands. Also, in the Swiss Alps temperatures fall by c.4˚C (Illyashuk et al., 2005) during GI-1b. [Fig.117]. This indicates that GI-1b was extended across N.W Europe and this event was a high amplitude cold phase. In N.W Europe, and in some N. American studies, this cold phase has been identified as being the Inter-Allerød Cold Period (Denniston et al., 2001) whereas in Greenland it has been called GI-1d (Rasmussen et al., 2014).

9.3.1.6 **Warmer phase (GI-1a)**

Abrupt warming occurs at c.12.9k cal BP in Caithness and Orkney. Temperatures rise to a high of 9.5˚C in Caithness and 11.5˚C in Orkney. In Shetland temperatures rise further to 13.5˚C at c.13.2k cal BP [Fig.115]. The LCA record from Caithness indicates that spring lake temperatures rose to 14.8˚C by c.12.6k cal BP. It is unlikely that lake temperatures were this high, as they indicate higher spring temperatures than in the summer but this does support the C-IT record which indicates that temperatures abruptly rose during this time. This warming in Orkney and Shetland is comparable to Abernethy Forest which shows there was a rise in mean July summer temperatures to 12˚C (Brooks et al., 2012). Loch Ashik and Whitrig Bog also show a rise to 11˚C (Brooks et al., 2012; Brooks et al., 2016) [Fig.116]. The record from Kråkenes, in N.W Norway, shows a rise in temperatures 9-10˚C. It is expected that Norway has colder temperatures during this time as it is found at a higher latitude and is in close proximity to the FIS.

However, it is unexpected that Caithness reports colder temperatures than those recorded in Orkney, Shetland and Norway as it is found at a lower latitude. This is likely a result of a poor fit to temperature and lack of modern analogues at this time. The abundance of the rare species *Corynocera ambigua* increases, constituting 40% of the overall assemblage. This species is rare in the Norwegian training set, with none being recorded in the 103 lakes. This same problem was recorded in Lake Egelsee in Switzerland, by Larocque-Tobler et al (2010). They recorded no good modern analogues where there was a high abundance of *Corynocera ambigua*.

9.3.1.7 **Loch Lomond Stadial**

At the onset of the Loch Lomond Stadial temperatures fall markedly to c.6˚C in Caithness (c.12.6k cal BP), Orkney (c.12.6k cal BP) and Shetland (c.13.2k cal BP) [Fig.115 & Fig.116]. This is the first time that all three sites record the same temperatures during the same event. The onset of the LLS in Shetland occurs approximately 600 years earlier than in the other sites from this research.

At the onset of the LLS there is a hiatus in the LCA record from Caithness. The environment became inhospitable for the haptophyte algae to thrive which resulted in no alkenones being deposited into the sediment. Longo et al (2016) suggests that this may be a result of freezing lakes which stopped the algae photosynthesising. This may also be due to an influx of freshwater, perhaps due to glacial melting which inhibited the growth of LCA producing algae. The geochemical markers from Caithness highlight a sharp increase in minerogenic in-washing. This highlights that there was abrupt instability in the catchment during this time which may have led to the hiatus in the record. Longo et al (2018) shows that changing pH levels in the lakes can influence the distribution and abundance of LCAs. With an increase in the amount of ice in the catchment, run-off, erosion and melting would have risen during this time altering the pH. This may also account for the break in the record. It is apparent that there was sufficient environmental change which inhibited the growth of the haptophyte algae during the first phase of the LLS.

Lane et al (2013) and Lowe et al (2019) highlight that there were two stages to the LLS in Scotland and the YD in N.W Europe. Temperatures in Shetland rise from 6˚C in stage one and rise to 7˚C in stage two. This mid-phase temperature change occurs at c.12.5k cal BP in Shetland. In Caithness temperatures range between 6-7˚C during the first stage and fall to 5-6˚C in the second stage. This mid-phase occurs at c.12.4k cal BP in Caithness. In Orkney temperatures range between 5.5-6˚C in the first stage and 4.8-5˚C in the second stage. This mid-phase occurs at c.12.3k cal BP.

Caithness and Orkney record a colder second phase which is similar to the record from Loch Ashik and Muir Park Reservoir (Brooks et al., 2012; Brooks et al., 2016) whereas, all of the other sites in Britain and Ireland record warming throughout the second phase of the LLS. Brooks et al (2016) attributes this to the close proximity of the sites to the LLS re-advance. As the sites were close to the LLS ice sheet, this likely caused a depression in atmospheric temperatures at this time. Where sites were further from the ice mass, atmospheric temperatures warmed e.g. at Lough

Nadourcan, Fidduan and Whitrig Bog (Brooks et al., 2016). Therefore, the LLS climate did not change synchronously or uniformly across Scotland and the Northern Isles [Fig.116].

Bakke et al (2009) suggests that this transition was synchronous across the North Atlantic Ocean. However, Lane et al (2013) has shown that the transition was time transgressive rather than one synchronous event across N.W Europe [Fig.122]. They highlight that the latter half of the YD was wetter than the first. This led to an increase in minerogenic in-washing which was reflected in a rise of titanium counts in the core (Kylander et al., 2011). They concluded that as the NPF increased in latitude it triggered the onset of wetter second stage YD.

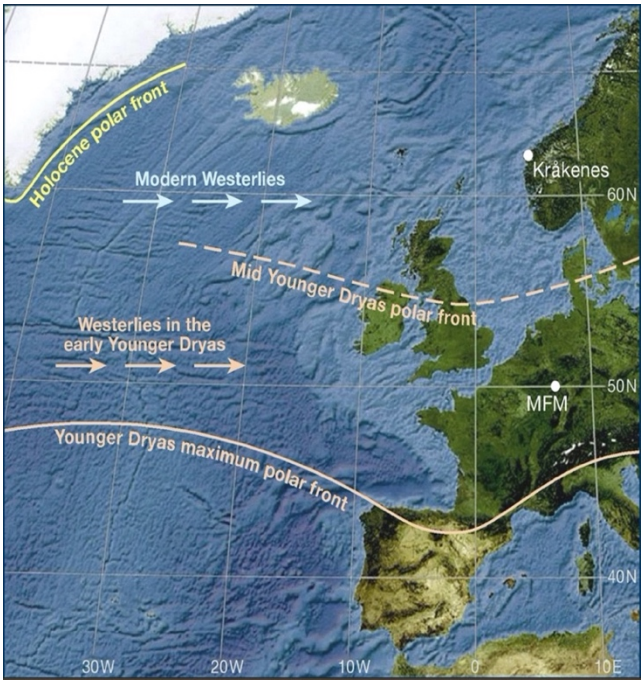

Figure 122. An illustration of the time transgressive Younger Dryas and the position of the North Polar Front (Lane et al, 2013)

They used the highly resolved Vedde ash layer as a tie point to track this transition. This layer has been identified in Meer Feld Maar (MFM) in Germany and Lake Kråkenes in Norway. They use this tie-point to constrain the timing and transgression of this transitional phase between these two sites. They showed that titanium counts rapidly rose 200 years prior to the deposition of the Vedde ash in MFM and 50 years after the deposition in Lake Kråkenes in Norway. They use titanium as a proxy of in-washing and concluded that the YD mid-phase occurred earlier in Germany than in Norway. Palaeo-precipitation levels have also been reconstructed for the LLS using glacial ELA calculations (Ballantyne, 2007).

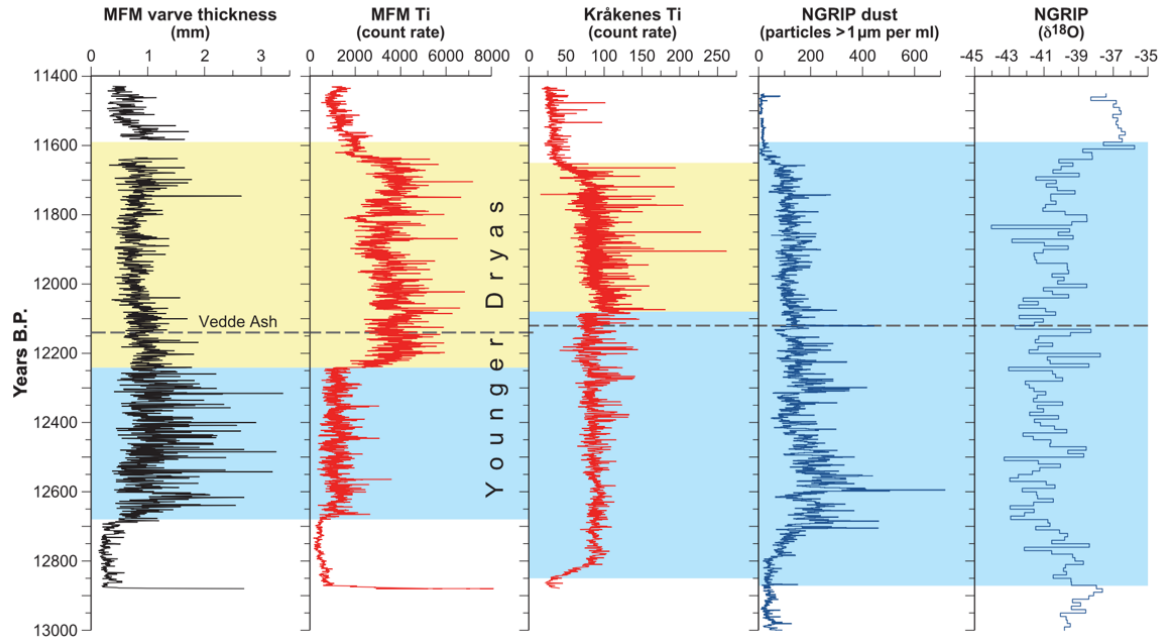

Figure 123. Time transgressive Younger Dryas (YD) based on Titanium counts and the position of the Vedde ash layer (Lane et al., 2013).

This is evidence of a time-transgressive mid-phase of the YD event rather than a synchronous transition across the North Atlantic postulated by Bakke et al (2009). Lane et al (2013) suggests the NPF cold air mass retreated at a rate of 10 km/y. between their two study sites. They suggest that if other sites were found, located between 50˚- 62˚ N, they will provide a clearer record of this transition across N.W Europe. The Northern Isles and Caithness fall within this zone and therefore can be a mid-point to track this transgressive movement of the NPF during the LLS/YD event.

The Vedde ash was identified in Loch of Sabiston on Orkney. However, the levels of titanium remain stable which suggests there was no change in the levels of in-washing meaning that this site could not be used to track the movement of the NPF following the reasoning of Lane et al (2013).

This led to Caithness being chosen, as there is a distinct rise in titanium counts, indicating minerogenic in-washing occurred during the mid-phase of the LLS. Although the Vedde ash layer has not been identified in Shebster it has been identified in Loch of Sabiston, Orkney. In the Orkney core there is a distinct brown stain in the minerogenic sediments of the LLS. This coincides spikes in calcium and iron with a reduction in potassium. These geochemical markers have also recorded in Caithness which has led to the assumption that this too is the Vedde ash. Future analysis will be done to geochemically analyse this brown layer for tephra shards to verify this. But

based on the lithostratigraphy, sediment characteristics and the XRF geochemistry one can be confident that this brown layer in Caithness is the Vedde Ash.

The figure below incorporates the work done by Lane et al (2013) with the results from Caithness. In the Shebster core it is evident that there is a sharp rise in the counts of titanium before the deposition of the 'proposed' Vedde ash which suggests that the transition to the second phase of the LLS occurred before the deposition of Vedde in Caithness. The Shebster core provides this intermediate stage of tracking the movement of the polar air mass northwards during the LLS [Fig 124].

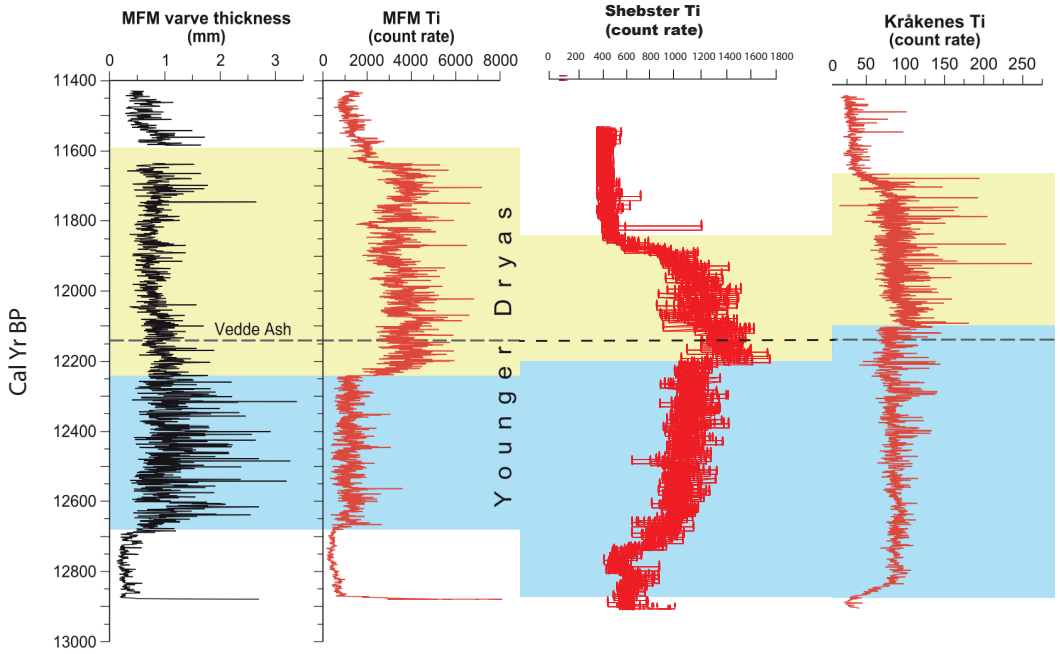

Figure 124. The counts of titanium for Meer Feld Maar (Germany) & Krakenes (Norway)(Adapted from Lane et al., 2013). Combined with the results from Shebster (Caithness). The position of the Vedde ash layer is highlighted. Age-depth model in cal yrs BP.

Based on the results above it is therefore possible to geospatially plot the movement of this air mass to highlight the asynchronies of the YD/LLS event in N.W Europe. Lane et al (2013) indicate that this transition first occurred at lower latitudes, in Meer Feld Maar (50˚N) at c.12.25k cal BP and then transitioned northwards, reaching Caithness by 12.2k cal BP and later reaching Kråkenes by 12.10k cal BP. There is no evidence of this transition in the Greenland ice core record (Rasmussen et al., 2006; Steffensen et al., 2008; Lane et al., 2013) which further suggests that the magnitude and timing of temperature change varied across the North Atlantic Ocean. Below the timing of the mid phase has been geospatially plotted, tracking the movement of the NPF across the LLS using Caithness as a mid-point [Fig.125]

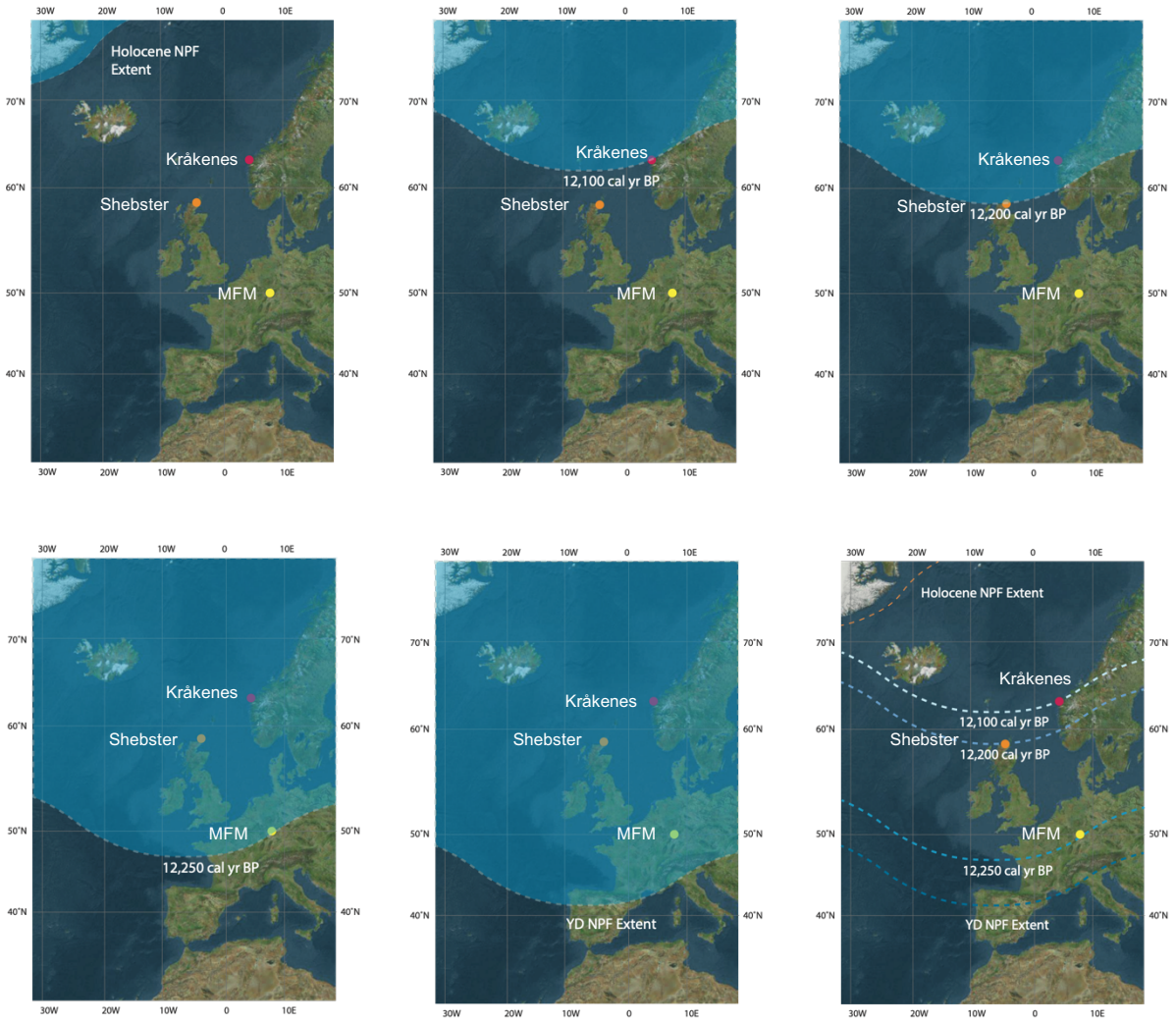

Figure 125. The counts of titanium for Meer Feld Maar (Germany) & Krakenes (Norway)(Adapted from Lane et al., 2013). Combined with the results from Shebster (Caithness). The position of the Vedde ash layer is highlighted. Age-depth model in cal yrs BP.

9.3.1.8 **Holocene Onset**

The onset of the Holocene period is marked by a sharp rise in atmospheric temperatures by 5˚C in Caithness (c.11.9k cal BP), 7˚C in Orkney (c.11.9k cal BP) and 5˚C in Shetland (c.11.4k cal BP) [Fig.115]. The transition is most abrupt in Orkney with temperatures rising by 7˚C within 50 years whereas, in Shetland it takes 600 years for temperatures to reach 12˚C (the same temperatures as Orkney). This suggests that the termination of LLS may have been less abrupt in Shetland than the rest of the British Isles. The FIS is believed to have advanced during the YD period and as a result would have slowed the warming into the Holocene in Shetland. In western Norway the maximum extent of the FIS and the Hardangerfjorden glacial lobe reached a maximum extent by the end of the YD and persisted into the early Holocene (Bondevik & Mangerud, 2002; Mangerud et al., 2016). This suggests that the cooling influence of the FIS may still be a factor controlling temperatures on the Isle of Shetland during this time.

The C-IT model from Loch Ashik records a sharp rise in temperatures from a low of 4.5˚C to 11˚C (Brooks et al., 2012) at the onset of the Holocene period [Fig.116]. This abrupt temperature increase is similar to that of Orkney. However, the record from Abernethy Forest is more similar to that found in Shetland as temperatures rose gradually until the onset of the Holocene. This further highlights that temperatures were not uniform across the N.W Atlantic and that the timing of atmospheric temperature change varied between localities.

The chronology for Orkney and Caithness is more robust due to the use of the Saksunarvatn tephra. Both of these sites record the 11.4k event, which was a short-lived cold phase in the early Holocene (Rasmussen et al., 2014). This event is not recorded in Shetland. In Orkney two previously unidentified cold reversals, at 11.0k cal BP and 10.2k cal BP, have been recorded [Fig.116]. The chironomid record from Orkney indicates there was a drop of temperatures of 4˚C during the 11.0k event and 5˚C during the 10.2k event. This coincides with a decrease in the oxygen isotope record of the Greenland ice cores (Blockley et al., 2014). The two cold reversals in Shetland dated at c.10.8k cal BP and c.10.55k cal BP likely correspond to the same two events at 11.0k cal BP and 10.2k cal BP in Orkney [Fig.126]. However, the lack of AMS dates in the top section of the Shetland core likely accounts for this temporal offset.

The onset of the Holocene period has been shown in all of the C-IT records across N.W Europe (Heiri et al., 2007; Illayshuk et al., 2009; Birks et al., 2014; Brooks et al., 2016) [Fig.117] highlighting, that this was a high magnitude, high amplitude and widespread warming event that spanned Norway, the Northern Isles, Scotland, England and to the interior of mainland Europe. For instance, in the Netherlands temperatures rise abruptly by 4˚C at the beginning of the Holocene period.

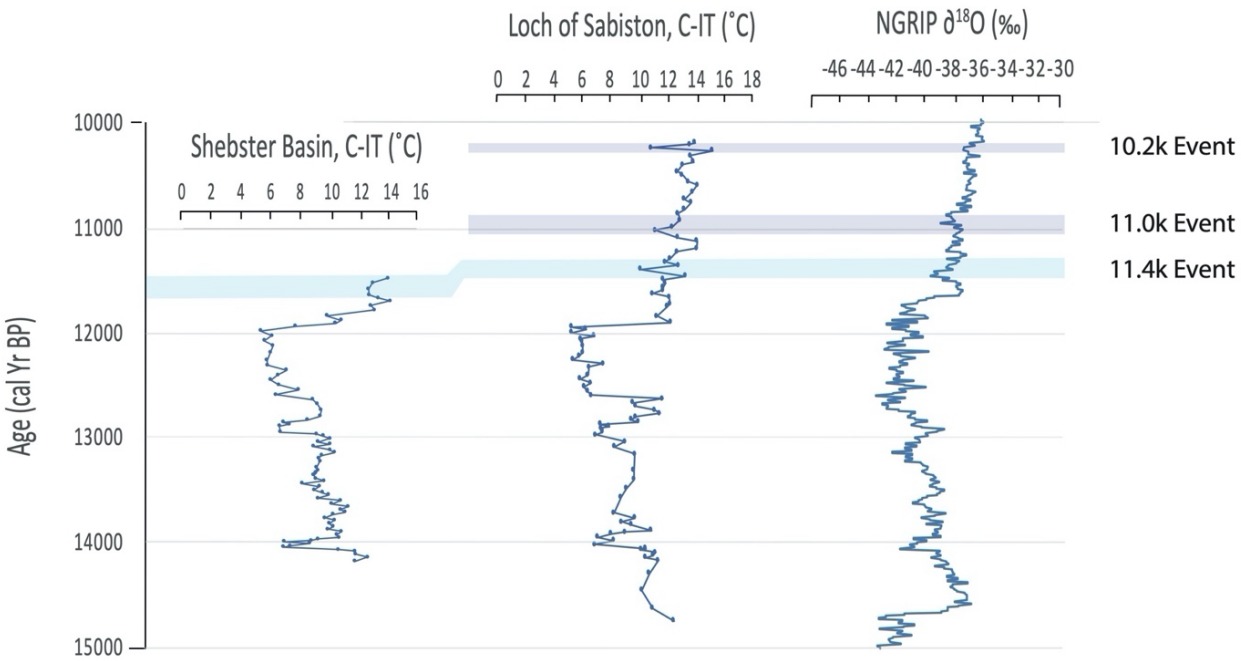

Figure 126 C-IT (˚C) temperature records for the Shebster basin and Loch of Sabiston compared to the NGRIP record (Grootes et al., 1997; Johnsen et al., 1997, Stuiver et al., 2000; North Greenland Ice Coreproject members, 2004; Rasmussen et al., 2014). The 11.4k event is highlighted in blue and the two new cold reversals are highlighted in purple (11.0k Event and the 10.2k Event)

9.3.2 **Summary**

High resolution and robust chironomid inferred mean July summer temperatures have been reconstructed for the Northern Isles of Scotland and Caithness. Combined, they provide an in-depth view of the palaeoclimate history of the north of Scotland. Below will complete the main aim of this research to reconstruct the palaeoclimate history of the Northern Isles of Scotland and Caithness. Furthermore, it will complete the aim of determining the magnitude and temporal scale of the warming and cooling events for during the LGIT for this region. See below the main findings from this chapter:

(1) **Termination of the LGM and Pre-interstadial**: Shetland is the only site in the Northern Isles record which records warming into the interstadial after the end of GS-2. The chironomid inferred temperatures suggest that mean July temperatures ranged between 5.5˚C to 10˚C, at c.15.88k cal BP, before the end of GS-2.

(2) **Climate warming (GI-1e**): Temperatures reach 12˚C in Caithness, c.14.7k cal BP, and 10.5˚C in Orkney, c.14.1k cal BP, whereas in Shetland temperatures are 8˚C at c.15.6k cal BP. In Caithness and Orkney temperatures appear more stable with values ranging between 12-12.5˚C and 10.5-12˚C respectively, whereas, on Shetland temperatures range between a low of 8.7˚C and high of 12.3˚C.

(3) **Abrupt cooling (GI-1d):** Temperatures fall from 11˚C to 6.8˚C at c.14.1k cal BP in Caithness. In Orkney, temperatures fall from 11˚C to 6.5˚C by c.14.1k cal BP. The LCA record from Caithness indicates that spring lake temperatures fell to a low of 8.7˚C by c.14.02k cal BP. The onset of GI-1d is more abrupt in Caithness and Orkney compared to Shetland.

(4) **Climate warming (GI-1c):** Abrupt warming occurs in Caithness and Orkney at c.13.9k cal BP. Temperatures rise to 10.6˚C and 10.7˚C respectively. In Shetland, temperatures rise to 8.9˚C by c.14.2k cal BP. The transition from cold to warmer climates is less abrupt in Shetland taking approximately 400 years. This event is split into three distinct phases.

a. **GI-1c(1)(c.13.9k cal BP).** In Caithness mean July summer temperatures were 11.3˚C and in Orkney temperatures were 10.7˚C. The LCA record from Shebster also records lake temperatures of 14˚C during GI-1c(1)
b. **GI-1c(2) (c.13.7k cal BP).** During this subtle cold phase temperatures fall to 8.1˚C in Caithness and 7.9˚C in Orkney. The LCA record from Shebster also records lake temperatures of 13˚C during GI-1c(2)

c. **GI-1c(3)(c.13.4k cal BP).** Temperatures begin to rise again to 10.4˚C in Caithness and 9.5˚C in Orkney. The LCA record from Shebster also records lake temperatures of 15˚C during GI-1c(3).

(5) **Abrupt cooling (GI-1b):** Climate cooling occurs in Caithness and Orkney at c. 13.0k cal BP. Mean July summer temperatures fall to a low of 6.6˚C in both locations. This abrupt cold phase occurs in Shetland at c.13.8k cal BP and temperatures drop to 6.11˚C. The LCA record from Caithness indicates an abrupt drop in spring lake temperatures to a low of 8˚C.

(6) Climate warming (GI-1a): Abrupt warming occurs at c.12.9k cal BP in Caithness and Orkney. Temperatures rise to a high of 9.5˚C in Caithness and 11.5˚C in Orkney. In Shetland temperatures rise further to 13.5˚C at c.13.2k cal BP. The LCA record from Caithness indicates that spring lake temperatures rose to 14.8˚C by c.12.6k cal BP.

(7) **Loch Lomond Stadial**: temperatures fall markedly to c.6˚C in Caithness (c.12.6k cal BP), Orkney (c.12.6k cal BP) and Shetland (c.13.2k cal BP). LLS mid-phase occurs in Meer Feld Maar (50˚N) at c.12.25k cal BP and then transitioned northwards, reaching Caithness by 12.2k cal BP and later reaching Kråkenes by 12.10k cal BP.

(8) **Holocene onset**. This time is marked by a sharp rise in atmospheric temperatures by 5˚C in Caithness (c.11.9k cal BP), 7˚C in Orkney (c.11.9k cal BP) and 5˚C in Shetland (c.11.4k cal BP). In Orkney two previously unidentified cold reversals, at 11.0k cal BP and 10.2k cal BP, have been recorded [Fig.108].

9.4. Was climate synchronous the across the North Atlantic during the LGIT?

For the past two decades the INTIMATE working group have been trying to synchronise the climate records across the North Atlantic and N.W Europe (Rasmussen et al., 2014). However, by doing so they assume that climate fluctuations were synchronous across the North Atlantic Ocean. With the high-resolution

chironomid inferred temperature records from this research, combined with a robustly constrained chronology it is possible to assess if mean July atmospheric temperatures were synchronous throughout the LGIT. However, this was only possible during intervals where the resolution of the age-depth model is high, and errors were low. To minimise uncertainty terrestrial plant fragments were preferentially chosen for AMS dating and well constrained tephra layers were identified. However, during periods between dated layers the errors and resolution is lower, and determinations of synchronicity were not possible.

Lane et al (2013) and Lowe et al (2019) have shown that there are local variations in climate which can influence the timing and magnitude of temperature change. Brooks et al (2012) assessed the similarity between Loch Ashik and Abernethy Forest with the Greenland ice core record. They showed that the main climate events in both records were also recorded in the Greenland ice core. However, to date no one has quantitatively assessed if atmospheric temperature changes were synchronous between Greenland, the Northern Isles and mainland Scotland, during the LGIT for the transitions between climate events.

In order to do this a high-resolution robust chronology is required. With the addition of tephra tie-points one can more reliably constrain the timing of climatic events through time. Loch of Sabiston from this project (Orkney), Loch Ashik (Skye) and Abernethy Forest, (Cairngorms) (Brooks et al., 2012) and the NGRIP record (Greenland) (Rasmussen et al., 2014) have a robust chronology with four tephra tie constraints found in each site [Fig.127]. As a result, each of the regions can be tied to one another and a quantitative analysis of synchronicity can be made. Brooks et al (2012) state that making robust comparisons between sites across the LGIT is difficult due to the lack of robust chronologies. However, where tephra tie-points are available isochronous markers make climatic and chronological comparisons possible. Below a comparison between each of the climatic stages of the LGIT will be shown highlighting the similarities and differences between each of the records. Statistical modelling in OxCal has been undertaken to assess the degree of synchronicity throughout the LGIT [Fig.128]:

- **GI-1e:** it is clear that the record for Loch of Sabiston spans GI-1e. However, at Abernethy Forest and Loch Ashik this warm period is missing. Brooks et al

(2012) suggests that the lakes were likely inhospitable due to the late withdrawal of ice in the area.

- **GI-1d:** Based on the age-depth model and age-difference calculations, there is a 98% (2 sigma) confidence that this cold phase is synchronous with the NGRIP record, Loch Ashik and Abernethy Forest.

- **GI-1c:** Based on the age-depth model age-difference calculations there is a 98% (2 sigma) confidence interval that this warm phase is synchronous with the NGRIP record, Abernethy Forest and Loch Ashik

- **GI-1b & G-1a:** There are clear climatic events, likely corresponding to GI-1a and GI-1b, which are apparent in Orkney that are not visible in the Cairngorms and the Isle of Skye. There is a 68% confidence that Greenland leads Orkney during these cold phases.

- **Loch Lomond Stadial:** Based on the age-depth model age-difference calculations there is a 98% (2 sigma) confidence interval that this warm phase is synchronous with the NGRIP record, Abernethy Forest and Loch Ashik. However, there is a 68% confidence interval that Orkney leads Abernethy Forest at the onset of the LLS. At the onset of the LLS, visually it is apparent that there was an offset between the onset the cold phase between Loch Ashik, Abernethy Forest and Loch of Sabiston. However, statistically only Abernethy Forest lags behind Loch of Sabiston. Brooks et al (2011) and Lang et al (2013) suggest that this is a result of local climate variability.

- **Early Holocene**: There is a 98% confidence that the onset of the Holocene period is synchronous between all of the 4 sites, although visually it is apparent that there is some offset between the records. With higher resolution dating it may be possible in the future to assess if this event is synchronous across the North Atlantic region.

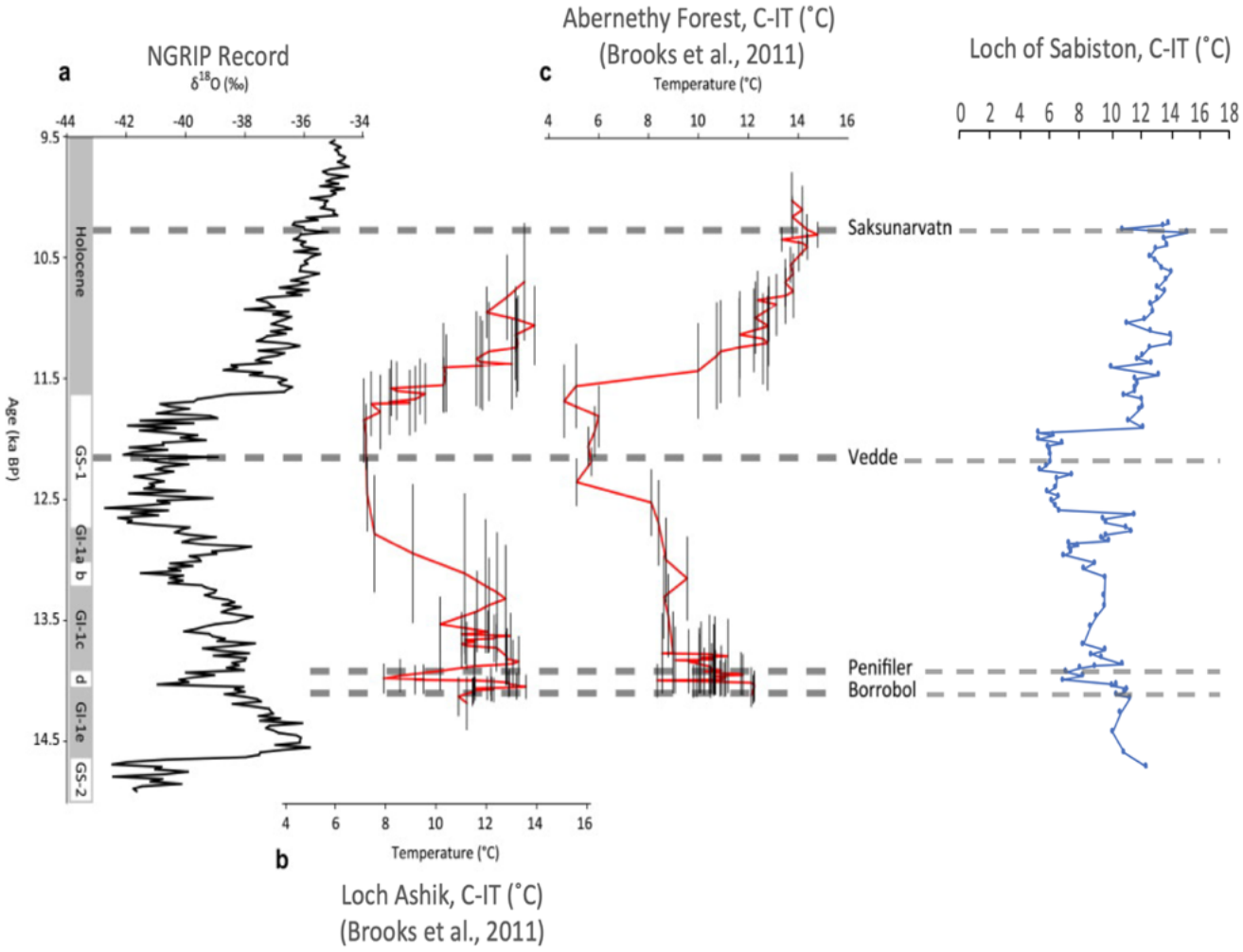

Figure 127. A comparison of the NGRIP record, the Loch Ashik & Abernethy Forest C-IT (˚C) models (Brooks et al., 2011) and Loch of Sabiston from Orkney. Constrained by the Saksunarvatn, Vedde, Borrobol and Penifiler tephra's.

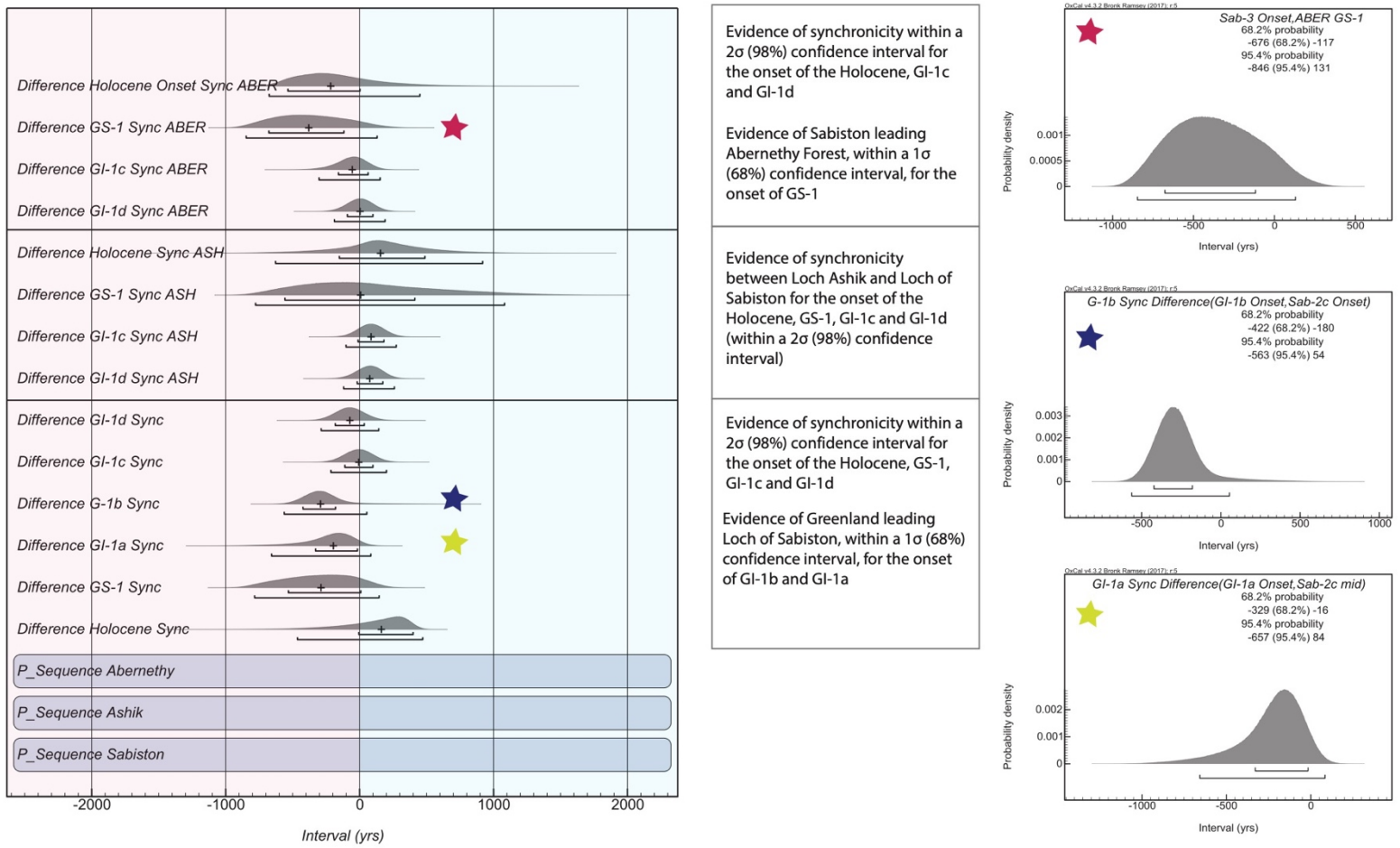

Figure 128. The diagram quantitatively assesses the synchronicity or a-synchronicity of mean July summer temperatures between Orkney (this research), Skye and the Cairngorms (Brooks et al., 2012), and the Greenland ice core (NGRIP) (Rasmussen et al., 2014).There is no evidence of climate a-synchronicity for GS-1, GI-1c and GI-1d between Orkney and Skye. There is evidence of climate a-synchronicity (68% confidence/two sigma) for the onset of GS-1 for Orkney and the Cairngorms. There is a 98% confidence that climate changes were synchronous for GS-1, the Holocene onset, GI-1c and GI-1d between Orkney and Greenland. There is evidence that Greenland led Orkney during the onset of GI-1b and GI-1a (68% confidence interval)

9.5 What was the nature of atmospheric temperature change across Scotland during the LGIT? What forced these changes?

Brooks and Langdon (2014) geospatially plotted the mean July summer temperatures for the British Isles, Ireland and the N.W European mainland throughout the LGIT. They were the first to do so for the region. However, they highlighted significant gaps in the records where temperatures were largely interpolated. These were N.W Scotland, the Faroes, south-west England, Wales, Denmark and the Baltic regions (Brooks and Langdon, 2014). This project fills the gap of the northern regions of Scotland. Based on their models they concluded that there was a strong W-E gradient across N.W Europe [Fig.129]. They highlight that this gradient is controlled primarily by the thermohaline circulation (THC). They show that going further east the influence of the THC reduces. This is supported by Coope and Lemdahl (1995) who emphasise the role of the North Atlantic thermohaline circulation and the Scandinavian ice sheet in controlling summer temperature change. Eastern sites in mainland Europe were shown to be influenced by the position of the Fennoscandinavian ice sheet and showed there was a N-S gradient. This research uses a similar approach, by geospatially plotting the extent of mean July summer temperatures. However, this research will only focus on the British Isles, with an emphasis on Scotland. This will be done to assess what drove mean July summer temperatures during the LGIT for this region and to assess if they were the same drivers suggested by Brooks and Langdon (2014).

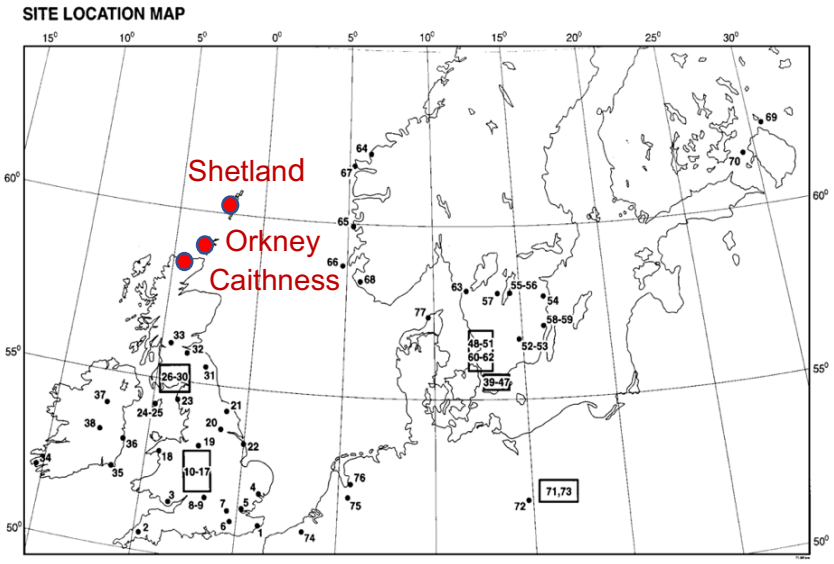

Figure 129. The 76 chironomid and coleoptera inferred temperature records for north-west Europe (adapted from Brooks and Langdon., 2014). The position of the Isle of Shetland, Orkney and Caithness are shown above (red dot).

9.5.1 **Isotherm gradients and climate drivers**

What drove climate fluctuations across the North Atlantic during the LGIT? How did the magnitude of temperature change, and the spatial extent, vary across Scotland? This research sets out to answer the questions above. Firstly, it is worth considering what drove other cold phases across the North Atlantic region.

The onset of the LGM was controlled by fluctuations in the North Atlantic Thermohalline Circulation (section 2.2) when cold saltwater flowed northwards and became denser, sinking beneath the arctic sea ice, limiting the transmission of heat from the ocean to the atmosphere (Serreze et al., 2007). McManus et al (2004) suggests that the Atlantic Meridional Overturning Circulation (AMOC) terminated at a lower latitude during the LGM, and as a result ice was found at lower latitudes. Both of these factors led to oceanic cooling in the North Atlantic and was a major control of the cold atmospheric temperatures seen in the region at this time. Were these controls on climate similar to those in the LGIT?

Eldevik et al (2014) suggests that oscillations in the THC were a dominant control of moderating climate change in N.W Europe during the LGIT. The warm and cold phases, recorded by Rasmussen et al (2014), are believed to be tightly constrained by the processes occurring in the THC (Rhines et al., 2008; Spielhagen et al., 2011). However, Lane et al (2013) has shown that the NPF was a major control of temperatures during the YD for N.W Europe. In addition, Brooks and Langdon (2014) show that the Fennoscandinavian ice sheet was a major control on temperatures in mainland Europe during the LGIT. Were these the same forcing mechanisms which controlled atmospheric temperatures in Scotland?

This research has modelled Isotherm gradients for the main climate events, spanning the Last Glacial – Interglacial Transition (LGIT) for Scotland to assess the main drivers of atmospheric temperature change and how temperature change, its spatial extent and magnitude varied between localities. The interpretations from the previous sections will be used to back-up the interpretations here. The Greenland ice core chronology has been used to constrain the timing of the events [Fig.130]

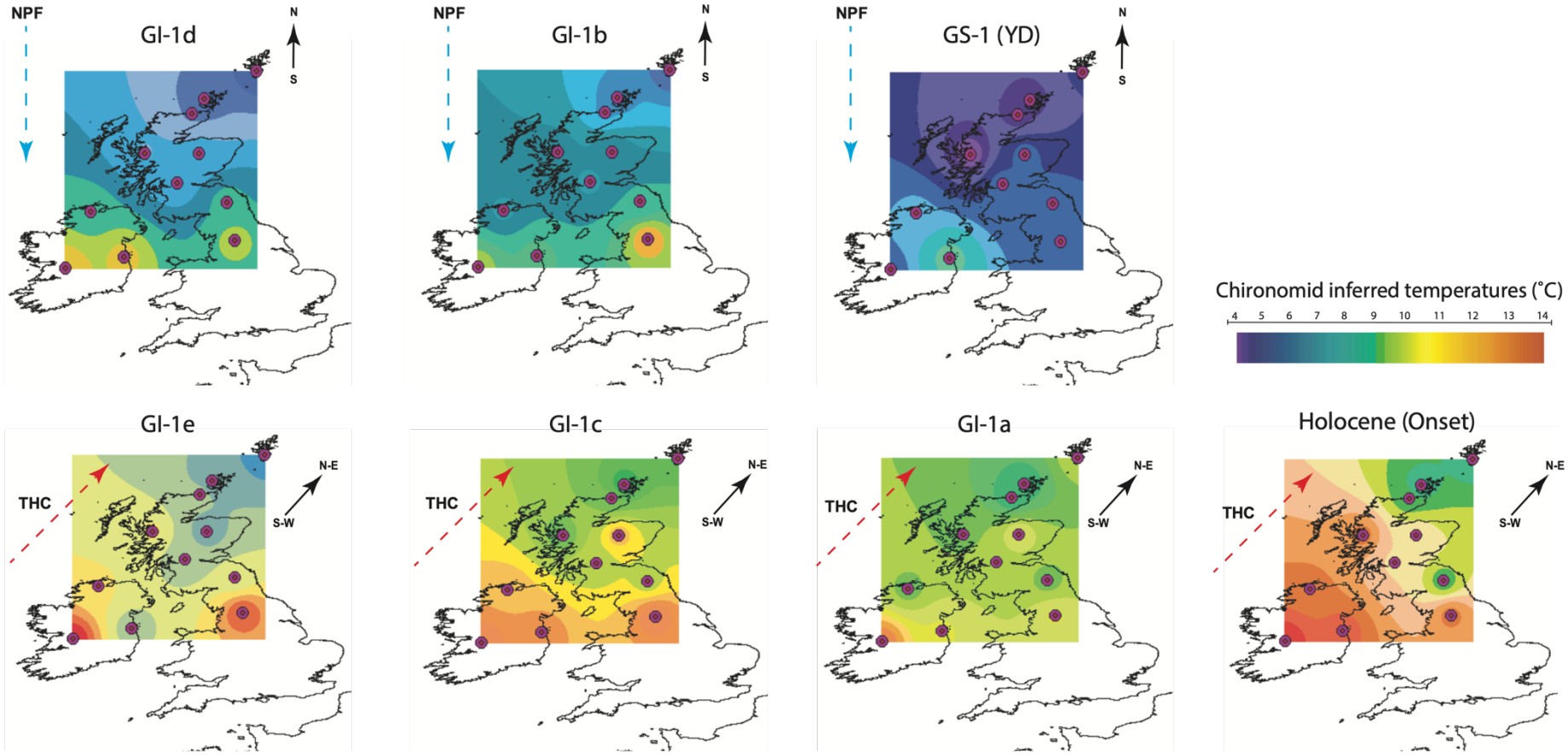

Figure 130 Temperature isotherms across the British Isles and Ireland during the LGIT. The INTIMATE chronology is used (Rasmussen et al., 2014). C-IT (˚C) models from Brooks et al (2011), Brooks et al (2016), van Asch et al (2015), Watson et al (2010) and the sites from this project.

9.5.1.1 **Climate warming (GI-1e)**

The chironomid inferred mean July summer isotherms highlight that there was a strong SW-NE gradient across Scotland at the onset of GI-1e [Fig.131]. The diagram below suggests that the THC was a major control of the spatial distribution of temperatures during this time. This is affirmed by McManus et al (2004) who attribute the onset of GI-1 to a is reignition of the AMOC at c.14.7k BP (McManus et al., 2004) combined with warming sea surface temperatures in N.W Europe (Rasmussen and Thomsen, 2008). This led to the retreat of the Fennoscandinavian Ice Sheet (FIS) and the British Ice Sheet (BIS) (Bradwell et al., 2019).

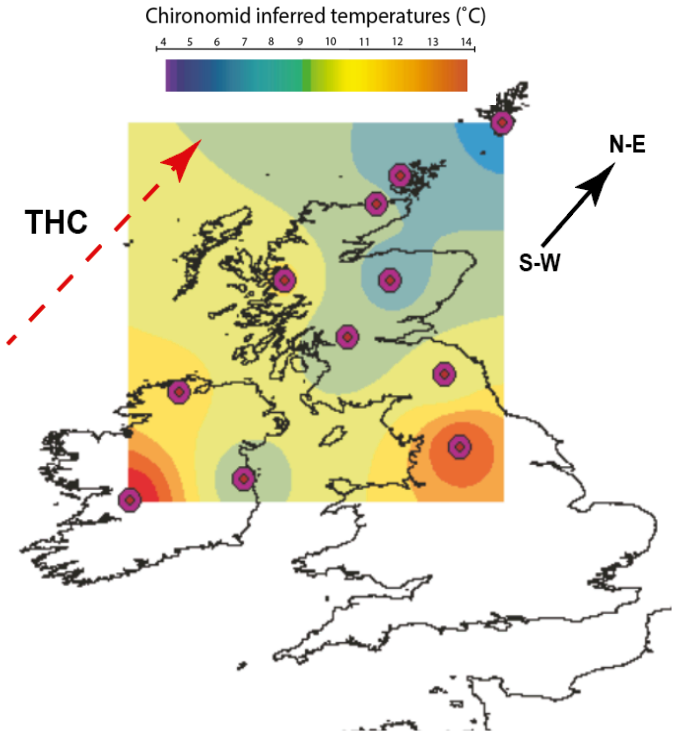

Figure 131. Chironomid inferred mean July summer palaeo-isotherms (°C) for the British Isles and Ireland (Brooks et al., 2016) and the sites from this research (Caithness, Orkney and Shetland) for GI-1e.

9.5.1.2 **Abrupt cooling (GI-1d)**

The mean July summer temperature isotherms record a strong N-S gradient across Scotland at the onset of the abrupt cold phase GI-1d [Fig.132]. However, for the Northern Isles of Scotland and Caithness the minimum temperatures recorded are the same. To date, the onset of the short-lived cold events GI-d and GI-b have not been attributed to a particular forcing mechanism. However, Andressen et al (2000) concludes that the onset of GI-1b cannot be associated with decreased solar insulation

as the concentration of ^{10}Be increases during this phase. Unlike the onset of the LLS, there is no sharp increase in ∆14C values at the onset of GI-1b (Hughen et al., 1998). This lends one to believe that deep ocean ventilation, and a weakening of the AMOC, was not the trigger to this cold phase.

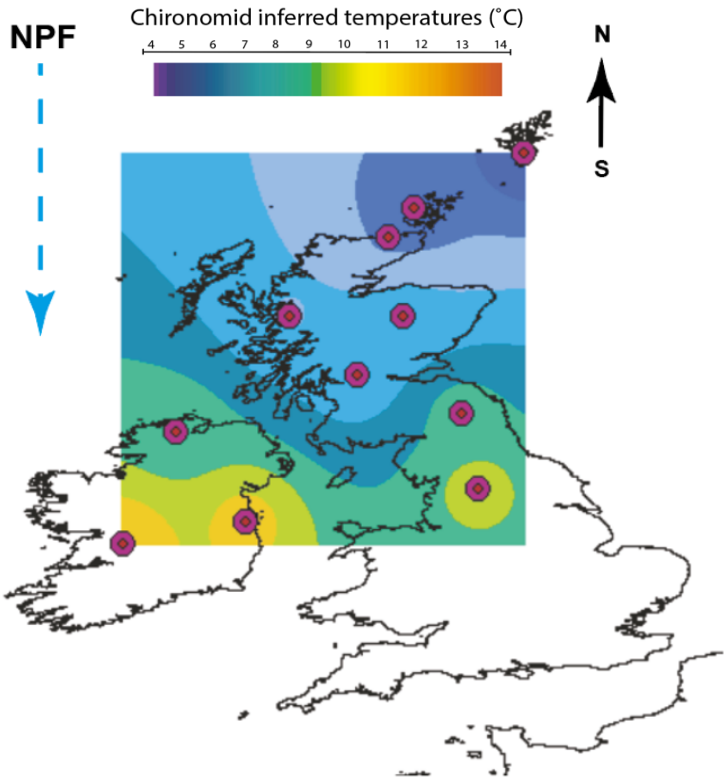

Figure 132. Chironomid inferred mean July summer palaeo-isotherms (˚C) for the British Isles and Ireland (Brooks et al., 2016) and the sites from this research (Caithness, Orkney and Shetland) for GI-1d.

Instead this research postulates that the onset of GI-1d in Scotland was linked to a southwards trend of the north polar front bringing cold dense air from the arctic to lower latitudes. As the polar front moved to lower latitudes, triggering GI-1d, Shetland would have been the first locality in the transect to experience climate cooling. Stewart et al (2017) highlights that Shetland today is located on the fringe between the maximum extent of the winter polar front which may account for the instability shown in the Shetland record [Fig.133].

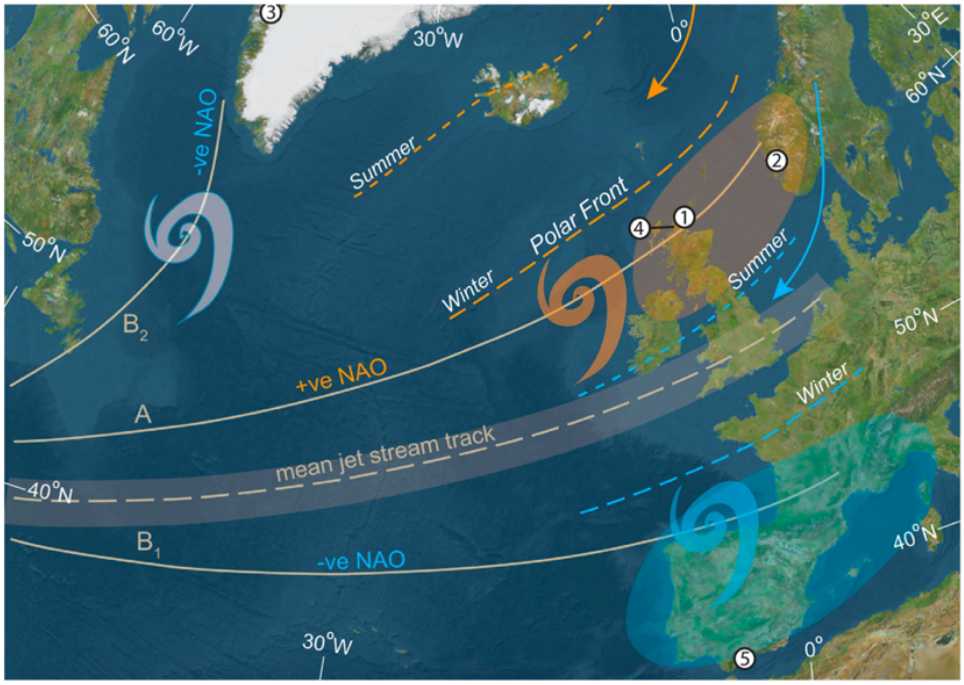

Figure 133. Position of the North Atlantic Oscillation, Winter Polar Front and Summer Polar Front (Stewart et al., 2017)

As the NPF moved to lower latitudes the chironomids record an early transgression of the polar front southwards, reaching Shetland first, thus affirming the hypothesis that Shetland was more unstable than the other two sites. The latitudinal position of Shetland, the lower latitude of the NPF and increased snowfall likely accounts for the colder temperatures recorded during this abrupt phase when compared to Orkney and Caithness.

When the Northern Isles are included in the isotherms there is a clear NE-SW deviation in the record. This suggests that whilst the NPF was the major control of temperatures in the region that perhaps the Fennoscandinavian ice sheet was also an important driver at the time. Brooks and Langdon (2014) suggests that this was the case for the eastern regions of mainland Europe during the cold phases of the LGIT. There is a clear difference in the spatial extent of GI-1d when compared to the previous warm phase GI-1e. This suggests that the THC was not the major control of temperatures for Scotland at this time, but rather the NPF and to an extent the position of the FIS.

9.5.1.3 **Climate warming (GI-1c)**

During the warm phase G1-1c there is a strong NE-SW gradient across Scotland [Fig.134]. This highlights that the THC was likely the same forcing mechanism triggering the onset of this event and the previous warm phase GI-1e. However, what is not clear is what caused the termination of the previous cold phase, why the THC became the dominant forcing mechanism again and what caused the NPF to increase in latitude. GI-1c is known to be split into three distinct phases and as a result in the future higher resolution isotherms could be modelled to assess the subtleties of climate change during this time. However, not all of the regions across the British Isles and Ireland record the three phased GI-1c.

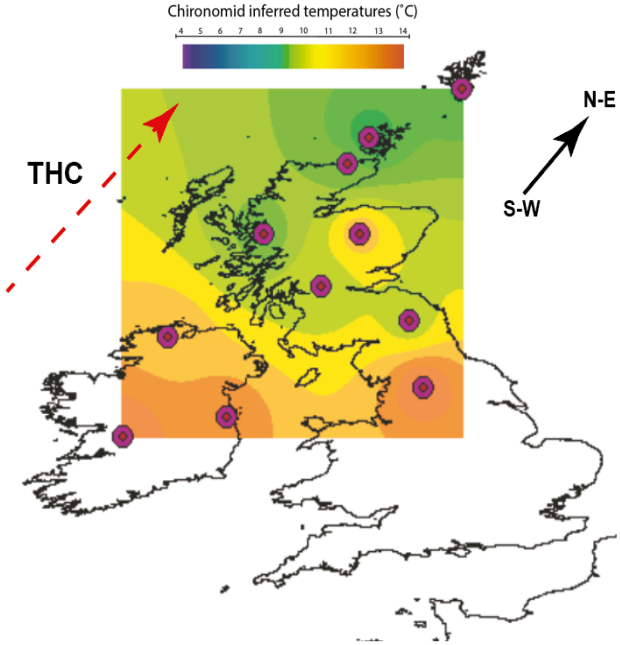

Figure 134. Chironomid inferred mean July summer palaeo-isotherms (°C) for the British Isles and Ireland (Brooks et al., 2016) and the sites from this research (Caithness, Orkney and Shetland) for GI-1c.

9.5.1.4 **Abrupt cooling (GI-1b)**

The chironomid inferred palaeo-isotherms for the onset of GI-1b indicates that there is a strong N-S gradient [Fig.135]. Similar to the cold phase GI-1d, there is an apparent NE-SW deviation in the trend of cooling in the Northern Isles and Caithness. This indicates that this region was also controlled by the position of the FIS. It is clear that the minimum temperatures inferred in GI-1b are significantly lower than the previous cold phase GI-1d. This research suggests that this cold phase was linked to a southward transgression of the NPF bringing cold air from the arctic.

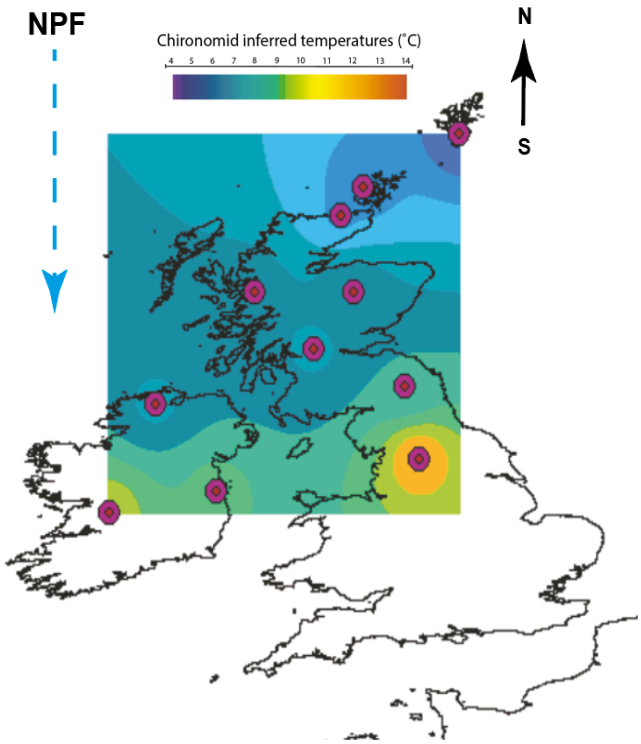

Figure 135. Chironomid inferred mean July summer palaeo-isotherms (°C) for the British Isles and Ireland (Brooks et al., 2016) and the sites from this research (Caithness, Orkney and Shetland) for GI-1b.

There was little retreat of the western edge of the FIS between 10-11.5 cal BP and as a result would have continued to be a major control of summer temperatures in the Northern Isles, particularly for Shetland (Stroeven et al., 2016). During the cold phases of the LGIT this research suggests that the NPF and the location of large ice masses are a greater control of atmospheric temperature change than the THC.

9.5.1.5 **Climate warming (G-1a)**

The chironomid inferred temperatures, at the onset of GI-1a, indicates there was a strong NE-SW trend where temperatures warmed from the west of the British Isles and cooled to the east [Fig.136]. This is similar to the previous warm phases GI-1e and GI-1c. Again, is not clear what caused the termination of the previous cold phase, why the THC became the dominant forcing again and what caused the NPF to increase in latitude. This highlights that the THC was likely the same forcing mechanism triggering the onset of this event and the previous warm phase GI-1e and GI-1c.

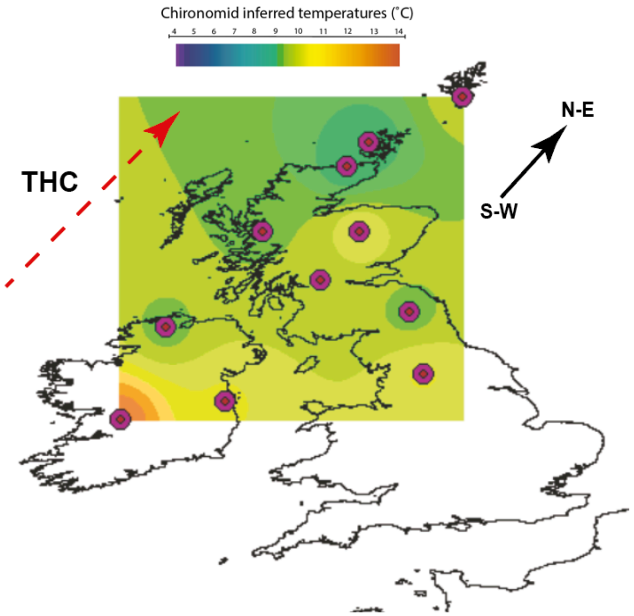

Figure 136. Chironomid inferred mean July summer palaeo-isotherms (˚C) for the British Isles and Ireland (Brooks et al., 2016) and the sites from this research (Caithness, Orkney and Shetland) for GI-1a.

9.5.1.6 **Loch Lomond Stadial/GS-1**

During the LLS/GS-1 there is a clear N-S gradient in mean July summer temperatures. This suggests that the NPF was the main control of temperature change across Scotland during this abrupt cold phase [Fig.137]. Again, there is an apparent NE-SW diversion in the temperature gradient. This suggests that the FIS was also a major control on temperature change in the Northern Isles. All of the available temperatures across the British Isles indicates that temperatures were <10˚C. It is evident that this cold phase was widespread during the LLS. Although similar to GI-1d and GI-1b there are subtle differences between the previous cold phases.

Over the western highlands and western isles of Scotland colder temperatures, range between 4-5˚C. This is not the case in the previous cold events. During the cold phases GI-1d and GI-1b the temperatures are still low however are higher than sites at higher latitudes. However, during the LLS there is a clear drop in temperatures at lower latitudes over the mountainous regions of Scotland. This suggests that there were local forcing mechanisms at play during this time. The LLS ice sheet was located in this region of Scotland. It is likely that these lower temperatures, over this area, were a result of the glacial ice creating a cooler microclimate. Brooks et al (2016) postulates that the closer an ice mass is to the site; the more depressed atmospheric temperatures are.

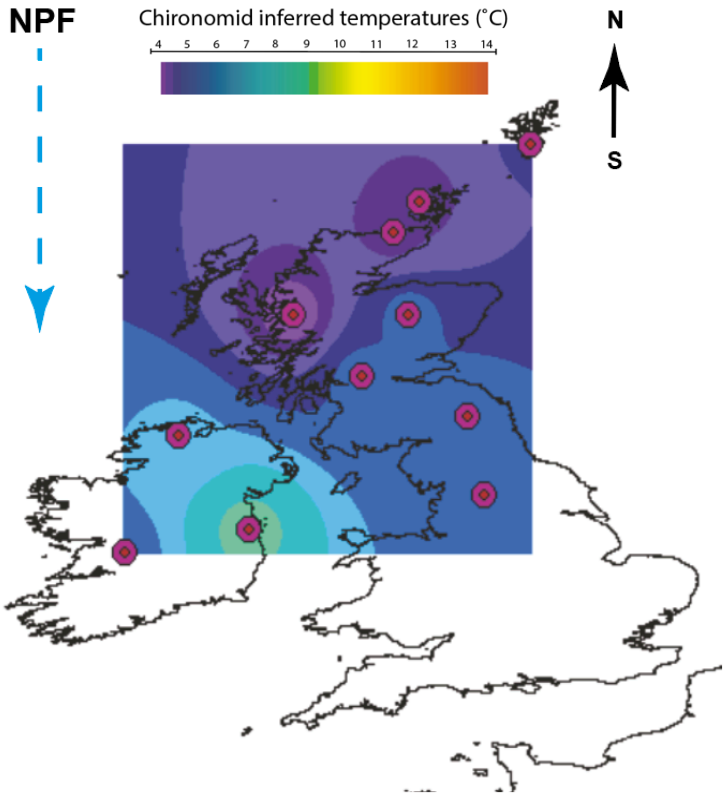

Figure 137. Chironomid inferred mean July summer palaeo-isotherms (˚C) for the British Isles and Ireland (Brooks et al., 2016) and the sites from this research (Caithness, Orkney and Shetland) for the LLS.

The onset of the LLS/GS-1, c.12.9-11.7k BP, coincides with a weakening of the AMOC (McManus et al., 2004). The reason for this weakening is contentious, with some studies suggesting it was caused by freshwater inundation from Lake Agassiz due to the destabilisation of the Laurentide Ice Sheet (Murton et al., 2010), whilst Tarasov and Peltier (2005) suggests it was a combination of this and vast iceberg/ice-sheet melting in the Arctic Ocean. However, Wunsch (2006) proposes that the onset of this cold phase was due to fluctuating atmospheric circulations. However, it may be combination of seasonal variations in atmospheric temperatures, atmospheric forcing and/or North Atlantic sea-ice (Denton et al., 2005; Brauer et al., 2008; Bakke et al., 2009). Cabedo-Sanz et al (2012) shows that midway through the GS-1 there was a sharp decrease in sea ice-cover and an increase in SST(˚C) during the latter phases. Bakke et al (2009) suggests that a sharp influx of warm salty water, into the North Atlantic Ocean, led to a southward transgression of the North Polar Front and westerly wind system leading to the termination of this cold phase. This affirms the research in this project which suggests that the NPF was the major control on temperatures in Scotland at this time.

A time slice of the LLS was taken using the available chironomid inferred temperatures from the literature, combined with the results from this project. The isotherms were plotted using IDW, the same method used in the previous subsection, layered with the glacial extent of the LLS re-advance from Golledge et al (2008). In this section the glacial extent and the mean July summer air temperatures (˚C) are compared to the precipitation levels reconstructed by Chandler et al (2019).

The combined C-IT (˚C) models indicate that there is a N-S gradient of temperatures across Scotland and Ireland during the LLS. With a deviation to a SW-NE trend across the Northern Isles of Scotland and Caithness. The coolest areas being the Isle of Orkney, Caithness, Isle of Skye and the Western Isles reaching average temperatures of 4-4.5˚C. Whereas, the central belt of Scotland, the Scottish borders and the North of England show a higher temperature averaging 7.5˚C for the whole region. Interestingly, the largest difference in temperatures are from the island of Ireland and the Scottish Highlands with temperatures exceeding 9˚C (an offset of 5˚C). It is worth reiterating that Shetland, being at a higher latitude, does not have the coldest temperatures (as explained in section 6.4.1). Shetland was not thought to have had any glaciers during this time (Bradwell et al., 2019). Due to the distance of Shetland to the LLS ice mass the cooling effect would be reduced compared to sites which were in closer proximity to the ice. This could account for the less cold temperatures seen in Shetland compared to sites in the Scottish Highlands. When comparing the chironomid inferred temperatures, with the precipitation levels modelled by Chandler et al (2019), one can see that the precipitation and temperatures are highest in the west and lowest in the east. Precipitation is lowest in the Cairngorms, reaching only 400-600mm a^{-1}, and highest on the Scottish west coast, Western isles and Inner Hebrides reaching a high of 2400mm a^{-1}(Chandler et al., 2019) [Fig.138]. Analysing both records more closely one can see that the centre of the LLS glacier is located in the coldest and wettest region of Scotland.

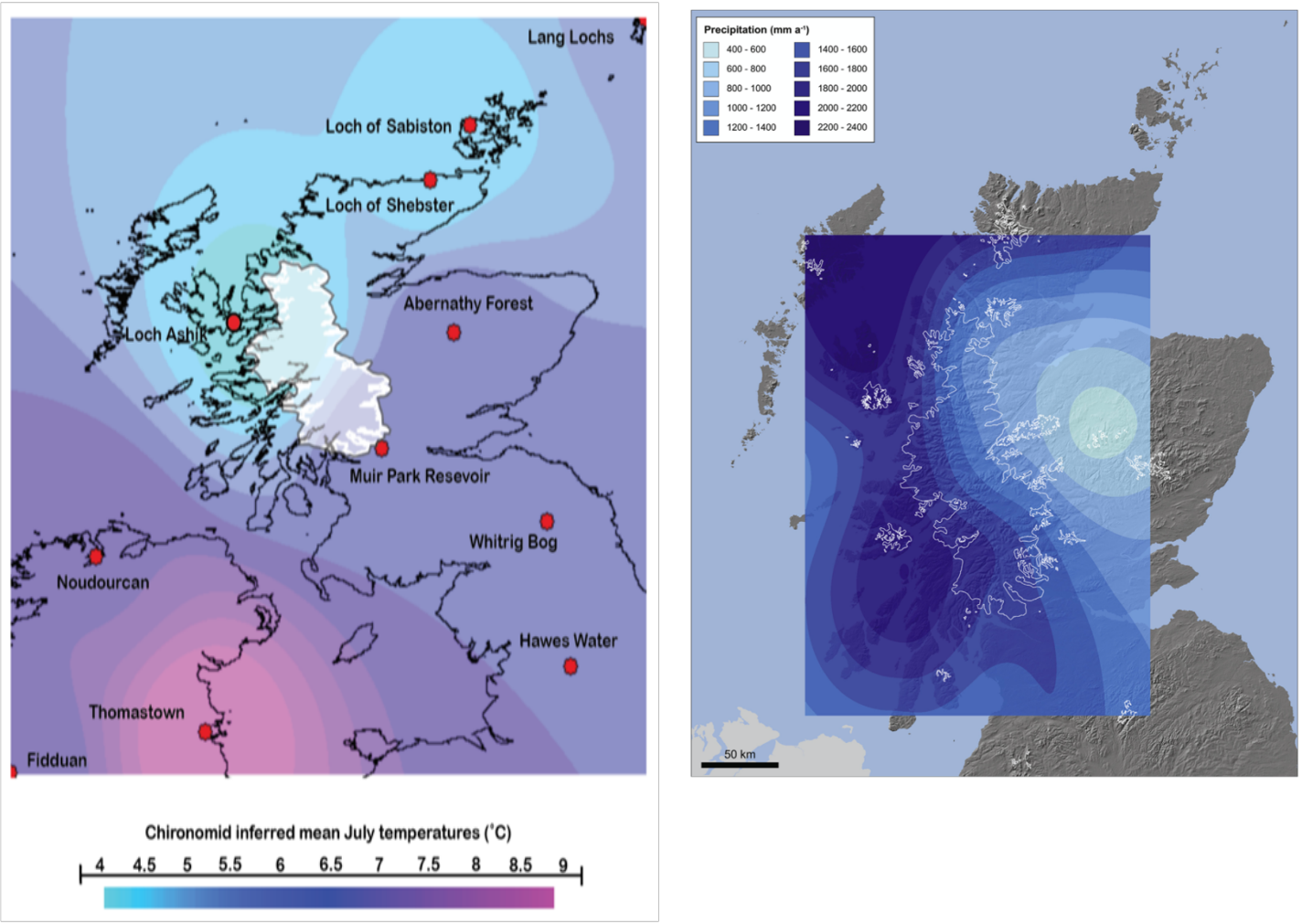

Figure 138. Chironomid inferred mean July summer temperatures (˚C) throughout the LGIT for the British Isles and Ireland (Watson et al., 2010; Brooks et al., 2012, Brooks et al., 2016). Temperatures are shown on a gradient ranging from 4-9˚C. Precipitation isopleth map showing the pattern across the Younger Dryas period for Scotland (Chandler et al., 2019)

9.5.1.7 **Onset of the Holocene**

There is a strong NE-SW gradient across Scotland at the onset of the Holocene period [Fig.139]. This has been explained by a reignition and reorganisation of the AMOC in the North Atlantic (Risebrobakken et al., 2011). There was an influx of warm salty water into the North Atlantic Ocean at this time which lead to the reinstation of the THC (Bakke et al., 2009). The THC is the dominant forcing mechanism in Scotland at this time for mean July summer temperature change.

However, the reignition of the THC also coincides with increased summer insolation in the northern hemisphere which is also believed to have triggered atmospheric warming during the Holocene Thermal Maximum (Calvo et al., 2002; Berner et al., 2011). However, the timing and spatial extent of this warming is also controlled by local melting of ice sheets and icecaps at the end of GS-1 (Kaufmen et al., 2004). This research suggests that the THC was the most dominant control of temperature change in Scotland. However, on a larger scale summer insolation was likely the greatest driver which caused the termination of the LLS/GS-1.

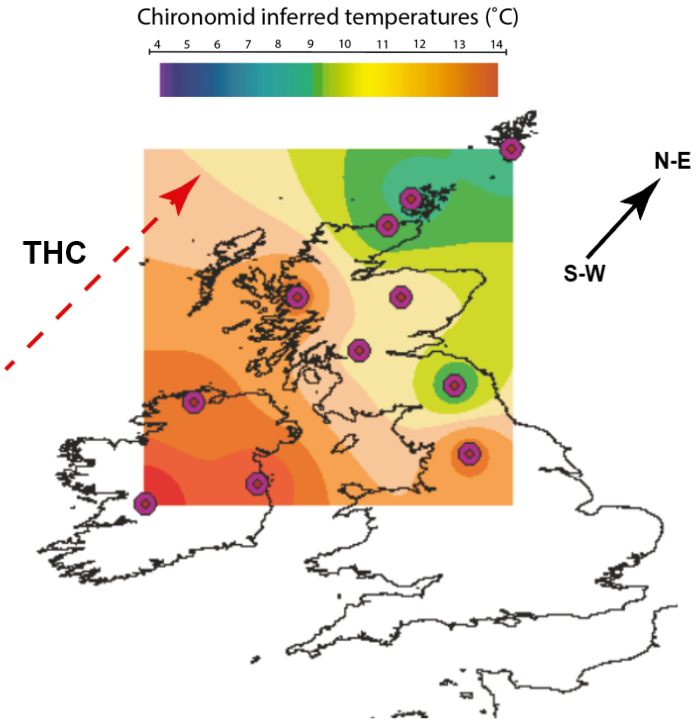

Figure 139 Chironomid inferred mean July summer palaeo-isotherms (˚C) for the British Isles and Ireland (Brooks et al., 2016) and the sites from this research (Caithness, Orkney and Shetland) for Holocene.

9.6 Chironomid inferred temperatures and palaeo-precipitation levels during the LLS

Ohmura et al (1992) was the first to pioneer the use of summer temperatures, to calculate the amount of winter accumulation at the Equilibrium Line Altitude (ELA). They used this relationship to reconstruct the temperature at the ELA which in turn can be used as a proxy for climate change. They found the following relationship:

$$(1)\ P_a = 645 + 296T_3 + 9T_3^2$$

P_a is the amount of winter accumulation plus summer precipitation (mma^{-1}) and T_3 is the 3-month average summer temperatures at the ELA. Ballantyne et al (2007) used this relationship to model glacial re-advance during the LLS for the Outer Hebrides of Scotland. Ballantyne et al (2007) highlights that this relationship can be used to calculate palaeo-precipitation levels if summer temperatures can be found. They used the palaeotemperatures inferred from Whitrig Bog, in south-east Scotland, reconstruct precipitation levels during the LLS for the Outer Hebrides. They extrapolated the chironomid inferred temperatures, from Whitrig Bog to the Outer Hebrides, using a latitude temperature gradient of 0.42˚C (100km^{-1}) which recorded the coldest phase of the LLS to be 7.2˚C. They calculated the T_3 to be 0.97 based on modern day meteorological datasets from Scotland and Scandinavia. The equation below is then used to calculate the T_3 at the Equilibrium Line Altitude 2 for the North Harris.

$$(2)\ T_3(ELA2) = \left[0.97\ Tj - \left(\Delta H\ x \frac{dt}{dH}\right)\right] - 1.11$$

The $T_3(ELA2)$ at the ELA2 considers glacial hypsometry, variable mass balance gradients and the ELA together (Benn and Gemmell., 1997). This has been shown to be a more reliable method than using a standard ELA. The ELA2 has a direct relationship with July summer temperatures (Tj) minus the difference in altitude, between Whitrig Bog and North Harris (ΔH), multiplied by the mean summer environmental lapse rate ($\frac{dt}{dH}$). Then subtracted by 1.11 which is the difference in summer temperatures between Whitrig Bog and the extrapolated temperatures in North Harris. Using the calculation above, combined with the chironomid inferred temperatures from Whitrig Bog they calculated the temperature at the Equilibrium Line Altitude ($T_3(ELA2)$) [Table.7].

Table 11. Assumed ELA(m), Lapse rate, T3(ELA)(˚C), winter accumulation (Pa)(mm) and the sea-level equivalent (P0) (mm) for North Harris, Outer Hebrides (Ballantyne et al., 2007)

Assumed ELA (m OD)	Lapse rate (°C m^{-1})	T_3 (ELA) (°C)	P_a (ELA) (mm)	P_0 (mm)
204	0.006	5.7	2625	2341
204	0.007	5.6	2585	2305
303	0.006	5.1	2389	1998
303	0.007	4.9	2319	1940
1971–1995 precipitation at Chliostair power station (45 m OD)				1933

At the time the Whitrig Bog record was the only C-IT record available. However, this project provides a closer reference which could be used to compare with glacier-inferred LLS palaeo-temperatures. Caithness is closer to the Outer Hebrides and has a high-resolution record of summer temperatures for the LLS. Based on the temperature record from Caithness, the coldest temperatures were closer to 5.3˚C, approximately 2˚C lower than Ballantyne et al (2007) extrapolated from Whitrig Bog. With temperatures being 2˚C lower than previously thought the amount of ice may actually be more during this time. As Caithness is located on the same latitude as North Harris no inferred temperature gradient is necessary. Therefore, the equation can be simplified:

$$(3)\ T_3(ELA2) = \left[0.97\ Tj - \left(\Delta H\ x \frac{dt}{dH}\right)\right]$$

The altitude of the Shebster basin (∆H) is 14m a.s.l, the ELA2 remains the same, at 303m (calculated by Ballantyne et al (2007)) and $\frac{dt}{dH}$, the mean environmental lapse rate also remains the same at 0.006 (Ballantyne, 2002). Using the updated variables and equation below the following was calculated:

$$T_3(ELA2) = [0.97\ x\ 5.3 - (289\ x\ 0.006)]$$

$$\boldsymbol{T_3 = 3.4^{\circ}}$$

$$P_a = 645 + 296T_3 + 9T_3^2$$

$$P_a = 645 + (296\ x\ 3.41) + (9\ x\ 3.41)^2$$

$$P_a = 645 + 1009.36 + 941.88$$

$$\boldsymbol{Pa = 2596.2mm}$$

The temperatures at the ELA2 have now been inferred to be 3.4˚C instead of 5.1˚C. Furthermore, the winter precipitation levels increase from 2389 mm to 2596 mm with the addition of the Caithness data. With an increase of 207 mm this highlights that precipitation levels during the LLS were greater than originally inferred by Ballantyne et al (2007). This shows the importance of using local chironomid inferred temperature records for glacial reconstructions and the limitation of using a latitudinal temperature gradient to infer atmospheric temperatures.

The same studies have been applied to the Loch Lomond Stadial using the temperatures inferred from Whitrig Bog (Brooks et al., 2000). Golledge et al (2010) proposes the use of the following equation to calculate the precipitation levels during the LLS:

$$(4)\ P = S(14.2T_a^2 + 248.2T_a + 213.5)$$

P is the effective precipitation, and *Ta* is the mean temperature during the season of ablation whilst *S* is the seasonality factor (S= 1.4 for summer, S=1 for neutral and S=0.8 for winter dominated ablation season). Ballantyne (2002) suggested that the temperatures in Whitrig Bog were not suggestive of a maritime climate so they were transformed into a sea surface temperature equivalents which increased the mean July summer temperatures by 3.5˚C. However, as Caithness is in close proximity to the North Atlantic it will therefore more closely resemble a maritime climate system. Although there are closer sites to the main LLS ice mass, these records are not dominated by a maritime climate system e.g. (Abernethy Forest is located in the heart of the Cairngorms (Brooks et al., 2012)). Also, Loch Ashik records cooling into the latter stages of the LLS as the chironomids are responding to microclimate cooling from the Skye ice cap (Brooks et al., 2012). Other sites in the British Isles record warming at the latter stage of the LLS. Therefore, it would be more appropriate to use the C-IT record from Caithness as it is controlled by a maritime system and is not influenced by a local ice-cap microclimate. This research suggests that the transformation into a sea temperature equivalent is not necessary. Therefore, that stage can be ignored and equation 4 from Golledge et al (2010) can be altered to equation (5). $T_{C\text{-}IT}$ is the mean July summer temperature record from Caithness.

$$(5)\ P = S(14.2T_{C-IT}^2 + 248.2T_{C-IT} + 213.5)$$

$$P = S(14.2T_{C-IT}^2 + 248.2T_{C-IT} + 213.5)$$

$$P = 1.4(14.2x5.3_{C-IT}^2 + 248.2x5.3_{C-IT} + 213.5)$$

$$P = \textbf{1926.3 mm a}^{\textbf{-1}}$$

The chironomid-inferred temperatures from Caithness and the relationship from Golledge et al (2010) were used instead of the C-IT record from Whitrig Bog, or the sea-level equivalents. A new precipitation value of 1926.3 mma^{-1} is now recorded for the LLS. If the Ohmura et al (1992) relationship is used instead the value is 2412.0 mma^{-1}.

$$(1)\quad P_a = 645 + 296T_{C-IT} + 9T_{C-IT}^2$$

$$P_a = 645 + (296\ x\ (0.97x5.3)) + (9\ x\ (0.97\ x\ 5.3^2))$$

$$P_a = 645 + (296\ x\ 5.14) + (9\ x\ 5.14)^2$$

$$P_a = 645 + 1521.74 + 245.23$$

$$P_a = \textbf{2412.0}\ \boldsymbol{mm}\ \textbf{a}^{\textbf{-1}}$$

It is therefore clear from the calculations that it is necessary to use local mean July summer temperature records, that are controlled by similar processes to the site in question, to more reliably reflect palaeo-glacial and palaeo-precipitation models. Present day annual precipitation for Tulloch Bridge (56.867N, -4.708W) in the Highlands is 1809mma^{-1} (Met Office, accessed April 2020). Therefore, this suggests that during the LLS there was more precipitation throughout the year compared to modern day

Chapter 10 – **Conclusion & Future Work**

High-resolution chironomid inferred mean July summer temperature records have been reconstructed for Caithness, Orkney and Shetland. This research is the first to do so for the region. Furthermore, it is the first to use long chain alkenones to infer spring lake temperatures for the Last Glacial – Interglacial Transition, in Scotland. A multi-proxy approach, combining chironomid assemblages, alkenones, micro-*XRF*, LOI, tephrochronology and AMS radiocarbon dating, has been used to better understand how the lake ecosystems changed during this time. These methods were employed to answer the following aims and objectives highlighted below:

(1) Reconstruct the palaeoclimate history of the Northern Isles of Scotland and Caithness during the LGIT. This was done through the use of high resolution chironomid assemblage records, and a Norwegian based transfer function, to infer mean July summer temperatures for the region.

(2) Assess the nature, magnitude and timing, of the cold and warm phases of the LGIT, to assess if climate changes were synchronous across the Northern Isles, Scotland and Greenland. In order to achieve this a high-resolution robust chronology for each site was built, using AMS radiocarbon dating and tephrochronology, to constrain the timings of the warm and cold events during this transition period. The high-resolution record from Loch of Sabiston (Orkney) was compared to the Greenland ice core record (NGRIP) (Rasmussen et al., 2014), and Loch Ashik and Abernethy Forest (Brooks et al., 2012) to model the levels of synchronicity between sites during phases of low error age-depth model reconstructions.

(3) Thirdly, this research aimed to understand how temperatures changed seasonally during the LGIT for Caithness. This was done by reconstructing the first long chain alkenone, spring lake temperature record for Scotland. By comparing the LCA record with the C-IT record it has now been possible to assess how the magnitude of atmospheric temperature change varied seasonally throughout the LGIT.

(4) Fourthly, this research aimed to assess how the nature and magnitude of summer temperatures varied spatially across Scotland during the LGIT, and to determine what the main climate forces were during this time. This was achieved by combining the chironomid inferred temperature records from the British Isles and Ireland with the three records from this project. Palaeo-isotherms were plotted to spatially assess the gradient and trends of temperature change across the region. Using the C-IT records it was possible to assess the relationship of temperature change with ice mass extent during the Loch Lomond Stadial.

10.1 Key findings

The key findings from this research are highlighted in this sub-section. Each heading corresponds to one of the four research aims set out at the onset of this study. They answer the main aims, and complete the intended objectives laid out in chapter 4.

10.1.1 Palaeoclimate history of the Northern Isles of Scotland and Caithness

The palaeoclimate history of the Northern Isles and Caithness has been reconstructed for the Last Glacial - Interglacial Transition. Novel, high-resolution, chironomid inferred mean July temperature reconstructions have been recorded for the LGIT. Combined with the first long chain alkenone spring lake temperature record for Scotland. Combining both proxies have provided an in-depth look at the complex palaeoclimate history of the region for the LGIT.

Shetland is the only site in this research which records warming into the interstadial at the end of GS-2. Mean July summer temperatures rise from a low of 5.5˚C to 10˚C by c.15.88k cal BP. However, there were two short-lived cooling events at c.15.6k cal BP and c15.3k cal BP where temperatures fell from 9˚ to 7.4˚C and 10.7˚C to 9˚C in Shetland before the onset of GI-1e. Highlighting that the warming into the interstadial was not rapid in this region. The C-IT from Caithness and Orkney begins at c.14.7k cal BP and c.14.1k cal BP respectively. This warming is thought to be synchronous with the GI-1e warm phase in Greenland (Rasmussen et al., 2014). Temperatures reach 12˚C in Caithness and 10.5˚C in Orkney during this time. This highlights that sedimentation began earlier in Shetland than in Caithness and Orkney. This affirms the work of Bradwell et al (2019) who records an early onset of

deglaciation at c.15-16k cal BP for mainland Shetland. The only other chironomid sites which record warming into the interstadial are from Whitrig Bog (Brooks et al., 2000); Lough of Nadourcan (Watson et al., 2010) and Fidduan (van Asch et al., 2012).

Abrupt cooling occurred in Caithness and Orkney at c.14.7k cal BP and c.14.1k cal BP respectively. This event is thought to be synchronous with GI-1d in Greenland (Rasmussen et al., 2014). Temperatures sharply fell from 11˚C to 6.8˚C in Caithness and in Orkney, temperatures fell from 11˚C to 6.5˚C. Furthermore, the LCA record from Caithness indicates that spring lake temperatures fell to a low of 8.7˚C by c.14.02k cal BP, highlighting that there was abrupt environmental and climate change during this time frame. The onset of GI-1d is more abrupt in Caithness and Orkney compared to Shetland. Temperatures gradually fall from the middle of GI-1e to the middle of GI-d.

Abrupt climate warming occurred in Caithness and Orkney at c.13.9k cal BP. Temperatures rose to 10.6˚C and 10.7˚C respectively. In Shetland, temperatures rose to 8.9˚C by c.14.2k cal BP. This warm phase is believed to be synchronous with GI-1c in Greenland (Rasmussen et al., 2014). The transition from cold to warmer climates is less abrupt in Shetland taking approximately 400 years in total. This warm phase has three distinct, yet subtle, sub-divisions recorded in Caithness and Orkney during this time. The same divisions have been recorded in Greenland (Rasmussen et al., 2014). This event was split into three distinct phases:

1. GI-1c (1) (c.13.9k cal BP). In Caithness temperatures were 11.3˚C and in Orkney temperatures were 10.7˚C. The LCA records lake temperatures of 14˚C during GI-1c (1).
2. GI-1c (2) (c.13.7k cal BP). During this subtle cold phase temperatures fall to 8.1˚C in Caithness and 7.9˚C in Orkney. The LCA records a drop to 13˚C during GI-1c (2).
3. GI-1c (3) (c.13.4k cal BP). Temperatures begin to rise again to 10.4˚C in Caithness and 9.5˚C in Orkney. The LCA record from Shebster also records warming to 15˚C.

Abrupt climate cooling occurs in Caithness and Orkney at c. 13.0k cal BP. Mean July summer temperatures fall to a low of 6.6˚C in both regions. This abrupt cold phase occurs in Shetland, at c.13.8k cal BP, approximately 800 years earlier than in the other sites. Temperatures fell to 6.11˚C during this cold phase in Shetland. The LCA record

from Caithness indicates an abrupt drop in spring lake temperatures to a low of 8˚C. This cold phase has been linked to GI-1b in Greenland (Rasmussen et al., 2014).

Abrupt warming occurred at c.12.9k cal BP in Caithness and Orkney. Temperatures rise to a high of 9.5˚C in Caithness and 11.5˚C in Orkney. In Shetland temperatures rose 13.5˚C by c.13.2k cal BP. This event The LCA record from Caithness indicates that spring lake temperatures rose to 14.8˚C by c.12.6k cal BP.

Mean July summer temperatures fell abruptly in all three sites at the onset of the LLS/GS-1. Temperatures fell markedly to c.6˚C in Caithness (c.12.6k cal BP), Orkney (c.12.6k cal BP) and Shetland (c.13.2k cal BP). There is evidence that the two-phased LLS/YD event proposed by Lane et al (2013) and Lowe et al (2019) was also recorded in the Northern Isles and Caithness. This event is split into two phases in Orkney and Caithness temperatures fell to a low of 6-7˚C during the first stage and later fell to 4.5˚C during the second stage. The opposite has been shown to be the case in Shetland. The latter stages of the LLS were warmer than the onset. Temperatures rose from a low of 5˚C to 7˚C in Shetland during this time.

Mean July summer temperatures abrupt rise at the onset of the Holocene onset. This time is marked by a sharp rise in atmospheric temperatures by 5˚C in Caithness (c.11.9k cal BP), 7˚C in Orkney (c.11.9k cal BP) and 5˚C in Shetland (c.11.4k cal BP). In Orkney two previously unidentified cold reversals, at 11.0k cal BP and 10.2k cal BP, have been recorded [Fig.]. The transition is most abrupt in Orkney with temperatures rising by 7˚C within 50 years. Whereas, in Shetland it takes 600 years for temperatures to reach the same temperatures as Orkney. This suggests that the termination of LLS may have been less abrupt in Shetland than the rest of the British Isles.

10.1.2 **Was climate synchronous during the LGIT across the North Atlantic?**

This is the first research to attempt to model synchronicity between Scotland and Greenland during the LGIT. The core from Loch of Sabiston (Orkney) had the highest most robust chronology out of the three sites. This site had four identified tephra tie-points and a robust AMS chronology. Therefore, this allowed age-depth modelling calculations to be performed to assess the level of synchronicity between other sites with the same tephra constraints. As previously stated, it is realistically only possible to reconstruct synchronicity between sites Loch of Sabiston (Orkney) was compared

to the sites from Brooks et al (2012) (Abernethy Forest and Loch Ashik in the Scottish Highlands and Isle of Skye). Using OxCal the following results were found:

Based on the age-depth model and age-difference calculations, there is a 98% (2 sigma) confidence that the cold phase (GI-1d) in Orkney was synchronous with the NGRIP record, Loch Ashik and Abernethy Forest (Brooks et al., 2012; Rasmussen et al., 2014). Furthermore, there is a 98% (2 sigma) confidence interval that the warm phase GI-1c in Orkney was synchronous with the NGRIP record, Abernethy Forest and Loch Ashik. There is a 68% confidence interval that there was a-synchronous climate change between Greenland and Orkney during the cold phases (GI-1b and GI-1d). The results indicate that Greenland led Orkney during these abrupt cold phases. Based on the age-depth model age-difference calculations there is a 98% (2 sigma) confidence interval that the warm phase (GI-1a) in Loch of Sabiston was synchronous with the NGRIP record, Abernethy Forest and Loch Ashik. There is a 68% confidence interval that Orkney leads Abernethy Forest at the onset of the LLS. There is a 98% confidence, that in Orkney, the onset of the Holocene period was synchronous between all of the 4 sites.

This research has provided evidence of a mid-LLS transition, previously recorded by Lane et al (2013) in Meer Feld Maar in Germany and Kråkenes in Norway. By combining the research from Caithness with these two sites, this transition has been shown to have first occurred at lower latitudes, in Meer Feld Maar (50˚N) at c.12.25k cal BP and then transitioned northwards, reaching Caithness by c.12.2k cal BP and later reaching Kråkenes by c.12.10k cal BP. This research has provided a mid-point tracking the movement of the north polar front northwards during the middle of the LLS/YD cold phase. This highlights that climate likely changed asynchronously between the Northern Isles and N.W Europe at the onset of the LLS.

10.1.3 **What were the seasonal variations in climate during the LGIT?**

This is the first study to directly compare the use of chironomid head capsules with long-chain Alkenones for the British Isles. Chironomids provide a mean July summer temperature record whilst alkenones provide a spring lake temperature record. This research aimed to assess seasonal variations in temperature change throughout the LGIT for Caithness.

Throughout the LGIT, the overall trend in temperatures is strikingly similar. This correlation between both records suggests that LCAs can be effective proxies for lake

temperature modelling in lacustrine environments (Toney et al., 2010). Whilst, the long chain alkenone record is in agreement with the chironomid record for the onset of the cold events it is apparent that there is a significant offset between the onset of warming between the two proxies. See below the main findings for each of the cold and warm phases spanning the LGIT.

During the onset of GI-e (c.14.2k cal BP) summer temperatures range between 12-12.5˚C. However, the LCA record shows that spring lake temperatures were significantly lower, reaching 3.8˚C. This research suggests that the LCA record is recording spring meltwater temperatures and not spring atmospheric temperatures.

There was abrupt cooling in the spring and summer during GI-1d. Between c.14.1-13.9k cal BP mean July summer temperatures fall markedly from a high of 11.8˚C to a low of 6.9˚C. There is an agreement with the spring lake temperatures during this cold phase as temperatures fell to 8.7˚C.

Abrupt warming occurred between c.13.9k cal BP and c.12.9k cal BP temperatures ranged between 8-11˚C. This event is split into three subtle distinct climatic phases. The LCA temperature record indicates that temperatures ranged between 14-15˚C. Both records indicate that the climate warmed during this time in the summer and spring. However, the temperatures in the spring appear larger than the summer. This research concludes that this is due to the lack of an independent lake calibration for the site. By using the calibrations from Norway and Alaska there will likely be inconsistencies in the temperature reconstructions as they assume that environmental conditions are the same to studied site. However, it does highlight that temperatures rose during this time. The LCA record also records the subtle three phases during GI-1c. Highlighting, that LCA temperature records are highly sensitive to environmental and climate change.

During the abrupt cool phase GI-1b, summer temperatures fell to a low of 6.6˚C between c.12.9-12.8k cal BP. The LCA records a drop-in spring temperature to 8˚C. This further suggests that during the cold phases of the LGIT the summer and spring temperatures are in agreement with one another. This also suggests that during this cold phase that temperatures were similar all year round leading to a lack of seasonality. There was abrupt warming into GI-1a (c.12.8-12.6k cal BP). Summer temperatures rose to a high of 9-9.5˚C during this warm phase. Spring temperatures also rose however the LCA record indicates higher temperatures ranging between 14-15˚C. Again, with an independent lake calibration this offset could be accounted for.

During the Loch Lomond Stadial there was a reduction in mean July summer temperatures, between c.12.6-11.9k cal BP, to a low of 6˚C. The LCA record also indicates a drop-in spring temperature to a low of 3.5-5˚C. There is a hiatus in the LCA record at the onset of the LLS. Mid-way though the LLS the LCA record restarts further suggesting that there were two stages during this cold phase. It is apparent that the LCA producing haptophytes were not present in the lake during the onset of the Loch Lomond Stadial indicating that significant environmental change occurred in the second phase of the LLS to support the growth of algae in the lake system. During this cold phase temperatures are significantly lower throughout the whole year. Again, during this cold phase there is a lack of seasonal variation between the summer and spring months. This research has shown that there was intense climate cooling during the LLS in Caithness all year round.

At the onset of the Holocene period there was a sharp transition to warmer climates (c.11.9k cal BP). Mean July summer temperatures rise from a low of 5.3˚C to 10.8˚C. The LCAs also show an abrupt rise in spring lake surface temperature from 2˚ to 12˚C. This research has shown that throughout the LGIT, long chain alkenones can be used effectively to reconstruct periods of warming and cooling, with the greatest reliability found during periods of climate cooling.

10.1.4 **The spatial extent and magnitude of climate changes during the LGIT, and their associated drivers**

This research has shown that throughout the LGIT the spatial distribution of mean July summer temperature change varied across the Northern Isles and mainland Scotland. and confirms that there was a significant temperature gradient shift between the warm and cold phases of the LGIT. Using palaeo-isotherms a better understanding of the main climate drivers has also been made possible. Below are the main findings for each of the warm and cold phases of the LGIT.

During GI-1e the chironomid inferred mean July summer isotherms highlight that there was a strong SW-NE gradient across Scotland. This research suggests that the THC was a major control of the spatial distribution of temperatures during this time. This is affirmed by McManus et al (2004) who attributes the onset of GI-1 to a is reignition of the AMOC at c.14.7k BP (McManus et al., 2004). This led to the retreat of the Fennoscandinavian Ice Sheet (FIS) and the British Ice Sheet (BIS) (Bradwell et al., 2019).

During the abrupt cold phase GI-1d is a strong N-S gradient and a clear shift in the spatial extent of climate cooling. Furthermore, this research has shown that during this time, in Northern Isles of Scotland and Caithness, the minimum temperatures recorded are the same. Moreover, this study shows that there is a slight SW-NE deviation in Northern Isles. This study proposes that the Northern Isles are being influenced by the close position of the Fennoscandinavian ice sheet during this time. This affirms the work of Brooks and Langdon (2014) who links the strong N-S gradient on mainland Europe to the position of the FIS. This study suggests the position of the NPF was the major control at the time for temperatures across N.W Europe, with the FIS playing a role locally.

During the warm phase G1-1c the temperature trend returns to a strong NE-SW gradient across Scotland. This research attributes this to the position and influence of the THC. The chironomid inferred palaeo-isotherms for the onset of GI-1b indicates that there is a return to a strong N-S gradient. Similar to the cold phase GI-1d, there is an apparent NE-SW deviation in the trend of cooling in the Northern Isles and Caithness. This indicates that this region was also controlled by the position of the FIS again. This research suggests that this cold phase was majorly controlled by a southward transgression of the NPF bringing cold air from the arctic.

During GI-1a the chironomid inferred temperatures indicates that there was a return of a strong NE-SW trend across Scotland. This is similar to the previous warm phases GI-1e and GI-1c. The position and influence of the THC has been attributed to the warming and was likely the same forcing mechanism triggering the onset of the previous warm phases, GI-1e and GI-1c.

During the LLS/GS-1 there is a clear N-S gradient in mean July summer temperatures. Again, the NPF was the main control of temperature change across Scotland during this time. There is a return to a NE-SW diversion in the temperature gradient of the Northern Isles suggesting that the FIS was a major control of summer temperature change. At the onset of the Holocene period there is a strong NE-SW gradient across Scotland. This has been explained by a reignition and reorganisation of the AMOC in the North Atlantic (Risebrobakken et al., 2011). This research suggests that the THC was the most dominant control of temperature change in Scotland during this time.

10.2. **Future Work**

Based on the research conducted for this PhD, apparent gaps in knowledge have become clear. See below the work required in the future to better understand the palaeoclimate and environmental history of the Northern Isles of Scotland and Caithness:

- An independent chronology for the Shebster basin is required to better constrain the palaeoclimate and environmental changes that occurred during the LGIT. Eleven AMS dates have been awarded by the NERC Radiocarbon Steering Committee (2019-20) and will be, with the aim to be submitted by the summer of 2020. These dates will be used for future publication. Furthermore, samples will be sub-sampled in order to find potential tephra layers for the Shebster basin. In the future, tephrochronolgies could be used to better constrain the timing of events on Shetland during the LGIT.
- An independent lake calibration should be built for the Shebster basin to overcome the need to use an LCA calibration from Norway and Alaska (D'Andrea et al., 2016; Longo et al., 2018). Furthermore, more LCA temperature reconstructions should be developed for the British Isles.
- When the long chain alkenones were analysed the N1, N3 and N4 algal fractions were collected. There are numerous biomarkers, such as N-alkanes, GDGTs and Long-chain Diols found in these archived fractions. As a result, they can be analysed at a later stage. The long-chain diols and glycerol dialkyl glycerol tetraethers (GDGTs) are able to reconstruct lake temperature records (Schouten et al., 2002). Whilst, the N-alkanes are able to reconstruct palaeo-precipitation levels (Toney pers comm).
- Brooks and Langdon (2014) state that there is a lack of chironomid inferred temperature records for the North Atlantic region. In the future, there should be a particular focus on the Faroe Islands, Iceland and Greenland. However, due to low species diversity in the regions there should be attempts to make a training set for the region. This will allow one to better understand the synchronicity of climate changes across the North Atlantic during the LGIT.

References

Abrook A.M , Matthews I.P , Milner A.M , Candy I , Palmer A.P , Timms R.G.O (2019) Environmental variability in response to abrupt climatic change during the Last Glacial-Interglacial Transition (16-8 cal. ka BP): evidence from Mainland, Orkney. Scottish Journal of Geology

Andersen, T., Sæther, O.A., Cranston, P.S. and Epler, J.H., 2013. The larvae of Orthocladiinae (Diptera: Chironomidae) of the Holarctic region-Keys and diagnoses. The larvae of Chironomidae (Diptera) of the Holarctic Region-Keys and diagnoses. Insect Systematics and Evolution Supplement, Lund, pp.189-386.

Andresen, C.S.A., 2000. What do Δ14C changes across the Gerzensee oscillation/GI-1b event imply for deglacial oscillations? Journal of Quaternary Science 15, 203–214. doi:10.1002/(SICI)1099-1417(200003)15:3<203:AID-JQS514>3.0.CO;2-8

Atkinson, T.C., Lawson, T.J., Smart, P.L., Harmon, R.S. and Hess, J.W., 1986. New data on speleothem deposition and palaeoclimate in Britain over the last forty thousand years. Journal of Quaternary Science, 1(1), pp.67-72.

Alley, R.B., Meese, D.A., Shuman, C.A., Gow, A.J., Taylor, K.C., Grootes, P.M., White, J.W.C., Ram, M., Waddington, E.D., Mayewski, P.A., Zielinski, G.A., 1993. Abrupt increase in snow accumulation at the end of the Younger Dryas event. Nature 362, 527}529.

Alley R.B (2000) The Younger Dryas cold interval as viewed from central Greenland Quaternary Science Reviews 19 (2000) 213}226

Álvarez-Solas, J., Montoya, M., Ritz, C., Ramstein, G., Charbit, S., Dumas, C., Nisanciogl, K., Dokken, T. and Ganopolski, A., 2011. Heinrich event 1: an example of dynamical ice-sheet reaction to oceanic changes.

ARCA (2014) The department of Archaeology, University of Winchester, Institute for Archaeology.

Ascough, P., Cook, G.T., Church, M.J., Dunbar, E., Einarsson, Á., McGovern, T.H., Dugmore, A.J., Perdikaris, S., Hastie, H., Friðriksson, A. and Gestsdóttir, H., 2010. Temporal and spatial variations in freshwater 14 C reservoir effects: Lake Mývatn, northern Iceland. Radiocarbon, 52(3), pp.1098-1112.

Ashe, P., 1983. A catalogue of chironomid genera and subgenera of the world including synonyms (Diptera: Chironomidae). Entomologica scandinavica. Supplementum, (17).

Atkinson, T.C., Briffa, K.R. and Coope, G.R., 1987 “Seasonal temperatures in Britain during the past 22,000 years reconstructed using beetle remains.” Nature 325, 587-592

Aufgebauer A, Panagiatopoulos K, Wagner B, Schaebitz F, Viehberg FA, Vogel H, Zanchetta G, Sulpizio R, Leng MJ, Damaschke M (2012) Climate and environmental change over the last 17 ka recorded in sediments from Lake Prespa (Albania/F.Y.R. of Macedonia/Greece). Quat Int 274:122–135. doi:10.1016/jquaint.2012.02.015

Ballantyne, C.K., 1989. The Loch Lomond Readvance on the Isle of Skye, Scotland: glacier reconstruction and palaeoclimatic implications. Journal of Quaternary Science, 4(2), pp.95-108.

Ballantyne, C.K., 2002. The Loch Lomond Readvance on the Isle of Mull, Scotland: glacier reconstruction and palaeoclimatic implications. Journal of Quaternary Science 17, 759–771.

Ballantyne, C.K., Hall, A.M., Phillips, W., Binnie, S., Kubik, P.W., 2007. Age and significance of former low-altitude corrie glaciers on Hoy, Orkney Islands. Scottish Journal of Geology, in press

Ballantyne, C.K., 2007. Loch Lomond Stadial glaciers in North Harris, Outer Hebrides, North-West Scotland: glacier reconstruction and palaeoclimatic implications. Quaternary Science Reviews, 26(25-28), pp.3134-3149.

Ballantyne, C.K. and Stone, J.O., 2012. Did large ice caps persist on low ground in north-west Scotland during the Lateglacial Interstade?. Journal of Quaternary Science, 27(3), pp.297-306.

Balascio, N.L., Zhang, Z., Bradley, R.S., Perren, B., Dahl, S.O. and Bakke, J., 2011. A multi-proxy approach to assessing isolation basin stratigraphy from the Lofoten Islands, Norway. Quaternary Research, 75(1), pp.288-300.

Bakke, J., Lie, Ø., Heegaard, E., Dokken, T., Haug, G.H., Birks, H.H., Dulski, P. and Nilsen, T., 2009. Rapid oceanic and atmospheric changes during the Younger Dryas cold period. Nature Geoscience, 2(3), pp.202-205.

Becker LWM, Sejrup HP, Hjelstuen BO, et al. 2018. Ocean–ice sheet interaction along the SE Nordic Seas margin from 35 to 15 ka BP. Marine Geology 402: 99–117, https://doi.org/10.1016/j.margeo. 2017.09.003

Bedford, A., Jones, R.T., Lang, B., Brooks, S. and Marshall, J.D., 2004. A Late-glacial chironomid record from Hawes Water, northwest England. Journal of Quaternary Science, 19(3), pp.281-290.

Bennett, K.D., Boreham, S., Sharp, M.J. and Switsur, V.R., 1992. Holocene history of environment, vegetation and human settlement on Catta Ness, Lunnasting, Shetland. Journal of Ecology, pp.241-273.

Bennett, K.D., Bunting, M.J. and Fossitt, J.A., 1997. Long-term vegetation change in the Western and Northern Isles, Scotland. Botanical Journal of Scotland, 49(2), pp.127-140.

Benn, D.I., Gemmell, A.M.D., 1997. Calculating equilibrium line altitudes of former glaciers: a new computer spreadsheet. Glacial Geology and Geomorphology. /http://ggg.qub.ac.uk/ggg/paper/full1997/tn011997/ tn0.1.htmS.
Benn,

Benn, D.I. and Ballantyne, C.K., 2005. Palaeoclimatic reconstruction from Loch Lomond readvance glaciers in the west Drumochter Hills, Scotland. Journal of Quaternary Science: Published for the Quaternary Research Association, 20(6), pp.577-592.

Berg, H. B., 1995, Larval food and feeding behaviour, pp. 136-168. In: P. D. Armitage, P. S. Cranston & L. C. V. Pinder (eds.), The Chironomidae: biology and ecology of non-biting midges. Chapman & Hall, London, 584p.

Berner, K.S., Koc, N., Godtliebsen, F., Divine, D., 2011. Holocene climate variability of the Norwegian Atlantic Current during high and low solar insolation forcing. Paleoceanography 26, PA2220. http://dx.doi.org/10.1029/2010PA002002.

Berry, R.J., 2000. Orkney nature. T & AD Poyser.

Bianchi, C. and Gersonde, R., 2004. Climate evolution at the last deglaciation: the role of the Southern Ocean. Earth and Planetary Science Letters, 228(3-4), pp.407-424.

Birse EL. 1974. Bioclimatic characteristics of Shetland. In: Goodier R, ed. The natural environment of Shetland. Edinburgh ; Nature Conservancy Council, 24—33.

Bilyj, B. and Davies, I.J., 1989. Descriptions and ecological notes on seven new species of Cladotanytarsus (Chironomidae: Diptera) collected from an experimentally acidified lake. Canadian Journal of Zoology, 67(4), pp.948-962.

Birks, H.J. and Ransom, M.E., 1969. An interglacial peat at Fugla Ness, Shetland. New Phytologist, 68(3), pp.777-796.

Birks, H.H. and Mathewes, R.W., 1978. Studies IN THE VEGETATIONAL HISTORY OF SCOTLAND: V. LATE DEVENSIAN AND EARLY FLANDRIAN POLLEN AND MACROFOSSIL STRATIGRAPHY AT ABERNETHY FOREST, INVERNESS-SHIRE. New Phytologist, 80(2), pp.455-484.

Birks, H.J. and Madsen, B.J., 1979. Flandrian vegetational history of Little Loch Roag, Isle of Lewis, Scotland. The Journal of Ecology, pp.825-842.

Birks, H.J. and Peglar, S.M., 1979. Interglacial pollen spectra from Sel Ayre, Shetland. New Phytologist, 83(2), pp.559-575.

Birks, H.H., 1984. Late-Quaternary pollen and plant macrofossil stratigraphy at Lochan An Druim, north-west Scotland. In:Haworth, E.Y., Lund, J.W.G. (Eds.), Lake Sediments and Environmental History. University of Leicester Press, Leicester,pp. 377–404

Birks, H.J.B., Juggins, S. and Line, J.M., 1990. Lake surface-water chemistry reconstructions from palaeolimnological data. The Surface Waters Acidification Programme. Cambridge University Press, Cambridge, pp.301-313.

Birks, H.H., 1994. Late-glacial vegetational ecotones and climatic patterns in Western Norway. Vegetation History and Archaeobotany, 3(2), pp.107-119.

Birks, H.J.B. 1998: Numerical tools in quantitative palaeolimnology–progress, potentials, and problems . Journal of Paleolimnology 20, 307–332

Birks, H.H., Birks, H.J.B., Mackay, A., Battarbee, R., Birks, J. and Oldfield, F., 2003. Reconstructing Holocene climates from pollen and plant macrofossils. Global change in the Holocene, pp.342-357.

Birks, Hilary H. "The importance of plant macrofossils in the reconstruction of Lateglacial vegetation and climate: examples from Scotland, western Norway, and Minnesota, USA." Quaternary Science Reviews 22.5-7 (2003(b): 453-473.

Birks, H.J.B., Heiri, O., Seppä, H. and Bjune, A.E., 2010. Strengths and weaknesses of quantitative climate reconstructions based on Late-Quaternary. The Open Ecology Journal, 3(1).

Birks, H.H., Aarnes, I., Bjune, A.E., Brooks, S.J., Bakke, J., Kühl, N. and Birks, H.J.B., 2014. Lateglacial and early-Holocene climate variability reconstructed from multi-proxy records on Andøya, northern Norway. Quaternary Science Reviews, 89, pp.108-122.

Birnie, J.F., 2000. Devensian Lateglacial palaeoecological changes in Shetland. Boreas, 29(3), pp.205-218s

Birse, E.L., 1971. Assessment of Climatic Conditions in Scotland: The Bioclimatic Subregions Map and Explanatory Pamphlet. Macaulay Institute for Soil Research..

Bishop, W.W. and Coope, G.R., 1977. Stratigraphical and faunal evidence for Lateglacial and early Flandrian environments in south-west Scotland. In Studies in the Scottish Lateglacial environment (pp. 61-88). Pergamon.

Bitušik, P. and Kubovcik, V., Sub-fossil chironomids (Dip- tera: Chironomidae) from the sediments of the Nižné Terianske pleso (High Tatra Mts., Slovakia), Dipterol. Bohemoslov., 1999, vol. 9, pp. 11–20.

Björck, S., Rundgren, M., Ingolfsson, O. and Funder, S., 1997. The Preboreal oscillation around the Nordic Seas: terrestrial and lacustrine responses. Journal of Quaternary Science: Published for the Quaternary Research Association, 12(6), pp.455-465.

Blaauw, M., Wohlfarth, B., Christen, J.A., Ampel, L., Veres, D., Hughen, K.A., Preusser, F. and Svensson, A., 2010. Were last glacial climate events simultaneous between Greenland and France? A quantitative comparison using non-tuned chronologies. Journal of Quaternary Science: Published for the Quaternary Research Association, 25(3), pp.387-394.

Blockley, S.P., Bourne, A.J., Brauer, A., Davies, S.M., Hardiman, M., Harding, P.R., Lane, C.S., MacLeod, A., Matthews, I.P., Pyne-O'Donnell, S.D. and Rasmussen, S.O., 2014. Tephrochronology and the extended intimate (integration of ice-core, marine and terrestrial records) event stratigraphy 8–128 ka b2k. Quaternary Science Reviews, 106, pp.88-100.

Boomer, I., von Grafenstein, U. and Moss, A., 2012. Lateglacial to early Holocene multiproxy record from Loch Assynt, NW Scotland. Proceedings of the Geologists' Association, 123(1), pp.109-116.

Bond, G., Broecker, W., Johnsen, S., McManus, J., Labeyrie, L., Jouzel, J. and Bonani, G., 1993. Correlations between climate records from North Atlantic sediments and Greenland ice. Nature, 365(6442), pp.143-147.

Bondevik, S. and Mangerud, J., 2002. A calendar age estimate of a very late Younger Dryas ice sheet maximum in western Norway. Quaternary Science Reviews, 21(14-15), pp.1661-1676

Bradley, S. L., Milne, G. A., Shennan, I. & Edwards, R. 2011. An improved glacial isostatic adjustment model for the British Isles. Journal of Quaternary Science 26, 541–52.

Bradwell T, Stoker MS, Golledge NR, et al. 2008. The northern sector of the last British Ice Sheet: maximum extent and demise. Earth- Science Reviews 88: 207–226, https://doi.org/10.1016/j.earscirev. 2008.01.008

Bradwell, T., Fabel, D., Stoker, M., Mathers, H., McHargue, L. and Howe, J., 2008. Ice caps existed throughout the Lateglacial Interstadial in northern Scotland. Journal of Quaternary Science: Published for the Quaternary Research Association, 23(5), pp.401-407.

Bradwell, T., Small, D., Fabel, D., Clark, C.D., Chiverrell, R.C., Saher, M.H., Dove, D., Callard, S.L., Burke, M.J., Moreton, S.G. and Medialdea, A., 2019. Pattern, style and timing of British–Irish Ice Sheet retreat: Shetland and northern North Sea sector. Journal of Quaternary Science.

Brassell, S.C., Eglinton, G., Marlowe, I.T., Pflaumann, U., Sarnthein, M., 1986. Molecular stratigraphy: a new tool for climatic assessment. Nature 320, 129–133.

Brauer, A., Gunter, C., Johnsen, S.J., Negendank, J.F.W., 2000. Land- ice teleconnections of cold climatic periods during the last Glacial/ Interglacial transition. Climate Dynamics 16, 229–239

Brauer, A., Haug, G.H., Dulski, P., Sigman, D.M. and Negendank, J.F., 2008. An abrupt wind shift in western Europe at the onset of the Younger Dryas cold period. Nature Geoscience, 1(8), pp.520-523.

Brodersen, K.P., Odgaard, B.V., Vestergaard, O. and Anderson, N.J., 2001. Chironomid stratigraphy in the shallow and eutrophic Lake Søbygaard, Denmark: chironomid–macrophyte co-occurrence. Freshwater Biology, 46(2), pp.253-267.

Brodin, Y.W., 1986. The postglacial history of Lake Flarken, southern Sweden, interpreted from subfossil insect remains. Internationale Revue der Gesamten Hydrobiologie und Hydrographie, 71(3), pp.371-432.

Brodin, Y.-W. 1990: Midge fauna development in acidified lakes in northern Europe. Philosophical Transactions of the Royal Society London (Series B) 327, 295–98.

Brodin, Y.W. and Gransberg, M., 1993. Responses of insects, especially Chironomidae (Diptera), and mites to 130 years of acidification in a Scottish lake. Hydrobiologia, 250(3), pp.201-212.

Broecker WS (1997) Thermohaline circulation, the Achilles Heel of our climate aystem: will man-made CO2 upset the current balance? Science 278:1582

Brooks, S. J., Lowe, J. J. & Mayle, F. E (1997). The Late Devensian Lateglacial palaeoenvironmental record from Whitrig Bog, SE Scotland

Brooks, S.J. and Birks, H.J.B., 2000. Chironomid-inferred Late-glacial air temperatures at Whitrig Bog, southeast Scotland. Journal of Quaternary Science: Published for the Quaternary Research Association, 15(8), pp.759-764.

Brooks, S.J. and Birks, H.J.B., 2001. Chironomid-inferred air temperatures from Lateglacial and Holocene sites in north-west Europe: progress and problems. Quaternary Science Reviews, 20(16-17), pp.1723-1741.

Brooks SJ, Langdon PG, Heiri O. 2007. The Identification and Use of Palaearctic Chironomidae Larvae in Palaeoecology. Quaternary Research Association Technical Guide no. 10: Cambridge.

Brooks SJ, Matthews IP, Birks HH et al. 2012b. High resolution Lateglacial and early-Holocene summer air temperature records from Scotland inferred from chironomid assemblages. Quaternary Science Reviews 41: 67–82.

Brooks, S.J. and Langdon, P.G., 2014. Summer temperature gradients in northwest Europe during the Lateglacial to early Holocene transition (15–8 ka BP) inferred from chironomid assemblages. Quaternary International, 341, pp.80-90.

Brooks, S. J., Davies, K. L., Mather, K. A., Matthews, I. P., & Lowe, J. J. (2016). Chironomid-inferred summer temperatures for the Last Glacial-Interglacial Transition from a lake sediment sequence in Muir Park Reservoir, west-central Scotland. Journal of Quaternary Science. https://doi.org/10.1002/jqs.2860

Brodersen, K.P. and Lindegaard, C., 1997. Significance of subfossile chironomid remains in classification of shallow lakes. In Shallow Lakes' 95 (pp. 125-132). Springer, Dordrecht.

Brodersen, K.P. and Lindegaard, C., 1999. Mass occurance and sporadic distribution of Corynocera ambigua Zetterstedt (Diptera, Chironomidae) in Danish lakes. Neo-and palaeolimnological records. Journal of Paleolimnology, 22(1), pp.41-52.

Brown, E.T., Johnson, T.C., Scholz, C.A., Cohen, A.S. and King, J.W., 2007. Abrupt change in tropical African climate linked to the bipolar seesaw over the past 55,000 years. Geophysical Research Letters, 34(20).

Brown E (2011) Lake Malawi's response to "megadrought" terminations: sedimentary records of flooding, weathering and erosion. Palaeogeogr Palaeoclimatol Palaeoecol 303:120–125. doi:10.1016/j.palaeo.2010.01.038

Brundin, L, 1949 Chironomiden und andere Bodentiere der südschwedischen Urbirgseen Ein Beitrag zug Kenntnis der bodenfaunistischen Charakterzüge schwedischer oligotropher Seen. Report of the Institute of Freshwater Research, Drottningholm 30: 1-914

Brundin, L., 1956. Zur Systematik der Orthocladiinae (Diptera, Chironomidae). Report of Institute of Freshwater Research, Drottningholm, 37, pp.5-185.

Buckley, M.W. and Marshall, J., 2016. Observations, inferences, and mechanisms of the Atlantic Meridional Overturning Circulation: A review. Reviews of Geophysics, 54(1), pp.5-63.

Buizert, C., Gkinis, V., Severinghaus, J. P., He, F., Lecavalier, B. S., Kindler, P., Leuenberger, M., Carlson, A. E., Vinther, B., Masson-Delmotte, V.,White, J. W. C. Liu, Z., Otto-Bliesner, B., Brook, E. J. (2014) 'Greenland temperature response to climate forcing during the last deglaciation. Science, v.345, pp.1177–80.

Bunting M.J (1994) Vegetation history of Orkney, Scotland; pollen records from two small basins in west Mainland. New Phytol. 128. 771-792

Bunting, M.J., 1996. The development of heathland in Orkney, Scotland: pollen records from Loch of Knitchen (Rousay) and Loch of Torness (Hoy). Holocene 6, 193e212.

Buskens, R.F.M., 1987. The chironomid assemblages in shallow lentic waters differing in acidity, buffering capacity and trophic level in the Netherlands. Entomologica Scandinavica, pp.217-224.

Cabedo-Sanz, P., Belt, S.T., Knies, J., Husum, K., 2012. Identification of contrasting seasonal sea ice conditions during the Younger Dryas. Quat. Sci. Rev.. Calvo,

Calvo, E., Grimalt, J., Jansen, E., 2002. High resolution Uk37 sea surface temperature reconstruction in the Norwegian Sea during the Holocene. Quat. Sci. Rev. 21, 1385e1394.

Campbell, J.M. and Clark, W.J., 1983. Effects of microhabitat heterogeneity on the spatial dispersion of small plant-associated invertebrates. Freshwater Invertebrate Biology, 2(4), pp.180-185.

Candy, I., Abrook, A., Elliott, F., Lincoln, P., Matthews, I. P. & Palmer, A. 2016. Oxygen isotopic evidence for high-magnitude, abrupt climatic events during the Lateglacial Interstadial in northwest Europe: analysis of a lacustrine sequence from the site of Tirinie, Scottish Highlands. Journal of Quaternary Science 31, 607–21.

Cacho, I., Grimalt, J.O., Pelejero, C., Canals, M., Sierro, F.J., Flores, J.A. and Shackleton, N., 1999. Dansgaard-Oeschger and Heinrich event imprints in Alboran Sea paleotemperatures. Paleoceanography, 14(6), pp.698-705.

Cao, Y., Zhang, E., Langdon, P.G., Liu, E. and Shen, J., 2014. Chironomid-inferred environmental change over the past 1400 years in the shallow, eutrophic Taibai Lake (south-east China): Separating impacts of climate and human activity. The Holocene, 24(5), pp.581-590.

Chafik ., L (2012) The response of the circulation in the Faroe-Shetland Channel to the North Atlantic Oscillation, Tellus A: Dynamic Meteorology and Oceanography, 64:1, DOI: 10.3402/tellusa.v64i0.18423

Chandler, B.M., Boston, C.M. and Lukas, S., 2019. A spatially-restricted Younger Dryas plateau icefield in the Gaick, Scotland: Reconstruction and palaeoclimatic implications. Quaternary Science Reviews, 211, pp.107-135.

Charman, D.J., West, S., Kelly, A. and Grattan, J., 1995. Environmental change and tephra deposition: the Strath of Kildonan, northern Scotland. Journal of Archaeological Science, 22(6), pp.799-809.

Chernovsky, A.A. 1949. Opredelitel' lichinok komarov semeistva Tendipedidae (Identification of larvae of the midge family Tendipedidae). - Opredeliteli po faune SSSR 31: 1-186.

Chiverrell, R.C. and Thomas, G.S., 2010. Extent and timing of the Last Glacial Maximum (LGM) in Britain and Ireland: a review. Journal of Quaternary Science: Published for the Quaternary Research Association, 25(4), pp.535-549.

Chu, G., Sun, Q., Li, S., Zheng, M., Jia, X., Lu, C., Liu, J., Liu, T., 2005. Long-chain alkenone distributions and temperature dependence in lacustrine surface sediments from China. Geochimica et Cosmochimica Acta 69, 4985–5003.

Clark, P.U., Marshall, S.J., Clarke, G.K.C., Hostetler, S.W., Licciardi, J.M., Teller, J.T., 2001.Freshwater forcing of abrupt climate change during the Last Glaciation. Science 293, 283–287.

Clark CD, Hughes ALC, Greenwood SL, et al. 2012. Pattern and timing of retreat of the last British–Irish Ice Sheet. Quaternary Science Reviews 44: 112–146, https://doi.org/10.1016/j.quascirev.2010. 07.019

Clark, R.M. and Renfrew, C., 1973. Tree-ring calibration of radiocarbon dates and the chronology of ancient Egypt. Nature, 243(5405), pp.266-270.

Cohen AS (2003) Paleolimnology: the history and evolution of lake systems. Oxford University Press, New York, p 528

Coolen, M., Muyzer, G., Rijpstra, W., Schouten, S., Volkman, J.K., Sinninghe Damsté, J.S., 2004. Combined DNA and lipid analyses of sediments reveal changes in Holocene haptophyte and diatom populations in an Antarctic lake. Earth and Planetary Science Letters 223, 225–239.

Coope GR (1977) Fossil Coleopteran assemblages as sensitive indicators of climatic changes during the Devensian (Last) cold stage. Philosophical Transactions of the Royal Society of London, Series B 280: 313–340.

Coope GR, Lemdahl G, Lowe JJ, and Walkling A (1998) Temperature gradients in northern Europe during the last glacial-Holocene transition (14–9 14Ckyr BP) interpreted from coleopteran assemblages. Journal of Quaternary Science13: 419–433.

Coope, G.R., Lemdahl, G., 1995. Regional differences in the Lateglacial climate of northern Europe based on coleopteran analysis. Journal of Quaternary Science 10, 391e395.

Coope, G.R. and Rose, J., 2008. Palaeotemperatures and palaeoenvironments during the Younger Dryas: arthropod evidence from Croftamie at the type area of the Loch Lomond Readvance, and significance for the timing of glacier expansion during the Lateglacial period in Scotland. Scottish Journal of Geology, 44(1), pp.43-49.

Cole, K.L. & Arundel, S.T. (2005) Carbon isotopes from fossil packrat pellets and elevational movements of Utah agave plants reveal Younger Dryas cold period in Grand Canyon, Arizona. Geology, 33, 713–716.

Corella J, Brauer A, Mangili C, Rull V, Vegas-Vilarrúbia T, Morellón M, Valero-Garcés B (2012) The 1.5-ka varved record of Lake Montcortès (southern Pyrenees, NE Spain). Quat Res 78:323–332. doi:10.1016/j.yqres.2012.06.002

Crampton, C.B. and Carruthers, R.G., 1914. The Geology of Caithness:(Sheets 110 and 116, with Parts of 109, 115, and 117.) (Vol. 110). HM Stationery Office.

Cranston, P.S., Tee, R.D., Credland, P.F. and Kay, A.B., 1983. Chironomid haemoglobins: Their detection and role in allergy to midges in the Sudan and elsewhere. Memoirs of the Entomological Society of America, 34, pp.71-87.

Cranston, P.S., 1995. Introduction to the Chironomidae. In: Armitage,P.D.,Cranston,P.S.,Pinder,L.C.V.(Eds.),TheChironomidae:TheBiologyandEcologyofNon-bitingMidges.Chapman&Hall,London,pp.1–7.

Cranston PS & Martin J. 1989. Family Chironomidae. In: Catalog of the Diptera of the Australasian and Oceanian Regions (ed. NL Evenhuis), pp. 252–274. Bishop Museum Press, Honolulu, USA and E.J. Brill, Leiden, Netherlands.

Cranston, P.S., 2013. The larvae of the Holarctic Chironomidae (Diptera: Chironomidae)—2. Morphological terminology and key to subfamilies. Chironomidae of the Holarctic Region: Keys and diagnoses. Part, 1, pp.13-24.

Cranwell, P.A., 1985. Long-chain unsaturated ketones in recent lacustrine sediments. Geochimica et Cosmochimica Acta 49, 1545–1551.

Croudace, I.W. and Rothwell, R.G. eds., 2015. Micro-XRF Studies of Sediment Cores: Applications of a non-destructive tool for the environmental sciences (Vol. 17). Springer.

Crucifix, M. and Loutre, F.M., 2002. Transient simulations over the last interglacial period (126–115 kyr BP): feedback and forcing analysis. Climate Dynamics, 19(5-6), pp.417-433.

Czymzik, M., Brauer, A., Dulski, P., Plessen, B., Naumann, R., von Grafenstein, U. and Scheffler, R., 2013. Orbital and solar forcing of shifts in Mid-to Late Holocene flood intensity from varved sediments of pre-alpine Lake Ammersee (southern Germany). Quaternary Science Reviews, 61, pp.96-110.

Dalton, C., Birks, H.J.B., Brooks, S.J., Cameron, N.G., Evershed, R.P., Peglar, S.M., Scott, J.A. and Thompson, R., 2005. A multi-proxy study of lake-development in response to catchment changes during the Holocene at Lochnagar, north-east Scotland. Palaeogeography, Palaeoclimatology, Palaeoecology, 221(3-4), pp.175-201.

D'Andrea, W.J., Lage, M., Martiny, J.B.H., Laatsch, A.D., Amaral-Zettler, L.A., Sogin, M.L., Huang, Y., 2006. Alkenone producers inferred from well-preserved 18S rDNA in Greenland lake sediments. Journal of Geophysical Research 111, G03013. http://dx.doi.org/10.1029/2005JG000121.

D'Andrea, W.J., Huang, Y., Fritz, S.C., Anderson, N.J., 2011. Abrupt Holocene climate change as an important factor for human migration in West Greenland. Proceedings of the National Academy of Sciences of the United States of America 108, 9765–9769.

D'Andrea, W.J., Theroux, S., Bradley, R.S. and Huang, X., 2016. Does phylogeny control U37K-temperature sensitivity? Implications for lacustrine alkenone paleothermometry. Geochimica et Cosmochimica Acta, 175, pp.168-180.

Dansgaard, W., Johnsen, S.J., Clausen, H.B., Dahl-Jensen, D., Gundestrup, N.S., Hammer, C.U., Hvidberg, C.S., Steffensen, J.P., Sveinbjörnsdottir, A.E., Jouzel, J. and Bond, G., 1993. Evidence for general instability of past climate from a 250-kyr ice-core record. Nature, 364(6434), pp.218-220.

Dawson A, Napier I, Davies N & McIlvenyJ (2010) A review of SOTEAG monitoring data and other long term environmental series from Shetland.

de Bar, M.W., Hopmans, E.C., Verweij, M., Dorhout, D.J., Damsté, J.S.S. and Schouten, S., 2017. Development and comparison of chromatographic methods for the analysis of long chain diols and alkenones in biological materials and sediment. Journal of Chromatography A, 1521, pp.150-160.

Delworth, T.L. and Zeng, F., 2012. Multicentennial variability of the Atlantic meridional overturning circulation and its climatic influence in a 4000 year simulation of the GFDL CM2. 1 climate model. Geophysical Research Letters, 39(13)

Delworth, T.L., Zeng, F., Vecchi, G.A., Yang, X., Zhang, L. and Zhang, R., 2016. The North Atlantic Oscillation as a driver of rapid climate change in the Northern Hemisphere. Nature Geoscience, 9(7), pp.509-512.

Denton, G. H., Alley, R. B., Comer, G. C., & Broecker, W. S. (2005). The role of seasonality in abrupt climate change. Quaternary Science Reviews. https://doi.org/10.1016/j.quascirev.2004.12.002

Denton, G.H., Anderson, R.F., Toggweiler, J.R., Edwards, R.L., Schaefer, J.M. and Putnam, A.E., 2010. The last glacial termination. science, 328(5986), pp.1652-1656.

Denniston R.F, Gonzalez L.A, Asmerom Y, Polyak V, Reagan M.K, Saltzman M.R (2001) A high-resolution speleothem record of climatic variability at the Allerød–Younger Dryas transition in Missouri, central United States, Palaeogeography, Palaeoclimatology, Palaeoecology,Volume 176, Issues 1–4,2001,147-155, ISSN 0031-0182,

Dokken, Trond; Andersson, Carin; Risebrobakken, Bjørg (2015): Relative abundance of planktic foraminifera and calculated SSTs and SST anomaly (0-25.5 ka BP) in sediment core MD99-2284. PANGAEA, https://doi.org/10.1594/PANGAEA.846924

Donner, J.J., 1958. XI.—The Geology and Vegetation of Late-glacial Retreat Stages in Scotland. Earth and Environmental Science Transactions of The Royal Society of Edinburgh, 63(2), pp.221-264.

Dunbar E, et al. 2016. AMS 14C Dating at the Scottish Universities Environmental Research Centre (SUERC) Radiocarbon Dating Laboratory 58(1):233.

Edwards KJ, WhittingtonG, Tipping RM. 2000. The incidence of microscopic charcoal in lateglacial deposits. Palaeogeography, Palaeoclimatology, Palaeoecology 164: 247–262.

Edwards, K.J., Whittington, G., 1997. A 12 000-year record of palaeoenvironmental change in the Lomond Hills, Fife, Scotland: vegetational and climatic variability. Veg. Hist. Archaeobot. 6, 133e152.

Eldevik, Tor; Risebrobakken, Bjørg; Bjune, Anne Elisabeth; Andersson, Carin; Birks, H John B; Dokken, Trond; Drange, Helge; Glessmer, Mirjam S; Li, Camille; Nilsen, Jan Even Ø; Otterå, Odd Helge; Richter, Kristin; Skagseth, Øystein (2014): A brief history of climate - the northern seas from the Last Glacial Maximum to global warming. Quaternary Science Reviews, 106, 225-246, https://doi.org/10.1016/j.quascirev.2014.06.028

Epler, J.H., Ekrem, T. and Cranston, P.S., 2013. The larvae of Chironominae (Diptera: Chironomidae) of the Holarctic region–keys and diagnoses. Chironomidae of the Holarctic region: Keys and diagnoses, Part, 1, pp.387-556.

Everest, J. and Kubik, P., 2006. The deglaciation of eastern Scotland: cosmogenic 10Be evidence for a Lateglacial stillstand. Journal of Quaternary Science: Published for the Quaternary Research Association, 21(1), pp.95-104.

Fabel, D., Ballantyne, C.K. and Xu, S., 2012. Trimlines, blockfields, mountain-top erratics and the vertical dimensions of the last British–Irish Ice Sheet in NW Scotland. Quaternary Science Reviews, 55, pp.91-102.

Ferreira, D., Cessi, P., Coxall, H.K., De Boer, A., Dijkstra, H.A., Drijfhout, S.S., Eldevik, T., Harnik, N., McManus, J.F., Marshall, D.P. and Nilsson, J., 2018. Atlantic-Pacific asymmetry in deep water formation. Annual Review of Earth and Planetary Sciences.

Fenton, A (1978). The Northern Isles: Orkney and Shetland. 1978.

Fiedel, S. J. (2011). The mysterious onset of the Younger Dryas. Quaternary International. https://doi.org/10.1016/j.quaint.2011.02.044

Finlay, T.M., Woodward, A.S. and White, E.I., 1926. XII.—The Old Red Sandstone of Shetland. Part I. South-Eastern Area. With an Account of The Fossil Fishes of the Old Red Sandstone of the Shetland Islands. Earth and Environmental Science Transactions of The Royal Society of Edinburgh, 54(3), pp.553-572.

Flinn D. 1964. Coastal and submarine features around the Shetland Islands. Proceeding of the Geologists Association 75: 321-329.

Ford, D.C., Smart, P.L. and Ewers, R.O., 1983. The physiography and speleogenesis of Castleguard Cave, Columbia Icefields, Alberta, Canada. Arctic and Alpine Research, 15(4), pp.437-450.

Francke, A., Wagner, B., Just, J., Leicher, N., Gromig, R., Baumgarten, H., Vogel, H., Lacey, J. H., Sadori, L., Wonik, T., Leng, M. J. et al (2016). Sedimentological processes and environmental variability at Lake Ohrid (Macedonia, Albania) between 637 ka and the present. Biogeosciences, 13 1179-1196.

Fritz, S.C. and Anderson, N.J., 2013. The relative influences of climate and catchment processes on Holocene lake development in glaciated regions. Journal of Paleolimnology, 49(3), pp.349-362.

Gajewski K (2008) Comment on ‘‘Abrupt environmental change in Canada’s northernmost lake inferred from fossil diatom and pigment stratigraphy’’ by Dermot Antoniades et al. GEOPHYSICAL RESEARCH LETTERS, VOL. 35, L08701, doi10.1029/2007GL032316, 2008

Gathorne-Hardy, F.J., Erlendsson, E., Langdon, P.G. and Edwards, K.J., 2009. Lake sediment evidence for late Holocene climate change and landscape erosion in western Iceland. Journal of Paleolimnology, 42(3), pp.413-426

Gilchrist, S.J.L., 2004. Late Quaternary palaeoclimatic reconstructions in Patagonia using chironomid analysis (Doctoral dissertation, University of Edinburgh).

Gilfedder, B.S., Petri, M., Wessels, M. and Biester, H., 2011. Bromine species fluxes from Lake Constance's catchment, and a preliminary lake mass balance. Geochimica et Cosmochimica Acta, 75(12), pp.3385-3401.

Godwin, H. and Willis, E.H., 1959. Radiocarbon dating of the Late-glacial period in Britain. Proceedings of the Royal Society of London. Series B-Biological Sciences, 150(939), pp.199-215.

Golledge, N.R., 2007. An ice cap landsystem for palaeoglaciological reconstructions: characterizing the Younger Dryas in western Scotland. Quaternary Science Reviews, 26(1-2), pp.213-229.

Golledge, N. R., Finlayson, A., Bradwell, T., & Everest, J. D. (2008). The last glaciation of Shetland, North Atlantic. Geografiska Annaler, Series A: Physical Geography. https://doi.org/10.1111/j.1468-0459.2008.00332.x

Golledge, N. R., Hubbard, A., & Sugden, D. E. (2008(b)). High-resolution numerical simulation of Younger Dryas glaciation in Scotland. Quaternary Science Reviews. https://doi.org/10.1016/j.quascirev.2008.01.019

Golledge N.R, McCulloch R, Finlayson A., J.D Everset (2009) A late glacial to modern palaeoenvironmental history for the Dounreay site area, reconstructed from a peat core from the Shebster basin. British Geological Survey Comissioned Report, CR/09/094 46pp

Golledge, N.R., 2010. Glaciation of Scotland during the Younger Dryas stadial: a review. Journal of Quaternary Science: Published for the Quaternary Research Association, 25(4), pp.550-566.

Goslar, T., Bałaga, K., Arnold, M., Tisnerat, N., Starnawska, E., Kuźniarski, M., Chróst, L., Walanus, A. and Więckowski, K., 1999. Climate-related variations in the composition of the Late Glacial and early Holocene sediments of Lake Perespilno (eastern Poland). Quaternary Science Reviews, 18(7), pp.899-911.

Goslar, T., Arnold, M., Tisnerat-Laborde, N., Czernik, J. and Więckowski, K., 2000. Variations of Younger Dryas atmospheric radiocarbon explicable without ocean circulation changes. Nature, 403(6772), pp.877-880.

Grootes PM, Stuiver M, White JW, Johnsen S, Jouzel J. 1993. Comparison of oxygen isotope results from the GISP2 and GRIP Greenland ice cores. Nature 366: 552–4.

Graham AGC, Stoker MS, Lonergan L, et al. 2011. The Pleistocene glaciations of the North Sea Basin. Developments in Quaternary Sciences 15: 261–278, https://doi.org/10.1016/B978-0-444-53447- 7.00021-0

Grachev, A.M., Severinghaus, J.P. (2005) A revised +10±4°C magnitude of abrupt change in Greenland temperature at the Younger Dryas termination using published GISP2 gas isotope data and air thermal diffusion constants. Quaternary Science Reviews, v.24, pp.513–519.

Grafenstein, U., Erlenkeuser, H., Brauer, A., Jouzel, J., Johnsen, S.J., 1999. A mid-European decadal isotope-climate record from 15,500 to 5000 years BP. Science 284, 1654–1657.

Greffard, M.H., Saulnier-Talbot, É. and Gregory-Eaves, I., 2012. Sub-fossil chironomids are significant indicators of turbidity in shallow lakes of northeastern USA. Journal of paleolimnology, 47(4), pp.561-581.

Grimm, E.C., 1987. TILIA and Tilia-Graph Software, Version 2.0.[WWW Document]. Grimm, EC.

Grimm EC, Watts WA, Jacobson GL, Hansen BCS, Almquist HR, and Dieffenbacher-Krall AC (2006) Evidence for warm wet Heinrich events in Florida.Quaternary Science Reviews 25: 2197–2211.

Gullan, P.J. and Cranston, P.S., 2010. The Insects: An Outline of Entomology. Willey.

Gusarov, V., 1995. Novye i maloizvestnye palearkticheskie stafilinidy (Coleoptera, Staphylinidae). Entomologicheskoe Obozrenie, 74(1), pp.81-96.

Haberzettl, T., Fey, M., Lücke, A., Maidana, N., Mayr, C., Ohlendorf, C., Schäbitz, F., Schleser, G.H., Wille, M. and Zolitschka, B., 2005. Climatically induced lake level changes during the last two millennia as reflected in sediments of Laguna Potrok Aike, southern Patagonia (Santa Cruz, Argentina). Journal of Paleolimnology, 33(3), pp.283-302.

Häkkinen, S., 2002. Freshening of the Labrador Sea surface waters in the 1990s: Another great salinity anomaly?. Geophysical Research Letters, 29(24), pp.85-1.

Hall, A. M. 1993: Clettnadal, West Burra. In Birnie, J. F., Gordon, J. E., Bennett, K. D. & Hall, A. M. (eds.): The Quaternary of Shetland: Field Guide, 48–50. Quaternary Research Association, Cambridge. Haworth,

Hall , A M 2013 , ' The last glaciation of Shetland : local ice cap or invasive ice sheet? ' , Norwegian Journal of Geology , vol. 93 , no. 3-4 , pp. 229-242 .

Hall, A.M., Riding, J.B. and Brown, J.F., 2016 (a). The last glaciation in Orkney, Scotland: glacial stratigraphy, event sequence and flow paths. Scottish Journal of Geology, 52(2), pp.90-101.

Hall, A.M. and Riding, J.B., 2016 (b). The last glaciation in Caithness, Scotland: revised till stratigraphy and ice-flow paths indicate multiple ice flow phases. Scottish Journal of Geology, 52(2), pp.77-89.

Hall, A.M. and Jarvis, J., 1989. A preliminary report on the late Devensian glaciomarine deposits around St. Fergus, Grampian Region. Quaternary Newsletter, 59(5), p.7.

Hall, A.M. and Whittington, G., 1989. Late Devensian glaciation of southern Caithness. Scottish Journal of Geology, 25(3), pp.307-324.

Hartz I and Milthers V (1901) Det senglacie ler i Allerød tegelværksgrav. Meddelelser Danks Geologisk Foreningen 8: 31–60.

Helmens KF, Johansson PW, Rasanen ME, Alexanderson H, Eskola KO (2007) Ice-free intervals at Sokli continuing into marine isotope stage 3 in the central area of the Scandinavian glaciations. Geol Surv Finl Bull 79:17–39

Henrikson, L., Olofsson, J.B. and Oscarson, H.G. 1982: The impact of acidification on Chironomidae (Diptera) as indicated by subfossil stratification. Hydrobiologia 86, 223–29.

Heiri, O. and Lotter, A.F., 2001. Effect of low count sums on quantitative environmental reconstructions: an example using subfossil chironomids. Journal of Paleolimnology, 26(3), pp.343-350.

Heiri, O. and Millet, L., 2005. Reconstruction of Late Glacial summer temperatures from chironomid assemblages in Lac Lautrey (Jura, France). Journal of Quaternary Science, 20(1), pp.33-44.

Heiri, O., Cremer, H., Engels, S., Hoek, W.Z., Peeters, W. and Lotter, A.F., 2007. Lateglacial summer temperatures in the Northwest European lowlands: a chironomid record from Hijkermeer, the Netherlands. Quaternary Science Reviews, 26(19-21), pp.2420-2437.

Heiri, O., Brooks, S.J., Birks, H.J.B., Lotter, A.F., 2011. A 274-lake calibration data-set and inference model for chironomid-based summer air temperature reconstruction in Europe. Quaternary Science Reviews 30, 3445–3456.

Heiri, O., Brooks, S. J., Renssen, H., Bedford, A., Hazekamp, M., Ilyashuk, B., … Samartin, S. (2014). ARTICLE Validation of climate model-inferred regional temperature change for late-glacial Europe. Heikki Seppä Spassimir Tonkov, 12(21). https://doi.org/10.1038/ncomms5914

Henrikson, L., Olofsson, J.B. and Oscarson, H.G., 1982. The impact of acidification on Chironomidae (Diptera) as indicated by subfossil stratification. Hydrobiologia, 86(3), pp.223-229.

Hoek Z (2008) The Last Glacial - Interglacial Transition. INTIMATE contribution. 226-229

Hofmann, W., 1984. Stratigraphie subfossiler Cladocera (Crustacea) und Chironomidae (Diptera) in zwei Sedimentprofilen des Meerfelder Maares. Courier Forschungs Institut Senckenberg, 65, pp.67-80.

Holliday, N.P., Bersch, M., Berx, B., Chafik, L., Cunningham, S., Florindo-López, C., Hátún, H., Johns, W., Josey, S.A., Larsen, K.M.H. and Mulet, S., 2020. Ocean circulation causes the largest freshening event for 120 years in eastern subpolar North Atlantic. Nature communications, 11(1), pp.1-15.

Home, D.M., 1881. V.—On the Glaciation of the Shetlands. Geological Magazine, 8(5), pp.205-212.

Hulme, P.D. and Shirriffs, J., 1994. The Late-glacial and Holocene vegetation of the Lang Lochs Mire area, Gulberwick, Shetland: a pollen and macrofossil investigation. New phytologist, 128(4), pp.793-806.

Hughen, K., Overpeck, J., Lehman, S. J., Kashgarians, M., Southons, J., Peterson, L. C., Alley, R. and Sigman, D. M. 1998. Deglacial changes in ocean circulation from an extended radiocarbon calibration. Nature, 391, 65–68.

Hughen, K., Southon, J., Lehman, S., Bertrand, C. and Turnbull, J., 2006. Marine-derived 14C calibration and activity record for the past 50,000 years updated from the Cariaco Basin. Quaternary Science Reviews, 25(23-24), pp.3216-3227.

Hurrell, J.W. and Deser, C., 2010. North Atlantic climate variability: the role of the North Atlantic Oscillation. Journal of marine systems, 79(3-4), pp.231-244.

Il'yashuk B.P and Il'yashuk E.A 2000 Palaeocological analysis of chironomid assemblages of a mountain lake as a source of information for biomonitoring. Russian Journal of Ecology 31: 353-358

Ilyashuk, B., Gobet, E., Heiri, O., Lotter, A.F., van Leeuwen, J.F., van der Knaap, W.O., Ilyashuk, E., Oberli, F. and Ammann, B., 2009. Lateglacial environmental and climatic changes at the Maloja Pass, Central Swiss Alps, as recorded by chironomids and pollen. Quaternary Science Reviews, 28(13-14), pp.1340-1353.

Isarin, R. F. B., & Rensse, H. (1999). Reconstructing and modelling Late Weichselian climates: the Younger Dryas in Europe as a case study. Earth-Science Reviews, 48, 1–38. Retrieved from www.elsevier.comrlocaterearscirev

Iversen, J., 1954. The Late Glacial flora of Denmark and its relations to climate and soil. Danmarks Geol. Unders 80, 87e119

Iversen, J., 1958. The bearing of glacial and interglacial epochs on the formation and extinction of plant taxa. Uppsala Univ. Arsskr, 6, p.210.

Johansen J. 1975, Pollen diagrams from the Shetland and Faroe Islands. Neu-Phytotogist 75: 369-387.

Johnsen, S.J., Clausen, H.B., Dansgaard, W., Fuhrer, K., Gundestrup, N., Hammer, C.U., Iversen, P., Jouzel, J., Stau!er, B., Stefensen, J.P., 1992. Irregular glacial interstadials recorded in a new Green- land ice core. Nature 359, 311}313.

Johnsen, S.J., Dahl-Jensen, D., Gundestrup, N., Steffensen, J.P., Clausen, H.B., Miller, H., Masson-Delmotte, V., Sveinbjörnsdottir, A.E. and White, J., 2001. Oxygen isotope and palaeotemperature records from six Greenland ice-core stations: Camp Century, Dye-3, GRIP, GISP2, Renland and NorthGRIP. Journal of Quaternary Science: Published for the Quaternary Research Association, 16(4), pp.299-307.

Johnsen, S.J., Clausen, H.B., Dansgaard, W., Gundestrup, N.S., Hammer, C.U., Andersen, U., Andersen, K.K.,Hvidberg, C.S., Dahl-Jensen, D., Steffensen, J.P., Shoji, H., Sveinbjörnsdóttir, Á.E., White, J., Jouzel, J., Fisher,D., 1997. The δ18O record along the Greenland Ice Core Project deep ice core and the problem of possibleEemian climatic instability. Journal of Geophysical Research 102, 26397-26410.

Jouve, G., Francus, P., Lamoureux, S., Provencher-Nolet, L., Hahn, A., Haberzettl, T., Fortin, D., Nuttin, L. and Team, T.P.S., 2013. Microsedimentological characterization using image analysis and μ-XRF as indicators of sedimentary processes and climate changes during Lateglacial at Laguna Potrok Aike, Santa Cruz, Argentina. Quaternary Science Reviews, 71, pp.191-204.

Jones, G., Davies, S.M., Farr, G.J. and Bevan, J., 2017. Identification of the Askja-S Tephra in a rare turlough record from Pant-y-Llyn, south Wales. Proceedings of the Geologists' Association, 128(4), pp.523-530.

Juggins, S., 2005. C2 Data Analysis, v. 1.5. 1. University of Newcastle, UK.

Kaufman, D.S., Ager, T.A., Anderson, N.J., Anderson, P.M., Andrews, J.T., Bartlein, P.J., Brubaker, L.B., Coats, L.L., Cwynar, L.C., Duvall, M.L., Dyke, A.S., Edwards, M.E., Eisner, W.R., Gajewski, K., Geirsdottir, A., Hu, F.S., Jennings, A.E., Kaplan, M.R., Kerwin, M.W., Lozhkin, A.V., MacDonald, G.M., Miller, G.H., Mock, C.J.,

Oswald, W.W., Otto-Bliesner, B.L., Porinchu, D.F., Rühland, K., Smol, J.P., Steig, E.J., Wolfe, B.B., 2004. Holocene thermal maximum in the western Arctic (0e180?W). Quat. Sci. Rev. 23, 529e560.

Karpuz, N.K. and Jansen, E., 1992. A high-resolution diatom record of the last deglaciation from the SE Norwegian Sea: Documentation of rapid climatic changes. Paleoceanography, 7(4), pp.499-520.

Korhola, A., Olander, H. and Blom, T., 2000. Cladoceran and chironomid assemblages as qualitative indicators of water depth in subarctic Fennoscandian lakes. Journal of Paleolimnology, 24(1), pp.43-54.

Kingsbury 2018 A multiproxy palaeolimnological reconstruction of the nature and timing of climatic changes in the Northern Isles from the end of the last glaciation through the early Holocene. Thesis. University of Stirling.

Klink A 2002 Determineersleutel voor de larven can de in Nedlerland vookomende soorten Polypedilum. STOWA concetuitgave 2002/06 18pp

Kylander ME, Ampel L, Wohlfarth B, Veres D (2011) High resolution X-ray fluorescence core scanning analysis of Les Echets (France) sedimentary sequence: new insights from chemical proxies. Journal of Quaternary Science 26: 109-117

Knight, J.R., Allan, R.J., Folland, C.K., Vellinga, M. and Mann, M.E., 2005. A signature of persistent natural thermohaline circulation cycles in observed climate. Geophysical Research Letters, 32(20).

Kylander, M.E., Lind, E.M., Wastegård, S. and Löwemark, L., 2012. Recommendations for using XRF core scanning as a tool in tephrochronology. The Holocene, 22(3), pp.371-375.

Lane, C.S., Brauer, A., Blockley, S.P. and Dulski, P., 2013. Volcanic ash reveals time-transgressive abrupt climate change during the Younger Dryas. Geology, 41(12), pp.1251-1254.

Lang, B., Bedford, A., Brooks, S.J., Jones, R.T., Richardson, N., Birks, H.J.B. and Marshall, J.D., 2010. Early-Holocene temperature variability inferred from chironomid assemblages at Hawes Water, northwest England. The Holocene, 20(6), pp.943-954.

Langdon, P.G., Holmes, N. and Caseldine, C.J., 2008. Environmental controls on modern chironomid faunas from NW Iceland and implications for reconstructing climate change. Journal of Paleolimnology, 40(1), pp.273-293.

Larocque-Tobler, I., Heiri, O. and Wehrli, M., 2010. Late Glacial and Holocene temperature changes at Egelsee, Switzerland, reconstructed using subfossil chironomids. Journal of Paleolimnology, 43(4), pp.649-666.

Lauterbach, S., Brauer, A., Andersen, N., Danielopol, D.L., Dulski, P., Hüls, M., Milecka, K., Namiotko, T., Obremska, M., Von Grafenstein, U. and Declakes Participants, 2011. Environmental responses to Lateglacial climatic fluctuations recorded in the sediments of pre-Alpine Lake Mondsee (northeastern Alps). Journal of Quaternary Science, 26(3), pp.253-267.

Lindegaard, C.B., Brodersen, K.P., 1995. Distribution of Chironomidae (Diptera) in the River Continuum. In: Cranston, P. (Ed.), Chironomids: From Genes to Ecosystems. CSIRO Publications, Melbourne, pp. 257–271.

Lisiecki, L. E., and Raymo, M. E. (2005), A Pliocene-Pleistocene stack of 57 globally distributed benthic δ18O records, Paleoceanography, 20, PA1003, doi:10.1029/2004PA001071.

Liu Z and Broeker (2008) Rock varnish microlamination dating of late Quaternary geomorphic features in the drylands of western USA Geomorphology 93 (2008) 501–523

Longo, W.M., Theroux, S., Giblin, A.E., Zheng, Y., Dillon, J.T. and Huang, Y., 2016. Temperature calibration and phylogenetically distinct distributions for freshwater alkenones: Evidence from northern Alaskan lakes. Geochimica et Cosmochimica Acta, 180, pp.177-196.

Longo, W.M., Huang, Y., Yao, Y., Zhao, J., Giblin, A.E., Wang, X., Zech, R., Haberzettl, T., Jardillier, L., Toney, J. and Liu, Z., 2018. Widespread occurrence of distinct alkenones from Group I haptophytes in freshwater lakes: Implications for paleotemperature and paleoenvironmental reconstructions. Earth and Planetary Science Letters, 492, pp.239-250.

Lotter, A.F., Heiri, O., Brooks, S., van Leeuwen, J.F., Eicher, U. and Ammann, B., 2012. Rapid summer temperature changes during Termination 1a: high-resolution multi-proxy climate reconstructions from Gerzensee (Switzerland). Quaternary Science Reviews, 36, pp.103-113.

Lowe, J.J., Ammann, B., Birks, H.H., Björck, S., Coope, G.R., Cwynar, L., De Beaulieu, J.L., Mott, R.J., Peteet, D.M. and Walker, M.J.C., 1994. Climatic changes in areas adjacent to the North Atlantic during the last glacial-interglacial transition (14-9 ka BP): a contribution to IGCP-253. Journal of Quaternary Science, 9(2), pp.185-198

LoweJJ, Rasmussen S O, Bjorck Setal.2008 .Synchronisation of palaeoenvironmental events in the North Atlantic region during the Last Termination: a revised protocol recommended by the INTI- MATE group. Quaternary Science Reviews 27: 6–17.

Lowe, J., Matthews, I., Mayfield, R., Lincoln, P., Palmer, A., Staff, R. and Timms, R., 2019. On the timing of retreat of the Loch Lomond ('Younger Dryas') Readvance icefield in the SW Scottish Highlands and its wider significance. Quaternary Science Reviews, 219, pp.171-186.

Lowe J & Walker M (2014) Reconstructing Quaternary Environments. Routledge 1317753712, 9781317753711

MacLeod, A., Palmer, A., Lowe, J., Rose, J., Bryant, C. and Merritt, J., 2011. Timing of glacier response to Younger Dryas climatic cooling in Scotland. Global and Planetary Change, 79(3-4), pp.264-274.

Magny, M., Aalbersberg, G., Bégeot, C., Benoit-Ruffaldi, P., Bossuet, G., Disnar, J.R., Heiri, O., Laggoun-Defarge, F., Mazier, F., Millet, L. and Peyron, O., 2006. Environmental and climatic changes in the Jura mountains (eastern France) during the Lateglacial–Holocene transition: a multi-proxy record from Lake Lautrey. Quaternary Science Reviews, 25(5-6), pp.414-445.

Mangerud J, Inge Aarseth, Anna L.C. Hughes, Øystein S. Lohne, Kåre Skår, Eivind Sønstegaard, John Inge Svendsen,A major re-growth of the Scandinavian Ice Sheet in western Norway during Allerød-Younger Dryas,Quaternary Science Reviews,Volume 132,2016,Pages 175-205,ISSN 0277-3791,

Marcott, S.A., Clark, P.U., Padman, L., Klinkhammer, G.P., Springer, S.R., Liu, Z., Otto-Bliesner, B.L., Carlson, A.E., Ungerer, A., Padman, J. and He, F., 2011. Ice-shelf collapse from subsurface warming as a trigger for Heinrich events. Proceedings of the National Academy of Sciences, 108(33), pp.13415-13419.

Martín-Puertas, C., Valero-Garcés, B.L., Mata, M.P., Moreno, A., Giralt, S., Martínez-Ruiz, F. and Jiménez-Espejo, F., 2011. Geochemical processes in a Mediterranean Lake: a high-resolution study of the last 4,000 years in Zonar Lake, southern Spain. Journal of Paleolimnology, 46(3), pp.405-421.

Marty, J. and Myrbo, A., 2014. Radiocarbon dating suitability of aquatic plant macrofossils. Journal of paleolimnology, 52(4), pp.435-443.

Marshall, J.D., Jones, R.T., Crowley, S.F., Oldfield, F., Nash, S. and Bedford, A., 2002. A high resolution late-glacial isotopic record from Hawes Water, northwest England: Climatic oscillations: Calibration and comparison of palaeotemperature proxies. Palaeogeography, Palaeoclimatology, Palaeoecology, 185(1-2), pp.25-40.

Marshall M, Schlolaut G, Nakagawa T, Lamb H, Brauer A, Staff R, Ramsey C, Tarasov P, Gotanda K, Haraguchi T, Yokoyama Y, Yonenobu H, Tada R (2012) A novel approach to varve counting using μXRF and X-radiography in combination with thin-section microscopy, applied to the Late Glacial chronology from Lake Suigetsu, Japan. Quat Geochronol 13:70–80. doi:10.1016/j.quageo.2012.06.002

McKirdy. A (2010) Orkney and Shetland. Scottish National Heritage ISBN-10: 1853976024

McManus, J.F., Francois, R., Gherardi, J.-M., Keigwin, l.D., Brown-Leger, S., 2004. Collapse and rapid resumption of Atlantic meridional circulation linked to deglacial climate changes. Nature 428, 834e837.

McVean, D.N. and Ratcliffe, D.A., 1962. Plant communities of the Scottish Highlands. A study of Scottish mountain, moorland and forest vegetation. Plant communities of the Scottish Highlands. A study of Scottish mountain, moorland and forest vegetation.

Meehl GA, Stocker TF, Collins WD et al. 2007. Global climate projections. In Climate Change 2007: The Physical Science Basis. Contribution of Working Group I to the Fourth Assessment Report of the Intergovernmental Panel on Climate Change, Solomon S, Qin D, Manning M, et al. (eds) Cambridge University Press: Cambridge; 749–844.

Merritt, J.W., Coope, G.R., Taylor, B.J. and Walker, M.J.C., 1990. Late Devensian organic deposits beneath till in the Teith Valley, Perthshire. Scottish Journal of Geology, 26(1), pp.15-24.

Merritt, J.W., Auton, C.A. and Firth, C.R., 1995. Ice-proximal glaciomarine sedimentation and sea-level change in the Inverness area, Scotland: a review of the deglaciation of a major ice stream of the British Late Devensian ice sheet. Quaternary Science Reviews, 14(3), pp.289-329.

Merritt, J. W., E. R. Connell, and D. R. Bridgland. Quaternary of the Banffshire coast and Buchan. Quaternary Research Association, 2000.

Merritt, J.W., GORDON, J.E. and CONNELL, E.R., 2019. Late Pleistocene sediments, landforms and events in Scotland: a review of the terrestrial stratigraphic record. Earth and Environmental Science Transactions of the Royal Society of Edinburgh, 110(1-2), pp.39-91.

Metcalfe, S.E., Jones, M.D., Davies, S.J., Noren, A. and MacKenzie, A., 2010. Climate variability over the last two millennia in the North American Monsoon region, recorded in laminated lake sediments from Laguna de Juanacatlán, Mexico. The Holocene, 20(8), pp.1195-1206.

Millet, L., Rius, D., Galop, D., Heiri, O. and Brooks, S.J., 2012. Chironomid-based reconstruction of Lateglacial summer temperatures from the Ech palaeolake record (French western Pyrenees). Palaeogeography, Palaeoclimatology, Palaeoecology, 315, pp.86-99.

Moreno A, Lopéz-Merino L, Leira M, Marco-Barba M, González-Sampériz P, Valero-Garcés BL, Lopéz-Saez J, Santos L, Mata P, Ito E (2011) Revealing the last 13,500 years of environmental history from the multi-proxy record of a mountain lake (Lago Enol, northern Iberian Peninsula). J Paleolimnol 46:327–349. doi:10.1007/s10933-009-9387-7

Moar, N.T., 1969. Two pollen diagrams from the Mainland, Orkney Islands. New Phytologist, 68(1), pp.201-208.

Moller Pillot H.K.M and Buskens R.F.M 1990 De larven der Nederlandse Chironomidae. Autoecologie en verspreiding. Nederlandse Faunistische Mededelingen Ic: 1-87

Murton, J.B., Bateman, M.D., Dallimore, S.R., Teller, J.T., Yang, Z., 2010. Identification of Younger Dryas outburst flood path from Lake Agassiz to the Arctic Ocean. Nature 464, 740e743.

Mykura W. 1976. British regional geology : Orkney and Shetland. Edinburgh: HMSO.

Mysterud, A., Stenseth, N.C., Yoccoz, N.G., Ottersen, G. and Langvatn, R., 2003. The response of terrestrial ecosystems to climate variability associated with the North Atlantic Oscillation. Geophysical Monograph-American Geophysical Union, 134, pp.235-262.

Nakamura, H., Sawada, K., Araie, H., Suzuki, I., Shiraiwa, Y., 2014. Long chain alkenes, alkenones and alkenoates produced by the haptophyte alga Chrysotila lamellosa CCMP1307 isolated from a salt marsh. Organic Geochemistry 66, 90–97.

Nagell B and Landahl C C. (1978). Resistance to anoxia of Chironomus plumosus and Chironomus anthracinus (Diptera) larvae. Holarctic Ecology 1(4): 333–336.

Naughton, F., Bourillet, J.-F., Goñi, m.f.S., Turon, J.-L., Jouanneau, J.-M., 2007a. Long- term and Millennial-scale climate variability in northwestern France during the last 8850 years. The Holocene 17, 939e953.

Neugebauer, I., Brauer, A., Dräger, N., Dulski, P., Wulf, S., Plessen, B., Mingram, J., Herzschuh, U. and Brande, A., 2012. A Younger Dryas varve chronology from the Rehwiese palaeolake record in NE-Germany. Quaternary Science Reviews, 36, pp.91-102.

North Greenland Ice Core Project members, 2004. High-resolution record of Northern Hemisphere climate extending into the last interglacial period. Nature 431, 147-151.

Nyman, M., Korhola, A. and Brooks, S.J., 2005. The distribution and diversity of Chironomidae (Insecta: Diptera) in western Finnish Lapland, with special emphasis on shallow lakes. Global Ecology and Biogeography, 14(2), pp.137-153.

Østbye E, Hågvar S. 1996. Pitfall catches of surface-active arthropods in high mountain habitats at Finse, south Norway. IV. Coleoptera. Fauna Norvegica B43: 1–18.

Ohmura, A., Kasser, P., Funk, M., 1992. Climate at the equilibrium line of glaciers. Journal of Glaciology 38, 397–411.

Ólafsson, J., 1999. Connections between oceanic conditions off N-Iceland, Lake Myvatn temperature, regional wind direction variability and the North Atlantic Oscillation. Rit Fiskideild, 16, pp.41-58.

Oliver, D. R., 1983. The larvae of Diamesinae (Diptera: Chironomidae) of the Holarctic region — Keys and diagnoses. Ent. scand. Suppl. 19: 115–138.

Paus, A., 2010. Vegetation and environment of the Rødalen alpine area, Central Norway, with emphasis on the early Holocene. Vegetation History and Archaeobotany, 19(1), pp.29-51.

Peacock, J.D. and Long, D., 1994. Late-Devensian glaciation and deglaciation of Shetland.

Pearce, T. J., and I. Jarvis (1995), High-resolution chemostratigraphy of Quaternary distal turbidites: A case study of new methods for the analysis and correlation of barren sequences, in Non-Biostratigraphical Methods of Dating and Correlation, Geol. Soc. Spec. Publ., vol. 89,edited by R. E. Dunay, and E. A. Hailwood, pp. 107–143, Geol. Soc. of London, London, U. K.

Pearson, E.J., Juggins, S., Farrimond, P., 2008. Distribution and significance of long-chain alkenones as salinity and temperature indicators in Spanish saline lake sediments. Geochimica et Cosmochimica Acta 72, 4035–4046.

Peglar, S., 1979. A radiocarbon-dated pollen diagram from Loch of Winless, Caithness, north-east Scotland. New Phytologist, 82(1), pp.245-263.

Pennington, W., Haworth, E.Y., Bonny, A.P. and Lishman, J.P., 1972. Lake sediments in northern Scotland. Philosophical Transactions of the Royal Society of London. B, Biological Sciences, 264(861), pp.191-294.

Pentecost, A. (2009). The marl lakes of the British Isles. Freshwater Reviews 2, 167-197.

Peterson, L.C., Haug, G.H., Hughen, K.A., Rohl, U., 2000. Rapid changes in the hydrologic cycle of the tropical atlantic during the Last Glacial. Science 290 (5498), 1947e1951

Phillips, W.M., Hall, A.M., Ballantyne, C.K., Binnie, S., Kubik, P.W. and Freeman, S., 2008. Extent of the last ice sheet in northern Scotland tested with cosmogenic 10Be exposure ages. Journal of Quaternary Science: Published for the Quaternary Research Association, 23(2), pp.101-107.

Philippsen Bente (2013) The freshwater reservoir effect in radiocarbon dating. Heritage Science 2013, 1:24

Pinder, L.C.V. and Reiss, F., 1983. The larvae of Chironominae: keys and diagnoses. Chironomidae of the Holarctic Region. Keys and Diagnoses, Part, 1, pp.293-435.

Pinder,L.C.V.,1995.The habitats of chironomid larvae. In:Armitage, P.D., Cranston, P.S., Pinder, L.C.V. (Eds.), The Chironomidae: TheBiologyandEcologyofNon-bitingMidges.Chapman&Hall, London, pp. 107–135.

Pinder, L.C.V. and Morley, D.J., 1995. Chironomidae as indicators of water quality with a comparison of the chironomid faunas of a series of contrasting Cumbrian Tarns.

Pilcher, J.R. and Hall, V.A., 1992. Towards a tephrochronology for the Holocene of the north of Ireland. The Holocene, 2(3), pp.255-259.

Plancq J, Cavazzin B, Juggins S, Haig H.A,Leavitt P.R, Toney J.L, (2018)Assessing environmental controls on the distribution of long-chain alkenones in the Canadian Prairies,Organic Geochemistry,Volume 117,Pages 43-55,ISSN 0146-6380,

Porinchu, D.F. and MacDonald, G.M. 2003: The use and application of freshwater midges (Chironomidae: Insecta: Diptera) in geographical research. Progress in Physical Geography 27, 378 /422.

Porinchu, D., Rolland, N. and Moser, K., 2009. Development of a chironomid-based air temperature inference model for the central Canadian Arctic. Journal of Paleolimnology, 41(2), pp.349-368.

Prahl, F., Muehlhausen, L., Zahnle, D., 1988. Further evaluation of long-chain alkenones as indicators of paleoceanographic conditions. Geochimica et Cosmochimica Acta 52, 2303–2310.

Prahl, F.G., Wakeham, S.G., 1987. Calibration of unsaturation patterns in long- chain ketone compositions for palaeotemperature assessment. Nature 330, 367–369.

Ramsey, C.B., Albert, P.G., Blockley, S.P., Hardiman, M., Housley, R.A., Lane, C.S., Lee, S., Matthews, I.P., Smith, V.C. and Lowe, J.J., 2015. Improved age estimates for key Late Quaternary European tephra horizons in the RESET lattice. Quaternary Science Reviews, 118, pp.18-32.

Ramsey, C., 2017. OxCal Program, Version 4.3. Oxford Radiocarbon Accelerator Unit: University of Oxford.

Rasmussen K & Lindegaard C (1988) Effects of iron compounds on macroinvertbrate communities in a Danish Lowland River System - Water Research 22: 1101-1108

Rasmussen, S.O., Andersen, K.K., Svensson, A.M., Steffensen, J.P., Vinther, B.M., Clausen, H.B., Siggaard-Andersen, M.L., Johnsen, S.J., Larsen, L.B., Dahl-Jensen, D. and Bigler, M., 2006. A new Greenland ice core chronology for the last glacial termination. Journal of Geophysical Research: Atmospheres, 111(D6).

Rasmussen, S.O., Vinther, B.M., Clausen, H.B. and Andersen, K.K., 2007. Early Holocene climate oscillations recorded in three Greenland ice cores. Quaternary Science Reviews, 26(15-16), pp.1907-1914.

Rasmussen, T.L., Thomsen, E., 2008. Warm Atlantic surface water inflow to the Nordic Seas 34e10 calibrated ka B.P. Paleoceanography 23, PA1201. http:// dx.doi.org/10.1029/2007PA001453.

Rasmussen SO, Bigler M, Blockley SP et al. 2014a. A stratigraphic framework for abrupt climatic changes during the last glacial period based on three synchronized Greenland ice-core records: refining and extending the INTIMATE event stratigraphy. Quater- nary Science Reviews 106: 14–28.

Renssen, H., Isarin, R.F.B., 2001. The two major warming phases of the last deglaciation ate14.7 ande11.5 ka cal BP in Europe: climate reconstructions and AGCM experiments. Global and Planetary Change 30, 117e153

Rhines, P., Hakkinen, S., Josey, S., 2008. Is oceanic heat transport significant in the climate system? In: Dickson, B., Meincke, J., Rhines, P. (Eds.), Arctic e Subarctic Ocean Fluxes: Defining the Role of the Northern Seas in Climate, pp. 87e109.

Rieradevall, M. and Brooks, S.J., 2001. An identification guide to subfossil Tanypodinae larvae (Insecta: Diptera: Chrironomidae) based on cephalic setation. Journal of paleolimnology, 25(1), pp.81-99.

Risebrobakken, B., Dokken, T., Smedsrud, L.H., Andersson, C., Jansen, E., Moros, M., Ivanova, E.V., 2011. Early Holocene temperature variability in the Nordic Seas: the role of oceanic heat advection versus changes in orbital forcing. Paleoceanography 26, PA4206. http://dx.doi.org/10.1029/2011PA002117.
Risebrobakken,

Robinson, M. 2004. A Late glacial and Holocene diatom record from Clettnadal, Shetland Islands, northern Scotland. Journal of Paleolimnology 31, 295–319.

Rodrigues, T., Grimalt, J. O., Abrantes, F., Naughton, F., & Flores, J. A. (2010). The last glacial-interglacial transition (LGIT) in the western mid-latitudes of the North Atlantic: Abrupt sea surface temperature change and sea level implications. Quaternary Science Reviews. https://doi.org/10.1016/j.quascirev.2010.04.004

Romundset, A., Lakeman, T.R. and Høgaas, F., 2019. Coastal lake records add constraints to the age and magnitude of the Younger Dryas ice-front oscillation along the Skagerrak coastline in southern Norway. Journal of Quaternary Science, 34(2), pp.112-124.

Ross, H., 1997. The last glaciation of Shetland (Doctoral dissertation, University of St Andrews).

Sæther, O.A., 1975. Nearctic chironomids as indicators of lake typology: With 1 figure and 2 tables in the text. Internationale Vereinigung für theoretische und angewandte Limnologie: Verhandlungen, 19(4), pp.3127-3133.

Saether, O.A., 1979. Chironomid communities as water quality indicators. Ecography, 2(2), pp.65-74.

Saether, O.A & Andersen T: 7. The larvae of Diamesinaw (Diptera: CHironomidae) of the Holarctic Region – Keys and diagnoses, In: Andresen, T, Cranston, P.S & Epler J.H (cie eds): The larvae of Chironomididae (Diptera) of the Holarctic Region – keys and diagnoses. Insect Systematics & Evolution. 66:145-178 Lund, Sweden 17 June 2013. ISSN 2001-4945

Schouten, S., Hopmans, E.C., Schefuß, E. and Damste, J.S.S., 2002. Distributional variations in marine crenarchaeotal membrane lipids: a new tool for reconstructing ancient sea water temperatures?. Earth and Planetary Science Letters, 204(1-2), pp.265-274.

Seager, R. and Battisti, D.S., 2007. Challenges to our understanding of the general circulation: Abrupt climate change. Global Circulation of the Atmosphere, pp.331-371

Sejrup, H.P., Nygård, A., Hall, A.M. and Haflidason, H., 2009. Middle and Late Weichselian (Devensian) glaciation history of south-western Norway, North Sea and eastern UK. Quaternary Science Reviews, 28(3-4), pp.370-380.

Seppä H* and Bennett K (2003) Quaternary pollen analysis: recent progress in palaeoecology and palaeoclimatology. Progress in Physical Geography 27,4 (2003) pp. 548–579

Shane P & Smith I (2000) Geochemical fingerprinting of basaltic tephra deposits in the Auckland Volcanic Field, New Zealand Journal of Geology and Geophysics, 43:4, 569-577, DOI: 10.1080/00288306.2000.9514909

Shakun, J. D., & Carlson, A. E. (2010). A global perspective on Last Glacial Maximum to Holocene climate change. Quaternary Science Reviews. https://doi.org/10.1016/j.quascirev.2010.03.016

Shennan, I., Bradley, S., Milne, G., Brooks, A., Bassett, S. and Hamilton, S., 2006. Relative sea-level changes, glacial isostatic modelling and ice-sheet reconstructions from the British Isles since the Last Glacial Maximum. Journal of Quaternary Science: Published for the Quaternary Research Association, 21(6), pp.585-599.

Serreze, M.C., Holland, M.M., Stroeve, J., 2007. Perspectives on the Arctic's rapidly shrinking sea-ice cover. Science 315, 1533e1536.
Shakun,

Sissons, J.B., 2017. The Lateglacial lakes of glens Roy, spean and vicinity (Lochaber district, Scottish Highlands). Proceedings of the Geologists' Association, 128(1), pp.32-41.

Small, D., Rinterknecht, V., Austin, W., Fabel, D., Miguens-Rodriguez, M. and Xu, S., 2012. In situ cosmogenic exposure ages from the Isle of Skye, northwest Scotland: implications for the timing of deglaciation and readvance from 15 to 11 ka. Journal of Quaternary Science, 27(2), pp.150-158.

Small, D., Rinterknecht, V., Austin, W. E. N., Bates, R., Benn, D. I., Scourse, J. D., Bourle`s, D. L. & Hibbert, F. D. 2016. Implica- tions of 36Cl exposure ages from Skye, northwest Scotland for the timing of ice stream deglaciation and deglacial ice dynamics. Quaternary Science Reviews 150, 130–45.

Smeed, D.A., Josey, S.A., Beaulieu, C., Johns, W.E., Moat, B.I., Frajka-Williams, E., Rayner, D., Meinen, C.S., Baringer, M.O., Bryden, H.L. and McCarthy, G.D., 2018. The North Atlantic Ocean is in a state of reduced overturning. Geophysical Research Letters, 45(3), pp.1527-1533.

Spielhagen, R.F., Werner, K., Aagaard-Sørensen, S., Zamelczyk, K., Kandiano, E.S., Budeus, G., Husum, K., Marchitto, T.M., Hald, M., 2011. Enhanced modern heat Transfer to the arctic by warm Atlantic water. Science 331, 450e453.
Stanford,

Stansell, N.D., Rodbell, D.T., Abbott, M.B. and Mark, B.G., 2013. Proglacial lake sediment records of Holocene climate change in the western Cordillera of Peru. Quaternary Science Reviews, 70, pp.1-14.

Steffensen, J.P., Andersen, K.K., Bigler, M., Clausen, H.B., Dahl-Jensen, D., Fischer, H., Goto-Azuma, K., Hansson, M., Johnsen, S.J., Jouzel, J. and Masson-Delmotte, V., 2008. High-resolution Greenland ice core data show abrupt climate change happens in few years. Science, 321(5889), pp.680-684.

Stenseth, N.C., Ottersen, G., Hurrell, J.W., Mysterud, A., Lima, M., Chan, K.S., Yoccoz, N.G. and Ådlandsvik, B., 2003. Studying climate effects on ecology through the use of climate indices: the North Atlantic Oscillation, El Nino Southern Oscillation and beyond. Proceedings of the Royal Society of London. Series B: Biological Sciences, 270(1529), pp.2087-2096.

Stewart, H., Bradwell, T., Bullard, J., Davies, S.J., Golledge, N. and McCulloch, R.D., 2017. 8000 years of North Atlantic storminess reconstructed from a Scottish peat

record: implications for Holocene atmospheric circulation patterns in Western Europe. Journal of Quaternary Science, 32(8), pp.1075-1084.

Straile, D., Livingstone, D.M., Weyhenmeyer, G.A. and George, D.G., 2003. The response of freshwater ecosystems to climate variability associated with the North Atlantic Oscillation.

Stroud, D.A., Reed T.M. Pienkowski M.W., Lindsay, R.A. Stroud, D. A., Reed, T. M., Pienkowski, M. W., & Lindsay, R. A. 1987. Birds, Bogs and Forestry. The peatlands of Caithnesss and Sutherland. Tech. rept. Nature Conservancy Council, Peterborough.

Stroeven, A.P., Hättestrand, C., Kleman, J., Heyman, J., Fabel, D., Fredin, O., Goodfellow, B.W., Harbor, J.M., Jansen, J.D., Olsen, L. and Caffee, M.W., 2016. Deglaciation of fennoscandia. Quaternary Science Reviews, 147, pp.91-121.

Stuiver, M., Reimer, P., RW, R., 2013. CALIB 7.0 (program and documentation).

Tarasov, L., Peltier, W.R., 2005. Arctic freshwater forcing of the Younger Dryas cold reversal. Nature 435, 662e665.

Thiagarajan N, A.V. Subhas, J.R. Southon, J.M. Eiler, J.F. Adkins (2014) Abrupt pre-Bolling-Allerod warming and circulation changes in the deep ocean Nature, 511 (2014), pp. 75–78

Thiel, V., Jenisch, A., Landmann, G., Reimer, A., Michaelis, W., 1997. Unusual distributions of long-chain alkenones and tetrahymanol from the highly alkaline Lake Van, Turkey. Geochimica et Cosmochimica Acta 61, 2053–2064.

Timms, R.G.O., Matthews, I.P., Lowe, J.J., Palmer, A.P., Weston, D.J., MacLeod, A., and Blockley, S.P.E. (2019). „Establishing tephrostratigraphic frameworks to aid the study of abrupt climatic and glacial transitions: a case study of the Last Glacial-Interglacial Transition in the British Isles (c. 16-8 ka BP)." Earth-Science Reviews https://doi.org/10.1016/j.earscirev.2019.01.003

Timms, R.G.O., Matthews, I.P., Palmer, A.P., and Candy, I. (2018). „Toward a tephrostratigraphic framework for the British Isles: A Last Glacial to Interglacial Transition (LGIT c. 16-8 ka) case study from Crudale Meadow, Orkney.‟ Quaternary Geochronology, 46, pp. 28-44.

Tipping, R., 1991. The climatostratigraphic subdivision of the Devensian Lateglacial: evidence from a pollen site near Oban, western Scotland. Journal of biogeography, pp.89-101.

Toney, J.L., Huang, Y., Fritz, S.C., Baker, P.A., Grimm, E., Nyren, P., 2010. Climatic and environmental controls on the occurrence and distributions of long chain alkenones in lakes of the interior United States. Geochimica et Cosmochimica Acta 74, 1563–1578.

Toney, J.L., Leavitt, P.R., Huang, Y., 2011. Alkenones are common in prairie lakes of interior Canada. Organic Geochemistry 42, 707–712.

Toney, J.L., Theroux, S., Andersen, R.A., Coleman, A., Amaral-Zettler, L.A., Huang, Y., 2012. Culturing of the first 37:4 predominant lacustrine haptophyte: Geochemical, biochemical, and genetic implications. Geochimica et Cosmochimica Acta 78, 51–64.

Turner, J. N., Holmes, N., Davis, S. R., Leng, M. J., Langdon, C., & Scaife, R. G. (2015). A multiproxy (micro-XRF, pollen, chironomid and stable isotope) lake sediment record for the Lateglacial to Holocene transition from Thomastown Bog, Ireland. Journal of Quaternary Science. https://doi.org/10.1002/jqs.2796

Turney, C.S.M., Harkness, D.D., and Lowe, J.J. (1997). The use of microtephra horizons to correlate Late-glacial lake sediment successions in Scotland, Journal of Quaternary Science, 12(6), pp. 525–531.

Turney, C. S. M., Harkness, D. D. & Lowe, J. J. 1998. Carbon isotope variations and chronology of the Last Glacial–Interglacial Transi- tion (14-9 ka BP). Radiocarbon 40, 873–81.

Uutala, A. J., 1986. Paleolimnological assessment of the effects of lake acidification on Chironomidae (Diptera) assemblages in the Adirondack region of New York. Ph.D. thesis, State Univ. of N.Y., Coll. Environ. Sci. For., Syracuse, U.S.A.

Vallenduuk (1999) Key to the larvae Glyptotendipes (Diptera: Chironomidae) in Western Europe. Schijindel. 51pp

Vallenduuk, H.J. and Pillot, H.K.M., 2007. Chironomidae Larvae, Vol. 1: Tanypodinae: General Ecology and Tanypodinae. Brill.

van Asch, N., Lutz, A.F., Duijkers, M.C., Heiri, O., Brooks, S.J., and Hoek, W.Z. (2012). „Rapid climate change during the Weichselian Late-Glacial in Ireland: chironomid-inferred summer temperatures from Fiddaun, Co. Galway. Palaeogeography, Palaeoclimatology, Palaeoecology, 315-316, pp. 1-11.

Velle, G., Brooks, S.J., Birks, H.J.B. and Willassen, E., 2005. Chironomids as a tool for inferring Holocene climate: an assessment based on six sites in southern Scandinavia. Quaternary Science Reviews, 24(12-13), pp.1429-1462.

Vojtech J, C. M. Farrow, Vojtech E, Interpretation of Whole-rock Geochemical Data in Igneous Geochemistry: Introducing Geochemical Data Toolkit (GCDkit), Journal of Petrology, Volume 47, Issue 6, June 2006, Pages 1255–1259, https://doi.org/10.1093/petrology/egl013

Volkman, J.K., Eglinton, G., Corner, E.D.S., Forsberg, T.E.V., 1980. Long chain alkenes and alkenones in the marine coccolithophorid Emiliania huxleyi. Phytochemistry19, 2619–2622.

Wagner-Cremer, F. and Lotter, A.F., 2011. Spring-season changes during the Late Pleniglacial and Bølling/Allerød interstadial. Quaternary Science Reviews, 30(15-16), pp.1825-1828.

Wang, G. and Schimel, D., 2003. Climate change, climate modes, and climate impacts. Annual Review of Environment and Resources, 28(1), pp.1-28.

Walker, G.T., 1924. Correlations in seasonal variations of weather. I. A further study of world weather. Mem. Indian Meteorol. Dep., 24, pp.275-332.

Walker, I.R., Smol, J.P., Engstrom, D.R. and Birks, H.J.B., 1991. An assessment of Chironomidae as quantitative indicators of past climatic change. Canadian Journal of Fisheries and Aquatic Sciences, 48(6), pp.975-987.

Walker, I.R. and MacDonald, G.M., 1995. Distributions of Chironomidae (Insecta: Diptera) and other freshwater midges with respect to treeline, Northwest Territories, Canada. Arctic and Alpine Research, 27(3), pp.258-263.

Walker, M.J. and Lowe, J.J., 1990. Reconstructing the environmental history of the last glacial-interglacial transition: evidence from the Isle of Skye, Inner Hebrides, Scotland. Quaternary Science Reviews, 9(1), pp.15-49.

Walker, I.R., 2001. Midges: Chironomidae and related diptera. In Tracking environmental change using lake sediments (pp. 43-66). Springer, Dordrecht.

Walker, M.J.C., Bryant, C., Coope, G.R., Harkness, D.D., Lowe, J.J. and Scott, E.M., 2001. Towards a radiocarbon chronology of the Late-Glacial: sample selection strategies. Radiocarbon, 43(2B), pp.1007-1019.

Walker, M., Johnsen, S., Rasmussen, S.O., Steffensen, J.P., Popp, T., Gibbard, P., Hoek, W., Lowe, J., Andrews, J., Björck, S., Cwynar, L.C., Hughen, K., Kershaw, P., Kromer, B., Litt. T., Lowe, D.J., Nakagawa, T., Newnham, R., Schwander, J. (2009) Formal definition and dating of the GSSP (Global Stratotype Section and Point) for the base of the Holocene using the Greenland NGRIP ice co, and selected auxiliary records. Journal of Quaternary Science, v.24, pp.3–17.

Walker, M., Gibbard, P., Head, M.J., Berkelhammer, M., Björck, S., Cheng, H., Cwynar, L.C., Fisher, D., Gkinis, V., Long, A. and Lowe, J., 2019. Formal subdivision of the Holocene series/epoch: a summary. Journal of the Geological Society of India, 93(2), pp.135-141.

Walker, M. and John, Lowe., 2019. Lateglacial environmental change in Scotland. Earth and Environmental Science Transactions of the Royal Society of Edinburgh, 110(1-2), pp.173-198.

Walshe, B. M. (1948): The oxygen requirements and thermal resistance of chironomid larvae from flowing and from still waters.- The Journal of Experimental Biology 25: 35-44,...

Wallace, J.M., Panetta, R.L. and Estberg, J., 1993. Representation of the equatorial stratospheric quasi-biennial oscillation in EOF phase space. Journal of the atmospheric sciences, 50(12), pp.1751-1762.

Watson, J., Brooks, S. J., Whitehouse, N., Reimer, P., Birks, H. J. B., & Turney, C. S. M. (2010). Chironomid- inferred Late-Glacial Summer Air Temperatures From Lough Nadourcan, Co. Donegal, Ireland. Journal of Quaternary Science, 25(8), 1200. DOI: 10.1002/jqs.1399

Weckström, K., Weckström, J., Yliniemi, L.M. and Korhola, A., 2010. The ecology of Pediastrum (Chlorophyceae) in subarctic lakes and their potential as paleobioindicators. Journal of Paleolimnology, 43(1), pp.61-73.

Whittington, G. and Edwards, K.J., 1993. Vegetation change on Papa Stour, Shetland, Scotland: a response to coastal evolution and human interference?. The Holocene, 3(1), pp.54-62.

Whittington, G., Fallick, A.E. and Edwards, K.J., 1996. Stable oxygen isotope and pollen records from eastern Scotland and a consideration of Late-glacial and early Holocene climate change for Europe. Journal of Quaternary Science: Published for the Quaternary Research Association, 11(4), pp.327-340.

Whittington, G., Buckland, P., Edwards, K.J., Greenwood, M., Hall, A.M. and Robinson, M., 2003. Multiproxy Devensian Late-glacial and Holocene environmental

records at an Atlantic coastal site in Shetland. Journal of Quaternary Science: Published for the Quaternary Research Association, 18(2), pp.151-168.

Whittington, G., Edwards, K.J., Zanchetta, G., Keen, D.H., Bunting, M.J., Fallick, A.E., and Bryant, C. L. (2015). „Lateglacial and early Holocene climates of the Atlantic margins of Europe: Stable isotope, mollusc and pollen records from Orkney, Scotland." Quaternary Science Reviews, 122, pp. 112-130.

Wiersma, A.P. and Renssen, H., 2006. Model–data comparison for the 8.2 ka BP event: confirmation of a forcing mechanism by catastrophic drainage of Laurentide Lakes. Quaternary Science Reviews, 25(1-2), pp.63-88.

Willby, N. (2005). Macrophyte inferred reference conditions and supporting chemistry for marl lakes. Technical report, Environment Agency Paper TAG/LTT 91.

Wiik E., Bennion H., Sayer C.D. & Willby N.J. (2013) Chemical and biological responses of marl lakes to eutrophica- tion. Freshwater Reviews, 6, 35–62.

Williams, K. A. (1981). Population dynamics of epiphytic chironomid larvae in a chalk stream. University of Reading. PhD Thesis, 317 pp.

Willis, K.J. and MacDonald, G.M., 2011. Long-term ecological records and their relevance to climate change predictions for a warmer world. Annual Review of Ecology, Evolution, and Systematics, 42, pp.267-287.

Wijk, S., 1986. Performance of Salix herbacea in an alpine snow-bed gradient. The Journal of Ecology, pp.675-684.

Windfinder (2020) https://www.windfinder.com/windstatistics/kirkwall (Accessed March 25th 2020)

Wu, M.S., Zong, Y., Mok, K.M., Cheung, K.M., Xiong, H. and Huang, G., 2017. Holocene hydrological and sea surface temperature changes in the northern coast of the South China Sea. Journal of Asian Earth Sciences, 135, pp.268-280.

Wunsch, C., 2006. Abrupt climate change: an alternative view. Quat. Res. 65, 191e203.

Yamamoto, M. 1986: Study of Japanese Chironomus inhabiting high acidic water (Diptera: Chironomidae) I. Kontyû, Tokyo 54 324-32

Zhang, E., Langdon, P., Tang, H., Jones, R., Yang, X. and Shen, J., 2011. Ecological influences affecting the distribution of larval chironomid communities in the lakes on Yunnan Plateau, SW China. Fundamental and Applied Limnology/Archiv für Hydrobiologie, 179(2), pp.103-113.

Zhou, W., An, Z., Jull, A.T., Donahue, D.J. and Head, M., 1997. Reappraisal of Chinese Loess Plateau stratigraphic sequences over the last 30,000 years: precursors of an important Holocene monsoon climatic event. Radiocarbon, 40(2), pp.905-913.

Zink, K., Leythaeuser, D., Melkonian, M., Schwark, L., 2001. Temperature dependency of long-chain alkenone distributions in Recent to fossil limnic sediments and in lake waters. Geochimica et Cosmochimica Acta 65, 253–265.

Zumaque, J., Eynaud, F., Zaragosi, S., Marret, F., Matsuzaki, K.M., Kissel, C., Roche, D.M., Malaizé, B., Michel, E., Billy, I. and Richter, T., 2012. An ocean-ice coupled response during the last glacial: a view from a marine isotopic stage 3 record south of the Faeroe Shetland Gateway. Climate of the Past, 8(6).

Appendix

Table 12.BECS ID, depth (cm) UK37 index and the inferred temperatures based on the UK37 and Norwegian calibration only.

BECS ID	Depth	UK37	*Norway Temps (D'Andrea et al.,2016) UK = 0.0284 (T) – 0.655*
3464	964	-0.1427907	18.03553984
3465	956	-0.0753189	20.41130667
3466	950	-0.0451713	21.47284016
3467	946	-0.0072971	22.80644187
3468	945	-0.105076	19.3635219
3469	944	-0.1973955	16.11283534
3470	943	-0.1035963	19.41562356
3472	941	-0.4071308	8.727787271
3473	938	-0.1461533	17.91713726
3474	920	-0.024335	22.20651299
3475	912	-0.0886028	19.94356501
3476	904	-0.0455897	21.45810941
3477	900	-0.1676395	17.16058022
3478	899	-0.1287792	18.52890079
3479	898	-0.1185185	18.89019301
3480	896	-0.1635252	17.30545012
3481	895	-0.1655221	17.23513864
3482	892	-0.2079208	15.74222563
3483	884	-0.2300157	14.96423683
3484	876	-0.2569821	14.01471642
3485	868	-0.2804205	13.18941958
3486	865	-0.2740465	13.41385444
3487	864	-0.2285192	15.01692973
3488	863	-0.3562448	10.51955067
3489	862	-0.3357143	11.24245473
3490	861	-0.4271084	8.024350925
3491	860	-0.1586043	17.47872245
3492	856	-0.1655058	17.23571186
3493	852	-0.2350771	14.78601868
3494	848	-0.0127685	22.61378516
3497	842	0.46887603	39.57309965
3498	840	-0.5672269	3.090602438
3499	838	-0.5472619	3.793593441
3500	836	-0.4125461	8.537108258
3504	828	-0.0702479	20.58986148
3505	826	-0.0317417	21.94571653
3506	824	-0.6770251	-0.775533087
3507	822	-0.2651646	13.72659702
3508	820	-0.3842365	9.533927704
3509	819	-0.4628975	6.764171602
3510	811	-0.331307	11.39764117
3512	795	-0.4622853	6.785729312

Table 13. The samples for the Shebster basin including the depth (cm), UK37 index and the peak areas for the 37:4, 37:3a, 37:3b and the 37:32 Alkenones present.

BECS ID	Depth	UK37	37.4 (Area)	37.3a (Area)	37.3b (Area)	37.(a+b)(Area)	37.2 (Area)
3464	964	-0.1427907	128.5	152.9	120.58	273.48	62.217
3465	956	-0.0753189	310.7	643.2	328.7	971.9	199.1
3466	950	-0.0451713	148.6	387.3	187.8	575.1	110.9
3467	946	-0.0072971	205.96	294.5	420	714.5	197.8
3468	945	-0.105076	82.6	81.4	95.2	176.6	50.1
3469	944	-0.1973955	99	69.5	81.9	151.4	41.4
3470	943	-0.1035963	55.16	154.88	135.88	290.76	17.51
3471	942	**No Alkenones Present in this sample**					
3472	941	-0.4071308	125.31	35.94	56.4	92.34	26.08
3473	938	-0.1461533	77.3	98.08	71.2	169.28	36
3474	920	-0.024335	36.4	48.6	59.6	108.2	32.1
3475	912	-0.0886028	162.8	364.5	163.8	528.3	93.3
3476	904	-0.0455897	19.7	39.8	26.3	66.1	15.1
3477	900	-0.1676395	162.5	185.92	145.2	331.12	68.3
3478	899	-0.1287792	170.4	195.06	175	370.06	89.3
3479	898	-0.1185185	29.1	46.5	31.2	77.7	14.7
3480	896	-0.1635252	112.1	136.8	95.8	232.6	47.9
3481	895	-0.1655221	137.1	181.74	110.9	292.64	56.6
3482	892	-0.2079208	105.4	105	74.6	179.6	38.2
3483	884	-0.2300157	86.3	79.7	61.6	141.3	27.6
3484	876	-0.2569821	135.3	115.78	87.1	202.88	38.5
3485	868	-0.2804205	130.2	104.36	71.3	175.66	34.7
3486	865	-0.2740465	123	108.22	70.7	178.92	31.6
3487	864	-0.2285192	54.5	54.6	38	92.6	17
3488	863	-0.3562448	80.9				38.4
3489	862	-0.3357143	12	13.4		13.4	2.6
3490	861	-0.4271084	93.5		49.9	49.9	22.6
3491	860	-0.1586043	83.2	115.14	69.1	184.24	35.2
3492	856	-0.1655058	92.1	109.08	71.5	180.58	40.3
3493	852	-0.2350771	110.3	120.96	73.5	194.46	31.3
3494	848	-0.0127685	49.86	52.84	84.6	137.44	46.87
3495	846	**No Alkenones Present in this sample**					
3496	844	**No Alkenones Present in this sample**					
3497	842	0.46887603	11.59	7.11		7.11	38.33
3498	840	-0.5672269	28.6	4.8	5.14	9.94	4.3
3499	838	-0.5472619	19	2.2	4.16	6.36	3.31
3500	836	-0.4125461	16.19	2.1	3.8	5.9	5.01
3501	834	**No Alkenones Present in this sample**					
3502	832	**No Alkenones Present in this sample**					
3503	830	**No Alkenones Present in this sample**					
3504	828	-0.0702479	4.42	6.7		6.7	3.4
3505	826	-0.0317417	25.41	19.2	42.12	61.32	21.96
3506	824	-0.6770251	22.19	3.65		3.65	2.8
3507	822	-0.2651646	2.6	2.1		2.1	1.07
3508	820	-0.3842365	10.14	2.2		2.2	3.9
3509	819	-0.4628975	17	3.2	4.2	7.4	3.9
3510	811	-0.331307	17.8	8.2		8.2	6.9
3511	804	**No Alkenones Present in this sample**					
3512	795	-0.4622853	14.04	6.9	4.18	11.08	1.66
3513	787	**No Alkenones Present in this sample**					

Table 14. Depth of samples and the refined temperature reconstructions using the UK37 and R3b indices

Depth	LCA + RB3
964	8.72173585
956	9.84944643
950	3.4440288
946	9.57531008
941	8.72778727
920	14.7366308
899	13.2531869
892	15.6091637
884	14.9642368
876	14.0147164
868	13.1894196
865	13.4138544
864	15.0169297
863	10.5195507
862	11.2424547
861	8.02435092
852	14.7860187
840	3.09060244
838	3.79359344
836	8.53710826
822	12.8259275
820	12.6165803
819	12.1825432
811	11.3976412

OXCal Output: Shebster basin

```
Plot()
{
P_Sequence("",1,1,U(-2,2))
{
Boundary();
R_Date("Sheb-9",14180,70)
{
z=936;
};
R_Date("Sheb-15",11320,60)
{
z=875;
};
R_Date("Sheb-8",11020,50)
{
z=859;
};
R_Date("Sheb-14",10260,60)
{
z=848;
};
Boundary();
};
};
```

OxCal AMS Input: Loch of Sabiston

```
P_Sequence("Sabiston",1,0.5,U(-2,2))
 {
  Boundary("Core Base")
  {
   z=432;
  };
  Date("BORO-TEPHRA", N(calBP(14098),47))
  {
   z=383;
  };
  Date("PEN-TEPHRA", N(calBP(13939),66))
  {
   z=361;
  };
  R_Date("SUERC-67380",11988,48)
  {
   z=355;
  };
  R_Date("SUERC-67381",11074,44)
  {
   z=330;
  };
  Date("VEDDE-TEPHRA", N(calBP(12023),43))
  {
   z=293;
  };
  Date("SASK-TEPHRA", N(calBP(10176),49))
  {
   z=212;
  };
  R_Date("SUERC-67388",4790,38)
  {
   z=115;
  };
  R_Date("SUERC-67389",3460,36)
  {
   z=100;
  };
  Boundary();
 };
```

Oxcal out put for Lang Lochs

```
Plot()
{
P_Sequence("Lang Lochs",1,0.9,U(-2,2))
{
Boundary(Basal)
{
z=420;
};
R_Date("SUERC-87010",13410,52)
{
z=395;
};
R_Date("SUERC-87014",11790,46)
{
z=377;
};
R_Date("SUERC-87018",11479,45)
{
z=341;
};
R_Date("SUERC-87019",11402,45)
{
z=337;
};
R_Date("SUERC-87020",11236,44)
{
z=328;
};
R_Date("SUERC-87021",10003,42)
{
z=320;
};
R_Date("SUERC-87022",8825,40)
{
z=265;
};
R_Date("SUERC-87023",7325,39)
{
z=249;
};
Boundary(Top)
{
z=240;
};
};
```

Table 15. Sea Surface Temperatures (˚C) Globigerina pacaderma based inference model. Against age (cal yr BP) (Dokken et al (2015)

Ag	SST	Ag	SST	Ag	SST
9.983	10.6	11.791	9.1	12.063	3.2
10.022	11.3	11.807	6.2	12.068	4
10.034	11.2	11.812	5.2	12.073	4.6
10.124	11.8	11.817	6.8	12.073	3.6
10.162	12.1	11.827	2.5	12.078	3.5
10.209	11.3	11.832	4.3	12.083	3.1
10.218	11	11.838	5.1	12.088	1.2
10.256	10.3	11.843	3.5	12.093	1.9
10.275	10.4	11.848	4.5	12.098	3.3
10.303	11.1	11.853	3.3	12.114	3.2
10.312	10.4	11.858	3.6	12.129	4.2
10.341	10.7	11.863	3.9	12.134	3.8
10.35	10.3	11.868	6.4	12.144	3.3
10.446	9.9	11.873	4.7	12.155	3.7
10.47	9.5	11.878	4.5	12.16	1.7
10.566	9.8	11.884	3.7	12.17	3.6
10.59	9.4	11.889	4.3	12.187	3.3
10.71	10.1	11.894	4.3	12.204	2.1
10.734	9.7	11.899	3.3	12.221	3.6
10.758	10.1	11.904	5.2	12.247	2.4
10.782	9.9	11.909	3.1	12.264	3.6
10.806	9.4	11.919	2.6	12.289	3.6
10.83	9.7	11.93	3.6	12.298	1.9
10.854	8.8	11.935	2.3	12.315	2.7
10.878	8.9	11.94	3.7	12.332	3.1
10.902	9	11.945	6.2	12.349	2.8
10.926	9.3	11.95	1.7	12.366	2.7
10.974	9.5	11.96	4.3	12.391	3.4
11.022	10	11.971	6.5	12.417	3.3
11.038	9.4	11.976	7	12.442	2.8
11.054	7.5	11.986	8.1	12.451	4.2
11.07	7.9	11.991	8.3	12.519	2.1
11.085	8.6	11.996	8.5	12.527	3.8
11.101	7.3	12.001	7.5	12.545	3.9
11.117	8.2	12.006	5.8	12.57	3.3
11.133	7.7	12.011	6.3	12.578	2.8
11.149	8	12.017	5.4	12.595	3.5
11.165	7.2	12.027	5.4	12.604	3.7
11.18	7	12.032	3.9	12.629	3.4
11.196	8.3	12.037	3.2	12.646	3.4
		12.042	4.6	12.655	3.8
		12.047	3.1	12.672	3.3
		12.052	2.8	12.68	3.7

12.689	3.3
12.716	2.8
12.769	5.6
12.795	3.8
12.822	5.5
12.848	5.3
12.901	5.4
12.928	5.9
12.954	5.9
12.981	6.3
13.034	3.6
13.06	4.1
13.113	3.4
13.166	4.4
13.219	3.3
13.299	4.5
13.352	4
13.418	4.1
13.431	3.9
13.482	5.5
13.508	4.4
13.547	4.1
13.573	4.3
13.612	4.3
13.663	4.5
13.718	4.2
13.776	4
13.82	3.3
13.849	3.9
13.908	3.7
13.937	3.6
13.966	4.3
13.98	4.4
14.039	4.6
14.082	3.5
14.111	3.9
14.133	2.7
14.161	3.8
14.175	3.8
14.189	3.1
14.202	4.7
14.216	6.5
14.23	3.7
14.244	2.7
14.265	3.6
14.279	4
14.3	4.2
14.314	4.4
14.328	4.6
14.348	7.5
14.362	6.9
14.369	6.3
14.383	7.8
14.438	9.3
14.505	6.1
14.554	8.6
14.583	5.4
14.612	5.6
14.656	5.3
14.701	6.2
14.73	6.8
14.774	7.2
14.803	6.4
14.847	5.7
14.877	5.7
14.921	5.2
14.98	6.4
15.024	4.5
15.053	3.5
15.082	5
15.126	3.1
15.156	5.1
15.2	3.7
15.229	5.7
15.259	4.5
15.273	7.6
15.332	6.5
15.337	3.9
15.342	4.5
15.347	4.9
15.352	5.6
15.355	3
15.357	3.9
15.36	3.5
15.362	3.7
15.369	4.2
15.372	3.9
15.374	3.9
15.377	4.3
15.38	3
15.383	4
15.388	3.4
15.393	4.2
15.397	4.2
15.4	3.5
15.403	3.4
15.408	4.1
15.412	3
15.421	3.3
15.469	4.9
15.505	4
15.517	3.8
15.523	1.6
15.541	3.5
15.565	5.6
15.583	3.5
15.601	5.3
15.619	6.4
15.651	4.1
15.706	3
15.734	4.3
15.761	4.4
15.789	3.4
15.872	4.9
15.913	3
15.996	3.8
16.081	3.2

Table 16. The identified chironomid taxa in the Shebster basin (%). The taxa names are shown on the left and the depth (cm) on the top.

Chironomids	Column1	Column2	Column3	Column4	Column5	Column6	786	788	790	792	794	796	798	801	804	806	808	810	813	816	818	820	822	824	826	828	830	833	836	838	840	8
Code	Name	Element	Units	Context	Taphonomy	Group																										
Insig	Microspectra insignilobus					B	0	0	0	0	0	0	0	0	0	0	0	0	0	2.2	6.8	0	13.2	3.2	0	6.1	5.9	5.2	5.6	1.9	13.2	2.8
Pedel	Microtendipes pedellus					C	9.4	0	5.2	6.9	8.2	2	3.3	8.9	20	12.5	15.7	8.3	3.4	16.4	1.6	9.4	4.3	0	0	0	0	0	0	0	0	0
Oliv	Corynocera oliveri					B	0	0	0	0	0	0	3.3	1.8	2	0	0	0	0	0	0	1.9	9.7	19.4	18.4	5.9	22.4	7.4	1.9	7.5	5.6
Nerv	Dicrotendipes nervosus					D	1.9	1.9	0	1.7	12.2	12.2	20	5.4	6	7.1	7.8	4.2	3.4	13.7	3.3	11.3	0	0	0	0	0	0	0	0	0	0
Proclad	Procladius					D	1.9	0	5.2	1.7	6.1	18.4	0	1.8	0	0	0	2.1	2.2	1.4	0	0	0	0	0	0	0	0	0	0	0	0
Glab	Tanytarsus glabrescens					D	17	20.4	6.9	0	0	0	0	0	8	3.6	11.8	0	0	0	0	0	0	0	0	0	0	0	0	0	0	0
TanyPall	Tanytarsus pallidicornis					D	1.9	5.6	5.2	10.3	26.5	6.1	0	7.1	4	1.8	9.8	2.1	7.9	4.1	0	7.5	0	0	0	0	0	0	0	0	0	0
Sordi	Psectorcladius sordidellus					B	28.3	31.5	17.2	6.9	10.2	4.1	16.7	8.9	6	8.9	7.8	35.4	50.6	8.2	41	22.6	3.2	0	0	0	0	0	0	1.9	0
Cricto	Crictopus intersectus					B	1.9	0	1.7	0	12.2	4.1	3.3	0	4	3.6	2	14.6	3.4	8.2	4.9	0	3.2	25.8	18.4	39.2	32.8	18.5	25	24.5	29.2
PsecSept	Psectrocladius septentrionalis					B	1.9	7.4	1.7	0	0	0	0	0	0	0	0	0	0	0	3.3	7.5	0	0	0	0	0	0	0	0	0	0
Ambig	Corynocera ambigua					B	0	1.9	13.8	62.1	6.1	2	10	14.3	16	21.4	0	8.3	0	19.2	0	3.8	48.4	1.6	0	0	0	0	0	0	0	0
Calc	Psectrocladius calcaratus					B	0	0	0	0	0	0	0	0	0	0	0	0	0	0	0	0	0	0	0	0	0	0	0	0	0	0
Lugens	Tanytarsus lugens					A	0	0	1.7	0	0	0	0	0	0	0	0	0	0	0	0	0	8.6	9.7	0	5.9	3.4	9.3	5.8	11.3	0
Sergent	Sergentia coracina					B	0	0	6.9	0	0	0	0	0	0	0	0	0	3.4	0	1.6	0	3.2	9.7	12.2	9.8	6.9	20.4	25	7.5	36.1
Conform	Hydrobeanus conformis					A	0	0	0	0	0	0	0	0	0	0	0	0	0	0	0	0	1.1	1.6	0	3.9	3.4	3.7	7.7	0	0
Pagast	Pagastiella					D	0	0	1.7	1.7	2	0	0	3.6	0	0	0	0	0	0	0	0	0	0	0	0	0	0	0	0	0
Paraclad	Paracladius					A	0	0	1.7	0	0	0	0	0	0	0	0	0	0	1.4	0	0	0	0	0	0	0	0	0	0	0
Barb	Psectrocladius barbimanus					B	0	0	0	0	0	0	0	0	0	0	0	0	0	0	0	0	0	0	0	0	0	0	0	0	0
Anthra	Chironomus anthracinus					D	1.9	0	0	0	0	0	0	0	2	0	2	0	6.7	1.4	19.7	1.9	3.2	0	0	0	0	0	0	0	0
Mendx	Tanytarsus mendax					D	11.3	13	6.9	1.7	2	16.3	16.7	17.9	12	16.1	25.5	8.3	2.2	9.6	8.2	3.8	2.2	0	0	0	0	0	0	0	1.4
Radial	Microspectra radialis					A	0	0	0	0	0	0	0	0	2	0	0	0	1.1	1.4	1.6	1.9	2.2	24.2	40.8	27.5	24.1	35.2	25	26.4	19.4
Syl	Crictopus sylvestris					C	0	1.9	0	1.7	0	0	0	0	0	0	0	0	0	0	0	0	0	0	0	0	0	0	0	0	0
Ablab	Ablabesmyia					D	15.1	13	13.8	1.7	0	2	0	3.6	0	0	3.9	8.3	10.1	5.5	0	13.2	4.3	0	0	0	0	0	0	0	0
OrthoS	Orthocladius S					A	0	0	1.7	0	0	0	0	0	0	0	2	0	0	0	9.8	0	0	0	0	0	0	0	0	0	0
OrthoTrig	Orthocladius trigonolabis					A	0	0	0	0	0	0	0	0	0	0	0	0	0	0	0	0	0	0	0	0	0	0	0	0	0
Smit	Smittia					C	0	0	0	0	0	0	0	0	0	0	0	0	0	0	0	0	0	0	0	0	0	0	0	0	0
Chaeotpig	Chaeotocladius piger					C	0	0	1.7	0	6.1	4.1	0	3.6	0	1.8	0	0	0	0	3.3	0	0	0	0	0	0	0	0	0	0
ParaAust	Paratanytarsus austriacus					C	0	0	0	0	0	0	0	0	0	0	0	2.1	0	2.7	1.6	1.9	1.1	8.1	2	0	0	0	5.8	3.8	0
CrictLar	Crictopus laricomalis					C	0	0	0	0	0	0	0	0	0	0	0	0	0	0	0	0	0	0	0	0	0	0	0	0	0
Sympo	Symposiocladius					C	0	0	0	0	2	0	0	3.6	2	0	2	0	0	0	0	0	0	0	0	0	0	0	0	0	0
CricoTri	Crictopus trifasciatus					C	0	0	0	0	0	0	0	0	0	0	0	0	0	0	0	0	0	0	0	0	0	0	0	0	0
Tanychin	Tanytarsus chinyensis					A	0	0	0	0	2	2	0	1.8	2	0	0	0	0	0	0	0	0	0	0	0	0	0	0	0	0
RheoChal	Rheocrictopus chalybeatus					C	0	0	0	0	0	0	0	0	0	0	0	0	0	0	0	0	0	0	0	0	0	0	0	0	0
Protany	Protanypus					A	0	0	0	0	0	0	0	0	0	0	0	0	0	0	0	0	1.1	0	2	0	1.7	0	1.9	0	1.4
Pseudodi	Pseudodiamesa					A	1.9	1.9	3.4	0	0	0	0	0	0	0	0	0	0	0	0	0	1.1	0	0	2	0	0	0	3.8	4.2
OrthoCon	Orthocladius consobrinus					A	0	0	0	0	0	0	0	0	0	0	0	0	0	0	0	0	0	0	0	0	0	0	0	0	0
CrictoC	Crictopus C					B	0	0	0	0	0	0	0	0	0	0	0	0	0	0	0	0	0	0	0	0	0	0	0	0	0
Synorth	Synorthocladius					B	0	0	0	0	0	0	0	0	0	1.8	0	0	0	0	0	0	0	0	0	0	0	0	0	0	0
Proplac	Propsilocerus lacustris					B	0	0	0	0	0	0	0	0	0	0	2	4.2	2.2	0	0	0	0	0	0	0	0	0	0	0	0
Endotend	Endochironomous tendens					C	0	0	0	0	0	0	0	0	0	0	0	2.1	1.1	0	0	0	0	0	0	0	0	0	0	0	0
Endoalb	Endochironomous albipennis					C	0	0	0	1.7	2	12.2	13.3	3.6	12	14.3	5.9	0	0	0	0	0	0	0	0	0	0	0	0	0	0
Cladolat	Cladopelma lateralis					C	0	0	0	0	0	0	0	0	2	7.1	2	0	0	0	0	0	0	0	0	0	0	0	0	0	0
Parapen	Paratanytarsus penicillatus					C	1.9	0	0	0	0	2	10	12.5	0	0	0	0	0	0	0	0	0	0	0	0	0	0	0	0	0
Polyped	Polypedilum nubifer					D	0	0	0	0	0	0	8.2	3.3	1.8	0	0	0	0	0	0	0	0	0	0	0	0	0	0	0	0
Paraalb	Paratentipes albimanus					D	0	0	1.7	0	0	2	0	0	0	0	0	0	0	0	0	0	0	0	0	0	0	0	0	0	0
Crypto	Cryptochironomous					D	0	0	0	0	0	0	2	0	0	0	0	0	0	0	0	0	0	0	0	0	0	0	0	0	0
Orthol	Orthocladius I					C	3.8	0	0	1.7	2	0	0	0	0	0	0	0	0	0	0	0	0	0	0	0	0	0	0	0	0
ChaetoB	Chaetocladius B					A	0	1.9	1.7	0	0	0	0	0	0	0	0	0	0	0	0	0	0	0	0	0	0	0	0	0	0

Chironomids	Column1	Column2	Column3	Column4	Column5	C	842	844	846	848	850	852	854	856	858	859	860	861	862	864	865	866	868	870	872	874	876	878	880	882	884	888	890	892	894	896	8
Code	Name	Element	Units	Context	Taphonomy																																
Insig	Microspectra insignilobus					Bi	0	3	1.6	0	11.7	0	1.7	0	10.7	6.8	11.4	18	6.1	8.4	4.2	7.3	11.4	10	3.1	1.6	7.9	1.4	0	7.4	1.4	2.2	0	3.8	7.4	7.3	
Pedel	Microtendipes pedellus					Ci	0	0	0	0	0	9.9	13.8	19.4	4.9	9.5	0	0	0	0	0	3.6	3.8	2.9	3.1	6.3	4.8	2.7	6.9	5.9	18.1	8.9	7.8	0	0	0	
Oliv	Corynocera oliveri					Bi	0	0	1.6	0	0	11.3	3.4	1	0	4.1	5.7	14	1	0	4.2	0	0	2.9	3.1	0	0	0	0	0	0	2.2	1.6	0	0	7.3	
Nerv	Dicrotendipes nervosus					Di	0	0	0	0	0	0	3.4	5.8	2.9	2.7	0	0	0	0	0	0	0	0	3.1	3.1	6.3	5.4	0	0	2.8	3.3	3.1	0	13	0	
Proclad	Procladius					Di	0	0	0	0	0	1.4	1.7	1	1	0	1.9	0	0	0	0	0	5.1	1.4	1.6	0	0	1.4	0	1.5	0	4.4	1.6	3.8	0	3.6	
Glab	Tanytarsus glabrescens					Di	0	0	0	0	0	0	0	0	0	0	0	0	0	0	0	0	0	0	0	0	0	0	0	0	0	0	1.6	0	0	0	
TanyPall	Tanytarsus pallidicornis					Di	0	0	0	0	0	1.4	1.7	1	1	0	0	2	0	0.8	1.4	0	5.1	2.9	1.6	0	1.6	0	3.4	1.5	0	0	0	5.7	3.7	12.7	
Sordi	Psectorcladius sordidellus					Bi	0	0	1.6	2.4	5	4.2	3.4	4.9	3.9	2.7	7.6	0	9.2	0.8	22.2	36.4	30.4	30	31.3	37.5	20.6	39.2	24.1	29.4	15.3	24.4	18.8	37.7	13	20	
Cricto	Crictopus intersectus					Bi	21.3	7.6	36.1	16.7	3.3	0	1.7	0	1	0	0	0	0	0.8	0	0	1.3	0	1.6	0	0	0	0	5.9	2.8	0	1.6	1.9	5.6	0	
PsecSept	Psectrocladius septentrionalis					Bi	0	0	0	0	0	0	0	1	0	4.1	0	0	0	0	0	3.6	3.8	1.4	4.7	1.6	0	2.7	1.7	0	4.2	0	6.3	1.9	3.7	5.5	
Ambig	Corynocera ambigua					Bi	0	0	0	0	41.7	32.4	36.2	35.9	29.1	44.6	50.5	60	64.3	69.7	27.8	7.3	5.1	10	3.1	6.3	4.8	4.1	3.4	5.9	1.4	10	12.5	7.5	13	18.2	
Calc	Psectrocladius calcaratus					Bi	0	0	0	0	0	0	0	0	0	0	0	0	0	0	0	0	0	0	0	0	0	0	0	0	0	1.1	0	0	0	0	
Lugens	Tanytarsus lugens					Al	0	0	1.6	0	1.7	1.4	0	2.9	6.8	1.4	3.8	0	3.1	1.7	4.2	7.3	0	2.9	1.6	3.1	0	0	1.7	0	0	0	1.6	0	0	0	
Sergent	Sergentia coracina					Bi	46.8	54.5	32.8	40.5	16.7	9.9	15.5	4.9	5.8	6.8	1	2	2	5	18.1	18.2	8.9	5.7	6.3	0	6.3	5.4	3.4	7.4	9.7	4.4	6.3	3.8	7.4	7.3	
Conform	Hydrobeanus conformis					Al	6.4	7.6	3.3	2.4	1.7	0	0	0	0	0	1	0	0	0	0	0	0	0	0	0	0	0	0	0	0	0	0	0	0	0	
Pagast	Pagastiella					Di	0	0	0	0	0	0	0	0	0	0	0	0	0	0	0	1.8	1.3	0	0	1.6	0	0	0	0	0	1.1	0	0	0	0	
Paraclad	Paracladius					Al	0	0	0	0	0	1.4	0	0	1	1.4	0	0	5.1	3.4	0	0	0	0	0	0	0	0	0	0	0	0	0	0	1.9	1.8	
Barb	Psectrocladius barbimanus					Bi	0	0	0	0	0	1.4	0	0	0	0	0	0	0	0	0	0	0	0	0	0	0	0	0	0	0	0	0	0	0	0	
Anthra	Chironomus anthracinus					Di	0	0	0	0	0	4.2	0	10.7	10.7	9.5	3.8	2	2	0.8	5.6	3.6	7.6	7.1	3.1	1.6	27	5.4	20.7	7.4	4.2	6.7	7.8	11.3	13	9.1	
Mendx	Tanytarsus mendax					Di	0	0	0	0	0	5.6	1.7	5.8	1.9	1.4	1.9	0	0	0	1.4	1.8	1.3	0	0	9.4	0	2.7	0	0	0	4.4	4.7	0	0	0	
Radial	Microspectra radialis					Al	19.1	19.7	9.8	14.3	6.7	0	0	2.9	1	0	1.9	0	1	0.8	0	0	0	1.4	0	4.7	0	0	0	2.9	1.4	0	0	0	0	3.6	
Syl	Crictopus sylvestris					Ci	0	0	0	0	0	1.4	0	0	0	0	0	0	0	0	0	0	0	0	0	0	0	0	0	0	0	0	0	0	1.9	0	0	
Ablab	Ablabesmyia					Di	0	0	0	0	0	1.4	1.7	1	0	0	0	0	0	0.8	0	0	3.8	1.4	6.3	1.6	1.6	4.1	3.4	4.4	4.2	0	1.6	0	0	0	
Ortho5	Orthocladius 5					Al	4.3	3	9.8	14.3	3.3	8.5	6.9	0	0	2.7	1.9	2	6.1	6.7	9.7	7.3	7.6	18.6	25	21.9	12.7	24.3	22.4	11.8	33.3	20	14.1	15.1	3.7	0	
OrthoTrig	Orthocladius trigonolabis					Al	0	0	0	0	0	0	0	0	0	0	0	0	0	0	0	0	0	0	0	0	0	0	0	0	0	0	3.1	5.7	0	0	
Smit	Smittia					Ci	0	0	0	0	0	0	0	0	0	0	0	0	0	0	0	0	0	0	0	0	0	0	0	0	0	0	0	0	0	0	
Chaeotpig	Chaeotocladius piger					Ci	0	0	0	2.4	0	0	1.7	0	1	0	0	0	0	0	0	0	0	0	0	0	0	0	0	0	0	0	0	0	0	0	
ParaAust	Paratanytarsus austriacus					Ci	0	1.5	0	0	1.7	2.8	5.2	1.9	12.6	2.7	7.6	0	0	0	0	0	1.3	0	0	0	3.2	0	6.9	5.9	1.4	5.6	4.7	0	9.3	0	
CrictLar	Crictopus laricomalis					Ci	0	0	0	0	0	0	0	0	0	0	0	0	0	0	0	0	0	0	0	0	0	0	0	0	0	0	0	0	3.7	1.8	
Sympo	Symposiocladius					Ci	0	0	0	4.8	0	0	0	0	0	0	0	0	0	0	0	0	2.5	0	0	0	3.2	0	1.7	1.5	0	1.1	1.6	0	1.9	1.8	
CricoTri	Crictopus trifasciatus					Ci	0	0	0	0	0	1.4	0	0	0	0	0	0	0	0	0	0	0	0	1.6	0	0	1.4	0	0	0	0	0	0	0	0	
Tanychin	Tanytarsus chinyensis					Al	0	0	0	0	0	0	0	0	0	0	0	0	0	0	0	1.8	0	1.4	0	0	0	0	0	1.5	0	0	0	0	0	0	
RheoChal	Rheocrictopus chalybeatus					Ci	0	0	0	0	0	0	0	0	0	0	0	0	0	0	1.4	0	0	0	0	0	0	0	0	0	0	0	0	0	0	0	
Protamy	Protanypus					Al	2.1	0	0	2.4	6.7	0	0	0	0	0	0	0	0	0	0	0	0	0	0	0	0	0	0	0	0	0	0	0	0	0	
Pseudodi	Pseudodiamesa					At	0	3	1.6	0	0	0	0	0	0	0	0	0	0	0	0	0	0	0	0	0	0	0	0	0	0	0	0	0	0	0	
OrthoCon	Orthocladius consobrinus					Al	0	0	0	0	0	0	0	0	1	0	0	0	0	0	0	0	0	0	0	0	0	0	0	0	0	0	0	0	0	0	
CrictoC	Crictopus C					Bi	0	0	0	0	0	0	0	0	3.9	0	0	0	0	0	0	0	0	0	0	0	0	0	0	0	0	0	0	0	0	0	
Synorth	Synorthocladius					Bi	0	0	0	0	0	0	0	0	0	0	0	0	0	0	0	0	0	0	0	0	0	0	0	0	0	0	0	0	0	0	
Proplac	Propsilocerus lacustris					Bi	0	0	0	0	0	0	0	0	0	0	0	0	0	0	0	0	0	0	0	0	0	0	0	0	0	0	0	0	0	0	
Endotend	Endochironomus tendens					Ci	0	0	0	0	0	0	0	0	0	0	0	0	0	0	0	0	0	0	0	0	0	0	0	0	0	0	0	0	0	0	
Endoalb	Endochironomus albipennis					Ci	0	0	0	0	0	0	0	0	0	0	0	0	0	0	0	0	0	0	0	0	0	0	0	0	0	0	0	0	0	0	
Cladolat	Cladopelma lateralis					Ci	0	0	0	0	0	0	0	0	0	0	0	0	0	0	0	0	0	0	0	0	0	0	0	0	0	0	0	0	0	0	
Parapen	Paratanytarsus penicillatus					Ci	0	0	0	0	0	0	0	0	0	0	0	0	0	0	0	0	0	0	0	0	0	0	0	0	0	0	0	0	0	0	
Polyped	Polypedulim nubifer					Di	0	0	0	0	0	0	0	0	0	0	0	0	0	0	0	0	0	0	0	0	0	0	0	0	0	0	0	0	0	0	
Paraalb	Paratentipes albimanus					Di	0	0	0	0	0	0	0	0	0	0	0	0	0	0	0	0	0	0	0	0	0	0	0	0	0	0	0	0	0	0	
Crypto	Cryptochironomous					Di	0	0	0	0	0	0	0	0	0	0	0	0	0	0	0	0	0	0	0	0	0	0	0	0	0	0	0	0	0	0	
Orthol	Orthocladius I					Oi	0	0	0	0	0	0	0	0	0	0	0	0	0	0	0	0	0	0	0	0	0	0	0	0	0	0	0	0	0	0	
ChaetoB	Chaetocladius B					Al	0	0	0	0	0	0	0	0	0	0	0	0	0	0	0	0	0	0	0	0	0	0	0	0	0	0	0	0	0	0	

Chironomids	Column1	Column2	Column3	Column4	Column5	C	898	900	902	904	906	908	910	912	914	916	918	920	922	924	926	928	930	932	934	936	938	939	940	941	942	943	944	945	946	948	950	952	954	956	958	960	962	964
Code	Name	Element	Units	Context	Taphonomy																																								
Insig	Microspectra insignilobus					B	7.3	10.5	6.7	6.2	7.8	5.6	2.5	0	0	9.1	4.7	0	3.8	1.4	0	0	0	0	1.5	4.8	1.4	1.9	31	45.9	30.4	38.8	45.2	21.4	3	0	1.6	0	0	0	0	0	0	0
Pedel	Microtendipes pedellus					C	3.6	0	3.3	0	15.7	9.7	2.5	5	0	6.8	9.3	0	1.3	4.2	8.6	7.7	0	3.2	0	6.3	1.4	1.9	0	0	0	0	0	8.3	12.1	24.2	13.1	9.9	5.1	17.7	5.8	7.2	11.9	14.9
Oliv	Corynocera oliveri					B	3.6	0	6.7	0	0	0	0	0	0	0	0	0	0	1.4	5.7	0	0	3.2	0	0	0	1	12.1	9.8	26.1	4.9	17.7	3.6	0	0	0	0	0	0	0	0.7	0	0
Nerv	Dicrotendipes nervosus					D	0	0	0	0	0	0	0	0	5.5	4.5	2.3	11.1	0	0	0	0	0	0	0	0	0	0	0	0	0	0	0	0	0	0	0	0	0	2.5	1.9	5.8	0	0
Proclad	Procladius					D	5.5	1.1	0	1.5	0	0	0	5	0	6.8	0	0	1.3	0	0	0	4.9	1.6	0	4.8	1.4	0	0	0	0	0	0	1.2	4.5	1.5	0	1.4	0	3.8	1	2.2	0.7	3.4
Glab	Tanytarsus glabrescens					D	0	0	0	0	0	0	0	0	0	0	0	0	0	0	0	0	0	0	0	0	0	8.6	0	0	0	0	0	0	0	0	0	0	0	0	0	0	0	0
TanyPall	Tanytarsus pallidicornis					D	5.5	4.2	10	0	0	4.2	0	10	3.6	11.4	2.3	13.3	6.4	14.1	5.7	3.1	8.2	11.3	8.8	14.3	8.5	1.9	6.9	0	1.4	0	0	14.3	9.1	9.1	16.4	4.2	16.5	3.8	3.9	6.5	8.1	12.6
Sordi	Psectorcladius sordidellus					B	23.6	13.7	26.7	50.8	31.4	30.6	42.5	32.5	34.5	29.5	46.5	35.6	46.2	26.8	37.1	24.6	26.2	43.5	44.1	15.9	60.6	20	12.1	0	7.2	0	0	10.7	28.8	22.7	39.3	23.9	31.6	27.8	37.9	33.8	38.5	35.6
Cricto	Cricotopus intersectus					B	0	0	5	1.5	3.9	1.4	0	0	5.5	0	0	0	0	1.4	2.9	6.2	6.6	4.8	0	0	0	4.8	5.2	9.8	10.1	6.8	9.7	1.2	3	12.1	0	9.9	8.9	1.3	1	3.6	4.4	0
PsecSept	Psectrocladius septentrionalis					B	1.8	2.1	1.7	1.5	0	0	0	0	0	0	9.3	2.2	5.1	2.8	0	0	0	0	0	0	0	0	0	0	0	0	0	0	0	1.5	0	0	0	0	0	0	0	1.1
Ambig	Corynocera ambigua					B	29.1	47.4	16.7	13.8	2	25	15	7.5	5.5	0	14	11.1	5.1	1.4	0	0	0	0	1.5	0	2.8	37.1	15.5	0	0	0	0	0	0	0	0	0	0	0	0	0	0	0	0	2.3
Calc	Psectrocladius calcaratus					B	0	0	0	1.5	0	0	0	0	0	0	0	0	0	1.4	0	0	1.6	0	11.8	0	0	0	1.7	0	0	0	0	0	0	0	0	0	0	2.5	8.7	11.5	0.7	1.1
Lugens	Tanytarsus lugens					A	0	6.3	1.7	4.6	13.7	1.4	0	0	0	0	0	0	0	0	0	0	0	0	0	0	0	11.4	3.4	1.6	0	13.6	0	4.8	0	0	0	0	0	1.3	0	0	0	0
Sergent	Sergentia coracina					B	7.3	0	3.3	4.6	2	9.7	0	10	5.5	0	0	0	0	1.4	0	0	0	0	0	0	0	0	1.7	9.8	17.4	17.5	1.6	6	0	0	0	0	0	0	0	0	0	0	0
Conform	Hydrobaenus conformis					A	0	0	0	0	0	0	0	0	0	0	0	0	0	0	0	1.5	0	0	0	0	0	0	0	0	0	0	0	0	0	0	0	0	0	0	0	0	0	0
Pagast	Pagastiella					D	0	0	1.7	1.5	0	0	0	0	9.1	2.3	0	2.2	3.8	1.4	0	0	0	0	0	0	0	0	0	0	0	0	0	0	0	0	0	0	0	0	0	0	0	0	0
Paraclad	Paracladius					A	1.8	5.3	0	0	0	0	0	0	0	0	0	0	0	1.4	0	4.6	1.6	3.2	1.5	0	0	0	1.7	4.9	7.2	3.9	11.3	0	0	0	0	0	0	0	4.9	0	3	2.3
Barb	Psectrocladius barbimanus					B	0	0	0	0	0	0	0	0	0	0	0	0	0	0	0	0	0	0	0	0	0	0	0	0	0	0	0	0	0	0	0	0	0	0	0	0	0	0
Anthra	Chironomus anthracinus					D	10.9	6.3	10	1.5	15.7	12.5	12.5	15	7.3	13.6	9.3	13.3	12.8	22.5	20	27.7	11.5	6.5	5.9	19	2.8	5.7	3.4	1.6	0	3.9	1.6	26.2	24.2	15.2	21.3	35.2	16.5	17.7	20.4	11.5	17.8	6.9
Mendx	Tanytarsus mendax					D	0	0	1.7	1.5	0	0	7.5	2.5	1.8	2.3	0	0	0	1.4	0	1.5	3.3	1.6	4.4	9.5	4.2	1.9	5.2	0	0	0	0	1.2	3	4.5	0	7	8.9	6.3	9.7	13.7	14.1	8
Radial	Microspectra radialis					A	0	0	0	0	0	0	0	0	0	0	0	0	0	9.9	2.9	9.2	1.6	6.5	0	4.8	0	0	0	0	8.2	0	10.7	12.9	0	0	1.5	0	0	0	0	0	0	0	0
Syl	Cricotopus sylvestris					C	0	0	0	0	0	0	0	0	0	0	0	0	0	0	0	0	0	0	0	0	0	0	0	0	0	0	0	0	0	7.6	1.5	0	0	0	0	0.7	0	0
Ablab	Ablabesmyia					D	0	1.1	0	1.5	0	0	0	5	7.3	4.5	2.3	6.7	1.3	0	2.9	6.2	16.4	6.5	17.6	7.9	9.9	1	0	0	0	0	0	0	4.5	6.1	8.2	1.4	8.9	10.1	1	0.7	0.7	9.2
OrthoS	Orthocladius S					A	0	2.1	1.7	7.7	7.8	0	17.5	7.5	7.3	9.1	0	4.4	12.8	0	0	0	0	0	2.9	0	7	2.9	0	0	0	0	0	0	0	0	0	7	3.8	5.1	3.9	2.2	0	0
OrthoTrig	Orthocladius trigonolabis					A	0	0	0	0	0	0	0	0	0	0	0	0	0	7	14.3	6.2	18	8.1	0	12.7	0	0	0	8.2	0	0	0	1.2	0	0	0	0	0	0	0	0	0	0
Smit	Smittia					C	0	0	0	0	0	0	0	0	0	0	0	0	0	0	0	1.5	0	0	0	0	0	0	0	0	0	0	0	0	0	0	0	0	0	0	0	0	0	0	0
Chaeotpig	Chaetocladius piger					C	0	0	0	0	0	0	0	0	0	0	0	0	0	0	0	0	0	0	0	0	0	0	0	0	0	0	0	0	0	0	0	0	0	0	0	0	0	2.3
ParaAust	Paratamytarsus austriacus					C	0	0	3.3	0	0	0	0	0	5.5	0	0	0	0	0	0	0	0	0	0	0	0	0	0	0	0	0	0	0	0	0	0	0	0	0	0	0	0	0	0
CrictLar	Cricotopus laricomalis					C	0	0	0	0	0	0	0	0	0	0	0	0	0	0	0	0	0	0	0	0	0	0	0	0	0	0	0	0	0	0	0	0	0	0	0	0	0	0
Sympo	Symposiocladius					C	0	0	0	0	0	0	0	0	1.8	0	0	0	0	0	0	0	0	0	0	0	0	0	0	0	0	0	0	0	0	0	0	0	0	0	0	0	0	0
CricoTri	Cricotopus trifasciatus					C	0	0	0	0	0	0	0	0	0	0	0	0	0	0	0	0	0	0	0	0	0	0	0	0	0	0	0	0	0	0	0	0	0	0	0	0	0	0
Tanychin	Tanytarsus chinyensis					A	0	0	0	0	0	0	0	0	0	0	0	0	0	0	0	0	0	0	0	0	0	0	0	0	0	0	0	0	0	0	0	0	0	0	0	0	0	0
RheoChal	Rheocricotopus chalybeatus					C	0	0	0	0	0	0	0	0	0	0	0	0	0	0	0	0	0	0	0	0	0	0	0	0	0	0	0	0	0	0	0	0	0	0	0	0	0	0
Protany	Protanypus					A	0	0	0	0	0	0	0	0	0	0	0	0	0	0	0	0	0	0	0	0	0	0	0	0	0	0	0	0	0	0	0	0	0	0	0	0	0	0
Pseuddi	Pseudodiamesa					A	0	0	0	0	0	0	0	0	0	0	0	0	0	0	0	0	0	0	0	0	0	0	0	0	0	0	0	0	0	0	0	0	0	0	0	0	0	0
OrthoCon	Orthocladius consobrinus					A	0	0	0	0	0	0	0	0	0	0	0	0	0	0	0	0	0	0	0	0	0	0	0	0	0	0	0	0	0	0	0	0	0	0	0	0	0	0
CrictoC	Cricotopus C					B	0	0	0	0	0	0	0	0	0	0	0	0	0	0	0	0	0	0	0	0	0	0	0	0	0	0	0	0	0	0	0	0	0	0	0	0	0	0
Synorth	Synorthocladius					B	0	0	0	0	0	0	0	0	0	0	0	0	0	0	0	0	0	0	0	0	0	0	0	0	0	0	0	0	0	0	0	0	0	0	0	0	0	0
Proplac	Propsilocerus lacustris					B	0	0	0	0	0	0	0	0	0	0	0	0	0	0	0	0	0	0	0	0	0	0	0	0	0	0	0	0	0	0	0	0	0	0	0	0	0	0
Endotend	Endochironomous tendens					C	0	0	0	0	0	0	0	0	0	0	0	0	0	0	0	0	0	0	0	0	0	0	0	0	0	0	0	0	0	0	0	0	0	0	0	0	0	0
Endoalb	Endochironomous albipennis					C	0	0	0	0	0	0	0	0	0	0	0	0	0	0	0	0	0	0	0	0	0	0	0	0	0	0	0	0	0	0	0	0	0	0	0	0	0	0
Cladolat	Cladopelma lateralis					C	0	0	0	0	0	0	0	0	0	0	0	0	0	0	0	0	0	0	0	0	0	0	0	0	0	0	0	0	0	0	0	0	0	0	0	0	0	0
Parapen	Paratamytarsus penicillatus					C	0	0	0	0	0	0	0	0	0	0	0	0	0	0	0	0	0	0	0	0	0	0	0	0	0	0	0	0	0	0	0	0	0	0	0	0	0	0
Polyped	Polypedilum nubifer					D	0	0	0	0	0	0	0	0	0	0	0	0	0	0	0	0	0	0	0	0	0	0	0	0	0	0	0	0	0	0	0	0	0	0	0	0	0	0
Paraalb	Paratentipes albimanus					D	0	0	0	0	0	0	0	0	0	0	0	0	0	0	0	0	0	0	0	0	0	0	0	0	0	0	0	0	0	0	0	0	0	0	0	0	0	0
Crypto	Cryptochironomous					D	0	0	0	0	0	0	0	0	0	0	0	0	0	0	0	0	0	0	0	0	0	0	0	0	0	0	0	0	0	0	0	0	0	0	0	0	0	0
Orthol	Orthocladius I					C	0	0	0	0	0	0	0	0	0	0	0	0	0	0	0	0	0	0	0	0	0	0	0	0	0	0	0	0	0	0	0	0	0	0	0	0	0	0
ChaetoB	Chaetocladius B					A	0	0	0	0	0	0	0	0	0	0	0	0	0	0	0	0	0	0	0	0	0	0	0	0	0	0	0	0	0	0	0	0	0	0	0	0	0	0

Table 17. The identified chironomid taxa from Loch of Sabiston (%). Depth in cm shown above with the taxa name on the left.

Chironomids	Column1	Column2	Column3	Column4	Column5	Column6	182	198	214	216	218	220	222	224	226	228	230	232	234	236	23
Code	Name	Element	Units	Context	Taphonomy	Group															
Insig	Microspectra insignilobus					B	0	0	0	0	3.3	1.7	1.4	8.3	3.2	4.5	0	0	1	1.9	
Pedel	Microtendipes pedellus					C	0	0.8	0	7.3	4.9	8.5	6.8	10.4	4.8	0	0	13.1	6.2	5.6	
Oliv	Corynocera oliveri					B	0	0	1.6	0	0	0	0	0	0	0	3.9	0	0	0	
Macpel	Macropelopia					C	0	0	0	0	0	0	0	0	0	0	3.9	0	0	0	
Monopel	Monopelopia					C	0	0	0	0	0	0	0	0	0	0	0	0	0	0	
Lars	Larsia					C	0.7	0	4.8	0	0	0	0	0	0	0	0	0	0	0	
Nerv	Dicrotendipes nervosus					D	9.5	3.2	1.6	1.8	4.9	1.7	2.7	4.2	0	0	0	0	7.2	0	
Ryd	Microtendipes rydalensis					C	0	0	0	0	0	0	0	0	0	0	2	0	0	0	
Proclad	Procladius					D	5.1	7.9	8.1	0	0	0	5.5	4.2	1.6	3	21.6	3.3	2.1	3.7	
Cons	Orthocladius consobrinus					A	0	0	0	0	0	0	0	0	0	0	0	0	0	0	
Glab	Tanytarsus glabrescens					D	0.7	0	9.7	56.4	18	15.3	11	25	21	51.5	0	24.6	17.5	28.7	
MicroA	Microspectra A					B	0	0	0	0	0	0	0	0	0	0	3.9	0	0	0	
Glypto	Glyptotendipes pallens					D	0	0	0	0	0	0	0	0	0	0	2	0	0	0	
TanyPall	Tanytarsus pallidicornis					D	0	0	0	0	0	3.4	0	2.1	9.7	0	2	0	7.2	0	
Sordi	Psectorcladius sordidellus					B	2.2	0	0	0	0	0	0	0	0	0	0	0	0	0	
Cricto	Crictopus intersectus					B	0	0	6.5	1.8	0	0	2.7	0	1.6	0	0	1.6	0	0	
PolyA	Polypedilum A					C	0	0	0	0	0	0	0	0	0	0	0	0	0	0	
TanyChi	Tanytarsus chinyensis					A	0.7	2.4	0	0	1.6	0	0	0	0	0	0	0	2.1	1.9	
PsecSept	Psectrocladius septentrionalis					B	0.7	3.2	16.1	3.6	8.2	23.7	12.3	33.3	6.5	9.1	39.2	18	15.5	24.1	
Ambig	Corynocera ambigua					B	0	0	0	0	0	0	0	0	3.2	0	0	0	0	0	
Impar	Endochironomous impar					D	0	0	0	0	0	0	0	0	0	0	2	0	0	0	
Albipen	Endochironomous albipennis					D	0	0	0	1.8	6.6	0	0	0	1.6	1.5	5.9	0	0	5.6	
Calc	Psectrocladius calcaratus					B	0.7	10.3	0	0	14.8	6.8	5.5	4.2	12.9	4.5	3.9	0	14.4	0	
ParaCric	Paracricotopus					C	0	0	0	0	0	0	0	0	0	0	2	0	0	0	
Notal	Dicrotendipes notalus					D	0	0	1.6	0	0	0	0	0	0	0	2	0	0	0	
Sticto	Stictochironomous rosenschoeldi					D	0	0	0	0	0	0	0	0	0	0	2	0	0	0	
Labrund	Labrundinia					D	0	0	0	0	0	0	0	0	0	0	2	0	0	0	
Lugens	Tanytarsus lugens					A	0	0	3.2	0	0	0	0	0	0	1.5	2	0	0	0.9	
Lact	Tanytarsus lactescens					D	19	39.7	25.8	1.8	19.7	3.4	28.8	0	11.3	0	0	0	2.1	0	
CM	Ceratopogondiae Midge					D	43.8	12.7	12.9	0	0	10.2	4.1	0	0	0	0	0	0	0	
Albiman	Paratendipes albimanus					D	0	0	4.8	0	0	0	0	0	0	0	0	0	0	0	
Sergent	Sergentia coracina					B	0	0	0	0	0	0	0	0	0	0	0	0	0	0.9	
Conform	Hydrobeanus conformis					A	0	0	0	0	0	0	0	0	0	0	0	0	0	0	
Oliverid	Oliveridia					D	0	0	0	0	0	0	0	0	0	0	0	0	0	0	
Nubifer	Polypedilum nubifer					D	12.4	12.7	0	1.8	3.3	11.9	6.8	4.2	8.1	7.6	0	3.3	7.2	5.6	
Pagast	Pagastiella					D	1.5	1.6	0	5.5	8.2	3.4	2.7	0	1.6	6.1	0	0	3.1	0.9	
Paraclad	Paracladius					A	0	0	0	0	0	0	0	0	0	0	0	0	0	0	
Smit	Smittia					A	0	0	0	0	0	0	0	0	0	0	0	0	0	0	
Barb	Psectrocladius barbimanus					B	0	0	0	0	0	0	0	0	0	0	0	0	0	0	
Artica	Corynoneura artica					B	0	0	0	0	0	0	0	0	0	0	0	0	0	0	
Effusuus	Rheocrictopus effusus					C	0	0	0	0	0	0	0	0	0	0	0	0	0	0	
Lateral	Cladopelma lateralis					C	0	0	1.6	0	0	0	0	0	0	0	0	0	0	0	
StictoCh	Stictochironomous B					C	0	0	1.6	0	0	0	0	0	0	0	0	0	0	0	
Rivul	Orthocladius rivulorum					A	0	0	0	0	0	0	0	0	0	0	0	0	0	0	
Anthra	Chironomus anthracinus					D	0	0	0	1.8	0	0	0	0	3.2	1.5	0	9.8	0	8.3	
Mendx	Tanytarsus mendax					D	0	0	0	0	0	0	0	0	0	0	0	6.6	0	1.9	
Radial	Microspectra radialis					A	0	0	0	0	0	0	0	0	0	0	0	0	0	0	
Conv	Polypedilum convictum					D	0	0	0	0	0	0	0	0	0	0	0	0	0	0	
Paramet	Parametriocnemus					D	0	0	0	0	0	0	0	0	0	0	0	0	0	0	
Syl	Crictopus sylvestris					C	0	0	0	0	0	0	0	0	0	0	0	0	0	0	
Ablab	Ablabesmyia					D	2.9	4	0	10.9	3.3	6.8	9.6	4.2	8.1	9.1	0	13.1	12.4	3.7	
CricC	Crictopus C					C	0	0.8	0	5.5	0	3.4	0	0	0	0	0	4.9	0	2.8	
CricTri	Crictopus trifascia					B	0	0	0	0	0	0	0	0	0	0	0	0	0	0	
OrthoTr	Orthocladius trigonobalis					A	0	0.8	0	0	3.3	0	0	0	0	0	0	0	0	2.8	
CriptoCh	Criptochironomous					C	0	0	0	0	0	0	0	0	1.6	0	0	1.6	2.1	0.9	
OrthoC	Orthocladius S					A	0	0	0	0	0	0	0	0	0	0	0	0	0	0	
Chaet	Chaetocladius piger					A	0	0	0	0	0	0	0	0	0	0	0	0	0	0	
Obnix	Cricoptous obnixus					C	0	0	0	0	0	0	0	0	0	0	0	0	0	0	
OrthoO	Orthocladius oliveri					A	0	0	0	0	0	0	0	0	0	0	0	0	0	0	

Chironomids	Column1	Column2	Column3	Column4	Column5	Column6	238	240	242	244	246	248	250	252	254	256	258	260	261	262	263	264	266	267	268	270	271	272	274	276	278	282	284	286	288	290	294	296	298	300	302	303	304	306	307	309	310	311	312	314	315	31
Code	Name	Element	Units	Context	Taphonomy	Group																																														
Insig	Microspectra insignilobus					B	6.7	1.6	4.4	2	1.6	7.9	0	0	0	1.6	0	1.5	1.3	8.9	0	1.5	0	1.2	2.4	1.7	3.8	6.3	3.8	14.3	23.7	14.5	25.4	18.6	26.2	15.1	6.6	8.8	9.1	8	8.2	22.8	9.8	6.8	1.2	23.4	15.3	9.7	12.3	0	0
Pedel	Microtendipes pedellus					C	10.7	9.7	9.9	9.8	9.4	6.6	17.4	10.9	9	19.7	15.1	25.4	16.9	6.7	13.6	26.2	16.4	4.9	4.9	18.3	26	27.4	21.8	0	22	0	0	0	0	0	0	0	0	0	0	1.8	0	0	0	0	0	0	0	5.4	10.3
Oliv	Oxynocera oliveri					B	0	0	0	0	0	0	0	0	0	0	0	0	0	4.4	0	0	0	0	0	0	1	0	0	3.2	1.7	0	0	0	0	0	0	0	0	0	0	0	0	0	0	2.8	4.2	1.8	0	2.6
Macpel	Macropelopia					C	0	0	0	0	0	0	0	0	0	0	0	0	0	0	0	0	0	0	0	0	0	0	0	0	3.4	0	0	0	0	0	0	0	0	0	0	0	0	0	0	0	0	0	1.8	0
Monopel	Monopelopia					C	0	0	0	0	0	0	0	0	0	0	0	0	0	0	0	0	0	0	0	0	0	0	0	0	1.7	0	0	0	0	0	0	0	0	0	0	0	0	0	0	0	0	0	0	0
Lars	Larsia					C	0	0	0	0	0	0	0	0	0	0	0	0	0	2.2	0	0	0	0	0	0	0	0	0	0	5.1	0	0	0	0	0	0	0	0	0	0	0	0	0	0	0	0	0	0	0	0
Nerv	Dicrotendipes nervosus					D	2.7	1.6	1.1	2	0	1.3	5.1	1.6	6	0	0	9	1.3	0	4.5	4.6	1.6	1.2	4.9	3.5	1.9	1.1	3.8	1.6	6.8	0	0	0	0	0	0	0	0	0	0	0	0	0	0	0	0	0	0	0	0
Ryd	Microtendipes rydalensis					C	0	0	0	0	4.7	0	0	0	0	0	0	0	0	2.2	0	0	0	0	0	0	0	0	0	0	0	0	0	0	0	0	0	0	0	0	0	0	0	0	0	0	0	0	0	1.8	0
Proclad	Procladius					D	6.7	1.6	1.1	2	6.3	0	7.2	3.1	11.3	3.3	5.6	3	1.3	15.6	10.6	4.6	19.7	1.2	1.2	0.9	1	0	0	0	6.8	0	0	0	0	0	0	0	0	0	0	0	0	0	0	0	0	0	0	13.5	7.7
Cons	Orthocladius consobrinus					A	0	0	0	0	0	0	0	0	0	0	0	0	0	0	0	0	0	0	0	0	0	0	0	0	1.7	11.3	3.2	20.3	0	0	0	11.8	0	9.8	8.2	0	0	0	0	22.2	5.6	0	0	0
Glab	Tanytarsus glabrescens					D	24	37.1	24.2	27.5	0	22.4	13.8	29.7	9.8	11.5	4.8	10.4	13	0	3	6.2	4.9	3.7	0	0.9	7.7	4.2	7.7	3.2	0	0	0	0	0	0	0	0	0	0	0	0	0	0	0	0	0	0	0	0	0
MicroA	Microspectra A					B	0	0	0	0	0	0	0	0	0	0	0	0	0	0	0	0	0	0	0	0	0	0	0	0	1.7	0	0	0	0	0	0	0	0	0	0	0	0	0	0	0	0	0	1.8	0
Glypto	Glyptotendipes pallens					D	0	0	0	0	0	0	0	0	0	0	0	0	0	0	0	0	0	0	0	0	0	0	0	0	0	0	0	0	0	0	0	0	0	0	0	0	0	0	0	0	0	0	0	0	0
TanyPall	Tanytarsus pallidicornis					D	0	0	1.1	0	0	0	0	0	8.3	8.2	9.5	1.5	2.6	0	15.2	9.2	8.2	8.6	22	22.6	0	18.9	25.6	9.5	0	0	0	0	0	0	0	0	0	0	0	0	0	0	0	0	0	0	0	0	0	0
Sordi	Psectrocladius sordidellus					B	0	0	0	0	4.7	0	0	1.6	0	0	0	0	2.6	2.2	0	1.6	1.2	1.2	0	0	0	0	0	0	1.7	0	0	0	1.6	0	0	0	0	0	0	0	0	0	0	0	0	0	0	0	0
Cricto	Cricotopus intersectus					B	0	0	0	0	0	2.6	2.2	1.6	1.5	1.6	2.4	0	1.3	0	1.5	1.5	0	1.2	0	2.6	0	3.2	3.8	14.3	1.7	6.5	4.8	3.4	13.1	5.7	1.6	0	15.9	0.9	0	12.3	9.8	11.4	18.1	31.9	0	1.4	12.3	0	0
PolyA	Polypedilum A					C	0	0	0	0	0	0	0	0	0	0	0	0	0	0	0	0	0	0	0	0	0	0	0	0	1.7	0	0	0	0	0	0	0	0	0	0	0	0	0	0	0	0	0	0	0	0
TanyChi	Tanytarsus chinyensis					A	2.7	1.6	4.4	0	0	2.6	0.7	0	0.8	0	0.8	3	5.2	2.2	0	3.1	0	6.2	2.4	0.9	2.9	7.4	3.8	7.9	0	0	0	0	0	0	0	0	0	0	0	0	0	0	0	0	0	0	0	0	0	0
PsecSept	Psectrocladius septentrionalis					B	6.7	24.2	9.9	19.6	28.1	21.1	13.8	20.3	5.3	32.8	14.3	19.4	31.2	17.8	24.2	21.5	3.3	30.9	12.2	4.3	10.6	9.5	0	3.2	0	0	0	0	0	0	0	0	2.7	0	5.3	3.3	4.5	1.2	0	8.3	2.8	1.8	16.2	28.2
Ambig	Oxynocera ambigua					B	0	0	0	0	1.6	0	0	0	2.3	0	9.5	3	2.6	2.2	3	6.2	4.9	19.8	23.2	22.6	0	0	1.3	3.2	0	0	0	1.7	0	0	0	0	0	0	0	0	0	3.6	0	5.6	22.2	8.8	8.1	3.8
Impar	Endochironomus impar					D	0	0	0	0	0	0	0	0	0	0	0	0	0	0	0	0	0	0	0	0	0	0	0	0	0	0	0	0	0	0	0	0	0	0	0	0	0	0	0	0	0	0	0	0	0
Albipen	Endochironomus albipennis					D	2.7	0	2.2	0	1.6	1.3	2.9	1.6	0	1.6	0	3	0	0	1.5	0	1.6	0	0	0	0	0	0	0	1.7	0	0	0	0	0	0	0	0	0	0	0	0	0	0	0	0	0	0	0.9	0
Calc	Psectrocladius calcaratus					B	12	0	19.8	11.8	4.7	0	5.8	0	20.3	1.6	16.7	7.5	0	11.1	0	3.1	23	0	0	6.1	0	0	0	2.6	0	0	0	0	1.6	0	0	0	2.9	0	0	0	0	0	0	0	0	0	0	5.4	0
ParaCric	Paracricotopus					C	0	0	0	0	0	0	0	1.6	0	0	0	0	0	0	0	0	0	0	0	0	0	0	0	0	0	0	0	0	0	0	0	0	0	0	0	0	0	0	0	0	0	0	0	0	0
Notal	Dicrotendipes notalus					D	0	0	0	0	0	0	0	0	0	0	0	0	0	0	0	0	0	0	0	0	0	0	0	0	0	0	0	0	0	0	0	0	0	0	0	0	0	0	0	0	0	0	0	0	0
Stictoc	Stictochironomus rosenschoeldi					D	0	0	0	0	0	0	0	0	0	0	0	0	0	0	0	0	0	0	0	0	0	0	0	0	0	0	0	0	0	0	0	0	0	0	0	0	0	0	0	0	0	0	0	0	0
Labrund	Labrundinia					D	0	0	0	0	0	0	0	0	0	0	0	0	0	0	0	0	0	0	0	0	0	0	0	0	0	0	0	0	0	0	0	0	0	0	0	0	0	0	0	0	0	0	0	0	0
Lugens	Tanytarsus lugens					A	2.7	4.8	1.1	2	4.7	2.6	0	0	0	1.6	0.8	0	5.2	11.1	0	4.6	0	7.4	1.2	2.6	19.2	8.4	2.6	6.3	1.7	1.6	4.8	0	0	5.7	0	4.4	2.3	4.5	1	0	0	0	0	2.1	1.4	4.2	0	0	2.6
Lact	Tanytarsus lactescens					D	12	6.5	6.6	5.9	21.9	6.6	16.7	4.7	18	9.8	9.5	3	0	2.2	6.1	0	4.9	1.2	4.9	1.7	0	0	0	1.6	0	0	0	0	0	0	0	0	0	0	0	0	0	0	0	0	0	0	0	0	0	0
CM	Ceratopogonidae Midge					D	0	0	0	0	2	0	0	0	0	0	0	0	0	0	0	0	0	0	0	0	0	0	0	0	0	0	0	0	0	0	0	0	0	0	0	0	0	0	0	0	0	0	0	0	0
Albiman	Paratendipes albimanus					D	0	0	0	0	0	0	0	0	0	0	0	0	0	0	0	0	0	0	0	0	0	0	0	0	0	0	0	0	0	0	0	0	0	0	0	0	0	0	0	0	0	0	0	0	0
Sergent	Sergentia coracina					B	0	0	0	0	0	0	0	0	0	0	0	0	0	2.2	0	0	0	1.2	2.4	3.5	5.8	0	3.8	1.6	0	4.8	12.7	3.4	13.1	7.5	18	17.6	13.6	11.6	8.2	17.5	8.2	13.6	8.4	8.5	9.7	12.5	24.6	31.5	24.4
Conform	Hydrobaenus conformis					A	0	0	0	0	1.6	0	0	0	0	0	0	0	0	0	0	0	0	0	0	0	0	0	0	0	0	0	0	0	0	1.6	0	6.6	4.4	0	8	5.2	0	19.7	9.1	32.5	21.3	23.6	19.4	3.5	0	0
Oliverid	Oliveridia					D	0	0	0	0	0	0	0	0	0	0	0	0	0	0	0	0	0	0	0	0	0	0	0	0	0	0	0	0	0	0	0	0	0	0	0	0	0	0	0	0	0	0	0	0	0
Nubifer	Polypedilum nubifer					D	0	3.2	0	2	0	2.6	5.8	3.1	0.8	0	4	0	2.6	0	1.5	0	0	3.7	2.4	1.7	5.8	4.2	1.3	7.9	0	0	0	0	0	0	0	0	0	0	0	0	0	0	0	0	0	0	0	0	0
Pagast	Pagastiella					D	1.3	1.6	5.5	0	0	1.3	0	3.1	0	3.3	0.8	1.5	1.3	0	0	1.5	0	0	0	0	0	0	0	1.6	0	0	0	0	0	0	0	0	0	0	0	0	0	0	0	0	0	0	0	0	0
Paraclad	Paracladius					A	0	0	0	0	0	0	0	0	0	0	0	0	0	0	0	0	0	0	0	0	0	0	0	0	0	0	0	5.1	0	0	4.9	1.5	4.5	0	0	0	0	2.3	0	0	1.4	0	0	0	0
Smit	Smittia					A	0	0	0	0	0	0	0	0	0	0	0	0	0	0	0	0	0	0	0	0	0	0	0	0	0	0	0	0	0	0	0	0	0	0	0	0	0	0	0	0	0	0	0	0	0
Barb	Psectrocladius barbimanus					B	0	0	0	0	0	0	0	0	0	0	0	0	0	0	0	0	0	0	0	0	0	0	0	0	0	0	0	0	0	0	0	0	0	0	0	0	0	0	0	0	0	0	0.9	0
Artica	Corynoneura artica					B	0	0	0	0	0	0	0	0	0	0	0	0	0	0	0	0	0	0	2.4	0.9	0	0	0	0	0	0	0	0	0	0	0	0	0	0	0	0	0	0	0	0	0	0	0	0
Effusus	Rheocricotopus effusus					C	0	0	0	0	0	0	0	0	0	0	0	0	0	0	0	0	0	0	0	0	0	0	0	0	0	0	0	0	0	0	0	0	0	0	0	0	0	0	0	0	0	0	0	0	0
Lateral	Cladopelma lateralis					C	0	0	0	0	0	0	0	0	0	0	0	0	0	0	0	0	0	0	0	0	0	0	0	0	0	0	0	0	0	0	0	0	0	0	0	0	0	0	0	0	0	0	0	0	0
StictoCh	Stictochironomus B					C	0	0	0	0	0	0	0	0	0	0	0	0	0	0	0	0	0	0	0	0	0	0	0	0	0	0	0	0	0	0	0	0	0	0	0	0	0	0	0	0	0	0	0	0	0
Rivul	Orthocladius rivulorum					A	0	0	0	0	1.6	0	0	0	0	0	0	0	0	0	0	0	0	0	0	0	0	0	0	0	0	0	0	0	0	0	0	0	0	0	0	0	0	0	0	0	0	0	0	0	0
Anthra	Chironomus anthracinus					D	0	0	0	0	1.6	1.3	0.7	3.1	0.8	0	1.6	0	0	9.1	0	0	0	0	0	0	1.7	1	4.2	12.8	4.8	5.1	0	0	0	0	0	0	0	0	0	0	0	0	0	0	0	0	0	0	1.3
Mendx	Tanytarsus mendax					D	0	0	0	0	1.6	0	0	4.7	0	0	0	0	6.5	2.2	0	0	0	3.7	1.2	0	10.6	0	0	0	5.1	0	0	0	0	0	0	0	0	0	0	0	0	1.6	0	0	0	0	0	6.3	5.1
Radial	Microspectra radialis					A	0	0	0	0	0	0	0	0	0	0	0	0	0	0	0	0	1.6	0	0	0.9	0	1.1	3.8	1.6	0	38.7	41.3	30.5	21.3	28.3	39.3	29.4	34.1	38.4	37.1	19.3	29.5	25	26.5	4.3	6.9	6.9	10.5	0	1.3
Conv	Polypedilum convictum					D	0	0	0	0	0	0	0	0	0	0	0	0	0	0	0	0	0	0	0	0	0	0	0	0	0	0	0	0	0	0	0	0	0	0	0	0	0	0	0	0	0	0	0	0.9	0
Paramet	Parametriocnemus					D	0	0	0	0	0	0	0	0	0	0	0	0	0	0	0	0	0	0	0	0	0	0	0	0	0	0	0	0	0	0	0	0	0	0	0	0	0	0	0	0	0	0	0	0	0
Syl	Cricotopus sylvestris					C	0	0	0	0	0	0	0	0	0	0	0	0	0	0	0	0	0	0	0	0	0	0	0	0	0	0	0	0	0	0	0	0	0	0	0	0	0	0	0	0	0	0	0	0	0
Ablab	Ablabesmyia					D	8	6.5	7.7	11.8	4.7	11.8	7.2	6.3	6	1.6	4	7.5	5.2	6.7	4.5	3.1	6.6	0	4.9	1.7	1	3.2	0	6.3	6.8	0	0	0	0	0	0	0	0	0	0	0	0	0	0	0	0	0	0	0.9	3.8
CricC	Cricotopus C					C	0	0	0	0	0	2.6	0	3.1	0	0	0	0	0	0	0	0	0	2.5	1.2	0	1.9	0	0	0	0	0	0	0	0	0	0	0	0	0	0	0	0	0	0	0	0	0	0	0.9	0
CricTri	Cricotopus trifascia					B	1.3	0	0	0	0	0	0	0	0	0	0	0	0	0	1.5	0	0	0	1.2	0	0	0	0	1.6	0	0	0	0	0	0	0	0	0	0	0	0	0	0	0	0	0	0	0	0
OrthoTr	Orthocladius trigonolabis					A	0	0	0	0	0	2.6	0	0	0	0	0	0	0	0	0	0	0	0	0	0	0	0	1.1	0	4.8	0	22.6	6.3	16.9	21.3	37.7	23	19.1	20.5	16.1	32	21.1	18	27.3	8.4	8.5	2.8	6.9	24.6	3.6	9
CriptoCh	Criptochironomus					C	0	0	0	2	0	1.3	0.7	0	0	0	0	0	0	0	0	0	1.6	0	0	0	0	0	1.3	0	0	0	0	0	0	1.6	0	0	0	0	0	0	0	0	0	0	0	0	0	0	0
OrthoC	Orthocladius S					A	0	0	1.1	0	0	1.3	0	0	0	1.6	0.8	1.5	0	0	0	0	0	0	1.2	0.9	0	0	0	0	0	0	0	0	0	0	0	0	0	0	0	0	0	0	0	0	0	0	0	0	0
Chaet	Chaetocladius piger					A	0	0	0	0	0	0	0	0	0	0	0	0	0	0	0	3.1	0	0	2.4	0	0	0	0	0	0	0	0	0	0	0	0	0	0	0	0	0	0	0	0	0	0	0	0	0	0
Obnix	Cricoptous obnixus					C	0	0	0	0	0	0	0	0	0	0	0	0	0	0	0	0	0	0	0	0	0	0	0	1.6	0	0	0	0	0	0	0	0	0	0	0	0	0	0	0	0	0	0	0	0	0
OrthoO	Orthocladius oliveri					A	0	0	0	0	0	0	0	0	0	0	0	0	0	0	0	0	0	0	0	0	0	0	0	0	0	0	0	0	0	0	0	0	0	0	0	0	0	0	0	0	0	4.2	0	0	0

Chironomids	Column1	Column2	Column3	Column4	Column5	Column6	315	316	317	318	319	320	322	323	324	325	326	327	328	329	330	332	334	336	338	340	342	344	346	348	350	352	354	356	358	360	363	368	372	376	380	382	384	386	388	392	396	400	404	408	420
Code	Name	Element	Units	Context	Taphonomy	Group																																												
Insig	Microspectra insignilobus					B	0	1.4	0	1.8	3	0	3	1.2	5.6	2.1	1.1	7.5	6.5	0	1.7	1.4	0	3	0	1.2	2.3	0	2.4	0	0	3	4.6	3.3	8.2	17.9	15.6	2	0	4.3	0	1.4	1.4	0	0	0	0	0	1.1	0	0
Pedel	Microtendipes pedellus					C	10.3	16.4	18.2	0.9	0	1.3	0	0	0	0	0	0	0	0	5	0	1	3	3.8	2.4	1.5	4.3	6.1	9.3	18.8	3	12.3	10.8	0	2.1	0	38.8	10.1	21.7	26.2	13.9	13.7	19.6	13.1	34.4	53.8	41	4.3	48.3	1.4
Oliv	Corynocera oliveri					B	2.6	1.4	0	0	0	0	0	2.4	0	2.1	5.7	0	0	4.1	0	0	1	0	0	0	1.5	1.4	0	0	3.5	0	10.8	1.7	24.6	8.4	10.1	0	9	4.3	0	4.2	1.4	15.5	16.6	3.3	3.1	4.8	6.4	4.5	0
Macpel	Macropelopia					C	0	0	0	0	0	0	0	0	0	0	0	0	0	0	0	0	0	0	0	0	0	0	0	0	0	0	0	0	0	0	0	0	0	0	0	0	0	0	0	0	0	0	0	0
Monopel	Monopelopia					C	0	0	0	0	0	0	0	0	0	0	0	0	0	0	0	0	0	0	0	0	0	0	0	0	0	0	0	0	0	0	0	0	0	0	0	0	0	0	0	0	0	0	0	0
Lars	Larsia					C	0	0	0	0	0	0	0	0	0	0	0	0	0	0	0	0	0	0	0	0	0	0	0	0	0	0	0	0	0	0	0	0	0	0	0	0	0	0	0	0	0	0	0	0
Nerv	Dicrotendipes nervosus					D	0	1.4	0	0	0	0	1	0	0	0	0	0	0	0	0	0	5.9	3	0	0	0	0	0	0	0	0	0	0	0	0	0	5.6	0	0	0	0	0	0	14.3	0	0	0	3.2	0	7.2
Nyd	Microtendipes nydalensis					C	0	0	0	0	0	0	0	0	0	0	0	0	0	0	0	0	0	0	0	0	0	0	0	0	0	0	0	0	0	0	0	0	0	0	0	0	0	0	0	0	0	0	0	0
Procfad	Procladius					D	7.7	4.1	1.8	11.9	4.5	5.1	8	1.2	5.6	0	3.4	0	0	1	1.7	2.9	7.8	3	9.6	3.6	6.1	0	3.7	4.2	14.1	2	1.5	0	0	0	0	5.6	1.4	0	1.4	0	0	2.9	0	0	0	11.7	2.2	20.3
Cons	Orthocladius consobrinus					A	0	0	0	0	0	0	0	0	0	0	8	0	0	0	0	0	0	0	0	0	0	0	0	0	0	0	0	0	0	0	0	0	0	0	0	0	0	0	0	0	0	0	0	0
Glab	Tanytarsus glabrescens					D	0	0	0	0	0	0	0	0	0	0	0	0	0	0	0	0	0	0	0	0	0	0	0	0	0	0	0	0	0	0	0	0	0	0	0	0	0	0	0	0	0	0	0	0
MicroA	Microspectra A					B	0	0	0	0	0	0	0	0	0	0	0	0	0	0	0	0	0	0	0	0	0	0	0	0	3.5	0	0	0	0	0	0	3.4	0	0	0	0	0	0	0	0	0	0	0	0
Glypto	Glyptotendipes pallens					D	0	0	0	0	0	0	0	0	0	0	0	0	0	0	0	0	0	0	0	0	0	0	0	0	0	0	0	0	0	0	0	0	0	0	0	0	0	0	0.6	0	0	0	0	0	1.4
TanyPall	Tanytarsus pallidicornis					D	0	4.1	5.5	0	1.5	0	0	0	0	0	0	0	0	0	0	0	0	0	0	0	0	4.3	0	0	1.2	29	12.3	0	0	2.1	0	14.3	14.6	4.3	24.6	19.4	15.1	18.6	4	3.3	7.7	8.6	0	15.7	0
Sordi	Psectorcladius sordidellus					B	0	0	0	0	0	0	0	0	0	0	2.3	0	0	0	0	2.9	0	0	0	3.1	1.4	0	0	0	1	0	0	1.6	0	0	6.1	0	0	0	0	0	1	0.6	0	1.5	0	2.1	0	0
Cricto	Criotopus intersectus					B	0	1.4	5.5	0	0	0	0	3.5	1.9	12.5	0	0	0	1	0	0	1	1.5	1.9	0	0	0	0	0	0	3	0	2.5	1.6	5.3	4.6	0	0	10.1	0	4.2	0	1	0.6	0	0	0	2.1	0	1.4
PolyA	Polypedilum A					C	0	0	0	0	0	0	0	0	0	0	0	0	0	0	0	0	0	0	0	0	0	0	0	0	0	0	0	0	0	0	0	0	0	0	0	0	0	0	0	0	0	0	0	0
TanyChi	Tanytarsus chinyensis					A	0	0	0	0.9	0	0	0	0	0	0	0	0	0	0	0	0	0	0	0	0	0	0	0	0	0	1	0	0	0	0	2	0	0	0	0	1.4	0	0.6	1.6	7.7	1.9	0	2.2	0
PsecSept	Psectrocladius septentrionalis					B	28.2	31.5	20	14.7	29.9	51.3	17	0	9.3	0	2.3	3	1.6	1	20	10	2.9	6	19.2	20.2	4.6	4.3	31.7	16.9	7.1	15	9.2	0	3.3	3.2	1.8	10.2	3.4	2.9	3.1	0	2.7	2.1	4	11.5	3.1	5.7	2.1	0	17.4
Ambig	Corynocera ambigua					B	3.8	2.7	1.8	7.3	9	14.1	23	65.9	44.4	27.1	47.7	41.8	58.1	66	11.7	44.3	30.4	23.9	21.2	36.9	38.9	65.7	30.5	37.3	8.2	5	9.2	66.7	1.6	0	1.8	0	0	0	0	0	1.6	0	0	5.3	0	23.2
Impar	Endochironomus impar					D	0	0	0	0	0	0	0	0	0	0	0	0	0	0	0	0	0	0	0	0	0	0	0	0	0	0	0	0	0	0	0	0	0	0	0	0	0	0	0	0	0	0	0	0
Albipen	Endochironomus albipennis					D	0	0	0	1.8	0	0	0	0	0	0	0	0	0	0	0	0	0	0	0	0	0	0	0	0	0	0	0	0	0	0	0	0	1.4	0	0	0	0	0	0	0	0	0	0	0	0
Calc	Psectrocladius calcaratus					B	0	0	0	17.4	0	0	23	0	0	0	0	0	0	0	0	0	20.6	3	0	0	14.5	0	0	0	2.4	0	0	0	0	1.1	0	0	0	0	3.1	0	0	0	0	0	0	0	10.6	0	1.4
ParaOric	Paracricotopus					C	0	0	0	0	0	0	0	0	0	0	0	0	0	0	0	0	0	0	0	0	0	0	0	0	0	0	0	0	0	0	0	0	0	0	0	0	0	0	0	0	0	0	0	0
Notal	Dicrotendipes notalis					D	0	0	0	0	0	0	0	0	0	0	0	0	0	0	0	0	0	0	0	0	0	0	0	0	0	0	0	0	0	0	0	0	0	0	0	0	0	0	0	0	0	0	0	0
Sticho	Stictochironomus rosenschoeldi					D	0	0	0	0	0	0	0	0	0	0	0	0	0	0	0	0	0	0	0	0	0	0	0	0	0	0	0	0	0	0	0	0	0	0	0	0	0	0	0	0	0	0	0	0
Labrund	Labrundinia					D	0	0	0	0	0	0	0	0	0	0	0	0	0	0	0	0	0	0	0	0	0	0	0	0	0	0	0	0	0	0	0	0	0	0	0	0	0	0	0	0	0	0	0	0
Lugens	Tanytarsus lugens					A	2.6	2.7	0	0	0	1.3	0	0	1.9	0	3.4	0	1.6	0	0	0	0	0	1.9	1.2	0	0	2.4	0	20	1	4.6	1.7	9.8	11.6	0	2	18	1.4	3.1	1.4	4.1	5.2	19.4	8.2	0	4.8	18.1	4.5	0
Lact	Tanytarsus lactiscens					D	0	0	0	0	0	0	0	0	0	0	0	0	0	0	0	0	0	0	0	0	0	0	0	0	0	0	0	0	0	0	0	0	0	0	0	0	0	0	0	0	0	0	0	0
CM	Ceratopogonidae Midge					D	0	0	0	0	0	0	0	0	0	0	0	0	0	0	0	0	0	0	0	0	0	0	0	0	0	0	0	0	0	0	0	0	0	0	0	0	0	0	0	0	0	0	0	0
Albiman	Paratendipes albimanus					D	0	0	0	0	0	0	0	0	0	0	0	0	0	0	0	0	0	0	0	0	0	0	0	0	0	0	0	0	0	0	0	0	0	0	0	0	0	0	0	0	0	0	0	0
Serigent	Sergentia coracina					B	24.4	21.9	34.5	32.1	43.3	16.7	20	22.4	16.7	12.5	5.7	13.4	11.3	4.1	45	12.9	17.6	31.3	19.2	10.7	25.2	11.4	19.5	21.2	4.7	17	3.1	0	11.5	6.3	4.6	0	0	0	0	2.7	2.1	0	0	0	1	10.6	1.1	13
Conform	Hydrobaenus conformis					A	0	0	0	0	1.5	0	0	0	0	0	0	0	0	1	0	0	0	0	0	0	0	0	0	0	0	0	0	4.6	1.7	1.6	2.1	0.9	6.1	0	0	0	0	0	0	0	1.5	0	0	0
Oliverid	Oliveridia					D	0	0	0	0	0	0	0	0	0	0	0	0	0	0	0	0	0	0	0	0	0	0	0	0	0	0	0	0	0	0	0	0	0	0	0	0	0	0	0	0	0	0	0	0
Nubifer	Polypedilum nubifer					D	0	0	0	0	0	0	0	0	0	0	0	0	0	0	0	0	0	0	0	0	0	0	0	0	0	0	0	0	0	0	0	0	0	0	0	0	0	0	0	0	0	0	0	0
Pagast	Pagastiella					D	0	1.4	1.8	0.9	0	0	0	0	0	0	0	0	0	0	0	0	1	0	0	0	0	0	0	0	0	0	0	0	0	0	0	0	0	0	0	0	0	0	0	0	0	0	0	0	1.4
Paraclad	Paracladius					A	0	0	0	0	0	0	0	0	7.4	18.8	5.7	7.5	6.5	2.1	0	0	0	0	0	0	0	0	0	0	0	0	0	0	13.1	9.5	25.7	2	0	0	3.1	0	0	1	0	0	0	1	0	0	0
Smit	Smittia					A	0	0	0	0	0	0	0	0	0	0	0	0	0	0	0	0	0	0	0	0	0	0	0	0	0	0	0	0	6.6	0	0	0	0	0	0	0	0	0	0	0	0	0	0	0	0
Barb	Psectrocladius barbimanus					B	0	0	0	0	0	1.3	0	0	0	0	0	0	0	0	0	11.4	1	3	0	6	0	0	0	0	0	0	0	0	0	0	0	0	0	0	3.1	2.8	1.4	0	0	1.6	1.5	0	0	3.4	1.4
Artica	Corynoneura artica					B	0	0	0	0	0	0	3	0	0	0	0	0	0	0	0	0	0	0	0	0	0	0	0	0	0	0	0	0	0	0	0	0	0	0	0	0	0	0	0.6	0	0	0	0	2.9
Effusus	Rheocricotopus effusus					C	0	0	0	0	0	0	0	0	0	0	0	0	0	0	0	0	0	0	0	0	0	0	0	0	0	0	0	0	0	0	0	0	1.1	0	0	0	0	0	0	0	0	0	1.1	0	0
Lateral	Cladopelma lateralis					C	0	0	0	0	0	0	0	0	0	0	0	0	0	0	0	0	0	0	0	0	0	0	0	0	0	0	0	0	0	0	0	0	0	0	0	0	0	0	0	0	0	0	0	0
SticteCh	Stictochironomus B					C	0	0	0	0	0	0	0	0	0	0	0	0	0	0	0	0	0	0	0	0	0	0	0	0	0	0	0	0	0	0	0	0	0	0	0	0	0	0	0	0	0	0	0	0
Rivul	Orthocladius rivulorum					A	0	0	0	0	0	0	0	0	0	0	0	0	0	0	0	0	0	0	0	0	0	0	0	0	0	0	0	0	0	0	0	0	0	0	0	0	0	0	0	0	0	0	0	0
Anthra	Chironomus anthracinus					D	1.3	0	3.6	1.8	0	0	2	1.2	1.9	2.1	4.5	4.5	6.5	6.2	1.7	2.9	2.9	13.4	7.7	8.3	0	0	2.4	1.7	4.7	13	1.5	3.3	0	13.7	1.8	6.1	18	20.3	12.3	26.4	38.4	17.5	12	19.7	12.3	12.4	18.1	6.7	1.4
Mendx	Tanytarsus mendax					D	5.1	0	5.5	7.3	0	1.3	0	0	0	0	0	1.5	0	1	0	0	0	0	0	1.2	0	0	0	0	4.7	1	9.2	2.5	0	0	0	0	1.1	17.4	0	0	9.6	9.3	0	0	4.6	2.9	0	0	0
Radial	Microspectra radialis					A	1.3	6.8	1.8	0	0	0	0	1.2	5.6	12.5	8	6	8.1	7.2	3.3	1.4	0	1.5	0	1.2	0	2.9	0	2.5	4.7	1	1.5	0	16.4	14.7	26.6	2	7.9	0	0	1.4	0	0	10.9	0	0	0	0	0	1.4
Conv	Polypedilum convictum					D	0	0	0	0	0	0	0	0	0	0	0	0	0	0	0	0	0	0	0	0	0	0	0	0	0	0	0	0	0	0	0	0	0	0	0	0	0	0	0	0	0	0	0	0
Paramet	Parametriocnemus					D	0	0	0	0	0	0	0	0	0	0	0	0	0	0	0	0	0	0	0	0	0	0	0	0	1.2	0	0	0	0	0	0	0	0	0	0	0	0	0	0	0	0	0	0	0
Syl	Criotopus sylvestris					C	0	0	0	0	0	0	0	0	0	0	0	0	0	0	0	0	0	0	0	0	0	0	0	0	0	0	0	0	0	0	0	0	1.1	0	0	0	0	0	0	0	2.9	0	1.1	0
Ablab	Ablabesmyia					D	3.8	1.4	0	0.9	6	2.6	0	0	0	0	0	0	0	0	1.4	0	0	3.8	1.2	0	1.4	1.2	0	1.2	2	6.2	1.7	0	1.1	0	2	1.1	1.4	7.7	8.3	1.4	6.2	0	9.8	3.1	1.9	2.1	0	0
CricC	Criotopus C					C	0	0	0	0	0	0	0	0	0	2.1	0	0	0	0	0	0	0	0	0	0	0	0	0	0	0	0	0	0	0	0	0.9	0	0	0	0	0	0	0	0	0	5.7	0	7.9	0
CricTri	Criotopus trifascia					B	0	0	0	0	0	0	0	0	0	0	0	0	0	0	0	0	0	0	0	0	0	0	0	0	0	0	0	0	0	0	0	0	0	0	0	0	0	0	0	0	0	0	0	0
OrthoTr	Orthocladius trigonolabis					A	9	1.4	0	0	0	0	0	0	0	8.3	2.3	14.9	0	5.2	10	11.4	3.9	0	11.5	6	2.3	0	0	0	0	0	0	0	0	0	5.5	0	0	0	0	0	0	0	0	0	0	0	1.1	0	4.3
CriptoCh	Criptochironomus					C	0	0	0	0	0	0	0	0	0	0	0	0	0	0	0	0	0	0	0	0	0	0	0	0	0	0	0	0	0	0	0	0	0	0	0	0	0	0	0	0	0	0	0	0
OrthoC	Orthocladius S					A	0	0	0	0	1.5	5.1	0	1.2	0	0	0	0	0	0	0	0	0	4.5	0	0	0	2.9	0	6.8	0	3	9.2	4.2	0	1.1	0	6.1	0	8.7	13.8	15.3	6.8	1	0	4.9	0	5.7	0	2.2	0
Chaet	Chaetocladius piger					A	0	0	0	0	0	0	0	0	0	0	0	0	0	0	0	0	0	0	0	0	0	0	0	0	0	0	0	0	0	0	0	0	0	0	0	0	0	0	0	0	0	0	0	0
Obnix	Cricoptous obnixus					C	0	0	0	0	0	0	0	0	0	0	0	0	0	0	0	0	0	0	0	0	0	0	0	0	0	0	0	0	0	0	0	0	0	0	0	0	0	0	0	0	0	0	0	0
OrthoO	Orthocladius oliveri					A	0	0	0	0	0	0	0	0	0	0	0	0	0	0	0	0	0	0	0	0	0	0	0	0	0	0	0	0	0	0	0	0	0	0	0	0	0	0	0	0	0	0	0	0

Table 18. The chironomid taxa identified in the Lang Lochs core shown as a percentage of the assemblage (%). The sample depth is shown on above (cm) with species on the left.

Pollen	Column1	Column2	272	274	277	285	288	291	295	299	304	309	316	318	320	321	323	326	329	331	333	334	336	338	339	340	342	344	347	350	352
Code	Name	Group																													
Lugens	Tanytarsus lugens	A	0	0	0	0	0	3.6	2.6	0	0	0	0	0	5.2	5.1	32.6	13.3	0	0	1.5	0	1.4	0	0	0	0	0	0	0	0
Conform	Hydrobeanus con	A	0	0	0	0	0	0	0	0	0	0	0	0	0	0	0	0	0	0	0	0	0	0	0	0	0	1.8	0	0	0
Paraclad	Paracladius	A	0	0	0	0	0	0	0	0	0	0	0	0	0	0	0	0	0	0	0	0	1.4	0	0	1.9	0	0	0	0	0
Radial	Microspectra rad	A	0	0	0	0	0	0	0	3.5	0	0	0	2.8	0	5.1	0	2.4	11.9	15.6	9	6.1	13.7	17.3	0	0	5.6	0	0	0	0
OrthoS	Orthocladius S	A	0	0	0	0	0	0	0	0	0	0	0	0	0	0	0	0	0	0	0	0	0	0	0	0	0	0	3.7	0	0
Tanychin	Tanytarsus chiny	A	0	0	0	0	0	0	0	0	0	0	0	0	0	0	0	0	0	0	0	0	0	0	0	0	0	0	0	0	0
Protany	Protanypus	A	0	0	0	0	0	0	0	0	0	0	0	0	0	0	0	0	0	0	0	0	0	0	0	0	0	0	0	0	0
Pseudodi	Pseudodiamesa	A	0	0	0	0	0	0	0	0	0	2.7	0	0	0	0	2.2	2.4	0	0	0	0	0	0	0	0	0	0	0	0	0
OrthoCon	Orthocladius con	A	0	0	0	0	0	0	0	0	7.1	0	0	1.7	2.6	8.7	8.4	11.9	0	10.4	10.2	4.1	0	0	0	0	0	0	0	0	0
ChaetoB	Chaetocladius B	A	0	0	0	0	0	0	0	0	0	0	5.6	1.7	5.1	2.2	6	0	0	0	0	0	0	0	0	0	0	0	0	0	0
Diamab	Diamesa aberata	A	0	0	0	0	0	0	0	0	0	0	0	1.7	5.1	2.2	3.6	0	0	0	0	0	0	0	0	0	0	0	0	0	0
Insig	Microspectra insi	B	0	0	0	0	0	0	0	0	0	2.7	0	5.2	10.3	0	15.7	15.3	2.2	9	18.4	21.9	21.2	30.6	46.2	24.1	0	1.9	15	1.7
Oliv	Corynocera olive	B	0	4.6	0	2.4	0	0	2.6	0	2.2	0	0	5.2	5.1	0	7.2	8.5	4.4	11.9	14.3	6.8	3.8	0	0	0	7	9.3	5	16.7
Sordi	Psectorcladius so	B	5.9	13.8	1.5	0	0	0	5.1	1.8	8.9	11.9	0	0	0	5.1	4.3	0	1.7	2.2	4.5	0	1.4	3.8	2	7.7	1.9	5.3	5.6	8.3	3.3
Cricto	Crictopus interse	B	0	0	0	0	0	0	0	0	2.2	0	0	5.6	5.2	7.7	0	3.6	1.7	11.1	11.9	0	13.7	17.3	32.7	17.3	16.7	0	0	0	0
PsecSept	Psectrocladius se	B	0	0	0	0	0	0	0	0	0	0	0	0	0	0	0	0	0	0	0	0	0	0	0	0	0	0	0	0	0
Ambig	Corynocera ambi	B	0	0	0	0	0	0	0	0	0	0	0	0	0	0	0	0	0	0	0	0	0	0	0	0	0	0	0	0	0
Calc	Psectrocladius ca	B	2	0	1.5	0	0	0	0	0	0	0	0	0	0	0	0	0	0	0	0	0	0	0	0	1.9	0	1.8	0	0	0
Sergent	Sergentia coracin	B	0	0	0	11.9	47.2	21.4	0	26.3	6.7	21.4	13.5	19.4	22.4	10.3	0	13.3	8.5	0	19.4	26.5	21.9	30.8	32.7	19.2	20.4	7	0	13.3	5
Barb	Psectrocladius ba	B	0	0	0	0	0	0	0	0	0	0	0	0	0	0	0	0	0	0	0	0	0	0	0	0	0	0	0	0	0
ParaAust	Paratanytarsus a	B	0	0	0	9.5	36.1	0	2.6	8.8	24.4	31	48.6	44.4	46.6	33.3	28.3	8.4	18.6	51.1	13.4	14.3	1.4	0	0	0	0	0	0	0	0
CrictoC	Crictopus C	B	0	0	0	0	0	0	0	0	0	0	0	0	0	0	0	0	0	0	0	0	0	0	0	0	0	0	0	0	0
Synorth	Synorthocladius	B	0	0	0	0	0	0	0	0	0	0	0	0	0	0	0	0	0	0	0	0	0	0	0	0	0	0	0	0	0
Proplac	Propsilocerus lac	B	0	0	0	0	0	0	0	0	0	0	0	0	0	0	0	0	0	0	0	0	0	0	0	0	0	0	0	0	0
CoryA	Coryneura artica	B	0	0	0	0	0	0	0	0	0	0	0	0	0	0	0	0	0	0	0	0	0	0	0	0	0	0	0	0	0
OrthoTrig	Orthocladius trig	B	0	0	0	0	0	0	0	0	0	2.7	0	3.4	5.1	0	3.6	16.9	4.4	9	4.1	11	5.8	0	0	0	0	0	0	0	0
MicroCon	Microspectra con	B	0	0	0	0	0	0	0	0	0	0	0	0	0	0	0	0	0	0	0	0	0	0	0	0	0	0	3.7	0	0
ParaCric	Paracricotopus	B	0	0	0	0	0	0	0	0	0	0	0	0	0	0	0	0	0	0	0	0	0	0	0	0	0	0	0	0	0
EukClar	Eukiefferiella clar	B	0	0	0	0	0	0	0	0	0	0	0	0	0	0	0	0	0	0	0	0	0	0	0	0	0	0	0	0	0
Pedel	Microtendipes pe	C	9.8	18.5	10.3	52.4	8.3	21.4	12.8	31.6	15.6	7.1	18.9	16.7	0	0	6.5	3.6	0	4.4	0	2	0	0	0	1.9	0	29.8	11.1	5	5
Syl	Crictopus sylvest	C	0	0	0	0	0	0	0	0	0	0	0	0	0	0	4.3	0	0	0	0	0	0	0	0	0	0	0	0	0	0
Smit	Smittia	C	0	0	0	0	0	0	0	0	0	0	0	0	0	0	0	0	0	0	0	0	0	0	0	0	0	0	0	0	0
CrictLar	Crictopus laricor	C	0	0	0	0	0	0	0	0	0	0	0	0	0	0	0	0	0	0	0	0	0	0	0	0	0	0	0	0	0
Sympo	Symposiocladius	C	0	0	0	0	0	0	0	0	0	0	0	0	0	0	0	0	0	0	0	0	0	0	0	0	0	0	0	0	0
CricoTri	Crictopus trifasci	C	0	4.6	0	0	2.8	7.1	7.7	3.5	6.7	4.8	5.4	0	0	0	0	0	0	0	0	0	0	0	2	0	0	1.8	5.6	1.7	8.3
RheoChal	Rheocrictopus ch	C	0	0	0	0	0	0	0	0	0	0	0	0	0	0	0	0	0	0	0	0	0	0	0	0	0	0	0	0	0
Endotend	Endochironomus	C	0	0	0	0	0	0	0	0	0	0	0	0	0	0	0	0	0	0	0	0	0	0	0	0	0	0	0	0	0
Endoalb	Endochironomus	C	0	0	0	0	0	0	0	0	0	0	0	0	0	0	0	0	0	0	0	0	0	0	0	0	0	3.5	13	0	0
Cladolat	Cladopelma later	C	2	0	0	0	0	0	0	0	2.2	0	0	0	0	0	0	0	0	0	0	0	0	0	0	0	0	0	0	0	0
Parapen	Paratanytarsus pe	C	11.8	15.4	29.4	0	0	35.7	33.3	7	0	0	0	0	0	0	0	0	0	0	0	0	0	0	0	0	0	15.8	24.1	41.7	43.3
OrthoI	Orthocladius I	C	0	0	0	0	0	0	0	0	0	0	0	0	0	0	0	0	0	0	0	0	0	0	0	0	0	0	0	0	0
ParaChe	Parachaetocladiu	C	0	0	0	0	0	0	0	0	0	0	0	0	0	0	0	0	0	0	0	0	0	0	0	0	0	0	0	0	0
HeteroG	Heterotrissocladi	C	0	0	0	0	0	0	0	0	0	0	0	0	0	0	0	0	0	0	0	0	0	0	0	0	0	0	0	0	0
Rheoeff	Rheocrictopus eff	C	0	0	0	0	0	0	0	0	0	0	0	0	0	0	0	0	0	0	0	0	0	0	0	0	0	0	1.9	0	0
OrthoO	Orthocladius oliv	C	0	0	0	0	0	0	0	0	0	0	0	0	0	0	0	0	0	0	0	0	0	0	0	0	0	0	1.9	5	6.7
CricOb	Crictopus obnixu	C	0	1.5	1.5	2.4	5.6	0	2.6	1.8	0	0	0	0	0	0	0	0	0	0	0	0	0	0	0	0	0	0	0	0	0
Nerv	Dicrotendipes ne	D	0	0	0	0	0	0	0	0	0	0	0	0	0	0	0	0	0	0	0	0	0	0	0	0	0	0	0	0	0
Proclad	Procladius	D	0	4.6	2.9	7.1	0	0	5.1	5.3	6.7	7.1	0	0	0	0	6.5	3.6	0	0	0	1.4	0	0	0	0	0	0	0	0	3.3
Glab	Tanytarsus glabre	D	0	0	0	0	0	0	0	0	0	0	0	0	0	0	0	0	0	0	0	0	0	0	0	0	0	0	7.4	0	0
TanyPall	Tanytarsus pallidi	D	3.9	0	0	0	0	0	0	0	0	0	0	0	0	0	0	0	0	0	0	0	0	0	0	0	31.5	19.3	7.4	3.3	6.7
Pagast	Pagastiella	D	0	0	0	0	0	0	0	0	0	0	0	0	0	0	0	0	0	0	0	0	0	0	0	0	0	0	0	0	0
Anthra	Chironomus anth	D	3.9	0	5.9	2.4	0	0	2.6	5.3	17.8	7.1	0	5.6	1.7	0	0	1.2	5.1	4.4	0	2	0	0	0	0	0	1.8	0	1.7	0
Mendx	Tanytarsus mend	D	0	1.5	0	2.4	0	0	2.6	1.8	0	0	0	0	0	0	0	0	0	0	0	0	0	0	0	1.9	0	5.3	1.9	0	0
Ablab	Ablabesmyia	D	0	1.5	0	2.4	0	7.1	2.6	3.5	6.7	2.4	5.4	0	0	0	2.2	0	0	0	0	2	0	0	0	1.9	0	0	1.9	0	0
Polyped	Polypedulim nub	D	47.1	20	26.5	4.8	0	0	5.1	0	0	0	0	0	0	0	0	0	0	0	0	0	0	0	0	0	0	0	0	0	0
Paraalb	Paratentipes albi	D	0	0	4.4	0	0	0	0	0	0	0	0	0	0	0	0	0	0	0	0	0	0	0	0	0	0	0	0	0	0
Crypto	Cryptochironom	D	0	0	0	0	0	0	0	0	0	0	0	0	0	0	0	0	0	0	0	0	0	0	0	0	0	0	0	0	0
Glypto	Glyptotendipes p	D	13.7	13.8	14.7	2.4	0	3.6	12.8	0	0	0	0	0	0	0	0	0	0	0	0	0	0	0	0	0	0	0	0	0	0
Glyptsv	Glyptotendipes s	D	0	0	1.5	0	0	0	0	0	0	0	0	0	0	0	0	0	0	0	0	0	0	0	0	0	0	0	0	0	0
SUM(A)	Ultra-cold	T	0	0	0	0	0	3.6	2.6	3.5	0	7.1	2.7	8.3	10.3	23.1	47.8	39.8	23.7	15.6	20.9	16.3	20.5	17.3	0	1.9	5.6	1.8	3.7	0	0
SUM(B)	Cold	T	7.8	18.5	2.9	23.8	83.3	21.4	10.3	36.8	44.4	64.3	67.6	69.4	87.9	76.9	32.6	51.8	71.2	75.6	79.1	77.6	78.1	82.7	98	92.3	63	21.1	20.4	41.7	26.7
SUM(C)	Temperate	T	23.5	40	41.2	54.8	16.7	64.3	56.4	43.9	24.4	11.9	24.3	16.7	0	0	10.9	3.6	0	4.4	0	2	0	0	2	1.9	0	50.9	57.4	53.3	63.3
SUM(D)	Warm	T	68.6	41.5	55.9	21.4	0	10.7	30.8	15.8	31.1	16.7	5.4	5.6	1.7	0	8.7	4.8	5.1	4.4	0	4.1	1.4	0	0	3.8	31.5	26.3	18.5	5	10
SSUM(T)	Total Chironomi	A;B;C;D	51	65	68	42	36	28	39	57	45	42	37	36	58	39	46	83	59	45	67	49	73	52	49	52	54	57	54	60	60

Pollen	Column1	Column2	353	354	355	356	357	358	359	360	361	362	364	365	366	367	368	369	372	375	377	379	380	381	382	384	386	387	389	390	391	392	393	394	396	397	399	405
Code	Name	Group																																				
Lugens	Tanytarsus lugen	A	1.8	5	2.5	0	0	3.3	1.6	12.5	0	0	0	8.9	0	0	0	5.4	1.6	2.4	4.5	0	0	5.8	0	5.7	0	10.2	0	10.7	0	10.4	0	2	2.3	5.5	7.5	13.3
Conform	Hydrobeanus con	A	0	0	0	0	0	0	0	0	0	0	0	0	0	0	0	0	0	1.2	4.5	0	0	0	1.9	0	0	0	0	0	0	0	0	2	0	0	6	2.2
Paraclad	Paracladius	A	0	0	0	0	0	0	0	0	0	0	0	0	0	0	0	2.7	0	0	0	0	0	0	0	0	0	0	0	0	0	0	0	0	0	1.8	0	0
Radial	Microspectra rad	A	0	7.5	0	0	0	20	26.6	13.9	0	0	0	0	0	0	0	0	0	2.4	7.6	16.2	1.5	0	5.7	0	2	0	0	0	0	0	0	2	2.3	0	4.5	4.4
OrthoS	Orthocladius S	A	0	0	0	0	0	0	0	0	0	7.6	0	0	0	2.4	4.3	0	1.6	0	1.5	0	0	0	0	0	0	2	0	0	0	0	2.5	2	0	0	1.5	0
Tanychin	Tanytarsus chiny	A	0	0	0	0	0	0	0	0	0	0	0	0	0	0	0	0	0	0	0	0	0	0	0	0	0	0	0	0	0	0	0	0	0	0	0	0
Protany	Protanypus	A	0	0	0	0	0	0	0	0	0	0	0	0	0	0	0	0	0	0	0	0	0	0	0	0	0	0	0	0	0	0	0	0	0	0	0	0
Pseudodi	Pseudodiamesa	A	0	0	1.3	0	0	1.7	1.6	0	1.4	1.5	0	0	0	0	2.1	0	1.6	0	0	0	0	0	0	0	0	0	0	0	0	0	0	4	0	0	0	0
OrthoCon	Orthocladius con	A	17.5	12.5	20.3	2.2	15.6	11.7	0	2.8	0	1.5	0	0	0	0	2.1	16.2	4.8	9.5	1.5	0	6.2	7.7	7.5	10	0	0	0	0	0	0	0	2	0	9.1	13.4	17.8
ChaetoB	Chaetocladius B	A	0	0	0	0	0	0	1.6	0	0	0	0	0	0	0	0	0	0	0	0	5.4	0	0	0	0	4.1	0	0	0	0	0	2.5	0	0	0	1.5	0
Diamab	Diamesa aberata	A	0	0	0	0	0	0	0	0	0	0	0	0	0	0	0	0	0	0	0	0	0	0	0	0	0	0	0	0	0	0	0	0	0	0	0	0
Insig	Micropsectra insi	B	1.8	0	0	2.2	2.2	3.3	4.7	4.2	0	3	0	0	10.6	23.8	0	0	4.8	2.4	0	0	4.6	3.8	3.8	2.9	6.1	6.1	0	7.1	4.7	8.3	10	4	0	9.1	9	0
Oliv	Corynocera olive	B	12.3	7.5	8.9	0	0	1.7	3.1	4.2	0	6.1	4.5	1.8	6.4	4.8	0	2.7	6.5	4.8	10.6	8.1	15.4	11.5	0	0	2	2	0	8.9	2.3	6.3	2.5	4	13.6	0	6	6.7
Sordi	Psectorcladius so	B	5.3	0	3.8	0	0	0	1.6	1.4	1.4	0	0	0	2.1	0	8.5	10.8	4.8	19	0	0	9.2	7.7	7.5	11.4	4.1	10.2	6.6	10.7	4.7	8.3	0	0	18.2	10.9	3	0
Cricto	Crictopus interse	B	0	0	3.8	0	0	8.3	7.8	2.8	1.4	1.5	13.6	0	4.3	2.4	0	0	1.6	6	6.1	54.1	16.9	3.8	5.7	2.9	0	0	0	1.8	0	8.3	0	2	0	7.3	0	0
PsecSept	Psectrocladius se	B	0	0	0	0	0	0	0	0	0	0	0	0	0	0	0	0	0	0	0	0	0	0	0	0	0	0	0	0	0	0	0	0	0	0	0	0
Ambig	Corynocera ambi	B	0	0	0	0	0	1.7	0	0	0	0	0	0	0	0	0	0	0	0	0	0	0	0	0	0	0	0	0	0	0	0	0	0	0	0	0	0
Calc	Psectrocladius ca	B	0	0	0	0	0	0	0	0	0	0	0	0	0	0	0	0	0	0	0	0	0	0	0	0	2	2	0	0	0	2.1	0	0	0	0	0	0
Sergent	Sergentia coracin	B	5.3	15	29.1	13.3	22.2	20	9.4	26.4	12.9	6.1	27.3	3.6	19.1	2.4	12.8	18.9	6.5	9.5	3	0	0	0	0	0	0	0	0	0	0	0	0	4	0	0	0	4.4
Barb	Psectrocladius ba	B	0	0	0	0	0	0	0	0	0	0	0	0	0	0	0	0	0	0	0	0	0	0	0	0	0	0	0	0	0	0	0	0	0	0	0	0
ParaAust	Paratanytarsus au	B	0	50	21.5	77.8	55.6	11.7	37.5	19.4	72.9	54.5	50	66.1	44.7	0	66	40.5	9.7	42.9	56.1	13.5	41.5	46.2	3.8	0	16.3	0	0	0	55.8	0	10	38	22.7	25.5	17.9	33.3
CrictoC	Crictopus C	B	0	0	0	0	0	0	0	0	0	0	0	0	0	0	0	0	0	0	0	0	0	0	0	0	0	0	0	0	0	0	0	0	0	0	0	0
Synorth	Synorthocladius	B	0	0	0	0	0	0	0	0	0	0	0	0	0	0	0	0	0	0	0	0	0	0	1.9	0	0	0	0	0	0	0	0	0	0	0	0	0
Proplac	Propsilocerus lac	B	0	0	0	0	0	0	0	0	0	0	0	0	0	0	0	0	0	0	0	0	0	0	0	0	0	0	0	0	0	0	0	0	6.8	0	6	0
CoryA	Coryneura artica	B	0	0	0	0	0	0	0	0	0	0	0	0	0	0	0	0	0	0	0	0	0	0	0	1.4	0	0	0	0	0	0	0	2	2.3	0	7.5	6.7
OrthoTrig	Orthocladius trig	B	0	0	3.8	0	2.2	15	4.7	8.3	4.3	0	2.3	0	0	0	0	0	0	0	0	2.7	0	0	0	0	0	0	0	0	0	0	0	24	0	0	7.5	0
MicroCon	Micropsectra con	B	0	0	0	0	0	0	0	0	0	0	0	0	0	0	0	0	0	0	0	0	0	0	0	0	0	0	0	0	0	0	0	0	0	0	0	0
ParaCric	Paracricotopus	B	0	0	0	0	0	0	0	0	0	0	0	0	0	0	0	0	0	0	1.5	0	1.5	1.9	1.9	0	0	0	0	0	0	0	0	0	0	0	0	0
EukClar	Eukiefferiella clar	B	0	0	0	0	0	0	0	0	0	0	0	0	0	0	0	0	0	0	0	0	0	0	0	0	0	0	0	0	0	0	0	0	0	0	0	0
Pedel	Microtendipes pe	C	36.8	0	1.3	2.2	0	0	0	0	2.9	1.5	0	3.6	0	0	0	0	3.2	0	0	0	0	0	3.8	0	0	0	0	5.4	4.7	4.2	0	0	15.9	29.1	4.5	4.4
Syl	Crictopus sylvest	C	0	0	0	0	0	0	0	0	0	0	0	0	0	0	0	0	0	0	0	0	0	0	0	0	0	0	0	0	0	0	2.5	0	0	0	0	0
Smit	Smittia	C	0	0	0	0	0	0	0	0	0	0	0	0	0	0	0	0	0	0	0	0	0	0	0	1.4	0	0	0	0	0	0	0	0	0	0	0	0
CrictLar	Crictopus laricon	C	0	0	0	0	0	0	0	0	0	0	0	0	0	0	0	0	0	0	0	0	0	0	0	0	0	0	0	0	0	0	0	0	0	0	0	0
Sympo	Symposiocladius	C	0	0	0	0	0	0	0	0	0	0	0	0	0	0	0	0	0	0	0	0	0	0	0	0	0	0	0	0	0	0	0	0	2.3	0	0	2.2
CricoTri	Crictopus trifasci	C	1.8	0	0	0	0	0	0	0	0	0	0	5.4	0	2.4	0	0	1.6	0	0	0	0	1.9	0	4.3	2	2	4.9	1.8	2.3	2.1	0	6	0	0	0	0
RheoChal	Rheocrictopus ch	C	0	0	0	0	0	0	0	0	0	0	0	0	0	0	0	0	0	0	0	0	0	0	0	0	0	0	0	0	0	0	0	0	0	0	0	0
Endotend	Endochironomus	C	0	0	0	0	0	0	0	0	0	0	0	0	0	0	0	0	0	0	0	0	0	0	0	0	0	0	0	0	0	0	0	0	0	0	0	0
Endoalb	Endochironomus	C	0	0	0	0	0	0	0	0	0	0	0	0	0	0	0	0	0	0	0	0	0	0	0	0	0	0	0	0	0	0	0	0	0	0	0	0
Cladolat	Cladopelma later	C	0	0	0	0	0	0	0	0	0	0	0	0	0	0	0	0	0	0	0	0	0	0	0	0	0	0	0	0	0	0	0	0	0	0	0	0
Parapen	Paratanytarsus pe	C	15.8	0	0	0	0	0	0	0	0	6.1	0	3.6	12.8	47.6	4.3	2.7	45.2	0	0	0	0	0	24.5	40	42.9	51	59	50	11.6	27.1	35	0	0	0	0	0
OrthoI	Orthocladius I	C	0	0	0	0	0	0	0	0	0	0	0	0	0	0	0	0	0	0	0	0	0	0	0	0	0	0	0	0	0	0	0	0	0	0	0	0
ParaChe	Parachaetocladiu	C	0	0	0	0	0	0	0	0	0	0	0	0	0	0	0	0	0	0	0	0	0	0	0	0	0	0	0	0	0	0	0	0	0	0	1.5	0
HeteroG	Heterotrissocladi	C	0	0	0	0	0	0	0	0	0	0	0	0	0	0	0	0	0	0	0	0	0	0	0	0	0	0	0	0	0	0	0	0	2.3	0	0	0
Rheoeff	Rheocrictopus eff	C	0	0	0	0	0	0	0	0	0	0	0	0	0	0	0	0	0	0	0	0	0	0	0	0	0	0	0	0	0	0	0	0	0	0	0	0
OrthoO	Orthocladius oliv	C	0	0	0	0	0	0	0	0	0	0	0	0	0	0	0	0	6.5	0	1.5	0	1.5	5.8	28.3	18.6	18.4	12.2	29.5	3.6	7	0	35	0	0	0	0	0
CricOb	Crictopus obnixu	C	0	0	0	0	0	0	0	0	0	0	0	0	0	0	0	0	0	0	0	0	0	0	0	1.4	0	0	0	0	0	0	0	0	0	0	0	0
Nerv	Dicrotendipes ne	D	0	0	0	0	0	0	0	0	0	0	0	0	0	0	0	0	0	0	0	0	0	0	0	0	0	0	0	0	0	0	0	0	0	0	0	2.2
Proclad	Procladius	D	0	0	2.5	0	0	0	0	0	0	0	0	1.8	0	2.4	0	0	0	0	0	0	0	0	0	0	0	0	0	0	7	2.1	0	0	0	0	0	0
Glab	Tanytarsus glabr	D	0	0	0	0	0	0	0	0	0	0	0	0	0	0	0	0	0	0	0	0	0	0	0	0	0	0	0	0	0	0	0	0	0	0	0	0
TanyPall	Tanytarsus pallidi	D	0	0	0	0	0	0	0	0	0	0	0	0	0	0	0	0	0	0	0	0	0	0	0	0	0	0	0	0	0	2.1	0	0	0	0	0	0
Pagast	Pagastiella	D	0	0	0	0	0	0	0	0	0	0	0	0	0	0	0	0	0	0	0	0	0	0	0	0	0	0	0	0	0	0	0	0	0	0	0	0
Anthra	Chironomus anth	D	1.8	2.5	0	2.2	2.2	0	0	4.2	2.9	10.6	2.3	5.4	0	11.9	0	0	0	0	0	0	0	1.9	1.9	0	0	2	0	0	0	0	0	2	0	1.8	0	2.2
Mendx	Tanytarsus mend	D	0	0	1.3	0	0	0	0	0	0	0	0	0	0	0	0	0	0	0	0	0	0	0	0	0	0	0	0	0	0	16.7	0	0	6.8	0	1.5	0
Ablab	Ablabesmyia	D	0	0	0	0	0	1.7	0	0	0	0	0	0	0	0	0	0	0	0	1.5	0	1.5	1.9	1.9	0	0	0	0	0	0	2.1	0	0	4.5	0	1.5	0
Polyped	Polypedilum nub	D	0	0	0	0	0	0	0	0	0	0	0	0	0	0	0	0	0	0	0	0	0	0	0	0	0	0	0	0	0	0	0	0	0	0	0	0
Paraalb	Paratentipes albi	D	0	0	0	0	0	0	0	0	0	0	0	0	0	0	0	0	0	0	0	0	0	0	0	0	0	0	0	0	0	0	0	0	0	0	0	0
Crypto	Cryptochironomu	D	0	0	0	0	0	0	0	0	0	0	0	0	0	0	0	0	0	0	0	0	0	0	0	0	0	0	0	0	0	0	0	0	0	0	0	0
Glypto	Glyptotendipes p	D	0	0	0	0	0	0	0	0	0	0	0	0	0	0	0	0	0	0	0	0	0	0	0	0	0	0	0	0	0	0	0	0	0	0	0	0
Glyptsv	Glyptotendipes s	D	0	0	0	0	0	0	0	0	0	0	0	0	0	0	0	0	0	0	0	0	0	0	0	0	0	0	0	0	0	0	0	0	0	0	0	0
SUM(A)	Ultra-cold	T	19.3	25	24.1	2.2	15.6	36.7	31.3	29.2	1.4	10.6	0	8.9	0	2.4	8.5	24.3	9.7	15.5	19.7	21.6	7.7	13.5	15.1	15.7	6.1	12.2	0	10.7	0	10.4	5	14	4.5	16.4	34.3	37.8
SUM(B)	Cold	T	24.6	72.5	70.9	93.3	82.2	61.7	68.8	66.7	92.9	71.2	97.7	71.4	87.2	33.3	87.2	73	33.9	84.5	77.3	78.4	89.2	75	24.5	18.6	30.6	20.4	6.6	28.6	67.4	33.3	22.5	78	63.6	52.7	56.7	51.1
SUM(C)	Temperate	T	54.4	0	1.3	2.2	0	0	0	0	2.9	7.6	0	12.5	12.8	50	4.3	2.7	56.5	0	1.5	0	1.5	7.7	56.6	65.7	63.3	65.3	93.4	60.7	25.6	33.3	72.5	6	20.5	29.1	6	6.7
SUM(D)	Warm	T	1.8	2.5	3.8	2.2	2.2	1.7	0	4.2	2.9	10.6	2.3	7.1	0	14.3	0	0	0	0	1.5	0	1.5	3.8	3.8	0	0	2	0	0	7	22.9	0	2	11.4	1.8	3	4.4
SSUM(T)	Total Chironomi	A;B;C;D	57	40	79	45	45	60	64	72	70	66	44	56	47	42	47	37	62	84	66	37	65	52	53	70	49	49	61	56	43	48	40	50	44	55	67	45